

J. Wijker

Spacecraft Structures

 Springer

Spacecraft Structures

Jacob Job Wijker

Spacecraft Structures

With 199 Figures and 106 Tables



Jacob Job Wijker
Dutch Space BV
P.O. Box 32070
NL-2303 DB Leiden
The Netherlands
www.dutchspace.nl

ISBN 978-3-540-75552-4 e-ISBN 978-3-540-75553-1

DOI 10.1007/978-3-540-75553-1

Library of Congress Control Number: 2007939115

© 2008 Springer-Verlag Berlin Heidelberg

This work is subject to copyright. All rights are reserved, whether the whole or part of the material is concerned, specifically the rights of translation, reprinting, reuse of illustrations, recitation, broadcasting, reproduction on microfilm or in any other way, and storage in data banks. Duplication of this publication or parts thereof is permitted only under the provisions of the German Copyright Law of September 9, 1965, in its current version, and permission for use must always be obtained from Springer. Violations are liable to prosecution under the German Copyright Law.

The use of general descriptive names, registered names, trademarks, etc. in this publication does not imply, even in the absence of a specific statement, that such names are exempt from the relevant protective laws and regulations and therefore free for general use.

Typesetting: perform electronic publishing GmbH, Heidelberg
Production: LE-TEX Jelonek, Schmidt & Voeckler GbR, Leipzig
Cover design: eStudio Calamar S.L., F. Steinen-Broo, Girona, Spain

Printed on acid-free paper SPIN: 12094448 60/3180/YL

9 8 7 6 5 4 3 2 1

springer.com

To my wife Wil

Preface

This book about spacecraft structures design reflects my experiences gained at Dutch Space B.V., formerly Fokker Space B.V., Fokker Space & Systems B.V. and the Space Division of Fokker Aircraft B.V., over a period of about 35 years.

I work as a part-time associate professor at the Chair Aerospace Structures, Faculty of Aerospace Engineering, Delft University of Technology, and lecture “Spacecraft Structures” in the Master’s program. The scientific environment at the university, in combination with my work in the aerospace industry, has amplified the wish to write a book about spacecraft structures design.

I would like to express my admiration for the patient attitude of my wife Wil during the time I was preparing the manuscript of this book.

I would also like to acknowledge my colleagues at Dutch Space and the Delft University of Technology, for all the discussions within the framework of spacecraft structures projects.

Velserbroek 2007

Jaap Wijker

Contents

1 General	1
1.1 Introduction	1
1.2 Literature	3
2 Design Process.....	5
2.1 Introduction	5
2.2 Design criteria	5
2.3 Design specification	5
2.4 Design	6
2.5 Design control	6
2.6 Exercises	7
2.6.1 Design and development	7
3 Launch Vehicle Systems.....	9
3.1 Introduction	9
3.1.1 Launch Vehicle User's manual	10
3.2 Literature	11
3.3 Exercises	11
3.3.1 Definition the mechanical design specification.....	11
4 Spacecraft Subsystems	13
4.1 Introduction	13
4.2 Power Supply.....	14
4.3 Attitude Control system.....	14
4.4 Data Systems	14
4.5 Thermal Control System	14
4.6 Telecommunication Systems.....	15

4.7 Propulsion System	15
4.8 Structure	15
4.9 Mutual Interaction of Subsystems	15
4.9.1 Power Supply versus Attitude control System	15
4.9.2 Power Supply versus Thermal Control System	16
4.9.3 Attitude Control System versus Thermal Control System	16
4.9.4 Thermal Control System versus Structure	16
4.10 Literature	17
5 Design and Safety factors	19
5.1 Introduction	19
5.2 Terminology	19
5.2.1 Flight Limit Load	19
5.2.2 Design Limit Load	19
5.2.3 Ultimate Load	20
5.2.4 Buckling Load	20
5.2.5 Yield Load	20
5.2.6 Proof Load	20
5.2.7 Allowable stress	20
5.2.8 Material Strength	20
5.2.9 A-value (A basis)	21
5.2.10 B-value (B basis)	21
5.2.11 S-Value (S-basis)	22
5.2.12 Qualification Loads	23
5.2.13 Flight Acceptance Loads	23
5.2.14 Margin of Safety	23
5.2.15 Fail-Safe	23
5.2.16 Safe-life	23
5.3 Factors of Safety for Spacecraft	24
5.4 Literature	25
5.5 Exercises	25
5.5.1 Survey of Applied Factors of Safety	25
6 Spacecraft Design Loads	27
6.1 Introduction	27
6.2 Transportation load factors	29
6.3 Steady-State Loads	29
6.4 Mechanical Dynamic loads	30
6.4.1 Sinusoidal loads	30
6.4.2 Random loads	38

6.5	Acoustic loads	45
6.5.1	Sound Pressure Level	46
6.5.2	Octave band	49
6.5.3	Centre frequency	49
6.5.4	Relative bandwidth	49
6.5.5	Power Spectral Density	51
6.5.6	Conversions of SPL	52
6.5.7	Acoustic Fill Factor	55
6.6	Shock loads	56
6.6.1	Introduction	56
6.6.2	Enforced acceleration	58
6.6.3	Shock Attenuation Rules	61
6.6.4	SRS Tolerance Limit	62
6.7	Static pressure variations	62
6.8	Micro-meteorites / Orbital Debris	63
6.8.1	Introduction	63
6.8.2	Simple Micro Meteoroid Flux Model	64
6.8.3	Simple Debris flux Model	64
6.9	Literature	66
6.10	Exercises	66
6.10.1	Sinusoidal Vibrations	66
6.10.2	Tuned Damper	67
6.10.3	Calculation of PSD's and Grms	68
6.10.4	Prove of conversion formulae	69
	6.10.5 Calculation of OASPL and conversion to 1/3-octave band	69
7	Test Verification	71
7.1	Introduction	71
7.2	Tests	71
7.3	Goal of the tests	72
7.4	Test Plan	73
7.5	Test Procedure	74
7.6	Model philosophy	74
7.7	Static Test	75
7.7.1	Sine-burst test	76
7.7.2	Sine-dwell test	77
7.8	Mechanical Vibration/Acoustic Tests	77
7.8.1	Sine Vibration Test	78
7.8.2	Random Vibration Test	82
7.8.3	Acoustic Vibration Test	83

7.8.4 Shock test.	85
7.8.5 Modal Survey/Modal Analysis Test	85
7.9 Notching	86
7.9.1 Notching at Equipment Level	86
7.9.2 Notching at main resonances on basis of quasi-static loads	93
7.9.3 Force Limiting Vibration Testing	96
7.10 Plots	97
7.11 Test Facilities West-Europe	98
7.12 Literature	99
8 Design of Spacecraft structure	101
8.1 Introduction	101
8.2 Determination of Spacecraft Configuration	101
8.2.1 Boundary Conditions Launch Vehicle	103
8.2.2 Launch mass	103
8.2.3 Available Launch Volume	103
8.2.4 Launch Vehicle Adapter (LVA)	104
8.2.5 Payload Separation System	104
8.2.6 Functional requirements spacecraft	105
8.3 First Design Spacecraft Structure	105
8.3.1 Design Loads	106
8.3.2 Stiffness requirements (natural frequencies)	107
8.3.3 Quasi-static loads	108
8.3.4 Mass Acceleration Curve (MAC)	109
8.3.5 Random Loads	110
8.3.6 Factors of Safety	110
8.4 Basic Design Supporting Structure	111
8.4.1 Design criteria	111
8.4.2 Standard structural elements of spacecraft structures	112
8.4.3 Selection of materials	114
8.5 Detailed Analyses	116
8.5.1 Finite Element Model	117
8.5.2 Finite Element Model Verification	117
8.5.3 Finite Element Analyses	118
8.6 Manufacturing of the spacecraft structure	119
8.7 Testing	120
8.8 Literature	121
8.9 Exercises	121
8.9.1 Use of the User's Manual of ARIANE 5	121

9 Strength and Stiffness of Structural Elements	123
9.1 Introduction	123
9.2 Trusses and Truss frames	124
9.3 Bending of Beams, Myosotis Method	127
9.3.1 Bending of Beams by transverse forces and bending moments	127
9.3.2 Buckling of Struts	128
9.3.3 Bending stresses in beams	133
9.3.4 Shear stresses in beams	134
9.3.5 Torsion of Beams	136
9.3.6 Local buckling of thin-walled tubes	139
9.3.7 Rings	141
9.4 Platforms	142
9.5 Panels	142
9.6 Shells of revolution: cylinders / cones	143
9.6.1 Stability of Cylinders	143
9.6.2 Stiffness of Cylinders	145
9.6.3 Running Loads in Cylinder	146
9.6.4 Stiffness of Cones	147
9.6.5 Stability of Cones	149
9.7 Stresses in Lap Joints	150
9.8 Literature	151
9.9 Exercises	152
9.9.1 Deflection of truss frame	152
9.9.2 Deflection of a beam	152
9.9.3 Deflection and bending moment in a clamped-clamped beam	153
9.9.4 Buckling of Beam with Variable Cross-section	153
9.9.5 Buckling of Square Tube	154
9.9.6 Torsion and Shear Force	155
9.9.7 Stiffness and Buckling of a Cone	155
10 Sandwich Construction	157
10.1 Introduction	157
10.1.1 Design aspects	158
10.2 Optimum design: Determination of core and face sheet thickness for minimum mass	159
10.3 Stresses	160
10.3.1 Stresses in face sheets	161
10.3.2 Shear stress	162
10.3.3 Failure modes	162
10.4 Buckling Sandwich Columns	163

10.5 Global Buckling Cylinder	164
10.6 Local Buckling	166
10.6.1 Combined Loads	168
10.7 Inserts	168
10.8 Honeycomb mechanical properties	170
10.9 Typical connections	171
10.10 Literature	172
10.11 Exercises	172
10.11.1 Stiffness Sandwich Beam	172
11 Finite Element Analysis	175
11.1 Introduction	175
11.2 Theory	175
11.2.1 Static Calculations	176
11.2.2 Dynamic Calculations	181
11.3 Mathematical Model	184
11.4 Finite element type	185
11.5 Number of degrees of freedom	186
11.6 Joints	186
11.7 Damping	186
11.7.1 Spacecraft	188
11.7.2 Launch vehicles	188
11.8 Modifications	188
11.9 Finite element model to be delivered	189
11.9.1 Coordinate systems	189
11.9.2 Units	189
11.9.3 Numbering schemes	190
11.9.4 Reaction forces in case unit forces of inertia occur	190
11.9.5 Elastic Energy as Rigid Body	190
11.9.6 Reduced finite element model	193
11.9.7 Reports regarding the finite element model	193
11.9.8 Electronic Carrier	194
11.10 Literature	195
11.11 Exercises	195
11.11.1 Application Lagrange's Equations	195
11.11.2 Deployed Natural Frequency	196
11.11.3 Natural frequency cantilever beam	196

12 Stiffness/Flexibility Analysis	199
12.1 Introduction	199
12.2 Examples	200
12.2.1 ATV Cargo Carrier	200
12.2.2 ARIANE 5 Bati-Moteur (BME)	200
12.3 The unit force method	201
12.4 Reduced stiffness matrix	202
12.5 Unit displacement	202
12.6 Principal directions	203
12.7 Literature	206
12.8 Exercises	206
12.8.1 Stiffness Pin-joined Frame	206
13 Material Selection	207
13.1 Introduction	207
13.2 Metal alloys	207
13.3 Composite materials	208
13.3.1 Physical-mechanical properties of fillers	209
13.3.2 Properties of Non-metal Matrices	210
13.3.3 Properties of Metal Matrices	211
13.4 Sandwich Honeycomb Core	211
13.5 Design considerations	212
13.6 Literature	224
14 Spacecraft Mass	215
14.1 Introduction	215
14.2 Structure Mass	217
14.3 Total Mass Calculation	217
14.3.1 Mass Matrix	217
14.3.2 Mass matrix with respect to the centre of mass	223
14.3.3 Centre of mass	223
14.3.4 Second Moments of Mass	224
14.3.5 Finite Element Model Mass Matrix	225
14.4 Literature	228
14.5 Exercises	228
14.5.1 Mass computer programme	228
15 Natural Frequencies, an Approximation	229
15.1 Introduction	229

15.2 Static Displacement Method	229
15.3 Rayleigh's Quotient	232
15.4 Dunkerley's Method	234
15.5 Literature	241
15.6 Exercises	241
15.6.1 Natural frequency of airplane	241
15.6.2 Rayleigh's method	241
15.6.3 Rayleigh's method	241
15.6.4 Equations of motion and natural frequencies	242
15.6.5 Calculation natural frequencies	243
15.6.6 Equations of motion and natural frequencies	244
15.6.7 Deployed Natural Frequency	245
16 Modal Effective Mass	247
16.1 Introduction	247
16.2 Enforced Acceleration	247
16.3 Modal Effective Masses of an MDOF System	250
16.4 Literature	259
16.5 Excercises	259
16.5.1 Large mass solution	259
16.5.2 Calculation modal effective masses cantilevered beam	260
16.5.3 Modal Effective Mass of a Cantilevered Beam	261
16.5.4 Calculation of Base Force	262
17 Dynamic Model Reduction Methods	265
17.1 Introduction	265
17.2 Static Condensation Method	266
17.3 Craig–Bampton Reduced Models	271
17.4 System Equivalent Reduction Expansion Process (SEREP)	274
17.5 Conclusion	277
17.6 Literature	278
17.7 Exercises	278
17.7.1 Reduction Finite Element Model	278
17.7.2 Reduction of dynamic 10 DOF model	279
18 Dynamic Substructuring, Component Mode Synthesis	281
18.1 Introduction	281
18.2 Special CMS Methods	282
18.2.1 Craig–Bampton Fixed-Interface Method	282

18.2.2 Free-Interface Method	287
18.2.3 General-Purpose CMS Method	294
18.3 Literature	299
18.4 Exercises	299
18.4.1 Substructure Analysis 1	299
18.4.2 Substructure Analysis	300
19 Output Transformation Matrices	303
19.1 Introduction	303
19.2 Reduced Free-Free Dynamic Model	304
19.3 References	310
19.4 Exercises	310
19.4.1 Problem 1	310
19.4.2 Problem 2	311
20 Coupled Dynamic Loads Analysis	313
20.1 Introduction	313
20.2 Finite Element Validation	315
20.3 Literature	318
20.4 Exercises	318
20.4.1 Internet search	318
21 Random Vibrations Simplified Response Analysis	319
21.1 Introduction	319
21.2 Low frequency	319
21.2.1 The response of a single mass-spring system due to a random force or base excitation	320
21.2.2 Damping	325
21.2.3 Static Assumed Mode Random Vibration Response Analysis	325
21.2.4 Passages	326
21.2.5 Calculation of the rms stresses / forces	329
21.2.6 Reaction Forces	333
21.3 Acoustic Analysis	334
21.3.1 Introduction	334
21.3.2 Acoustic loads transformed into mechanical random vibrations	335
21.3.3 Component Vibration Requirements	337
21.3.4 Static approach	339
21.3.5 The stress in an acoustically loaded panel	340
21.4 Literature	344

21.5 Exercises	345
21.5.1 Calculation of PSD Function.	345
21.5.2 Peak Pressure Values	345
21.5.3 Simply Supported Plate [Blevins 1989]	346
21.5.4 Waves	346
22 Fatigue Life Prediction	349
22.1 Introduction	349
22.2 Palmgren-Miner Linear Cumulative Damage Rule.	349
22.3 Analysis of Load-time Histories	351
22.4 Failure due to Sinusoidal Vibrations	353
22.5 Failure due to Narrow-banded Random Vibrations.	355
22.6 Literature	363
22.7 Internet.	363
22.8 Exercises	363
22.8.1 Fatigue life prediction sinusoidal vibration.	363
22.8.2 Fatigue life prediction random vibration.	365
23 Shock-Response Spectrum	367
23.1 Introduction	367
23.2 Enforced Acceleration.	368
23.3 Numerical Calculation of the SRS, the Piece wise Exact Method	370
23.4 Response Analysis in Combination with Shock-Response Spectra	375
23.5 Matching Shock Spectra with Synthesised Time Histories.	385
23.6 Literature	396
23.7 Exercises	396
23.7.1 Calculation of Shock Response Curves.	396
23.7.2 Problem 2.	398
24 Damage to Spacecraft by Meteoroids and Orbital Debris	399
24.1 Introduction	399
24.2 Micro-Meteoroids and Space Debris Environment.	400
24.2.1 Micro-Meteoroids Environment	400
24.2.2 Orbital debris Environment.	402
24.3 Hyper Velocity Impact Damage Models	405
24.3.1 Single Plate Penetration Equations	405
24.3.2 Multi-shock shield.	406
24.4 Probability of Impacts	409
24.5 Literature	411

25 Prescribed Averaged Temperatures	413
25.1 Introduction	413
25.2 PAT method	413
25.3 PAT Method Applied to a Simplified Solar Array.....	418
25.4 Literature	430
25.5 Exercises	430
25.5.1 Temperature interpolation in finite element model.....	430
26 Thermal-elastic Stresses	433
26.1 Introduction	433
26.2 Material properties.....	439
26.3 Literature	440
26.4 Exercises	440
26.4.1 Thermal stress in beam	440
26.4.2 Self Strained Structure.....	440
27 Coefficients of thermal & moisture expansion	443
27.1 Introduction	443
27.2 Coefficient of thermal expansion	443
27.2.1 The CTE as a derivative of the thermal expansibility.....	443
27.2.2 The Secant CTE.....	444
27.3 Moisture coefficient of expansion (CME).....	445
28 Venting Holes	447
28.1 Introduction	447
28.2 Venting Holes	447
28.2.1 Beryline method	447
28.2.2 The convergent Nozzle	449
28.2.3 Rule of Thumb.....	450
28.3 Literature	451
29 Examples.....	453
29.1 Introduction	453
29.2 Natural Frequencies, an Approximation	454
29.2.1 Displacement method	454
29.3 Design Example Fixed-Free Beam	455
29.3.1 Introduction	455
29.3.2 Stiffness calculations.....	456
29.3.3 Strength calculations	458

29.3.4 Effective stress.....	459
29.3.5 Iterations	460
29.4 Equivalent dynamic systems	462
29.4.1 Introduction	462
29.5 Random Vibrations	464
29.5.1 Comparison of two random vibration specifications.	464
29.5.2 Enforced random Acceleration	467
29.6 Strength and Stiffness Analysis SIMPSAT	476
29.6.1 Introduction	476
29.6.2 Design Philosophy.....	477
29.6.3 Quasi-Static Loads (QSL).....	478
29.6.4 Minimum Natural Frequencies	478
29.6.5 Material properties.	478
29.6.6 Natural Frequencies.....	478
29.6.7 Selection of the type of structure.....	481
29.6.8 Strength aspects.....	482
29.6.9 Summary MS values	487
29.7 Stiffnes calculations using Castiglano's second theorem.....	487
29.8 Modal Effective Mass of a Cantilevered Beam.....	490
29.9 Component Mode Synthesis (Craig-Bampton Method)	492
Subject Index	497

1 General

1.1 Introduction

Space flight yields results in both the field of knowledge as well as in practical applications. Space flight is of most importance to scientific research. Since the atmosphere of the Earth blocks out most kinds of radiation, research into space (planets, stars, the universe as a whole) is more feasible from space than it is from Earth.

Research in space is particularly interesting due to the lack of gravity.

Research from space, amongst others, offers the possibility to study Earth, as a whole, at a fast pace. Environmental changes as well as meteorological processes can be monitored from space in an effective and economical way.

Practical applications of space flight have become part of our lives in the form of weather and environmental satellites as well as communication satellites. The latter usually circle in a geostationary orbit at 36.000 km above the equator.

Space flight produces new technologies and has become economically viable. There is, for example, a great need for communication satellites as well as rockets to carry them into orbit.

Space flight is a comprehensive and innovative part of technology. It encompasses many fields of technology, some of which will be dealt with in this book.

This book presents a cross section of the total field of expertise that is called “space flight” and aims to provide insight into the design, construction and analysis aspects of spacecraft. Spacecraft includes satellites as well as launch vehicles, with a distinction between manned or unmanned. The International Space Station (ISS), Russian MIR the American shuttle and the European Spacelab are examples of manned space flight, whereas communication satellites for radio and television and meteorological satellites are examples of unmanned space flight. This book does not cover all aspects of manned and unmanned space missions, spacecraft and launch vehicles [Fortescue 1990, Griffin 1991, Marty 1994, Wertz 1999]. Emphasis will be on unmanned space flight, particularly on the construction of spacecraft rather than the construction of launch vehicles.

The nature of the satellite is dependent on the task that is set for that satellite. The spacecraft can be used as:

- Communication satellite (TELECOM, INTELSAT, DRS)
- TV Satellite
- Weather satellite (METEOSAT, GOES, NOAA)
- Navigation satellite (INMARSAT)
- Astronomical satellite (ANS, IRAS, ISO, Hubble Space Telescope (HST))
- Military satellite (espionage)
- Earth observation satellite (SPOT, ERS1, Landsat, RADARSAT, ENVISAT)
- Scientific satellite (EURECA, GIOTTO, CLUSTER)
- Manned space flight (Shuttle, Spacelab, MIR, Spacestation ISS)
- Micro gravitation (EURECA)
-

A spacecraft orbiting the earth, another planet in our solar system or even beyond that, is a part of a complex infrastructure consisting of the launch vehicle, which positions the spacecraft in a certain orbit and ground based stations that cater for the communications. This book will only deal with the structural aspects of spacecraft design.

A spacecraft is generally divided into two parts:

- Payload
- Service modules

The payload carries out the set task, i.e. the radio communications in a communication satellite. The spacecraft bus consists of several support systems (subsystems), such as attitude control, propulsion, power supply, thermal control, structure, deployable mechanisms (solar arrays) and telemetry.

According to H. Öry [Öry 1991], seven main parts can be distinguished in the design of a spacecraft construction:

- Load assumptions, environment
- Design criteria
- Design details, construction features, manufacturing methods
- Material selection
- Static and dynamic analysis
- Failure analyses, load bearing capacity
- Qualification and verification tests

The above mentioned parts are like the links of a chain; where it is only as strong as its weakest link. This book will discuss all of these parts in spacecraft construction design.

1.2 Literature

- Fortescue, P. and Star, J., 1990, *Spacecraft Systems Engineering*, Wiley, ISBN 0 471 92794 5.
- Griffin, D.G. and French, J.R., *Space Vehicle Design*, AIAA Education Series, 1991, ISBN 0-930403-90-8.
- Marty, D., 1994, *Systems Spatiaux, Conception et Technology*, Masson, ISBN 2-225-84460-7.
- Öry, H., 1991, *Structural Design of Aerospace Vehicles I*, Space Course, Institut fur Leichtbau, RWTH, Achen.
- Wertz, J. and Larson, J.W., 1999, *Space Mission Analysis and Design*, third edition, Space technology Library, ISBN 1-881883-10-8.

2 Design Process

2.1 Introduction

The process of designing and developing spacecraft is characterised by the fact that it concerns single and “one-off” time product, that have to be produced within a given amount of time.

Requirements of the principal and subsequent testing of test models lead to the final design. This final design is then laid down in working drawings and other documents, all of which define the final product or flight model.

2.2 Design criteria

Any design is led by the design criteria (mass, stiffness, shape, etc.). The proposal phase is intended to leave room for negotiations on any alterations of the design criteria. Depending on the kind of project, it may be necessary to derive further specifications for subsystems, such as the solar arrays, from the design criteria.

2.3 Design specification

The first step of the design process is to derive the design specification. This needs to comply with demands concerning:

- functioning with regard to primary tasks
- mechanical loads
- environmental influences
- material properties
- weight and balance
- reliability and lifetime

- safety
- exchangeability, repairs and maintenance
- manageability
- interactions

Based on the design specification, a design and development plan is worked out and work packages are defined. A work package describes the activities to be performed, the available time and the resources available. It also includes the necessary input and the expected output.

2.4 Design

Based on the design and development plan, the design specifications are further tested and elaborated on during the design process by means of design studies, computer simulations, analyses, trade-off studies, detailed testing, as well as designing and testing test models.

During each step of the process the level of detail is increased in such a way that, through design drawings, the design can be finalised in production documents (drawings, manufacturing sheets), test plans and procedures.

Testing and studying certain aspects by means of test models form an important part of the design process. These are not complete models. In most cases the following will be used:

- the structural model (SM, dynamic aspects)
- the thermal model (TM, thermal behaviour in vacuum)
- the electrical model (EM, the electrical behaviour of all systems combined and in relation to the ground testing equipment or EGSE: Electrical Ground Support Equipment)
- the qualification model (QM, qualification of the design for production of the flight model, FM)

For the development of attitude control systems an attitude control model is added.

Tests on the test models may lead to changes in the design. Deviations from the design specifications need to be approved by the client.

2.5 Design control

The design process consists of several steps in which the design is laid down in more detail. These steps are usually concluded with a number of reviews. In most cases these are:

- a preliminary design review (PDR) for the release of the preliminary design, in general before starting production of the test models
- a critical design review (CDR) before the release of qualification and flight models, preferably before the start of flight model production.

2.6 Exercises

2.6.1 Design and development

Find somewhere a design and development plan of ESA and NASA spacecraft.

3 Launch Vehicle Systems

3.1 Introduction

A launch system is a launch vehicle comprised of one or more stages, and the infrastructure for support from the ground. The launch vehicle positions the spacecraft in the required orbit and attitude. During launch, the spacecraft is exposed to loads (which will be discussed later) and protected from the environment by the nose cone (fairing).

Therefore the choice of the launch vehicle is of course dependent on the spacecraft mission. The launch vehicle sets restrictions for the spacecraft, such as the possible launch mass and the available volume.

It was Robert H. Goddard, on 16 March 1926, who successfully launched the first rocket with liquid fuel. Goddard was one of the driving forces behind rocket propulsion in the USA. He died on 10 August 1945, and on 1th of May 1959. The Goddard Space Flight Centre (GSFC), Greenbelt, Maryland, USA, was established in his memory.

Launch vehicles can be divided into two groups: Expendable launch vehicles (ELV) (where the rocket is used once) and Reusable Launch Vehicles, (RLV) (where parts can be used several times). The space transportation system (STS) is an example of a reusable launch system. Expendable and reusable launch vehicles are listed in [ESA 2002]. It is possible to purchase launch capacity already in the following countries:

- Europe
- USA
- CIS
- Japan
- China
- India
- Brazil
- Israel

In Europe the ARIANE 5 and SOYUZ launch vehicles are well known while in the USA the Shuttle, the DELTA family, the ATLAS family and the TITAN family of launch vehicles are well known.

3.1.1 Launch Vehicle User's manual

The purpose of the user's manual of a launch vehicle is to provide (to the potential user) information on the launch vehicle. Generally, it contains information on the performance, environment and interfaces, defines the spacecraft design and operation constraints imposed by the launch vehicle, and the operations on the range. It also describes the launch operations and documentation procedure.

In general, the following chapters and appendices may be found in the User's manual [Arianespace 1998, 2002]:

- The introduction
- The general characteristics and brief description of the launch vehicle
- The performance of the launch vehicle. In this section the performance data of the launch vehicle are presented. Typical missions are outlined (GTO, SSO, LEO, etc.) and performance data in terms of spacecraft mass are given
- The environmental conditions. In this section the mechanical, thermal, radio and electromagnetic environment is presented as well the variation in static pressure within the payload volume during launch and the contamination and cleanliness.
- The spacecraft design and sizing data. This section is very important within the frame of spacecraft structural design and verification. This section contains information about safety regulations and selection of spacecraft construction materials regarding outgassing criteria. It also covers the dimensioning of the spacecraft concerning the location of the centre of gravity, spacecraft balancing, minimum natural frequencies, dimensioning loads, spacecraft qualification and acceptance tests related to static loads, sinusoidal vibrations, acoustic loads, shocks, interfaces, etc.
- The mechanical interface. This section describes the interfaces of the spacecraft with the launch vehicle with regards to fairing, payload adapters and accessibility.
- The electrical and radio electrical interface
- The launch operations
- The documentation. In this section the documentation which will be used when the launch vehicle system is adopted by the user. i.e. safety documents, mission analysis documents, launch preparation and range operations, launch vehicle and payload review documentation.
- In the appendices the dynamic space under the fairing will be described as well the payload adaptors to be used. In general the design of the payload adaptor is described together with the load capability of the adaptor, the expected shock response spectrum, mechanical and electrical interface drawings.

3.2 Literature

ESA, December 2004, *Launch Vehicles Catalogue*, Volume 1 and Volume 2, revision number 15, ESA contract no. 8152/88/F/BL.

Arianespace, November 2004, *ARIANE 5 User's manual*, Issue 4, revision 0.

Arianespace, September 2004, *VEGA User's manual*, Issue 2, revision 0.

3.3 Exercises

3.3.1 *Definition the mechanical design specification*

Suppose a spacecraft of 8000 kg is launched into a low earth orbit of 400 km. Assuming that an ARIANE 5 launch vehicle will be used and that it will be launched from the ARIANE 5 launch complex in Kourou. Check the launch capability of ARIANE 5

- Define the mechanical design specifications for the 8 Tons spacecraft
- Define the qualification programme
- Select a proper payload adaptor system (PAS)
- Define the mechanical interfaces with the spacecraft

The ARIANE 5 User's manual can be downloaded from www.arianespace.com/cite/documents.

4 Spacecraft Subsystems

4.1 Introduction

Space vehicles are often characterized by the conflicting requirements that are demanded from them: strong and light, accurate, reliable and low-cost [Laan 1986].

Next to the general requirements such as low weight, low price, high reliability, etc., there are also demands with respect to specific components. In this regard, the temperature range within which the temperature of the battery must remain may be entirely different from that of a tank with liquid fuel.

To function properly, each element sets requirements to its environment and also influences it: it uses space, requires energy, gives off heat and create a magnetic field, etc.

Since all the elements are packed close to each other, they must function in each others environment. That has positive consequences but may also lead to problems.

Subsystems complement each other and, in some cases, are also meant for each other. For instance, the structure maintains the equipment in a fixed position, carries loads and ensures heat is conducted from warm to cold surfaces.

Problems occur when subsystems set requirements to their environment that are incompatible, such as when two elements next to each other must operate at different temperatures.

In general, a compromise is required. In most cases one subsystem is not optimal, since it is more important that the entire system operates in harmony.

Due to the fact the number of possible variations and combinations of systems used in a spacecraft are very large, it is impossible to make a brief general analysis that covers all these combinations.

In order to get an idea of the mutual interaction of subsystems, the most important subsystems and their mutual interaction will dealt with briefly.

4.2 Power Supply

The power supply is designed to deliver electrical energy to the other subsystems. There are a number of types:

- Batteries
- Solar cells
- Isotopic Reactors
- Fuel Cells

4.3 Attitude Control system

The attitude control system consists of:

- Active systems that require an energy source, in which a control circuit of sensors and actuators determine the attitude.
- Passive systems that do not require an energy source, such as gyro stabilisation or gravity-gradient stabilisation.

An attitude control system is necessary to eliminate the influence of external disturbance moments and to set instruments, antennas, nozzles, etc.

4.4 Data Systems

This concerns the control of information flows that originate from sensors, instruments, antennas, etc.

Often the information is stored temporarily into computer memory. Information is processed by means of software in the on board computer.

This system is in contact with ground stations on earth through a communication system (telemetry).

4.5 Thermal Control System

Since the proper functioning of certain elements is only possible within a certain temperature range, the temperature range must also be regulated during flight. This sets requirements on the conduction of heat between different parts.

Energy absorption from outside (sun and albedo) and emission to the outside (cold space) takes place through radiation. In a spacecraft both radiation and conduction play a part. Here, one also distinguishes between passive and active systems.

4.6 Telecommunication Systems

The telecommunication system maintains contact with ground stations on Earth. This is usually referred to as telemetry or telecommand. The former refers to signals emitted by the spacecraft, the latter to signals that the spacecraft receives from the ground station.

Transmitters and receivers often use the same antenna.

4.7 Propulsion System

The propulsion system is used when the orbit needs to be changed during flight.

Change of orbit is done through a change in velocity, an impulse that must be delivered by the rocket engine. A chemical engine may be ignited for a short period of time, such as in the transition to a geostationary orbit.

4.8 Structure

Even though in a gravitation free environment the forces exerted on a spacecraft are very small, the spacecraft must be designed to withstand high loads. These forces occur during lift-off. Besides high acceleration, severe vibrations also play an important role.

The structure consists of platforms, cylinders and rods, where sandwich structures are often used because they combine low weight with high stiffness. Other frequently used materials are aluminium and fibre-reinforced plastics.

4.9 Mutual Interaction of Subsystems

The subsystems interact, although it is better avoided.

4.9.1 Power Supply versus Attitude control System

Unfolding the solar panels disturbs the attitude. Solar panels also experience disturbance forces (sunlight,...) that disturb the attitude of the spacecraft. Large solar panels exhibit flexible behaviour that interact with the attitude control system.

The attitude control system points the solar panels continually in the direction of the sun.

Active attitude control systems require energy.

The discharge of reaction wheels with the help of magnetic spools requires a strong electric current.

4.9.2 Power Supply versus Thermal Control System

The solar panels require a complex construction so that the temperature remains low and unwanted radiation is reflected. A low operating temperature of the solar panels leads to a high efficiency.

The performance and the lifetime of the batteries depend strongly on the temperature as they are based on chemical reactions.

All the dissipated energy is radiated to space by the thermal system.

4.9.3 Attitude Control System versus Thermal Control System

In the case where gyroscopes are used as attitude sensors the temperature must be maintained as constant as possible.

However, optical sensors usually don't deviate due to thermal deformations.

4.9.4 Thermal Control System versus Structure

Heat is conducted through the structure and this sets requirements for the construction/shape and the choice of materials. To a great extent, the shape determines the flow of energy that occurs due to the radiation of surfaces to each other and to space.

4.10 Literature

Laan, van der, F.H., 1986, Het natuurlijke ruimtemilieu en de schade die het kan veroorzaken aan ruimtevoertuigen, Thesis work Technical University Delft, Faculaty of Aerospace Engineering.

5 Design and Safety factors

5.1 Introduction

Factors of safety are used in space projects to account for uncertainties with regards to the prediction of loads, structural analysis, the fabrication process and material properties.

In this chapter the terminology for different loads, allowable stress, design approaches and factors of safety and the relation between both will be given.

5.2 Terminology

In the design process of spacecraft and launch vehicles the following terminology is frequently used (see also Fig. 5.1).

5.2.1 Flight Limit Load

The flight limit load for a given design condition is the maximum occurring load with, for example, a probability of 97.7% (2σ). This usually holds for spacecraft. The stress that is calculated with applied flight limit loads is called the limit stress.

5.2.2 Design Limit Load

The design limit load is the limit load multiplied by the design factor to avoid risks during the design and the test phase. Design limit load is also known as qualification load.

5.2.3 *Ultimate Load*

In general, the ultimate load is the design load multiplied by a factor of safety (FOS). The ultimate loads are the most critical loads for the design.

The structure must be able to support this load without failing. The calculated stresses when the ultimate loads were applied are known as ultimate stress.

5.2.4 *Buckling Load*

The buckling load is the design load multiplied by the buckling safety factor. The most unfavourable combination of buckling loads must not lead to buckling or failure of the structure. Imperfections should also be accounted for (knock down factors).

5.2.5 *Yield Load*

The yield load is the design load multiplied by a yield safety factor. The structure must be able to support this load without permanent deformation.

5.2.6 *Proof Load*

The proof load is the limit load multiplied by the proof factor. The proof load is used to test parts of the structure before the entire spacecraft or launch vehicle is tested. An example of a proof load is the testing of fuel tanks at a certain internal pressure.

5.2.7 *Allowable stress*

The allowable stress is the maximum stress that can be applied without breakage, failure or any other detrimental deformation occurring.

5.2.8 *Material Strength*

The material strength is the level of stress that a certain material can support in a part of a structure under the expected loads.

5.2.9 A-value (*A* basis)

The A-value is referred to as the value above which at least 99% of the population is expected with a reliability of 95%. This means that there is 95% certainty that at least 99% of the individual measured characteristic is higher than the A-value.

5.2.10 B-value (*B* basis)

The B-value is referred to as the value above which at least 90% of the population is expected with a reliability of 95%. This means that there is 95% certainty that at least 90% of the individual measured characteristic is higher than the "B" value.

To determine the A and the B value of a strength property of a certain material, a sample of size n with results x_i , $i = 1, 2, \dots, n$, is carried out. It is assumed that x_i is normally distributed, however, the mean μ and the standard deviation σ are unknown. Subsequently, a mean \bar{x}

$$\bar{x} = \frac{1}{n} \sum_{i=1}^n x_i, \quad (5.1)$$

and standard deviation s

$$s = \sqrt{\sqrt{\frac{\sum_{i=1}^n (x_i - \bar{x})^2}{n-1}}}, \quad (5.2)$$

are calculated from the sample. The A-value and the B-value are dependent on the number of samples n , the mean of the sample \bar{x} , the standard deviation of the sample s , the one-sided confidence interval $1 - \alpha = 0.95$ and the percentage $1 - \gamma = 0.99, 0.90$ (one-sided) of the population that is greater than or equal to the A-value and the B-value respectively. The A-value and the B-value are determined with the help of the following expressions respectively:

- A-value: $x_A = \bar{x} - k_A s$
- B-value: $x_B = \bar{x} - k_B s$

In general, one looks for $n \geq 10$.

The weight factors k_A and k_B can be found in Table 5.1.

Table 5.1 Weight factors A and B values

$1 - \alpha = 0.95$	$1 - \gamma = 0.90$	$1 - \gamma = 0.99$
n	k_B	k_A
5	3.407	5.741
6	3.006	5.062
7	2.755	4.642
8	2.582	4.354
9	2.454	4.143
10	2.355	3.981
15	2.068	3.520
20	1.926	3.295
30	1.777	3.064
∞	1.282	2.326

The factors k_A and k_B can be approximated with the following formula [Stange 1970 and A5-SG-1-X-10-ASAI-2003]:

$$k = \frac{2(n-1)}{2(n-1) - u_{1-\alpha}^2} \left[u_{1-\gamma} + \frac{u_{1-\alpha}}{\sqrt{2(n-1)}} \sqrt{\frac{2(n-1)}{n} + u_{1-\gamma}^2 - \frac{u_{1-\alpha}^2}{n}} \right]. \quad (5.3)$$

The fractiles u_p for the standard normal distribution are given in the following Table 5.2.

Table 5.2 Fractions, Fractiles

$1 - \alpha , 1 - \gamma$	P=0.90	P=0.95	P=0.99
u_p	1.2816	1.6449	2.3263

5.2.11 S-Value (S-basis)

Minimum mechanical property values specified by various agencies [Peery 1982].

5.2.12 Qualification Loads

The loads that are applied during the qualification tests are called the qualification loads.

5.2.13 Flight Acceptance Loads

The flight model (FM) of the spacecraft will be tested against flight acceptance loads before it will be launched.

5.2.14 Margin of Safety

The margin of safety (*MS* or *MoS*) is defined as the ratio between the allowable strength or stresses (*A*, *B* or other) and the actual stresses multiplied by a safety factor minus one. This means that the value of the margin of safety must be greater than or equal to zero.

$$MS = \frac{s_r}{FoS \times s_a} - 1 \geq 0, \quad (5.4)$$

where s_r is the permissible strength (stress), s_a is the actual stress due to the design limit loads and FoS is the factor of safety (yield, ultimate, buckling, etc.)

5.2.15 Fail-Safe

A structure is designed to be fail-safe when the total structure does not fail after the failure of one structural element.

5.2.16 Safe-life

A structure has been designed to be safe-life if the largest possible undetectable crack in a structural element does not augment under oscillating and main loads.

5.3 Factors of Safety for Spacecraft

The relation of the loads and the factors of safety is illustrated in Fig. 5.1. This diagram is taken from [ECSS-E-30 Part 2A].

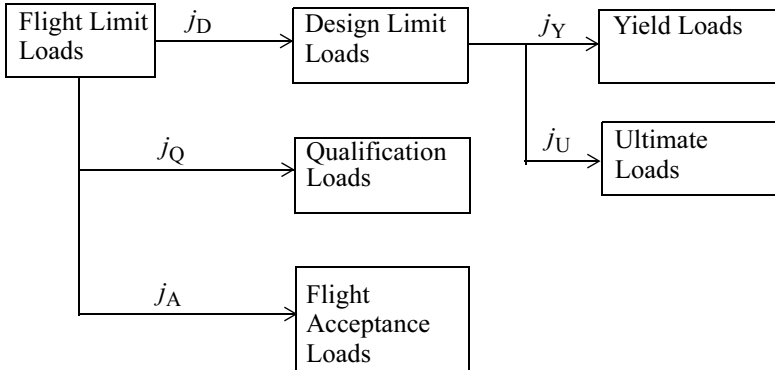


Fig. 5.1 Loads and factors of safety relationship

The factors of safety j_D , j_Q and j_A represent a probability level (reliability) with respect to the flight limit loads. The factor of safety j_Y ensures an acceptable risk of yielding and the factor of safety j_U ensures an acceptable risk of ultimate failure during test at design flight loads.

The following factors are commonly used within the frame of ESA projects:

- j_D 1.4 to 1.5
- j_Q 1.25 for ARIANE family
- j_A 1.1 for ARIANE family
- j_Y 1.1 to 1.25
- j_U 1.25 to 1.5

The structural design and test factors of safety for NASA space flight hardware are presented and discussed in [NASA-STD-5001].

5.4 Literature

- A5-SG-1-X-10-ASAI, 2003, *Specification de Conception de Dimensionnement et d'Essais des Structures*, Edition 5, Revision 12, April 8th, 2003.
- ECSS-E-30 Part 2A, April 25, 2000, *Space Engineering, Mechanical-Part 2: Structural*.
- Stange, K., 1970, *Angewandte Statistik, Eindimensionale Probleme*, Erster Teil, Springer-Verlag, ISBN 3-540-05256-9.
- NASA-STD-5001, June 21, 1996, *Structural Design and test Factors of Safety for Space flight Hardware*.
- Peery, D.J., Azar, J.J., 1982, *Aircraft Structures*, ISBN 0-07-049196, McGraw-Hill Book Company.

5.5 Exercises

5.5.1 Survey of Applied Factors of Safety

Perform a literature survey about the factors of safety used by ESA in European projects and present them in the following table format (Table 5.3).

Table 5.3 List of applied factors of safety

Qualification	Type	L/V ^a	Factors of safety employed in S/C ^b projects as related to flight limit loads				
			Structure of S/C project	j_D	j_Y	j_U	j_Q, j_A
SM ^c							
FM ^d							

- a. Launch Vehicle
- b. Spacecraft
- c. Structural model
- d. Flight Model

6 Spacecraft Design Loads

6.1 Introduction

Launch vehicle and spacecraft low frequency loads are driven by transients such as engine ignition, engine shutdowns, wind gusts or wind shears, and quasi-static loads. Other environments are acoustics, random vibration, sine vibration, and shock.

These environments are driven by the ascent profile, which includes the events listed in Table 6.1.

Table 6.1 Sources of launch vehicle environments [Yunis 2005]

	Acoustics	Random Vibration	Sine Vibration	Shock
Lift-off	X	X		
Aerodynamics /Buffet	X	X		
Separation (stage, fairing, spacecraft)				X
Motor burn /Combustion/ POGO		X	X	

The maximum loads (flight limit loads) at any stage in the life cycle of a spacecraft or other space system are used to design and dimension the primary, secondary and other parts.

The dynamic mechanical loads that occur during the lifetime of a spacecraft are:

- Handling loads
- Transportation loads
- Vibration tests required for the qualification of the spacecraft structure
 - Sinusoidal vibrations
 - Random vibrations
 - Acoustic pressures

- Dynamic loads during launch
 - Steady-state acceleration (inertia loads)
 - Sinusoidal vibrations
 - Random vibrations
 - Acoustic loads
 - Shock loads
 - Pressure variations
- Re-entry loads
- (Emergency) landing loads (STS)
- Loads following launch
 - Transfer orbit loads
- Loads/influences on the spacecraft in orbit (In-service loads)
 - Extension of folded elements, such as solar panels, antennas, etc.
 - Temperature gradients
 - 0g loads
 - Micro-meteorites / Debris

The dynamic loads during launch of the spacecraft are generally the highest for the basic structure. The test loads are dealt with in a later chapter.

Foldable structures experience different loads during launch than in orbit around the earth.

In the following sections launch loads and micro-meteoroid / debris will be covered, and specifically:

- Steady-state static loads as a result of:
 - The propulsion of the engine
 - Crosswind loads
 - Manoeuvres
- Mechanical dynamic loads that are a result of unsteady combustion of the engine(s), the turbulent flows along the rocket and the noise of the exhaust (especially during the initial phase of launch). These enforced mechanical vibrations (base excitation) transferred via the interface of the spacecraft with the Launch Vehicle, are in general:
 - Sinusoidal vibrations
 - Random vibrations
 - Shock loads
- Acoustic loads (sound pressures) as a result of exhaust noises and the turbulent flows along the launch vehicle.
- Shock loads as a result of the separation of the stages and the separation of the spacecraft from the launch vehicle, the ignition and the stopping of the engines. The separation of the spacecraft results in the highest shock load.
- Pressure changes. The absolute pressure decreases during launch, which can influence the systems unless suitable ventilation systems have been fitted.
- Micro-meteorites/Debris. Parts, boxes and instruments mounted on the outside of the spacecraft are exposed to micro meteorites and man-made debris.

6.2 Transportation load factors

The typical transportation and handling load factors are given in Table 6.2.

Table 6.2 Transportation limit load factors [NASA-HDBK-7005]

Medium/Mode	Longitudinal load factors	Lateral load factors	Vertical load factors
Water	± 0.5	± 2.5	± 2.5
Air	± 3.0	± 1.5	± 3.0
Ground			
• Truck	± 3.5	± 2.0	± 6.0
• Rail (humping shocks)	± 6.0 to ± 30.0	± 2.0 to ± 5.0	± 4.0 to ± 15.0
• Rail (rolling)	± 0.25 to ± 3.0	± 0.25 to ± 0.75	± 0.2 to ± 3.0
• Slowly moving dolly	± 3.1	± 0.75	± 2.0

The transportation loads should be included in the design analysis unless special protection is provided to assure that they contribute negligible damage compared with the other (flight) loads.

6.3 Steady-State Loads

The maximum steady-state acceleration in the launch direction occur at the end of the propulsion phase of a rocket stage. The acceleration increases because the mass of the launch vehicle decreases, while the overall thrust remains the same. An example of the acceleration is illustrated in Fig. 6.1.

The vibrations are superimposed on the steady state acceleration.

The lateral steady-state accelerations are usually much smaller than the acceleration in the launch direction.

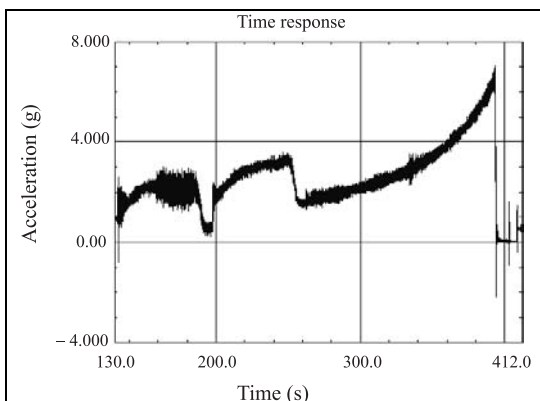


Fig. 6.1 Acceleration versus time Delta 2 launch vehicle (courtesy FEMCI, NASA GSFC)

The maximum steady state accelerations of various launch vehicles are shown in Table 6.3.

Table 6.3 Maximum steady-state acceleration

Launch vehicle	Maximum steady-state acceleration	
	Longitudinal [g]	Lateral [g]
Ariane 4	4.5	0.2
Ariane 5	4.25	0.2
Atlas	5.5	0.4
Delta 2	5.5–7 ^a	0
Pegasus	7–10	0
Proton	4	0
Long March 2E	5.2	0.6
Long March 3	5.5	0.6

a. Depends on mass of spacecraft

6.4 Mechanical Dynamic loads

The mechanical dynamic loads during launch can subdivided into:

- Low frequency sinusoidal vibrations in a frequency domain of 5–100 Hz.
- Random vibrations in a frequency range of 20 – 2000 Hz.

An example of the low frequency acceleration is illustrated in Fig. 6.2 and an example of high frequency acceleration is shown in Fig. 6.3.

6.4.1 Sinusoidal loads

Low frequency sinusoidal vibrations occur as a result of the interaction between launch vehicle mode forms and loads occurring during [NASA Practice No. PT-TE-1406, Lalanne 2002a]:

- Lift-off, the fast build-up of thrust causes a shock load that excites the low frequency domain.
- Combustion of the engines, during combustion of the engines sinusoidal vibrations occur, both in, and adjacent to, the launch direction.

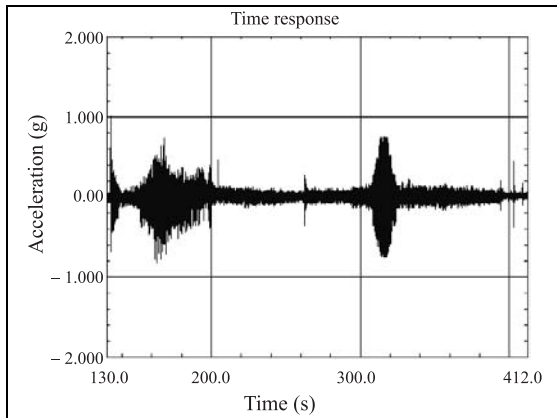


Fig. 6.2 Low frequency acceleration versus time (courtesy FEMCI, NASA GSFC)

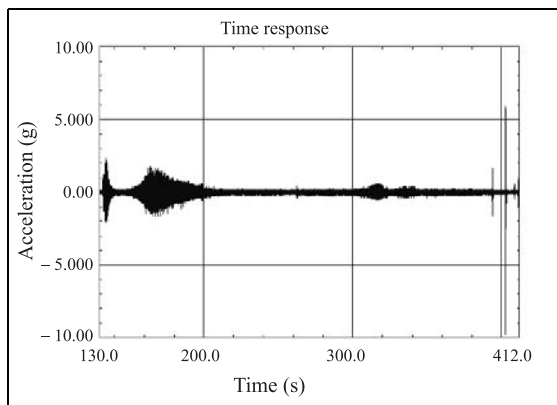


Fig. 6.3 High frequency acceleration versus time (courtesy FEMCI, NASA GSFC)

- POGO (a stick with a spring on the bottom). Even though engineers will go to great lengths to reduce the effects of POGO vibrations, they are still observed just before the burn up of a stage.

The maximum sinusoidal vibrations for a DELTA 7925 L/V are summarized in Table 6.4:

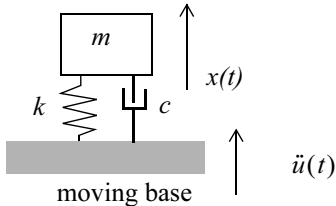
Table 6.4 Sinusoidal vibrations

	Frequency (Hz)	Acceleration (g)
Launch direction	5 – 6.2	12.7 mm double amplitude
	6.2 – 100	1.0
Lateral direction	5 – 100	0.7

Enforced accelerations

A SDOF system with a discrete mass m , a damper element c and a spring element k , is placed on a moving base which is accelerated with an acceleration $\ddot{u}(t)$. The resulting displacement of the mass is $x(t)$. A relative motion $z(t)$ is introduced which is the displacement of the mass with respect to the base. This is defined as:

$$z(t) = x(t) - u(t). \quad (6.1)$$

**Fig. 6.4** Enforced acceleration

The equation of motion for $z(t)$ can be written as

$$\ddot{z}(t) + 2\zeta\omega_n\dot{z}(t) + \omega_n^2 z(t) = -\ddot{u}(t). \quad (6.2)$$

The enforced acceleration of the SDOF system is transformed into an external force. The absolute displacement $x(t)$ can be calculated with (6.1) or

$$\ddot{x}(t) = \ddot{z}(t) + \ddot{u}(t) = -2\zeta\omega_n\dot{z}(t) - \omega_n^2 z(t). \quad (6.3)$$

Using the initial conditions, the displacement $z(0)$ and the velocity $\dot{z}(0)$, the solution of (6.2) for $z(t)$ is

$$\begin{aligned} z(t) &= z(0)e^{-\zeta\omega_n t} \left(\cos\omega_d t + \frac{\zeta}{\sqrt{1-\zeta^2}} \sin\omega_d t \right) \\ &\quad + \dot{z}(0)e^{-\zeta\omega_n t} \frac{\sin\omega_d t}{\omega_d} - \int_0^t e^{-\zeta\omega_n \tau} \frac{\sin\omega_d \tau}{\omega_d} \ddot{u}(t-\tau) d\tau. \end{aligned} \quad (6.4)$$

The first part of (6.4) is dependent on the initial conditions and will damp out very quickly. Therefore we will focus on the particular (or steady-state) solution.

Generally, the harmonic vibration is expressed in complex numbers ($j = \sqrt{-1}$)

$$z(t) = Z(\omega)e^{j\omega t}, \quad (6.5)$$

with the following definition of the Fourier transform pair

$$Z(\omega) = \int_{-\infty}^{\infty} z(t)e^{-j\omega t} dt, \quad (6.6)$$

and

$$z(t) = \frac{1}{2\pi} \int_{-\infty}^{\infty} Z(\omega)e^{j\omega t} d\omega. \quad (6.7)$$

The velocity becomes

$$\dot{z}(t) = j\omega Z(\omega)e^{j\omega t} = \dot{Z}(\omega)e^{j\omega t}, \quad (6.8)$$

and the acceleration will be

$$\ddot{z}(t) = (j\omega)^2 Z(\omega)e^{j\omega t} = -\omega^2 Z(\omega)e^{j\omega t} = \ddot{Z}(\omega)e^{j\omega t}. \quad (6.9)$$

The multiplication with j will rotate the vector (e.g $Z(\omega)$) 90° in the positive direction in the Argand diagram (Wessel's geometry, [Nahin 1998]).

The complex number $j = \sqrt{-1}$ is called the rotation operator.

Equation (6.2) becomes

$$(-\omega^2 + 2j\zeta\omega\omega_n + \omega_n^2)Z(\omega) = -\ddot{U}(\omega), \quad (6.10)$$

or

$$\ddot{Z}(\omega) = \frac{\omega^2 \ddot{U}(\omega)}{(-\omega^2 + 2j\zeta\omega\omega_n + \omega_n^2)} = H(\omega)(\ddot{U}(\omega)), \quad (6.11)$$

and

$$\ddot{X}(\omega) = \ddot{Z}(\omega) + \ddot{U}(\omega) = \{H(\omega) + 1\}\ddot{U}(\omega), \quad (6.12)$$

$$H_{\ddot{x}}(\omega) = H(\omega) + 1 = \frac{\omega^2}{\omega_n^2} \frac{1}{\left(1 - \frac{\omega^2}{\omega_n^2}\right) + 2j\zeta\frac{\omega}{\omega_n}} + 1. \quad (6.13)$$

From this, three response regions can be determined:

1. $\frac{\omega}{\omega_n} < 1$ the transfer function $H_{\ddot{x}}\left(\frac{\omega}{\omega_n}\right) \approx 1$, this is called stiffness controlled
2. $\frac{\omega}{\omega_n} = 1$ the transfer function $H_{\ddot{x}}\left(\frac{\omega}{\omega_n}\right) = \frac{1}{2j\zeta} + 1 \approx \frac{1}{2j\zeta}$, this is called damping controlled
3. $\frac{\omega}{\omega_n} > 1$ the transfer function $H_{\ddot{x}}\left(\frac{\omega}{\omega_n}\right) \approx 0$, this is called mass controlled

The transfer function $\left|H_{\ddot{x}}\left(\frac{\omega}{\omega_n}\right)\right|$ is plotted in Fig. 6.5.

The sinusoidal or harmonic displacement $x(t)$ can be written as

$$x(t) = D e^{j\omega t}, \quad (6.14)$$

where D is the amplitude of the sinusoidal displacement and ω is the excitation frequency (Rad/s). The radian frequency ω can be expressed as a number of cycles per second f (cps) or (Hz) with $\omega = 2\pi f$.

The velocity $\dot{x}(t)$ is the time derivative of the displacement

$$\dot{x}(t) = j\omega D e^{j\omega t}. \quad (6.15)$$

It is observed that the velocity $\dot{x}(t)$ has a phase shift of $\frac{\pi}{2}$ radians with respect to the displacement $x(t)$.

The acceleration $\ddot{x}(t)$ is the time derivative of the displacement

$$\ddot{x}(t) = -\omega^2 D e^{j\omega t}. \quad (6.16)$$

Similarly, it is also observed that the acceleration $\ddot{x}(t)$ has a phase shift of $\pm\pi$ radians with respect to the displacement $x(t)$.

At a frequency $f = 6.2$ Hz and an amplitude $D = \frac{0.0127}{2} = 0.00635$ m, the amplitude $\omega^2 D$ of the harmonic acceleration becomes

$$\omega^2 D = (2\pi 6.2)^2 0.00635 = 9.64 \text{ m/s}^2 (\approx 1)g$$

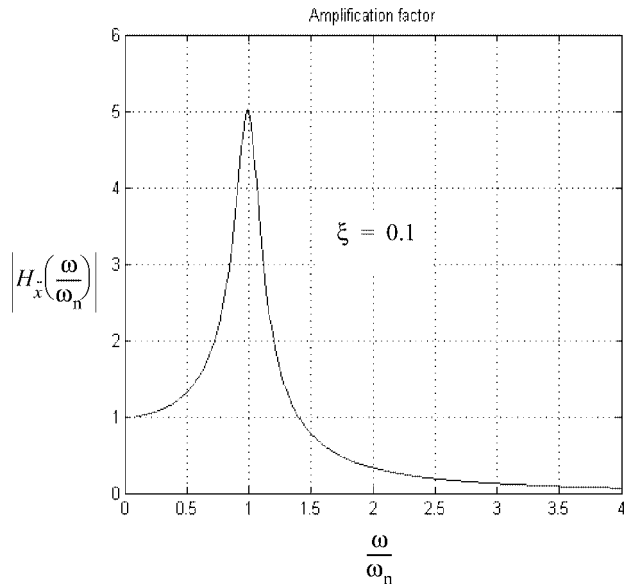


Fig. 6.5 Transfer function $\left|H_x\left(\frac{\omega}{\omega_n}\right)\right|$

Influence of the Natural Frequency

A two mass–spring system is illustrated in Fig. 6.6. The system with m_1 and k_1 represents a spacecraft, instrument or box, and the system with m_2 and k_2 represents the launch vehicle or spacecraft.

The application of the quasi-static loads is only allowed if the natural frequency of the combination of spacecraft & launch vehicle or the combination of spacecraft & instrument or box is well separated. In that case, the system with the highest natural frequency

$$f_1 = \frac{1}{2\pi} \sqrt{\frac{k_1}{m_1}}, \quad (6.17)$$

is significantly higher than the lowest natural frequency of the total system.

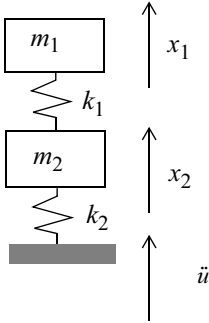


Fig. 6.6 Two mass–spring system

The lowest frequency of the total system can be estimated with Dunkerly's equation

$$\frac{1}{f_{\text{tot}}^2} = \frac{1}{f_1^2} + \frac{1}{f_2^2}, \quad (6.18)$$

with $f_2 = \frac{1}{2\pi} \sqrt{\frac{k_2}{m_1 + m_2}}$. f_2 is the natural frequency of the total system with the system m_1 and k_1 acting as a rigid body. If f_1 and f_2 are far apart then lowest natural frequency of the total system becomes approximately $f_{\text{tot}} \approx f_2$. The motion is stiffness driven (see Fig. 6.5).

Another method to approximate the lowest natural frequency is with the Rayleigh Quotient

$$\omega^2 \approx R(q) = \frac{\{q\}^T [K] \{q\}}{\{q\}^T [M] \{q\}}, \quad (6.19)$$

where $[M]$ and $[K]$ are the mass and stiffness matrix respectively and $\{q\}$ is an assumed mode. We can take the static displacement under 1-g

$$\begin{Bmatrix} q_1 \\ q_2 \end{Bmatrix} = g \begin{Bmatrix} \frac{m_1 + m_1 + m_2}{k_1} \\ \frac{m_1 + m_2}{k_2} \end{Bmatrix} = \begin{Bmatrix} \frac{1}{f_1^2} + \frac{1}{f_2^2} \\ \frac{1}{f_2^2} \end{Bmatrix} = \begin{Bmatrix} \frac{f_2^2 + 1}{f_1^2} \\ 1 \end{Bmatrix} \quad (6.20)$$

If the ratio $\frac{f_2^2}{f_1^2} < 1$ then the ratio $\frac{q_1}{q_2} \approx 1$, the system m_1 and k_1 will act as a rigid

body with respect to the system m_2 and k_2 . In the case where $\frac{f_2^2}{f_1^2} \approx 1$ the system m_1 and k_1 will act as a mass-spring damper and will amplify considerably.

Example

A dynamic system is assumed to have $m_1 = 10 \text{ kg}$, $m_2 = 150 \text{ kg}$ with

$$f_2 = \frac{1}{2\pi}\sqrt{\frac{k_2}{m_1 + m_2}} = 15 \text{ Hz}. \text{ It is also assumed that } f_1 = \frac{1}{2\pi}\sqrt{\frac{k_1}{m_1}} = 40 \text{ Hz}.$$

The spring stiffness can then be calculated by $k_1 = (2\pi f_1)^2 m_1$ and $k_2 = (2\pi f_2)^2 (m_1 + m_2)$. The base excitation $\ddot{u} = 1 \text{ m/s}^2$ over the frequency domain. The modal damping ratio is $\zeta = 0.02$. The transfer functions $|H_1(\omega)|$ and $|H_2(\omega)|$ will be calculated.

We see from Fig. 6.7 that the system m_1 and k_1 moves with about the same amplitude compared to the mass m_2 .

Assuming $f_1 = f_2 = 15 \text{ Hz}$, the transfer functions $|H_1(\omega)|$ and $|H_2(\omega)|$ will be calculated again.

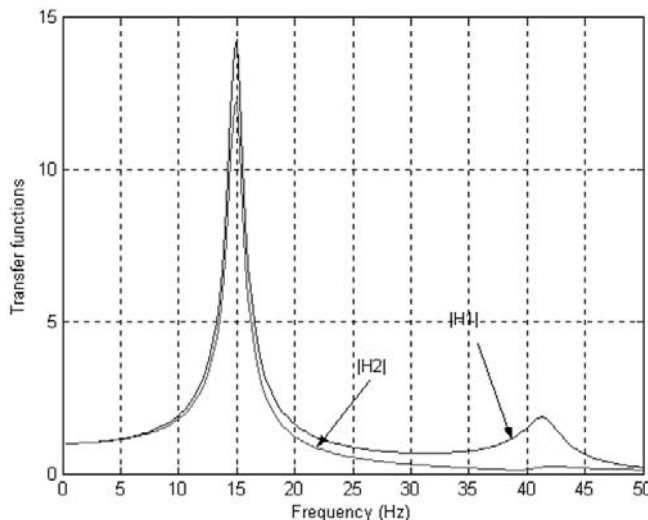


Fig. 6.7 Transfer functions

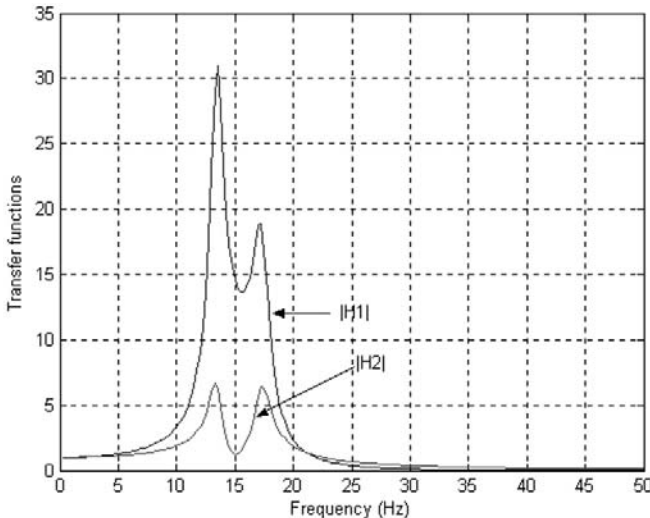


Fig. 6.8 Frequency transfer funtions

We see from Fig. 6.8 that the system m_1 and k_1 moves with much higher amplitude compared with the mass m_2 . The system m_1 and k_1 acts as a tuned mass–spring system with the same natural frequency as the mass m_2 , however, the peak of mass m_2 is divided into two peaks with lower amplitude.

End of example

6.4.2 Random loads

Acoustic loads and boundary layer turbulence are transformed into mechanical vibrations in the launch vehicle, which affect the spacecraft at its base.

In the ARIANE 5 User's Manual no random mechanical vibrations are specified. It is assumed that the acoustic loads will cover the random mechanical vibrations. There are many textbooks about random vibration, i.e. [Lalanne 2002c, Newland 1975].

In general random vibration loads are specified for instruments and equipment boxes, etc. Random mechanical loads are specified for the ARIANE 4 L/V (Table 6.5). These are valid at the base of the spacecraft.

It is assumed that the random accelerations are stationary and ergodic.

Table 6.5 Random vibrations

Frequency range (Hz)	Power Spectral Density (g ² /Hz)	rms acceleration (g)
20–150	+6dB/octave	
150–700	0.04	7.3
700–2000	–3dB/octave	

Power Spectral Density

The root mean square value (rms) value of a periodic signal $x(t)$ with a period

$T = \frac{1}{f}$ (s) is defined by:

$$x_{\text{rms}} = \left[\frac{1}{T} \int_{t_o}^{t_o + T} \{x(t)\}^2 dt \right]^{\frac{1}{2}}, \quad (6.21)$$

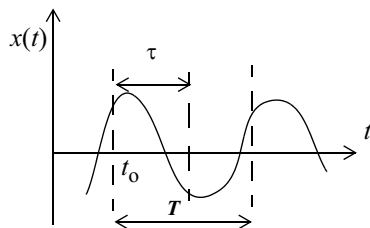
where t_o is an arbitrary starting time.

For a random signal $x(t)$ the x_{rms} is defined by

$$x_{\text{rms}} = \left[\lim_{T \rightarrow \infty} \frac{1}{T} \int_{-\frac{T}{2}}^{\frac{T}{2}} x^2(t) dt \right]^{\frac{1}{2}}. \quad (6.22)$$

The auto-correlation function of $x(t)$ is defined by

$$R_{xx}(\tau) = \lim_{T \rightarrow \infty} \frac{1}{T} \int_{-\frac{T}{2}}^{\frac{T}{2}} x(t)x(t + \tau) dt. \quad (6.23)$$

**Fig. 6.9** Periodic signal $x(t)$

The time shift τ is illustrated in Fig. 6.9

It can be observed from the (6.21) and (6.23) that

$$R_{xx}(0) = \lim_{T \rightarrow \infty} \frac{1}{T} \int_{-\frac{T}{2}}^{\frac{T}{2}} x(t)x(t)dt = \lim_{T \rightarrow \infty} \frac{1}{T} \int_{-\frac{T}{2}}^{\frac{T}{2}} x^2(t)dt = x_{\text{rms}}^2. \quad (6.24)$$

Example

A harmonic displacement is defined as $x(t) = D \sin(\omega t)$. Calculate the root mean square value of the displacement x_{rms} . The period time is $T = \frac{2\pi}{\omega}$, and is illustrated in Fig. 6.9. With use of (6.21) we calculate for x_{rms}

$$x_{\text{rms}} = \left[\frac{D^2 \omega}{2\pi} \int_{t_o}^{t_o + \frac{2\pi}{\omega}} \{ \sin(\omega t) \}^2 dt \right]^{\frac{1}{2}} = \sqrt{\frac{D^2 \omega t}{2\pi}} \Big|_{t_o}^{t_o + \frac{2\pi}{\omega}} = \frac{1}{2} D \sqrt{2}.$$

The auto-correlation of the signal $x(t)$ becomes

$$R_{xx}(\tau) = \frac{\omega D^2}{2\pi} \int_0^{\frac{2\pi}{\omega}} \sin \omega t \sin \omega(t + \tau) dt = \frac{D^2}{2} \cos \omega \tau,$$

and

$$R_{xx}(0) = x_{\text{rms}}^2 = \frac{D^2}{2}.$$

End of Example

With the aid of the Parseval's theorem the average power of $x(t)$ can be expressed in the frequency domain [Papoulis 1962]

$$\lim_{T \rightarrow \infty} \frac{1}{T} \int_{-\frac{T}{2}}^{\frac{T}{2}} x^2(t)dt = \lim_{T \rightarrow \infty} \frac{1}{2\pi T} \int_{-\frac{T}{2}}^{\frac{T}{2}} X(\omega) X^*(\omega) d\omega = \lim_{T \rightarrow \infty} \frac{1}{2\pi} \int_{-\frac{T}{2}}^{\frac{T}{2}} \frac{|X(\omega)|^2}{T} d\omega, \quad (6.25)$$

where $|X(\omega)|^2$ is the power spectrum, with

$$|z|^2 = z z^* = (x + jy)(x - jy) = x^2 + y^2, X^*(\omega) = \int_{-\infty}^{\infty} x(t) e^{j\omega t} dt \text{ and}$$

$\lim_{T \rightarrow \infty} \frac{|X(\omega)|^2}{T}$ the power spectral density (PSD function) in general denoted with

$$S_{xx}(\omega) = \lim_{T \rightarrow \infty} \frac{|X(\omega)|^2}{T} \geq 0. \text{ The dimension of the PSD function is unit}^2/\text{Rad.}$$

Equation (6.25) can be written as follows

$$x_{\text{rms}}^2 = R_{xx}(0) = \lim_{T \rightarrow \infty} \frac{1}{T} \int_{-\frac{T}{2}}^{\frac{T}{2}} x^2(t) dt = \frac{1}{2\pi} \int_{-\infty}^{\infty} S_{xx}(\omega) d\omega. \quad (6.26)$$

The power spectral density (PSD) function $S_{xx}(\omega)$ of the function $x(t)$ is defined as the Fourier transform of its auto correlation function $R_{xx}(\tau)$, thus

$$S_{xx}(\omega) = \int_{-\infty}^{\infty} R_{xx}(\tau) e^{-j\omega\tau} d\tau, \quad (6.27)$$

and

$$R_{xx}(\tau) = \frac{1}{2\pi} \int_{-\infty}^{\infty} S_{xx}(\omega) e^{j\omega\tau} d\omega. \quad (6.28)$$

The relations (6.27) and (6.28) form the Wiener–Kintchine relationship [Harris 1974].

The PSD function is symmetric with respect to $\omega = 0$, $S(\omega) = S(-\omega)$, thus

$$R_{xx}(\tau) = \frac{1}{2\pi} \int_0^{\infty} 2S_{xx}(\omega) e^{j\omega\tau} d\omega = \frac{1}{2\pi} \int_0^{\infty} 2S_{xx}(\omega) \cos \omega t d\omega. \quad (6.29)$$

It is more practical to define the power spectral density in cycles per second (Hz, cps)

$$R_{xx}(\tau) = \int_0^{\infty} 2S_{xx}(\omega) \cos(2\pi f t) df = \int_0^{\infty} W_{xx}(f) \cos(2\pi f \tau) df, \quad (6.30)$$

where $W_{xx}(f) = 2S_{xx}(\omega)$ is the PSD function in the frequency domain (Hz, cps). The dimension of $W_{xx}(f)$ is unit²/Hz (e.g. Pa²/Hz, g²/Hz, etc.).

The square root of the mean value $x(t)$ then is, see (6.26) and (6.30):

$$x_{\text{rms}} = \sqrt{R_{xx}(0)} = \sqrt{\int_0^{\infty} W_{xx}(f) df} \quad (6.31)$$

Example

The PSD $W(f)$ of a signal is a band-limited white noise with a constant value W_o in the frequency band $[f_1, f_2]$, as shown in Fig. 6.10.

Calculate the auto correlation function and the rms value of the signal.

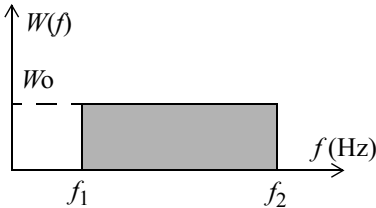


Fig. 6.10 Band limited white noise

The auto correlation function $R(\tau)$ is defined by (6.30)

$$R(\tau) = \int_0^{\infty} W(f) \cos(2\pi f\tau) df = W_0 \int_{f_1}^{f_2} \cos(2\pi f\tau) df,$$

$$R(\tau) = \frac{W_0}{2\pi\tau} [\sin(2\pi f_2\tau) - \sin(2\pi f_1\tau)].$$

Using the well-known limit $\lim_{x \rightarrow 0} \frac{\sin x}{x} = 1$ the rms value of the signal becomes

$$\text{rms} = \sqrt{R(0)} = \sqrt{W_0[f_2 - f_1]}.$$

The rms value of the signal can also be calculated with (6.31), as follows

$$\text{rms} = \sqrt{\int_0^{\infty} W_{xx}(f) df} = \sqrt{W_0[f_2 - f_1]}.$$

End of example

The definition of the unit decibel per octave (dB/oct) is given by

$$10 \log \left[\frac{W(f_2=2f)}{W(f_1=f)} \right] = r \quad (\text{dB/oct}). \quad (6.32)$$

An octave band is given by

$$\frac{f_2}{f_1} = 2^1. \quad (6.33)$$

One octave is in fact the doubling of the frequency.

When the ratio between the frequency is not exactly a factor of 2 but slightly more or less, then the number of octaves is calculated in the following way:

$$\frac{f_y}{f_{\text{ref}}} = 2^y, \quad (6.34)$$

with f_y the considered frequency (Hz), f_{ref} the reference frequency (Hz) and y the number of octaves (Oct). Then y can be obtained as follows

$$y = \frac{\log\left(\frac{f_y}{f_{\text{ref}}}\right)}{\log 2} \approx 3.322 \log\left(\frac{f_y}{f_{\text{ref}}}\right). \quad (6.35)$$

In the case where the number of octaves y and the number of decibels r per octave are known, one can easily calculate the increase or decrease of the power spectral density (see (6.32)):

$$10\log\left[\frac{W(f_y)}{W(f_{\text{ref}})}\right] = yr \quad (\text{dB}). \quad (6.36)$$

Then one can calculate the PSD function $W(f_y)$

$$W(f_y) = W(f_{\text{ref}})10^{\frac{yr}{10}} = W(f_{\text{ref}})10^{\frac{r\log\left(\frac{f_y}{f_{\text{ref}}}\right)}{10\log 2}}. \quad (6.37)$$

Elaborating (6.37) gives:

$$W(f_y) = W(f_{\text{ref}})\left(\frac{f_y}{f_{\text{ref}}}\right)^{\frac{r}{3}}, \quad (6.38)$$

with $\log 2 \approx 0.30 \approx \frac{1}{3}$.

Example

As an example the power spectral density $W_{xx}(f= 20)$ is calculated, when the PSD function at $f = 150 \text{ Hz}$ is $W_{xx}(f= 150) = 0.04 \text{ g}^2/\text{Hz}$. The slope is $r = 6 \text{ dB/Oct}$. using (6.38)

$$W(f= 20) = W(f= 150)\left(\frac{20}{150}\right)^{\frac{6}{3}} = 0.04\left(\frac{20}{150}\right)^2 = 0.0007 \text{ g}^2/\text{Hz}.$$

End of example

The root mean square (rms) value is representative value of a random power spectrum. An example spectrum is illustrated in Fig. 6.11.

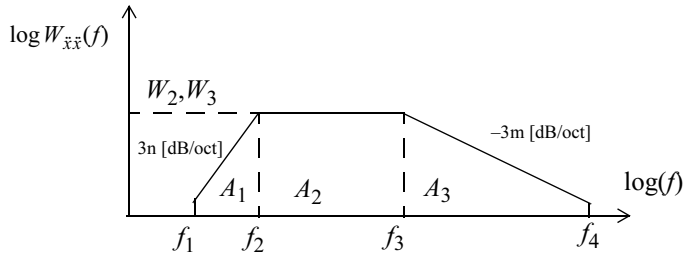


Fig. 6.11 PSD function $W_{\ddot{x}\ddot{x}}(f)$ versus frequency f (Hz) (very usual spectrum for Europe and USA)

The rms value of the acceleration \ddot{x}_{rms} is determined by:

$$\ddot{x}_{\text{rms}} = \sqrt{A_1 + A_2 + A_3} \quad (6.39)$$

where

$$A_1 = \frac{W_2 f_2}{n+1} \left[1 - \left(\frac{f_1}{f_2} \right)^{n+1} \right], \quad n > 0,$$

$$A_2 = W_2 (f_3 - f_2),$$

$$A_3 = \frac{W_3 f_3}{m+1} \left[\left(\frac{f_4}{f_3} \right)^{m+1} - 1 \right], \quad m < 0, \quad (m \neq -1).$$

For $m = -1$ (with the help of the rule of l'Hôpital):

$$A_3 = W_3 f_3 \ln \left(\frac{f_4}{f_3} \right) = 2.303 W_3 f_3 \log \left(\frac{f_4}{f_3} \right),$$

where W_2, W_3 are the power spectral densities (g^2/Hz) at the frequencies f_2 and f_3 (Hz) respectively, r_{12} is the slope (dB/Oct) between the frequencies f_1 and f_2 (Hz), and r_{34} is the slope (dB/Oct) between the frequencies f_3, f_4 (Hz),

$$n = \frac{\log \frac{W_2}{W_1}}{\log \frac{f_2}{f_1}} = \frac{\log \left(\frac{f_2}{f_1} \right)^{\frac{r_{12}}{3}}}{\log \frac{f_2}{f_1}} = \frac{r_{12}}{3} \quad \text{and} \quad m = \frac{\log \frac{W_4}{W_3}}{\log \frac{f_4}{f_3}} = \frac{\log \left(\frac{f_4}{f_3} \right)^{\frac{r_{34}}{3}}}{\log \frac{f_4}{f_3}} = \frac{r_{34}}{3}.$$

Example

Random accelerations at the base of the spacecraft for the ARIANE 4 are specified. The rms value for the acceleration spectrum below will be calculated (Table 6.6).

Table 6.6 Calculation of rms value

Frequency range (Hz)	Power Spectral Density (g^2/Hz)	Slope (dB/oct)	Area's (g^2)
20–150	+6dB/octave	$n = 2$	$A_1 = 2.0$
150–700	0.04		$A_2 = 22.0$
700–2000	-3dB/octave	$m = -1$	$A_3 = 29.4$
rms			$\sqrt{A_1 + A_2 + A_3} = 7.3$

End of example

6.5 Acoustic loads

The noise of the launch vehicle engines, the separation of the airflow along the launch vehicle and the aerodynamic noise generate acoustic loads in a broad frequency spectrum from 20–10000 Hz.

The acoustic loads also result in high frequency random vibration. The noise level is at its peak during lift-off and transonic flight of the launch vehicle.

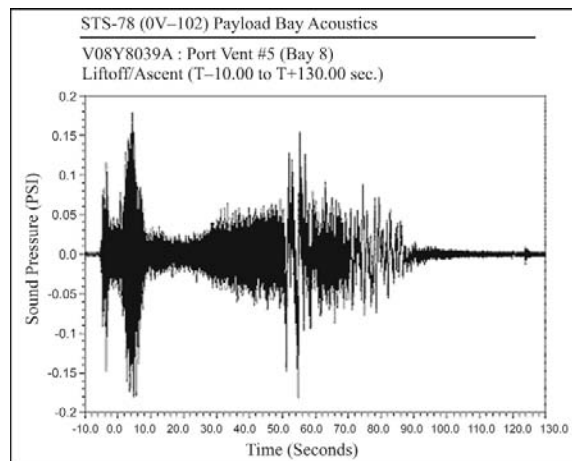


Fig. 6.12 High frequency sound pressures versus time (courtesy FEMCI, NASA GSFC)

An example of measured acoustic pressures is shown in Fig. 6.12 and an example of a specified acoustic load spectrum is illustrated in Fig. 6.13.

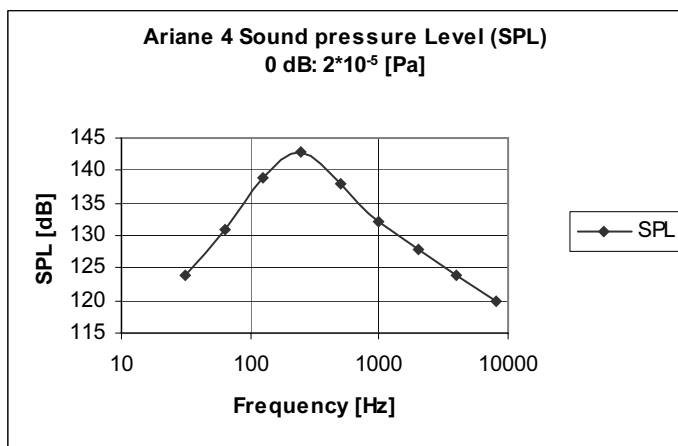


Fig. 6.13 Ariane 4 Acoustic loads, qualification level

The sound pressure level (SPL) is expressed in decibels (dB) and depends on the frequency. Various basic concepts will be explained in the following sections.

6.5.1 Sound Pressure Level

The sound pressure level (SPL) is generally given in decibels. The SPL gives an indication of the strength of the noise source but nothing about the direction.

In fact, a noise field is governed by two quantities: the sound pressure level and the direction. In a free space, a vibrating sphere will radiate sound in all directions, while in a closed space the noise field will reflect off the walls from several sides.

A noise field is called reverberant or diffuse when the noise strength is equally high from all directions. In the case of a reverberant noise field, the direction of sound is insignificant and only the noise strength is important.

The sound in a room consists of that coming directly from the source plus sound reflected or scattered by the walls and by objects in the room. Sound is called reverberant after having undergone one or more reflections [Pierce 1981].

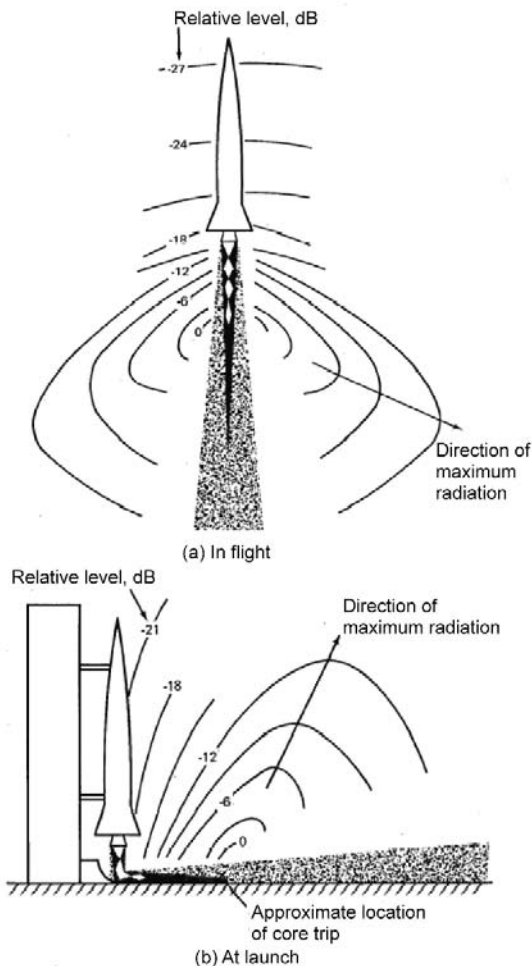


Fig. 6.14 Sketch of the rocket flow and contour overall sound-pressure level for flight and launch cases [NASA SP-8072]

Relative noise levels around a launch vehicle during lift-off and flight are shown in Fig. 6.14.

Examples of sound pressure levels are given in Table 6.7, [Pierce 1981].

Table 6.7 Examples

SPL (dB) $p_{\text{ref}} = 2 \times 10^{-5}$ Pa	Examples
140	Near jet engine (at 3 m)
130	Threshold of pain
120	Rock concert
110	Accelerating motorcycle (at 5 m)
100	Pneumatic hammer (at 2 m)
90	Noisy factory
80	Vacuum cleaner
70	Busy traffic

The exhaust noise of the engines causes considerable acoustic loads within the nose cone of the launch vehicle. The highest acoustic loads occur during lift-off and in transonic flight. Generally, a reverberant noise field is assumed. The strength of the noise field (SPL) is expressed in (dB), depending on the frequency. The frequency band is the octave- or one-third octave band. An example of a definition of acoustic loads is given in the following Table 6.8:

Table 6.8 Sound pressure level

Octave band	Sound Pressure Level (SPL) (dB) ref.: 0 (dB) = 2×10^{-5} (Pa)
31.5	124
63	130
125	135
250	139
500	134
1000	128
2000	124
4000	120
8000	116
Overall Sound Pressure Level (OASPL)	142

The sound pressure level (SPL) is defined in the following way:

$$SPL = 10 \log \left(\frac{p^2}{p_{\text{ref}}^2} \right), \quad (6.40)$$

where the reference value of the sound pressure, $p_{\text{ref}} = 2 \times 10^{-5}$ Pa and p is the effective value of the occurring sound pressure.

The sound pressure is measured in a certain centre frequency with associated bandwidth.

In acoustics it is common to work with a constant relative bandwidth (the so-called octave or one-third octave band filters).

6.5.2 Octave band

For a constant relative bandwidth, the ratio between two consecutive frequencies is defined as:

$$\frac{f_x}{f_{\text{ref}}} = 2^x. \quad (6.41)$$

In which case it yields for x :

- $x = 1$ one speaks of an octave band, $\frac{f_x}{f_{\text{ref}}} = 2^1$ and when
- $x = \frac{1}{3}$ one speaks of a one-third octave band, $\frac{f_x}{f_{\text{ref}}} = 2^{\frac{1}{3}} = 1.260$

The centre frequencies in an octave- and one-third octave band are given in Table 6.9

6.5.3 Centre frequency

The centre frequency f_{cent} is the geometric mean of the minimum frequency f_{min} and the maximum frequency f_{max} in the relative frequency band, and is of course dependent on the octave band used. The centre frequency is:

$$f_{\text{cent}} = \sqrt[f]{f_{\text{min}} f_{\text{max}}}. \quad (6.42)$$

6.5.4 Relative bandwidth

The bandwidth Δf is the difference between the maximum frequency f_{max} and the minimum frequency f_{min} and is given by:

$$\Delta f = f_{\max} - f_{\min}. \quad (6.43)$$

The ratio between the extreme frequencies in the band is $\frac{f_{\max}}{f_{\min}} = 2^x$. It is then easy to derive the expression for the bandwidth in terms of the centre frequency:

$$\Delta f = \left(2^{\frac{x}{2}} - 2^{-\frac{x}{2}}\right) f_{\text{cent}}. \quad (6.44)$$

Any proportional frequency band is defined by its centre frequency and by x . An octave band ($x = 1$) with a centre frequency 1000 Hz, the extreme frequencies of the frequency band are $f_{\min} = 707$ Hz and $f_{\max} = 1414$ Hz respectively and the relative bandwidth is $\Delta f = 707$ Hz.

Table 6.9 Centre frequencies octave and one-octave frequency bands

Octave frequency band (Hz)	One-third octave frequency band (Hz)	Octave frequency band (Hz)	One-third octave frequency band (Hz)
31.5	25	1000	800
	31.5		1000
	40		1250
63	50	2000	1600
	63		2000
	80		2500
125	100	4000	3150
	125		4000
	160		5000
250	200	8000	6300
	250		8000
	315		10000
500	400		
	500		
	630		

The relative bandwidth for the one-octave and one-third octave bands are given in Table 6.10.

Table 6.10 Relative bandwidth

x st -Octave band	Bandwidth (Hz)
$x = 1$	$\Delta f = 0.7071f_{\text{cent}}$
$x = \frac{1}{3}$	$\Delta f = 0.2316f_{\text{cent}}$

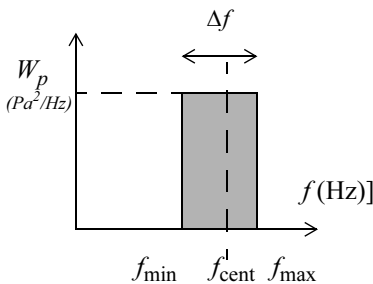
6.5.5 Power Spectral Density

The power spectral density of the effective (rms) sound pressure for a certain centre frequency with relative bandwidth Δf , is calculated as follows:

$$W_p(f_{\text{cent}}) = \frac{p^2}{\Delta f}, \quad (6.45)$$

in which $W_p(f_{\text{cent}})$ is the power spectral density of the sound pressure (Pa^2/Hz) and p^2 is the effective sound pressure.

The SPL is constant in the frequency bandwidth, hence the pressure is constant in the frequency bandwidth. That means that the power spectral density of the sound pressure is constant in the frequency bandwidth. This is illustrated in Fig. 6.15.

**Fig. 6.15** Calculation power spectral density

The square root of the mean value of the noise strength over the entire frequency band is calculated with (see (6.31)):

$$p_{\text{rms}} = \sqrt{\int_{f_{\text{lower}}}^{f_{\text{upper}}} W_p(f) df}. \quad (6.46)$$

Equation (6.46) can be simplified using (6.45):

$$p_{\text{rms}} = \sqrt{\int_{f_{\text{lower}}}^{f_{\text{upper}}} W_p(f) df} = \sqrt{\sum_k \frac{p_k^2}{\Delta f_k} \Delta f_k} = \sqrt{\sum_k p_k^2}. \quad (6.47)$$

The effective pressure p can be calculated with (6.40):

$$p_k^2 = p_{\text{ref}}^2 10^{\frac{SPL_k}{10}}. \quad (6.48)$$

The reference pressure is $p_{\text{ref}} = 2.0 \times 10^{-5}$ Pa, thus p_k can be written as follows:

$$p_k^2 = 10^{\frac{SPL_k - 94}{10}}. \quad (6.49)$$

The overall sound pressure level (OASPL) is calculated as follows:

$$OASPL = 10 \log \left(\frac{p_{\text{rms}}^2}{p_{\text{ref}}^2} \right). \quad (6.50)$$

This is in accordance with (6.40).

We may rewrite (6.50)

$$OASPL = 10 \log p_{\text{rms}}^2 + 94. \quad (6.51)$$

An example of a calculation of the OASPL is given in the following Table 6.11.

6.5.6 Conversions of SPL

The following relation determines the conversion of the 1/3-octave band to the one-octave band:

$$SPL_{1-\text{octave}} = 10 \log \left\{ \sum_{k=1}^3 10^{\frac{SPL_{\frac{1}{3}-\text{octave}}}{10}} \right\}. \quad (6.52)$$

One octave frequency band contains three 1/3-octave bands (see Table 6.9). The mean pressure in the octave band is equal to the sum of the mean square pressure in the 1/3-octave band (see (6.47)).

Table 6.11 Calculation OASPL

Octave band	Sound Pressure Level (SPL) (dB)		Sound pressure p_k^2 (Pa ²)
	ref: 0 [dB] = 2*10 ⁻⁵ (Pa)		
31.5	124		1.005×10 ³
63	130		4.000×10 ³
125	135		1.265×10 ⁴
250	139		3.177×10 ⁴
500	134		1.005×10 ⁴
1000	128		2.524×10 ³
2000	124		1.005×10 ³
4000	120		4.000×10 ²
8000	116		1.592×10 ²
		$p_{rms}^2 = \sum_k p_k^2$	6.356×10 ⁴
Overall Sound Pressure level (OASPL)	$OASPL = 10\log\left(\frac{p_{rms}^2}{p_{ref}^2}\right)$		142 [dB]
Overall Sound Pressure level (OASPL)	142		

$$p_{octave}^2 = \sum_{k=1}^3 p_{\frac{1}{3}-octave,k}^2 = \sum_{k=1}^3 p_{ref}^2 10^{\frac{SPL_{\frac{1}{3}-octave,k}}{10}}. \quad (6.53)$$

Dividing both sides of (6.53) by p_{ref}^2 then

$$\frac{p_{octave}^2}{p_{ref}^2} = \sum_{k=1}^3 10^{\frac{SPL_{\frac{1}{3}-octave,k}}{10}}. \quad (6.54)$$

By taking the 10 logarithm (log) for both sides and multiplying with 10, (6.54) becomes

$$SPL_{octave} = 10 \log \left(\frac{P_{octave}^2}{P_{ref}^2} \right) = 10 \log \left(\sum_{k=1}^3 10^{\frac{SPL_{\frac{1}{3}-octave, k}}{10}} \right). \quad (6.55)$$

The following relation determines the conversion of the 1-octave band to the 1/3-octave band:

$$SPL_{\frac{1}{3}-octave} = SPL_{1-octave} + 10 \log \left\{ \frac{\Delta f_{\frac{1}{3}-octave}}{\Delta f_{1-octave}} \right\}. \quad (6.56)$$

Example

The conversion of the 1-octave band to the 1/3-octave band is given Table 6.12. An example conversion of the 1/3-octave band to the 1-octave band is illustrated in Table 6.13

Table 6.12 Example conversion calculation 1–1/3 octave band

Octave band (Hz)	SPL _{1-octave} (dB)	Δf _{1-octave} (Hz)	1/3-octave band (Hz)	Δf _{\frac{1}{3}-octave} (Hz)	SPL _{\frac{1}{3}-octave} (dB)
125	135	88.4	100	23.2	129.2
			125	28.9	130.1
			160	37.1	131.2

Table 6.13 Example conversion calculation 1/3–1 octave band ($p_{ref} = 2 \times 10^{-5}$ Pa)

1/3-octave band (Hz)	SPL _{\frac{1}{3}-octave} (dB)	SPL _{\frac{1}{3}-octave} 10	Octave band (Hz)	SPL _{1-octave} (dB)
100	129.2	12.92	125	135
125	130.1	13.01		
160	131.2	13.12		

End of example

6.5.7 Acoustic Fill Factor

Often, the acoustic environment for launch vehicles is representative for the unfilled or empty environment. It becomes necessary to account for the presence of the payload fill and its effects on the interior sound pressure level, [Hughes 1994].

The fill factor FF is given by the following expression [Hughes 1994]

$$FF(f) = 10 \log \left[\frac{\left\{ 1 + \frac{c}{2fH} \right\}}{1 + \left\{ \frac{c}{2fH} (1 - V_{ratio}) \right\}} \right] (\text{dB}) \quad (6.57)$$

where

- c is the speed of sound in air (m/s^2)
- f is the **one third octave band center frequency** (Hz)
- H is the gap distance between the payload and the fairing/cargo bay wall (m)
- V_{ratio} is the volume ratio of the payload volume to the empty fairing/cargo bay volume, for a given payload zone length.

Add the fill factor effect to the acoustic levels specified for the empty fairing/cargo bay. If the sound pressure levels are specified in the octave band a conversion to the one third octave band is needed to add the fill factor. After that, the octave band specification may be converted to the octave band.

Example

Let the factor $\frac{c}{fH} = 100$ and the volume ratio $V_{ratio} = 0.70$ then the fill factor

$FF = 5 \text{ dB}$. The empty volume $SPL(f) = 130 \text{ dB}$. The total filled sound pressure level at the one third octave band center frequency f (Hz) becomes $SPL(f) = 135 \text{ dB}$.

End of example

6.6 Shock loads

6.6.1 Introduction

Separation of stages and the separation of the spacecraft from the last stage of the launch vehicle will induce very short duration loads in the internal structure of the spacecraft, these are the shock loads. The duration of the shock load is in general very short with respect to the duration associated with the fundamental natural frequencies of the loaded dynamic mechanical system.

The effects of the shock loads are generally represented in a Shock Response Spectrum (SRS). The SRS is essentially a plot that shows the responses of a number of single degree of freedom (SDOF) systems to an excitation.

The excitation is usually an acceleration time history. This process is illustrated in Fig. 6.16.

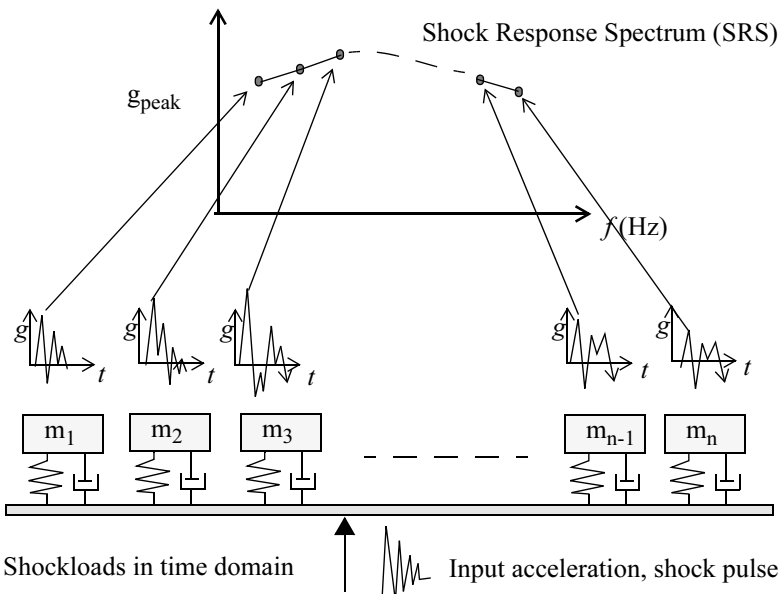


Fig. 6.16 The SRS (Shock Response Spectrum) concept. An input transient acceleration to be analysed is processed mathematically in a way that simulates the process represented here.

The spacecraft is generally loaded by the heaviest loads when the nose cone is fired away and when the spacecraft separates from the last stage of the launch vehicle. The combustion and the burn-up of the engines generally result in lower shock loads.

The launch authorities specify the shock load with a “shock spectrum”. An example of an ARIANE 4 shock spectrum is given in Fig. 6.17. The damping factor (Quality factor Q) must be specified.

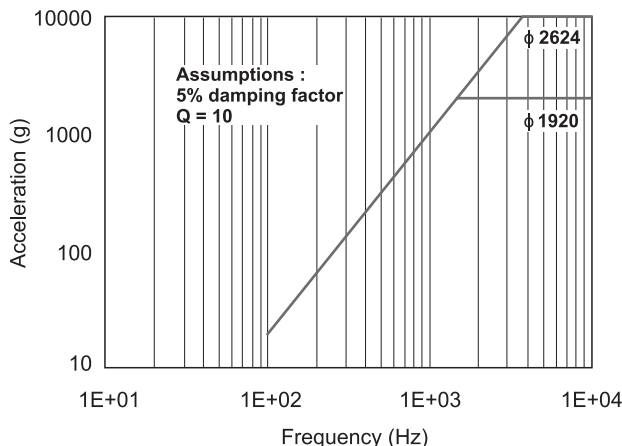


Fig. 6.17 Ariane 4 Shock Response Spectrum (SRS)

A SRS is generated by calculating the maximum response of a SDOF system to a particular base transient excitation. Many SDOF systems tuned to a range of natural frequencies are assessed using the same input time history. A damping value must be selected in the analysis. A damping ratio of $\zeta = 0.05$, $Q = 10$, is commonly used.

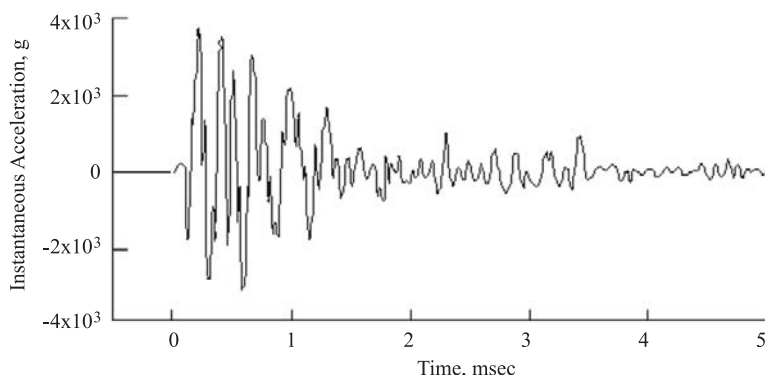


Fig. 6.18 Typical Pyroshock acceleration Time History [NASA-STD-7003]

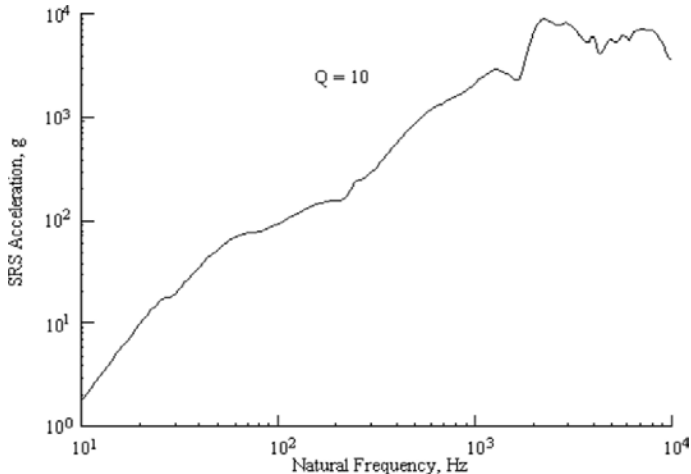


Fig. 6.19 Typical Pyroschock Maximum Shock Response Spectrum (SRS) [NASA-STD-7003]

The final SRS plot looks like a frequency domain plot. It shows the largest absolute response encountered for a particular SDOF system anywhere within the analysed time. Therefore the SRS provides an estimate of the response of an actual product and its various components to a given transient input (i.e. shock pulse). A typical example of a time history acceleration and associated SRS as illustrated in Fig. 6.18 and Fig. 6.19, are extracted from NASA-STD-7003.

In this section the response of a SDOF system, due to enforced acceleration, will be recapitulated.

6.6.2 Enforced acceleration

A SDOF system with a discrete mass m , a damper element c and a spring element k is placed on a moving base which is accelerated with an acceleration $\ddot{u}(t)$. The resulting displacement of the mass is $x(t)$. We introduce the natural (circular) frequency $\omega_n = \sqrt{\frac{k}{m}}$, the damped circular frequency $\omega_d = \omega_n \sqrt{1 - \zeta^2}$, the critical damping constant $c_{\text{crit}} = 2\sqrt{km}$ and the damping ratio $\zeta = \frac{c}{c_{\text{crit}}}$. The amplification factor is defined as $Q = \frac{1}{2\zeta}$ where $Q = 10$ is generally assumed.

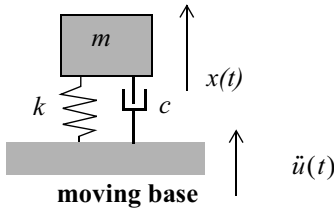


Fig. 6.20 Enforced acceleration on a damped SDOF system

We introduce a relative motion $z(t)$, which is the displacement of the mass with respect to the base. The relative displacement is

$$z(t) = x(t) - u(t). \quad (6.58)$$

The equation of motion for the relative motion $z(t)$ is

$$\ddot{z}(t) + 2\zeta\omega_n\dot{z}(t) + \omega_n^2 z(t) = -\ddot{u}(t). \quad (6.59)$$

The enforced acceleration of the SDOF system is transformed into an external force. The absolute displacement $x(t)$ can be calculated with

$$\ddot{x}(t) = \ddot{z}(t) + \ddot{u}(t) = -2\zeta\omega_n\dot{z}(t) - \omega_n^2 z(t). \quad (6.60)$$

The solution of (6.59), using initial conditions with respect to displacement $z(0)$ and velocity $\dot{z}(0)$ is

$$z(t) = z(0)e^{-\zeta\omega_n t} \left(\cos \omega_d t + \frac{\zeta}{\sqrt{1-\zeta^2}} \sin \omega_d t \right) + \dots$$

$$\dots + \dot{z}(0)e^{-\zeta\omega_n t} \frac{\sin \omega_d t}{\omega_d} - \int_0^t e^{-\zeta\omega_n \tau} \frac{\sin \omega_d \tau}{\omega_d} \ddot{u}(t-\tau) d\tau. \quad (6.61)$$

For SRS calculations $z(0) = \dot{z}(0) = 0$, hence

$$z(t) = - \int_0^t e^{-\zeta\omega_n \tau} \frac{\sin \omega_d \tau}{\omega_d} \ddot{u}(t-\tau) d\tau = - \int_0^t e^{-\zeta\omega_n(t-\tau)} \frac{\sin \omega_d(t-\tau)}{\omega_d} \ddot{u}(\tau) d\tau. \quad (6.62)$$

After differentiation of (6.62) with respect to time, the relative velocity $\dot{z}(t)$ becomes

$$\dot{z}(t) = - \int_0^t e^{-\zeta\omega_n(t-\tau)} \cos(\omega_d(t-\tau)) \ddot{u}(\tau) d\tau - \zeta\omega_n z(t). \quad (6.63)$$

The absolute acceleration $\ddot{x}(t)$ can be obtained applying (6.60)

$$\ddot{x}(t) = 2\zeta\omega_n \int_0^t e^{-\zeta\omega_n(t-\tau)} \cos(\omega_d(t-\tau)) \ddot{u}(\tau) d\tau + \omega_n(2\zeta^2 - 1)z(t). \quad (6.64)$$

The maximum acceleration $\ddot{x}(t)$ can be calculated by inserting the natural frequency $\omega_n = 2\pi f_n$ (Rad/s) of the SDOF system for every natural frequency. The maximum acceleration $\ddot{x}(t)$ will be plotted against the number of cycles per second f_n (Hz). This plot is called the Shock Response Spectrum (SRS) of the base excitation $\ddot{u}(t)$.

For the calculation of the SRS the following parameters are important:

1. The damping ratio ζ of the SDOF dynamic system.
2. The number of SDOF systems for which the maximum response is calculated
3. The minimum time frame of the transient period T_{\min} [s]. The minimum time frame is the larger of either $T_{\min} \geq \frac{1}{f_{\min}}$ or twice the maximum shock time $T_{\min} \geq 2t_{\text{shock}}$.
4. The time increment Δt must be less than 10% of the reciprocal value of the maximum frequency f_{\max} (Hz) involved in the calculation of the SRS, i.e. $\Delta t \leq \frac{0.1}{f_{\max}}$. The minimum number of time steps n within the time frame T_{\min} is $n = \frac{T_{\min}}{\Delta t} = 10 \frac{f_{\max}}{f_{\min}}$.

Example

A half sine pulse $\ddot{u}_{\text{base}} = 200 \sin \frac{\pi t}{\tau}$, $0 \leq t \leq \tau = 0.0005$ (s) and

$\ddot{u}_{\text{base}} = 0$, $t < 0$, $t > \tau$ is applied to the base of series of SDOF dynamic systems to calculate the SRS of the HSP. The total time is $t_{\text{end}} = 0.05$ s and

$\Delta t = 0.00001 \leq \frac{0.1}{f_{\max}} = \frac{0.1}{3000} = 0.00003$ s. The damping ratio $\zeta = 0.05$, $Q = 10$.

The calculated SRS (absolute acceleration) is illustrated in Fig. 6.21.

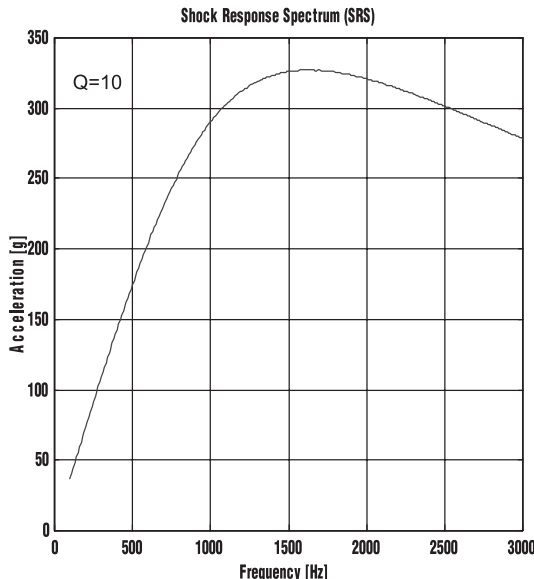


Fig. 6.21 The SRS of a Half Sine pulse (HSP) with amplitude $A=200\text{g}$ and a time duration $\tau = 0.0005\text{s}$

6.6.3 Shock Attenuation Rules

A number of empirically derived shock attenuation rules have been proposed over the years by NASA and ESA. It is important to note that this assessment of attenuation is only valid for prediction of the shock environment induced by clampband separation.

The following scaling relationships are proposed [Kryenko 2004] by NASA and ESA respectively

$$att_{\text{NASA}} = e^{\left[\left(-8 \times 10^{-4} f^{\frac{2.4f^{0.105}}{}} \right) d \right]}, \quad (6.65)$$

and

$$att_{\text{ESA}} = e^{\left[\left(-8 \times 10^{-4} f^{\frac{2.515f^{0.115}}{}} \right) (0.0144d^3 - 0.2d^2 + 0.93d + 0.024) \right]}, \quad (6.66)$$

where d (m) is the distance between the point of interest and the shock source and f is the frequency (Hz). These rules must be used with great care.

6.6.4 SRS Tolerance Limit

The SRS tolerance limit Tol_{SRS} is specified in (dB) and defined as follows

$$Tol_{SRS} = 20 \log \left\{ \frac{SRS_{Tol}}{SRS_{Nominal}} \right\}, \quad (6.67)$$

where SRS_{Tol} is the extreme value of the SRS defined by the tolerance band and $SRS_{Nominal}$ is the nominal specified value of the SRS. A very usual tolerance limit is $Tol_{SRS} = \pm 3$ dB.

6.7 Static pressure variations

During the launch phase, the pressure will decrease within the payload volume. Air cavities must be designed to have sufficient venting to prevent damage to the closing (surrounding) structure due to high pressure differences (pressure vessel).

The variation of the static pressure during launch is illustrated in Fig. 6.22.

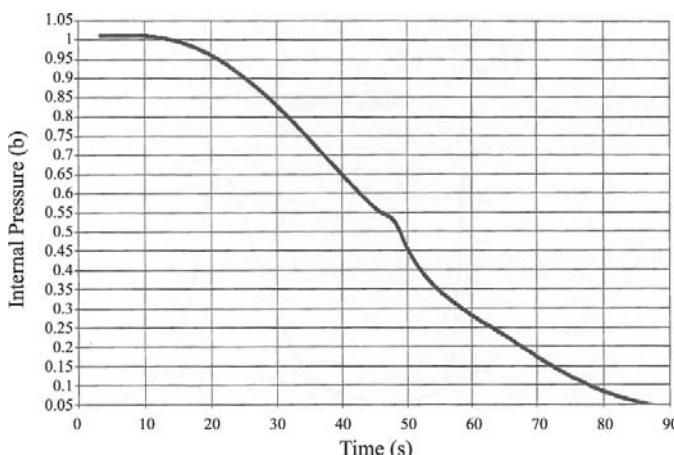


Fig. 6.22 Variation of static pressure within payload volume (Ariane 5)

As a rule of thumb sufficient venting will be provided if (ENVISAT-1 experience):

$$\frac{A}{V} \geq 20 \times 10^{-4} \text{ m}^{-1} \quad (6.68)$$

where A is the total area of the venting holes (m^2) and V the total volume to be vented (m^3).

6.8 Micro-meteorites / Orbital Debris

6.8.1 Introduction

Space surrounding Earth is full of millions of micro meteoroids and man-made orbital debris. In the last 30 years that humans have been exploring space, much orbital debris has been created that poses a serious threat to spacecraft orbiting the earth. Orbital debris consists not only of large redundant stages of rockets and old spacecraft but, also small parts such as bits of paint and other fragments. Even minute parts can seriously damage a spacecraft because these parts move at very high velocities. Orbital debris flies with a velocity of 7.5 km/s (27000 km/h) in an orbit around the earth. If two parts have a frontal collision the crash velocity is therefore 15 km/s.

Micro meteorites usually circle the sun with speeds that can exceed 70 km/s. However, they are much smaller and their density is less than that of orbital debris.

Orbital debris is still increasing. Every year more and more spacecraft are launched into space, which then results in even more orbital debris. “Dead” spacecraft explode or disintegrate which results in thousands of new pieces of orbital debris.

Large parts can be traced by radar so that one can map the positions of orbital debris. The small parts that cannot be observed by radar however, are, nevertheless, dangerous for spacecraft.

Spacecraft must be designed against the impact of small parts at extremely high velocities.

In an orbit around the Earth, the parts (solar panels, antennas, radiators, etc.), boxes, and instruments mounted on the outside of the spacecraft are exposed to micro meteorites and man-made debris. In some cases protective measures must be taken.

A meteorite flux model describes the number of micro meteorites. The flux F of the micrometric is given as a function of the “particle” mass m (gram).

A debris flux model describes the debris. The flux F of the debris is given as a function of the “particle” diameter D (cm). The flux F describes the number of particles per m^2 , per year.

The density of the meteorites is $\rho = 0.5$ gram/cm³ for all sorts of meteorites and all existing sizes. The density of the debris with a diameter $D \leq 1$ cm is $\rho = 2.8$ gram/cm³. The density of the debris decreases as the diameter D increases.

A more detailed discussion about micro-meteoroids and space debris is given chapter 24 "Damage to Spacecraft by Meteoroids and Orbital Debris", page 399.

6.8.2 Simple Micro Meteoroid Flux Model

The micro meteoroid flux model is limited by a "particle" mass $10^{-12} \leq m \leq 1$ gram.

For a "particle" mass $10^{-12} \leq m \leq 10^{-6}$ grams the following micro meteorites flux model may be used:

$$\log F = -0.063(\log m)^2 - 1.584\log m - 14.339 \text{ (Particles/m}^2/\text{year}), \quad (6.69)$$

and for a "particle" mass $10^{-6} \leq m \leq 1$ gram the following micro meteorites flux model may be used:

$$\log F = -1.213\log m - 14.37 \text{ (Particles/m}^2/\text{year}), \quad (6.70)$$

where F is the average number of particles, with mass m or larger, per m² of surface area and per second and m the mass of the "particle" in grams.

6.8.3 Simple Debris flux Model

Orbital debris is defined as any man-made object in orbit about the Earth which no longer serves a useful purpose.

The higher the altitude, the longer the orbital debris will generally remain in Earth orbit. Debris left in orbits below 600 km normally fall back to Earth within a few years. At altitudes of 800 km, the time for orbital decay is often measured in decades. Above 1000 km, orbital debris will normally continue circling the Earth for a century or more.

The debris flux model is limited by a "particle" diameter $D \leq 2$ (cm).

For a "particle" $D \leq 1$ (cm) the following debris flux model may be used:

$$\log F = -2.52\log D - 5.46 \text{ (Particles/m}^2/\text{year}). \quad (6.71)$$

For a “particle” diameter $1 \leq D \leq 2$ cm the following debris flux model may be used:

$$\log F = -1.395 \log D - 5.46 \text{ (Particles/m}^2/\text{year}), \quad (6.72)$$

where F is the average number of particles, with diameter D (cm) or larger, per m^2 of surface area and per year and D the size of the “particle” in (cm).

Much more information about Orbital debris can be read in [NRC 1995].

6.9 Literature

- Harris, R.W. and Ledwith, T.J., 1974, *Introduction to Noise Analysis*, Pion Limited, ISBN 0 85086 041 5.
- Kyryenko, S., 2004, *Sloshsat Shock Mapping, Shock induced by Spacecraft Separation from Launcher*, Memorandum:TEC-MCS/2004/1026/In/SK.
- Lalanne, C., 2002a, *Mechanical Vibration & Shock Volume 1, Sinusoidal Vibration*, HPS, ISBN 1 9039 9603 1.
- Lalanne, C., 2002b, *Mechanical Vibration & Shock Volume 2, Mechanical Shock*, HPS, ISBN 1 9039 9604 X.
- Lalanne, C., 2002c, *Mechanical Vibration & Shock Volume 3, Random Vibration*, HPS, ISBN 1 9039 9605 8.
- Nahin, P.J., 1998, *An Imaginary Tale, The Story of $\sqrt{-1}$* , Princeton University Press, ISBN 0-691-02795-1.
- NASA SP-8072, 1971, *Acoustic Loads Generated by the Propulsion System*, NASA Space Vehicle Design Criteria.
- Hughes, W.O., McNelis, M.E., Manning, J.E., 1994, NASA TM-106688, *NASA LeRC's Acoustic Fill Effect Test Program and Results*, Lewis Research center.
- NASA Practice No. PD-EC-1102, *Meteoroids & Space debris*, Preferred Reliability Practices, JPL.
- NASA Practice No. PD-ED-1211, *Combination Methods for Deriving Structural Design Loads Considering Vibro-Acoustic, Etc., Responses*, Preferred Reliability Practices, JPL.
- NASA Practice No. PT-ET-1406, *Sinusoidal Vibration*, Preferred Reliability Practices, JPL.
- National Research Council (NRC), 1995, *Orbital Debris, A Technical Assessment*, National Academic press, ISBN 0-309-0515-8.
- Newland, D.E., 1975, *An Introduction to Random Vibrations and Spectral Analysis*, Longman, ISBN 0 582 46335-1.
- <http://see.msfc.nasa.gov/mod/modpub.html>, Space Environments & Effects (SEE) Program, Meteoroids and Orbital Debris, SEE related NASA Publications.

6.10 Exercises

6.10.1 Sinusoidal Vibrations

The maximum sinusoidal vibrations are specified by the acceleration levels in Table 6.14. Answer the following questions:

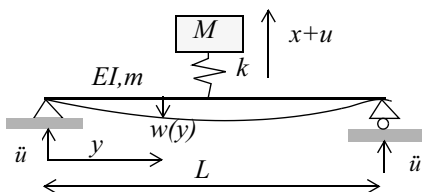
- Why is the acceleration in the launch direction, between 4–7 Hz specified in mm?
- Calculate the acceleration in (g), in the launch direction, at 4 Hz.
- Is the acceleration specification in lateral direction properly specified? If not, update the specification in the lateral direction.

Table 6.14 Sinusoidal vibrations

	Frequency (Hz)	Acceleration (g)
Launch direction	4–7	10 mm double amplitude
	7–100	1.0
Lateral direction	4–100	0.6

6.10.2 Tuned Damper

A simply supported beam is damped by a tuned damper placed in the mid of the beam. The system is illustrated in Fig. 6.23.

**Fig. 6.23** Beam and tuned damper

The beam is excited by a enforced harmonic acceleration $\ddot{u}(t)$. The bending stiffness of the beam is EI , the mass per unit of length is $m = 2 \text{ kg/m}$ and the total length is $L = 0.5 \text{ m}$. The tuned damper is placed at the mid of the beam and has a mass $M = \gamma \frac{mL}{2}$ and spring stiffness k .

The deflection of the beam $w(y, t)$ is with respect to the base and is given by $w(y, t) = \eta(t) \sin\left(\frac{\pi y}{L}\right)$ (assumed mode) and the relative displacement of the discrete mass M of the tuned damped is given by $x(t)$.

- Set up the undamped equations of motion.
- Assume a zero spring stiffness of the tuned damper $k = 0$ and calculate the natural frequency of the simply supported beam.
- Calculate the bending stiffness EI of the beam assuming a natural frequency $f_{n,beam} = 50 \text{ Hz}$.
- Vary $\gamma = 0.01, 0.1, 1.0$ and calculate the spring stiffness of the SDOF system assuming a natural frequency $f_{n,sdof} = 50 \text{ Hz}$

- Vary $\gamma = 0.01, 0.1, 1.0$ and calculate the natural frequency f_1 and f_2 (Hz) and associated mode shapes.
- Vary $\gamma = 0.01, 0.1, 1.0$ and calculate the frequency responses

$$\ddot{w}\left(\frac{L}{2}, f\right) = \ddot{\eta}(f)) \text{ and } \ddot{x}(f), \text{ assuming}$$

$\ddot{u}(f) = 1 \text{ m/s}^2$, applying the modal approach using a constant modal damping ratio $\zeta = 0.05$ for both modes.

Answers:

- $$\begin{bmatrix} M & 0 \\ 0 & mL \end{bmatrix} \begin{Bmatrix} \ddot{x} \\ \ddot{\eta} \end{Bmatrix} + \begin{bmatrix} k & -k \\ -k & k + \left(\frac{\pi}{L}\right)^4 EIL \end{bmatrix} \begin{Bmatrix} x \\ \eta \end{Bmatrix} = -\begin{Bmatrix} M \\ 2mL \end{Bmatrix} \ddot{u}$$
- $$f_{n,\text{beam}} = \frac{\pi}{2} \sqrt{\frac{EI}{mL^4}}$$

6.10.3 Calculation of PSD's and Grms

A specified power spectral density of the enforced acceleration is given in Table 6.15, however, with three unknowns: the PSD levels at 20 and 2000 Hz and the Grms value.

- Calculate the PSD over the acceleration at 20 Hz.
- Calculate the PSD over the acceleration at 2000 Hz.
- Calculate the Grms value of the random vibration spectrum

Table 6.15 .PSD random vibrations levels

Frequency (Hz)	PSD Level (g^2/Hz)
20	?
20–50	2.3 dB/Oct
50–800	0.02
800–2000	-2.3 db/Oct
2000	?
Overall	? Grms

Answers: 0.01 g^2/Hz , 0.01 (g^2/Hz), 5.7 Grms

6.10.4 Prove of conversion formulae

The conversion of the SPL from the one-octave band to the SPL in the 1/3-octave band can be done using (6.56). Prove this equation (6.56).

6.10.5 Calculation of OASPL and conversion to 1/3-octave band

The SPL specification is specified in Table 6.16. Carry out following assignments:

- Calculate the OASPL of the specified SPLs in the one-octave band.
- Convert the SPLs to the 1/3-octave band and recalculate the OASPL.

Table 6.16 Specification SPL

Octave band	Sound Pressure Level (SPL) (dB) ref: 0 [dB] = 2×10^{-5} (Pa)
31.5	125
63	132
125	136
250	140
500	134
1000	130
Overall Sound Pressure level (OASPL)	? (dB)

7 Test Verification

7.1 Introduction

The objectives of structural tests are to gain confidence in the analytical predictions which support spacecraft development, and ultimately to support the qualification and flight acceptance of the spacecraft system. The types and purposes of the different tests are described in this chapter.

7.2 Tests

The following mechanical tests are usually performed:

- **Static test** is achieved by subjecting the structure to static loads (wiffle tree), or by a centrifuge test, or quasi-static testing on a shaker to facilitate the load introduction. The static tests provide insight into the validity of the stiffness matrix, but are used mainly to qualify the strength adequacy of the primary structure and critical structural interfaces e.g. spacecraft/launcher and spacecraft/payload interfaces.
- **Modal survey** (also called modal analysis) tests are achieved by exciting the structure with small excitors (or on the shaker) to determine the modal characteristics of the spacecraft, e.g. natural frequencies, mode shapes, damping, etc. Since the applied excitation forces at resonance are compensated only by damping, high responses can be achieved with small excitation forces. The results of the modal survey tests determine the dynamic compatibility of the spacecraft with the launcher. They also support the verification of the mathematical model (in general the finite element model) which is used in launch vehicle spacecraft coupled loads dynamic analysis (CLDA) in the loads cycle assessment, and to tailor the vibration test level.
- **Shaker vibration sine test** supports the verification of the mathematical model used in forced frequency response predictions, and it particularly useful in determining the amplification of the excitation input from the launcher space-

craft interface on various elements of the spacecraft (amplification factor Q=output/input). The main purpose of the shaker vibration sine test is to qualify the adequacy of the secondary structures when subjected to a dynamic environment, and to verify the adequacy of the spacecraft system by performing functional tests after the spacecraft system qualification and flight acceptance shaker tests.

- **Shaker vibration random test** supports the verification of spacecraft units subjected to a random dynamic environment which might be experienced during flight. The latter usually results from acoustic excitation of structural surfaces.
- **Shock test** supports the verification and qualification of the spacecraft structure and instruments when subjected to a shock environment due to pyrotechnics and latching loads e.g. release of launcher spacecraft interface clamp band, and release of booms, solar panels, antennas, etc.
- **Acoustic test** supports the verification of the spacecraft against the specified acoustic loads under the fairing of the launch vehicle. The acoustic test is done in a reverberant chamber.

Many loads (jet engines, wind loads, turbulence, transonic velocity, noise loads, ...) occur simultaneously. Currently, however, no test apparatus is available that can apply these loads simultaneously on the structure that is to be tested. For that reason the loads are applied according to type and according to coordinate-axis.

The spacecraft stiffness, the mass and the centre of gravity also influence the induced dynamic loads. The test directions cannot account for these parameters and serve to design a large range of spacecraft. This means that the test requirements can be significantly more stringent than the loads that are actually induced.

7.3 Goal of the tests

The tests are carried out to qualify the design of the spacecraft structure (qualification test) and to accept the flight hardware (acceptance test). The qualification tests are usually carried out at the ‘design limit loads’ level while the acceptance tests are usually carried out at the ‘flight limit loads’ level.

The qualification tests are used to prove that the structure can withstand the qualification loads. The applied loads are often a factor greater (i.e. design loads) than the expected flight limit loads.

The acceptance test is carried out to discover production deviations (workmanship) that were not discovered during the inspections. The applied loads are equivalent to the expected flight limit loads. The acceptance test is often used to control the integrity of the mechanical system.

The structural model (basically the primary structure) is usually subjected to a static test to verify the strength and stiffness requirements.

The complete qualification model of the spacecraft will be tested with enforced sine vibrations and an acoustic test in a reverberant chamber to verify sinusoidal and acoustic specified loads respectively.

The secondary structure is generally subjected to a sine test and a random test. Acoustic loads are converted to random structural vibrations which must be verified by test.

Light structures with large surface areas (such as solar panels, antennas, etc.) are usually subjected to acoustic tests. The acoustic test loads generally envelop the mechanical stochastic loads. Therefore, acoustic loads are considered the design driving loads.

Deployable structures are tested for shock loads during deployment.

Small and very stiff structures such as electronic boxes are mainly tested for random vibrations loads. Acoustic loads are converted to random structural vibrations which must be verified by tests.

Separation tests on deployable structures are also done to verify the release and deployment systems.

7.4 Test Plan

The test is carried out according to the test plan, in which the order of the tests (qualification, acceptance) has been established.

In the test plan the objectives of the tests and the test success criteria must be discussed.

A measurement plan (location of the accelerometers, strain gauges, etc.) is generally included.

Test predictions of the spacecraft to be tested (including the test fixtures) are a part of the test plan.

The requested output (accelerations, strains, displacements, etc.) must be defined in the test plan.

Low level sine sweep tests with a low sweep rate are performed before and after the dynamic tests to detect failures after the test. In case of no failure, the low level sine responses should be equal, and the resonances must be at about the same locations.

One part of the test plan is the test sequence. Such a test sequence is illustrated in following Table 7.1. The sequence may be applied per axis and the load levels specified in the test plan.

Table 7.1 Test sequence

Test #	Test description	Specifications	Comments
1	Low level sine sweep	Input: 0.15 g , 20–2000 Hz, 2 oct./min	Signature test
2	Sinusoidal vibration	5–100 Hz	Qualification level
3	Low level sine sweep	Input: 0.15 g , 20–2000 Hz, 2 oct./min	
4	Random Vibration	Input: 20–2000 Hz	120 s
5	Low level sine sweep	Input: 0.15 g , 20–2000 Hz, 2 oct./min	
6	Sine burst	Input: ± 8.5 g, 24.5–25.5 Hz	10 full cycles
7	Low level sine sweep	Input: 0.15 g , 20–2000 Hz, 2 oct./min	Signature test

7.5 Test Procedure

The test procedure is, in general, an answer of the test house to the test plan in which the qualification philosophy had been explained.

In the test procedure, the test article, the test description, responsibilities, the test personnel and QA management will be briefly outlined.

The general test conditions and safety measures with respect to the potential expected hazards (i.e. pressurised tanks) must be identified. Project and QA plan and the safety plan must be met.

The test facility, adapters, the control system, the instrumentation (Pilot and Co-pilot sensors, measurement points), the data acquisition and processing system, and system tolerances must be described.

Furthermore, within the frame of the test performance, the test sequence, the input levels, the vibration control and safety aspects during the test, data handling and reduction must be described, followed by a step by step procedure which describes all relevant activities for each test.

7.6 Model philosophy

The number of test models has decreased over time. In the past, three models were in use:

- STM (Structural Test Model) is used to carry out static and dynamic tests (qualification level).
- QM (Qualification Model) is used to carry out dynamic tests with qualification loads. This second model is necessary because of lack of confidence in the analytic approach.
- FM (Flight Model) is dynamically loaded with acceptance loads.

Presently, the number of test models in use is as follows:

- STM to apply the qualification loads during static and dynamic tests.
- PFM / QM (Proto Flight Model). The first FM (Flight Model) is used to apply qualification loads during dynamic tests, but for a time duration equal to those for the acceptance loads. The PFM will be refurbished to a FM.
- FM (Flight Model) are used to apply the acceptance loads during dynamic tests.

The first FM is used to qualify the satellite. The risk is higher and the chance that the FM must be repaired is high. This approach is based on sufficient confidence in the analytic calculation of the design loads.

In the new philosophy, the STM is excluded and is called the protoflight approach.

- PFM / QM. The first FM is subjected to qualification loads, for static and dynamic loads. The PFM will be refurbished to a FM.
- FM is loaded with acceptance loads.

The qualification of the satellite is done directly on the PFM and increases the probability of failure. This approach is used more and more to limit the development costs. More trust is put in analytic calculations.

The qualification of the structure is possible because:

- The structure was qualified during a static test carried out beforehand. This is known as the “BUS” approach when a family of like satellites are developed.
- Large components of the structure are tested separately. Critical parts are qualified separately.

7.7 Static Test

The static test is carried out to qualify the strength of the primary structure and the most important adjacent structures; spacecraft / launch vehicle and satellite / payload interface.

In addition, the stiffness properties of the primary structure are measured. The stiffness matrix can be measured to control the stiffness matrix of the finite element model.

The static test can be carried out:

- On a centrifuge
- In a test rig (the forces are applied with the aid of whiffle trees)
- With a “sine-burst” test
- With a “sine-dwell” test

In Table 7.2 an evaluation of the pro’s and con’s between a centrifuge test and a test rig static test are given. The static test is usually applied on very large and heavy structures with a low natural frequency.

The inertial load of the electronic boxes etc. is simulated by a complex whiffle tree. This whiffle tree becomes way too complicated if every box would be simulated. That is why the large masses are simulated and the small masses are not simulated.

A centrifuge commonly loads appendages such as solar panels and antennas.

Table 7.2 Centrifuge / Test rig evaluation

Type of test	Advantages	Disadvantages
Centrifuge test	<ul style="list-style-type: none"> • All (dummy) mass can be mounted on the spacecraft structure and will transfer inertia loads into the structure. • Relatively cheap if there is a centrifuge available 	<ul style="list-style-type: none"> • Inertia field varying over the spacecraft • No visual observation during the test (during failure) • Less information due to a limited number of strain gauges, etc.
Static test within test rig (whiffle trees)	<ul style="list-style-type: none"> • A lot of information because there are no limitations for strain gauges, etc. • Visual observation during the test 	<ul style="list-style-type: none"> • Not all masses can be mounted due to the limitations of load introduction. Masses must be lumped.

7.7.1 Sine-burst test

The ‘sine burst’ test was developed by the GSFC (NASA) in order to cheaply induce the quasi-static qualification loads and, in doing so, qualify the strength of the structure. Sine-burst means that the input signal g_{sb} (accelerations) is made up of a sinusoidal signal $A_{sb} \sin(2\pi f_{sb})$ with a certain frequency $\omega_{sb} = 2\pi f_{sb}$ and amplitude A_{sb} on which a gradient filter $f(t)$ has been placed. The sine-burst signal is then $g_{sb} = f(t)A_{sb} \sin(2\pi f_{sb})$. Starting at zero, the ascending slope of $f(t)$ reaches the maximum value after a number of cycles. The amplitude then remains constant for 5 to 10 cycles followed by a descending slope and after a number of cycles approaches zero. The maximum amplitude of the input signal remains constant for 5 to 10 cycles and is equal to the quasi-static loads. The frequency f_{sd} of

the sinusoidal signal $\sin(2\pi f_{sb})$ must be smaller than $f_{sb} \leq \frac{f_n}{3}$ where f_n is the smallest natural frequency associated with the lowest significant vibration form. In that case, the effective mass will have to be a significant fraction of the total mass of the spacecraft.

It is difficult to apply the sine-burst to very large structures that often have low natural frequencies.

7.7.2 Sine-dwell test

The sine-dwell test was developed in order to cheaply induce the quasi-static qualification loads, and in doing so, qualify the strength of the structure. The ‘sine-dwell’ test is also known as the quasi-static test on a vibration table. ‘Sine-dwell’ means that the input signal g_{sd} (accelerations) is a sinusoidal signal $A_{sd} \sin(2\pi f_{sd})$ with a certain frequency $\omega_{sd} = 2\pi f_{sd}$ and amplitude A_{sd} which is maintained during a certain period of time. The maximum amplitude of the input signal is equal to the ultimate quasi-static loads. The frequency f_{sd} of the sinusoidal signal $\sin(2\pi f_{sd})$ must be smaller than $f_{sd} \leq \frac{f_n}{3}$, where f_n is the smallest natural frequency associated with the lowest significant vibration mode. In that case, the effective mass will have to be a significant fraction of the total mass of the satellite. The sine-dwell test is also simulated by scanning the frequency band $[f_n - \delta, f_n + \delta]$ with a certain linear sweep velocity n (for example, 1 Hz / min), where $\delta = 0.5$ Hz. The number of cycles depends strongly on the frequency bandwidth and the sweep velocity.

It is difficult to apply the sine-dwell to very large structures due to the fact that they often have low natural frequencies.

7.8 Mechanical Vibration/Acoustic Tests

The goal of the vibration tests on a satellite is to check whether all the systems on board still function properly after the mechanical vibration tests.

A design qualification test can be carried out on a prototype of a satellite, while for a flight acceptance test the satellite that is to be launched (flight model) is used. During the flight acceptance test the “real” dynamic load is applied, while for the qualification test the applied load is generally higher and the test lasts longer.

The results of the mechanical vibration tests can be used to correct the dynamic mathematical models, for example the damping- and the mass matrices.

The mechanical vibration tests that are generally required are:

- Sine test
- Stochastic (random) test
- Shock test
- Acoustic test

The aforementioned tests are carried out on the shaker table. Shock tests are also done especially for equipment designed to introduce heavy shocks (i.e. shock separation induced shocks).

7.8.1 Sine Vibration Test

The sine vibration test simulates the low frequency sinusoidal dynamic loads. The main goal of the sinusoidal test is to expose and test the secondary structure (mounted or not to the satellite) for sinusoidal loads and determine whether the systems are still functioning after the sine test.

The boundary conditions at the base of the satellite on the vibration table deviate from the boundary conditions when the spacecraft is mounted on the launch vehicle. These deviating boundary conditions generally manifest themselves unfavourably. The high impedance of the vibration table causes an excessive load in the spacecraft structure when it is excited in the vicinity of a resonant frequency. The launch vehicle with the spacecraft adapter on which the spacecraft is mounted, has lower impedance than the vibration table. If it turns out that by using the Coupled Loads Dynamic Analysis (CDLA) the spacecraft is loaded too heavily on the vibration table, then excessive loading of the spacecraft must be prevented.

Another criteria to notch the input level is the load carrying capability of the payload adapter. The shaker system can put more load in the system than the payload adapter can carry. Adaptations for the input levels must be made.

The low level sine sweep test must be used to define the resonance frequencies and amplification factors of the maximum expected acceleration levels and interface (I/F) loading must somehow be calculated to define the notches.

Sometimes to ensure an intermediate acceleration level, a sine vibration test is done. Again the results of this test may be used to adapt (notch) input levels.

To maintain the dynamic response of spacecraft values within certain values, the prescribed base excitation must be decreased. Decreasing the base input is known as 'notching'. In practice, notching is only applied to resonant frequencies associated with high modal effective mass. Notching must usually be applied to the appendages (solar panels, antennas) and may only be carried out with the consent of the main contractor. The test levels for the sinusoidal vibration test for the ARI-ANE 5 are given in the following Table 7.3.

Table 7.3 Sinusoidal accelerations

	Frequency (Hz)	Qualification level (0-peak) (g)	Acceptance level (0-peak) (g)
Launch direction	4–200	1.25	1.0
Lateral	2–18	1.0	0.8
	18–100	0.8	0.6
Sweep rate	2 oct./min.		4 oct./min.

First some concepts need to be explained:

Zero to peak

The term zero to peak refers to the amplitude of the sinusoidal acceleration.

Sweep rate

On a shaker, the sinusoidal enforced acceleration is applied to a structure with a certain (proto flight) sweep rate with the unit octave/min.

The sweep rate is the velocity at which the frequency domain is scanned. This sweep rate is given by n octaves per minute, that means that the relation between time t and the frequency $f(t)$ is logarithmic:

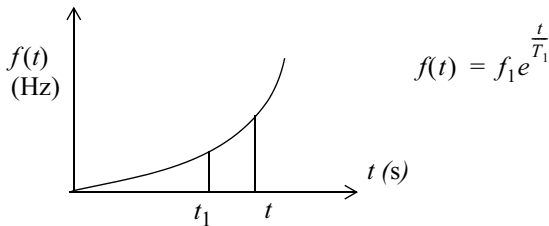


Fig. 7.1 Sweep rate

The logarithmic ratio of the frequency ratio is equal to a constant times the time difference [Lalanne 2002, Volume 1]

$$f(t) = f_1 e^{K(t-t_1)} = f_1 e^{\frac{t}{T_1}}. \quad (7.1)$$

From (7.1) we derive that

$$f(t)dt = \frac{df}{K} = T_1 df. \quad (7.2)$$

The sweeprate is defined as the number of octaves per minute, i.e. n Oct/min. If we have n Oct/min (7.1) can be written $\ln(2^n) = K60 = \frac{60}{T_1}$. Thus we get for the constants K and T_1

$$K = \frac{1}{T_1} = \frac{n \ln(2)}{60} = 0.0116n. \quad (7.3)$$

The number of cycles in a certain time domain can be obtained by

$$N(t) = \int_{t_{\text{ref}}}^t f(t)dt = \frac{1}{K} \int_{f_{\text{ref}}}^f df = \frac{f - f_{\text{ref}}}{K} = \frac{\Delta f}{K} = T_1 \Delta f \quad (7.4)$$

The number of cycles is constant all over the frequency range and is given by

$$N(\Delta f=1) = \frac{1}{K} = T_1 = \frac{86.6}{n} \quad (7.5)$$

The number of cycles ΔN between the half power points around the natural frequency f_o in a bandwidth with the amplification factor Q

$$\Delta f = \frac{f_o}{Q} = 2\zeta f_o, \quad (7.6)$$

where ζ is the damping ratio. The number of cycles is given by

$$\Delta N = \frac{\Delta f}{K} = T_1 \Delta f = \frac{T_1 f_o}{Q}. \quad (7.7)$$

The time to sweep from 4–100 Hz with a sweep rate $n = 2$ can be calculated very easily using (7.1)

$$\Delta t = \frac{1}{K} \ln \left\{ \frac{f_2}{f_1} \right\} = T_1 \ln \left\{ \frac{f_2}{f_1} \right\} = \frac{86.6}{n} \left\{ \frac{f_2}{f_1} \right\} = \frac{86.6}{2} \ln \left\{ \frac{100}{4} \right\} = 140 \text{ s} \quad (7.8)$$

A swept sine enforced acceleration $\ddot{u}(t)$ can be defined as a function characterised by [Lalanne 2002, Volume 1]

$$\ddot{u}(t) = U(f) \sin \left\{ \frac{d}{dt} E(t) + \alpha \right\}, \quad (7.9)$$

where $U(f)$ is the frequency dependent amplitude of the acceleration, $E(t)$ is a time function defining the sweep mode and α is a phase shift which is, in general zero. The radian frequency Ω is give by

$$\Omega = 2\pi f = \frac{dE(t)}{dt}. \quad (7.10)$$

Hence

$$E(t) = 2\pi \int_0^t f_1 e^{\frac{t}{T_1}} dt = 2\pi f_1 T_1 \left(e^{\frac{t}{T_1}} - 1 \right). \quad (7.11)$$

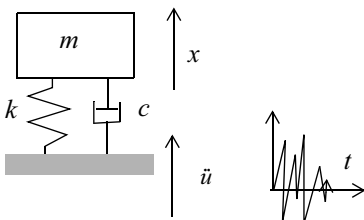


Fig. 7.2 Enforced acceleration

The relative displacement with respect to the base is

$$z(t) = x(t) - u(t). \quad (7.12)$$

The equation of motion for the relative displacement $z(t)$ is given by

$$\ddot{z}(t) + 2\zeta\omega_0\dot{z}(t) + \omega_0^2 z(t) = -\ddot{u}(t) = -\ddot{U}(f)\sin\left\{\frac{d}{dt}E(t) + \alpha\right\}, \quad (7.13)$$

with α the phase shift. The acceleration $\ddot{x}(t)$ is further obtained by

$$\ddot{x}(t) = -2\zeta\omega_0\dot{z}(t) - \omega_0^2 z(t), \quad (7.14)$$

and

$$E(t) = 2\pi f_1 T_1 \left(e^{\frac{t}{T_1}} - 1 \right).$$

Introducing the parameter η

$$\eta = \frac{Q^2}{f_o T_1}, \quad (7.15)$$

the reduction in amplitude, for increasing frequencies, compared with the stationary frequency response analysis is given by, [Lalanne 2002, Volume 1]

$$G_{up}(\eta) = 1 - e^{(-2.55\eta^{-0.39})} - 0.0025\eta^{0.79}, \quad 0 \leq \eta \leq 100, \quad (7.16)$$

and the reduction for decreasing frequencies

$$G_{down}(\eta) = 1 - e^{(-3.18\eta^{-0.38})}, \quad 0 \leq \eta \leq 100. \quad (7.17)$$

Example

Table 7.4

Sweep rate n (oct/min)	Q	f_o (Hz)	T_1	$\eta = \frac{Q^2}{f_o T_1}$	$G_{up}(\eta)$	$G_{down}(\eta)$
2	25	25	43.281	0.578	0.956	0.980
4	25	25	21.64	1.15	0.907	0.951

End of example

7.8.2 Random Vibration Test

The random vibration test is primarily used to test and to qualify spacecraft parts: electronic boxes, tanks, etc.

The random vibration loads for the qualification of the spacecraft or a subsystem generally last 120 seconds and are applied to the qualification model. The duration of the random test for acceptance is 60 sec. The input during a random test consists of a mix of frequencies between 20 and 2000 Hz.

The following random vibration specification for the fuel tank of the ARTEMIS spacecraft are given for the random test in Table 7.5.

Table 7.5 Random vibration specification (ARTEMIS)

Application	Axis	Frequency (Hz)	PSD Acceleration (g ² /Hz)	Duration (s)
Fuel tank	x,y,z	20–110	+3 dB/oct.	120
		110–700	0.09	
		700–2000	–3 dB/oct	

The input PSD is measured with the aid of one or more “pilot” accelerometers. The input definition can be the maximum, minimum or average value of the PSD of “pilots”. The test tolerance is determined by means of “abort limits”, for example:

$$10\log\left(\frac{PSD_{\max,\min}}{PSD_{\text{nominal}}}\right) = \pm 3 \text{ dB} \quad (7.18)$$

The total signal is decoded with the aid of filters with a “centre frequency” f_1 , f_2 , ... and associated bandwidth Δf_i . The signal coming from each filter band is statistically distributed and the grms-values can be determined with the help of a voltmeter; g_{rms,f_1} , g_{rms,f_2} , etc. or the mean values of the acceleration in the frequency bands g_{rms,f_1}^2 , g_{rms,f_2}^2 , etc.

The value $\frac{g_{\text{rms},f_i}^2}{\Delta f_i}$ is known as the Power Spectral Density (PSD). The mean square value of the acceleration along the entire frequency domain is then equal to:

$$g_{\text{rms}}^2 = \sum_{i=1}^n \frac{g_{\text{rms},f_i}^2}{\Delta f_i} \Delta f_i = \sum_{i=1}^n g_{\text{rms},f_i}^2. \quad (7.19)$$

7.8.3 Acoustic Vibration Test

Acoustic loads are important loads for the external subsystems of the spacecraft, i.e. solar arrays, antenna dishes, etc.. The acoustic vibration test is carried out to simulate the sound vibrations in the frequency band.

The test is carried out in a reverberation chamber. That means that the sound level at every point in the chamber has an equal spectrum and is moreover, the same in all directions. The walls in the reverberant chamber have been made as hard and as reflective as possible. None of the walls are parallel to each other.

As for a random test where g_{rms} -values are measured by accelerometers, the rms pressure fluctuations p_{rms} are measured by microphones.

The pressure level is measured with respect to a reference pressure $p_{\text{ref}} = 2 \times 10^{-5}$ Pa. The sound pressure levels are given in dB. For a frequency band i holds:

$$SPL_i = 10 \log \left(\frac{p_{\text{rms},i}}{p_{\text{ref}}} \right)^2. \quad (7.20)$$

Since it is not easy to set up the sound spectrum in the reverberation chamber exactly, a test tolerance is defined for each frequency band. An example of a test input is given in the following Table 7.6.

The input is defined by the average of a number of microphone signals. This average is based on the equivalent power for microphone k . The average dB in the reverberation chamber is determined by:

$$SPL_{\text{av}} = 10 \log \left(\frac{1}{n} \sum_{k=1}^n 10^{\frac{SPL_k}{10}} \right) \quad (7.21)$$

Table 7.6 SPL specifications.

Octave band (Hz)	Qualification (dB)	Acceptance (dB)	Test tolerances (dB)
31.5	118	114	-2, +4
63	124	120	-1, +3
125	135	131	-1, +3
250	140	136	-1, +3
500	143	139	-1, +3
1000	137	133	-1, +3
2000	132	128	-1, +3
4000	125	121	-4, +4
8000	124	120	-4, +4
OASPL	146	142	-1, +3
Duration (s)	120	60	

A series of measurements during the qualification acoustic test of the MAQSAT-B2&Sloshsat on six control microphone positions is given as an example (see Table 7.7)

Table 7.7 Measured sound pressure levels

Octave band (Hz)	Pos 1 (dB)	Pos 2 (dB)	Pos 3 (dB)	Pos 4 (dB)	Pos 5 (dB)	Pos 6 (dB)	ASPL ^a (dB)
31.5	124.6	125.0	126.0	122.2	123.1	124.1	124.3
63	128.9	126.1	128.3	128.1	128.0	129.5	128.3
125	129.2	129.5	128.4	129.7	128.9	130.0	129.3
250	127.6	127.2	127.2	128.9	127.8	128.1	127.8
500	127.3	127.9	127.6	127.6	127.5	127.2	127.5
1000	122.2	123.3	121.6	121.8	121.8	122.0	122.2
2000	113.1	114.8	112.7	112.9	112.9	113.5	113.4
OASPL	135.1	134.8	134.8	135.1	134.7	135.4	135.0
Octave band (Hz)	SSPL ^b (dB)	TSPL ^c (dB)	ASPL (dB)	DSPL ^d (dB)			
31.5	125.0	+4/-2	124.3	-0.7			
63	128.0	+3/-1	128.3	0.3			
125	129.0	+3/-1	129.3	0.3			
250	127.0	+3/-1	127.8	0.6			
500	127.0	+3/-1	127.5	0.8			
1000	121.0	+3/-1	122.2	0.5			
2000	114.0	+3/-1	113.4	1.2			
OASPL	134.6	+1/-1	135.0	0.4			

a. Averaged Sound Pressure level

b. Specified Sound Pressure level

c. Tolerances specified

d. Deviation (ASPL-SSPL)

Pre-tests in the empty chamber are done both at low and at test levels.

The test sequence has, in general, first a low level acoustic test to calibrate the SPL levels in the frequency band. After that, the real test (qualification or flight acceptance) is done, and, after that again a low level test is performed to show if any failures have occurred. The results of the pre-test are matched with the results of the post-test.

The data reduction for each respective channel is, in general, performed in the following form:

- 1/3 and 1/1 Octave band analysis and OASPL indicating tolerance, average and difference SPL for the microphone signals.
- PSD-plots in the test band (i.e. 10–2500 Hz) for a given Δf (i.e. 5 Hz) and RMS value for the response channels (accelerometers, straingauges).

7.8.4 Shock test

A shock test is used to prove that part of the spacecraft (such as the instruments, electronic boxes, etc.) can withstand the shock loads caused by the separation of the spacecraft from the rocket, the burn up of the rocket stages, deployment of the solar panels, etc.

For parts of a spacecraft the Shock Response Spectrum (SRS) is replaced by an equivalent half sine pulse (HSP) for a duration of 0.5 ms, at an amplitude of 200 g for example. Small parts (for example up to 30 kg) can, if deemed necessary, be subjected to shock loads on shock tables. The shock loads are introduced in various ways:

- A pendulum with a weight attached to both ends that strikes an anvil on which the test unit is mounted. By modifying the weight and the drop height of the pendulum the SRS can be changed.
- By mounting the unit that is to be tested on a ringing plate. The plate is excited by a falling weight. The SRS can be modified by varying the location where the falling weight falls.

7.8.5 Modal Survey/Modal Analysis Test

The measurement of the modal characteristics of a spacecraft structure actually requires that structure. The structure, however, only becomes available at a late stage in the project.

The dynamic characteristics of the structure are measured with the help of modal survey:

- Resonant frequencies
- Vibration modes or mode shapes
- Generalised masses
- Modal effective masses
- Modal damping ratio's

Using the data obtained from the modal survey test, the finite element model of the spacecraft is updated, if necessary. The corrected finite element model of the spacecraft may then be used for a coupled loads dynamic analysis of the spacecraft / launch vehicle.

In practice the frequency response functions of the dynamic system are measured for a modal survey test.

The frequency response function is measured between a point that is excited and another point where the response (acceleration) is measured.

An accelerometer is mounted (glued) at one point while other defined points are excited (excitation point) by a hammer stroke for instance, where the dynamic

force is measured with the help of a dynamometer. With modern methods various points can be excited simultaneously with small shakers. The excitation can be a force in a certain frequency band, a block sine, a shock or white noise. Both the excitation and the measured response are converted into the frequency domain using fast fourier transform techniques, after which the frequency response functions can be determined.

The modal survey test can be divided into three phases:

- Test preparation phase
- Measurement of the FRFs
- Determination of the modal characteristics; natural frequencies, vibration modes, etc.

In the test preparation phase the configuration of the structure, the location of the acceleration transmitters and force excitors, and the magnitude of the forces (measurement plan) are determined.

For spacecraft systems it must be proven that the cross-orthogonality between the calculated and the measured mode shapes is acceptable. Therefor a condensed matrix corresponding with the instrumentation plan must be provided to be used for the orthogonality tests.

7.9 Notching

The first objective of notching is to reduce the excitation level during sine or random vibration testing in order to not exceed the sizing loads at the interfaces. This is called primary notching.

Secondary notching is sometimes necessary to avoid unrealistic overtesting of items within internal structures of units if it is felt that the test may damage the unit, the sub-contractor may request a secondary notch to the prime-contractor. This applies only if the primary notching is not sufficient and if the sub-contractor can show strong evidence that the equipment will suffer damage.

7.9.1 Notching at Equipment Level

In this chapter we will give some guidelines to perform vibration sine and random tests at equipment level.

During the test the design loads must not be exceeded. The impedance of the shaker must be greater than the impedance of the real spacecraft structure, so the shaker system is able to introduce significant more dynamic loads in the equipment than the real supporting vibrating structure. To prevent overloading the vibration inputs must be decreased during the tests. Assume the following test levels for the particular equipment, [Mansholt 1985], shown in Table 7.8 and Table 7.9.

Table 7.8 Sine input specification

Frequency range (Hz)	Qualification level (0-peak)
	Sweep rate 2 Oct/min. (duration 1 sweep)
5–19	10.3 mm
19–22	10.3 mm
22–100	20 g

Table 7.9 Random test specification

Frequency range (Hz)	Qualification level (duration 120 s for each axis)
	PSD (g^2/Hz)
20–60	6 dB/oct
60–700	0.2
700–2000	−3 dB/oct
Grms	16.6

The load restraint is given in Table 7.10.

Table 7.10 Sine test restraints

Equipment tests	Qualification output
Sine test maximum acceleration output	24 g
Random test maximum acceleration output	8 grms

To get a good overview of the dynamic behaviour of the test specimen concerning natural frequencies and amplification factors a low level sine sweep test must be done. For example, the following low level sine sweep can be done, see Table 7.11.

Table 7.11 Low level sine sweep

Low level sine input	0.2 g
Frequency range	5–2000 Hz
Sweep rate	2 Oct/min

Sine Vibration Test Notching

The harmonic response acceleration $\ddot{X}_i(f)$ at a certain position due to the acceleration base excitation $\ddot{U}(f)$ of the equipment can be written as

$$\ddot{X}_i(f) = H_i(f)\ddot{U}(f), \quad (7.22)$$

where $H_i(f)$ is the frequency response function. This is illustrated in Fig. 7.3.

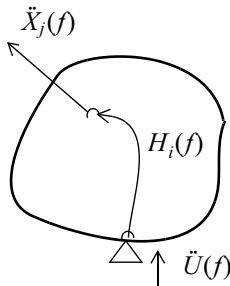


Fig. 7.3 Acceleration excited equipment

For linear structures a reduction of the harmonic response $\alpha\ddot{X}_i(f)$ can be achieved when the base excitation is reduced to $\alpha\ddot{U}_i(f)$. That means that the notching curve must be an image of the output curve as shown in Fig. 7.4 which applies for forces also. The resonance frequency f_r and amplification factor are detected by the low level sine sweep run.

Random Vibration Test Notching

The notching profile for random vibration tests must be based on the low level sine sweep test results (resonant frequencies f_r (Hz), amplification factors Q). The discussion of the notching procedure for random vibration test has been based on [Mansholt 1985].

The notching level is defined by the input level for the random vibration test devided by the amplification factor squared

$$W_{\tilde{u}, \text{notch}}(f_r) = \frac{W_{\tilde{u}}(f_r)}{Q^2} \quad (7.23)$$

The frequency band Δf

$$\Delta f = \frac{f_r}{Q} = 2\zeta f_r, \quad (7.24)$$

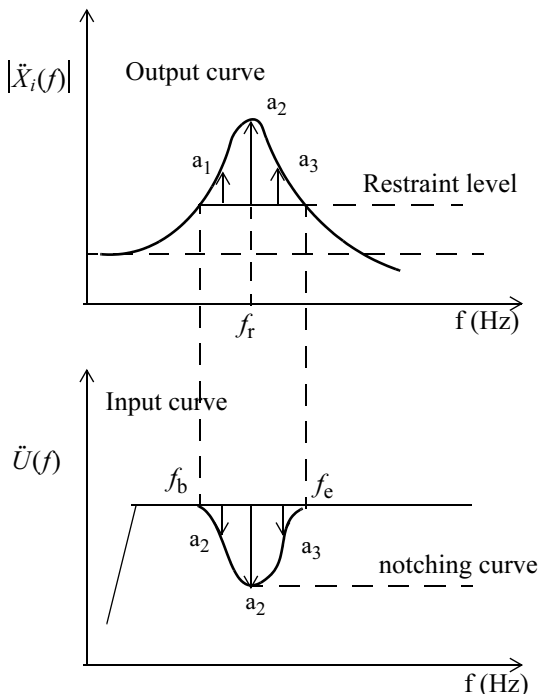


Fig. 7.4 Notch definition for sine vibration test

where ζ the damping ratio. The lower and upper bounds of the notch are defined as

$$f_{lo} = f_r - \frac{\Delta f}{2} \text{ and } f_{hi} = f_r + \frac{\Delta f}{2}. \quad (7.25)$$

The frequency range between f_b and f_e must be in the area, therefore the amplification factor of the low level sine sweep is $Q \geq 2$.

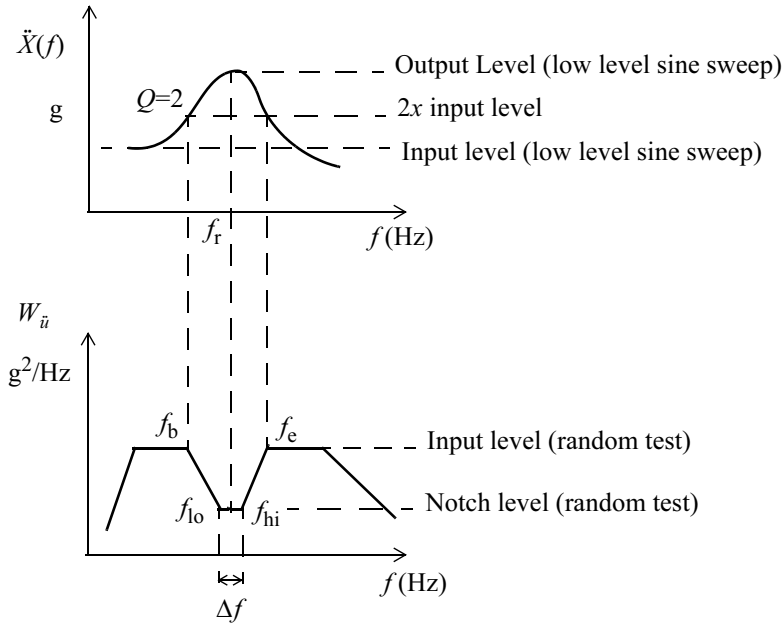


Fig. 7.5 Random vibration test notching

The steepness of the slopes of the notch can be calculated with

$$k_1 = \frac{\ln\left(\frac{W_{\ddot{u}, \text{notch}}(f_r)}{W_{\ddot{u}}(f_{lo})}\right)}{\ln\left(\frac{f_{lo}}{f_b}\right)} \quad \text{and} \quad k_2 = \frac{\ln\left(\frac{W_{\ddot{u}}(f_e)}{W_{\ddot{u}, \text{notch}}(f_r)}\right)}{\ln\left(\frac{f_e}{f_{hi}}\right)}. \quad (7.26)$$

The area below the input of the random test can be calculated with

$$A_i = \begin{cases} \frac{W_1 f_1}{3} \left[\left(\frac{f_2}{f_1} \right)^{\frac{k_i}{3} + 1} - 1 \right] & (k_i \neq -3) \\ W_1 f_1 \ln\left(\frac{f_2}{f_1}\right) & (k_i = -3) \end{cases} g^2, \quad (7.27)$$

for a constant power spectral density of the random accelerations $k = 0$.
The RMS value of the random input can now be calculated

$$\ddot{u}_{rms} = \sqrt{\sum_{i=1}^n A_i g_{rms}}. \quad (7.28)$$

The rms value for the input spectrum of the notched random input can be obtained, and will be denoted by $\ddot{u}_{rms,\text{notch}}$.

Example

For this example a qualification random vibration test on equipment in one direction is presented.

The results of the low level sine sweep, from 5–2000 Hz with a sweep of 2 Oct/min and an acceleration level of 0.2 g, are presented in Table 7.12.

Table 7.12 Resonant frequencies and amplification factors

# Resonance frequency (Hz)	Resonance frequency f_r (Hz)	Amplification factor Q	f_b (Hz)	f_e (Hz)
1	325	25.5	240	400
2	584	8.5	530	650
3	1407	3.7	—	—

The third resonance frequency will not be considered because the amplification is low and is beyond the turning point at 700 Hz.

The notching calculations are presented in Table 7.13 and Table 7.14.

Table 7.13 Calculations of notch input levels

# Notch	f_r (Hz)	Amplification factor Q	PSD $W_{\ddot{u}}(f_r)$ ($\frac{g^2}{Hz}$)	PSD $W_{\ddot{u}}(f_r)$ ($\frac{g^2}{Hz}$) $\frac{f_r}{Q^2}$	$\Delta f = \frac{f_r}{Q}$ (Hz)
1	325	25.5	0.2	0.00031	12.7
2	584	8.5	0.2	0.0027	68.7

Table 7.14 Calculation of notch width

# Notch	$\Delta f = \frac{f_r}{Q}$ (Hz)	$f_{lo} = f_r - \frac{\Delta f}{2}$ (Hz)	$f_{hi} = f_r + \frac{\Delta f}{2}$ (Hz)
1	12.7	319	331
2	68.7	550	618

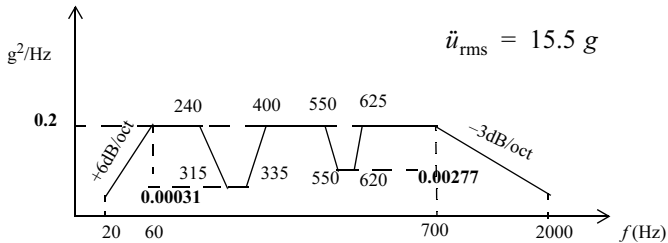


Fig. 7.6 Notched random acceleration input

We proceed now with a low level random test with an input level much lower than the previous discussed level with notches. Assume a test level factor $ZL = -10$ dB. The associated g_{rms} value of the low level input becomes

$$\ddot{u}_{rms,ZL} = \ddot{u}_{rms,notch} 10^{\frac{ZL}{20}} = 15.5 \times 10^{\frac{-10}{20}} = 4.9 \text{ g.}$$

The rms response acceleration $\ddot{x}_{rms,ZL}$ of a certain location had been provided by the test facility and is given by

$$\ddot{x}_{rms,ZL} = 5.6 \text{ g.}$$

The output power level for random qualification tests for the equipment must in the range of 8 to 1.1×8 Grms. With help of the low level random test results, the input for the random test and the expected power level $\ddot{x}_{rms,Z}$ can be calculated and defined.

The inputs for the calculation are:

- $\ddot{u}_{rms,notch} = 15.5 \text{ g}$, the input specification test profile with notches
- $\ddot{x}_{rms,ZL} = 5.6 \text{ g}$, output low level random test with $ZL = -10$ dB.

The control values

- $W_{\ddot{u},max} = 0.2 \text{ g}^2/\text{Hz}$, maximum PSD-input of specification input curve
- $\ddot{x}_{rms,Z} = 8.0 \text{ g}$, maximum power-output for random test.

The calculation sequence is as follows.

1. The rms value for the low level random test is

$$\ddot{u}_{rms,ZL} = \ddot{u}_{rms,notch} 10^{\frac{ZL}{20}} = 15.5 \times 10^{\frac{-10}{20}} = 4.9$$

2. The expected rms output for a test with nominal values (with notches)

$$\ddot{x}_{rms,notch} = \frac{\ddot{x}_{rms,ZL}}{10^{\frac{ZL}{20}}} = \frac{5.6}{10^{\frac{-10}{20}}} = 17.7 \text{ g.}$$

3. The test level factor Z , with regard to the maximum allowable rms level of $\ddot{x}_{\text{rms},Z} = 8.0 \text{ g}$.

$$Z = 10 \log \left(\frac{\ddot{x}_{\text{rms},Z}}{\ddot{x}_{\text{rms,notch}}} \right)^2 = 10 \log \left(\frac{8}{17.7} \right)^2 = -6.89 \text{ dB.}$$

4. Expected rms output level $\ddot{x}_{\text{rms},Z}$ for a test with a Z -factor of -6.89 dB can be calculated

$$\ddot{x}_{\text{rms},Z} = \ddot{x}_{\text{rms,notch}} \times 10^{\frac{Z}{20}} = 17.7 \times 10^{-\frac{6.89}{20}} = 8.0 \text{ g.}$$

5. Expected rms input level $\ddot{u}_{\text{rms},Z}$ for a test with a Z -factor of -6.89 dB can be calculated

$$\ddot{u}_{\text{rms},Z} = \ddot{u}_{\text{rms,notch}} \times 10^{\frac{Z}{20}} = 15.5 \times 10^{-\frac{6.89}{20}} = 7.0 \text{ g.}$$

6. Expected power spectral density input level $W_{\ddot{u},\text{max},Z}$ for a test with a Z -factor of -6.89 dB can be calculated

$$W_{\ddot{u},\text{max},Z} = W_{\ddot{u},\text{max}} \left(\frac{\ddot{u}_{\text{rms},Z}}{\ddot{u}_{\text{rms,notch}}} \right)^2 = 0.2 \left(\frac{7.0}{15.5} \right)^2 = 0.04 \text{ g}^2/\text{Hz.}$$

7. We have to decrease the specified input PSD curve with a factor χ

$$\chi = \frac{W_{\ddot{u},\text{max}}}{W_{\ddot{u},\text{max},Z}} = \frac{0.2}{0.04} = 5$$

End of example

7.9.2 Notching at main resonances on basis of quasi-static loads

The random input spectrum for large equipment may be notched so that the total interface load at 3σ value is not higher than the quasi-static loads at qualification level. The input spectrum shall be notched at main resonances.

For small equipment, the random input spectrum may be notched on the basis of quasi-static loads, however, minimum input levels are required over the whole frequency range. This means the random test may be a design load case for some equipment.

The box in Fig. 7.7 is exposed to a random enforced acceleration with power spectral density $W_{\ddot{u}}(f)$ (g^2/Hz) which will cause a random reaction force with the power spectral density $W_F(f)$ (N^2/Hz). The quasi-static load factor in the direction of the enforced acceleration is given by $\gamma(\text{g})$. The mass of the box is given by M (kg).

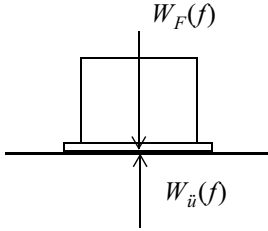


Fig. 7.7 Box exposed to random enforce acceleration

The notch criteria with regard to the quasi-static load factor is defined as

$$3 \sqrt{\int_{f_{\min}}^{f_{\max}} W_F(f) df} < M\gamma. \quad (7.29)$$

That means the $3\sigma = 3x_{\text{rms}}$ value of the reaction force must be less than the reaction force caused by the quasi-static load. (7.29) can be written as

$$3 \sqrt{\int_{f_{\min}}^{f_{\max}} M^2 |H(f)|^2 W_{\ddot{u}}^*(f) df} < M\gamma, \quad (7.30)$$

where $H(f)$ is the frequency response function between the base and the centre of gravity of the box and $W_{\ddot{u}}^*(f)$ an adapted input power spectral density. Applying Miles' equation (SDOF) we can rewrite (7.30) as follows

$$3M \sqrt{\frac{\pi}{2} f_n Q W_{\ddot{u}}^*(f_n)} < M\gamma. \quad (7.31)$$

For a multi-resonance structure, the notching criteria must take into account the following relation

$$3 \sqrt{\sum_{i=1}^n m_{\text{eff},i}^2 \frac{\pi}{2} f_i Q W_{\ddot{u}}^*(f_i) + M_{\text{res}}^2 \int_{f_{\min}}^{f_{\max}} W_{\ddot{u}}^*(f) df} < M\gamma, \quad (7.32)$$

where $m_{\text{eff},i}$ is the modal effective mass associated with mode i , the natural frequency is f_i , and M_{res} is the residual mass. The total mass M can be written as

$$M = \sum_{i=1}^n m_{\text{eff},i} + M_{\text{res}} \quad (7.33)$$

where $\sum_{i=1}^n m_{\text{eff},i}$ is the participation of the modal effective masses in the frequency range of interest.

We assume that the modal power contribution per mode i is related to the power spectral density $W_{\ddot{u}}(f_i)$ at the natural frequency f_i . The power is defined as the force ($m_{\text{eff},i}a_{\text{rms},i}$) times the velocity $v_{\text{rms},i}$. The modal power contribution is given by

$$m_{\text{eff},i}a_{\text{rms},i}v_{\text{rms},i} = CW_{\ddot{u}}(f_i), \quad (7.34)$$

or

$$m_{\text{eff},i} \frac{a_{\text{rms},i}^2}{2\pi f_i} = CW_{\ddot{u}}(f_i). \quad (7.35)$$

Finally we obtain

$$\frac{\frac{\pi}{2}f_i Q_i W_{\ddot{u}}^*(f_i)}{2\pi f_i} = \frac{m_{\text{eff},i}}{4} Q_i W_{\ddot{u}}^*(f_i) = CW_{\ddot{u}}(f_i). \quad (7.36)$$

We assume the constant C is the same for all modes in the frequency range of interest, hence we can write

$$\frac{m_{\text{eff},i} Q_i W_{\ddot{u}}^*(f_i)}{W_{\ddot{u}}(f_i)} = 4C = \text{constant} = \bar{C} \quad (7.37)$$

Assume all modes are in the frequency range of interest. That means the residual mass $M_{\text{res}} = 0$ and (7.32) becomes

$$3 \sqrt{\sum_{i=1}^n m_{\text{eff},i}^2} \frac{\pi}{2} f_i Q_i W_{\ddot{u}}^*(f_i) < M\gamma. \quad (7.38)$$

After substituting (7.37) into (7.38) the following relation is obtained

$$3 \sqrt{\frac{\pi}{2} \bar{C}} \sqrt{\sum_{i=1}^n m_{\text{eff},i}^2} f_i W_{\ddot{u}}(f_i) < M\gamma. \quad (7.39)$$

The constant \bar{C} can be calculated using the following equation

$$\bar{C} = \frac{(M\gamma)^2}{\frac{9\pi}{2} \left(\sum_{i=1}^n m_{\text{eff},i} f_i W_{\ddot{u}}(f_i) \right)} . \quad (7.40)$$

If the residual mass is not negligible (say >20%) (7.32) must be applied to obtain a reduced power spectral density of the enforced acceleration $W_{\ddot{u}}^*(f_n)$. This is an iterative process.

The width of the notch around the resonance is dependent upon the amplification factor Q and is equal to

$$\Delta f_i = \frac{3f_n}{Q_i}, \quad (7.41)$$

and the slope k of the power spectral density acceleration function will be approximately

$$k_i = \pm Q_i (\text{dB/oct}). \quad (7.42)$$

The resonance frequencies and associated amplification factor can be extracted from the low level sine sweep test.

The bandwidth and the slopes of the notch are illustrated in Fig. 7.8.

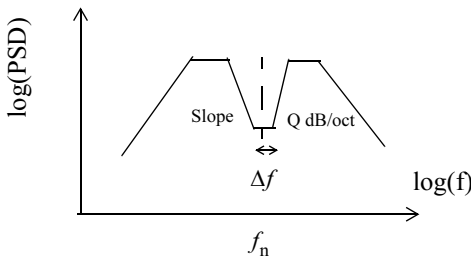


Fig. 7.8 Illustration width and slope of notch

7.9.3 Force Limiting Vibration Testing

Flight equipment is exposed to a random vibration environment and is required to survive the vibration testing. In flight, the mechanical impedance (force over velocity) of the equipment and the supporting structure is comparable, and results in modest interface forces and responses. In vibration tests, the shaker impedance is very high and could provide an almost unlimited driving force. To reduce forecasting, the acceleration input must be notched by specifying a force limit according to that predicted for flight.

The load at the equipment interface is related to the interface acceleration as

$$W_{FF}(f) = |M_d(f)|^2 W_{aa}(f), \quad (7.43)$$

where $W_{FF}(f)$, $W_{aa}(f)$ are the power spectral densities of the interface force and enforced acceleration respectively and $M_d(f)$ the dynamic mass (Also mentioned apparent mass [Cote 2004]).

For SDOF system with mass m , a natural frequency f_o , and a damping ratio ζ , the dynamic mass m_d is, [Wijker 2004]

$$m_d = m \left[1 + \left(\frac{f}{f_o} \right)^2 \frac{1}{1 - \left(\frac{f}{f_o} \right)^2 + 2j\zeta \left(\frac{f}{f_o} \right)} \right]. \quad (7.44)$$

Enveloping the force at the fundamental resonance frequency (maximum response) and replacing the dynamic mass by the rigid body mass ($\frac{f}{f_o} \rightarrow \infty$), the following semi-empirical force limiting loads are specified, [Chang 2002, Scharton 1997].

$$\begin{aligned} W_{FF}(f) &= C^2 M^2 W_{aa}(f) \quad f < f_o \\ W_{FF}(f) &= C^2 M^2 W_{aa}(f) \left(\frac{f_o}{f} \right)^2 \quad f \geq f_o \end{aligned} \quad (7.45)$$

where f_o is the fundamental resonance (significant modal effective mass) of the test item on the shaker and C^2 is a constant factor which defines the conservatism in the force limit specification. It is advised to use $C^2 = 5$ for directly mounted lightweight loads and for heavy strut mounted equipment a factor $C^2 = 2$ is recommended.

To perform the random vibration test, load cells between the test item and the shaker are required.

The semi-empirical force limit specification is developed and successfully applied by the Jet Propulsion Laboratory.

7.10 Plots

The response signals, originating from strain gauges, accelerometers, etc. can be represented by:

- Filtered amplitude spectrum plots (fundamental). All frequencies outside a “narrow-band” around the excitation frequency are removed.
- Unfiltered amplitude spectrum plots (rms). The results are displayed broad-banded, all frequencies included.
- Phase and transfer functions
- Universal files (i.e. ASCI) for further processing

7.11 Test Facilities West-Europe

Everywhere in West-Europe there are small or larger test facilities, where it is possible to carry out various mechanical tests. Four institutes and companies in West-Europe, however, are specialized in carrying out mechanical dynamic tests with regards to space projects.

- ESA/ESTEC in Noordwijk, the Netherlands
- Industrieanlagen-Betriebsgesellschaft mbH (IABG) in Ottobrun (in the vicinity of München) in Bavaria, Germany
- Ingénierie Tests en Environment Spatial (Interspace) in Toulouse, France
- Centre Spatial de Liège (CSL), Université de Liège, Belgium

The test installations of ESA/ESTEC are used for space projects. They fall under the umbrella of ESA. The three other institute and companies are more commercial, although Interspace is located on the same location as the French space organisation CNES.

Aforementioned institutes and companies offer the following test facilities:

- Acoustic chamber(s)
- Shaker(s)
- Modal survey facilities
- Measurement of mass properties
- Thermal vacuum test / space simulation
- EMC test facilities
- Magnetic test facilities
- Outgassing testing facilities
- ...

Static loads can also be applied with the help of a centrifuge. CEA-CESTA (Centre du Commissariat à l'Energie Atomique-Centre d'Etudes Scientifiques et Techniques d'Aquitaine) has the largest centrifuge (SILAT 265) of Europe. The centrifuge is 10 m long and weighs 40 tons. A test object weighing 2000 kg can be loaded up to 200 g and a test object weighing 4600 kg can be loaded up to 42 g.

7.12 Literature

- Chang, K.Y., 2002, *Structural Loads Prediction in Force-Limited Vibration Testing*, JPL, California Institute of Technology, Paper presented at Spacecraft & Launch vehicle Dynamic Environments Workshop The Aerospace Corporation, June 25-27.
- ESA PSS-01-802, Draft 1, September 1993, *Test Requirements Specifications for Space Equipment*, chapter 4.2.7.
- Cote, A. et al 2004, *Force-Limited Vibration Complex Two-Degree-of Freedom System System Method*, AIAA Journal, Vol 42, No.6, pages 1208-1218
- NASA-TM-86538, *Design and Verification Guidelines for Vibroacoustic and Transient Environments*, March 1986.
- GEVS-STRUCTURAL ELEMENT, 1990, *General Environmental Verification Specification for STS & ELV Payloads, Subsystems and Components*, NASA Goddard Space Flight Center.
- Lalanne, C., 2002, *Mechanical Vibration & Shock, Sinusoidal Vibration, Volume 1*, ISBN 1 9039 9603 1, HPS.
- Lefevre, Y.M., Boueilh, D., 1994, *Notching Guidelines for Mechanical Tests*, MSG-NNT-SE-TN-0742, Matra Marconi Space.
- Mansholt, U., 1985, *Guideline for the performance of vibration tests at equipment level*, Matra report MAT-HIP-19233.
- Rice, C.E., Buehrle, R.D., 2003, *Validation of Force Limited Vibration Testing at NASA Langley Research Center*, NASA/TM-2003-212404.
- Scharton, T.D., 1997, *Force Limited Vibration Testing Monograph*, NASA RP-1403.
- Schweikert, G, The Dornier Shocktable – A New Facility for Shocktesting of Components, SP-408, 1997, Environmental Testing for Space Programmes, ESTEC, Noordwijk.
- Tustin Institute of Technology, 1971, *Vibration and Shock Test Fixture Design, Design, Fabrication and Evaluation*.
- NASA “*Guidelines for Loads Analyses and Dynamic Model Verification of Shuttle Cargo Elements*”, MSFC-HDBK-1974, October 15, 1991.
- Friswell, M.I., Mottershead, J.E., 1995, *Finite Element Updating in Structural Dynamics*, Kluwer, ISBN 0792334310.
- Wijker, J.J., 2004, *Mechanical Vibrations in Spacecraft Design*, Springer, ISBN 3-540-40530-5.

8 Design of Spacecraft structure

8.1 Introduction

The various design elements of a spacecraft structure are illustrated in Fig. 8.1, [Agrawal 1986, chapter 4].

The design of a spacecraft structure can be subdivided into five phases.

1. Determination of spacecraft configuration
2. Initial design of the spacecraft structure
3. Detailed analyses
4. Production of the spacecraft structure
5. Testing

All phases will be discussed in this chapter.

8.2 Determination of Spacecraft Configuration

As part of the determination of the spacecraft configuration the following may be involved:

- Boundary Conditions Launch Vehicle
 - Launch weight
 - Available volume
 - Adapter
 - Payload separation system
 - Launch costs
- Functional requirements
- Mission time (duration)

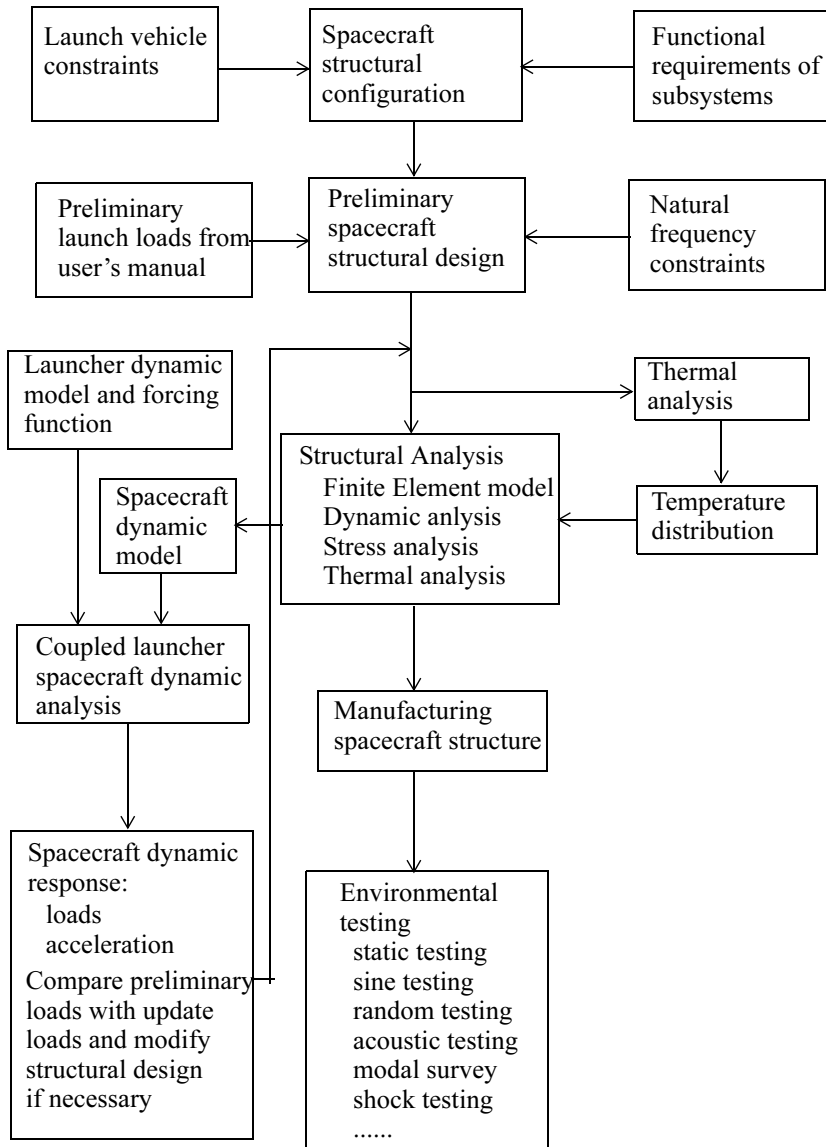


Fig. 8.1 Design flows spacecraft structure design and verification [Agrawal 1986]

8.2.1 Boundary Conditions Launch Vehicle

All the requirements and constraints are extensively covered in the user manuals of the associated launch vehicles. These include requirements and constraints concerning:

- The mass to be launched
- The available volume within the nose cone
- Launch vehicle adapter
- Vibrations
- Acoustic loads
- Safety factors

The mechanic and acoustic loads and the safety factors are discussed in previous chapters

8.2.2 Launch mass

The mass (spacecraft + adapter) that can be launched depends on the launch mission. The following general/common launch missions are mentioned below, i.e. ARIANE 5.

- The launching of spacecraft in a Geostationary Transfer Orbit (GTO).
- The launching of spacecraft in a Sun Synchronous Orbit (SSO).
- The launching of spacecraft in a Low Earth Orbit (LEO).
- The launching of spacecraft in an elliptic orbit around the earth.
- The escape of a spacecraft from the gravitation of the earth (escape mission).

The launch possibilities of the standard version of the ARIANE 5 launch vehicle with regards to a certain launch mission are given in the following Table 8.1.

Table 8.1 ARIANE 5 Launch capabilities

Geostationary Transfer Orbit (GTO) (kg)	Low Earth Orbit (LEO) (kg)	Sun-Synchronous Orbit (SSO) (kg)
6800	18000	10000

8.2.3 Available Launch Volume

The volume of the spacecraft that can fit inside the adapter of the launch vehicle depends on the diameter of the adapter and on the size of the fairing. If one spacecraft is being launched then the available volume is obviously the largest. When

several spacecraft are launched at once, the volume must be shared. The available volume is extensively covered in the user manual of the launch vehicle.

The space inside the fairing of the Taurus launch vehicle is illustrated in Fig. 8.2.

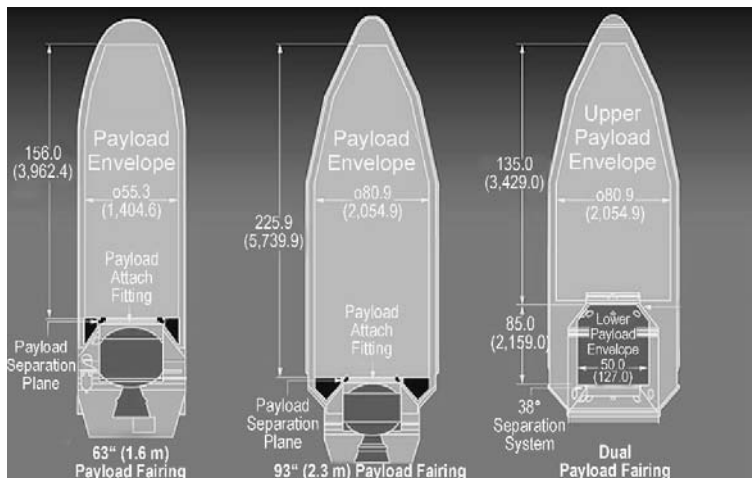


Fig. 8.2 Taurus Fairing Accommodations (courtesy Taurus Launch Systems)

8.2.4 Launch Vehicle Adapter (LVA)

Usually there are various launch adapters and or coupling structures available on which the spacecraft can be placed. The dimensions of the adapters and coupling structures are outlined extensively in the user's manual of the launch vehicle.

8.2.5 Payload Separation System

The payload separation system consists of either:

- Pyrotechnique cutting device(s).
- Clampband. The Clamp Band (CB) consists of two halves of steel bands fixed by two connecting bolts. The tensile stress in the band exerts pressure on the clamp that connects the adapter with the spacecraft. The Pyro Bolt Cutters cut through the connecting bolts so that the half bands come loose. The separation springs are loaded in such a way that the spacecraft can separate safely from the adapter. The Clamp Band grasping system grasps the two halves of the Clamp Band and thus prevents the spacecraft from clinging behind it.

Both systems will introduce high shock loads on the spacecraft.

8.2.6 Functional requirements spacecraft

The functional requirements can vary immensely and are strongly dependent on the mission. The various missions can be:

- Sun-observation
- Planetary
 - Fly-by
 - Orbiter
 - Lander
- Geostationary spacecraft
 - Communication
 - Television
 - Meteorological
 - Earth observation
 - Navigation
- LEO spacecraft
 - Telecommunications
 - Meteorological
 - Earth observation
 - Navigation
 - Micro-gravity
- Astronomy
 - Space observatory
- Fields and particles
-

8.3 First Design Spacecraft Structure

For the initial preliminary design of the spacecraft structure, the following aspects must be considered:

- Design Launch Loads
- Factors of Safety
- Stiffness requirements
- Materials
- Basic Design

The preliminary sizing of the structural components is illustrated in Fig. 8.3.

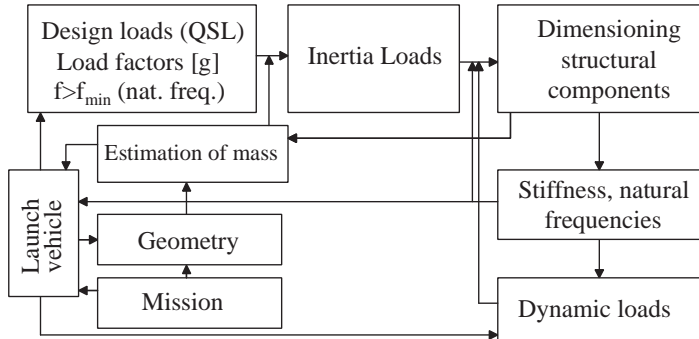


Fig. 8.3 Preliminary sizing structural components

The mission requirements in combination with the functional requirements will lead to a preliminary geometry and associated mass distribution. The selected launch vehicle will specify launch loads, stiffness, geometry constraints, etc. The quasi-static load factors will be applied assuming a minimum natural frequency compliance. The quasi-static loads factors applied to the mass distribution will result in internal load distribution. This load distribution is a starting point for sizing the structural members of the spacecraft primary and secondary structures. After that, the stiffness of the primary structure must be checked against launch vehicle stiffness requirements. If the minimum of the longitudinal and lateral natural frequencies comply with the requirements, dynamic loads may be applied.

8.3.1 Design Loads

The various mechanical loads are not all equally important and depend on the type of the mechanical structure: i.e. does it concern a primary structure, the spacecraft structure or other secondary structures (such as solar panels, antennas, instruments and electronic boxes). Preparations on the ground, the launch, and the operations in the orbit around the Earth set various types of requirements, such as [Sach 1988]:

- natural frequencies
- steady-state (semi-static) acceleration
- sine excitation
- random excitation
- acoustic noise
- transient loads
- shock loads
- temperatures

Natural frequencies

The natural frequency is a governing design requirement for all parts of the spacecraft. This requirement is imposed in order to limit the dynamic coupling of the spacecraft with the launch vehicle.

Semi-static and low frequency sinusoidal loads

The design of the primary structure is determined to a large extent by the semi-static and low frequency sinusoidal loads (up to approximately 50Hz).

Sinusoidal and random loads

To a large extent, the sinusoidal and random loads determine the design of secondary structures (solar panels, antennas, electronic boxes).

Acoustic loads

Light structural parts with relatively large surface areas (such as solar panels and spacecraft antennas) are more sensitive to acoustic loads than sinusoidal and random base excitation.

Shock loads

Deployable structures experience high shock loads; for example during latch-up of hinges in the required final position of these mechanisms. This is especially the case when the deployment velocities are too high.

Temperatures

Temperature variations usually cause high thermal stresses in the structures. In general, the various coefficients of expansion are accounted for in the choice of the structural materials. Thermal deformations are taken into account when working with structures that must be aligned with each other.

Random Loads

The design of instruments and electronic boxes are determined by the random base excitation.

8.3.2 Stiffness requirements (natural frequencies)

Additionally, the natural frequencies of the spacecraft must be such that the fundamental natural (undamped) frequencies in all directions are larger than the lowest frequencies generated by the launch vehicle that excite the spacecraft. Due to the difference in natural frequencies, the spacecraft is dynamically uncoupled from the launch vehicle and will display rigid behaviour in the lower frequency regions.

In the Table 8.2 the required lowest frequencies in the lateral and the launch direction are given for various launch vehicles. In general, these frequencies are valid when the spacecraft is considered to be clamped at the interface between the spacecraft and the launch vehicle.

Table 8.2 Examples stiffness requirements (Continued)

Launch Vehicle Launch System	Required Lowest Natural frequencies (Hz)	
Direction	Launch direction	Lateral
STS	13	13
DELTA 6925/7925	35	15
ARIANE 5		9–10 ^a
<=4500 kg	31	
> 4500 kg	27	

a. Depends on the launcher spacecraft interface

8.3.3 Quasi-static loads

The structure of the spacecraft is designed to support the maximum quasi-static loads (QSL), including a factor of safety. The quasi-static loads are a combination of the steady-state static loads and the low frequency sinusoidal loads. Quasi-static loads can be used to dimension the spacecraft, provided the minimum frequency requirements with respect to mode shapes in the launch direction and the lateral direction are fulfilled.

In the ARIANE 5 user manual the sizing loads for spacecraft with a weight \leq 5000 kg are specified in the following way:

Table 8.3 Quasi-static load factors

Flight event	Load factors, acceleration (g)			
	Launch direction		Lateral	
	Static	Dynamic	Static	Dynamic
Lift-off	-1.7	± 1.5	0.0	± 1.5
Maximum dynamic pressure	-2.7	± 0.5	0.0	± 2.0
P230 Burn-out	-4.25	± 0.25	± 0.25	± 0.25
H155 Burn-out	-3.6	± 1.0	± 0.1	0.0
H155 Thrust tail-off	-0.7	± 1.4	0.0	0.0

- The minus sign refers to a pressure force in the launch direction.
- The quasi-static loads are applied for the centre of gravity of the spacecraft.
- Gravity has been taken into account.
- The spacecraft must fulfill the stiffness requirements.
- The centre of gravity of the spacecraft must be located in a certain area to prevent overloading of the spacecraft adapter. This depends of course on the adapter used.

8.3.4 Mass Acceleration Curve (MAC)¹

In Fig. 8.4, the design loads for the structural analyses, which depend on the effective masses, for the components and instruments are given. Components with a low effective mass experience higher acceleration. This observation is valid both for transient as well as random (stochastic) loads. The “mass acceleration curve” (MAC) is primarily based on experiences (data) from previous projects. In most cases, a MAC can be derived for a launch vehicle that can subsequently be used for most components and instruments. The MAC is an upper bound acceleration level for all components of a given mass, regardless of location, orientation, or frequency. In general, it is assumed that the lowest natural frequencies are $f_n \geq 100$ Hz.

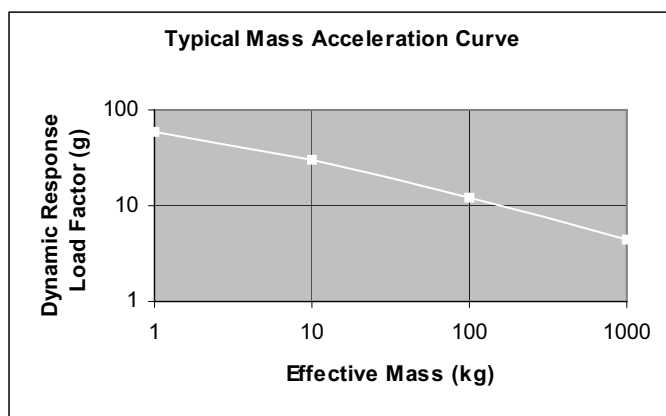


Fig. 8.4 Typical mass acceleration curve [NASA PD-ED-1211]

Example

We have a component of about 10 kg and the lowest natural frequencies are above 100Hz. The “static” load factors to design that component can be taken from the MAC (Fig. 8.4) and are about 40g.

End of example

1. The term “Mass Acceleration Curve” is frequently used by the NASA in many “Spacecraft loads” documents. MAC is also the abbreviation of the term “Modal Assurance Criteria”.

8.3.5 Random Loads

The (test) qualification random loads depend on the type of launch vehicle and spacecraft.

In the “General Environmental Verification Specification for STS & ELV, Payloads, Subsystems and Components”, [Baumann 1996], a distinction is made between:

- Spacecraft
- Instrument (subsystem) ($\leq 68\text{kg}$, 150lbs)
- Component ($\leq 22\text{kg}$, 50lbs)

In the following Table 8.4, Table 8.5 and Table 8.6 “Random vibration levels” are specified. It must be noticed that the higher the mass of the component the lower the random vibration levels.

Table 8.4 Spacecraft “Random Vibration Levels”

Frequency spectrum (Hz)	PSD acceleration (g^2/Hz)
20–800	0.008
800–1000	7.6 dB/octave
1000–1300	0.014
1300–2000	-13.6 dB/octave
2000	0.002
Grms	4.1 g

8.3.6 Factors of Safety

The factors of safety are used to account for uncertainties that cannot be fully analysed.

The qualification loads are often used as design loads, and subsequently the factors of safety for “yield” and “ultimate” are applied.

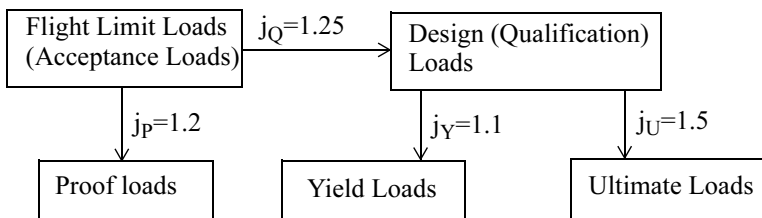
Table 8.5 Instrument “Random Vibration Levels”

Frequency spectrum (Hz)	PSD acceleration (g^2/Hz)
20	0.01
20–50	5.5 dB/octave
50–800	0.053
800–2000	-5.5 dB/octave
2000	0.01
Grms	8.26 g

Table 8.6 Component “Random Vibration Levels”

Frequency spectrum (Hz)	PSD acceleration (g^2/Hz)
20	0.026
20–50	6 dB/octave
50–800	0.16
800–2000	-6 dB/octave
2000	0.026
Grms	14.1 g

The factors of safety that were used in the ENVISAT spacecraft project are illustrated in Fig. 8.5.

**Fig. 8.5** ENVISAT Safety factor philosophy

8.4 Basic Design Supporting Structure

The spacecraft structure is designed to mechanically support the service systems, the payload or the instruments and is essentially the backbone of the spacecraft. In addition, the structure ensures that the instruments are properly aligned with each other and that the surfaces of certain structural elements are finished in such a way that they meet the requirements set by the thermal subsystem.

8.4.1 Design criteria

The design criteria for the structural elements are:

- Mass (minimum)
- Reliability
- Design costs (e.g. engineering hours)
- Production costs (including moulds and templates)
- Ease of inspection (e.g. NDI)
- Ease of reproduction

- Possibility to repair
- Modification possibilities of hardware (H/W) in a late design phase

These criteria have been presented in an arbitrary order. The mass is important, however, sometimes costs are even more important. Each product has its own order for these criteria.

8.4.2 Standard structural elements of spacecraft structures

A spacecraft is generally constructed with the following standard structural elements:

- Bending beams
- Tension and compression members (Struts)
- Ring frames
- Plates/panels
 - Rectangular
 - Circular
 - Annular
- Cylindrical and conical thin-walled shells
 - Monocoque
 - With rings and stiffeners
 - Corrugated
 - Composites
- Sandwich and composite structures
- Pressure vessels¹
- Fuel tanks
- ...

The design of a structural element is specified by three aspects [Ashly 2003]:

1. The functional requirements
2. The geometry
3. The properties of the materials used

The performance p of a structural element is described by the following equation

1. A pressure vessel stores 19130 J of energy or more. The energy is based on the adiabatic expansion of an ideal gas.

$$p = f\left[\begin{array}{c} \text{Functional} \\ \text{requirements, } F \end{array}\right], \left[\begin{array}{c} \text{Geometrical} \\ \text{parameters, } G \end{array}\right], \left[\begin{array}{c} \text{Material} \\ \text{properties, } M \end{array}\right] \quad (8.1)$$

Equation (8.1) is separable, hence

$$p = f_1(F)f_2(G)f_3(M) \quad (8.2)$$

where $f_1(F)f_2(G)$ is the structural index and $f_3(M)$ is the efficiency coefficient or material index.

The provisional sizing of a space structure can be done quickly and efficiently provided that straightforward methods (Manual, EXCEL®, Mathcad®, Maple®, MATLAB®, etc.) are used to calculate the aforementioned elements.

Important aspects for the determination of the dimensions of a space structure are:

- Design loads
 - Handling loads
 - Launch loads
 - In-orbit loads
- Test loads
- Internal pressures (i.e. fuel tanks)
- Minimum requirements with respect to natural frequencies
- Thermo-elastic deformations
- ...

The most important failure modes are:

- Exceeding the yield stress
- Exceeding the ultimate strength
- Stability (against buckling), locally or generally
- Fracture mechanics (pressure vessels, manned space flight)
- Fatigue
- ...

Margins of safety (MS, or MOS) and factors of safety have a different meaning. For a given factor of safety the “probability of failure” or in other words, the reliability of the structure, can be determined. With the aid of the concept of MS we determine the functionality of the structure. The MS is defined as follows:

$$\text{MS} = \frac{\sigma_{\text{allowable}}}{j\sigma_{\text{actual}}} - 1, \quad (8.3)$$

where MS is the margin of safety and $\sigma_{\text{allowable}}$ is the allowable stress. The allowable stress is the maximum permissible stress before failure. The σ_{actual} is the resulting stress from a certain load and j is the factor of safety.

At failure, the applied stress is larger than the allowable stress. The MS value is then negative. From this it follows that the MS value must be greater than zero.

In Table 8.7 the significance of the MS value is shown.

Table 8.7 Significance of MS values

Margin of safety	Significance
MS<0	Failure
0<MS<0.5	Optimal design
0.5<MS<1.5	Good design
MS>1.5	The design may be easily improved

For a combination of load conditions, the value for the MS can be determined as shown in Table 8.8.

Table 8.8 Combined loadcases

Margin of safety	Combined load cases
$MS = \frac{1}{j} \left(\frac{\sigma_{\text{compr}}^* + \sigma_{\text{bend}}^*}{\sigma_{\text{compr}} + \sigma_{\text{bend}}} \right)^{-1} - 1$	Combination of compression and bending loads
$MS = \frac{1}{j} \left(\frac{\sigma_{\text{compr}}^* + \sigma_{\text{tors}}^*}{\sigma_{\text{compr}} + \sigma_{\text{tors}}} \right)^{-1} - 1$	Combination of compression and torsion loads
$MS = \frac{1}{j} \left(\frac{\sigma_{\text{compr}}^* + \sigma_{\text{bend}}^* + \left\{ \frac{\sigma_{\text{tors}}^*}{\sigma_{\text{tors}}} \right\}^2}{\sigma_{\text{compr}} + \sigma_{\text{bend}}} \right)^{-1} - 1$	Combination of compression, bending and torsion loads

where σ_{\dots} is the resulting stress, σ_{\dots}^* is the allowable stress and j is the factor of safety.

8.4.3 Selection of materials

A very important step in the design process is the selection of materials for a spacecraft structure. The choice has significant consequences for the mass, the production costs, etc. The operational conditions of the spacecraft, the ability to retain its shape and the reliability of the structure are some of the parameters used for the selection of materials. The most important material properties are:

- Strength and stiffness
- Specific weight

- Ultimate strength
- Fatigue strength
- Technical constraints (elasticity, weldability, stress concentrations, etc.)
- Effect of the environment on the material properties
- Thermal conductivity
- Electrical conductivity or resistance
- Availability
- Costs

With regards to structural elements that are subjected to a tensile stress, the following simple expression can be derived:

$$M = AL\rho = j \frac{N}{\sigma_u} L\rho, \quad (8.4)$$

in which M is the mass of the structural element, A is the cross-section of the structural element, L is the length of the structural element, N is the normal (tension) force, σ_u is the ultimate stress of the applied material, ρ is the density of the applied material and j is the factor of safety.

It appears from the previous expression that the mass of the structural element decreases while the specific strength $\frac{\sigma_u}{\rho}$ increases.

For thin-walled structural elements (monocoque, sandwich, with stiffeners) subjected to an axial compression load, the mass M for various buckling conditions can be expressed as follows:

$$M = 2\pi R \sqrt{\frac{jN}{2\pi\psi E}}, \quad (8.5)$$

in which R is the radius of the monocoque shell and ψ is a constant that depends on the boundary conditions.

For thin-walled structural elements the mass of the structural element decreases while the specific stiffness $\frac{\sqrt{E}}{\rho}$ increases.

Analogous expressions can be derived for different loads and structural elements.

Ashly defines in [Ashly 2003] the structure efficiency (SE) or material index which stands for:

$$\text{Structure Efficiency} = \frac{\text{Load carried by the structure}}{\text{mass of the structure}}$$

$$SE = f\left(\frac{E^i}{\rho}\right), \quad i = 1, \frac{1}{2}, \frac{1}{3} \quad (8.6)$$

In Table 8.9 an example of the structure efficiency are given.

Table 8.9 Structural efficiency or material index (Continued)

Structural element	Load	SE	Remarks
Beam, Plates and shells	Tension and pure compression	$f\left(\frac{E}{\rho}\right)$	$L < L_{crit}$
Sandwich panels and shells (symmetric)	Tension and pure compression	$f\left(\frac{E}{\rho}\right)$	$L < L_{crit}$
	Bending	$f\left(\frac{E}{2\rho_f}\right)$	Strength
		$f\left(\frac{E}{3\rho_f}\right)$	Stiffness
Beams	Buckling and bending	$f\left(\frac{1}{\frac{E^2}{3\rho_f}}\right)$	
Plate and shells	Buckling and bending	$f\left(\frac{1}{\frac{E^2}{3\rho_f}}\right)$	

When assessing the material choice for the various structural elements, the effect of the temperature on the material properties must be taken into account. For this reason, lightweight metal alloys and composite materials are often used for the construction of a spacecraft.

8.5 Detailed Analyses

The structural analyses are, in general, done with the finite element method. There are many commercially available finite programmes that are used in conjunction with compatible pre- and post processors. Examples of commercially available finite element packages are:

- MSC.Nastran
- MSC.Marc
- ABAQUS
-

and examples of pre- and post processors are:

- MSC.Patran
- FEMAP

- ABAQUS/CAE
- ...

The objective of the analysis defines the detail of the finite element model; in terms of the number of nodes and finite elements, and therefore the number of degrees of freedom. The detail of the finite element model is also defined by the availability of geometric information, applied materials, mass distribution and loads.

8.5.1 Finite Element Model

If the geometry and applied materials and associated material properties are known with the aid of pre- and post processors, a finite element or mathematical model can be generated. This finite element model, in general, consists of the following:

- Nodes or nodal points, scalar points (one DOF).
- Finite elements, 0-D, 1-D, 2-D and 3-D
- Material properties (Young's modulus, Poisson's ratio, shear modulus, density, coefficient of thermal expansion (CTE), structural damping,...)
- Mass distribution (material density, non structural mass, discrete masses)
- Boundary conditions (clamped, simply supported, pinned, etc.)
- Constraint equations to relate DOFs with each other
- Applied loads
- Damping
- ...

The quality of the finite element model will be checked by performing dedicated finite element model checks later in the programme by tests (static, dynamic and modal survey).

8.5.2 Finite Element Model Verification

Finite element models shall be checked for:

- Rigid body strain energy to determine for hidden constraints in the finite element model. Theoretically the rigid body strain energy must be zero.
- Free-free modal analysis to determine for unwanted mechanisms in the finite model. A correct finite element will show six zero rigid body natural frequencies, three translations and three rotations.
- Stress free thermal-expansion to determine for bad elements in the finite element model. Bad aspect ratio elements, and warped plate elements, for example, will show non-zero stresses.

- In the case of pressure loads the normal vectors of the faces on which the pressures are applied must point in the same direction, otherwise forces due to pressures may be cancelled out.
- ...

8.5.3 Finite Element Analyses

Generally, the finite element models are used to perform the following types of analysis:

- Strength/stiffness
- Thermo-elastic
- Dynamic (e.g. modal response)
- Spacecraft / launch vehicle coupled load analysis
- Vibroacoustic
- ...

Strength analysis

The strength properties of the spacecraft structure (structural elements) shall be verified by finite element analysis and later in the programme by dedicated tests. The stress/load distribution in structural elements must be verified and compared with allowable stresses/loads (associated with identified failure modes) showing margins of safety greater than zero. A dedicated buckling analysis will give allowable buckling stresses/loads. Typical applied loads are the quasi-static inertia loads and combinations of them. If only dynamic loads factors are applicable, the stresses/load due dynamic load application must be verified against allowable stresses and loads (in general static). For random loads 3-sigma values of stresses must be compared with the allowable stresses (yield, ultimate).

Thermo-elastic Analysis

The thermal deformation and stress due to temperature gradients in the structure must be calculated to check alignment requirements. In spacecraft, thermal stresses in the structure are, in general, not important. One of the major tasks is to depict the temperature distribution on nodes in a finite element applied to structural analyses. The temperature distribution is mostly obtained from thermal analysers based on the lumped parameter method.

Dynamic Analysis

Dynamic analysis is done to check if the specifications for natural frequencies and dynamic responses are met. To check the requirements about minimum natural frequencies a modal analysis will be done. The outcomes of such analysis are primarily: the natural frequencies and the associated mode shapes, generalised masses and stiffnesses and the modal effective mass. The damping is mostly ignored during the eigenvalue extraction process because damping in spacecraft structures is low (2–10% damping ratio). The deviation between real and complex modes is small.

A spacecraft industry standard modal damping ratio of $\zeta = 0.015$ or $g = 0.03$ structural damping is used [Foist 2004]. The associated amplification factor is $Q \approx \frac{1}{2\zeta} = \frac{1}{g} = 33.33$.

Later in the programme, the modal properties are checked with modal analysis or with a low input frequency sweep with a low sweep rate on a shaker table.

After the calculation of the modal properties of the spacecraft, the response characteristics due to mechanical deterministic and random loads are calculated. This is mostly done in the frequency domain. The application of the finite element model to specified frequency ranges must be checked.

The statistical energy analysis (SEA) method can be applied in frequency ranges out of the scope of the finite element application [Wijker 2004].

Coupled Load Analysis

Early in the programme a spacecraft/launch vehicle coupled dynamic load analysis is done to analyse the dynamic loads during the launch of the spacecraft. This analysis is done to verify the preliminary design loads from the launch vehicle user's manual (which are conservative).

A complete or reduced finite element model, in combination with load transformation matrices, must be delivered to launcher authority. The outcome of the coupled load analysis may be used during vibration tests.

Vibroacoustic Analysis

Lightweight, large area structures, i.e. solar arrays and antenna reflectors, are very sensitive to acoustic loads (sound pressures) and are mounted outside the spacecraft. A combined finite element method and boundary element method analysis is needed to simulate the fluid structure interaction (FSI). The structural behaviour will be covered by the finite element method (modal base: natural frequencies, vibration modes, stress modes,...) and the influence of the fluid (added mass, radiation damping) and the acoustic loads are dealt with by the boundary element method.

8.6 Manufacturing of the spacecraft structure

The structural parts of the spacecraft structures may be produced by the responsible company or sub-contracted to other companies. The subcontracting of structural parts may either be based on the 'build to print' principle or risk sharing principle (which means that the design and production of a structural part is done under the responsibility of the subcontractor).

The assembly of the structure is mostly done at the premises of the company responsible for that spacecraft structure. The complete spacecraft is generally assembled at the premises of the prime contractor.

Mechanical ground support equipment (MGSE) must be produced to assemble mechanical parts to a complete structure and to transport the spacecraft or parts of the spacecraft.

8.7 Testing

Tests are applied to verify requirements posed on a spacecraft design. The general applied tests and the associated requirements are shown in Table 8.10.

Table 8.10 Test verification (Continued)

Type of test	Test verification
Static test and centrifuge test.	<ul style="list-style-type: none"> Check/qualification of structural strength in particularly the primary structure and critical interfaces Verify (partially) the stiffness matrix
Modal survey test	<ul style="list-style-type: none"> identify the natural frequencies ω_i, vibration modes $\{\phi_i\}$ and the modal damping ratios ζ_i to support the verification of the mathematical model which is used in loads cycles, and the CDLA
Shaker sine vibration test	<ul style="list-style-type: none"> Support the verification of the spacecraft mathematical model (amplification from launcher spacecraft interface input to various spacecraft parts) Qualification of secondary structures Qualification of the spacecraft system by performing functional tests after the shaker vibration at qualification test input Flight acceptance of the spacecraft system by performing functional tests often shaker vibration at flight test input
Acoustic test	<ul style="list-style-type: none"> Verification and qualification of spacecraft system to acoustic environment which might be experienced by the spacecraft during flight Qualification of the spacecraft system by performing functional tests after the acoustic test at qualification level. In case units are represented with dummies the random level is measured at unit dummy interfaces. Subsequently this input is employed for unit qualification at subsystem and unit level. Flight acceptance of the spacecraft system by performing functional test after acoustic tests at flight level.
Shaker random vibration test	<ul style="list-style-type: none"> Qualification of electronic units subjected to random (acoustically generated) flight environment
Shock test	<ul style="list-style-type: none"> Spacecraft verification and qualification due to shock type of loads (pyrotechnic and mechanically induced shocks)

8.8 Literature

- Agrawal, B.N., 1986, *Design of Geosynchronous Spacecraft*, ISBN 0-13-200114-4, Prentice-Hall.
- Ashby, M.F., 2003, *Materials Selection in Mechanical Design*, second edition, Buterworth Heinemann, ISBN 0 7506 4357 9.
- Baumann, R.C., 1996, *General Environmental Verification Specification for STS & ELV Payloads, Subsystems, and Components*, GEVS-SE, Rev A, June.
- Foist, B.L., Grau, E.L., Nejad, B.I., 2004, *Launch Loads Development Using Sine Vibration Methodology*, AIAA 2004-1800.
- NASA PD-ED-1211, *Combination Methods for Deriving Structural Design Loads considering Vibro-Acousti, etc., Responses*, Center of contact Jet Propulsion Laboratory (JPL)
- Sach, E.D., 1988, *Environmental testing- an approach to more efficiency*, ESA SP-289, pages 15–19.
- Wijker, J.J., 2004, *Mechanical Vibrations in Spacecraft Design*, ISBN 3-540-40530-5, Springer.

8.9 Exercises

8.9.1 Use of the User's Manual of ARIANE 5

Presume that two spacecraft will be launched at the same time. One spacecraft has a mass of 3500 kg and the other one has a mass of 4500 kg. The spacecraft with a mass of 3500 kg is placed ‘on top’ of the other one. Write down the design requirements for both spacecraft based on the user’s manual of ARIANE 5. There are no space limitations. (see www.arianespace.com for user’s manual ARIANE 5)

9 Strength and Stiffness of Structural Elements

9.1 Introduction

Before detailed strength and stiffness analysis of a spacecraft structure can be done, a preliminary sizing of all structural members constituting the spacecraft structure must be established. The preliminary sizing of spacecraft structural elements is illustrated in Fig. 9.1.

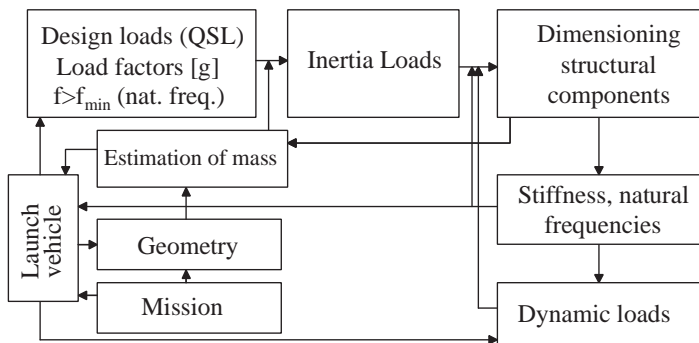


Fig. 9.1 Preliminary sizing of spacecraft structural elements

The quasi-static load factors (acceleration) are defined in the user's manual of the selected launch vehicle. The quasi-static load factors may be applied if the lowest and lower natural frequencies meet the requirement up to a specified value f_{min} (Hz). Within the frame of preliminary sizing of the spacecraft, the quasi-static load factors will first be applied, afterwards it will be verified if the stiffness requirements are met (natural frequencies).

The estimated mass distribution multiplied with the quasi-static load factors will give the distribution of internal loads within the spacecraft structure. These internal loads can be applied to obtain the preliminary dimensions of the spacecraft structural elements.

In this chapter we will provide the reader with strength and stiffness formulae to obtain the preliminary dimensions of the structural element by hand calculations. Afterwards, more advanced techniques (i.e. the finite element method) are applied to verify the stiffness assumption and the minimum required natural frequencies to prevent dynamic coupling of the spacecraft with the launch vehicle. Later in the project, dynamic structural analyses are performed to show dynamic loads can be taken by the spacecraft structural elements. The dynamic loads are beyond the scope of this chapter.

The following basic structural elements are discussed:

- Trusses and truss frames
- Bending beams (bending, Euler and lateral buckling, torsion, local buckling of tubes)
- Rings
- Panels
- Shear panels
- Shells of revolution; cylinders & cones (strength, stiffness)
- Stresses in lap joints

The structural elements made of sandwich construction are discussed in the chapter about sandwich structures.

Many textbooks about the strength of materials are written and some of them are referenced here [Benham 1987, Budynas 1999, Den Hartog 1967, Den Hartog 1987, Gere 1994, Klein 2001, Prescott 1961, Rivello 1969, Sechler 1963, Sechler 1968, Shanley 1967, Simitses 1976, Wang 2004].

9.2 Trusses and Truss frames

Structures built up out of trusses are called truss frames. A truss is a rod which only carries tension and compression loads. A truss will be defined as not being able to carry bending moments and torsion moments. An example of a simple truss frame is shown in Fig. 9.2. This truss frame is statically determinate. That means the reaction forces V_A , H_A and H_B can be calculated using the three available equations of equilibrium.

The equilibrium of the bending moments about point B will bring us

$$\sum M_B = 0, FL + H_A L \tan \alpha = 0, H_A = -F \cot \alpha. \quad (9.1)$$

The equilibrium in horizontal direction will give

$$\sum H = 0, H_A + H_B = 0, H_B = -H_A = F \cot \alpha, \quad (9.2)$$

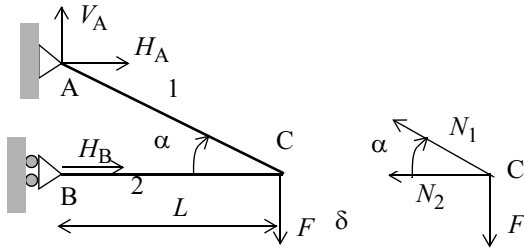


Fig. 9.2 Truss frame

and the equilibrium in vertical direction will result in

$$\sum V = 0 , \quad V_A - F = 0 , \quad V_A = F . \quad (9.3)$$

The equilibrium in node C is used to calculate the (normal) forces in the truss members 1 and 2.

$$\sum V = 0 , \quad N_1 \sin \alpha - F = 0 , \quad N_1 = \frac{F}{\sin \alpha} , \quad (9.4)$$

and from the horizontal equilibrium in node C \$N_2\$ can be calculated

$$\sum H = 0 , \quad N_1 \cos \alpha + N_2 = 0 , \quad N_2 = -N_1 \cos \alpha = -F \cot \alpha . \quad (9.5)$$

The elongation of a prismatic truss under a normal force \$N\$ is given by

$$\delta = \frac{NL}{EA} , \quad (9.6)$$

where \$L\$ is the length of the truss, \$A\$ the cross section of the truss and \$E\$ the Young's modulus of the material used to produce the truss. The normal averaged stress in the cross section is

$$\sigma = \frac{N}{A} , \quad (9.7)$$

and the strain becomes

$$\varepsilon = \frac{\sigma}{E} . \quad (9.8)$$

The strain energy in one truss is given by

$$U = \frac{1}{2} \int_V \sigma \varepsilon dV = \frac{1}{2} \frac{N^2 L}{EA} . \quad (9.9)$$

With Castigliano's first theorem [Castigliano 1966] we can obtain the displacement δ (see Fig. 9.2) which is in the direction of the force F . We assume the same cross section A and Young's modulus E for both trusses. The displacement δ becomes

$$\delta = \frac{\partial U}{\partial F} = \sum \left(\frac{N \frac{\partial N}{\partial F} L}{EA} \right)_i = \frac{FL}{EA} \left[\frac{1}{(\sin \alpha)^2 \cos \alpha} + (\cot \alpha)^2 \right]. \quad (9.10)$$

The stiffness k at node C in the direction of δ and F is defined as

$$k = \frac{F}{\delta}. \quad (9.11)$$

We proceed with an application of Castigliano's first theorem on an indeterminate structure illustrated in Fig. 9.3 and calculate the normal forces in both trusses 1 and 2. A cut through trusses 1 and 2 is made and equilibrium with a normal force N_2 in truss 1 is considered. The normal force in truss 2 becomes $F - N_2$.

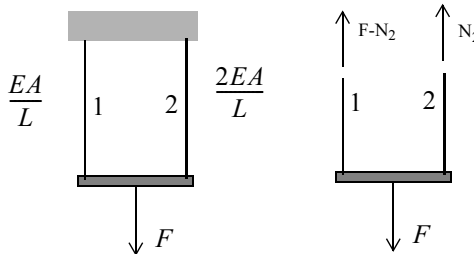


Fig. 9.3 Statically indeterminate structure

The total strain energy in the structure is

$$U = \frac{1}{2} \sum_{k=1}^2 \frac{N_k^2 L}{EA} = \frac{1}{2} \frac{L}{EA} \left[\frac{N_2^2}{2} + (F - N_2)^2 \right]. \quad (9.12)$$

Because a cut is made in the trusses it follows that

$$\frac{\partial U}{\partial N_2} = 0, \quad (9.13)$$

hence

$$\frac{N_2}{2} - (F - N_2) = 0, \quad N_2 = \frac{2}{3}F \text{ and } N_1 = \frac{1}{3}F. \quad (9.14)$$

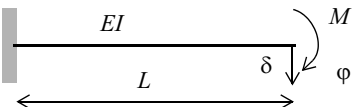
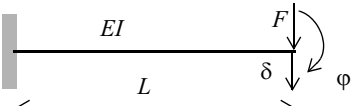
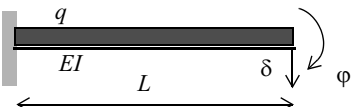
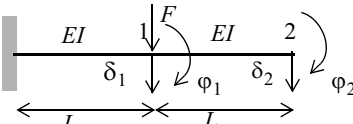
It can be concluded that stiff structural parts will attract internal forces.

9.3 Bending of Beams, Myosotis Method

9.3.1 Bending of Beams by transverse forces and bending moments

The bending beam is an important structural element. The six basic equations of the deflection and rotation at the free end of a clamped beam with basic loading conditions are the so-called Myosotis formulae [Den Hartog 1967] (Myosotis means forget-me-not). The Myosotis formulae are shown in Table 9.1. Most of the bending beam problems can be solved using the Myosotis formulae. The loads are applied in the shear centre of the cross section, therefore no additional torsion effects appear.

Table 9.1 Myosotis formulae

Load case #	δ	φ
	$\delta = \frac{ML^2}{2EI}$	$\varphi = \frac{ML}{EI}$
	$\delta = \frac{FL^3}{3EI}$	$\varphi = \frac{FL^2}{2EI}$
	$\delta = \frac{qL^4}{8EI}$	$\varphi = \frac{qL^3}{6EI}$
	$\delta_1 = \frac{FL^3}{3EI}$ $\delta_2 = \delta_1 + \varphi_1 L$	$\varphi_1 = \frac{FL^2}{2EI}$ $\varphi_2 = \varphi_1$

Example

An instrument whose mass $M = 20\text{ kg}$ must be mounted on a spacecraft through a cantilever arm of annular cross section made of Al-alloy with a Young's

modulus $E = 70 \text{ GPa}$ and density $\rho = 2700 \text{ kg/m}^3$. The length of the arm is $L = 600 \text{ mm}$. Choose the dimensions of the cross section in such a way that the first natural frequency is $f \geq 50 \text{ Hz}$. This example is taken from [Genta 1995].

The mass of the beam is neglected and a model with a SDOF is used, in order to obtain a natural frequency higher than 50Hz the stiffness of the beam must be $k \geq M(2\pi f)^2 = 20x(2\pi 50)^2 = 1.974 \times 10^6 \text{ N/m}$.

It can be modelled as a cantilever beam clamped at one side and loaded by the inertia force of the instrument at the other end. The well-known Myosotis formula giving its stiffness is $k = \frac{3EI}{L^3}$, where L and I are the length and second moment of area of the cross section, respectively.

The minimum value of the second moment of area I can be easily computed $I = \frac{kL^3}{3E} = 2.03 \times 10^{-6} \text{ m}^4$. The second moment of area of a tube is given by $I = \pi R^3 t$. Assuming $\frac{R}{t} = 20$ the radius R and the wall thickness t of the tube can be calculated. The radius R becomes $R = 60 \text{ mm}$ and the wall thickness $t = 3 \text{ mm}$.

The mass of the beam is $m = \pi R^2 t L \rho = 0.322 \text{ kg}$.

End of example

9.3.2 Buckling of Struts

For all possible boundary conditions the critical Euler load of a column is expressed by [Simitses 1976]:

$$F_{\text{Euler}} = C \frac{\pi^2 EI}{L^2}, \quad (9.15)$$

where E is the Young's modulus, I is the minimum second moment of area (also called the moment of inertia) and L is the length of the column. The constant C is given in the following Table 9.2

Table 9.2 .End Fixity Factors (Continued) [Simitses 1976]

Boundary conditions	C
Both ends simply supported (pinned-pinned)	1
One end fixed, the other free	0.25
Both ends fixed	4
One end fixed, the other simply supported	$\left(\frac{4.493}{\pi}\right)^2$

The critical stress σ_{Euler} becomes

$$\sigma_{\text{Euler}} = \frac{F_{\text{Euler}}}{A} = C \frac{\pi^2 EI}{AL^2} = C \frac{\pi^2 E}{\left(\frac{L}{\rho}\right)^2}, \quad (9.16)$$

where ρ is the radius of gyration, $\rho = \sqrt{\frac{I}{A}}$ (m).

Rankine's Formula [Prescott 1961]

The Euler buckling loads calculated by the several methods, are the loads at which the straight strut becomes unstable, assuming that it does not fail in any other way before buckling occurs. But a very short strut would clearly fail by crushing before it buckles. If σ_{yield} is the maximum intensity of the compression stress that the material can stand without permanent deformation, and if A is the area of the cross-section, the short rod will fail when

$$F_{\text{sc}} = A\sigma_{\text{yield}}. \quad (9.17)$$

A very long pinned strut will buckle at $F_{\text{Euler}} = \frac{\pi^2 EI}{L^2}$. Rankine's empirical

allowable compression force F is defined by [Prescott 1961]

$$\frac{1}{F} = \frac{1}{F_{\text{sc}}} + \frac{1}{F_{\text{Euler}}}. \quad (9.18)$$

Johnson Parabolic Formula [Sechler 1963]

The Johnson column equation approximates the tangent modulus curve in the intermediate region between the very short and the Euler long columns. The Johnson's equation gives the critical short column stress

$$\sigma_{Jc} = \sigma_Y - \frac{\sigma_Y^2 \left(\frac{L}{\rho}\right)^2}{4C\pi^2 E}. \quad (9.19)$$

The Euler buckling stress σ_{Euler} is equal to the Johnson stress σ_{Jc} when $\left(\frac{L}{\rho}\right)$ is

$$\left.\frac{L}{\rho}\right|_{crit} = \pi \sqrt{\frac{2CE}{\sigma_Y}}. \quad (9.20)$$

The critical Johnson's formula for the compression load F_{cr} for a column is

$$F_{cr} = \begin{cases} A\sigma_{Jc} & \left(\frac{L}{\rho}\right) \leq \pi \sqrt{\frac{2CE}{\sigma_Y}} \\ F_{Euler} & \left(\frac{L}{\rho}\right) > \pi \sqrt{\frac{2CE}{\sigma_Y}} \end{cases} \quad (9.21)$$

Example

The forces in the struts of a truss frame structure were calculated with a finite element programme. The longest strut has been selected to be investigated against Euler buckling. The idealised length of the strut is $L = 1100$ mm, the cross section $A = 44$ mm², the minimum second moment of area $I = 3092$ mm⁴ and the Young's modulus of the strut material is $E = 73200$ N/mm². The allowable yield stress of the applied material is $\sigma_y = 276$ N/mm², and allowable ultimate stress $\sigma_u = 441$ N/mm². The maximum calculated compression load in the selected strut is $F = 1250$ N.

The stress in the strut is

$$\sigma = \frac{F}{A} = \frac{1250}{44} = 28.41 \text{ N/mm}^2.$$

The strut is pinned on both sides, so the Euler buckling load can be calculated by the following formula

$$F_{Euler} = \frac{\pi^2 EI}{L^2} = \frac{\pi^2 73200 \times 3092}{1100^2} = 1861 \text{ N.}$$

The margin of safety against column buckling is

$$MS = \frac{F_{Euler}}{F} - 1 = \frac{1861}{1250} - 1 = 0.48.$$

Rankine Empirical Formula for Struts [Prescott 1961]

The yield load is

$$F_y = \sigma_y A = 276 \times 44 = 12144 \text{ N},$$

and the equivalent Rankine allowable load becomes

$$\frac{1}{F_{\text{Rankine}}} = \frac{1}{F_y} + \frac{1}{F_{\text{Euler}}} = \frac{1}{12144} + \frac{1}{1861}, F_{\text{Rankine}} = 1613 \text{ N}.$$

The margin of safety against the Rankine allowable load becomes

$$MS = \frac{F_{\text{Rankine}}}{F} - 1 = \frac{1613}{1250} - 1 = 0.29.$$

Johnson Parabolic Formula

The critical value for $\left. \frac{L}{\rho} \right|_{\text{crit}}$ is

$$\left. \frac{L}{\rho} \right|_{\text{crit}} = \pi \sqrt{\frac{2E}{\sigma_Y}} = 71.$$

The radius of gyration ρ is $\rho = \sqrt{\frac{I}{A}} = \sqrt{\frac{3092}{44}} = 8.38 \text{ mm}$, and therefore $\frac{L}{\rho}$

can be calculated $\frac{L}{\rho} = \frac{1100}{8.38} = 131 > 72$. The critical load must be based on the Euler compression load (see above calculations).

End of example

Tapered Struts

Frequently tapered struts are applied as a structural element in a spacecraft structure. If I_1 is the second moment of area of the end cross section and I_o the second moment of area in the middle of the strut the following expressions can be defined

$$\frac{I_1}{I_o} = \left(\frac{b}{a} \right)^m = \alpha. \quad (9.22)$$

The Euler buckling of the strut, shown in Fig. 9.4, simply supported (pinned-pinned) at both ends of the strut, is derived by [Abbassi 1958]

$$F_{\text{Euler}} = \left[\frac{\left(1 - \frac{m}{2}\right) \left(1 - \alpha^{\frac{1}{m}}\right)}{1 - \alpha^{\frac{1}{m} - \frac{1}{2}}} \right]^2 \frac{\pi^2 EI_o}{L^2}. \quad (9.23)$$

For $m = 1$ we get

$$F_{\text{Euler}} = \frac{1}{4} (1 + \sqrt{\alpha})^2 \frac{\pi^2 EI_o}{L^2}, \quad (9.24)$$

with $\alpha = 1$ we obtain the classical Euler buckling of a pinned-pinned strut.

$$F_{\text{Euler}} = \frac{\pi^2 EI_o}{L^2}. \quad (9.25)$$

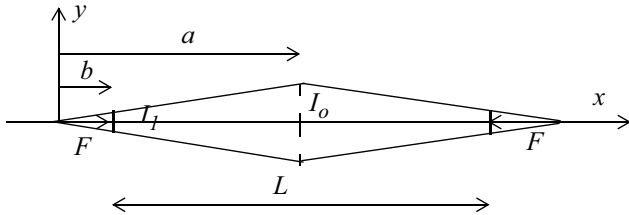


Fig. 9.4 Strut with variable cross section

Sechler in [Sechler 1968] proposed a Rayleigh like quotient to obtain the buckling load of a column with variable section moment of area $I(x)$, variable Young's modulus $E(x)$, and the deflection of the strut $w(x)$ is

$$F_{\text{critical}} = \frac{\int_0^L E(x)I(x) \left(\frac{d^2 w}{dx^2} \right)^2 dx}{\int_0^L \left(\frac{d^2 w}{dx^2} \right)^2 dx}, \text{ with } \left(w \frac{dw}{dx} \right)_0^L = 0. \quad (9.26)$$

Many examples of stability analysis using the Rayleigh's method are given in [Den Hartog 1987].

If a beam has a cross section with a width b that is small compared with the depth h , and both are very small with regard to the length L , it is possible to have a lateral instability of the beam under bending and shear loads as illustrated in Fig. 9.5.

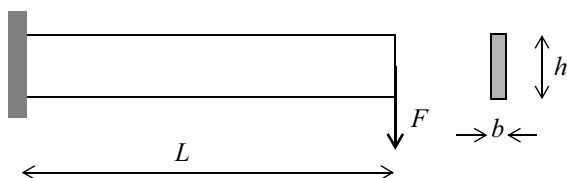


Fig. 9.5 Bending beam slender cross-section

For the situation as shown in Fig. 9.5, the critical load F_{critical} can be calculated by the following expression from the book of Sechler, [Sechler 1968]

$$F_{\text{critical}} = 0.415 \frac{hb^3 E}{L^2} \sqrt{\left(1 - 0.630 \frac{b}{h}\right)}, \quad (9.27)$$

where E is the Young's modulus of the material.

The Euler buckling of that beam is given by $F_{\text{critical}} = 0.206 \frac{hb^3 E}{L^2}$.

9.3.3 Bending stresses in beams

The normal stress caused by a pure bending moment M_z acting over the transverse surface is given by the bending stress formula [Budynas 1999]

$$\sigma_x = \frac{M_z y}{I_z} = \frac{M_z}{W}, \quad (9.28)$$

where y is the so-called fibre distance, $I_z = \int_{y_{\min}}^{y_{\max}} y^2 dA$ the second moment of area. If the extreme fibre distance is indicated with e , the associated maximum bending stress σ_{\max} can be written

$$\sigma_{\max} = \frac{M_z e}{I_z} = \frac{M_z}{W}, \quad (9.29)$$

where $W = \frac{I_z}{e}$ is the section modulus. The parameters are illustrated in Fig. 9.6.

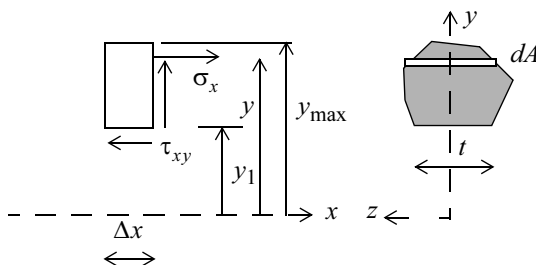


Fig. 9.6 Bending and transverse shear stresses

9.3.4 Shear stresses in beams

The shear stress in a cross-section of a beam can be written as

$$\tau_{xy} = \frac{D_y S}{I_z t}, \quad (9.30)$$

where D_y and I_z are the total shear force and the second moment of area (second-area moment), t is the width at $y = y_1$ where the shear stress τ_{xy} is being evaluated,

and $S = \int_{y_1}^{y_{\max}} y dA$ is the first moment of area (first-area moment). S is always a maximum at the neutral axis (neutral axis) where $y_1 = 0$. The parameters are illustrated in Fig. 9.6.

For long beams undergoing transverse loading, the shear stress is normally small compared to the bending stresses. For short beams with narrow widths at the neutral axis the shear stress can be significant [Budynas 1999].

For most cross sections, the ratio $\frac{S}{t}$ is maximum at the bending neutral axis. For a rectangular cross section, the maximum value of the shear stress is $\tau_{xy, \max} = \frac{3D_x}{2A} = \frac{3}{2}\tau_{xy, \text{average}}$. For a circular cross section the maximum shear stress is $\tau_{xy, \max} = \frac{4}{3}\tau_{xy, \text{average}}$.

Example

Find the maximum normal stress in the beam in Fig. 9.7 and the shear stress distribution over the cross section.

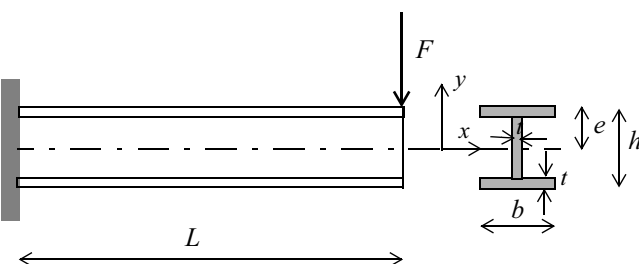


Fig. 9.7 Beam

The length of the cantilever beam $L = 500$ mm, the width of the flanges in the cross section $b = 75$ mm, the height of the cross section $h = 150$ mm, the extreme fibre distance $e = 75$ mm and the thickness of the flanges and span $t = 25$ mm. The applied force at the end of the beam $F = 2 \times 10^5$ N.

The maximum normal stress σ_{xx} due to bending will occur at the point of maximum bending moment, or at the fixed end of the beam. Since the shear force is constant throughout the beam span, the shear stress distribution will be the same at any cross section.

The second moment of area I_z for the cross section is obtained as follows

$$I_z = 2 \left[\frac{bt^3}{12} + bt \left(e - \frac{t}{2} \right)^2 \right] + \frac{t(h-2t)^3}{12} = 1.693 \times 10^{-5} \text{ m}^2.$$

The maximum bending moment at the fixation of the cantilever beam is

$$M_z = FL = 1 \times 10^5 \text{ Nm.}$$

The maximum bending stress becomes

$$\sigma_{xx} = \frac{M_z e}{I_z} = 4.431 \times 10^8 \text{ Pa.}$$

For a point $y = e - t$ below the top of the beam, the first moment of area

$$S(e-t) = \int_{e-t}^e y dA = b \int_{e-t}^e y dy = ebt - \frac{bt^2}{2} = 1.172 \times 10^{-4} \text{ m}^3.$$

The shear stress in the span at $y = e - t$ is given by

$$\tau_{yx}(e-t) = \frac{D_y S(e-t)}{I_z t} = \frac{FS(e-t)}{I_z t} = 5.538 \times 10^4 \text{ Pa.}$$

The first moment of area with respect to the neutral line ($y = 0$) is

$$S(0) = b \int_0^e (y + e - t) dy + t \int_0^{e-t} y dy = \frac{b}{2}(2et - t^2) + \frac{t}{2}(e^2 - 2et + t^2),$$

$$S(0) = 1.484 \times 10^{-4} \text{ m}^3.$$

The shear stress in the span at $y = 0$ is given by

$$\tau_{yx}(0) = \frac{D_y S(0)}{I_z t} = \frac{FS(0)}{I_z t} = 7.012 \times 10^4 \text{ Pa.}$$

The shear stress distribution in the lower part of the cross section is similar to the distribution over the upper half part due to the symmetry of the cross section.

This example is taken from [Peery 1982], however, the dimensions are adapted to the SI system.

End of example

9.3.5 Torsion of Beams

Torsion may be defined as the transmission of a torsion moment along an axis having the same direction as that of the moment vector.

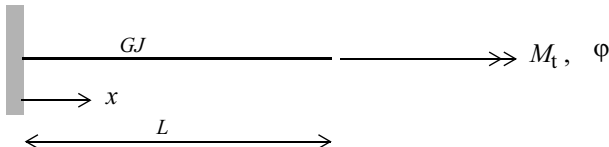


Fig. 9.8 Torsion of a beam

Classes of cross sections are

- Solid round bar
- Thin-walled; any shape
- Thick; non circular

Solid Round Bar

In a solid round bar (cross section) the maximum shear stress is given by [Shanley 1967]

$$\tau_{\max} = \frac{M_t R}{I_p}, \quad (9.31)$$

where M_t is the twisting moment, R the outside radius and I_p the polar moment of inertia. The polar moment of inertia is given by

$$I_p = \frac{\pi R^4}{2}. \quad (9.32)$$

The stiffness k_ϕ of the beam concerning the twist ϕ and the twisting moment M_t can be calculated by

$$k_\phi = \frac{G I_p}{L}, \quad (9.33)$$

where L is the length of the beam and G is the shear modulus. For an isotropic material the shear modulus G is related to the Young's modulus E and the Poisson's ratio ν and is given by

$$G = \frac{E}{2(1+\nu)}. \quad (9.34)$$

Torsion of thin-walled closed members

The tubular member must be closed, however, the thickness may vary around the periphery of the tube. The thickness is small compared with the outside dimension (width) of the tube.

The shear stress is uniformly distributed across the thickness, the shear flow is constant around the circumference of the cross section and acts at the mid-thickness, and warping is free at the ends of the tube.

The constant shear flow q is given by

$$q = \frac{M_t}{2\bar{A}}, \quad (9.35)$$

where \bar{A} is the entire area enclosed by the median line of the wall thickness. The shear stress is dependent on the wall-thickness t and becomes

$$\tau = \frac{q}{t}. \quad (9.36)$$

Example

A torsion box is constructed of an Al-alloy of $t=3$ mm sheet, with a rectangular cross section $b=250$ by $h=500$ mm (mean dimensions). A torque or twist moment $M_t = 100000$ Nm is applied. Find the shear stress in the sheet.

The shear flow can be calculated by

$$q = \frac{M_t}{2\bar{A}} = \frac{M_t}{2bh} = \frac{100000}{2 \times 0.25 \times 0.5} = 25000 \text{ N/m.}$$

The shear stress becomes

$$\tau = \frac{q}{t} = \frac{25000}{0.003} = 8.33 \times 10^6 \text{ Pa.}$$

End of example

The stiffness k_ϕ of the beam concerning the twist ϕ and the twisting moment M_t can be calculated by

$$k_\phi = \frac{GJ}{L}, \quad (9.37)$$

where the torsion constant J is given by

$$J = \frac{4\bar{A}^2}{\oint \frac{ds}{t}}. \quad (9.38)$$

When the thickness t is constant and the periphery of the median line is S than the torsion constant becomes

$$J = \frac{4\bar{A}^2 t}{S}. \quad (9.39)$$

Example

Find the shear stress and the torsion constant of an Al-alloy tube with a length $L=4$ m, having a diameter $D=100$ mm and a wall thickness of 3 mm. The applied torque $M_t = 3 \times 10^4$ Nm. The shear modulus is $G=27$ GPa.

The shear stress is

$$\tau = \frac{M_t}{2\bar{A}t} = \frac{3 \times 10^4}{2\pi(0.5)^2 \times 0.003} = 6.28 \times 10^7 \text{ Pa.}$$

The torsion constant J is

$$J = \frac{4\bar{A}^2}{S} = \frac{4\bar{A}^2 t}{\oint_S \frac{ds}{t}} = \frac{4(\pi R^2)t}{2\pi R} = 2Rt = 3 \times 10^{-4} \text{ m}^2.$$

The twisting/torsional can be obtained by

$$k_\phi = \frac{GJ}{L} = \frac{27 \times 10^9 \times 3 \times 10^{-4}}{4} = 2.025 \times 10^6 \text{ Nm/m.}$$

End of example

Torsion in noncircular members

We will start with a cross section for which the width b is much greater than the thickness t , thus $\frac{t}{b} \ll 1$.

The maximum stress in such a cross section is given by [Peery 1982]

$$\tau = \frac{3M_t}{bt^2}. \quad (9.40)$$

The torsion constant J is given by

$$J \approx \frac{bt^3}{3}, \quad (9.41)$$

and if a cross section is built up by a number of thin elements the torsion constant can be obtained by

$$J \approx \sum_k \frac{b_k t_k^3}{3}. \quad (9.42)$$

The shear stress in member k becomes

$$\tau = \frac{3M_t t_k}{\sum_k b_k t_k^3}. \quad (9.43)$$

For a rectangular cross section with $\frac{t}{b} \approx 1$ the shear stress is

$$\tau = \frac{M_t}{ab t^2}, \quad (9.44)$$

and the torsion constant J

$$J \approx \beta b t^3. \quad (9.45)$$

The values for α and β can be found in [Peery 1982], see Table 9.3.

Table 9.3 Constants

$\frac{b}{t}$	1.00	1.50	1.75	2.00	2.5	3.00	4	6	8	10	∞
α	0.208	0.231	0.239	0.246	0.258	0.267	0.282	0.299	0.307	0.313	0.333
β	0.141	0.196	0.214	0.229	0.249	0.263	0.281	0.299	0.307	0.313	0.333

For a cross section made up of several rectangular elements the torsion constant is given by

$$J \approx \sum_k \beta_k b_k t_k^3. \quad (9.46)$$

9.3.6 Local buckling of thin-walled tubes

The local buckling (crushing) of a metal circular tube with $\frac{D}{t}$ the diameter-thickness can be predicted by

$$\sigma_{lb} = \frac{K_c E}{\frac{D}{t}}, \quad (9.47)$$

where E is Young's modulus and K_c is theoretically 1.2, however, due the influence of imperfections it is observed [Shanley 1967] that $K_c = 0.4 \dots 0.8$. In

the inelastic range, an effective modulus equal to the geometric mean of the elastic and tangent moduli gives conservative results. So (9.47) becomes

$$\sigma_{lb} = \frac{K_c \sqrt{EE_t}}{\frac{D}{t}}, \quad (9.48)$$

where E_t is the tangent modulus at the stress σ_{lb} .

Example

A thin-walled tube has a mean diameter $D = 72$ mm, a wall thickness $t = 0.5$ mm, and a length $L = 2$ m is pin ended. The Euler stress can be calculated by

$$\sigma_{Euler} = \frac{\pi^2 EI}{AL^2} = \frac{\pi^2 E}{\left(\frac{L}{\rho}\right)^2}, \quad (9.49)$$

with the radius of gyration $\rho = \sqrt{\frac{I}{A}}$. The second moment of area of a thin walled tube is $I = \pi R^3 t$, $R = \frac{D}{2}$, and the area $A = 2\pi R t$. Thus the radius of gyration $\rho = \sqrt{\frac{I}{A}} = 0.7071R = 0.0255$. The slenderness of the tube (strut) $\lambda = \frac{L}{\rho} = \frac{2.0}{0.0255} = 78.4$. The strut is made of an Al-alloy with a Young's modulus $E = 70$ GPa. The Euler stress becomes $\sigma_{Euler} = \frac{\pi^2 E}{\left(\frac{L}{\rho}\right)^2} = 112.4$ MPa.

For local buckling, assuming $K_c = 0.6$ can be calculated by $\left(\frac{D}{t} = 144\right)$

$$\sigma_{lb} = \frac{K_c E}{\frac{D}{t}} = 291.7 \text{ MPa.}$$

The strut will collapse due to Euler instability of the column as a whole, not by local buckling of the wall. There is no need to consider inelastic effects.

End of example

9.3.7 Rings

Rings are used to improve the general instability of shells of revolution and to connect various shells of revolution: a cylinder, a cone and a platform for example. Rings are also used to mount fuel cells (Apogeeum Boost Motor) on a cylinder. Rings or ring frames are used to reduce the buckling length of shells of revolution. These rings must satisfy certain stiffness criteria. This criterion has been formulated by [Shanley 1949]:

$$(EI)_{\text{ringframe}} = \frac{NR^3}{8000L}, \quad (9.50)$$

with L the mutual distance between the rings, E the modulus of elasticity of the ring material, I the second moment of area of the ring, R the radius of the cylinder and N the load per unit length (running load).

Besseling in [Besseling 1975] discussed the strength and stiffness problem of a ring loaded with two opposite forces (Fig. 9.9). The following solution was derived.

$$M_\alpha = FR\left(\frac{1}{\pi} - \frac{1}{2}\cos\alpha\right). \quad (9.51)$$

Thus the maximum bending moment in the ring is given by

$$M_{\max} = \frac{1}{\pi}FR, \quad (9.52)$$

and the corresponding maximum bending stress can be calculated using

$$\sigma_{\max} = \frac{FRe}{\pi I}, \quad (9.53)$$

where e is the extreme fibre distance and I the second moment of area.

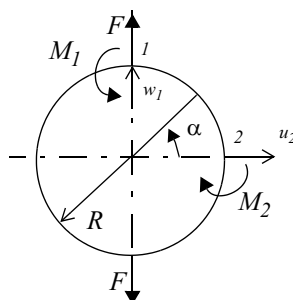


Fig. 9.9 Ring loaded in plane with concentrated forces

The displacements can be obtained by the following equations:

$$u_2 = -\frac{FR^3}{EI} \left(\frac{4-\pi}{\pi} \right), \quad w_1 = \frac{FR^3}{EI} \left(\frac{\pi^2 - 8}{8\pi} \right), \quad (9.54)$$

with E the Young's modulus of the ring material.

9.4 Platforms

Equipment, instruments, harness, etc. are mounted to platforms and are, in general, made of sandwich construction. The sizing of the platform is basically based on the stiffness (natural frequency). The mass of the equipment, instruments, harness, etc. is smeared out over the platform (panel) and handbooks about the natural frequency of structures are used to obtain values for the natural frequencies [Leissa 1969].

9.5 Panels

The linear elastic-buckling stress for the square flat panel can be written in a general form that applies to all types of plate buckling:

$$\sigma_{cr} = K_c E \left(\frac{t}{b} \right)^2, \quad (9.55)$$

where K_c is a constant depending on the edge constraint, t the plate thickness, b the plate width and L the length of the plate. The buckling coefficients for flat plates are listed in [Shanley 1967], see Table 9.4

Table 9.4 Buckling Coefficients for Flat Plates

Loading (across b)	Constraint	K_c
Compression	All edges pinned	3.62
Compression	Unloaded edges fixed, others pinned	6.3
Compression	One unloaded edge fixed, other free	1.10
Compression	One edge free, other pinned ($L \gg b$)	0.375
Pure shear	All edges pinned ($L \gg b$)	4.8
Pure shear	All edges fixed ($L \gg b$)	8.1
Pure bending	All edges pinned	21.5

9.6 Shells of revolution: cylinders / cones

Shells of revolution, often cones and cylinders, usually form the central part of the spacecraft structure. They can be constructed in various ways:

- Monocoque
 - metal Al-alloys
 - filament wound with GPRP, CFRP, ...
- Sandwich
 - Al-alloy honeycomb core with Al-alloy face sheets
 - Al-alloy honeycomb core with face sheets. The latter consists of a CFRP laminate that is made up of various layers of unidirectional composite material that is arranged in various directions. The face sheets can also be filament wound.
- Integrally stiffened shells
- Sheet stiffeners
 - Z-stiffeners
- Orthotropic

9.6.1 Stability of Cylinders

The axially symmetric buckling of a simply supported, circular, isotropic shell under axial compression load is given by, [NASA SP-8007, Vinson 1989]

$$N_{x,cr} = \frac{Et^2}{R\sqrt{3(1-v^2)}}, \quad (9.56)$$

for a length L of the shell

$$L \geq \pi \left[\frac{R^2 t^2}{12(1-v^2)} \right]^{\frac{1}{4}} \approx 1.72 \sqrt{Rt}, \quad (9.57)$$

where E is the Young's modulus, R is the radius of the cylinder, t is the wall thickness and v is the Poisson's ratio.

However, it is necessary to incorporate an empirical (knock down) factor in all equations in order to relate the theoretical values to the actual test data. From [NASA SP-8007] (9.56) is modified to become

$$\sigma_{x,cr} = \frac{\gamma Et}{R\sqrt{3(1-v^2)}}, \quad (9.58)$$

where in the case of compression (constant running load) loads

$$\gamma = 1 - 0.901(1 - e^{-\phi}), \text{ and } \phi = \frac{1}{16} \sqrt{\frac{R}{t}}. \quad (9.59)$$

The empirical factor γ is illustrated in Fig. 9.10.

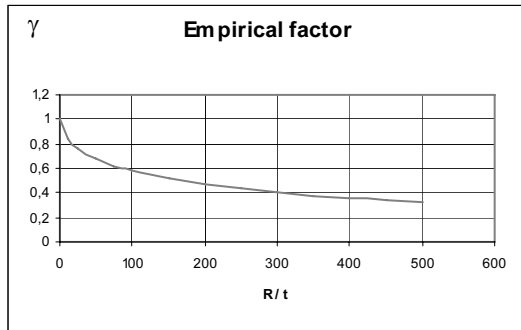


Fig. 9.10 Empirical (knock down) factor γ

Geometrically speaking, the buckle pattern that occurs is usually that of a diamond shape of dimensions small compared to the circumference of the shell length.

Example

Consider a cylindrical interstage structure of a missile system with $L \geq 1.72 \sqrt{Rt}$, yet $\frac{L}{R} \leq 5$ composed of an Al-alloy ($E = 70$ GPa, $v = 0.3$ and $\sigma_{yield} = 250$ MPa). If a shell of $R = 750$ mm and thickness $t = 2.5$ mm is subjected to an axial compression load, what will be the critical stress?

The ratio of radius over the thickness becomes $\frac{R}{t} = 300$, the value of

$\phi = \frac{1}{16} \sqrt{\frac{R}{t}} = 1.083$ and the knock down factor $\gamma = 1 - 0.901(1 - e^{-\phi}) = 0.4042$. The critical stress can be calculated by $\sigma_{x,cr} = \frac{\gamma Et}{R \sqrt{3(1-v^2)}} = 0.6052 \frac{\gamma Et}{R} = 57.08 \times 10^7$ Pa. This is below the yield stress of the Al-alloy.

End of example

9.6.2 Stiffness of Cylinders

The cylinder is fixed at the lower side, Fig. 9.11. The lateral and the bending flexibility of the fixed cylinder are given in (9.60) and (9.61), [Girard 1999].

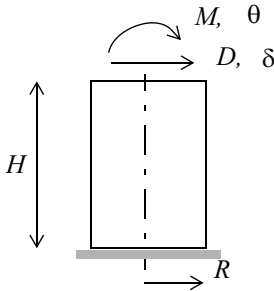


Fig. 9.11 Cylinder

The lateral deflection δ of the cylinder at the top due to the shear force D and bending moment M is given in the following expression, in which E is the Young's modulus and G is the shear modulus.

$$\delta = \left[\frac{\left(\frac{H}{R}\right)^3}{3\pi Et} + \frac{H}{R} \right] D + \left[\frac{\left(\frac{H}{R}\right)^2}{2\pi Re t} \right] M, \quad (9.60)$$

and the rotation θ due to the shear force D and bending moment M is given by

$$\theta = \left[\frac{\left(\frac{H}{R}\right)^2}{2\pi Re t} \right] D + \left[\frac{\left(\frac{H}{R}\right)}{\pi R^2 Et} \right] M. \quad (9.61)$$

In matrix notation

$$\begin{Bmatrix} \delta \\ \theta \end{Bmatrix} = \begin{bmatrix} G_{\delta\delta} & G_{\delta\theta} \\ G_{\theta\delta} & G_{\theta\theta} \end{bmatrix} \begin{Bmatrix} D \\ M \end{Bmatrix}. \quad (9.62)$$

Suppose a spacecraft has been firmly fixed on top of the cylinder with mass $M_{\text{spacecraft}}$, a second moment of mass $I_{\text{spacecraft}}$ and an off-set d from the top of the cylinder to the centre of mass or centre of gravity of the spacecraft the homogenous equations of motion can be written

$$\begin{bmatrix} M_{\text{spacecraft}} & 0 \\ 0 & I_{\text{spacecraft}} + d^2 M_{\text{spacecraft}} \end{bmatrix} \begin{Bmatrix} \ddot{\delta} \\ \ddot{\theta} \end{Bmatrix} + \begin{bmatrix} G_{\delta\delta} & G_{\delta\theta} \\ G_{\theta\delta} & G_{\theta\theta} \end{bmatrix}^{-1} \begin{Bmatrix} \delta \\ \theta \end{Bmatrix} = \begin{Bmatrix} 0 \\ 0 \end{Bmatrix}. \quad (9.63)$$

The natural frequency in launch direction is given by

$$f_{\text{ld}} = \frac{1}{2\pi} \sqrt{\frac{2\pi R E t}{H M_{\text{spacecraft}}}}. \quad (9.64)$$

9.6.3 Running Loads in Cylinder

The normal force N , the bending moment M and the shear force D , acting at the cross section of the cylinder, will introduce running loads (force per unit of length) along the circumference of the cylinder with radius R and wall thickness t . We assume that $\frac{t}{R} \ll 1$.

The running load q_N associated with the normal force (perpendicular to the cross section) is given by

$$q_N = \frac{N}{A} = \frac{N}{2\pi R}. \quad (9.65)$$

The running load q_M due with the normal force (perpendicular to the cross section) is given by

$$q_M(\theta) = \frac{M t y}{I} = \frac{M t R \sin \theta}{\pi R^3 t} = \frac{M \sin \theta}{\pi R^2}. \quad (9.66)$$

$$\text{The maximum running load } q_{M,\max} = \frac{M \sin \frac{\pi}{2}}{\pi R^2} = \frac{M}{\pi R^2}.$$

The maximum running load of the normal load N and bending moment M can be written

$$q_{\max} = \frac{N}{2\pi R} + \frac{M}{\pi R^2}. \quad (9.67)$$

The running shear force q_D (see (9.30)) is given by

$$q_D = \frac{D S}{I} = \frac{2 D R^2 t \cos \theta}{2\pi R^3 t} = \frac{D \cos \theta}{\pi R}. \quad (9.68)$$

The maximum running load q_D at $\theta = 0$ now becomes

$$q_D = \frac{D}{\pi R}. \quad (9.69)$$

The constant running shear flow q_T due to a torsion moment M_T is given by [Rivello 1969]

$$q_T = \frac{M_T}{2A_{\text{enclosed}}} = \frac{M_T}{2\pi R^2}. \quad (9.70)$$

The previous calculations to obtain running loads for cylinders can also be used for conical shells.

9.6.4 Stiffness of Cones

The lateral and bending flexibility of a fixed cone can be calculated with (9.71) and (9.72). The meanings of all parameters are illustrated in Fig. 9.12.

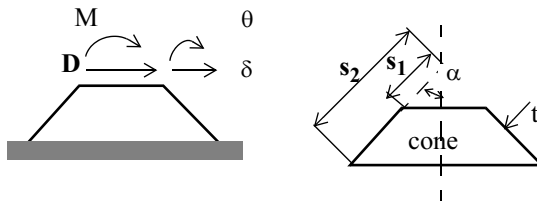


Fig. 9.12 Description of cone

The lateral displacement δ , due to the external force D and the bending moment M , can be calculated by the following equation, in which E the Young's modulus and ν the Poisson's ratio, [Seide 1972]

$$\delta = \frac{1 - \frac{s_1}{s_2}}{\pi Et(\sin\alpha)^3} \left\{ \frac{\ln \frac{s_2}{s_1}}{1 - \frac{s_1}{s_2}} - 2 + \left(1 + \frac{s_1}{s_2}\right) \left[\frac{1}{2} + (1 + v)(\sin\alpha)^2 \right] \right\} D \\ + \frac{1 - \frac{s_1}{s_2}}{\pi Et(\sin\alpha)^3} \left\{ 1 - \left(1 + \frac{s_1}{s_2}\right) \left[\frac{1}{2} + (1 + v)(\sin\alpha)^2 \right] \right\} \frac{M}{s_1 \cos\alpha}, \quad (9.71)$$

and the calculation of θ can be obtained by [Seide 1972]

$$\theta = \frac{1 - \frac{s_1}{s_2}}{\pi Ets_1(\sin\alpha)^3 \cos\alpha} \left\{ 1 - \left(1 + \frac{s_1}{s_2}\right) \left[\frac{1}{2} + (1 + v)(\sin\alpha)^2 \right] \right\} D \\ + \frac{1 - \frac{s_1}{s_2}}{\pi Ets_1(\sin\alpha)^3 \cos\alpha} \left\{ \left(1 + \frac{s_1}{s_2}\right) \left[\frac{1}{2} + (1 + v)(\sin\alpha)^2 \right] \right\} \frac{M}{s_1 \cos\alpha}. \quad (9.72)$$

In matrix notation

$$\begin{Bmatrix} \delta \\ \theta \end{Bmatrix} = \begin{bmatrix} G_{\delta\delta} & G_{\delta\theta} \\ G_{\theta\delta} & G_{\theta\theta} \end{bmatrix} \begin{Bmatrix} D \\ M \end{Bmatrix}. \quad (9.73)$$

Suppose a spacecraft has been firmly fixed on top of the cylinder with mass $M_{\text{spacecraft}}$, a second moment of mass $I_{\text{spacecraft}}$ and an off-set d from the top of the cylinder to the centre of mass or centre of gravity of the spacecraft the homogeneous equations of motion can be written

$$\begin{bmatrix} M_{\text{spacecraft}} & 0 \\ 0 & I_{\text{spacecraft}} + d^2 M_{\text{spacecraft}} \end{bmatrix} \begin{Bmatrix} \ddot{\delta} \\ \ddot{\theta} \end{Bmatrix} + \begin{bmatrix} G_{\delta\delta} & G_{\delta\theta} \\ G_{\theta\delta} & G_{\theta\theta} \end{bmatrix}^{-1} \begin{Bmatrix} \delta \\ \theta \end{Bmatrix} = \begin{Bmatrix} 0 \\ 0 \end{Bmatrix}. \quad (9.74)$$

The natural frequency in launch direction is given by

$$f_{ld} = \frac{1}{2\pi} \sqrt{\frac{2\pi \sin\alpha (\cos\alpha)^2 Et}{\ln\left(\frac{s_2}{s_1}\right) M_{\text{spacecraft}}}}. \quad (9.75)$$

9.6.5 Stability of Cones

The classical buckling load of a conical isotropic cone is given by the following equation

$$P_{\text{cr}} = \gamma \frac{2\pi Et^2(\cos\alpha)^2}{\sqrt{3(1-v^2)}}, \quad (9.76)$$

with $\rho_1 = \frac{R_1}{\cos\alpha}$ the knockdown factor γ for unstiffened cones is given by [Spagnoli 1999] and R_1 is the (small) radius at the top of the cone and α is the angle of the cone with the central axis.

$$\gamma = \begin{cases} \frac{0.83}{\sqrt{1 + 0.01 \frac{\rho_1}{t}}} & \text{for } \frac{\rho_1}{t} \leq 212 \\ \frac{0.70}{\sqrt{0.1 + 0.01 \frac{\rho_1}{t}}} & \text{for } \frac{\rho_1}{t} > 212 \end{cases} . \quad (9.77)$$

The knock down factors are illustrated in Fig. 9.13.

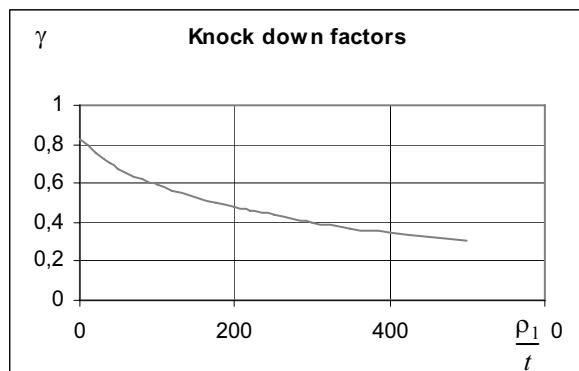


Fig. 9.13 Knock down factors γ [Spagnoli 1999]

In [NASA SP-8019] a knock down factor $\gamma = 0.33$ is recommended. This knock down factor is applicable for $10^\circ < \alpha < 75^\circ$.

9.7 Stresses in Lap Joints

In Fig. 9.14 a double lap joint is illustrated. The stresses are uniform over the thickness t_1 and $2t_2$ are σ_1 and σ_2 respectively. The Young's modulus of the strips is E_1 and E_2 . The adhesive is assumed to be subjected to shear stress, and the shear modulus of the adhesive is G .

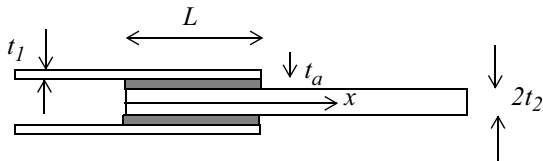


Fig. 9.14 Double lap joint

With the parameter

$$\lambda^2 = \frac{G}{t_a} \left(\frac{1}{E_1 t_1} + \frac{1}{E_2 t_2} \right). \quad (9.78)$$

the shear stress distribution $\tau(x)$, with the boundary conditions $\sigma_1(0) = \sigma_{10}$, $\sigma_1(L) = 0$, $\sigma_2(0) = 0$ and $\sigma_1(L) = \sigma_{20}$, becomes [Abrate 1998]

$$\tau(x) = \frac{G}{t_a \lambda} \left\{ \left(\frac{\sigma_{10}}{E_1 \tanh(\lambda L)} + \frac{\sigma_{20}}{E_2 \tanh(\lambda L)} \right) \cosh(\lambda x) - \frac{\sigma_{10}}{E_1} \sinh(\lambda x) \right\}. \quad (9.79)$$

Equation (9.79) shows that the shear stress in the adhesive is not uniformly distributed as might be expected.

9.8 Literature

- Abbassi, M.M., 1958, *Buckling of Struts of Variable Bending Rigidity*, Journal of Applied Mechanics, December 1958, pages 537–540.
- Abrate, S., 1998, *Impact on Composite Structures*, Cambridge University Press, ISBN 0 521 47389 6.
- Benham, P.P., Crawford, R.J., Armstrong, C.G., 1987, *Mechanics of Engineering Materials*, Second Edition, ISBN 0-582-25164-8, Longman.
- Besseling, J.F., 1975, *Stiffness and Strength 2, Applications* (in Dutch), ISBN 90 313 0040 3, Schelkema & Holkema.
- Budynas, R.G., 1999, *Advanced Strength and Applied Stress Analysis*, second edition, McGraw-Hill International editions.
- Besseling, J.F., 1975, *Stiffness and Strength 2, Applications* (in Dutch), ISBN 90 313 0040 3, Schelkema & Holkema.
- Castiglione, C.A.P., 1966, *The Theory of Equilibrium of Elastic Systems and its Applications*, Dover Publications.
- Den Hartog, J.P., 1967, *Sterkteleer (Strength of Materials)*, Prisma-Technica. The book is written in the dutch language.
- Den Hartog, J.P., 1987, *Advanced Strength of Materials*, ISBN 0-486-65407-9, Dover Publication.
- Genta, G., 1995, *Vibration of Structures and Machines*, Practical Aspects, second edition, Springer-Verlag, ISBN 0-387-94403-6.
- Gere, J.M., Timoshenko, S.P., 1994, *Mechanics of materials, Third SI edition*, ISBN 0 412 36880 3, Chapman.
- Girard, A., Pawłowski, M., 1999, *Optimum Conical Shells for Dynamic Behaviour*, Interspace, Toulouse, France.
- Klein, B., 2001, *Leichtbau-Konstruktion, Berechnunggrundlagen und Gestaltung*, 5. Auflage, ISBN 3-528-44115-1, Vieweg.
- Leissa, W., 1969, *Vibration of plates*, NASA SP-160.
- NASA SP-8019, 1968, *Buckling of Thin-Walled Truncated Cones*, NASA Space Vehicle Design Criteria (Structures).
- NASA SP-8007, 1968, *Buckling of Thin-Walled Circular Cylinders*, NASA Space Vehicle Design Criteria (Structures).
- Prescott, J., 1961, *Applied Elasticity*, Dover Publications, Inc.
- Rivello, R.M., 1969, *Theory and Analysis of Flight Structures*, McGraw-Hill.
- Sechler, E., Dunn, L.G. 1963, *Airplane Structural Analysis and Design*, Dover Publication.
- Sechler, E., 1968, *Elasticity in Engineering*, Dover Publication.
- Seide, P., 1972, *Influence Coefficients for End-Loaded Conical Fustrum*, AIAA Journal, Vol. 10, No. 12
- Shanley, F.R., 1949, *Simplified Analysis of general Instability of Stiffened Shells in Pure Bending*, Journal of the Aeronautical Sciences, October, pages 590–592.
- Shanley, F.R., 1967, *Mechanics of Materials*, McGraw-Hill.
- Simitses, G.J., 1976, *An Introduction to the Stability of Structures*, Prentice-Hall, ISBN 0-13-481200-X
- Spagnoli, A. and Chryssanthopoulos, K., 1999, *Buckling design of Stringer-Stiffened Conical Shells in Compression*, Journal of Structural Engineering, Vol 125, No. 1, January 1999, pages 40–48
- Vinson, J.R., 1989, *The Behavior of Thin Walled Structures, Beams, Plates, and Shells*, ISBN 90-247-3663-3, Kluwer Academic Publishers.
- Wang, C.M., Wang, C.Y., Reddy, J.N., 2004, *Exact Solutions for Buckling of Structural Members*, CRC, ISBN 0-8493-2222-7.

9.9 Exercises

9.9.1 Deflection of truss frame

All trusses in the truss frame illustrated in Fig. 9.15 have all the same length L and a stiffness EA .

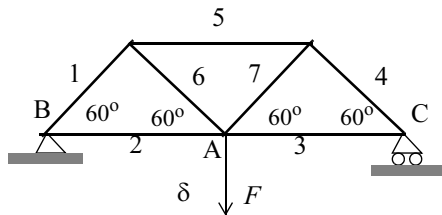


Fig. 9.15 Loaded truss frame

Perform the following analyses:

- Reaction forces at the locations B and C
- The internal loads in the trusses 1, 2, 3, 4, 5, 6 and 7
- The displacement δ at A.
- The stiffness k at position A

Answers: $V_B = V_C = \frac{F}{2}$, $N_1 = N_4 = -\frac{1}{3}F\sqrt{3}$, $N_2 = N_3 = \frac{1}{6}F\sqrt{3}$,

$$N_5 = -\frac{1}{3}F\sqrt{3}, N_6 = N_7 = \frac{1}{3}F\sqrt{3}, \delta = \frac{11FL}{6EA}, k = \frac{6EA}{11L}.$$

9.9.2 Deflection of a beam

A clamped-free beam is loaded with two forces F_1 and F_2 . The bending stiffness of the beam is EI , total length is L . The loaded beam is illustrated in Fig. 9.16. Calculate the deflection δ .

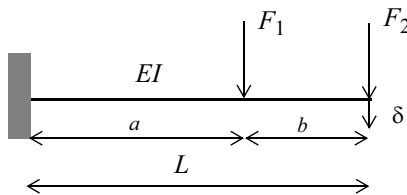


Fig. 9.16 Bending beam loaded with two forces

$$\text{Answer: } \delta = \left[\frac{(F_1 + F_2)a^3}{3EI} + \frac{(F_2 b)a^2}{2EI} \right] + \left[\frac{(F_1 + F_2)a^2}{2EI} + \frac{(F_2 b)a}{EI} \right] b + \frac{F_2 b^3}{3EI},$$

[Den Hartog 1967].

9.9.3 Deflection and bending moment in a clamped-clamped beam

A clamped-clamped beam is shown in Fig. 9.17.

- Derive the expression for the deflection $\delta = \frac{FL^3}{24EI}$ using the Myosotis formulae.
- Draw the shear diagram
- Draw the moment diagram
- Define the location(s) of the maximum bending moment

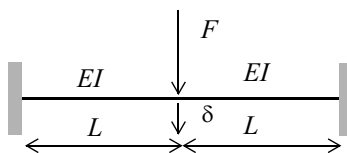


Fig. 9.17 Clamped-clamped beam

9.9.4 Buckling of Beam with Variable Cross-section

A strut with a variable cross-section is shown in Fig. 9.18.

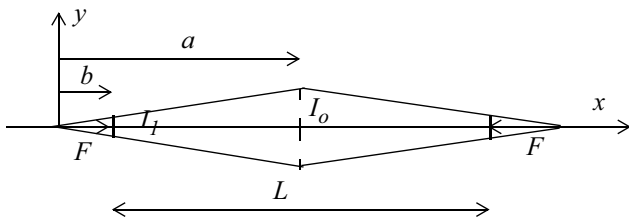


Fig. 9.18 Strut with variable cross-section

The second moment of area is given by

$$I(x) = I_1 + \frac{x}{a}(I_o - I_1), \quad b \leq x \leq a \quad \text{and} \quad I(x) = I_o + \frac{x}{a}(I_1 - I_o), \quad a \leq x \leq b + L.$$

The following deflection mode (assumed mode) $w(x)$ is taken

$$w(x) = w_o \sin \frac{\pi(x-b)}{L}, \quad b \leq x \leq a \quad \text{and} \quad w(x) = w_o \sin \frac{\pi(x-b)}{L},$$

$$b + \frac{L}{2} \leq x \leq b + L$$

Calculate with the aid of (9.26) the buckling load F_{cr}

$$\text{Answer: } F_{\text{cr}} = \frac{\pi^2 EI_o}{L^2} \left[\frac{1}{2} + \frac{L}{a} \left(\frac{1}{\pi^2} - \frac{1}{4} \right) \right] \quad [\text{Sechler 1968}]$$

9.9.5 Buckling of Square Tube

A square tube has a wall thickness $t = 2$ mm. The outside width is $b = 100$ mm.

The Young's modulus of the Al-alloy $E = 70$ GPa. Find the axial load at which a short specimen will begin to buckle locally.

Answer. $F_{\text{cr}} = 82743$ N.

9.9.6 Torsion and Shear Force

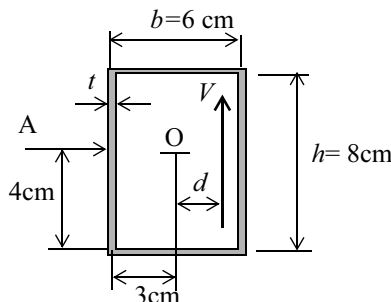


Fig. 9.19 Rectangular thin-walled cross section

A shear force V is applied to the rectangular thin-walled cross section as shown in Fig. 9.19. Calculate the distance d such that no shear stress acts at point A.

Answer: $d = 6.923 \text{ cm}$.

9.9.7 Stiffness and Buckling of a Cone

In Fig. 9.20 a cone is shown loaded by a compression force $N = 4 \text{ MN}$. The radius $R_1 = 1 \text{ m}$, the radius $R_2 = 1.5 \text{ m}$, the wall thickness is $t = 0.006 \text{ m}$. The cone is made of an Al-alloy with a Young's modulus $E = 70 \text{ GPa}$ and the Poisson's ratio is $\nu = 0.3$.

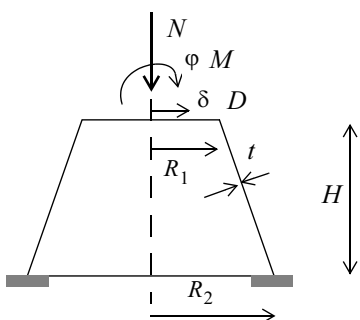


Fig. 9.20 Cone

Perform the following assignments:

- Calculate the flexibility matrix as given in (9.73)
- Calculate the allowable buckling load step by step procedure:
 - Define the knock down factor with (9.77).
 - Calculate the allowable buckling load.
- Calculate the margin of safety.

Answers: $[G] = 10^{-9} \begin{bmatrix} 3.345 & 0.676 \\ 0.676 & 0.2933 \end{bmatrix}$, $\gamma = 0.517$, $P_{cr} = 5.529 \times 10^6 \text{ N}$,

$MS = 0.382$.

10 Sandwich Construction

10.1 Introduction

A sandwich panel is a layered structure consisting of a thin facing material, or skin, bonded to either side of a thicker, low density, core. It is a type of stresses-skin construction with the skins carrying the major applied loads, in-plane loads and flat-wise bending moments. The stiffness, stability, configuration and strength of the panel are determined by the skins, stabilised by the core. In the literature [Allen 1969, Plantema 1966, TSB 124, Vinson 1999, Zenkert 1997] the analysis and design aspects of sandwich constructions, e.g. beams, panels, shells, are discussed in detail. A sandwich construction is shown in Fig. 10.1 and Fig. 10.2.

The sandwich constructions are frequently used because of the following characteristics:

- Mass savings with respect to conventional structures
- High specific stiffness (bending stiffness with respect to the mass)
- Good fatigue properties
- Sound-damping properties
- Good thermal and acoustical insulation properties

The sandwich construction is like an “I” cross-section where the face sheets are comparable with the flanges, carrying the tension and compression forces, and the core of sandwich construction is comparable with a web, carrying the shear forces.

Most times a honeycomb core, made of Al-alloy, is used as a core in sandwich construction applied for spacecraft and launch vehicles. More information about the mechanics of honeycombs can be find in [Gibson 1997].

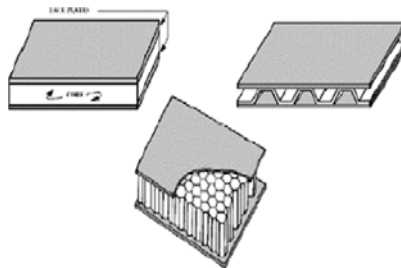


Fig. 10.1 Sandwich construction

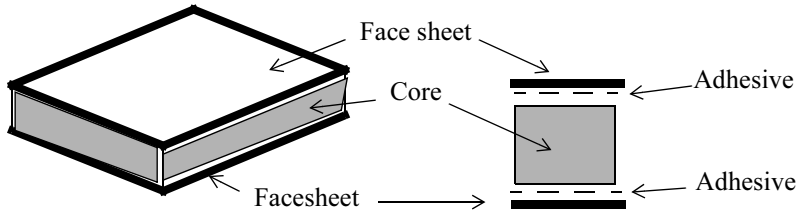


Fig. 10.2 Sandwich construction build up



Fig. 10.3 Honeycomb core

10.1.1 Design aspects

The major design aspects of sandwich constructions are:

- Attention shall be paid with respect to load introduction in the sandwich construction, either via the edges (edge members) or at discrete points, e.g. in and out of plane, bending, torque, etc.

- The face sheets (facings) shall have a thickness to carry the tensile, compression and shear forces (stresses) introduced in the sandwich structure.
- The core shall have adequate strength to carry the general shear forces and the local shear forces introduced via the inserts.
- The core shall have adequate strength and stiffness properties to prevent local and global buckling, e.g. wrinkling, shear crimpling, general buckling.
- The core shall have good compression properties to prevent crushing of the core. The crushing property is one of the design parameters to estimate the wrinkling of the face sheet.
- The diameter of the cells (in case of honeycomb core) shall be selected to prevent intercell buckling of the unsupported face sheet.
- The sandwich construction shall have good overall stiffness properties.
- The adhesive between the face sheets and the core shall have good strength properties

10.2 Optimum design: Determination of core and face sheet thickness for minimum mass

The optimum ratio between the core height h_c (m) and face sheet thickness t_f (m), $\frac{h_c}{t_f}$ can be optimised with respect to a minimum mass m_{sc} (kg/m) of the sandwich construction. The mass m_{sc} will be contributed by the mass of the face sheets $\rho_c h_c$ (kg/m), the mass of both face sheets (in this case equal face sheets) $2\rho_f t_f$ and the mass per unit of area of both adhesive layers $2\rho_a t_a$. The total mass per unit area becomes

$$m_{sc} = \rho_c h_c + 2\rho_f t_f + 2\rho_a t_a \quad (10.1)$$

During the optimisation the mass of the adhesive layers will be ignored.

The minimum mass optimization will be against:

- Bending stiffness
- Strength
- Face dimpling

In the following Table 10.1 equations for the minimum mass optimisation are given [Allen 1969].

Table 10.1 Optimum dimensions

Optimum ratio $\frac{h_c}{t_f}$, minimum mass		
Optimization		
Bending stiffness	$D = \frac{1}{2}E_f h_c^2 t_f$	$\frac{\rho_c h_c}{2\rho_f t_f} = 2$
General buckling	[Bladel 1995]	$\frac{h_c}{t_f} = \frac{4\rho_f - 3\rho_c}{\rho_c}$
Strength	$M = \sigma_{cr} t_f h_c$	$\frac{\rho_c h_c}{2\rho_f t_f} = 1$
Face dimpling	$\sigma_{cr} = C t_f^2$ $M = C t_f^3 h_c$	$\frac{\rho_c h_c}{2\rho_f t_f} = \frac{1}{3}$

where:

σ_{cr} the critical stress (Pa)

E_f Young's modulus of the face sheet material (Pa)

ρ_f mass density of face sheet material (kg/m^3)

ρ_c mass density of core material (kg/m^3)

M bending moment per unit length (Nm/m)

t_f face sheet thickness (m)

C is constant

10.3 Stresses

The stresses will occur both in the face sheets and in the core. The stress in the face sheets are caused by bending moments and in plane forces. Non uniform in plane forces will lead to shear stresses. The face sheets are in general very thin. That means that the stresses in the face sheets are more or less membrane stresses and we assume no stress variations in the face sheets through the thickness, when,

$\frac{h_c}{t_f} \gg 1$. The core will carry the out of plane shear forces.

10.3.1 Stresses in face sheets

Bending stresses

The bending stress σ_{fb} in the face sheets of a sandwich construction due to a bending moment per unit of width (Nm/m) is illustrated in Fig. 10.4.

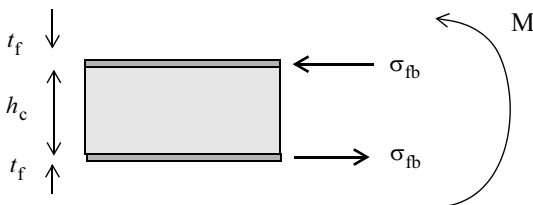


Fig. 10.4 Bending stress

The bending stress can be calculated with

$$\sigma_{fb} = \frac{Me}{I} \approx \frac{\frac{M}{2}h_c}{\frac{1}{2}h_c^2 t_f} = \frac{M}{h_c t_f}, \quad (10.2)$$

where e is the extreme fibre distance, I is the second moment of area.

In general the core is not able to carry in plane tension loads.

Tensile, compression stresses

The in plane stress σ_{fn} is caused by the in plane internal load N per unit of width [N/m]. This is shown in Fig. 10.5. The in plane loads are carried by both face sheets. The core will not carry the in plane loads. The in plane tensile or compression stress can be calculated with

$$\sigma_{fn} = \frac{N}{2t_f} \quad (10.3)$$

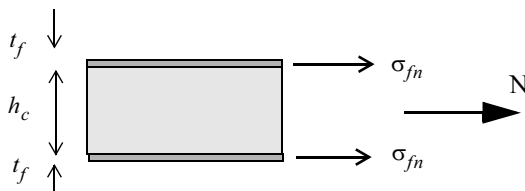


Fig. 10.5 In plane stress

Total stress in face sheets

The total stress σ_f in the face sheets in the superposition of the bending stress σ_{fb} with the in plane stress σ_{fn} . The total stress σ_f becomes

$$\sigma_f = \sigma_{fb} + \sigma_{fn} = \frac{M}{h_c t_f} + \frac{N}{2t_f} \quad (10.4)$$

10.3.2 Shear stress

The maximum shear τ stress, caused by the shear force D per unit width (N/m), can be calculated with the Jourawki method

$$\tau = \frac{DS_f}{I} \approx \frac{Dt_f \frac{1}{2}h_c}{\frac{1}{2}h_c^2 t_f} = \frac{D}{h_c}, \quad (10.5)$$

where S_f is the first moment of area per unit width of the face sheet with respect to the neutral line and I is the second moment of area per unit width of the face sheet with respect to the neutral line.

The shear stress τ is illustrated in Fig. 10.6.

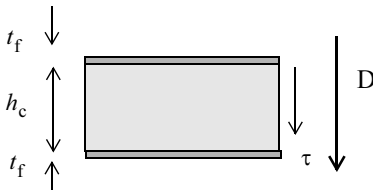


Fig. 10.6 Shear stress

10.3.3 Failure modes

Typical failure modes with respect to strength are:

- **Facing failure:** Initial failure may occur in either compression or tension in the face sheet caused by insufficient panel thickness, face sheet thickness or face sheet strength.
- **Transverse shear failure:** Caused by insufficient core strength or panel thickness.
- **Local crushing of core:** Caused by low core compression strength.

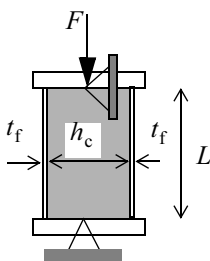
Table 10.2 Failure modes with respect to strength (Continued)

Failure modes of sandwich construction	
Failure mode	Design equation
Facing failure	$\sigma_f = \frac{M}{h_c t_f} + \frac{N}{2t_f}$
Transverse shear failure	$\tau_c = \frac{D}{h_c}$
Local crushing of core	$\sigma_c = \frac{F}{A}$

where A (m^2) is the area of load introduction and F local force (N).

10.4 Buckling Sandwich Columns

Let L denote the length of the column, F the axial compression force, the core thickness h_c and the shear modulus G_c , the face sheets have a thickness t_f , a width b and an axial elastic modulus E_f . The sandwich column is illustrated in Fig. 10.7.

**Fig. 10.7** Sandwich Column

The weakest bending stiffness of the sandwich column $E_f I$ can be approximated by

$$E_f I = 2E_f b t_f \left(\frac{h_c + t_f}{2} \right)^2 + \frac{1}{6} E_f b t_f^3 \approx \frac{E_f b t_f h_c^2}{2}, \quad t_f \ll h_c. \quad (10.6)$$

The shear stiffness of the sandwich column $G_c A$ is given by

$$G_c A = G_c b h_c. \quad (10.7)$$

The Euler buckling of a pinned-pinned column is

$$F_{\text{Euler}} = \frac{\pi^2 E_f I}{L^2} = \frac{\pi^2 E_f b t_f h_c^2}{2L^2} \quad (10.8)$$

In the paper of Bazant [Bazant 2003], two expressions are given to calculate the critical compression load for a sandwich column

$$F_{\text{cr}} = \frac{F_{\text{Euler}}}{1 + \frac{F_{\text{Euler}}}{G_c b h_c}}, \quad \text{Engesser type} \quad (10.9)$$

and

$$F_{\text{cr}} = \frac{G_c b h_c}{2} \left[\sqrt{1 + \frac{4F_{\text{Euler}}}{G_c b h_c}} - 1 \right], \quad \text{Haringx type.} \quad (10.10)$$

Engesser published his equation in 1889 and Haringx published his equation in 1942.

Equation (10.9) is also mentioned in the book of Allen [Allen 1969].

10.5 Global Buckling Cylinder

The compression stresses introduced into the faces of the sandwich cylinder subjected to an axial compression load F , where

$$F = 2\pi R N_x. \quad (10.11)$$

The compression stress $\sigma_{x,f}$ in the both equal thickness face sheets with thickness t_f is given by

$$\sigma_{x,f} = \frac{N_x}{2t_f}. \quad (10.12)$$

where N_x is the constant running load (N/m) and R is the mean radius of the cylinder. The critical value $N_{x,\text{cr}}$ of the running load per unit of circumference of a long cylinder, simply supported, is [Vinson 1999]

$$N_{x, \text{cr}} = \gamma \frac{2E_f}{\sqrt{(1-\nu_f^2)}} \frac{h_c t_f}{R} \left\{ 1 - \frac{E_f}{2\sqrt{(1-\nu_f^2)} R G_c} \frac{t_f}{h_c} \right\}, \quad (10.13)$$

where E_f is the Young's modulus, ν_f is the Poisson's ratio of the face sheet material and G_c is the shear modulus of the core.

γ is the knock down factor related to initial imperfections and is given by, [NASA SP-8007]

$$\gamma = 1 - 0.901(1 - e^{-\phi}), \quad (10.14)$$

where

$$\phi = \frac{\sqrt{2}}{29.8} \sqrt{\frac{R}{h_c}}. \quad (10.15)$$

In case $\sigma_{x, \text{cr}} = \frac{N_{x, \text{cr}}}{2t_f}$ is above the yield stress, the Young's modulus E_f shall be corrected with a plasticity factor η . In [NASA SP-8007] it is recommended to replace E_f with ηE_f , where

$$\eta = \frac{\sqrt{E_{\text{sec}} E_{\tan}}}{E_f}, \quad (10.16)$$

where E_{sec} is the secant and E_{\tan} is the tangent modulus of elasticity. The secant and the tangent modulus of elasticity are illustrated in Fig. 10.8 and can be found in material handbooks.

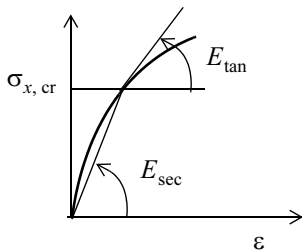


Fig. 10.8 Stress-strain curve

Example

We have a sandwich plate with Al-alloy face sheets and a Al-alloy honey comb core 1/4-5056-.0015p (Table 10.5)

where

- $t_f = 0.2$, $h_c = 20$, $d_c = 6.4$ mm
- $E_f = 70$ GPa
- $E_c = 2.17$ MPa
- $G_L = 345$, $G_T = 152$, $G_c = \sqrt{G_L G_T} = 229$ MPa

End of example

10.6 Local Buckling

The load carrying capability or strength properties of the sandwich construction are strongly influenced and reduced, due to local buckling. At local buckling the actual stress is beyond load carrying capability of sandwich construction, e.g. in the face sheets or in the core. The following local buckling (failure modes) can be identified:

- **Wrinkling of face sheets (faces):** The skin may buckle inwards or outwards, depending on the flatwise compression strength of the core flat-wise tensile strength of skin/core bond [Ley 1999]. A strong bond may cause a core tension failure. The skin flatness affects wrinkling load.
- **Dimpling of face sheets:** For cellular (honeycomb) or corrugated cores, where skins may buckle or dimple into the spaces between core walls or corrugations. Dimples may be permanent and grow across cell walls to form wrinkles.
- **Shear crimpling:** Appears as a local mode of failure, but is a general (global) form of buckling. Occurs suddenly, often with core failure at crimp; also may cause shear failure of skin/core bond.

The design equations for the mentioned local buckling failures are given in Table 10.3.

Table 10.3 Local buckling of sandwich construction

Local buckling of sandwich construction	
Failure mode	Design equation
Face sheet wrinkling ^a [Ley 1999]	$\sigma_{cr,w} = 0.5\sqrt[3]{\eta E_f E_c G_c}$
Face sheet dimpling (intercellular buckling)	$\sigma_{cr,d} = 2.0\eta \frac{E_f}{1 - v_f^2} \left(\frac{t_f}{d_c} \right)$
Shear crimpling	$\sigma_{cr,s} = 0.5 \left(\frac{h_c}{t_f} \right) G_c$

a. Minimum factor used

where:

d_c is the diameter of the cell (honeycomb core) (m)

σ_{cr} is the buckling stress (Pa)

η is the reduction factor when the buckling stress is beyond the yield stress.

The Young's modulus is corrected (reduced modulus). If the buckling stress is below the yield stress $\eta = 1$. The reduction factor may be

$$\eta = 2 \frac{E_{tan}}{E_{tan} + E_f} \text{ where } E_{tan} \text{ is the tangent modulus of elasticity at } \sigma_{cr}.$$

G_c is the shear modulus of the core, generally taken as $G_c = \sqrt{G_L G_T}$, (Pa)

Example

We have a sandwich plate with Al-alloy face sheets and an Al-alloy honeycomb core 1/4-5056-.0015p (Table 10.5)

with

- $t_f = 0.2$, $h_c = 20$, $d_c = 6.4$ mm
- $E_f = 70$ GPa
- $E_c = 2.17$ MPa
- $G_L = 345$, $G_T = 152$, $G_c = \sqrt{G_L G_T} = 229$ MPa

The calculated critical stresses become for:

- Wrinkling $\sigma_{cr,w} = 0.5\sqrt[3]{E_f E_c G_c} = 163$ MPa
- Dimpling $\sigma_{cr,d} = 2.0 \frac{E_f}{1 - v_f^2} \left(\frac{t_f}{d_c} \right) = 4.8$ GPa, plasticity factor η must be used

to correct (lower) the dimpling stress.

- Shear crippling $\sigma_{cr,s} = 0.5 \left(\frac{h_c}{t_f} \right) G_c = 11 \text{ GPa}$, thus no problem

End of example

10.6.1 Combined Loads

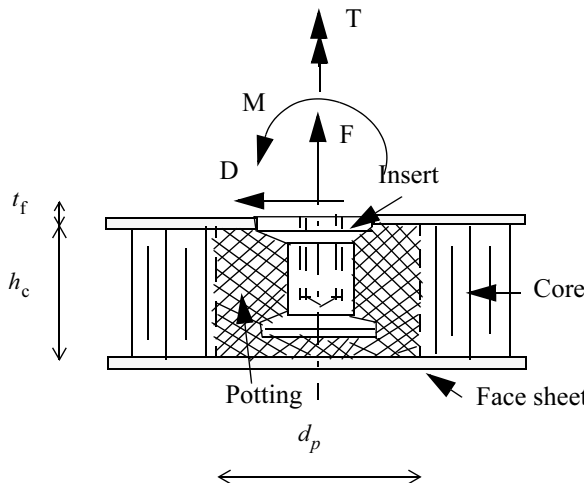
When two principal stresses are in compression the following interaction equation for wrinkling is suggested [Ley 1999] to calculate the margin of safety using

$$MS = \frac{1}{\left(\frac{\sigma_1}{\sigma_{cr,w1}} \right)^3 + \left(\frac{\sigma_2}{\sigma_{cr,w2}} \right)} - 1 \geq 0. \quad (10.17)$$

10.7 Inserts

Inserts are bonded in the sandwich construction core and used to introduce loads in the sandwich construction. The insert is embedded in a potting material, generally with a cylindrical shape. The potting shall be capable to transfer loads from the insert into the core. The insert configuration is shown in Table 10.9. Inserts are used to connect bracketery to the sandwich construction, e.g. boxes, cleats to connect panels to each other.

Inertia loads introduce the following loads via the inserts in the sandwich construction (Fig. 10.9), with D the shear force (N), F the pull out / compression load (N), M the bending moment (Nm) and T the torque (Nm).

**Fig. 10.9** Insert loads

The contribution of the typical sandwich element to load capability of inserts is indicated in Table 10.4, [Insert Design Handbook, ESA/PSS-03-1202].

Table 10.4 Contribution of sandwich components to insert's load capability

Load type	Contribution of Sandwich Components to Inserts' Load capability		
	Core	Face sheet	Core/face sheet adhesive
Tension F	major	medium	very little
Compression F	major	medium	little
Shear D	little	major	very little
Bending M	major	medium	little
Torsion T	major	little	little

The pre-stress in the bolts, due to prescribed torques, is taken by the winding of the threads and is not transferred into the sandwich construction.

The quasi-static loads are for boxes less critical than random loads caused by the random vibrations.

The 3σ acceleration $\ddot{x}_{3\sigma}$, caused by random vibrations, can be calculated with Miles' equation

$$\ddot{x}_{3\sigma} = 3 \sqrt{\frac{\pi}{2} f_n Q W(f_n)} . \quad (10.18)$$

with f_n the natural frequency of mode with significant effective mass of the mechanical system (e.g. spacecraft), Q the amplification factor (in general,

$\mathcal{Q} = \frac{1}{2\zeta} = 10$ is assumed) and $W(f_n)$ the power spectral density of the base acceleration at the natural frequency f_n , $\left(\frac{g^2}{Hz}\right)$.

The 3σ random inertia load $F_{3\sigma}$ can be obtained with

$$F_{3\sigma} = M\ddot{x}_{3\sigma}, \quad (10.19)$$

where M is the mass (kg) of the box.

10.8 Honeycomb mechanical properties

The mechanical properties of frequently applied Al-alloy 5056 honeycomb cores are illustrated in Table 10.5. These material properties are taken from [TSB 120, TSB 124].

Table 10.5 Honeycomb core properties

Type of Honey-comb core	d_c cell (mm)	ρ_c (kg/m^3)	Compr. strength E_c	Shear modulus		Shear strength	
				(MPa)	(MPa)	(MPa)	(MPa)
1/4-5056-.002p	6.4	69	3.21	462	186	2.24	1.31
3/8-5056-.0007p	9.6	16	0.24	103	62	0.31	0.17
1/4-5056-.0015p	6.4	54	2.17	345	152	1.59	0.90
1/4-5056-.0007p	6.4	26	0.55	138	83	0.54	0.26
3/16-5056-.002p	4.8	91	5.07	648	248	3.31	1.93

10.9 Typical connections

Some examples of sandwich construction connection are illustrated in Fig. 10.10.

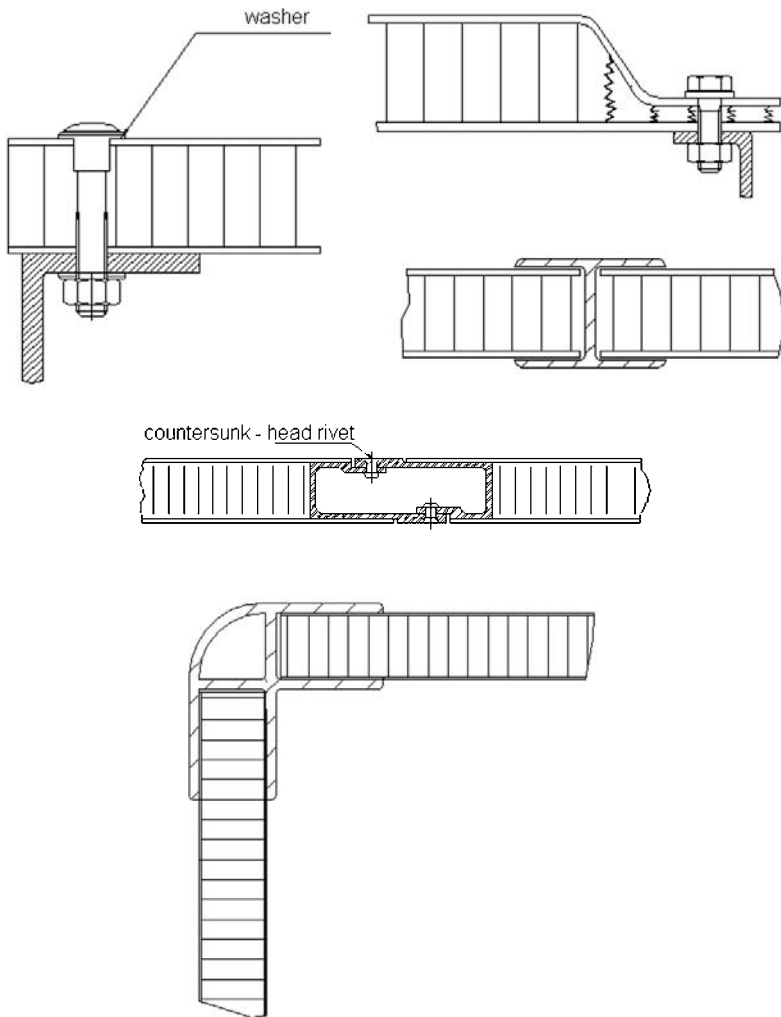


Fig. 10.10 Typical sandwich edge connections

10.10 Literature

- Allen, Howard, G., 1969, *Analysis and Design of Structural Sandwich Panels*, Pergamon Press.
- Bazant, Z.P., 2003, *Shear Buckling of Sandwich Fiber Composite and Lattice Columns, Bearings, and Helical Springs: Paradox Resolved*, Journal of Applied Mechanics, Vol. 70, pages 70–83
- Bladel van, P.G., 1995, *Design of Fibre Reinforced Composite Panels for Aerospace Applications*, ISBN 90-900838-X, PhD work, Delft University of Technology, Faculty of Aerospace Engineering, The Netherlands.
- Gibson, L.J., Ashby, M.F., 1997, *Cellular Solids: structure & properties*, Cambridge University Press, ISBN 0521 499119 9 (paperback).
- Hexcel company, TSB 120, 1992, *Mechanical Properties of Hexcel Honeycom Materials*.
- Hexcel company, TSB 124, 1991, *Bonded Honeycom Sandwich Construction*.
- Klein, B., 2001, *Leichtbau-Konstruktion, Berechnunggrundlagen und Gestaltung*, 5. Auflage, ISBN 3-528-44115-1, Vieweg.
- Ley, R.P., Lin, W. and Mbanefo, U., 1999, *Facesheets Wrinkling in Sandwich Structures*, NASA/CR-1999-208994.
- NASA SP-8007, August 1968, *Buckling of Thin-Walled Circular Cylinders*, NASA Space Vehicle Design Criteria (Structures).
- Peters, S.T.(editor), 1998, *Handbook of composites*, second edition, ISBN 0 412 54020 7, Chapman & Hall.
- Plantema, Frederik, J., 1966, *Sandwich Construction, The bending of buckling of sandwich beams, plates, and shells*, Wiley.
- Vinson, J.R., 1999, *The Behaviour of sandwich Structures of Isotropic and Composite Materials*, ISBN 1-56676-699-0, Technomic Publishing Company Inc.
- Zenkert, Dan, 1997, *An Introduction to Sandwich Construction*, Emas Publishing, ISBN 0 947817 77 8.

10.11 Exercises

10.11.1 Stiffness Sandwich Beam

A sandwich beam is simply supported at both ends as illustrated in Fig. 10.11.

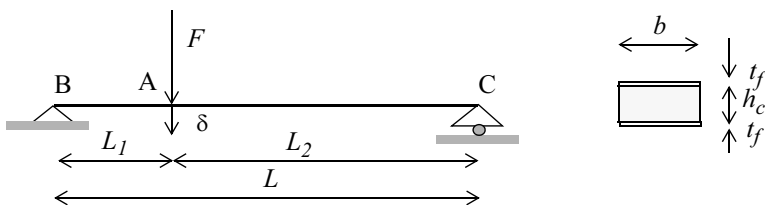


Fig. 10.11 Sandwich beam

The face sheets are made of an Al-alloy with a Young's modulus E_f . The shear modulus of the honeycomb core is G_c . Work out the following assignments:

- Calculate bending stiffness D of the beam and neglect higher order terms of t_f .
- Calculate the shear stiffness V of the beam neglecting the shear stiffness of the face sheets.
- Calculate the displacement δ_b due to pure bending.
- Calculate the displacement δ_s due to pure shear.
- Calculate the stiffness k at point A.
- Design the edge members at the point B and C.

Answers: $D = \frac{1}{2}E_f h_c^2 t_f$, $V = G_c b h_c$, $\delta_b = \frac{FL_1^2 L_2^2}{3DL}$, $\delta_s = \frac{FL_1 L_2}{VL}$, $k = \frac{F}{\delta_b + \delta_s}$

11 Finite Element Analysis

11.1 Introduction

After the initial sizing of the spacecraft structure, the strength- and stiffness characteristics are usually calculated with the finite element method. Since the structure of the spacecraft is complicated, it is almost impossible to solve the strength problems only with pure analytical solutions. There are many commercial finite element method programmes available on the market.

Important points of consideration for static and dynamic calculations with finite element models are:

- the theory
- number of nodes
- number of degrees of freedom
- choice of element type
- boundary conditions
- damping
- joints
- applied loads
- mass distribution
- material properties

11.2 Theory

The theory of the finite element method is summarised briefly for static and dynamic analyses. For static analyses the equilibrium equations are derived using the minimum principle of potential energy, and the equations of motion are derived using the equations of Lagrange.

It is recommended to look into the literature regarding the finite element method [NAFEMS 1992, Cook 1989, Crisfield 1986]. The finite element method is only touched upon briefly in the next sections.

11.2.1 Static Calculations

The energy method is applied frequently in the theory of the finite element method. To this end, the minimum principle of the potential energy is used. For the kinematic permissible displacement function u , a function u is chosen that makes the total potential energy $V(u)$ stationary. Mathematically this means that:

$$\delta V(u) = 0. \quad (11.1)$$

Where static analyses are concerned, the potential energy is given by:

$$V(u) = U(u) - W(u) \quad (11.2)$$

where U is the strain energy, $U = \frac{1}{2} \int_V \{\varepsilon\}^T [C] \{\varepsilon\} dV$, W is the work done by

the external load vector $\{F\}$; $W = \int_V \{F\}^T \{u\} dV$, $\{\varepsilon\}$ is the strain vector (6*1),

$[C]$ is the general constitutive matrix, with $\{\sigma\} = [C]\{\varepsilon\}$, V is the volume and $\{\sigma\}$ the stress vector (6*1).

When the elastic system is divided up into finite elements, then:

$$U = \sum_n U_e, \quad (11.3)$$

and

$$W = \sum_n W_e, \quad (11.4)$$

where n is the number of elements, U_e is the finite element strain energy

$U_e = \frac{1}{2} \int_{V_e} \{\varepsilon_e\}^T [C_e] \{\varepsilon_e\} dV_e$ and W_e is the finite element work done

$$W_e = \int_{V_e} \{F_e\}^T \{u_e\} dV_e.$$

In an element we assume a displacement (shape) function $\lfloor H \rfloor$ in such a way that

$$u_e = \lfloor H \rfloor \{\delta_e\}. \quad (11.5)$$

The vector $\{\delta_e\}$ represents the displacements and the rotations in the nodes of the element. The strain vector is obtained by differentiating the displacement function.

$$\{\varepsilon_e\} = \delta u_e = \delta(\lfloor H \rfloor \{\delta_e\}) = \delta \lfloor H \rfloor \{\delta_e\} = [B] \{\delta_e\}, \quad (11.6)$$

where δ is a differential operator and the matrix $[B]$ is the strain-displacement matrix.

Example

A simple truss finite element (only tension/compression) has two nodes and two degrees of freedom. This 1-D element is shown in Fig. 11.1.

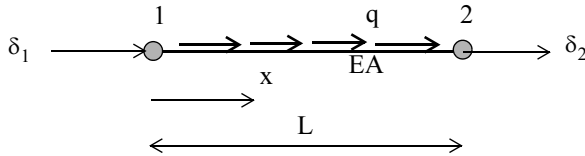


Fig. 11.1 Truss finite element

The displacement function $u(x)$ is defined as

$$u_e(x) = \lfloor H \rfloor \{\delta_e\} = \begin{bmatrix} 1 & -\frac{x}{L} & \frac{x}{L} \end{bmatrix} \begin{Bmatrix} \delta_1 \\ \delta_2 \end{Bmatrix}.$$

The strain $\varepsilon_e(x)$ in the truss is

$$\varepsilon_e(x) = \frac{du_e(x)}{dx} = \begin{bmatrix} 0 & 1 & 1 \end{bmatrix} \begin{Bmatrix} \delta_1 \\ \delta_2 \end{Bmatrix} = \lfloor B \rfloor \begin{Bmatrix} \delta_1 \\ \delta_2 \end{Bmatrix} = \frac{\delta_2 - \delta_1}{L}.$$

The strain is constant along the length of the truss finite element.

End of example

Substituting (11.6) in the element strain energy the strain energy becomes

$$U_e = \frac{1}{2} \int_{V_e} \{\varepsilon_e\}^T [C_e] \{\varepsilon_e\} dV_e = \frac{1}{2} \{\delta_e\}^T \int_{V_e} \{B\}^T [C_e] \{B\} dV_e \{\delta_e\}. \quad (11.7)$$

The stiffness matrix of the finite element is defined as

$$[K_e] = \int_{V_e} \{B\}^T [C_e] \{B\} dV_e. \quad (11.8)$$

The work done by the forces $\{F_e\}$, using (11.5), can be expressed as

$$W_e = \int_{V_e} \{F_e\}^T \{u_e\} dV_e = \int_{V_e} \{u_e\}^T \{F_e\} dV_e = \int_{V_e} \{H\}^T \{F_e\} dV_e \{\delta_e\}. \quad (11.9)$$

The nodal force vector $\{F_{\delta_e}\}$ is now defined by

$$\{F_{\delta_e}\} = \int_{V_e} \{H\}^T \{F_e\} dV_e. \quad (11.10)$$

Continuation of example

The matrix $[C]$ is for the 1-D case is the Young's modulus E , because there is a simple one dimensional stress-strain relation

$$\sigma = E\varepsilon = C\varepsilon.$$

The stiffness matrix $[K_e]$ becomes

$$[K_e] = \int_{V_e} \{B\}^T [C_e] \{B\} dV_e = A \int_0^L \begin{Bmatrix} -\frac{1}{L} \\ \frac{1}{L} \end{Bmatrix} E \left\{ -\frac{1}{L}, \frac{1}{L} \right\} dx,$$

thus

$$[K_e] = EA \int_0^L \begin{Bmatrix} \left(\frac{1}{L}\right)^2 & -\left(\frac{1}{L}\right)^2 \\ -\left(\frac{1}{L}\right)^2 & \left(\frac{1}{L}\right)^2 \end{Bmatrix} dx = \frac{EA}{L} \begin{bmatrix} 1 & -1 \\ -1 & 1 \end{bmatrix}. \quad (11.11)$$

The truss is loaded with a uniform load along the length of the truss q (N/m).

The nodal force vector $\{F_{\delta_e}\}$ becomes with

$$\{F_{\delta_e}\} = \int_{V_e} \{H\}^T \{F_e\} dV_e = \int_0^L \begin{Bmatrix} 1 - \frac{x}{L} \\ \frac{x}{L} \end{Bmatrix} q(x) dx,$$

furthermore

$$\{F_{\delta_e}\} = q \int_0^L \begin{Bmatrix} 1 - \frac{x}{L} \\ \frac{x}{L} \end{Bmatrix} dx = q \begin{Bmatrix} \frac{L}{2} \\ \frac{L}{2} \end{Bmatrix}. \quad (11.12)$$

The rigid body mode $\{\phi_r\}$ of the truss with two DOFs is

$$\{\phi_r\} = \begin{Bmatrix} 1 \\ 1 \end{Bmatrix}.$$

The strain energy associated with the rigid mode $\{\phi_r\}$ is defined as

$$U_{rb} = \frac{1}{2} \{\phi_r\}^T [K_e] \{\phi_r\} = \frac{EA}{2L} \begin{bmatrix} 1 & 1 \end{bmatrix} \begin{bmatrix} 1 & -1 \\ -1 & 1 \end{bmatrix} \begin{Bmatrix} 1 \\ 1 \end{Bmatrix} = 0.$$

This result has been expected! No strain will occur when the truss moves as a rigid body.

End of example

Suppose that the displacement vector $\{\delta_e\}$ is related to a global system of nodal displacements $\{\delta\}$, then:

$$\{\delta_e\} = [T_e]\{\delta\}, \quad (11.13)$$

where $[T_e]$ is the transformation matrix.

The potential energy can be written

$$V(\delta) = \frac{1}{2} \sum_n \{\delta_e\}^T [K_e] \{\delta_e\} - \sum_n \{\delta_e\}^T \{F_e\}. \quad (11.14)$$

Introducing (11.13) in (11.14) the potential energy of the complete system will result in

$$V(\delta) = \frac{1}{2} \sum_n \{\delta\}^T [T_e]^T [K_e] [T_e] \{\delta\} - \sum_n ([T_e]^T \{F_e\}) \{\delta\}, \quad (11.15)$$

hence

$$V(\delta) = \frac{1}{2} \{\delta\}^T \left(\sum_n [T_e]^T [K_e] [T_e] \right) \{\delta\} - \left(\sum_n [T_e]^T \{F_e\} \right) \{\delta\}, \quad (11.16)$$

and

$$V(\delta) = \frac{1}{2} \{\delta\}^T [K] \{\delta\} - \{F\} \{\delta\} . \quad (11.17)$$

The stationary value of the potential energy becomes

$$\partial V(\delta) = [K]\{\delta\} - \{F\} = 0, \quad (11.18)$$

and finally the equilibrium equations of the finite element method are obtained

$$[K]\{\delta\} = \{F\} . \quad (11.19)$$

Example

In Fig. 11.2 two simple rod elements are coupled to 3 nodes, node 1, 2 and 3. The model has 3 DOFs; δ_1 , δ_2 and δ_3 . The stiffness matrix of one element is given by (11.11). The elements are loaded by the uniform load q . The associated load vector is given by (11.12).

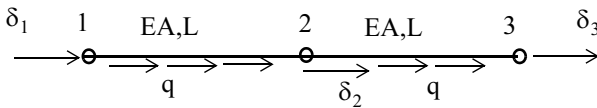


Fig. 11.2 Two element finite element model

The transformation matrices for both elements are

$$[T_{e,1}]^T = \begin{bmatrix} 1 & 0 \\ 0 & 1 \\ 0 & 0 \end{bmatrix}, [T_{e,2}]^T = \begin{bmatrix} 0 & 0 \\ 1 & 0 \\ 0 & 1 \end{bmatrix}.$$

The total stiffness matrix $[K]$ becomes

$$[K] = [T_{e,1}]^T [K_{e,1}] [T_{e,1}] + [T_{e,2}]^T [K_{e,2}] [T_{e,2}],$$

so

$$[K] = \frac{AE}{L} \begin{bmatrix} 1 & -1 & 0 \\ -1 & 1 & 0 \\ 0 & 0 & 0 \end{bmatrix} + \frac{AE}{L} \begin{bmatrix} 0 & 0 & 0 \\ 0 & 1 & -1 \\ 0 & -1 & 1 \end{bmatrix} = \frac{AE}{L} \begin{bmatrix} 1 & -1 & 0 \\ -1 & 2 & -1 \\ 0 & -1 & 1 \end{bmatrix}.$$

The total load vector $\{F\}$ becomes

$$\{F\} = [T_{e,1}]^T [F_{e,1}] + [T_{e,2}]^T [F_{e,2}],$$

and therefore

$$\{F\} = qL \begin{bmatrix} \frac{1}{2} \\ \frac{1}{2} \\ \frac{1}{2} \\ 0 \end{bmatrix} + qL \begin{bmatrix} 0 \\ \frac{1}{2} \\ \frac{1}{2} \\ \frac{1}{2} \end{bmatrix} = qL \begin{bmatrix} \frac{1}{2} \\ \frac{1}{2} \\ 1 \\ \frac{1}{2} \end{bmatrix}.$$

End of example

11.2.2 Dynamic Calculations

Where dynamic finite element analyses are concerned, besides the potential energy $V(u)$, the kinetic energy $T(\dot{u})$, the damping energy $D(u, \dot{u}, ..)$ and the work performed by the forces $W(F, u)$ must be considered. The kinetic energy contains the mass- and velocity terms. The damping energy is extracted from the total energy of the dynamic system. To begin with, the assumption is made that the dynamic systems are undamped.

For a displacement function u the Lagrangian function (Kinetic Potential) $L(u, \dot{u})$ is defined as follows:

$$L(u, \dot{u}) = T(\dot{u}) - V(u), \quad (11.20)$$

and the work done by the applied forces is $W(u)$.

Example

For a SDOF system with spring stiffness k and mass m with a motion x the Lagrangian becomes

$$L(x, \dot{x}) = \frac{1}{2}m\dot{x}^2 - \frac{1}{2}kx^2.$$

End of example

The equations of Lagrange are (without damping energy):

$$\frac{d}{dt} \left(\frac{\partial L(u, \dot{u})}{\partial \dot{u}} \right) - \left(\frac{\partial L(u, \dot{u})}{\partial u} \right) = \frac{\delta W(F, u)}{\delta u}, \quad (11.21)$$

where $\delta W(F, u) = \sum_l F_l \delta u_l$ is the virtual work done by the external forces.

Example

For a SDOF system with a displacement x and an external force F , the virtual work done by the external force is

$$\delta W = F\delta x.$$

End of example

The kinetic energy $T(\dot{u})$ of a body with volume V can be written as

$$T(\dot{u}) = \frac{1}{2} \int_V m(x, y, z) \dot{u}^2(x, y, z) dV. \quad (11.22)$$

When the elastic system is divided up into finite elements, then

$$T_{system}(\dot{u}) = \sum_e T_e(\dot{u}_e), \quad (11.23)$$

with

$$T_e(\dot{u}) = \frac{1}{2} \int_{V_e} m(x, y, z) \dot{u}_e^2(x, y, z) dV_e. \quad (11.24)$$

In an element we assume a displacement (shape) function $\lfloor H \rfloor$ in such a way that (see (11.5))

$$u_e = \lfloor H \rfloor \{\delta_e\}.$$

The vector $\{\delta_e\}$ represents the displacements and the rotations in the nodes of the element.

The kinetic energy in an element then becomes:

$$T_e(\dot{u}) = \frac{1}{2} \int_{V_e} m(x, y, z) \dot{u}_e^2(x, y, z) dV_e = \frac{1}{2} \int_{V_e} \{\dot{\delta}_e\}^T \{H\} m(x, y, z) \lfloor H \rfloor \{\dot{\delta}_e\} dV_e, \quad (11.25)$$

or

$$T_e(\dot{u}) = \frac{1}{2} \int_{V_e} \{\dot{\delta}_e\}^T \{H\} m(x, y, z) \lfloor H \rfloor \{\dot{\delta}_e\} dV_e = \frac{1}{2} \{\dot{\delta}_e\}^T [M_e] \{\dot{\delta}_e\}. \quad (11.26)$$

The mass matrix of the element is:

$$[M_e] = \int_{V_e} \{H\} m(x, y, z) \lfloor H \rfloor dV_e. \quad (11.27)$$

Example

A simple truss finite element (only tension/compression) has two nodes and two degrees of freedom. This 1-D element is shown in Fig. 11.1. The mass per unit of length is m (kg/m)

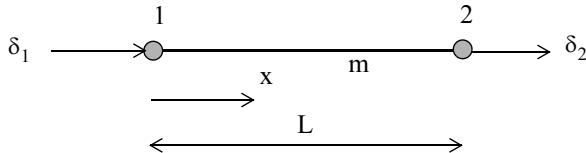


Fig. 11.3 Truss finite element

The displacement function $u(x)$ is defined as

$$u_e(x) = \lfloor H \rfloor \{ \delta_e \} = \begin{bmatrix} 1 - \frac{x}{L} & \frac{x}{L} \end{bmatrix} \begin{Bmatrix} \delta_1 \\ \delta_2 \end{Bmatrix}.$$

The mass matrix $[M_e]$ can be obtained by

$$[M_e] = \int_{V_e} \{H\}^T m \lfloor H \rfloor dV_e = \int_0^L \begin{Bmatrix} 1 - \frac{x}{L} \\ \frac{x}{L} \end{Bmatrix} m \left\{ 1 - \frac{x}{L} \frac{x}{L} \right\} dx,$$

and finally the mass matrix $[M_e]$ becomes

$$[K_e] = m \int_0^L \begin{Bmatrix} \left(1 - \frac{x}{L}\right)^2 & \left(\frac{x}{L}\right)\left(1 - \frac{x}{L}\right) \\ \left(\frac{x}{L}\right)\left(1 - \frac{x}{L}\right) & \left(\frac{x}{L}\right)^2 \end{Bmatrix} dx = \frac{mL}{6} \begin{bmatrix} 2 & 1 \\ 1 & 2 \end{bmatrix}.$$

The rigid body mode $\{\phi_r\}$ of the truss with two DOFs is

$$\{\phi_r\} = \begin{Bmatrix} 1 \\ 1 \end{Bmatrix}.$$

The total mass M_{tot} of the truss element can be calculated using the rigid body mode $\{\phi_r\}$

$$M_{tot} = \{\phi_r\}^T [M_e] \{\phi_r\} = \frac{mL}{6} \begin{bmatrix} 1 & 1 \end{bmatrix} \begin{bmatrix} 2 & 1 \\ 1 & 2 \end{bmatrix} \begin{Bmatrix} 1 \\ 1 \end{Bmatrix} = mL$$

This result has been expected!

End of example

The Lagrangian function for the entire dynamic system is given by:

$$L(u, \dot{u}) = \frac{1}{2} \{\dot{\delta}\}^T \left[\sum_n [T_e]^T [M_e] [T_e] \right] \{\dot{\delta}\} - \frac{1}{2} \{\delta\}^T \left[\sum_n [T_e]^T [K_e] [T_e] \right] \{\delta\}, \quad (11.28)$$

or

$$L(u, \dot{u}) = \frac{1}{2} \{\dot{\delta}\}^T [M] \{\dot{\delta}\} - \frac{1}{2} \{\delta\}^T [K] \{\delta\}. \quad (11.29)$$

The virtual work of the external forces are

$$\delta W = \{F\}^T \delta \{\delta\}. \quad (11.30)$$

From the Lagrange equation (11.21) it follows that:

$$\frac{d}{dt} \left(\frac{\partial L(u, \dot{u})}{\partial \dot{u}} \right) = [M] \{\ddot{\delta}\},$$

and

$$\frac{\partial L(u)}{\partial u} = [K] \{\delta\}.$$

The force vector will be extracted from the virtual work.

The undamped equations of motion of the dynamic system now become

$$[M] \{\ddot{\delta}\} + [K] \{\delta\} = \{F\}. \quad (11.31)$$

Now we proceed with the modelling aspects of the finite element method.

11.3 Mathematical Model

In order to analyse the structure of a spacecraft or another sub-systems with all of its experiments, antennas, solar panels, etc., a mathematical model or a finite element model must first be created. This mathematical model serves as the input for the finite element programme, and is divided up into a grid made up of nodes, between which there are, supposedly, finite elements that describe the geometry and the stiffness characteristics of the structure. The mathematical model of the spacecraft, however, is no more than a good approximation of reality even though advanced techniques (such as a combination of a pre-processor, finite element pro-

gramme and post-processor) are used. The displacement method is generally used. The force method has become dated. When modelling the structure one must take care in selecting the type of finite element, the number of degrees of freedom, load and mass distributions, joints and assumed values for the damping, the viscous or the hysteresis model.

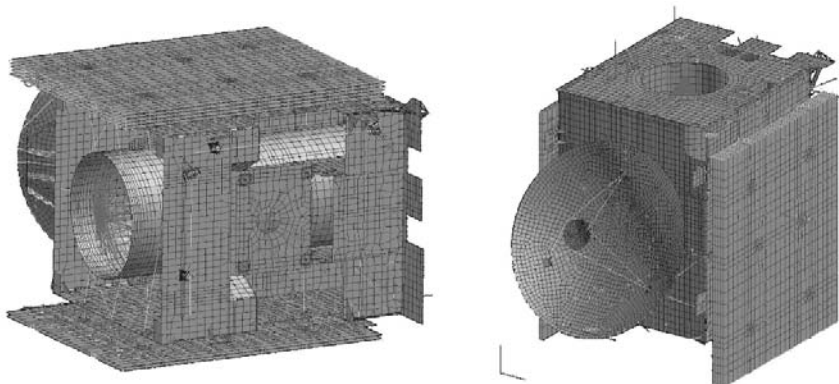


Fig. 11.4 Rosetta finite element model [FEM]

A MSC.Nastran® finite element model of the Rosetta spacecraft is shown in Fig. 11.4. The Rosetta mission is an interplanetary mission whose main objective is to rendezvous with and make in-situ measurements of comet 46 P/Wirtanen, in August 2012. The spacecraft will also carry the Rosetta Lander (Surface Science Package) to the nucleus and deploy it onto the comet's surface. The Lander is provided by a German-led consortium of European institutes

11.4 Finite element type

The choice of the element type (one-, two-, or three dimensional) is closely related to the construction of the structure. In general, one chooses membrane elements for very thin sheets, sandwich elements for sandwich structures and a bending beam to model the stiffeners and the rings.

When composite materials are used, the finite element is chosen such that it can adequately represent the material properties.

In the idealisation of the model, more elements are used where stress concentrations are expected and fewer elements are used where stress variations are minimal. The displacement functions that are used in the elements also determine the number of elements. Recent developments in the theory of the finite element methods allow the accuracy of the finite element analyses to be determined afterwards.

Boundary elements are gaining popularity for “voluminous” structures. The advantage of these types of elements is that only the surface area of the sheet of the structure needs to be modelled. The use of boundary elements limits the number of degrees of freedom, but the system matrices are completely filled; there is no matrix band structure.

11.5 Number of degrees of freedom

The accuracy and the costs of the analysis are more or less governed by the number of degrees of freedom (DOF) or equilibrium equations of the mathematical model of the satellite structure. The number of degrees of freedom per node is usually six; three translations (displacements) and three rotations. The number of degrees of freedom in the calculation of the dynamic characteristics of the satellite structure is an important aspect in the costs.

Eigenvalue analyses demand relatively large amounts of computer time as compared to static analyses. In order to decrease the costs of the relatively expensive eigenvalue analyses, the number of “dynamic” degrees of freedom is usually limited. The total number of degrees of freedom is reduced or condensed to a limited number of “dynamic” degrees of freedom.

11.6 Joints

Connections between the various structural parts are generally roughly included or completely left out of the mathematical model of the total structure. If one desires to do so, this will usually lead to an excessive number of nodes. Joints are sometimes a weak link in the structure, so that the stiffness of the structure is usually slightly overestimated.

11.7 Damping

The response of structures, as a result of the dynamic loads, depends strongly on the damping properties. It is therefore very important to be aware of the damping properties of the structure. The mechanisms that cause damping in a satellite structure are difficult to understand. The most important causes of damping are; damping in the material, damping in the joints, damping due to effects of the air. Efforts have been made to model the damping mathematically with viscous-, structural-, visco-elastic-, Coulomb-, or general non-linear damping.

For space purposes damping models are generally used in which the damping is proportional to the velocity $\dot{x}(t)$:

$$F_{damping} = c\dot{x}(t), \quad (11.32)$$

with c the damping constant (Ns/m).

The damping is proportional to the velocity and can be expressed as a function of the critical damping:

$$c = \zeta c_{critical} = 2\zeta\sqrt{km}, \quad (11.33)$$

where k is the spring constant (N/m), m is the discrete mass (kg) and ζ is the damping ratio. The damped equation of motion of the damped mass-spring system then becomes:

$$\ddot{x}(t) + 2\zeta\omega_o\dot{x}(t) + \omega_o^2x(t) = \frac{F(t)}{m}, \quad (11.34)$$

where ω_o is the natural frequency (Rad/s), $\omega_o = \sqrt{\frac{k}{m}}$, $F(t)$ is the external force (N), $x(t)$ is the displacement (m), $\dot{x}(t)$ is the velocity (m/s) and $\ddot{x}(t)$ is the acceleration (m/s²).

Otherwise the damping is proportional to the elastic force $kX(\omega)$, yet 90° out of phase with the displacement $X(\omega)$:

$$F_{damping}(\omega) = jgkX(\omega), \quad (11.35)$$

where $X(\omega)$ is the displacement in frequency domain, $x(t) = X(\omega)e^{j\omega t}$, $j = \sqrt{-1}$ is the complex number and g is the structural damping (-).

The (hysteresis) damped equation of motion of the mass-spring system then becomes:

$$\ddot{X}(\omega) + \omega_o^2(1+jg)X(\omega) = \frac{F(\omega)}{m}, \quad (11.36)$$

with $F(\omega)$ is the external force in frequency domain, $F(t) = F(\omega)e^{j\omega t}$.

Both damping models are mainly used because the mathematical model is simple, they are, however, far-removed from physical reality. The structural damping model can only be applied when harmonic vibrations are considered.

Even though damping is important for response calculations of structures, a priori we know little about damping characteristics. The applied value for damping is difficult to obtain, even with the availability of hardware. This is because damping depends strongly on the applied loads. Damping values obtained with "modal analyses" are frequently too low because the excitation forces are low. Damping values obtained from mechanical vibration tests are more reliable. Variations of more than 100% are possible.

Averages for the value (modal ζ) of damping are given in the following table (Dornier study: “Study on damping representation related to spacecraft structural design”):

Table 11.1 Typical damping ratio's

Type of damping	Modal viscous damping ratio ζ %
Material damping	0.1–1
Air radiation damping	0.1–2
Damping in joints	2–5
Equipment damping	2–8
Damping materials	1–50

In his AIAA paper AIAA-98-1718 Kabe [Kabe 1998] gives an indication for the modal viscous damping in satellite- and rocket structures:

11.7.1 *Spacecraft*

In the beginning of a spacecraft project, when damping has not yet been measured, it is recommended to use $\zeta = 1\%$. It is recommended to use a $\zeta = 2 – 3\%$ for vibration modes where hinges, etc. move.

If light appendages are sturdily attached to the primary structure, then it is recommended to use $\zeta = 0.2\text{--}0.3\%$ for the appendages.

11.7.2 *Launch vehicles*

Rocket vibration modes typically have a damping ratio $\zeta = 1 – 2\%$.

11.8 Modifications

Modifications of the satellite structure are undesirable, since the mathematical model also has to be modified. Subdividing the mathematical model in sub models (substructures) can offer advantages. Changes in a number of sub models are more straightforward than changes in the entire mathematical model. The substructure technique can offer advantages.

11.9 Finite element model to be delivered

If necessary, each subsystem provides a finite element model (mathematical model) that is then integrated in the satellite system in order to carry out complete static or dynamic analyses. The primary contractor carries out the analyses on the satellite level. The desired finite element model must meet the established requirements. The following issues are usually mentioned in the requirements.

- Purpose of Finite Element Analysis (FEA)
- Coordinate system
- Units
- Node numbering scheme
- Element numbering scheme
- Material properties.
- Loads
- Boundary conditions
- Various tests on the finite element model
- Description finite element model
- Accuracy reduced model
- Electronic carrier and file structure

In this section the above mentioned topics will be dealt with in detail.

11.9.1 Coordinate systems

The primary contractor establishes the basic coordinate system wherein the coordinates of the nodes must be given. Local coordinate systems can always be linked to the basic coordinate system.

11.9.2 Units

It is a good practice to use the “SI” or “MKS” units:

- Length meters (m)
- Mass kilogram (kg)
- Time second (s)
- Force Newtons (N)
- Modulus of elasticity (Pa, N/m²)
- Density (kg/m³)

It is advisable to make use of the (m, kg, N, s) units as much as possible.

If one prefers to use millimetres (mm) instead of meters (m) then it is advisable to use the following units:

- Length millimeters (mm)
- Mass kilogram (T, 1000 kg)
- Time second (s)
- Force Newtons (N)
- Modulus of elasticity,
Young's modulus (N/mm²)
- Density (T/m³)

11.9.3 Numbering schemes

In general, in a finite element programme (such as MSC.Nastran®), all the numbers that refer to nodes, material references, element references, etc. must be numbered uniquely. To facilitate this, the primary contractor will provide intervals for numbering systems. For example; the numbers 16000 till 18500 must be used for the nodes of the solar panel.

11.9.4 Reaction forces in case unit forces of inertia occur

The finite element model is restrained statically determinate. Subsequently, a unit force of inertia is applied in each direction separately. The reaction forces in the restrained point act in the direction of translation, but with opposite sign, equal to the masses, determined as for the mass matrix as rigid body. The reaction moments are equal to the static moments.

$-S_{xy}$ is the reaction moment of unit forces of inertia in the x-direction, but about the y-direction.

11.9.5 Elastic Energy as Rigid Body

One way of testing the quality of a finite element model is by controlling the elastic energy as rigid body. The elastic (strain) energy “ U ” of a finite element model that experiences motion as rigid body must be equal to zero ($U=0$). The binary representation of a word in a computer is finite, for example 32–64 Bit. Round-off errors will therefore occur when carrying out matrix operations, such that the elastic energy, as a result of the motion as rigid body, is not exactly equal to zero. Thus the following requirement is set:

$$U = \delta \leq \varepsilon. \quad (11.37)$$

For example, $\varepsilon = 10 \times 10^{-3}$ is a requirement. Where reduced models are concerned, often a larger value is assigned because after reducing the mass- and stiffness matrix, greater round-off errors are permitted.

For $[M]$ the mass matrix and $[K]$ the stiffness matrix and ω_k^2 the eigenvalue and $\{\phi_k\}$ the associated mode form, the eigenvalue problem is defined as follows:

$$(-\omega_k^2[M] - [K])\{\phi_k\} = \{0\}. \quad (11.38)$$

If motion as rigid body is concerned, then, $\omega_{R,k}^2 = 0$ $k = 1, 2, \dots, 6$ the natural frequency equals to zero. The associated mode form is referred to as $\{\varphi_{R,k}\}$. A finite element model usually has six eigenvalues equal to zero (the six degrees of freedom for a rigid body in space). If there are more than six eigenvalues equal to zero then the finite element model has hidden or other mechanisms that are generally not allowed. If there are less than 6 degrees of freedom then it is possible that hidden boundary conditions were applied at some point.

Thus for the motion as rigid body it holds that

$$[K]\{\varphi_{R,k}\} = \{0\}. \quad (11.39)$$

The result of the previous matrix multiplication is a vector. Multiplication (11.39) by $\frac{1}{2}\{\varphi_{R,k}\}^T$ gives the elastic energy U of a finite element model subjected to a motion $\{\varphi_{R,k}\}$ as rigid body:

$$\frac{1}{2}\{\varphi_{R,k}\}^T [K]\{\varphi_{R,k}\} = \delta \leq \varepsilon \quad (11.40)$$

The motion matrix as rigid body can be determined in three ways:

1. Using the coordinates of the nodes obtained from the geometry of the finite element model. For each node “ n ” with coordinates x_n , y_n and z_n , the following holds:

$$[\Phi_R]_n = \begin{bmatrix} 1 & 0 & 0 & 0 & z_n & -y_n \\ 0 & 1 & 0 & -z_n & 0 & x_n \\ 0 & 0 & 1 & y_n & -x_n & 0 \\ 0 & 0 & 0 & 1 & 0 & 0 \\ 0 & 0 & 0 & 0 & 1 & 0 \\ 0 & 0 & 0 & 0 & 0 & 1 \end{bmatrix} \quad (11.41)$$

This must be repeated for all the nodes.

2. The second option is to determine $[\Phi_R]$ with the aid of the stiffness matrix. We define a statically determined set of degrees of freedom R -set (R -set = 6). The other remaining degrees of freedom are referred to with E -set. When $[K]\{\phi_{R,k}\} = \{0\}$ holds for a motion as rigid body, then:

$$\begin{bmatrix} K_{EE} & K_{ER} \\ K_{RE} & K_{RR} \end{bmatrix} \begin{Bmatrix} \Phi_{EE} \\ \Phi_{RR} \end{Bmatrix} = \begin{Bmatrix} 0 \\ 0 \end{Bmatrix}. \quad (11.42)$$

Assume that:

$$[\Phi_{RR}] = \begin{bmatrix} 1 & 0 & 0 & 0 & 0 & 0 \\ 0 & 1 & 0 & 0 & 0 & 0 \\ 0 & 0 & 1 & 0 & 0 & 0 \\ 0 & 0 & 0 & 1 & 0 & 0 \\ 0 & 0 & 0 & 0 & 1 & 0 \\ 0 & 0 & 0 & 0 & 0 & 1 \end{bmatrix} = [I], \quad (11.43)$$

then with the first equation of (11.42):

$$[K_{EE}][\Phi_{EE}] + [K_{ER}][\Phi_{RR}] = [0]. \quad (11.44)$$

Thus $[\Phi_{EE}]$ now becomes:

$$[\Phi_{EE}] = -[K_{EE}]^{-1}[K_{ER}][\Phi_{RR}] = -[K_{EE}]^{-1}[K_{ER}] = [D]. \quad (11.45)$$

The motion vectors $[\Phi_R]$ as rigid body are then expressed as:

$$[\Phi_R] = \begin{bmatrix} \Phi_{EE} \\ \Phi_{RR} \end{bmatrix} = \begin{bmatrix} D \\ I \end{bmatrix} [\Phi_{RR}] = \begin{bmatrix} D \\ \Phi_{RR} \end{bmatrix}. \quad (11.46)$$

Then the following holds (second equation of (11.42)):

$$[K_{RE}][D] + [K_{RR}][\Phi_{RR}] = [0]. \quad (11.47)$$

Introducing (11.45) into (11.47) yields

$$([K_{RR}] - [K_{RE}][K_{EE}]^{-1}[K_{ER}])[\Phi_{RR}] = 0. \quad (11.48)$$

Since $[\Phi_R] = [I] \neq [0]$, the following must hold:

$$([K_{RR}] - [K_{RE}][K_{EE}]^{-1}[K_{ER}]) = 0. \quad (11.49)$$

3. Solve the eigenvalue problem (11.38) $(-\omega_k^2[M] - [K])\{\phi_k\} = \{0\}$ and obtain $[\Phi_R]$.

11.9.6 Reduced finite element model

If the finite element models of the subsystems are included one by one in the entire finite element model of the entire satellite, then the complete model can turn out to be rather large. The primary contractor or the one responsible for the complete finite element model therefore requires that a reduced model (of the subsystem) with a limited number of degrees of freedom is provided. The number of degrees of freedom is then specified.

The client also requires a certain accuracy with respect to the natural frequency, mode forms, etc. of the reduced model in comparison with the reference model (complete model of the subsystem), for example:

Less than $\pm 3.0\%$ for the natural frequencies.

Less than $\pm 10.0\%$ for the effective masses.

In case a “cross orthogonality” test is concerned, then the diagonal terms must be $\text{ortho} \leq 0.95$ and the other terms in the matrix must be $\text{ortho} \leq 0.05$. The “modal assurance criteria” (MAC) value must be $\text{MAC} \leq 0.95$.

Sometimes requirements are set with regards to the accuracy of the amplifications of the reduced model and the reference model.

The primary contractor usually demands the number of degrees of freedom of the total subsystem. This can be done using the Static Condensation Method (Guyan Reduction) in which the finite element model is reduced to the desired number of degrees of freedom. In chapter 17 "Dynamic Model Reduction Methods", page 265 the reduction methods are discussed in detail.

11.9.7 Reports regarding the finite element model

The primary contractor requires a clear description of the reference and reduced finite element models. In the description of the finite element models at least the following must be included:

- The description of the coordinate systems and the numbers that refer to them
- A list of nodes and the associated coordinates
- The boundary conditions that have been applied
- The material properties used and for which type of finite elements
- The mass distribution used and the mass matrix as rigid body with respect to the calculated centre of gravity (complete and reduced model). Furthermore, the main axes of inertia must be calculated
- Description of the interface of the subsystem with another (sub)system
- The elastic energy of the finite element model with a motion as rigid body
- The modal characteristics of the complete and reduced finite element model and a list with the analysis-set degrees of freedom

- A list containing the applied input of the finite element programme (Bulk Data Deck for MSC.Nastran®), preferably accompanied with explanatory text.

11.9.8 Electronic Carrier

The complete and reduced finite element model can be saved on a CD-Rom, mostly in ASCI format. Binary information is of course dependent on the computer used to carry out the computations.

FTP and E-mail are good alternatives to transfer mathematical models over the internet.

11.10 Literature

- Crisfield, M.A., *Finite Elements and Slution Procedures for Structural Analysis, Vol. I Linear Analysis*, Pineridge Press, ISBN 0-906674-53-0, 1986
 NAFEMS, *Guidelines to Finite Element Practice*, 1992
 NAFEMS, *A Finite Element Primer*, 1992
 NAFEMS, *A Finite Element Dynamics Primer*, 1992
 Cook, R.D., Malkus, D.S., Plesha, M.E., *Concepts and Applications of Finite Element Analysis*, third edition, ISBN0-471-84788-7, John Wiley & Sons, 1989

11.11 Exercises

11.11.1 Application Lagrange's Equations

Two equal masses, each of mass m , are connected by a spring with spring stiffness k while each mass is connected to a fixed wall by a spring with stiffness k . The kinetic energy T and potential (strain) energy U of this 2 DOF problem are:

$$T = \frac{m}{2}(\dot{x}_1^2 + \dot{x}_2^2),$$

$$U = \frac{k}{2}\{x_1^2 + x_2^2 + (x_1 - x_2)^2\}.$$

Derive the undamped equations of motion and compute both natural frequencies $\{\omega_n\}$ and associated vibration modes $[\Phi]$ such that the generalized masses are unity.

There are two grounded dampers with damping constant c attached to the masses. The damping (dissipated energy) D is given by

$$D = \frac{c}{2}\{\dot{x}_1^2 + \dot{x}_2^2\}$$

Derive the state space equation of damped motion. Compute the damped natural frequencies $\{\omega_d\}$ undamped natural frequencies $\{\omega_n\}$ and the modal damping $\{\zeta_n\}$ ratio assuming $k = m = c = 1$.

Answers: $\{\omega_n\} = \sqrt{\frac{k}{m}} \begin{Bmatrix} 1.0000 \\ 1.7321 \end{Bmatrix}, \quad [\Phi] = \frac{1}{\sqrt{m}} \begin{pmatrix} 0.7071 & -0.7071 \\ 0.7071 & 0.7071 \end{pmatrix},$

$$\{\omega_d\} = \begin{Bmatrix} 0.8660 \\ 1.6583 \end{Bmatrix}, \quad \{\omega_n\} = \begin{Bmatrix} 1.0000 \\ 1.7321 \end{Bmatrix}, \quad \{\zeta_n\} = \begin{Bmatrix} 0.2887 \\ 0.5000 \end{Bmatrix}.$$

11.11.2 Deployed Natural Frequency

A deployed solar array has the following simplified analysis model, as shown in Fig. 11.5. The solar array is allowed to rotate, however, a rotational spring with spring stiffness $K = 50000 \text{ Nm/rad}$ prevents that. The elastic beam has a length $L = 7 \text{ m}$, a bending stiffness $EI = 2.73 \times 10^5 \text{ Nm}^2$ and a total mass $M_1 = 14 \text{ kg}$. The tip mass $M_2 = 50 \text{ kg}$. Calculate the lowest natural frequency by modelling the beam as one beam finite element.

Check this answer using the Dunkerley's approach.

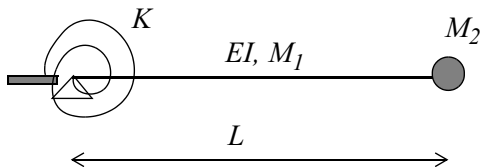


Fig. 11.5 Simplified analysis model deployed solar array

The bending beam finite element has four DOFs, at the left side a translation u_1 and a rotation φ_1 . At the right side of the bending beam finite element we have two DOFs also, a translation u_2 and a rotation φ_2 . The element stiffness and mass matrix are given by [Cook 1989].

$$[k] = \begin{bmatrix} \frac{12EI}{L^3} & \frac{6EI}{L^2} & -\frac{12EI}{L^3} & \frac{6EI}{L^2} \\ \frac{6EI}{L^2} & \frac{4EI}{L} & -\frac{6EI}{L^2} & \frac{2EI}{L} \\ -\frac{12EI}{L^3} & -\frac{6EI}{L^2} & \frac{12EI}{L^3} & -\frac{6EI}{L^2} \\ \frac{6EI}{L^2} & \frac{2EI}{L} & -\frac{6EI}{L^2} & \frac{4EI}{L} \end{bmatrix}, [m] = \frac{M_1}{420} \begin{bmatrix} 156 & 22L & 54 & -13L \\ 22L & 4L^2 & 13L & -3L^2 \\ 54 & 13L & 156 & -22L \\ -13L & -3L^2 & -22L & 4L^2 \end{bmatrix}.$$

Answers: Lowest natural frequency finite element approach $f = 0.5780 \text{ Hz}$, Dunkerley's method $f = 0.5776 \text{ Hz}$.

11.11.3 Natural frequency cantilever beam

The cantilever beam is shown in Fig. 11.6. The length of the beam is $L = 1.00 \text{ m}$. The cross-section has a width $b = 0.01 \text{ m}$ and the height is $h = 0.01 \text{ m}$. The den-

sity of the beam material is $\rho = 2700 \text{ kg/m}^3$ and the Young's modulus $E = 70 \text{ GPa}$.

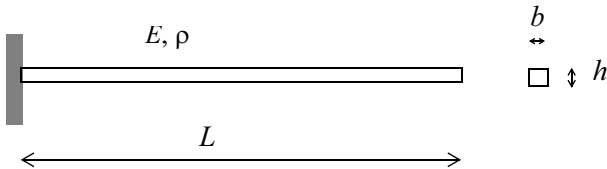


Fig. 11.6 Cantilever beam

Find the lowest natural frequency(ies):

- Theoretical solution of the equation of motion $EI \frac{\partial^4 w}{\partial x^4} + \rho A \frac{\partial^2 w}{\partial t^2} = 0$.
- Rayleigh's quotient $R(\omega) \approx \omega_0^2 = \frac{EI \int_0^L \left(\frac{d^2 u}{dx^2} \right)^2 dx}{\rho A \int_0^L u^2 dx}$, where the shape function is $u(x) = 2\left(\frac{x}{L}\right)^2 - \frac{4}{3}\left(\frac{x}{L}\right)^3 + \frac{1}{3}\left(\frac{x}{L}\right)^4$.
- Using the following finite element model consisting of two beam elements and using the element mass and stiffness matrices as given in section 11.11.2, however, in the mass matrix we replace $M_1 = A\rho L$. The finite element model is illustrated in Fig. 11.7.

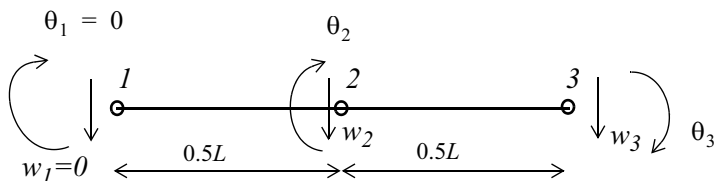


Fig. 11.7 Finite element model cantilever beam

- Check if the calculated modes are orthogonal with respect to the mass and stiffness matrix.

12 Stiffness/Flexibility Analysis

12.1 Introduction

The prime contractor specifies a minimum stiffness (matrix) or flexibility (matrix), for a given node(s) and for a specific degree(s) of freedom. The stiffness or flexibility must be calculated for certain boundary conditions, for example:

$$[K]\{x\} = \{F\}, \quad (12.1)$$

or if the stiffness matrix $[K]$ is regular by suppressing rigid body motion with adequate boundary conditions

$$\{x\} = [K]^{-1}\{F\} = [G]\{F\}, \quad (12.2)$$

where $\{x\}$ is the displacement vector, $\{F\}$ is the force vector and $[G]$ is the flexibility matrix.

A finite element model [Przemieniecki 1985] can be used to determine the stiffness characteristics in several ways:

1. Apply an **unit force** in a specific direction (degree of freedom) and solve the equation of equilibrium. The required stiffness is given by the reciprocal value of the calculated displacement or rotation of that degree of freedom.
2. Static **condensation the stiffness matrix** of the finite element model to the required degrees of freedom. The condensed stiffness matrix is the required stiffness.
3. Apply a **unit displacement** and with the aid of the equations of equilibrium, calculate the resulting reaction force in the degrees of freedom concerned.

If the minimum stiffness is known but the direction is not, then with the aid of the minimum eigenvalues, an approximation of the required stiffness can be made.

12.2 Examples

12.2.1 ATV Cargo Carrier

A global stiffness requirement is set in the specifications (Alenia) of the “External Structure” of the ATV Cargo Carrier (ATV stands for Automatic Transfer Vehicle and is the supply satellite of the International Space Station (ISS)). The external structure is cylindrical and contains 10 fuel tanks.

The stiffness requirement is valid in the middle (centre) of the upper plane of the cylinder while the lower plane of the cylinder is restrained (see Fig. 12.1). The specification is the flexibility matrix $[G]$:

$$\{x\} = \begin{Bmatrix} \eta \\ \delta \\ \phi \end{Bmatrix} = [G][F] = [G] \begin{Bmatrix} N \\ T \\ M \end{Bmatrix} \text{ with}$$

$$[G] = \begin{bmatrix} 0.2371 \times 10^{-9} & 0 & 0 \\ 0 & 0.1235 \times 10^{-8} & -0.3514 \times 10^{-10} \\ 0 & -0.3514 \times 10^{-10} & 0.1065 \times 10^{-9} \end{bmatrix}$$

with N, η the force and the displacement in the longitudinal direction of the cylinder, T, δ the transverse force and the associated displacement and M, ϕ the bending moment and the associated rotation

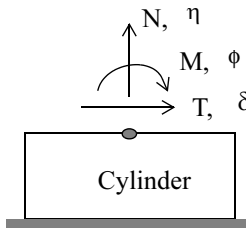


Fig. 12.1 Stiffness/flexibility specification illustration

12.2.2 ARIANE 5 Bati-Moteur (BME)

The flexibility, for example, of the Centre Cardan of the Bati-Moteur of the ARIANE 5 has been specified (see Fig. 12.2).

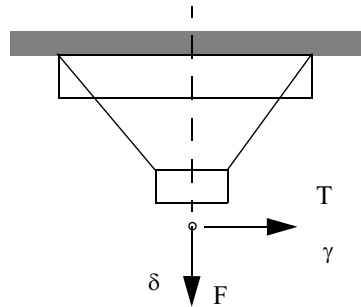


Fig. 12.2 Flexibility of motor support

The specifications for the stiffness/flexibility in the x-direction are:

$$\frac{\gamma}{T} \leq 5.5 \times 10^{-9} \text{ m/N},$$

and the specifications for the stiffness or flexibility in the lateral direction is

$$\frac{\delta}{F} \leq 37.0 \times 10^{-9} \text{ m/N}.$$

12.3 The unit force method

The equations of equilibrium for a static problem are, see (12.1):

$$[K]\{x\} = \{F\}$$

where $[K]$ is the stiffness matrix that was composed with the aid of the finite element method. The boundary conditions have been included such that the inverse of the stiffness matrix, the flexibility matrix $[G] = [K]^{-1}$, exists. $\{x\}$ is the vector composed of the unknown degrees of freedom and $\{F\}$ is the vector composed of the applied loads

If it is required to calculate the stiffness of the degrees of freedom $\{x_i\}$, then one unit of force $\{F_i\} = \{I\}$ must be applied on the equivalent position in the load vector.

$$\begin{bmatrix} K_{ii} & K_{ij} \\ K_{ji} & K_{jj} \end{bmatrix} \begin{Bmatrix} x_i \\ x_j \end{Bmatrix} = \begin{Bmatrix} F_i \\ 0 \end{Bmatrix}. \quad (12.3)$$

From the second part of the previous (12.3) it follows that:

$$\{x_j\} = -[K_{jj}]^{-1}[K_{ji}]\{x_i\}. \quad (12.4)$$

The result for $\{x_j\}$ ((12.4)) substituted in the first part of the partitioned equilibrium equations ((12.3)) gives:

$$([K_{ii}] - [K_{ij}][K_{jj}]^{-1}[K_{ji}])\{x_i\} = \{F_i\} = \{I\}, \quad (12.5)$$

or in other words

$$[\bar{K}_{ii}]\{x_i\} = \{I\} \quad (12.6)$$

Thus

$$\{x_i\} = [\bar{K}_{ii}]^{-1} = [\bar{G}_{ii}] \quad (12.7)$$

The resulting displacement due to the unit force $\{F_i\} = \{I\}$ is equal to the reduced flexibility matrix $\{x_i\} = [\bar{G}_{ii}]$.

12.4 Reduced stiffness matrix

The reduced stiffness matrix $[\bar{K}_{ii}]$, (12.6), is the required stiffness matrix.

12.5 Unit displacement

Say that the displacement vector is $\{x_i\} = [I]$, then:

$$\begin{bmatrix} K_{ii} & K_{ij} \\ K_{ji} & K_{jj} \end{bmatrix} \begin{Bmatrix} x_i = I \\ x_j \end{Bmatrix} = \begin{Bmatrix} R_i \\ 0 \end{Bmatrix} \quad (12.8)$$

The reaction forces $[R_i]$, due to the unit displacements $\{x_i\} = [I]$, are representative for the stiffness, see (12.5):

$$([K_{ii}] - [K_{ij}][K_{jj}]^{-1}[K_{ji}]) = [R_i] \quad (12.9)$$

The condensed stiffness matrix is $[\bar{K}_{ii}]$.

12.6 Principal directions

The principal directions of the stiffness matrix are equal to the eigenvectors and the associated stiffness (equal to the eigenvalues of the stiffness matrix):

$$([\bar{K}_{ii}] - \lambda_i [I]) \{\hat{x}_i\} = \{0\} \quad (12.10)$$

or

$$\left(\frac{1}{\lambda_i} [I] - [\bar{K}_{ii}]^{-1} \right) \{\hat{x}_i\} = \{0\}, \quad (12.11)$$

or using the flexibility matrix $[\bar{G}_{ii}]$ we obtain

$$(\gamma_i [I] - [\bar{G}_{ii}]) \{\hat{x}_i\} = \{0\}. \quad (12.12)$$

where λ_i is the principal stiffness, γ_i is the principal flexibility and $\{\hat{x}_i\}$ is the associated directions (eigenvectors).

The eigenvectors are orthonormal [Strang 1988].

Example

Let's look at a simple truss with six tension- and compression members and 4 nodes. The degrees of freedom of nodes 3 and 4 have all been specified. 4 degrees of freedom remain. Degrees of freedom 1 and 2 remain for node 1 and degrees of freedom 3 and 4 remain for node 2. The truss frame is illustrated in Fig. 12.3.

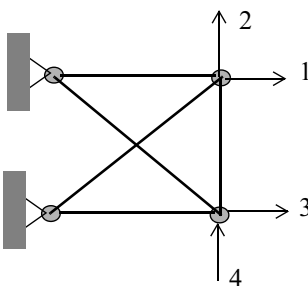


Fig. 12.3 Truss-frame, 4 DOFs

Leaving out the specified degrees of freedom, the stiffness matrix $[K]$ of the truss-frame is:

$$[K] = 0.125 \cdot 10^6 \begin{bmatrix} 5 & 1 & 0 & 0 \\ 1 & 5 & 0 & -4 \\ 0 & 0 & 5 & -1 \\ 0 & -4 & -1 & 5 \end{bmatrix} \text{ N/m}$$

Determine the stiffness characteristic of the first degree of freedom x_1 .

Unit force

A unit force is applied in the direction of x_1 , therefore the force vector $\{F\}$ is, specifically:

$$\{F\} = \begin{Bmatrix} 1 \\ 0 \\ 0 \\ 0 \end{Bmatrix} \text{ N.}$$

With $\{x\} = [K]^{-1}\{F\}$, the displacement vector $\{x\}$ becomes

$$\{x\} = 10^{-5} \begin{Bmatrix} 0.1818 \\ -0.1091 \\ -0.0182 \\ -0.0909 \end{Bmatrix} \text{ m.}$$

The flexibility term in the direction of the first degree of freedom x_1 becomes

$$g_{11} = x_1 \text{ m/N and } k_{11} = \frac{1}{x_1} = 55000 \text{ N/m.}$$

Unit displacement

With a unit displacement $x_1 = 1 \text{ m}$, the vector with reaction forces R_1 is equal to the stiffness in that direction. With:

$$K_{ii} = 5 \cdot 0.125 \cdot 10^6, [K_{jj}] = 0.125 \cdot 10^6 \begin{bmatrix} 5 & 0 & -4 \\ 0 & 5 & -1 \\ -4 & -1 & 5 \end{bmatrix} \text{ and } [K_{ij}] = 0.125 \cdot 10^6 \begin{Bmatrix} 1 \\ 0 \\ 0 \end{Bmatrix}$$

The condensed stiffness matrix \overline{K}_{ii} becomes

$$\overline{K}_{ii} = R_i = ([K_{ii}] - [K_{ij}][K_{jj}]^{-1}[K_{ji}]) = 55000 \text{ N/m.}$$

Subsequently, calculate the stiffness matrix for the degrees of freedom x_1, x_2 . This can be achieved by calculating the condensed stiffness matrix. With:

$$[K_{ii}] = 0.125 \cdot 10^6 \begin{bmatrix} 5 & 1 \\ 1 & 5 \end{bmatrix}, [K_{jj}] = 0.125 \cdot 10^6 \begin{bmatrix} 5 & -1 \\ -1 & 5 \end{bmatrix} \text{ and}$$

$$[K_{ij}] = 0.125 \cdot 10^6 \begin{bmatrix} 0 & 0 \\ 0 & -4 \end{bmatrix},$$

the condensed stiffness matrix becomes

$$[\bar{K}_{ii}] = ([K_{ii}] - [K_{ij}][K_{jj}]^{-1}[K_{ji}]) = 1 \times 10^5 \begin{bmatrix} 6.2500 & 1.2500 \\ 1.2500 & 2.0833 \end{bmatrix}.$$

The principal directions of the stiffness matrix can then be solved with the eigenvalue problem (12.10), that is

$$([\bar{K}_{ii}] - \lambda_i[I])\{\hat{x}_i\} = \{0\}.$$

The eigenvalues and the associated eigenvectors are

$$\{\lambda\} = \{\gamma\}^{-1} = 1 \times 10^5 \begin{bmatrix} 1.7371 & 0 \\ 0 & 6.5902 \end{bmatrix} \text{ and } \{\hat{x}\} = \begin{bmatrix} 0.2669 & -0.9637 \\ -0.9637 & -0.2669 \end{bmatrix}$$

The first eigenvector $\{\hat{x}_1\}$ has the largest displacement in the x_2 direction. This implies that the stiffness in the x_1 direction is higher than in the x_2 direction.

12.7 Literature

- Megson, T.H.G., 1999, *Aircraft Structures for Engineering Students*, third edition, Butterworth & Heinemann, ISBN 0 340 70588 4.
- Przemieniecki, J.S., 1985, *Theory of Matrix Structural Analysis*, Dover, ISBN 0-486-64948-2.
- Strang, G., 1988, *Linear Algebra and its Applications*, third edition, Harcourt Brace Jovanovich, ISBN 0-15-551005-3.

12.8 Exercises

12.8.1 Stiffness Pin-joined Frame

Calculate the stiffness of the pin-joined frame at point C in the direction of the force F as illustrated in Fig. 12.4, [Megson 1999]. The stiffness of the members is

$$\frac{EA}{L} = 20 \text{ (N/mm).}$$

Perform the following steps:

1. Calculate the internal forces in the frame members
2. Calculate the complete strain energy expressed in F
3. Calculate the displacement in the direction of the force F using first Castiglione's theorem
4. Calculate the stiffness in the direction of the force F
5. Set up the finite element model and calculate the condensed stiffness matrix at C (vertical and horizontal)
6. Calculate the minimum and maximum stiffness at C

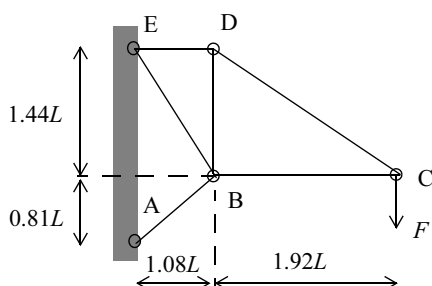


Fig. 12.4 Frame

13 Material Selection

13.1 Introduction

A very important step in the design process is the selection of materials for a spacecraft structure. The choice has significant consequences on the mass, the production costs, etc. The operational conditions of the spacecraft, the ability to retain its shape and the reliability of the structure are some of the parameters used for the selection of materials. In the following sections, properties of metal alloys, composite materials, metal and non-metal matrices, and metal aluminium honeycomb cores are discussed.

This chapter will end with a discussion about the design considerations.

A good reference about materials selection in mechanical design can be found in [Ashbey 2003, Derby 1992].

13.2 Metal alloys

Magnesium alloys ($\rho = 1760\text{--}2000 \text{ kg/m}^3$, $E = 41 \text{ GPa}$, temperature range $T \leq 125^\circ \text{ C}$) have a high specific strength, are easy to weld, however they are sensitive to corrosion.

Aluminium alloys ($\rho = 2700\text{--}2900 \text{ kg/m}^3$, $E = 70 \text{ GPa}$, temperature range $T \leq 200\text{--}350^\circ \text{ C}$). They form a large group of structural materials for spacecraft structures. They have a wide range of mechanical characteristics and can be used in heavily loaded structures in circumstances ranging from cryogenic conditions up to relatively high temperatures.

Titanium alloys ($\rho = 4500\text{--}4800 \text{ kg/m}^3$, $E = 115\text{--}120 \text{ GPa}$, temperature range $T \leq 500^\circ \text{ C}$) are characterised by a high mechanical strength and good resistance against corrosion for temperatures up to $450\text{--}500^\circ \text{ C}$. The good mechanical properties are, however, accompanied by poor ductile properties and sensitivity to cracking in a welded state.

Beryllium alloys ($\rho = 1850\text{--}2300 \text{ kg/m}^3$, $E = 190 \text{ GPa}$, temperature range $T \leq 600^\circ \text{ C}$) have unique thermal properties and good resistance against corrosion. Beryllium alloys are found in a limited number of applications due to their high toxicity. Additionally, they are sensitive to stress concentrations and brittleness.

Steel ($\rho = 7800\text{--}8000 \text{ kg/m}^3$, $E = 185\text{--}200 \text{ GPa}$) Traditional structural material for heavily loaded structures in, for example, aggressive environments (chemically active gases and fluids).

In the following table various mechanical properties (at room temperature) for the metal alloys are shown. The mechanical properties of the metal alloys are usually dependent on the environmental temperature.

Table 13.1 Typical material properties

Material	Density ρ (kg/m^3)	σ_v (MPa)	σ_y (MPa)	E (GPa)
Aluminium				
2014-T6	2.80	441	386	72
2024-T36	2.77	482	413	72
6061-T6	2.71	289	241	67
7075-T6	2.80	523	448	71
Magnesium				
AZ31B	1.77	221	110	44
AZ31B-H24	1.77	269	199	44
Titanium				
Ti6Al-4V	4.43	1103	999	110
Steel				
RH1050	7.60	1310	1170	200
D6AC	7.80	1600	1200	200
AMS-6434	7.88	2100	1400	200
Beryllium				
Lockalloy	2.10	426	310	203

13.3 Composite materials

Composite materials consist of dissimilar systems made of two or more components that retain their individual properties. Composite materials consist of filler with high strength, high elasticity modulus and low specific weight, embedded in a matrix of homogeneous material. The fillers used in space structures are fibres and threads. The length of the fibres can range from micrometers up to meters, with diameters ranging from several micrometers up to several millimetres. The matrix material used is usually epoxy and organic polymers, ceramics, metals and their alloys. For composite materials, the final form of the structure is made immedi-

ately, so that a large part of the machining can be omitted, such as with conventional alloys. Composite materials are generally an-isotropic.

13.3.1 Physical-mechanical properties of fillers

The fillers that are often used together with synthetic matrices are: glass-, carbon-organic- and boron fibres. Generally thin threads of steel, titanium, boron, niobium or wolfram are used in metal matrices.

Glass fibres are the most common fibre for composite materials. They have a relatively low specific weight of 2400–2600 kg/m³, high strength, low thermal conductivity and a high resistance to thermal, chemical and biological effects.

Organic fibres are made by drawing a polyamide polymer with a fluid-crystal structure. Organic fibres possess high strength, high elasticity modulus and minor creep properties. Aramid fibres have a low specific weight (1300–1400 kg/m³) and a high specific strength σ_u/ρ .

Carbon fibres have some very good mechanical and physicochemical properties, such as good thermal stability, a small expansion coefficient, high resistance to ambient effects, high strength and elasticity modulus. Carbon fibres can be subdivided into two groups: carbonised (80–90% carbon) and with graphite (99% carbon). Carbon fibres are made by the complicated thermochemical processing of polynitrilate (polyacrylonitrile (PAN)).

Boron fibres are continuous an-isotropic fibres with a diameter ranging from 5–200 µm. At high temperatures, boron fibres in a gas mixture of $BCl_2 + H_2$ settle on a thread of wolfram with a diameter of 12 µm. Composites with boron fibres can be used at temperatures of 600° K and higher and are processed in a normal way.

Sicilian carbide fibres are composite materials with a metal matrix and are suitable for use at very high temperatures.

Metal threads are very “cost” effective fibres, usually made of corrosion-resistant steel, wolfram, beryllium, niobium, etc. Some mechanical properties of metal and non-metal fibres are given in the following tables.

Table 13.2 Typical material properties non-metal fibres

Material	Young's modulus E (GPa)	Ultimate strength σ (MPa)	Density ρ kg/m ³
E-Glass fiber*	72.3	3170	2550
S-Glass fibre*	82.7	4130	2500
E-Glass in epoxy	51.7	1380	1940
S-Glass in epoxy	51.7	2070	1940
Aramid fibre*	137.8	3445	1690
Aramid fibre in epoxy	82.7	1930	1400
HM graphite fibre*	379	2070	1900
HT graphite fibre*	241	2410	1770
AS or T-300 fibre*	207	2760	1850
HM graphite in epoxy	207	930	1610
HT graphite in epoxy	152	1410	1500
AS or T-300 in epoxy	117	1580	1550
Boron filaments*	143	2760	2630
Boron in epoxy	214	1520	2080

13.3.2 Properties of Non-metal Matrices

The function of the matrix is to ensure that the fibres work simultaneously when the fibres are subjected to a load. The modulus of elasticity of the matrix must be as high as possible, and the relative strain must be as close to the fibres as possible. Presently, the following thermo sets are used: epoxy, phenol, polymide and bis-maleimide. The following thermoplastics are used: Polyetherether Ketone (PEEK), Polyether Imide (PEI), Polyethersulfone (PES), Polyamide Imide (Torlon), Polyamylene Sulphide (PAS) matrices. The most important advantages of epoxy resin are its good adhesion properties, the fact that processing requires low pressure and also only a little amount of gas is produced as a side-effect when the epoxy resin polymerises. The composite materials have a clear an-isotropic character. The properties in a longitudinal direction are different from those in a transverse direction. In practice, the uni-directional intersectional reinforced composite materials are most often used. The fibres give the best result when they are positioned in the same direction as the applied force.

Carbon-Carbon consists of carbon fibres in a pyrocarbon used as matrix material. The composite material has a specific weight of 1800–1900 kg/m³ and can be used for applications at ambient temperatures of 2500–3000° C.

13.3.3 Properties of Metal Matrices

Boron, carbon and beryllium are generally used as fibre material and aluminium, magnesium and titanium as matrix. The most promising composite material with excellent mechanical properties is carbon-aluminium. Some characteristics of composite materials with a metal matrix are given in the following Table 13.3.

Table 13.3 Mechanical properties metal-metal composites

Material	Young's modulus E (GPa)	Ultimate strength σ (GPa)	Density ρ (kg/m ³)
Boron-Aluminum	235	1.25	2650
Boron-Magnesium	220	1.2	2150
Carbon-Aluminum	230	0.9	2250
Steel-Aluminum	117	1.55	4470
Boron-Titanium	270	1.4	3500

13.4 Sandwich Honeycomb Core

The mechanical properties of frequently applied Al-alloy 5056 honeycomb cores are illustrated in Table 13.4.

Table 13.4 Honeycomb core properties

Type of Honeycomb core	d_c cell (mm)	ρ (kg/m ³)	Compr. strength E_c (MPa)	Shear modulus (MPa)		Shear strength (MPa)	
				G _L	G _T	τ_L	τ_T
1/4-5056-.002p	6.4	69	3.21	462	186	2.24	1.31
3/8-5056-.0007p	9.6	16	0.24	103	62	0.31	0.17
1/4-5056-.0015p	6.4	54	2.17	345	152	1.59	0.90
1/4-5056-.0007p	6.4	26	0.55	138	83	0.54	0.26
3/16-5056-.002p	4.8	91	5.07	648	248	3.31	1.93

13.5 Design considerations

The primary structural elements of a spacecraft are the hermetically sealed pressurized bays for the crew and instrumentation, the fuel tanks, the heavily loaded thin-walled monocoque structures, trusses and supporting beams, the panels on which the instrumentation is mounted, rods, pipes, rings, etc.

Pressurised compartments are subjected to internal pressure and must be hermetically sealed. The structure is made of an Aluminium- or Magnesium alloy.

Highly loaded thin-walled cylinders and cones make up the central structure of the spacecraft. They are designed to support axial pressure loads and bending moments. The primary failure mode is due to buckling of thin-walled shells. Light-weight and stiff structures can be obtained by using materials with a high modulus of elasticity, such as beryllium with carbon and boron reinforced epoxies. Thin-walled shells, cylinders and cones (monocoque type) are traditionally reinforced with longitudinal stiffeners and rings or a sandwich construction.

Rods, trusses and pipes are usually designed to support buckling loads.

The most promising materials are carbon/epoxy, boron/epoxy, beryllium, fibre-glass and Kevlar. Connecting the rods may be problematic and may cancel out the advantage of the lighter mass of the trusses.

The lowest natural frequency of the panels on which instruments are mounted must be as high as possible. A standard design of a panel is a sandwich structure with facings made of aluminium or magnesium of a composite material.

Fuel tanks are traditionally made of materials with high strength properties such as aluminium or titanium alloys.

In the following table various specific applications and constraints for metals are given.

Table 13.5 Material Applications

Material	Application	Important constraints
Steel	<ul style="list-style-type: none"> • Pressure stabilised cryogenic fuel tanks • Solid rocket booster casings • Fuel lines • Sandwich facesheets in heavy loaded structures • Hot structures 	<ul style="list-style-type: none"> • High density
Aluminum	<ul style="list-style-type: none"> • Cryogenic applications • Fuel tanks • Primary structures (<200°C) • Struts • Sandwich construction facesheets and cores 	<ul style="list-style-type: none"> • Sensitive for moisture
Titanium	<ul style="list-style-type: none"> • Homogeneous lightweight structures with a complex shape • Truss and nodes in truss frames • Struts under compression • Pressure tanks • Cryogenic applications (tanks) • Fuel lines • Hot structures (<500°C) • Bolts 	
Beryllium	<ul style="list-style-type: none"> • Stiff lightweight structures in compression (<530°C) • Construction under thermal shock • Increasing the natural frequency of structures • Low coefficient of thermal expansion 	<ul style="list-style-type: none"> • brittle • toxic • expensive
Magnesium	<ul style="list-style-type: none"> • Lightweight structures with many material involved • Truss frames • Low level loaded structural parts 	<ul style="list-style-type: none"> • Low toughness • Stress corrosion

13.6 Literature

- Ashby, M.F., 2003, *Materials Selection in Mechanical design*, second edition, Butterworth Heinemann, ISBN 0 7506 4357 9.
- Matthews, F.L., Davies, G.A.O., Hitchings, D., Soutis, C., 2000, *Finite Element modelling of composite materials and structures*, Woodhouse Publishing Limited, ISBN 0-8493-08461.
- Derby, B. Hills, D., Ruiz, C., 1992, *Materials for Engineering, A Fundamental Design Approach*, Longman, ISBN 0-582-03185.

14 Spacecraft Mass

14.1 Introduction

The design of a spacecraft is largely determined by the available mass budget. The following mass characteristics play an important role:

- mass of spacecraft that is to be launched
- the position of the centre of gravity or centre of mass
- the second moment of mass (moment of inertia, MOI)

The mass characteristics are always important. The level of importance of the other characteristics depends on the mission.

The calculation of the mass characteristics will be discussed in detail in the following sections.

The position of the centre of gravity is often of crucial importance because it is of great importance during launch. During lateral acceleration the spacecraft exerts a bending moment on the payload adapter. This bending moment depends on the mass of the spacecraft and the position of the centre of gravity. The launch authority specifies the permissible bending moment, from which the position of the centre of gravity can be calculated. The offset d with respect to the launch axis is also specified, for example $d \leq 3$ mm. The position of the centre of gravity is also important for the attitude control system (AOCS subsystem).

The second moments of mass are also important for the attitude control system.

The mutual relation between the mass moments of inertia is important for spinning satellites.

Satellites are classified according to weight (definition by the Surrey Satellite Technology Ltd (SSTL) , University of Surrey, Guildford, UK):

- Large spacecraft > 1000 kg
- Medium sized spacecraft 500–1000 kg
- Mini spacecraft 100–500 kg
- Micro spacecraft 10–100 kg

- Nano spacecraft 1–10 kg
- Pico spacecraft < 1 kg

Spacecraft that belong to the category 500–1000 kg are often referred to as “Small spacecraft” or “Smallsats” and are associated with cheap spacecraft that can be produced quickly (“Faster, Better, Smaller and Cheaper”).

The “US Advanced Research Projects Agency” refers to the “Smallsats” as “Lightsats, while the “US Naval Command” refers to the “Smallsats” as “SPIN-Sat’s” (Single Purpose Inexpensive Satellite Systems).

The principle of a mass budget is a method of bookkeeping: each subsystem is designed according to the goals set by the mass budget so that the mass can be monitored during the spacecraft project. In order to do this, a detailed list is used to record the mass of all the components of the spacecraft. At the beginning of the project the list consists mainly of the calculated masses, some multiplied with uncertainty factors. During the proposal phase 35% contingency is taken into account, at the preliminary design review (PDR) 15% contingency and at the critical design review 5% contingency is included in the mass analysis. As the design of the spacecraft is more and more frozen the uncertainties decrease and when hardware becomes available the measured weights can be included in the list.

In the following Table 14.1 the relative masses of the subsystems are given in terms of percentages. The percentages are averaged out over a number of spacecraft. This only concerns the dry mass of the spacecraft. The balance weight of approximately 1% is included. The fuel required to position a spacecraft in a geostationary orbit (GEO) and the fuel needed for the attitude control system can double the total weight with respect to the dry mass.

Table 14.1 Mass allocation budgets

Subsystem	Mass budget (dry mass)	
	3-axis stabilised spacecraft (%)	Spinning spacecraft
Structure	18	21
Propulsion (AKM+RCS)	12	11
AOCS	7	5
Power	23	24
TT&C	4	5
Thermal	4	5
Payload (incl. antennae)	28	25
Wiring	4	4
Total	100	100

14.2 Structure Mass

The structure of a spacecraft makes up in average about 20–21% of the total dry mass [Saleh 2002]. Mark Williamson [Williamson 1990] gives a mathematical relation for the percentage of the total mass that the structure mass, depending on the total dry mass, for a spacecraft stabilised along three axes as well as a spinning spacecraft:

The percentage of the structure mass with respect to the total dry mass of a spacecraft stabilised along three axes is:

$$p = -16\log(G) + 60, \quad (14.1)$$

with G the total dry mass of the spacecraft and p the percentage of structural mass of the total spacecraft mass.

The percentage of the structure mass with respect to the total dry mass of a spinning spacecraft is:

$$p = 16\log(G) - 60. \quad (14.2)$$

Below $G = 500$ kg the structural weight of a spinning spacecraft is lower than that of a spacecraft stabilised along three axes. Above 500 kg the structural weight of a spacecraft stabilised along three axes is lower than that of a spinning spacecraft.

In his book, B.N. Agrawal also gives an estimate for the structural weight, but with respect to the entire spacecraft weight (dry mass + fuel mass). For a spinning spacecraft that is 8.7% and for a spacecraft stabilised along three axes that is 9.7%.

14.3 Total Mass Calculation

The total mass of the spacecraft is of great importance and must therefore be calculated accurately. The following mass characteristics are important for the design of a spacecraft structure:

- The 6 x 6 mass matrix as rigid body
- The centre of gravity of the spacecraft: The first moments of mass are zero (kgm)
- The principal second moments of mass and the associated axes of inertia: The cross second moments of mass are zero (kgm)

14.3.1 Mass Matrix

The 6x6 diagonal mass matrix of a rigid body (instrument, box, etc.) [M_{RB}] is generally presented with respect to the centre of mass and in an orientation (local coor-

dinate system) of the principle second moments of mass. The diagonal mass matrix $[M_{RB}]$ is

$$[M_{RB}] = \begin{bmatrix} m & 0 & 0 & 0 & 0 & 0 \\ 0 & m & 0 & 0 & 0 & 0 \\ 0 & 0 & m & 0 & 0 & 0 \\ 0 & 0 & 0 & I_{\bar{x}} & 0 & 0 \\ 0 & 0 & 0 & 0 & I_{\bar{y}} & 0 \\ 0 & 0 & 0 & 0 & 0 & I_{\bar{z}} \end{bmatrix}. \quad (14.3)$$

This mass matrix $[M_{RB}]$ will be transformed in a mass matrix with respect to the reference coordinate system x, y and z . The local coordinate system of the rigid body \bar{x}, \bar{y} and \bar{z} will be expressed in the reference coordinate system

$$\begin{Bmatrix} \bar{x} \\ \bar{y} \\ \bar{z} \end{Bmatrix} = [T] \begin{Bmatrix} x \\ y \\ z \end{Bmatrix}, \quad (14.4)$$

where the rectangular matrix $[T]$ is an orthogonal transformation matrix with orthonormal columns and has special properties, $[T]^T [T] = [I]$ and $[T]^T = [T]^{-1}$, the left-inverse matrix [Strang 1988]. The reference coordinate system will be expressed in the local coordinate system of the rigid body

$$\begin{Bmatrix} x \\ y \\ z \end{Bmatrix} = [T]^{-1} \begin{Bmatrix} \bar{x} \\ \bar{y} \\ \bar{z} \end{Bmatrix} = [T]^T \begin{Bmatrix} \bar{x} \\ \bar{y} \\ \bar{z} \end{Bmatrix}. \quad (14.5)$$

A point P with coordinates (x, y, z) will be represented by a vector. The vector from the origin to the point P can be written as

$$\{P\} = xe_1 + ye_2 + ze_3 = x \begin{Bmatrix} 1 \\ 0 \\ 0 \end{Bmatrix} + y \begin{Bmatrix} 0 \\ 1 \\ 0 \end{Bmatrix} + z \begin{Bmatrix} 0 \\ 0 \\ 1 \end{Bmatrix} = \begin{Bmatrix} x \\ y \\ z \end{Bmatrix}, \quad (14.6)$$

with $e_j, j = 1, 2, 3$ as the unit orthonormal vectors representing the reference coordinate system.

The point P may also be expressed in the local coordinate system, however, the origin is the same.

$$\{P\} = \bar{x}\bar{e}_1 + \bar{y}\bar{e}_2 + \bar{z}\bar{e}_3. \quad (14.7)$$

The unit vectors \bar{e}_i , $i = 1, 2, 3$ may be expressed in the reference coordinate system.

$$\bar{e}_1 = \begin{Bmatrix} x_1 \\ y_1 \\ z_1 \end{Bmatrix}, \bar{e}_2 = \begin{Bmatrix} x_2 \\ y_2 \\ z_2 \end{Bmatrix} \text{ and } \bar{e}_3 = \begin{Bmatrix} x_3 \\ y_3 \\ z_3 \end{Bmatrix}. \quad (14.8)$$

We know that the length of the vectors $|\bar{e}_1| = |\bar{e}_2| = |\bar{e}_3| = 1$, the inner-product of vectors $\bar{e}_i \cdot \bar{e}_j = \delta_{ij}$, and the cross-product of vectors $\bar{e}_1 \times \bar{e}_2 = \bar{e}_3$, $\bar{e}_2 \times \bar{e}_3 = \bar{e}_1$ and $\bar{e}_3 \times \bar{e}_1 = \bar{e}_2$

The coordinates of point P are written as follows (see (14.7))

$$\begin{Bmatrix} x \\ y \\ z \end{Bmatrix} = \begin{bmatrix} x_1 & y_1 & z_1 \\ x_2 & y_2 & z_2 \\ x_3 & y_3 & z_3 \end{bmatrix} \begin{Bmatrix} \bar{x} \\ \bar{y} \\ \bar{z} \end{Bmatrix} = [T]^T \begin{Bmatrix} \bar{x} \\ \bar{y} \\ \bar{z} \end{Bmatrix}. \quad (14.9)$$

It is noticed that

$$x_i = \bar{e}_i \cdot e_1, y_i = \bar{e}_i \cdot e_2 \text{ and } z_i = \bar{e}_i \cdot e_3. \quad (14.10)$$

The inner product of two vectors $x_i = \bar{e}_i \cdot e_1$ is defined as

$$x_i = \bar{e}_i \cdot e_1 = \left[\begin{array}{ccc} x_i & y_i & z_i \end{array} \right] \begin{Bmatrix} 1 \\ 0 \\ 0 \end{Bmatrix}. \quad (14.11)$$

The translational velocities and angle velocities of a rigid body about the centre of mass of the rigid body can be defined for the local coordinate system

$$[\dot{\bar{x}}] = \begin{bmatrix} \dot{u} & \dot{v} & \dot{w} & \dot{\varphi}_{\bar{x}} & \dot{\varphi}_{\bar{y}} & \dot{\varphi}_{\bar{z}} \end{bmatrix} \quad \text{and for the reference coordinate system}$$

$$[\dot{x}] = \begin{bmatrix} \dot{u} & \dot{v} & \dot{w} & \dot{\varphi}_x & \dot{\varphi}_y & \dot{\varphi}_z \end{bmatrix}.$$

The relation between the velocities in the local and reference coordinate system is

$$\{\dot{\bar{x}}\} = \begin{bmatrix} T & 0 \\ 0 & T \end{bmatrix} \{\dot{x}\} = [T_{LR}] \{\dot{x}\} \text{ and } \{\dot{x}\} = [T_{LR}]^T \{\dot{\bar{x}}\}. \quad (14.12)$$

The kinetic energy is a scalar, thus

$$T = \frac{1}{2} \{\dot{\bar{x}}\}^T [M_{RB}] \{\dot{\bar{x}}\} = \frac{1}{2} \{\dot{x}\}^T [M_{RB,ref}] \{\dot{x}\}. \quad (14.13)$$

It can be seen that after the transformation from the local coordinate system to the reference coordinate system, the mass matrix of the rigid body $[M_{\text{RB,ref}}]$ becomes

$$[M_{\text{RB,ref}}] = [T_{\text{LR}}][M_{\text{RB}}][T_{\text{LR}}]^T. \quad (14.14)$$

Example

The local coordinate is with respect to the reference coordinate system rotated 45° about the x-axis. The transformation matrix T will be

$$[T] = \begin{bmatrix} 1 & 0 & 0 \\ 0 & \frac{1}{2}\sqrt{2} & -\frac{1}{2}\sqrt{2} \\ 0 & \frac{1}{2}\sqrt{2} & \frac{1}{2}\sqrt{2} \end{bmatrix}$$

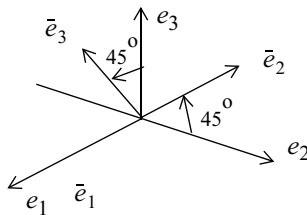


Fig. 14.1 Coordinate transformation

The mass matrix of the rigid body in the coordinate system is given by

$$[M_{\text{RB}}] = \begin{bmatrix} 10 & 0 & 0 & 0 & 0 & 0 \\ 0 & 10 & 0 & 0 & 0 & 0 \\ 0 & 0 & 10 & 0 & 0 & 0 \\ 0 & 0 & 0 & 1 & 0 & 0 \\ 0 & 0 & 0 & 0 & 2 & 0 \\ 0 & 0 & 0 & 0 & 0 & 3 \end{bmatrix}.$$

The mass matrix with respect to the reference coordinate system can be calculated using (14.14)

$$[M_{RB,ref}] = [T_{LR}][M_{RB}][T_{LR}]^T = \begin{bmatrix} 10 & 0 & 0 & 0 & 0 & 0 \\ 0 & 10 & 0 & 0 & 0 & 0 \\ 0 & 0 & 10 & 0 & 0 & 0 \\ 0 & 0 & 0 & 1 & 0 & 0 \\ 0 & 0 & 0 & 0 & 2.5 & -0.5 \\ 0 & 0 & 0 & 0 & -0.5 & 2.5 \end{bmatrix}.$$

End example

The mass matrix as rigid body with respect to an arbitrary point and coordinate system or for example the origin of the reference coordinate system is given by:

$$[M_{ref}] = \begin{bmatrix} m_{xx} & 0 & 0 & 0 & S_{xy} & S_{xz} \\ 0 & m_{yy} & 0 & S_{yx} & 0 & S_{yz} \\ 0 & 0 & m_{zz} & S_{zx} & S_{zy} & 0 \\ 0 & S_{yx} & S_{zx} & I_{xx} & I_{xy} & I_{xz} \\ S_{xy} & 0 & S_{zy} & I_{yx} & I_{yy} & I_{yz} \\ S_{xz} & S_{yz} & 0 & I_{zx} & I_{zy} & I_{zz} \end{bmatrix}, \quad (14.15)$$

with m_{ii} the mass as rigid body in the i -direction, S_{ij} the first moment of mass in the i -direction about the j -direction and I_{ij} the second moment of mass in the i -direction about the j -direction. Normally $m_{xx} = m_{yy} = m_{zz} = m$.

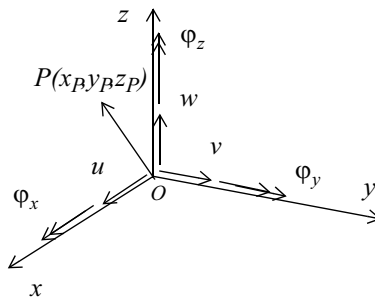


Fig. 14.2 Transformation of displacement vector

The coordinate system of point P is in the reference coordinate system. The displacement vector $[x_P] = [u \ v \ w \ \varphi_x \ \varphi_y \ \varphi_z]$ at P will be expressed in the displacement vector $[x_O]$ as follows

$$\begin{Bmatrix} u_P \\ v_P \\ w_P \\ \Phi_{x,P} \\ \Phi_{y,P} \\ \Phi_{z,P} \end{Bmatrix} = \begin{bmatrix} 1 & 0 & 0 & 0 & z_p & -y_p \\ 0 & 1 & 0 & -z_p & 0 & x_p \\ 0 & 0 & 1 & y_p & -x_p & 0 \\ 0 & 0 & 0 & 1 & 0 & 0 \\ 0 & 0 & 0 & 0 & 1 & 0 \\ 0 & 0 & 0 & 0 & 0 & 1 \end{bmatrix} \begin{Bmatrix} u_O \\ v_O \\ w_O \\ \Phi_{x,O} \\ \Phi_{y,O} \\ \Phi_{z,O} \end{Bmatrix} = [T_P] \begin{Bmatrix} u_O \\ v_O \\ w_O \\ \Phi_{x,O} \\ \Phi_{y,O} \\ \Phi_{z,O} \end{Bmatrix}, \quad (14.16)$$

where the matrix $[T_P]$ is called the geometric matrix.

The inverse transformation of the geometric matrix $[T_P]$ is

$$\begin{Bmatrix} u_O \\ v_O \\ w_O \\ \Phi_{x,O} \\ \Phi_{y,O} \\ \Phi_{z,O} \end{Bmatrix} = [T_P]^{-1} \begin{Bmatrix} u_P \\ v_P \\ w_P \\ \Phi_{x,P} \\ \Phi_{y,P} \\ \Phi_{z,P} \end{Bmatrix} = \begin{bmatrix} 1 & 0 & 0 & 0 & -z_p & y_p \\ 0 & 1 & 0 & z_p & 0 & -x_p \\ 0 & 0 & 1 & -y_p & x_p & 0 \\ 0 & 0 & 0 & 1 & 0 & 0 \\ 0 & 0 & 0 & 0 & 1 & 0 \\ 0 & 0 & 0 & 0 & 0 & 1 \end{bmatrix} \begin{Bmatrix} u_P \\ v_P \\ w_P \\ \Phi_{x,P} \\ \Phi_{y,P} \\ \Phi_{z,P} \end{Bmatrix}. \quad (14.17)$$

The kinetic energy of the general rigid body at point P is given by

$$T = \frac{1}{2} \{\dot{x}_P\}^T [M_{RB,P}] \{\dot{x}_P\} = \frac{1}{2} \{\dot{x}_O\}^T [T_P]^T [M_{RB,P}] [T_P]^{-1} \{\dot{x}_O\}, \quad (14.18)$$

or

$$T = \frac{1}{2} \{\dot{x}_O\}^T [T_P]^T [M_{RB,P}] [T_P]^{-1} \{\dot{x}_O\} = \frac{1}{2} \{\dot{x}_O\}^T [M_{RB,O,P}] \{\dot{x}_O\}. \quad (14.19)$$

Thus the transformed mass matrix in the origin of the reference coordinate system becomes

$$[M_{RB,O,P}] = [T_P]^T [M_{RB,P}] [T_P]^{-1}, \quad (14.20)$$

and the inverse transformation is

$$[M_{RB,P}] = [T_P]^T [M_{RB,O,P}] [T_P]. \quad (14.21)$$

This will be repeated for all N_P mass systems, thus

$$[M_{RB,O}] = \sum_{P=1}^{N_P} [M_{RB,O,P}]. \quad (14.22)$$

14.3.2 Mass matrix with respect to the centre of mass

The mass matrix of a spacecraft is calculated with respect to the centre of mass and with axes parallel to the reference coordinate system.

$$[M_{RB,CG}] = [T_{CG}]^{-T} [M_{RB,O}] [T_{CG}]^{-1}. \quad (14.23)$$

The transformation matrix $[T_{CG}]$ is defined as follows:

$$[T_{CG}] = \begin{bmatrix} 1 & 0 & 0 & 0 & z_{CG} & -y_{CG} \\ 0 & 1 & 0 & -z_{CG} & 0 & x_{CG} \\ 0 & 0 & 1 & y_{CG} & -x_{CG} & 0 \\ 0 & 0 & 0 & 1 & 0 & 0 \\ 0 & 0 & 0 & 0 & 1 & 0 \\ 0 & 0 & 0 & 0 & 0 & 1 \end{bmatrix}. \quad (14.24)$$

This is in accordance with (14.16). The inverse of $[T_{CG}]$ is in accordance with (14.17).

14.3.3 Centre of mass

If the mass matrix is given with respect to the origin of the coordinate system, with respect to the centre of gravity, the first order moments of mass S_{ij} , $i = 1, 2, 3$ $j = 1, 2, 3$ will vanish.

If (14.22) is substituted in the upper-right position of the first moments of mass we find the following values

$$[M_{RB,CG}] = \begin{bmatrix} \dots & 0 & mz_{CG} + S_{xy} & -my_{CG} + S_{xz} \\ \dots & -mz_{CG} + S_{yx} & 0 & mx_{CG} + S_{yz} \\ \dots & my_{CG} + S_{zx} & -mx_{CG} + S_{zy} & 0 \\ \dots & \cdot & \cdot & \cdot \\ \dots & \cdot & \cdot & \cdot \\ \dots & \cdot & \cdot & \cdot \end{bmatrix}. \quad (14.25)$$

The first moments of mass must vanish at the centre of mass.

The coordinates of the centre of gravity with respect to the reference coordinate system are:

$$x_{\text{CG}} = \frac{-S_{yz}}{m_{yy}} = \frac{S_{zy}}{m_{zz}}, \quad (14.26)$$

$$y_{\text{CG}} = \frac{-S_{zx}}{m_{zz}} = \frac{S_{xz}}{m_{xx}}, \quad (14.27)$$

$$z_{\text{CG}} = \frac{-S_{xy}}{m_{xx}} = \frac{S_{yx}}{m_{yy}}. \quad (14.28)$$

14.3.4 Second Moments of Mass

The symmetric second moments of mass $[I_{\text{CG}}]$ of the spacecraft with respect to the centre of gravity and with axes parallel to the reference coordinate system are:

$$[I_{\text{CG}}] = \begin{bmatrix} \bar{I}_{xx} & \bar{I}_{xy} & \bar{I}_{xz} \\ \bar{I}_{zx} & \bar{I}_{yy} & \bar{I}_{yz} \\ \bar{I}_{zx} & \bar{I}_{zy} & \bar{I}_{zz} \end{bmatrix}. \quad (14.29)$$

The principal second moments of mass $[I_{\text{principal}}]$ with respect to the centre of gravity and the associated principal axes of inertia $[Q]$ are:

$$[I_{\text{principal}}] = \begin{bmatrix} I_{11} & 0 & 0 \\ 0 & I_{22} & 0 \\ 0 & 0 & I_{33} \end{bmatrix}, [Q] = \begin{bmatrix} q_{11} & q_{12} & q_{31} \\ q_{12} & q_{22} & q_{32} \\ q_{11} & q_{23} & q_{33} \end{bmatrix}. \quad (14.30)$$

The theory in this subsection will be illustrated by an example.

Example

There are three identical mass point $N_P = 3$ with the following mass matrix

$$[M_{\text{RB},P}] = \begin{bmatrix} 10 & 0 & 0 & 0 & 0 & 0 \\ 0 & 10 & 0 & 0 & 0 & 0 \\ 0 & 0 & 10 & 0 & 0 & 0 \\ 0 & 0 & 0 & 2 & 0 & 0 \\ 0 & 0 & 0 & 0 & 2 & 0 \\ 0 & 0 & 0 & 0 & 0 & 2 \end{bmatrix}.$$

The coordinates of the mass points are with respect to the origin of the global coordinate system.

- $P_1 \lfloor x, y, z \rfloor = \lfloor 0.5, 0, 0 \rfloor$
- $P_2 \lfloor x, y, z \rfloor = \lfloor 0, 0.5, 0 \rfloor$
- $P_3 \lfloor x, y, z \rfloor = \lfloor 0, 0, 0.5 \rfloor$

The total mass matrix at the origin becomes

$$[M_{RB,O}] = \begin{bmatrix} 30 & 0 & 0 & 0 & 0 & -5 & 5 \\ 0 & 30 & 0 & 5 & 0 & 0 & -5 \\ 0 & 0 & 30 & -5 & 5 & 0 & 0 \\ 0 & 5 & -5 & 8 & 0 & 0 & 0 \\ -5 & 0 & 5 & 0 & 8 & 0 & 0 \\ 5 & -5 & 0 & 0 & 0 & 0 & 8 \end{bmatrix}.$$

The centre of mass is given by $P_{CG} \lfloor x, y, z \rfloor_{CG} = \lfloor 0.1667, 0.1667, 0.1667 \rfloor$.

The mass matrix with respect to the centre of gravity becomes

$$[M_{RB,CG}] = \begin{bmatrix} 30 & 0 & 0 & 0 & 0 & 0 \\ 0 & 30 & 0 & 0 & 0 & 0 \\ 0 & 0 & 30 & 0 & 0 & 0 \\ 0 & 0 & 0 & 6.3333 & 0.8333 & 0.8333 \\ 0 & 0 & 0 & 0.8333 & 6.3333 & 0.8333 \\ 0 & 0 & 0 & 0.8333 & 0.8333 & 6.3333 \end{bmatrix}.$$

The principle second moments of mass is now

$$[I_{\text{principle}}] = \begin{bmatrix} 5.5 & 0 & 0 \\ 0 & 5.5 & 0 \\ 0 & 0 & 8.0 \end{bmatrix},$$

and the associated eigenvectors $[Q]$

$$[Q] = \begin{bmatrix} 0.7071 & 0.4082 & 0.5774 \\ -0.7071 & 0.4082 & 0.5774 \\ 0 & -0.8165 & 0.5774 \end{bmatrix}.$$

End of example

14.3.5 Finite Element Model Mass Matrix

The finite element mass matrix will be calculated, in general, in a local coordinate system. The element mass matrix will be transformed in the global system and added to the global mass matrix $[M]$. The transformation of the global mass matrix $[M]$ into a 6x6 rigid body mass matrix can be done using the rigid body

modes with respect to the origin of the global coordinate system. The stiffness matrix $[K]$ and the geometric matrices are used to calculate the rigid body modes.

Afterwards the centre of mass and the principal second moments of mass can be obtained using (14.25) and (14.29).

The rigid body modes can be calculated as follows.

Rigid-Body Modes

If the linear dynamic system is not constrained the system can move as a rigid body. This means that during the movement as a rigid body no elastic forces will occur in the dynamic system. If this is the case, the stiffness matrix $[K]$ is singular (semi-positive-definite). In general, there are 6 possible motions as rigid-body; three translations and three rotations. The six rigid-body modes can be calculated very easily using the stiffness matrix $[K]$. The free-free system (with n degrees of freedom) is constrained at one node (i.e. the origin of the global system) with 6 degrees of freedom; three translations and three rotations. The set of degrees of freedom is called the R -set. The other elastic degrees of freedom are placed in the E -set, such that $n = R + E$. The constrained R-set is determinate, so no strains will be introduced in the elastic system. The R-set (origin) consists of 6 unit displacement and rotations and those will be enforced on the system. The rigid body motion can be calculated with the following equation

$$\begin{bmatrix} K_{EE} & K_{ER} \\ K_{RE} & K_{RR} \end{bmatrix} \begin{Bmatrix} \Phi_{R,E} \\ I \end{Bmatrix} = \begin{Bmatrix} 0 \\ 0 \end{Bmatrix}, \quad (14.31)$$

where $[I]$ is the identity matrix and $[\Phi_{R,E}]$ the E -set part of the rigid-body motion.

From the first equation of (14.31) the E -set part of the rigid-body mode can be solved

$$[\Phi_{R,E}] = -[K_{EE}]^{-1}[K_{ER}]. \quad (14.32)$$

The complete matrix of the 6 rigid body modes becomes

$$[\Phi_R] = \begin{bmatrix} -[K_{EE}]^{-1}[K_{ER}] \\ I \end{bmatrix}. \quad (14.33)$$

The rigid-body mode may be either extracted from the eigenvalue problem or calculated by partitioning the stiffness matrix in E -set and R -set submatrices. Using the geometric information of the nodes with coordinates (x,y,z) there is another way to calculate the rigid-body mode.

The geometric matrix

The geometric matrix of a node is obtained by translations along the x -, y - and z -axis and rotations about the x -, y - and z -axis. In fact, in the geometric matrix the motion of point P with respect to origin O is given with matrix $[T_P]$ (see (14.16)).

The rigid-body mode is built up from the geometric matrices of all nodes with respect to the origin of the global coordinate system. There are six rigid-body modes. The rigid body motion with respect to the origin is a column assembly of the node geometric matrices

$$[\Phi_R] = \begin{bmatrix} T_1 \\ \cdot \\ \cdot \\ T_N \end{bmatrix}, \quad (14.34)$$

where N is the number of nodes.

The 6×6 rigid body matrix with respect to the origin of the global system can be obtained by

$$[M_{RB,O}] = [\Phi_R]^T [M] [\Phi_R]. \quad (14.35)$$

Afterwards the centre of mass and the principle second moments of mass can be obtained using (14.25) through (14.29).

14.4 Literature

- Agrawal, B.N., 1986, *Design of Geosynchronous Spacecraft*, Prentic-Hall.
- Saleh J.H., Hastings, D.E. and Newman, D.J., 2002, *Spacecraft Design Lifetime*, Journal of Spacecraft and Rockets, Vol. 39, No. 2, March-April 2002.
- Strang, G., 1988, *Linear Algebra and its Applications*, third edition, Harcourt Brace Jovanovich publishers, ISBN 0-15-551005-3.
- Williamson, M., 1990, *The Communication Satellite*, Adam Hilger, chapter A2.

14.5 Exercises

14.5.1 Mass computer programme

Set up an EXCEL® sheet to calculate the global matrix from a number of boxes with a certain off set from the origin and box coordinate system. The box coordinate system is referred to the global coordinate system. The mass and principal second moments of mass of the boxes are given (measured elsewhere). After that, calculate the centre of mass and the mass matrix with respect to the centre of mass. Calculate the principal second moments of mass and associated eigenvectors. Re-do the last example.

15 Natural Frequencies, an Approximation

15.1 Introduction

Generally, when calculating the natural frequencies of complex dynamic linear systems the finite element analysis method is applied. However, it is good practice to first apply a method to approximately calculate the natural frequency of that system to get a feel for the value of the natural frequency. The system will be simplified as much as possible in order to be able to use an approximate method. In this chapter, the following methods used to quickly obtain the value of the natural frequency will be discussed:

- Static displacement method
- Rayleigh's¹ quotient [Temple 1956]
- Dunkerley's equation [Anderson 1967]

The theory will be illustrated with examples.

15.2 Static Displacement Method

The natural frequency of an SDOF system, as shown in Fig. 15.1, is given by

$$f_n = \frac{1}{2\pi} \sqrt{\frac{k}{m}}. \quad (15.1)$$

If a 1g acceleration is acting on the mass m (kg) the inertia force mg (N) will compress the spring with a spring stiffness k (N/m) with a static displacement x_{stat}

1. Lord Rayleigh, whose given name was John William Strutt (1842–1919)]

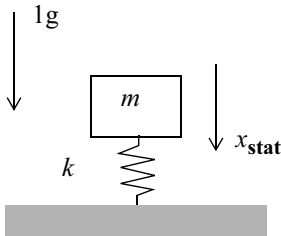


Fig. 15.1 Undamped SDOF system

$$x_{\text{stat}} = \frac{mg}{k}. \quad (15.2)$$

The static displacement x_{stat} has the dimension (m). This means that we can rewrite (15.1) as follows

$$f_n = \frac{1}{2\pi} \sqrt{\frac{k}{m}} = \frac{1}{2\pi} \sqrt{\frac{g}{x_{\text{stat}}}}. \quad (15.3)$$

The approximation of the natural frequency, using the static displacement method, is only applicable if the dynamic system has a dominant lumped (discrete) mass with respect to the distributed mass.

If we calculate the static displacement Δ per 1 m/s^2 the approximation of the natural frequency is

$$f_n = \frac{1}{2\pi} \sqrt{\frac{k}{m}} = \frac{1}{2\pi} \sqrt{\frac{1}{\Delta}}. \quad (15.4)$$

A spacecraft placed on a payload adapter is such a system. The mass of the payload adapter is (much) less than the lumped mass of the spacecraft in the centre of gravity (centre of mass). The static displacement of the centre of gravity, due to the unit acceleration inertia loads, can be used to calculate the natural frequencies of the spacecraft placed on the payload adapter.

Given a spacecraft with a total mass of $M_{\text{tot}} = 2500 \text{ kg}$. The centre of gravity of the spacecraft is located at $h = 1.5 \text{ m}$ above the interface with the conical payload adapter. The diameter at the top of the cone of the payload adapter is $d = 1.2 \text{ m}$. The configuration of the spacecraft is shown in Fig. 15.2. The diameter at the lower side is $D = 3 \text{ m}$. The height of the cone is $H = 1.5 \text{ m}$. The cone is made of CFRP with an isotropic Young's modulus $E = 120 \text{ GPa}$ and a Poisson's ratio $\nu = 0.3$. The thickness of the cone is $t = 5 \text{ mm}$.

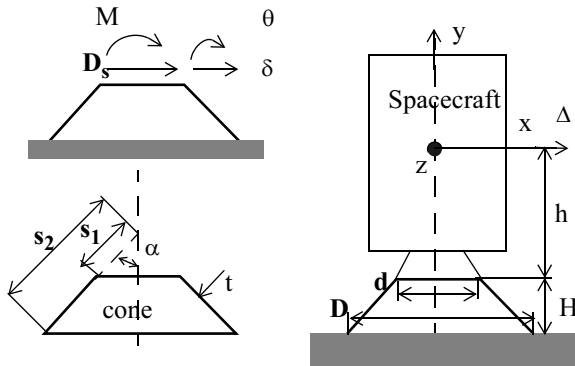


Fig. 15.2 Spacecraft mounted on a conical payload adapter

Calculate the natural frequency, associated with the first bending mode in the x–y plane, when the spacecraft has been placed on the conical payload adapter that is clamped at the lower side of the cone. The spacecraft is very well connected with the payload adapter and discontinuities do not exist.

In [Seide 1972] the following influence coefficients can be found

$$\delta = \frac{1 - \frac{s_1}{s_2}}{\pi E t (\sin \alpha)^3} \left\{ \frac{\ln \frac{s_2}{s_1}}{1 - \frac{s_1}{s_2}} - 2 + \left(1 + \frac{s_1}{s_2} \right) \left[\frac{1}{2} + (1 + \nu)(\sin \alpha)^2 \right] \right\} D_s + \frac{1 - \frac{s_1}{s_2}}{\pi E t (\sin \alpha)^3} \left\{ 1 - \left(1 + \frac{s_1}{s_2} \right) \left[\frac{1}{2} + (1 + \nu)(\sin \alpha)^2 \right] \right\} \frac{M}{s_1 \cos \alpha} , \quad (15.5)$$

and

$$\theta = \frac{1 - \frac{s_1}{s_2}}{\pi E t s_1 (\sin \alpha)^3 \cos \alpha} \left\{ 1 - \left(1 + \frac{s_1}{s_2} \right) \left[\frac{1}{2} + (1 + \nu)(\sin \alpha)^2 \right] \right\} D_s + \frac{1 - \frac{s_1}{s_2}}{\pi E t s_1 (\sin \alpha)^3 \cos \alpha} \left\{ \left(1 + \frac{s_1}{s_2} \right) \left[\frac{1}{2} + (1 + \nu)(\sin \alpha)^2 \right] \right\} \frac{M}{s_1 \cos \alpha} . \quad (15.6)$$

The shear force is $D_s = M_{\text{tot}}$ (N) and the bending moment $M = M_{\text{tot}}h$ (Nm). The total static displacement Δ (m), of the centre of gravity, due to 1m/s^2 acceleration in the x-direction is

$$\Delta = \delta + h\theta$$

The natural frequency f_n , corresponding to a bending mode shape in the x -direction is

$$f_n = \frac{1}{2\pi\sqrt{\Delta}} = \frac{1}{2\pi\sqrt{\frac{1}{1.8086 \times 10^{-5}}}} = 37.42 \text{ Hz}$$

In our calculations we have neglected the mass of the payload adapter. The spacecraft on top of the payload adapter was assumed to be rigid. The influence of a flexible spacecraft on top of the flexible payload adapter can be calculated using Dunkerley's method.

15.3 Rayleigh's Quotient

We define Rayleigh's quotient as [Temple 1956]

$$R(u) = \frac{\{u\}^T [K] \{u\}}{\{u\}^T [M] \{u\}}, \quad (15.7)$$

where $\{u\}$ is an admissible vector (assumed mode shape) that fulfils the boundary conditions, $[M]$ the positive-definite mass matrix, $\{u\}^T [M] \{u\} > 0$ and $[K]$ the stiffness matrix.

The minimum stationary value of Rayleigh's quotient $R(u)$ can be found when

$$\delta R(u) = 0. \quad (15.8)$$

Thus

$$\delta R(u) = \delta \{u\}^T 2 \left\{ \frac{[K] \{u\}}{\{u\}^T [M] \{u\}} - \frac{\{u\}^T [K] \{u\} [M] \{u\}}{(\{u\}^T [M] \{u\})^2} \right\} = 0. \quad (15.9)$$

In general, the “kinetic energy” (generalised mass) is $\{u\}^T [M] \{u\} \neq 0 = m_g$, thus (15.9) can be rewritten as

$$[K] \{u\} - R(u) [M] \{u\} = 0. \quad (15.10)$$

Rayleigh's quotient is analogous to the eigenvalue problem

$$([K] - \lambda[M]) \{\phi\} = 0. \quad (15.11)$$

Rayleigh's quotient $R(u)$ is equal to the eigenvalue λ only if $\{u\} = \{\phi\}$. We normalise the mode shapes $[\Phi]$ such that

$$[\Phi]^T [M] [\Phi] = [I] \text{ and } [\Phi]^T [K] [\Phi] = \langle \lambda \rangle.$$

We can express the assumed vector $\{u\}$ as follows

$$\{u\} = [\Phi]\{\eta\}. \quad (15.12)$$

Equation (15.7) can then be written

$$R(u) = \frac{\{u\}^T [K] \{u\}}{\{u\}^T [M] \{u\}} = \frac{\sum_j \eta_j^2 \lambda_j}{\sum_j \eta_j^2}. \quad (15.13)$$

Assume the mode shape $\{\phi_i\}$ is dominant with respect to the other mode shapes, then $\eta_j = \varepsilon_j \eta_i$ with $\varepsilon_j \ll 1$. When $\{\phi_i\} = \{\phi_1\}$ and $(\lambda_j - \lambda_1) \geq 0$ (15.13) becomes [Meirovitch 1975]

$$R(u) = \frac{\sum_j \eta_j^2 \lambda_j}{\sum_j \eta_j^2} = \frac{\eta_i^2 \lambda_1 + \eta_i^2 \sum_{j:j \neq i} \varepsilon_j^2 \lambda_j}{\eta_i^2 + \eta_i^2 \sum_{j:j \neq i} \varepsilon_j^2} \approx \lambda_1 + \sum_{j:j \neq i} \varepsilon_j^2 (\lambda_j - \lambda_1) \geq \lambda_1. \quad (15.14)$$

Rayleigh's quotient $R(u)$ will result in an upper bound value of the eigenvalue λ_i corresponding with the assumed mode shape $\{u\}$. Rayleigh's quotient is never below λ_1 and never above λ_n , with n the numbers of DOFs, [Sprang 1988].

A 1 g gravitational field is applied to the masses of the system, shown in Fig. 15.3. The static displacement vector $\{x\}$ becomes

$$\{x\} = \frac{mg}{k} \begin{Bmatrix} 1 & -1 & 0 \\ -1 & 3 & -2 \\ 0 & -2 & 5 \end{Bmatrix}^{-1} \begin{Bmatrix} 1 \\ 1 \\ 1 \end{Bmatrix} = \frac{mg}{k} \begin{Bmatrix} 1.8533 \\ 0.8533 \\ 0.3333 \end{Bmatrix}.$$

We take as admissible vector $\{u\}$

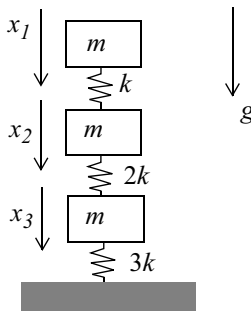


Fig. 15.3 3 DOFs MDOF linear system

$$\{u\} = \begin{Bmatrix} 1.8533 \\ 0.8533 \\ 0.3333 \end{Bmatrix}.$$

Rayleigh's quotient $R(u)$ now becomes

$$R(u) = \frac{\{u\}^T [K] \{u\}}{\{u\}^T [M] \{u\}} = 0.4400 \frac{k}{m}.$$

The lowest theoretical eigenvalue is $\lambda_1 = 0.41587 \frac{k}{m}$.

Rayleigh's quotient of a bending beam is defined as

$$R(u) = \frac{\int_0^L EI(u'')^2 dx}{\int_0^L mu^2 dx}, \quad (15.15)$$

where EI the bending stiffness of the beam (Nm^2), m the mass per unit of length (kg/m), $u(x)$ the assumed mode and L the length of the beam (m).

For a beam, simply supported at both ends, we take the assumed mode $u(x)$

$$u(x) = \frac{x}{L} \left(1 - \frac{x}{L}\right).$$

Rayleigh's quotient becomes

$$R(u) = 120 \frac{EI}{mL^4}.$$

The theoretical value for the eigenvalue $\lambda_1 = \pi^4 \frac{EI}{mL^4}$.

15.4 Dunkerley's Method

Dunkerley published his equation in 1894 [Brock 1976].

The equation of Dunkerley is a method to estimate the lowest natural frequency of a dynamic system, which is composed of substructures (components) of which the lowest and lower natural frequencies are known. The damping is not involved in the equation of Dunkerley. The equation of Dunkerley will predict an accurate lowest natural frequency when this frequency is far removed from the next natural frequencies.

The eigenvalue problem of an undamped dynamic system can be written as

$$(-\omega^2[M] + [K])\{\phi\} = \{0\}, \quad (15.16)$$

with $[M]$ is the mass matrix, and $[K]$ is the positive-definite stiffness matrix. The inverse of the stiffness matrix, the flexibility matrix $[G] = [K]^{-1}$ exists and $\{\phi\}$ the mode shape corresponding the natural frequency $\omega > 0$.

We can rewrite (15.16) as follows

$$\left(\frac{1}{\omega^2}[I] - [G][M]\right)\{\phi\} = \{0\}. \quad (15.17)$$

The solution of the determinant of (15.17), with n DOFs, can be formally written as

$$\left(\frac{1}{\omega^2} - \frac{1}{\omega_1^2}\right)\left(\frac{1}{\omega^2} - \frac{1}{\omega_2^2}\right)\dots\left(\frac{1}{\omega^2} - \frac{1}{\omega_n^2}\right) = 0, \quad (15.18)$$

with $\frac{1}{\omega_1^2}, \frac{1}{\omega_2^2}, \dots, \frac{1}{\omega_n^2}$ the solution, roots, of the characteristic equation

$$\left|\left(\frac{1}{\omega^2}[I] - [G][M]\right)\right| = 0. \quad (15.19)$$

The sum of the n eigenvalues of (15.19) equals the sum of the n diagonal terms of the matrix $[G][M]$ [Strang 1988]. This sum is known as the trace of $[G][M]$, thus

$$\text{trace}([G][M]) = \sum_{k=1}^n g_{kk}m_{kk} = \sum_{k=1}^n \left(\frac{1}{\omega_k^2}\right) \quad (15.20)$$

To estimate the lowest natural frequency ω_1 we may neglect the contribution of the higher natural frequencies ω_k , $k=2,3,\dots,n$. This approximation becomes more and more accurate if $\omega_1 \ll \omega_k$, $k=2,3,\dots,n$, then we obtain Dunkerley's equation

$$\frac{1}{\omega_1^2} \leq \sum_{k=1}^n g_{kk}m_{kk}. \quad (15.21)$$

The term $g_{kk}m_{kk}$ may be interpreted as a SDOF system with a discrete mass m_{kk} and a spring with spring stiffness g_{kk}^{-1} , as shown in Fig. 15.4. The natural frequency $\frac{1}{\omega_{kk}^2}$ of the equivalent SDOF system is

$$\frac{1}{\omega_{kk}^2} = g_{kk} m_{kk} = \frac{m_{kk}}{g_{kk}}. \quad (15.22)$$

Thus Dunkerley's equation, (15.21), becomes

$$\frac{1}{\omega_1^2} \leq \sum_{k=1}^n \frac{1}{\omega_{kk}^2}. \quad (15.23)$$

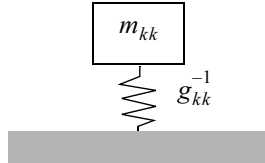


Fig. 15.4 Equivalent SDOF system in Dunkerley's equation

Consider one discrete mass at a time and neglect the other masses. The flexibility term g_{kk} can be calculated for the discrete mass by applying a unit load. The obtained displacement is, in fact, the flexibility g_{kk} . We shall illustrate that with an example.

Consider the dynamic system as shown in Fig. 15.3.

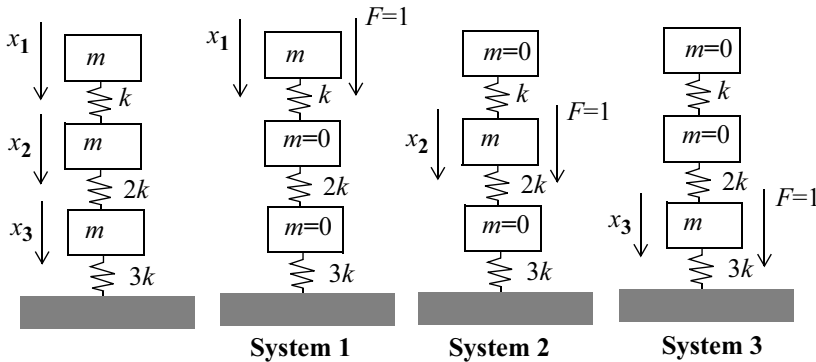


Fig. 15.5 Decomposition of the dynamic system in 3 systems

Equation (15.21) will be applied to calculate the lowest natural frequency of the complete dynamic system. The dynamic system has been decomposed into three systems; system 1, system 2 and system 3, as shown in Fig. 15.5.

Table 15.1 Example calculations Dunkerley's equation

System #	g_{kk}	m_{kk}
1	$\frac{1}{k} + \frac{1}{2k} + \frac{1}{3k} = \frac{11}{6k}$	m
2	$\frac{1}{2k} + \frac{1}{3k} = \frac{5}{6k}$	m
3	$\frac{1}{3k} = \frac{2}{6k}$	m
$\sum_{k=1}^3 g_{kk} m_{kk}$	$\frac{3m}{k}$	$\omega_1^2 = 0.3333 \frac{k}{m}$

The analysis procedure is illustrated in Table 15.1.

Suppose a dynamic system is built up of SDOFs on top of each other, as illustrated in Fig. 15.6. then we can derive an alternative equation of Dunkerley.

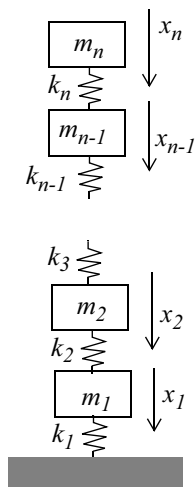


Fig. 15.6 n SDOF dynamic systems

The diagonal terms g_{kk} , $k = 1, 2, \dots, n$ of the flexibility matrix $[G] = [K]^{-1}$ ($[K]$ is a positive-definite matrix), can be written as follows

$$g_{kk} = \sum_{j=1}^k \frac{1}{k_j}. \quad (15.24)$$

Equation (15.21) becomes

$$\frac{1}{\omega_1^2} \leq \sum_{k=1}^n g_{kk} m_k = \sum_{k=1}^n m_k \sum_{j=1}^k \frac{1}{k_j} = \sum_{j=1}^n \frac{1}{k_j} \sum_{k=j}^n m_k. \quad (15.25)$$

The alternative equation of Dunkerley can be applied to the dynamic system as shown in Fig. 15.5. (15.25) will be applied to calculate the lowest natural frequency of a complete dynamic system. The dynamic system has been decomposed into three systems; system 1, system 2 and system 3, as shown in Fig. 15.7.

Table 15.2 Example calculations alternative Dunkerley's equation

System #	$n=3, j$	$\frac{1}{k_j}$	$\sum_{k=j}^n m_k$
1	3	$\frac{1}{k}$	m
2	2	$\frac{1}{2k}$	$2m$
3	1	$\frac{1}{3k}$	$3m$
$\sum_{j=1}^n \frac{1}{k_j} \sum_{k=j}^n m_k$		$\frac{3m}{k}$	$\omega_1^2 = 0.3333 \frac{k}{m}$

The procedure to calculate the lowest natural frequency, using the alternative equation of Dunkerley, is given in Table 15.2.

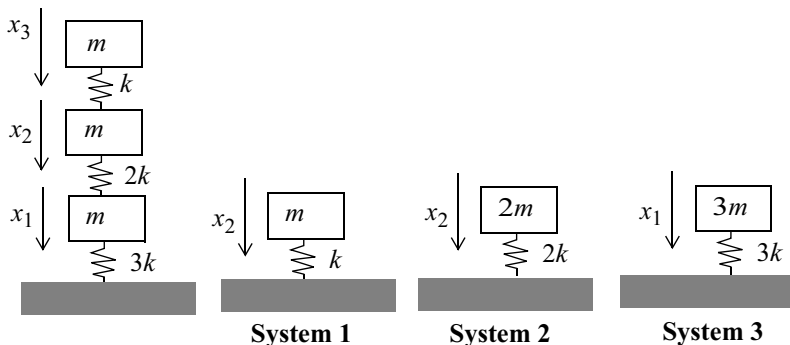


Fig. 15.7 Decomposition of dynamic system in 3 systems (alternative method)

The spacecraft mounted on the conical payload adapter is shown in Fig. 15.2. The spacecraft hardmounted at the interface between the spacecraft and the adapter has a lowest bending mode ($x-y$ plane) of $f_{sc} = 20$ Hz. Calculate the lowest natural frequency of the complete system (spacecraft and adapter). (15.25) will be applied to calculate the lowest natural frequency of a complete dynamic system. The dynamic system is composed of two systems; system 1 and system 2, as shown in Fig. . The procedure to calculate the lowest natural frequency, using the alternative equation of Dunkerley, is given in Table 15.3.

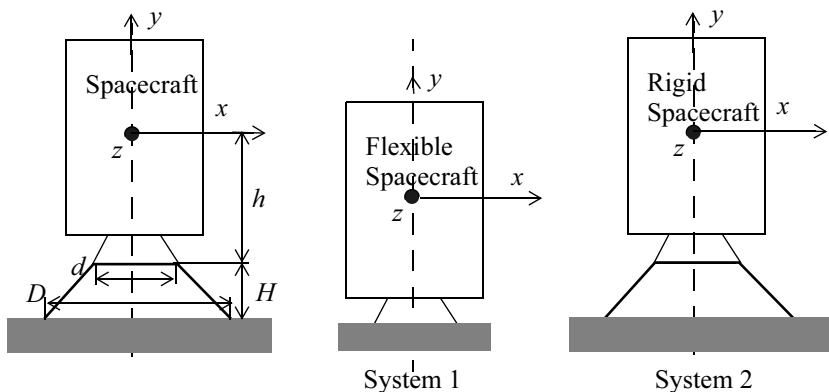


Fig. 15.8 Decomposition of dynamic system into 2 systems (alternative equation of Dunkerley)

Table 15.3 Spacecraft/payload adapter natural frequency calculations

System #	$n=2, j$	$\frac{(2\pi)^2}{\omega_j^2} = \frac{1}{k_j} \sum_{k=j}^n m_k$	$\sum_{k=j}^n m_k \text{ (kg)}$
1 Clamped flexible spacecraft	2	$\left(\frac{1}{f_{sc}}\right)^2 = \left(\frac{1}{20}\right)^2$	2500
2 Rigid spacecraft on payload adapter	1 result previous example	$\left(\frac{1}{37.42}\right)^2$	mass of payload adapter neglected
		$(2\pi)^2 \sum_{j=1}^n \frac{1}{k_j} \sum_{k=j}^n m_k$	$f = 17.64 \text{ Hz}$

15.5 Literature

- Anderson, R.A., 1967, *Fundamentals of Vibrations*, The Macmillan Company.
- Meirovitch, L., 1975, *Elements of Vibration Analysis*, McGraw-Hill, ISBN 0-07-041340-1.
- Seide P., 1972, *Influence Coefficients for End-Loaded Conical Shells*, AIAA Journal, Vol. 10, No. 12, pages 1717–1718.
- Strang, G., 1988, *Linear Algebra and its Applications*, Third edition, Harcourt Brace Javanovich Inc., ISBN 0-15551005-3.
- Temple, G., Bickley, W.G., 1956, *Rayleigh's principle, And Its Applications to Engineering*, Dover Publications.

15.6 Exercises

15.6.1 Natural frequency of airplane

An aeroplane settles 150 mm into its landing-gear springs when the aeroplane is at rest. What is the natural frequency f_n (Hz) for the vertical motion of the aeroplane with $g=9.81 \text{ m/s}^2$ [Moretti 2000]?

Answer: $f_n = 1.29 \text{ Hz}$.

15.6.2 Rayleigh's method

Demonstrate Rayleigh' method for estimating the fundamental frequency ω_n (Rad/s) of a uniform cantilever of length L (m), mass-per-unit-length m (kg/m), and a bending stiffness EI . Use the assumed deflection shape $w = \frac{x^3}{L}w_{\text{tip}}$.

15.6.3 Rayleigh's method

The considered structure is a bending beam supporting a discrete mass M , clamped at one side and simply supported at the other side. The mass per unit of length of the beam is m . Apply Rayleigh's method to approximate the natural frequency ω_o of the structure assuming a mode shape $\phi(x)) = \left(\frac{x}{L}\right)^2\left(\frac{x}{L} - 1\right)$.

$$\omega_o = \left(\frac{x}{L}\right)^2\left(\frac{x}{L} - 1\right)$$

$$\text{Answer: } R(\phi) \approx \omega_o^2 = \frac{\frac{2EI}{L^3}}{\frac{mL}{210} + \frac{1}{2}M\left[\frac{L_1^2}{L^2}\left(\frac{L_1}{L} - 1\right)\right]^2}.$$

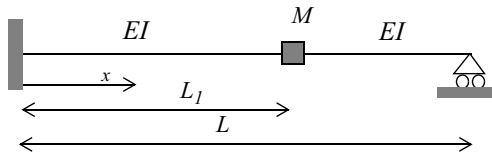


Fig. 15.9 Cantilevered structure with discrete mass

15.6.4 Equations of motion and natural frequencies

A dynamic system, as shown in Fig. 15.10, has 3 DOFs; w , φ and δ . The displacement δ is with respect to line A–B. Both DOFs w and φ are located in the middle of A–B. The structure in between A and B is rigid and has a mass m per unit of length (kg/m). The discrete mass M (kg) is coupled at the end of the massless elastic beam with a bending stiffness EI Nm². The beam is rigidly connected at point B. The complete dynamic system is supported by two spring with a springs stiffness k (N/m). The following values shall be used: $M = 0.15$ kg, $L_1=02$ m, $L_2=0.25$ m, $m=0.075$ kg/m, $\frac{3EI}{L_2^3} = (2\pi 100)^2 M$ and $k=10000$ N/m. The second moment of mass of the rigid beam A–B $I = \frac{1}{12}mL_1^3$ (kgm²).

1. Calculate the lowest natural frequency with the static displacement method, assuming $M \gg mL_1$.
2. Calculate the lowest natural frequency with Dunkerley's equation, using both the normal and the alternative equation.

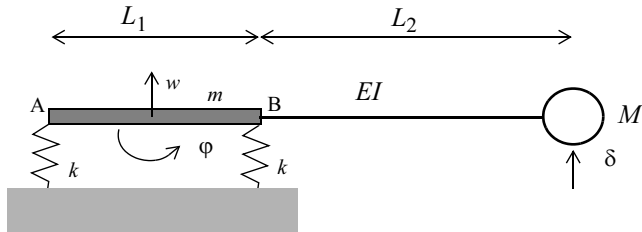


Fig. 15.10 Dynamic System with 3 DOFs

3. Calculate the lowest natural frequency using Rayleigh's quotient. Hint: use the deflection mode calculated in question 1.
4. Set up the equations of motion (e.g. using Lagrange's equations) and calculate the eigenvalues and compare these results with the approximations.

The homogeneous equations of motion are

$$\begin{bmatrix} mL_1 + M & M\left(\frac{1}{2}l_1 + l_2\right) & M \\ M\left(\frac{1}{2}l_1 + l_2\right) & I + M\left(\frac{1}{2}l_1 + l_2\right)^2 & M\left(\frac{1}{2}l_1 + l_2\right) \\ M & M\left(\frac{1}{2}l_1 + l_2\right) & M \end{bmatrix} \begin{Bmatrix} \ddot{w} \\ \ddot{\phi} \\ \ddot{\delta} \end{Bmatrix} + \begin{Bmatrix} 2k & 0 & 0 \\ 0 & kL_1 & 0 \\ 0 & 0 & \frac{3EI}{L_2^3} \end{Bmatrix} \begin{Bmatrix} w \\ \phi \\ \delta \end{Bmatrix} = \begin{Bmatrix} 0 \\ 0 \\ 0 \end{Bmatrix}$$

and the calculated natural frequencies $f = \begin{Bmatrix} 36.0 \\ 233.1 \\ 1577.5 \end{Bmatrix}$ Hz.

15.6.5 Calculation natural frequencies

A two mass system is illustrated in Fig. 15.11, Ceasar 1983]. Determine the natural frequency (Hz) of the two-mass system using.

1. the Dunkerly method
2. the Rayleigh method (use 1 g gravitation field to obtain displacement field)
3. exact method (4 DOFs)

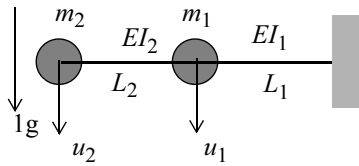


Fig. 15.11 Two-mass system

For numerical calculations use the following data:

- $E_1 = E_2 = 70 \text{ GPa}$
- $I_1 = 7.5 \times 10^{-6}, I_2 = 5.9 \times 10^{-6} \text{ m}^4$
- $L_1 = L_2 = 0.5 \text{ m}$

Answers: 14.02, 14.62, 14.50 Hz.

15.6.6 Equations of motion and natural frequencies

The MDOF system, as shown in Fig. 15.12, consists of five degrees of freedom.

- Derive the equations of motion using
 1. the equations of equilibrium (Newton's law)
 2. Lagrange's equations

The parameters have the following values; the masses (kg), $m_1 = 3, m_2 = 2, m_3 = 4, m_4 = 1$ and $m_5 = 4$, the spring stiffness (N/m), $k_1 = 3 \times 10^3, k_2 = 2 \times 10^3, k_3 = 5 \times 10^3, k_4 = 4 \times 10^3, k_5 = 6 \times 10^3, k_9 = 6 \times 10^3$ and $k_7 = 1 \times 10^3$.

First calculate the natural frequencies and associated normal modes and secondly calculate an approximation of the lowest natural frequency $\omega_{n,1}$ using the Rayleigh method. Use as assumed mode $\{\varphi_1\}$ the static deformation vector under a 1 g gravitation field.

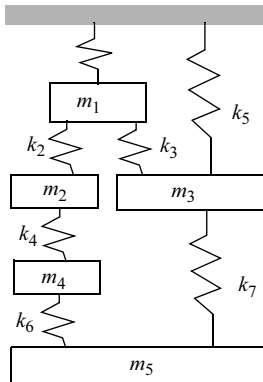


Fig. 15.12 MDOF dynamic system

Answer: Exact $\omega_{n,1} = 123.4 \text{ Rad/s.}$

15.6.7 Deployed Natural Frequency

A deployed solar array has the following simplified analysis model, as shown in Fig. 15.13. The solar is allowed to rotate, however, a rotational spring with spring stiffness $K = 50000 \text{ Nm/Rad}$ prevents that. The elastic beam has a length $L = 7 \text{ m}$, a bending stiffness $EI = 2.73 \times 10^5 \text{ Nm}^2$ and a total mass $M_1 = 14 \text{ kg}$. The tip mass $M_2 = 50 \text{ kg}$.

Calculate the lowest natural frequency using the Dunkerley's method. (hint: divide the system into three dynamic systems)

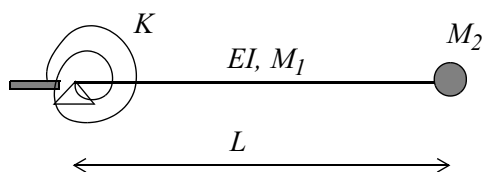


Fig. 15.13 Simplified analysis model deployed solar array

Answer: Dunkerley's method $f = 0.5776 \text{ Hz.}$

16 Modal Effective Mass

16.1 Introduction

The modal effective mass is a modal dynamic property of a structure associated with the modal characteristics; natural frequencies, mode shapes, generalised masses, and participation factors. The modal effective mass is a measure to classify the importance of a mode shape when a structure is excited by base acceleration (enforced acceleration). A high effective mass will lead to a high reaction force at the base, while mode shapes with low associated modal effective mass are barely excited by base acceleration and will give low reaction forces at the base. The effect of local modes is not well described with modal effective masses [Shunmugavel 1995, Witting 1996].

The modal effective mass matrix is a 6×6 mass matrix. Within this matrix the coupling between translations and rotations, for a certain mode shape, can be traced.

The summation over all modal effective masses will result in the mass matrix as a rigid-body.

In this chapter the theory behind the principle of the modal effective mass matrix will be discussed and the way in which the modal effective mass matrix can be obtained. The theory will be illustrated with an example.

16.2 Enforced Acceleration

An SDOF system with a discrete mass m , a damper element c and a spring element k is placed on a moving base that is accelerated with an acceleration $\ddot{u}(t)$. The resulting displacement of the mass is $x(t)$. The natural (circular) frequency

$\omega_n = \sqrt{\frac{k}{m}}$, the critical damping constant $c_{crit} = 2\sqrt{km}$ and the damping ratio $\zeta = \frac{c}{c_{crit}}$ are introduced. The amplification factor is defined as $Q = \frac{1}{2\zeta}$.

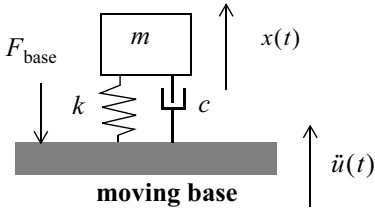


Fig. 16.1 Enforced acceleration of a damped SDOF system

A relative motion $z(t)$ is introduced, which is the displacement of the mass with respect to the base. The relative displacement is

$$z(t) = x(t) - u(t). \quad (16.1)$$

The equation of motion for the relative motion $z(t)$ is

$$\ddot{z}(t) + 2\zeta\omega_n\dot{z}(t) + \omega_n^2 z(t) = -\ddot{u}(t). \quad (16.2)$$

The enforced acceleration of the SDOF system is transformed into an external force. The absolute displacement $x(t)$ can be calculated from

$$\ddot{x}(t) = \ddot{z}(t) + \ddot{u}(t) = -2\zeta\omega_n\dot{z}(t) - \omega_n^2 z(t). \quad (16.3)$$

The reaction force $F_{base}(t)$, due to the enforced acceleration $\ddot{u}(t)$, is a summation of the spring force and the damping force

$$F_{base}(t) = kz(t) + c\dot{z}(t) = -m\{\ddot{z}(t) + \ddot{u}(t)\} = -m\ddot{x}(t). \quad (16.4)$$

Assuming harmonic vibration we can write the enforced acceleration

$$\ddot{u}(t) = \ddot{U}(\omega)e^{j\omega t}, \quad (16.5)$$

and also the relative motion $z(t)$

$$z(t) = Z(\omega)e^{j\omega t}, \dot{z}(t) = j\omega Z(\omega)e^{j\omega t} \text{ and } \ddot{z}(t) = -\omega^2 Z(\omega)e^{j\omega t} \quad (16.6)$$

and the absolute acceleration of the SDOF dynamic system is

$$\ddot{x}(t) = \ddot{X}(\omega)e^{j\omega t} = -\omega^2 X(\omega)e^{j\omega t}. \quad (16.7)$$

Equation (16.2) can be transformed in the frequency domain

$$[-\omega^2 + 2j\zeta\omega_n\omega + \omega_n^2]Z(\omega) = -\ddot{U}(\omega). \quad (16.8)$$

We are able to express the relative displacement $Z(\omega)$ in the enforced acceleration $\ddot{U}(\omega) = -\omega^2 U(\omega)$

$$Z(\omega) = \left(\frac{\omega}{\omega_n}\right)^2 H\left(\frac{\omega}{\omega_n}\right) U(\omega), \quad (16.9)$$

where $H(\omega) = \frac{1}{1 - \left(\frac{\omega}{\omega_n}\right)^2 + 2j\zeta\left(\frac{\omega}{\omega_n}\right)}$ is the frequency response function.

Using (16.3) we can write the absolute acceleration $\ddot{X}(\omega)$ as

$$\ddot{X}(\omega) = -\omega^2 [Z(\omega) + U(\omega)] = -\omega^2 \left[1 + \left(\frac{\omega}{\omega_n}\right)^2 H\left(\frac{\omega}{\omega_n}\right)\right] U(\omega), \quad (16.10)$$

or

$$\ddot{X}(\omega) = \left[1 + \left(\frac{\omega}{\omega_n}\right)^2 H\left(\frac{\omega}{\omega_n}\right)\right] \ddot{U}(\omega). \quad (16.11)$$

With the aid of (16.4) the reaction force at the base $F_{\text{base}}(\omega)$ now becomes

$$F_{\text{base}}(\omega) = m\ddot{X}(\omega) = m \left[1 + \left(\frac{\omega}{\omega_n}\right)^2 H\left(\frac{\omega}{\omega_n}\right)\right] \ddot{U}(\omega). \quad (16.12)$$

In this frame the mass m is the effective mass $M_{\text{eff}} = m$. The reaction force $F_{\text{base}}(\omega)$ is proportional to the effective mass M_{eff} and the base excitation $\ddot{U}(\omega)$ multiplied by the amplification $1 + \left(\frac{\omega}{\omega_n}\right)^2 H\left(\frac{\omega}{\omega_n}\right)$. Similar relations will be derived for multi-degrees of freedom (MDOF) dynamic systems.

When the excitation frequency is equal to the natural frequency of the SDOF $\omega = \omega_n$, the reaction force becomes

$$|F_{\text{base}}(\omega_n)| = \left|m \left[1 + \frac{1}{2j\zeta}\right] \ddot{U}(\omega_n)\right| \approx M_{\text{eff}} Q \ddot{U}(\omega_n). \quad (16.13)$$

(16.12) can then be written in a dimensionless form

$$\frac{F_{\text{base}}(\omega)}{m \ddot{U}(\omega)} = \left[1 + \left(\frac{\omega}{\omega_n}\right)^2 H\left(\frac{\omega}{\omega_n}\right)\right]. \quad (16.14)$$

16.3 Modal Effective Masses of an MDOF System

The undamped (matrix) equations of motion for a free-free elastic body can be written as

$$[M]\{\ddot{x}(t)\} + [K]\{x(t)\} = \{F(t)\}. \quad (16.15)$$

The external or boundary degrees of freedom are denoted with the index j and the internal degrees of freedom with the index i . The structure will be excited at the boundary DOFs; 3 translations and 3 rotations.

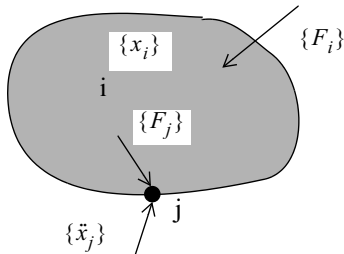


Fig. 16.2 Enforced structure

The number of boundary degrees of freedom is less than or equal to 6. The DOFs and forces are illustrated in Fig. 16.2. The matrix (16.15) may be partitioned as follows

$$\begin{bmatrix} M_{ii} & M_{ij} \\ M_{ji} & M_{jj} \end{bmatrix} \begin{Bmatrix} \ddot{x}_i \\ \ddot{x}_j \end{Bmatrix} + \begin{bmatrix} K_{ii} & K_{ij} \\ K_{ji} & K_{jj} \end{bmatrix} \begin{Bmatrix} x_i \\ x_j \end{Bmatrix} = \begin{Bmatrix} F_i \\ F_j \end{Bmatrix}. \quad (16.16)$$

In [Craig 1968] it is proposed to depict the displacement vector $\{x(t)\}$ on a basis of 6 rigid-body modes $[\Phi_r]$ with $\{x_j\} = [I]$ and elastic mode shapes $[\Phi_p]$ with fixed external degrees of freedom $\{x_j\} = \{0\}$ calculated from the eigenvalue problem $([K_{ii}] - \langle \lambda_p \rangle [M_{ii}])[\Phi_{ri}] = [0]$. $\{x\}$ can be expressed as

$$\{x\} = [\Phi_r]\{x_j\} + [\Phi_p]\{\eta_p\} = [\Phi_r, \Phi_p] \begin{Bmatrix} x_j \\ \eta_p \end{Bmatrix} = [\Psi]\{X\}. \quad (16.17)$$

The static modes can be obtained, assuming zero inertia effects, and $\{F_i\} = \{0\}$, and prescribe successively a unit displacement for the 6 boundary DOFs, thus $\{x_j\} = [I]$. (16.16) may be written as follows

$$\begin{bmatrix} K_{ii} & K_{ij} \\ K_{ji} & K_{jj} \end{bmatrix} \begin{Bmatrix} x_i \\ x_j \end{Bmatrix} = \begin{Bmatrix} 0 \\ 0 \end{Bmatrix}. \quad (16.18)$$

Enforced displacement $\{x_j\}$ will not introduce reaction forces in boundary DOFs.

From the first equation of (16.18) we find for $\{x_i\}$

$$[K_{ii}]\{x_i\} + [K_{ij}][x_j] = 0, \quad (16.19)$$

hence

$$\{x_i\} = -[K_{ii}]^{-1}[K_{ij}]\{x_j\}, \quad (16.20)$$

and therefore

$$[\Phi_{ij}] = -[K_{ii}]^{-1}[K_{ij}][I] = -[K_{ii}]^{-1}[K_{ij}]. \quad (16.21)$$

The static transformation now becomes

$$\{x\} = \begin{Bmatrix} x_i \\ x_j \end{Bmatrix} = \begin{bmatrix} \Phi_{ij} \\ I \end{bmatrix} \{x_j\} = [\Phi_r]\{x_j\}. \quad (16.22)$$

Using (16.18) it follows that

$$[K][\Phi_r] = \{0\}. \quad (16.23)$$

Assuming fixed external degrees of freedom $\{x_j\} = \{0\}$ and also assuming harmonic motions $x(t) = X(\omega)e^{j\omega t}$ the eigenvalue problem can be stated as

$$([K_{ii}] - \lambda_{k,p}[M_{ii}])\{X(\lambda_{k,p})\} = \{0\}, \quad (16.24)$$

or more generally as

$$([K_{ii}] - \langle \lambda_k \rangle [M_{ii}])[\Phi_{ip}] = \{0\}, \quad (16.25)$$

where λ_k the eigenvalue associated with the mode shape $\{\phi_{ip,k}\}$, $k = 1, 2, \dots, j$.

The internal degrees of freedom $\{x_i\}$ will be projected on the set of orthogonal mode shapes (modal matrix) $[\Phi_{ip}]$, thus

$$\{x_i\} = [\Phi_{ip}]\{\eta_p\}. \quad (16.26)$$

The modal transformation becomes

$$\{x\} = \begin{Bmatrix} x_i \\ x_j \end{Bmatrix} = \begin{bmatrix} \Phi_{ip} \\ 0 \end{bmatrix} \{\eta_p\} = [\Phi_p] \{\eta_p\}. \quad (16.27)$$

The Craig–Bampton (CB) transformation matrix $[\Psi]$ is

$$\{x\} = [\Phi_r, \Phi_p] \begin{bmatrix} x_j \\ \eta_p \end{bmatrix} = [\Psi] \{\chi\}, \quad (16.28)$$

where $[\Phi_r]$ the rigid body modes, $[\Phi_p]$ the modal matrix, $\{x_j\}$ the external or boundary degrees of freedom ($j \leq 6$) and $\{\eta_p\}$ the generalised coordinates. In general, the number of generalised coordinates p is much less than the total number of degrees of freedom $n = i + j$, $p \ll i$.

The CB transformation (16.28) will be substituted into (16.15) assuming equal potential and kinetic energies, hence

$$[\Psi]^T [M][\Psi] \{\ddot{\chi}\} + [\Psi]^T [K][\Psi] \{\chi\} = [\Psi]^T \{F(t)\} = \{f(t)\}, \quad (16.29)$$

further elaborated it is found

$$\begin{bmatrix} M_{rr} & M_{jp} \\ M_{pj} & \langle m_p \rangle \end{bmatrix} \begin{Bmatrix} \ddot{x}_j \\ \ddot{\eta}_p \end{Bmatrix} + \begin{bmatrix} \tilde{K}_{jj} & K_{jp} \\ K_{pj} & \langle k_p \rangle \end{bmatrix} \begin{Bmatrix} x_j \\ \eta_p \end{Bmatrix} = \begin{bmatrix} \Phi_{ij} & \Phi_p \\ I & 0 \end{bmatrix}^T \begin{Bmatrix} F_i \\ F_j \end{Bmatrix}, \quad (16.30)$$

with

- $[M_{rr}]$ the 6×6 rigid body mass matrix with respect to the boundary DOFs
- $[\tilde{K}_{jj}]$ the Guyan reduced stiffness matrix (j -set)
- $\langle m_p \rangle$ the diagonal matrix of generalised masses, $\langle m_p \rangle = [\Phi_p]^T [M][\Phi_p]$
- $\langle k_p \rangle$ the diagonal matrix of generalised stiffnesses,

$$\langle k_p \rangle = [\Phi_p]^T K [\Phi_p] = \langle \lambda_p \rangle \langle m_p \rangle = \langle \omega_p^2 \rangle \langle m_p \rangle$$

- $[K_{ip}] = [\Phi_{ij}]^T [K_{ii}] [\Phi_p] + [K_{ji}] [\Phi_p] = (-[K_{ij}]^T [K_{ii}]^{-1} [K_{ii}] + [K_{ji}]) [\Phi_p] = [0]$
- $[K_{pi}] = [K_{ip}]^T = [0]$
- $[\tilde{K}_{jj}] = [\Phi_r]^T [K][\Phi_r] = [0]$

Thus (16.30) becomes

$$\begin{bmatrix} M_{rr} & L^T \\ L & \langle m_p \rangle \end{bmatrix} \begin{Bmatrix} \ddot{x}_j \\ \ddot{\eta}_p \end{Bmatrix} + \begin{bmatrix} 0 & 0 \\ 0 & \langle m_p \lambda_p \rangle \end{bmatrix} \begin{Bmatrix} x_j \\ \dot{\eta}_p \end{Bmatrix} = \begin{bmatrix} \Phi_{ij} & \Phi_p \\ I & 0 \end{bmatrix}^T \begin{Bmatrix} 0 \\ F_j \end{Bmatrix} = \begin{Bmatrix} F_j \\ 0 \end{Bmatrix}, \quad (16.31)$$

where $[M_{jp}] = [\Phi_r]^T [M] [\Phi_p] = [L]^T$, $[L]^T$ is the matrix with the modal participation factors, $L_{kl} = \{\phi_{r,k}\}^T [M] \{\phi_{p,l}\}$, $k = 1, 2, \dots, 6$, $l = 1, 2, \dots, p$.

The matrix of modal participation factors couples the rigid-body modes $[\Phi_r]$ with the elastic modes $[\Phi_p]$ and $\{F_i\} = \{0\}$. No internal loads are applied.

Introducing the modal damping ratios ζ_p (16.31) can be written as follows

$$\begin{bmatrix} M_{rr} & L^T \\ L & \langle m_p \rangle \end{bmatrix} \begin{Bmatrix} \ddot{x}_j \\ \ddot{\eta}_p \end{Bmatrix} + \begin{bmatrix} 0 & 0 \\ 0 & \langle 2m_p \zeta_p \omega_p \rangle \end{bmatrix} \begin{Bmatrix} \dot{x}_j \\ \dot{\eta}_p \end{Bmatrix} + \begin{bmatrix} 0 & 0 \\ 0 & \langle m_p \lambda_p \rangle \end{bmatrix} \begin{Bmatrix} x_j \\ \eta_p \end{Bmatrix} = \begin{Bmatrix} F_j \\ 0 \end{Bmatrix} \quad (16.32)$$

(16.32) can be divided into two equations

$$[M_{rr}]\{\ddot{x}_j\} + [L]^T\{\ddot{\eta}_p\} = \{F_j\}, \quad (16.33)$$

and

$$[L]\{\ddot{x}_j\} + \langle m_p \rangle \{\ddot{\eta}_p\} + \langle 2m_p \zeta_p \omega_p \rangle \{\dot{\eta}_p\} + \langle m_p \lambda_p \rangle \{\eta_p\} = \{0\}. \quad (16.34)$$

(16.33) and (16.34), when transformed in the frequency domain, give

$$[M_{rr}]\{\ddot{X}_j\} + [L]^T\{\ddot{\Pi}_p\} = \{F_j\}, \quad (16.35)$$

and

$$[L]\{\ddot{X}_j\} + \langle m_p \rangle \{\ddot{\Pi}_p\} + \langle 2m_p \zeta_p \omega_p \rangle \{\dot{\Pi}_p\} + \langle m_p \lambda_p \rangle \{\Pi_p\} = \{0\}, \quad (16.36)$$

with

- $x(t) = X e^{j\omega t}$, $\ddot{X} = -\omega^2 X$
- $\eta(t) = \Pi e^{j\omega t}$, $\dot{\Pi} = j\omega \Pi$ and $\ddot{\Pi} = -\omega^2 \Pi$
- $F(t) = \hat{F} e^{j\omega t}$

With (16.36) we express $\{\Pi_p\}$ in $\{X_j\}$

$$m_p[-\omega^2 + 2j\zeta_p \omega_p \omega + \omega_p^2] \Pi_p = -[L_p]\{\ddot{X}_j\}, \quad (16.37)$$

where $[L_k] = \{\phi_{p,k}\}^T [M] [\Phi_r]$ is the 1×6 vector with modal participation factors and $L_{kj} = \{\phi_{p,k}\}^T [M] \{\Phi_{r,j}\}$ participation factor with $k = 1, 2, \dots, p$ and $j = 1, 2, \dots, 6$.

Thus (16.37) becomes

$$\Pi_k = -\frac{[L_k]\{\ddot{X}_j\}}{m_k \omega_k^2} \left[\frac{1}{1 - \left(\frac{\omega}{\omega_k} \right)^2 + 2j\zeta_k \frac{\omega}{\omega_k}} \right] = -\frac{[L_k]\{\ddot{X}_j\}}{m_k \omega_k^2} H_k\left(\frac{\omega}{\omega_k}\right). \quad (16.38)$$

(16.38) will be substituted into (16.35) giving

$$[M_{rr}]\{\ddot{X}_j\} + [L_1^T, \dots, L_p^T] \left\{ \left(\frac{\omega}{\omega_k} \right)^2 \frac{[L_k]}{m_k} H_k\left(\frac{\omega}{\omega_k}\right) \right\} \{\ddot{X}_j\} = \{\hat{F}_j\}, \quad k=1, 2, \dots, p \quad (16.39)$$

$$\left[[M_{rr}] + \sum_{k=1}^p \frac{[L_k]^T [L_k]}{m_k} \left\{ \left(\frac{\omega}{\omega_k} \right)^2 H_k\left(\frac{\omega}{\omega_k}\right) \right\} \right] \{\ddot{X}_j\} = \{\hat{F}_j\}. \quad (16.40)$$

We can prove that

$$[M_{rr}] = \sum_{k=1}^p \frac{[L_k]^T [L_k]}{m_k}, \quad (16.41)$$

because

$$[M_{rr}] = [\Phi_r]^T [M] [\Phi_p] ([\Phi_{ip}]^T [M_{ii}] [\Phi_{ip}])^{-1} [\Phi_p]^T [M] [\Phi_r] = [\Phi_r]^T [M] [\Phi_r], \quad (16.42)$$

or

$$[M_{rr}] = [\Phi_{ij}^T, I][M] \begin{bmatrix} \Phi_{ip} \\ 0 \end{bmatrix} ([\Phi_{ip}]^T [M_{ii}] [\Phi_{ip}])^{-1} [\Phi_{ip}^T, 0][M] \begin{bmatrix} \Phi_{ij} \\ 0 \end{bmatrix} = [\Phi_r]^T [M] [\Phi_r].$$

Assuming the inverse of $[\Phi_{ip}]$ exists. The modal effective mass $[M_{\text{eff},k}]$ is defined as follows

$$[M_{\text{eff},k}] = \frac{[L_k]^T [L_k]}{m_k}, \quad (16.43)$$

where $[L_k] = \{\phi_{p,k}\}^T [M] [\Phi_r]$ and $m_k = \{\phi_{p,k}\}^T [M] \{\phi_{p,k}\}$.

The summation over all modal effective masses $[M_{\text{eff},k}]$ will result in the rigid-body mass matrix $[M_{rr}]$ with respect to $\{x_j\}$. (16.41) becomes

$$[M_{rr}] = \sum_{k=1}^{p=i} [M_{\text{eff},k}], \quad (16.44)$$

Therefore (16.40) can be written

$$\left[\sum_{k=1}^p [M_{\text{eff},k}] \left\{ 1 + \left(\frac{\omega}{\omega_k} \right)^2 H_k \left(\frac{\omega}{\omega_k} \right) \right\} \right] \{\ddot{X}_j\} = \{\hat{F}_j\} \quad (16.45)$$

(16.45) can be decomposed into modal reaction forces $\{F_{\text{base},k}\}$

$$\sum_{k=1}^p \{F_{\text{base},k}\} = \{\hat{F}_j\}, \quad (16.46)$$

with

$$\{F_{\text{base},k}\} = [M_{\text{eff},k}] \left\{ 1 + \left(\frac{\omega}{\omega_k} \right)^2 H_k \left(\frac{\omega}{\omega_k} \right) \right\} \{\ddot{X}_j\}. \quad (16.47)$$

(16.47) is very similar to (16.12).

Example

For the dynamic system, as illustrated in Fig. 16.3, the effective masses $[M_{\text{eff},k}]$ will be calculated. The parameters m (kg) and k (N/m) are, respectively, $m = 1$ and $k = 100000$. The set of internal DOFs is $\{x_i\} = \{x_1, x_2, x_3, x_4, x_5, x_6, x_7\}^T$ and the boundary DOF is $\{x_j\} = \{x_8\}$.

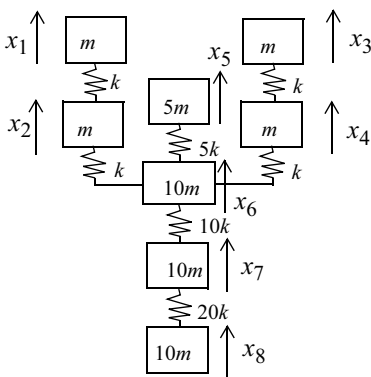


Fig. 16.3 8 DOFs dynamic system

The following procedure will be followed

1. $\{x_j\}$ will be assigned, $x_j = x_8$
2. Calculate the rigid-body modes $[\Phi_r] = \begin{bmatrix} -[K_{ii}]^{-1}[K_{ij}] \\ I \end{bmatrix}, x_j = x_8 = 1$
3. Fix the DOFs $\{x_j\}, x_j = x_8 = 0$
4. Calculate the natural frequencies and associated mode shapes $[\Phi_p], x_j = x_8 = 0$
5. Assemble $[\Psi] = [\Phi_r \Phi_p]$
6. Calculate $[\Psi]^T [M] [\Psi]$ and $[\Psi]^T [K] [\Psi]$
7. Calculate the modal effective masses per mode $[M_{\text{eff},k}] = \frac{[L_k]^T [L_k]}{m_k}$
8. Calculate the summation of modal effective masses $[M_{rr}] = \sum_{k=1}^p [M_{\text{eff},k}]$

The rigid-body mode $\{\phi_r\}$, is with respect to $x_8 = x_j = 1$, and the natural frequencies and associated mode shapes are with respect to $x_8 = x_j = 0$ are

$$\{f_n\} = \begin{Bmatrix} 24.4522 \\ 31.1052 \\ 36.6716 \\ 64.4657 \\ 81.4344 \\ 82.0637 \\ 95.9164 \end{Bmatrix}, [\phi_r] = \begin{Bmatrix} 1 \\ 1 \\ 1 \\ 1 \\ 1 \\ 1 \\ 1 \end{Bmatrix}$$

$$[\Phi_p] = \begin{bmatrix} 0.5347 & -0.6015 & -0.5781 & -0.3363 & -0.3717 & 0.3630 & -0.1343 \\ 0.4075 & -0.3717 & -0.2712 & 0.2155 & 0.6015 & -0.6022 & 0.3534 \\ 0.5347 & 0.6015 & -0.5781 & -0.3363 & 0.3717 & 0.3630 & -0.1343 \\ 0.4075 & 0.3717 & -0.2712 & 0.2155 & -0.6015 & -0.6022 & 0.3534 \\ 0.2407 & 0 & 0.3831 & -0.6458 & 0 & -0.0202 & 0.1681 \\ 0.1835 & 0 & 0.1797 & 0.4137 & 0 & 0.0336 & -0.4425 \\ 0.0664 & 0 & 0.0728 & 0.3044 & 0 & 0.0984 & 0.7001 \\ 0 & 0 & 0 & 0 & 0 & 0 & 0 \end{bmatrix}.$$

The mass matrix $[\Psi]^T [M] [\Psi]$ and the stiffness matrix $[\Psi]^T [K] [\Psi]$ become

$$[\Psi]^T [M] [\Psi] = \begin{bmatrix} 39 & 5.5874 & 0 & 2.7421 & 3.7104 & 0 & 0.7400 & 3.8552 \\ 5.5874 & 1.5746 & 0 & 0 & 0 & 0 & 0 & 0 \\ 0 & 0 & 1.0000 & 0 & 0 & 0 & 0 & 0 \\ 2.7421 & 0 & 0 & 1.9255 & 0 & 0 & 0 & 0 \\ 3.7104 & 0 & 0 & 0 & 5.0429 & 0 & 0 & 0 \\ 0 & 0 & 0 & 0 & 0 & 1.0000 & 0 & 0 \\ 0.7400 & 0 & 0 & 0 & 0 & 0 & 1.0989 & 0 \\ 3.8552 & 0 & 0 & 0 & 0 & 0 & 0 & 7.2863 \end{bmatrix}$$

$$[\Psi]^T [K] [\Psi] = 10^6 \begin{bmatrix} 0 & 0 & 0 & 0 & 0 & 0 & 0 & 0 \\ 0 & 0.0374 & 0 & 0 & 0 & 0 & 0 & 0 \\ 0 & 0 & 0.0382 & 0 & 0 & 0 & 0 & 0 \\ 0 & 0 & 0 & 0.1022 & 0 & 0 & 0 & 0 \\ 0 & 0 & 0 & 0 & 0.8274 & 0 & 0 & 0 \\ 0 & 0 & 0 & 0 & 0 & 0.2618 & 0 & 0 \\ 0 & 0 & 0 & 0 & 0 & 0 & 0.2922 & 0 \\ 0 & 0 & 0 & 0 & 0 & 0 & 0 & 2.6464 \end{bmatrix}.$$

The results of the calculations are summarised in Table 16.1.

Table 16.1 Calculation of the modal effective masses

Mode shape #	Natural frequency (Hz)	Modal participation factor $[L_k]^T$	Generalised masses $[m_k]$	Modal effective mass $[M_{\text{eff},k}]$ (kg)
1	24.5422	5.5874	1.5746	19.8271
2	31.1052	0.0000	1.0000	0.0000
3	36.6716	2.7421	1.9255	3.9048
4	64.4657	3.7104	5.0429	2.7300
5	81.4344	0.0000	1.0000	0.0000
6	82.0637	0.7400	1.0989	0.4983
7	95.9164	3.8552	7.2863	2.0398
Total mass (without $m_8 = 10m$)				29.0000

The mass $m_8 = 10m$ (connected to DOF x_8) is eliminated because the elastic modes are with respect to x_8 .

It appears that the modal effective mass of the first mode shape is already 68.37% of the total mass of 29 kg. The second and the fifth mode shapes have zero

modal effective mass. Modes with zero modal effective mass cannot be excited in the case of enforced acceleration.

The absolute value of the normalised base force $\left| \frac{F_{\text{base}}(\omega)}{\ddot{X}(\omega)} \right|$ can be written as

$$\left| \frac{F_{\text{base}}(\omega)}{\ddot{X}(\omega)} \right| = \left| \sum_{k=1}^J [M_{em,k}] \left\{ 1 + \left(\frac{\omega}{\omega_k} \right)^2 H_k \left(\frac{\omega}{\omega_k} \right) \right\} \right|,$$

and the calculations are illustrated in Fig. 16.4.

End of example

16.4 Literature

- Appel, S., 1992, *Calculation of Modal participation Factors and Effective Mass with the Large Mass Approach*, Fokker Space report FSS-R-92-0027.
- Craig, R.R, Jr. Bampton, M.C.C., 1968, *Coupling of Substructures for Dynamic Analysis*, AIAA Journal, Vol. 6 No. 7, pages 1313–1319.
- Shunmugavel, P., 1995, *Modal Effective Masses for Space Vehicles*, Rockwell Space Systems Division, Downey, California, AIAA-95-125.
- Witting M., Klein M., 1996, *Modal Selection by Means of Effective Masses and Effective Modal Forces an Application Example*, Proc. Conference on Spacecraft Structures, Materials & Mechanical Testing, 2729 March, (ESA SP-386, June 1996).

16.5 Exercises

16.5.1 Large mass solution

The problem is defined in the example Fig. 16.3, however, instead apply a large mass $M_{lm} = 10^6$ kg at x_8 . This method is discussed in [Appel 1992].

Calculate the following parameters:

- The free-free mode shapes $[\phi]$.
- Calculate $\frac{(M_{lm}\phi_{i,8})^2}{\phi_i^T[M]\phi_i}$ per mode “ i ” and compare the results with the modal effective masses as calculated in the example. What is your conclusion?

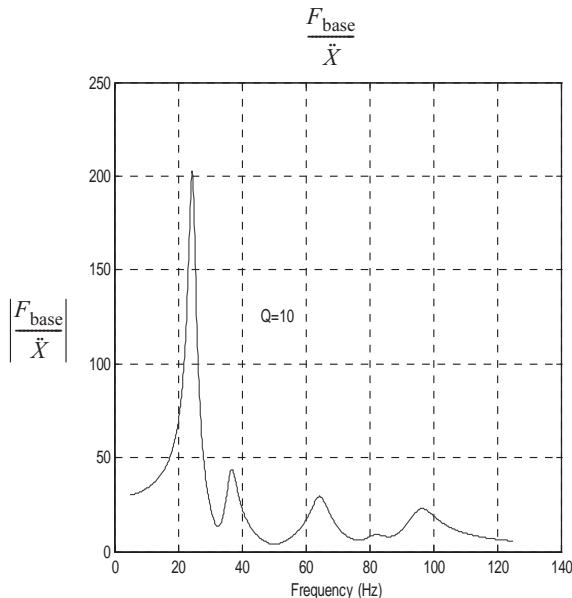


Fig. 16.4 $\left| \frac{F_{\text{base}}(f)}{\ddot{X}(f)} \right| = \left| \sum_{k=1}^7 [M_{\text{em},k}] \left\{ 1 + \left(\frac{f}{f_k} \right)^2 H_k \left(\frac{f}{f_k} \right) \right\} \right|$

16.5.2 Calculation modal effective masses cantilevered beam

A cantilevered beam, as illustrated in Fig. 16.5, has two discrete masses with mass m . The distance between the masses and the clamped interface is L .

A mode shape is assumed to be $\phi(x) = \left(\frac{x}{L}\right)^3$.

Using $\phi(x)$ calculate:

- the natural frequency using Rayleigh's Quotient.
- the generalised mass
- the modal participation factor with respect to clamped position A
- the effective mass

Answers: $\omega = 1.22 \sqrt{\frac{EI}{ml^3}}$, $\frac{65}{64}m$, $\frac{9}{8}m$ and $\frac{81}{65}m$.

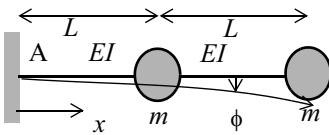


Fig. 16.5 Cantilevered beam

16.5.3 Modal Effective Mass of a Cantilevered Beam

A cantilevered beam with bending stiffness EI and length L is shown in Fig. 16.6. The modal deformation is given by

$$\phi(x) = 2\left(\frac{x}{L}\right)^2 - \frac{4}{3}\left(\frac{x}{L}\right)^3 + \frac{1}{3}\left(\frac{x}{L}\right)^4 \quad (16.48)$$

The mass per unit of length of the cantilevered beam is m (kg/m). The discrete mass at the end of the beam is M (kg).

- Calculate the natural frequency f_n (Hz) associated with the modal deformation $\phi(x)$ using the Rayleigh Quotient
- Calculate the modal participation vector $\{L\}^T$ with respect to point A respectively in w and Θ direction
- Calculate generalised mass m_g associated with the modal deformation $\phi(x)$.
- Calculate the 2×2 modal effective mass matrix $M_{eff}(\phi)$.

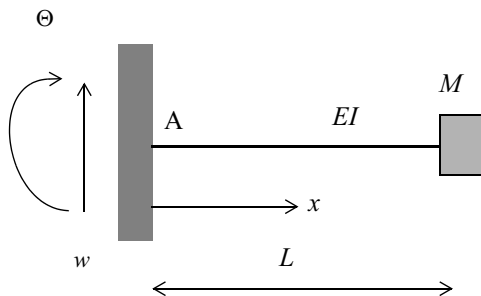


Fig. 16.6 Clamped beam

$$\text{Answers: } f_n = \frac{1}{2\pi}(\sqrt{R(\phi)}), \quad R(\phi) = \frac{16EI}{5\left(M + \frac{104}{405}mL\right)},$$

$$\{L\}^T = \begin{Bmatrix} M + \frac{6}{15}mL \\ ML + \frac{13}{45}mL^2 \end{Bmatrix}, \quad m_g = M + \frac{104}{405}mL \quad \text{and}$$

$$M_{eff}(\phi) = \frac{1}{M + \frac{104}{405}mL} \begin{Bmatrix} M + \frac{6}{15}mL \\ ML + \frac{13}{45}mL^2 \end{Bmatrix} \begin{Bmatrix} M + \frac{6}{15}mL & ML + \frac{13}{45}mL^2 \end{Bmatrix}.$$

16.5.4 Calculation of Base Force

During a sine vibration test the spacecraft, with a total mass of $M_{tot} = 6100 \text{ kg}$, will be excited with a constant enforced acceleration $\ddot{u} = 12.5 \text{ m/s}^2$ in the frequency range $f=5\text{-}100\text{Hz}$.

The most significant mode shape (mode 1) analysed has the following modal characteristics:

- Natural frequency $f_1 = 36 \text{ Hz}$
- Modal effective mass $M_{eff,1} = 2000 \text{ kg}$
- Generalised mass is $m_{p,1} = \{\phi_1\}^T [M] \{\phi_1\} = 1$, $[M]$ is the mass matrix and $\{\phi_1\}$ is the mode shape of mode 1
- Modal damping ratio $\zeta_1 = 0.02$
- Maximum modal displacement $\phi_{max,1} = 0.05$

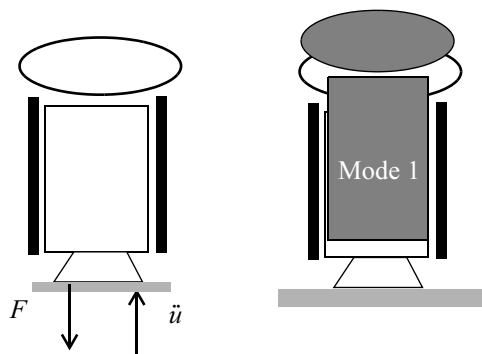


Fig. 16.7 Spacecraft sine testing

Solve the listed assignments:

- Calculate the modal participation factor L_1 .
- Set-up the two equations of motion expressed in the enforced acceleration $\ddot{u}(t) = \ddot{U}(\omega)e^{j\omega t}$ and the generalised co-ordinate $\eta_1(t) = \ddot{\Pi}(\omega)e^{j\omega t}$. (hint use (16.32))
- Calculate the acceleration of the generalised coordinate $\ddot{\Pi}(2\pi 36)$
- Calculate the maximum physical acceleration
- Calculate the absolute value of the force $|F(2\pi 36)|$ using (16.32)
- Calculate the absolute value of the force $|F(2\pi 36)|$ using (16.45)

Answers: 44.721 kg, $1.398 \times 10^4 j$, $689.771 j \text{ m/s}^2$, $6.296 \times 10^5 \text{ N}$, $6.255 \times 10^5 \text{ N}$.

17 Dynamic Model Reduction Methods

17.1 Introduction

The combining of unreduced finite element models (FEMs) of subsystems to a dynamic FEM of the complete system (spacecraft or launcher) will, in general, result in a finite element model with many degrees of freedom (DOFs) that is therefore difficult to handle. The responsible analyst, to manipulate the total dynamic model, will request for a reduced dynamic FEM description of the subsystem and will prescribe the allowed number of ‘left’ dynamic DOFs for the reduced dynamic model. The reduced dynamic model is, in general, a modal description of the system involved.

The customer will prescribe the required accuracy of the reduced dynamic model, more specifically the natural frequencies, mode shapes in comparison with the complete finite element model or reference model. For example the following requirements are prescribed:

- The natural frequencies of the reduced dynamic model shall than deviate less $\pm 3\%$ from the natural frequencies calculated with the reference model.
- The effective masses of the reduced dynamic model shall be within $\pm 10\%$ of the effective masses calculated with the reference model.
- The diagonal terms at the cross orthogonality check [Ricks 1991] shall be greater than or equal to 0.95 and the off-diagonal terms shall be less than or equal to 0.05. The cross orthogonality check is based upon the mass matrix.
- The diagonal terms at the modal assurance criteria (MAC) shall be greater than or equal to 0.95 and the off-diagonal terms less than or equal to 0.10.

Sometimes the requirements concern the correlation of the response curves obtained with the reduced dynamic model and the reference model.

Reduced models are also used to support the modal survey, the experimental modal analysis. The reduced dynamic model will be used to calculate the orthogonality relations between measured and analysed modes. This reduced model is called the test analysis model (TAM) [Kammer 1987].

In the following sections 3 reduction methods will be discussed:

- The static condensation method [Guyan 1968]
- Craig–Bampton (CB) reduction method [Craig 1968]
- System equivalent reduction expansion process (SEREPE) [Kammer 1987]

All reduction procedures mentioned are based upon the Ritz method [Michlin 1962].

This chapter is partly taken from [Wijker 2004].

17.2 Static Condensation Method

In general it is required to reduce the number of dynamic DOFs of a finite element model (dynamic model) by applying the static condensation method, often called the Guyan reduction [Guyan 1968], to a specified number of dynamic DOFs. A reduced dynamic model with 100 dynamic DOFs is quite suitable. The remaining (kept) DOFs will be denoted by $\{x_a\}$ and the eliminated DOFs by $\{x_e\}$. Furthermore we assume there are no applied external loads $\{F_e\}$.

The undamped equations of motion are

$$[M]\{\ddot{x}\} + [K]\{x\} = \{F\}. \quad (17.1)$$

In (17.1) the mass matrix $[M]$, the stiffness matrix $[K]$ and the displacement vector can be partitioned as follows

$$\begin{bmatrix} M_{aa} & M_{ae} \\ M_{ea} & M_{ee} \end{bmatrix} \begin{Bmatrix} \ddot{x}_a \\ \ddot{x}_e \end{Bmatrix} + \begin{bmatrix} K_{aa} & K_{ae} \\ K_{ea} & K_{ee} \end{bmatrix} \begin{Bmatrix} x_a \\ x_e \end{Bmatrix} = \begin{Bmatrix} F_a \\ F_e \end{Bmatrix} = \begin{Bmatrix} F_a \\ 0 \end{Bmatrix}. \quad (17.2)$$

The $\{x_a\}$ DOFs will represent large inertia forces with respect to the inertia forces related to the $\{x_e\}$ DOFs. The large masses and second mass moments of inertia are collected in the mass matrix $[M_{aa}]$. The inertia loads $[M_{aa}]\{\ddot{x}_a\}$ are significantly larger than the other inertia loads

$$[M_{ee}]\{\ddot{x}_e\}, [M_{ae}]\{\ddot{x}_e\}, [M_{ea}]\{\ddot{x}_a\} \ll [M_{aa}]\{\ddot{x}_a\}. \quad (17.3)$$

Only the inertia forces $[M_{aa}]\{\ddot{x}_a\}$ are maintained in (17.2), so

$$\begin{bmatrix} M_{aa} & 0 \\ 0 & 0 \end{bmatrix} \begin{Bmatrix} \ddot{x}_a \\ \ddot{x}_e \end{Bmatrix} + \begin{bmatrix} K_{aa} & K_{ae} \\ K_{ea} & K_{ee} \end{bmatrix} \begin{Bmatrix} x_a \\ x_e \end{Bmatrix} = \begin{Bmatrix} F_a \\ F_e \end{Bmatrix} = \begin{Bmatrix} F_a \\ 0 \end{Bmatrix}. \quad (17.4)$$

Using the equation related by the $\{x_e\}$ DOFs we are able to express the $\{x_e\}$ DOFs into the $\{x_a\}$ DOFs.

$$[K_{ea}]\{x_a\} + [K_{ee}]\{x_e\} = \{0\}. \quad (17.5)$$

The inertia loads in (17.5) are neglected. $\{x_e\}$ can be expressed into $\{x_a\}$

$$\{x_e\} = -[K_{ee}]^{-1}[K_{ea}]\{x_a\} = [G_{ea}]\{x_a\}. \quad (17.6)$$

Only the stiffness is involved in (17.6) and therefore static condensation can be considered.

The total displacement vector $\{x\}$ will be projected on the kept DOFs $\{x_a\}$

$$\{x\} = \begin{Bmatrix} x_a \\ x_e \end{Bmatrix} = \begin{bmatrix} I \\ G_{ea} \end{bmatrix}\{x_a\} = [T_{ea}]\{x_a\}. \quad (17.7)$$

The total kinetic energy in the dynamic system is

$$T = \frac{1}{2}\{\dot{x}\}^T[M]\{\dot{x}\} = \frac{1}{2}\{\dot{x}_a\}^T[T_{ea}]^T[M][T_{ea}]\{\dot{x}_a\}. \quad (17.8)$$

The reduced-mass matrix $[\bar{M}_{aa}]$ becomes

$$[\bar{M}_{aa}] = [T_{ea}]^T[M][T_{ea}]. \quad (17.9)$$

The total potential energy in the dynamic system is

$$U = \frac{1}{2}\{x\}^T[K]\{x\} = \frac{1}{2}\{x_a\}^T[T_{ea}]^T[K][T_{ea}]\{x_a\} \quad (17.10)$$

Analogous to the reduced-mass matrix $[\bar{M}_{aa}]$, the reduced-stiffness matrix $[\bar{K}_{aa}]$ becomes

$$[\bar{K}_{aa}] = [T_{ea}]^T[K][T_{ea}]. \quad (17.11)$$

The selection of the remaining DOFs $\{x_a\}$ is not always trivial. The remaining DOFs shall be selected in such a way that the mode shapes can be described as well as possible. The DOFs associated with large masses shall be selected. As a guideline the following mathematical selection may be used to select the $\{x_a\}$ DOFs. At least the DOFs shall be selected for which applies

$$\frac{1}{2\pi}\sqrt{\frac{k_{ii}}{m_{ii}}} \leq 1.5f_{\max} \quad (17.12)$$

where k_{ii} the diagonal term of the stiffness matrix $[K]$, translational and rotational, m_{ii} the diagonal term of the mass matrix $[M]$, translational and rotational and f_{\max} maximum frequency of interest.

Allen in [Allen 1993] described a more or less automatic way of selecting the analysis DOFs $\{x_a\}$, however, it is still based upon (17.12).

The reduced eigenvalue problem can now be written as

$$\{[\bar{M}_{aa}] - \lambda_a [\bar{K}_{aa}]\} \{\phi_a\} = 0, \quad (17.13)$$

with $\{\phi_a\}$ the eigenvector of the reduced eigenvalue problem and λ_a the eigenvalue associated with the eigenvector (mode shape) $\{\phi_a\}$.

The eigenvectors that belong to the complete set of DOFs, using (17.7), are

$$[\Phi_{GR}] = \begin{bmatrix} \Phi_a \\ \Phi_e \end{bmatrix} = \begin{bmatrix} I \\ G_{ea} \end{bmatrix} [\Phi_a], \quad (17.14)$$

where $[\Phi_e]$ the eigenvectors associated with the eliminated DOFs and $[G_{ed}]$ the transformation matrix as defined in (17.6).

Example

A 10 DOFs dynamic system (Fig. 17.1) will be used to illustrate the static condensation method. The constants are $m = 1$ and $k = 100000$. The dynamic system will be fixed in x_{10} . First, the natural frequencies and modes of the full system will be calculated.

The systems matrices are as follows

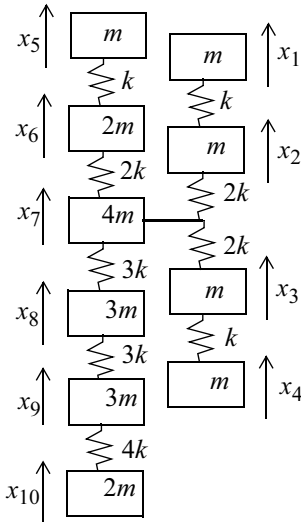


Fig. 17.1. 10 mass–spring dynamic system

The natural frequencies $\{f\}$ (Hz) calculated are

$$\{f\} = [14.25, 36.69, 38.52, 47.43, 63.69, 75.91, 90.25, 93.00, 106.51]^T.$$

The first four modes $[\Phi]$ are scaled such that

$$[\Phi]^T [M] [\Phi] = [I] \text{ and } [\Phi]^T [K] [\Phi] = \langle \omega^2 \rangle = \langle (2\pi f)^2 \rangle$$

$$[\Phi] = \begin{bmatrix} 0.3064 & -0.3878 & -0.6533 & -0.3762 \\ 0.2819 & -0.1817 & -0.2706 & -0.0421 \\ 0.2819 & -0.1817 & 0.2706 & -0.0421 \\ 0.3064 & -0.3878 & 0.6533 & -0.3760 \\ 0.3204 & 0.6591 & 0 & -0.3327 \\ 0.2948 & 0.3088 & 0 & -0.0373 \\ 0.2583 & -0.0304 & 0 & 0.1435 \\ 0.1750 & -0.0333 & 0 & 0.3417 \\ 0.0777 & -0.0185 & 0 & 0.2364 \\ 0 & 0 & 0 & 0 \end{bmatrix}.$$

We select the following DOFs to remain; $\{x_a\} = [x_1, x_4, x_5, x_7]$.

The natural frequencies $\{f_a\}$ of the reduced eigenvalue problem, (17.13), are

$$\{f_a\} = [14.39, 37.86, 38.98, 52.98]^T.$$

The modes $[\Phi_{GR}]$ are scaled such that $[\Phi_{GR}]^T [M] [\Phi_{GR}] = [I]$.

To compare the dynamic properties of the condensed dynamic system with the complete or reference dynamic system, we can compare the natural frequencies with each other and of course the mode shapes. To do so it is required to lengthen the mode shape of the reduced system (4 DOFs) to a total number of 10 DOFs.

$$[\Phi_{GR}] = \begin{bmatrix} 0.3134 & -0.4059 & -0.6708 & -0.4390 \\ 0.2802 & -0.1483 & -0.2236 & 0.0347 \\ 0.2802 & -0.1483 & 0.2236 & 0.0347 \\ 0.3134 & -0.4059 & 0.6708 & -0.4390 \\ 0.3269 & 0.7217 & 0 & -0.4577 \\ 0.2846 & 0.2276 & 0 & 0.0285 \\ 0.2635 & -0.0195 & 0 & 0.2716 \\ 0.1677 & -0.0124 & 0 & 0.1728 \\ 0.0719 & -0.0053 & 0 & 0.0741 \\ 0 & 0 & 0 & 0 \end{bmatrix}.$$

The modes of the reduced dynamic model will be compared to the complete dynamic model with three methods; the modal assurance criteria and the normalised cross orthogonality matrices [Friswell 1995, Maia 1997] and the cross orthogonality check [Ricks 1991]:

- The modal assurance criteria (MAC). The absolute value of the MAC is between 0 and 1. A value of 1 means that one mode shape is a multiple of the

other. The MAC matrix is defined as $MAC = \frac{([\Phi]^T [\Phi_{GR}])^2}{([\Phi]^T [\Phi])([\Phi_{GR}]^T [\Phi_{GR}])}$.

- The normalised cross orthogonality (NCO). The absolute values of the NCO are between 0 and 1. A value of 1 means that one mode shape is a multiple of the other. The modified MAC is defined as

$$NCO = \frac{([\Phi]^T [M] [\Phi_{GR}])^2}{([\Phi]^T [M] [\Phi])([\Phi_{GR}]^T [M] [\Phi_{GR}])}.$$

- Cross orthogonality check. $[C] = ([\Phi]^T [M] [\Phi_{GR}])$, $[\Phi]^T [M] [\Phi] = \langle I \rangle$ and the terms on the main diagonal of $([\Phi_{GR}]^T [M] [\Phi_{GR}])$ are one.

The MAC becomes

$$MAC = \frac{([\Phi]^T [\Phi_{GR}])^2}{([\Phi]^T [\Phi])([\Phi_{GR}]^T [\Phi_{GR}])} = \begin{bmatrix} 0.9980 & -0.0052 & 0.0000 & 0.0251 \\ -0.0017 & 0.9897 & 0.0000 & -0.0669 \\ 0.0000 & -0.0006 & 0.9950 & 0.0000 \\ -0.0540 & 0.0459 & 0.0000 & 0.8054 \end{bmatrix},$$

and the NCO

$$\text{NCO} = \frac{([\Phi]^T [M] [\Phi_{GR}])^2}{[\Phi]^T [M] [\Phi] ([\Phi_{GR}]^T [M] [\Phi_{GR}])} = \begin{bmatrix} 0.9995 & 0.0002 & 0.0000 & -0.0013 \\ -0.0004 & 0.9775 & 0.0000 & -0.0194 \\ 0.0000 & 0.0000 & 0.9950 & 0.0000 \\ -0.0019 & 0.0612 & 0.0000 & 0.7444 \end{bmatrix},$$

and finally the cross orthogonality

$$[C] = [\Phi]^T [M] [\Phi_{GR}] = \begin{bmatrix} -0.9996 & 0.0052 & 0.0000 & -0.0092 \\ -0.0004 & 0.9888 & 0.0000 & -0.0105 \\ 0.0003 & 0.0000 & -0.9975 & 0.0000 \\ -0.00151 & 0.0330 & 0.0000 & 0.8629 \end{bmatrix}.$$

The diagonal terms of the MAC, NCO and cross-pollination $[C]$ show us the correlation of the mode shapes of the reduced dynamic model with the reference model. The off-diagonal terms shows us the coupling between the correlated modes. The first 3 modes, of both the reduced and reference dynamic modes, do correlate very well. The fourth mode of the reduced model is less correlated with the fourth mode of the complete model.

End example

17.3 Craig–Bampton Reduced Models

The Craig–Bampton method is discussed in [Craig 1968] and many other publications and is one of the most favourite methods for reducing the size, number of degrees of freedom, of a dynamic model (finite element model). The undamped equations of motion are (17.1)

$$[M]\{\ddot{x}\} + [K]\{x\} = \{F(t)\}.$$

We denote the external or boundary degrees of freedom with the index j and the internal degrees of freedom with the index i . The matrix equations (17.1) may be partitioned as follows

$$\begin{bmatrix} M_{ii} & M_{ij} \\ M_{ji} & M_{jj} \end{bmatrix} \begin{Bmatrix} \ddot{x}_i \\ \ddot{x}_j \end{Bmatrix} + \begin{bmatrix} K_{ii} & K_{ij} \\ K_{ji} & K_{jj} \end{bmatrix} \begin{Bmatrix} x_i \\ x_j \end{Bmatrix} = \begin{Bmatrix} F_i \\ F_j \end{Bmatrix}. \quad (17.15)$$

In [Craig 1968] it is proposed to depict the displacement vector $\{x(t)\}$ on a basis of static or constraint modes $[\Phi_s]$ with $\{x_j\} = [I]$ and elastic mode shapes $[\Phi_p]$ with fixed external degrees of freedom $\{x_j\} = \{0\}$ and the eigenvalue problem $([K_{ii}] - \langle \lambda_p \rangle [M_{ii}])[\Phi_{ii}] = [0]$. We can express $\{x\}$ as

$$\{x\} = [\Phi_s]\{x_j\} + [\Phi_p]\{\eta_p\} = [\Phi_s, \Phi_p] \begin{Bmatrix} x_j \\ \eta_p \end{Bmatrix} = [\Psi]\{X\}. \quad (17.16)$$

The static modes can be obtained, assuming zero inertia effects, $\{F_i\} = \{0\}$, and successively prescribe a unit displacement for the boundary degrees of freedom, thus $\{x_j\} = [I]$. So we may write (17.15) as follows

$$\begin{bmatrix} K_{ii} & K_{ij} \\ K_{ji} & K_{jj} \end{bmatrix} \begin{Bmatrix} x_i \\ x_j \end{Bmatrix} = \begin{Bmatrix} 0 \\ R_j \end{Bmatrix}. \quad (17.17)$$

From the first equation of (17.17) we find for $\{x_i\}$

$$[K_{ii}]\{x_i\} + [K_{ij}]\{x_j\} = 0, \quad (17.18)$$

hence

$$\{x_i\} = -[K_{ii}]^{-1}[K_{ij}]\{x_j\}, \quad (17.19)$$

and therefore

$$[\Phi_{ij}] = -[K_{ii}]^{-1}[K_{ij}][I] = -[K_{ii}]^{-1}[K_{ij}]. \quad (17.20)$$

The static transformation now becomes

$$\{x\} = \begin{Bmatrix} x_i \\ x_j \end{Bmatrix} = \begin{bmatrix} \Phi_{ij} \\ I \end{bmatrix} \{x_j\} = [\Phi_s]\{x_j\}. \quad (17.21)$$

Assuming fixed external degrees of freedom $\{x_j\} = \{0\}$ and also assuming harmonic motions $x(t) = X(\omega)e^{j\omega t}$, the eigenvalue problem can be stated as

$$([K_{ii}] - \lambda_{i,p}[M_{ii}])\{X(\lambda_{i,p})\} = \{0\}, \quad (17.22)$$

or, more generally, as

$$([K_{ii}] - \langle \lambda_i \rangle [M_{ii}])[\Phi_{ip}] = \{0\}. \quad (17.23)$$

The internal degrees of freedom $\{x_i\}$ will be projected on the set of orthogonal mode shapes (modal matrix) $[\Phi_{ip}]$, thus

$$\{x_i\} = [\Phi_{ip}]\{\eta_p\}. \quad (17.24)$$

The modal transformation becomes

$$\{x\} = \begin{Bmatrix} x_i \\ x_j \end{Bmatrix} = \begin{bmatrix} \Phi_{ip} \\ 0 \end{bmatrix} \{\eta_p\} = [\Phi_p] \{\eta_p\}. \quad (17.25)$$

The Craig–Bampton (CB) transformation matrix is (17.16)

$$\{x\} = [\Phi_s, \Phi_p] \begin{Bmatrix} x_j \\ \eta_p \end{Bmatrix} = [\Psi] \{X\}$$

with

$[\Phi_s]$ the static or constraint modes

$[\Phi_p]$ the modal matrix

$\{x_j\}$ the external or boundary degrees of freedom

$\{\eta_p\}$ the generalised coordinates. In general, the number of generalised coordinates p is much less than the total number of degrees of freedom $n = i + j$, $p \ll n$.

The constraint modes will introduce displacements due to adjacent structures in a static way, while the elastic modes will introduce dynamic effects generated internally in the structure.

The CB transformation (17.16) will be substituted into (17.1) presuming equal potential and kinetic energies, hence

$$[\Psi]^T [M] [\Psi] \{\ddot{X}\} + [\Psi]^T [K] [\Psi] \{X\} = [\Psi]^T \{F(t)\}. \quad (17.26)$$

Further elaborated we find

$$\begin{bmatrix} \tilde{M}_{jj} & M_{jp} \\ M_{pj} & \langle m_p \rangle \end{bmatrix} \begin{Bmatrix} \ddot{x}_j \\ \ddot{\eta}_p \end{Bmatrix} + \begin{bmatrix} \tilde{K}_{jj} & K_{jp} \\ K_{pj} & \langle k_p \rangle \end{bmatrix} \begin{Bmatrix} x_j \\ \eta_p \end{Bmatrix} = \begin{bmatrix} \Phi_{ij} & \Phi_p \\ I & 0 \end{bmatrix}^T \begin{Bmatrix} F_i \\ F_j \end{Bmatrix}, \quad (17.27)$$

with

$[\tilde{M}_{jj}]$ the Guyan reduced mass matrix (j -set)

$[\tilde{K}_{jj}]$ the Guyan reduced stiffness matrix (j -set)

$\langle m_p \rangle$ the diagonal matrix of generalised masses, $\langle m_p \rangle = [\Phi_p]^T [M] [\Phi_p]$

$\langle k_p \rangle$ the diagonal matrix of generalised stiffnesses,

$$\langle k_p \rangle = [\Phi_p]^T K [\Phi_p] = \langle \lambda_p \rangle \langle m_p \rangle$$

$$[K_{ip}] = [\Phi_{ij}]^T [K_{ii}] [\Phi_p] + [K_{ji}] [\Phi_p] = (-[K_{ij}]^T [K_{ii}]^{-1} [K_{ii}] + [K_{ji}]) [\Phi_p] = [0] \\ (\text{see (17.20)})$$

$$[K_{pi}] = [K_{ip}]^T = [0]$$

Thus (17.27) becomes

$$\begin{bmatrix} \tilde{M}_{jj} & M_{jp} \\ M_{pj} & \langle m_p \rangle \end{bmatrix} \begin{Bmatrix} \ddot{x}_j \\ \ddot{\eta}_p \end{Bmatrix} + \begin{bmatrix} \tilde{K}_{jj} & 0 \\ 0 & \langle k_p \rangle \end{bmatrix} \begin{Bmatrix} x_j \\ \eta_p \end{Bmatrix} = \begin{bmatrix} \Phi_{ij} & \Phi_p \\ I & 0 \end{bmatrix}^T \begin{Bmatrix} F_i \\ F_j \end{Bmatrix}. \quad (17.28)$$

Finally

$$[M_{\text{CB}}]\{\ddot{X}\} + [K_{\text{CB}}]\{X\} = [\Psi]^T\{F\}, \quad (17.29)$$

with $[M_{\text{CB}}]$ the CB reduced-mass matrix and $[K_{\text{CB}}]$ the CB reduced-stiffness matrix.

The CB matrices are $j+p$, $j+p$ sized matrices. (17.29) is frequently applied for component-mode synthesis methods (dynamic substructuring).

The accuracy of the CB reduction technique is very satisfactory and was discussed in [Claessens 1996].

17.4 System Equivalent Reduction Expansion Process (SEREP)

The SEREP is proposed by [Kammer 1987] and is based upon a partitioning of the calculated mode shapes in combination with pseudo-inversion of matrices.

The displacement vector $x(t)$ is projected on the modal matrix $[\Phi]$. The number of m remaining mode shapes is much less than the total number of degrees of freedom n , hence $m \ll n$. The displacement vector can be written as

$$x(t)) = [\Phi]\{\eta(t)\}, \quad (17.30)$$

with $\{\eta(t)\}$ the vector of generalised coordinates.

The displacement vector $x(t)$ will be partitioned into two sets; the remaining set of degrees of freedom denoted by a and the eliminated set of degrees of freedom denoted by e , thus

$$\begin{Bmatrix} x_a \\ x_e \end{Bmatrix} = \begin{bmatrix} \Phi_a \\ \Phi_e \end{bmatrix} \{\eta\}, \quad (17.31)$$

We will express $\{x\}$ in $\{x_a\}$ as follows

$$\begin{Bmatrix} x_a \\ x_e \end{Bmatrix} = \begin{bmatrix} I \\ T_{ea} \end{bmatrix} \{x_a\} = [T_{\text{Kammer}}]\{x_a\}. \quad (17.32)$$

The a set of the displacement vector $\{x_a\}$ can be written as

$$\{x_a\} = [\Phi_a]\{\eta\} \quad (17.33)$$

We want to express the vector of generalised coordinates $\{\eta\}$ in $\{x_a\}$. However, the inverse of the rectangular matrix $[\Phi_a]$ does not exist. Both sides of (17.33) will be multiplied by $[\Phi_a]^T$, thus

$$[\Phi_a]^T\{x_a\} = [\Phi_a]^T[\Phi_a]\{\eta\}. \quad (17.34)$$

The matrix $[\Phi_a]^T[\Phi_a]$ is a square matrix and in general the inverse of that matrix exists. The generalised coordinates $\{\eta\}$ are expressed in $\{x_a\}$

$$\{\eta\} = ([\Phi_a]^T[\Phi_a])^{-1}[\Phi_a]^T\{x_a\} \quad (17.35)$$

The matrix $([\Phi_a]^T[\Phi_a])^{-1}[\Phi_a]^T$ is called the pseudo-inverse matrix of the modal matrix $[\Phi_a]$, hence

$$[\Phi_a]^{-1} = ([\Phi_a]^T[\Phi_a])^{-1}[\Phi_a]^T. \quad (17.36)$$

The displacement vector of eliminated degrees of freedom $\{x_e\}$ can be expressed in the set of kept degrees of freedom $\{x_a\}$. From (17.31) we can write

$$\{x_e\} = [\Phi_e]\{\eta\}, \quad (17.37)$$

and with (17.35) we obtain

$$\{x_e\} = [\Phi_e]([\Phi_a]^T[\Phi_a])^{-1}[\Phi_a]^T\{x_a\} = [T_{ea}]\{x_a\}. \quad (17.38)$$

The complete displacement vector $\{x\}$ can be expressed in $\{x_a\}$, see (17.32)

$$\begin{Bmatrix} x_a \\ x_e \end{Bmatrix} = \begin{bmatrix} I \\ [\Phi_e]([\Phi_a]^T[\Phi_a])^{-1}[\Phi_a]^T \end{bmatrix} \{x_a\} = \begin{bmatrix} I \\ T_{ea} \end{bmatrix} \{x_a\} = [T_{\text{Kammer}}]\{x_a\}. \quad (17.39)$$

The reduced-mass matrix $[M_{\text{SEREP}}]$ becomes

$$[M_{\text{SEREP}}] = [T_{\text{Kammer}}]^T[M][T_{\text{Kammer}}]. \quad (17.40)$$

Analogous to the reduced-mass matrix $[M_{\text{SEREP}}]$ the reduced-stiffness matrix $[K_{\text{SEREP}}]$ is

$$[K_{\text{SEREP}}] = [T_{\text{Kammer}}]^T[K][T_{\text{Kammer}}]. \quad (17.41)$$

The SEREP reduction method will provide ‘physical’ reduced matrices. In general, the kept degrees of freedom $\{x_a\}$ will correspond to measurement locations and directions.

Example

We select the following kept DOFs; $\{x_a\} = [x_1, x_4, x_5, x_7]^T$ (Fig. 17.1) and take into account the first and second modes to reduce the model with the SEREP method.

The modes $[\Phi]$ are scaled such that

$$[\Phi]^T [M] [\Phi] = [I] \text{ and } [\Phi]^T [K] [\Phi] = \langle \omega^2 \rangle = \langle (2\pi f)^2 \rangle$$

$$[\Phi] = \begin{bmatrix} 0.3064 & -0.3878 \\ 0.2819 & -0.1817 \\ 0.2819 & -0.1817 \\ 0.3064 & -0.3878 \\ 0.3204 & 0.6591 \\ 0.2948 & 0.3088 \\ 0.2583 & -0.0304 \\ 0.1750 & -0.0333 \\ 0.0777 & -0.0185 \\ 0 & 0 \end{bmatrix}.$$

The first two calculated natural frequencies of the reduced system are

$$\{f_d\} = [14.25, 36.69]^T.$$

Four natural frequencies are calculated but the third and the fourth natural frequencies have no physical meaning. Only two modes of the reference dynamic model are taken into account.

The modes $[\Phi_{\text{SEREP}}]$ are scaled such that $[\Phi_{\text{SEREP}}]^T [M] [\Phi_{\text{SEREP}}] = [I]$

$$[\Phi_{\text{SEREP}}] = \begin{bmatrix} -0.3064 & -0.3878 \\ -0.2819 & -0.1817 \\ -0.2819 & -0.1817 \\ -0.3064 & -0.3878 \\ -0.3204 & 0.6591 \\ -0.2948 & 0.3088 \\ -0.2583 & -0.0304 \\ -0.1750 & -0.0333 \\ -0.0777 & -0.0185 \\ 0 & 0 \end{bmatrix}.$$

The MAC and the modified MAC become

$$\text{MAC} = \frac{([\Phi]^T [\Phi_{\text{SEREP}}])^2}{([\Phi]^T [\Phi])([\Phi_{\text{SEREP}}]^T [\Phi_{\text{SEREP}}])} = \begin{bmatrix} 1.0000 & -0.0003 \\ -0.0006 & 1.0000 \end{bmatrix},$$

and

$$\text{NCO} = \frac{([\Phi]^T [M][\Phi_{\text{SEREP}}])^2}{[\Phi]^T [M][\Phi]([\Phi_{\text{SEREP}}]^T [M][\Phi_{\text{SEREP}}])} = \begin{bmatrix} 1.0000 & -0.0004 \\ -0.0004 & 1.0000 \end{bmatrix}.$$

The first two modes of the reduced model, associated with the first two natural frequencies, $\{f_a\} = \lfloor 14.25, 36.69 \rfloor^T$, do correlate very well with the first two modes of the reference model.

End of example

17.5 Conclusion

Reduced models are also used to support the modal survey, and the experimental modal analysis. The DOFs in the reduced dynamic model are related to measurements. The reduced dynamic model will be used to calculate the orthogonality relations between measured and analysed modes. This reduced model is called the test analysis model (TAM) [Kammer 1987]. Reduction methods that will give a TAM are:

- The static condensation technique [Guyan 1968]
- System equivalent reduction expansion process (SEREP) [Kammer 1987]
The other method:
- Graig–Bampton (CB) reduction method [Craig 1968]

will result in a hybrid reduced mathematical dynamic model; DOFs related to physical DOFs combined with mathematical (generalised) DOFs.

17.6 Literature

- Allen, T., April 1991, *Automatic ASET Selection for Dynamic Analysis*, Twenty-first NASTRAN User's conference, NASA CP-2303, pages 175–181.
- Claessens, G.J.T.J., Wijker, J.J., March 1996, *The Accuracy of Reduced Component Models*, Proc. Int. Conf.: 'Spacecraft Structures and Mechanical Testing', Noordwijk TheNetherlands, ESA SP-386, pages 533–547.
- Cook, R.D., Malkus, D.S., Plesha, E.M., 1989, *Concepts and Applications of Finite Element Analysis*, Third Edition, ISBN 0-471-84788-7, John Wiley.
- Craig, R.R., Jr., Bampton, M.C.C., July 1968, *Coupling of Substructures for Dynamic Analysis*, AIAA Journal, Vol. 6, No. 7, pages 1313–1319.
- Friswell, M.I., Mottershead, J.E., 1995, *Finite Element Updating in Structural Dynamics*, Kluwer, ISBN 0-7923-3431-0.
- Genta, G., 1995, *Vibration of Structures and Machines, Practical Aspects*, Second Edition, ISBN 0-387-94403-6, Springer Verlag.
- Guyan, R.J., 1968, *Reduction of Stiffness and Mass Matrices*, AIAA Journal, Vol. 3, No. 2, page 380.
- Kammer, D.C., October 1987, *Test-Analysis-Model Development using an Exact Modal Reduction*, Journal of Modal Analysis, pages 174–179.
- Maia, M.M.M., Silva, J.M.M., 1997, *Theoretical and Experimental Modal Analysis*, John Wiley, ISBN 0 47197067 0.
- Michlin, S.C., 1962, *Variationmethoden der Mathematischen Physik*, Akademie-Verlag, Berlin.
- Ricks, E.G., 1991, *Guidelines for Loads Analyses and Dynamic Verification of Shuttle Cargo Elements*, NASA-MSFC-HDBK-1974.
- Wijker, J.J., 2004, *Mechanical Vibrations in Spacecraft Design*, Springer, ISBN 3-54-40530-5.

17.7 Exercises

17.7.1 Reduction Finite Element Model

Compose the mass and stiffness matrices for the study of a simply supported beam additional supported in the middle [Genta 1995]. The system is illustrated in Fig. 17.2. The two beams are hinge connected at node 2.

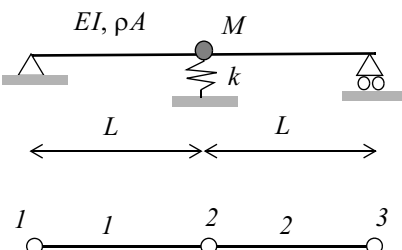


Fig. 17.2. Sketch of the system, finite element model based on two beams

Each node has two degrees of freedom: translation (flexure) w and rotation φ . Each beam “ i ” has four DOFs $[w_{i+1}, \varphi_{i1+1}, w_{i+2}, \varphi_{i+2}]$. The mass and stiffness matrices of the beam are [Cook 1989]

$$[M] = \frac{\rho AL}{420} \begin{bmatrix} 156 & 22L^2 & 54 & -13L \\ 22L^2 & 4L^2 & 13L & -3L^2 \\ 54 & 13L & 156 & -22L \\ -13L & -3L^2 & -22L & 4L^2 \end{bmatrix}, [K] = \frac{EI}{L^3} \begin{bmatrix} 12 & 6L & -12 & 6L \\ 6L & 4L^2 & -6L & 2L^2 \\ -12 & -6L & 12 & -6L \\ 6L & 2L^2 & -6L & 4L^2 \end{bmatrix}.$$

There are a total of seven DOFs in the unconstrained system. The connection between the elements is performed through a hinge that allows different rotations of the two elements at node 2.

Condense with the GR reduction technique the numbers of DOFs to one DOF representing the displacement at node 2. Calculate the natural frequency (Hz) of the condensed system.

17.7.2 Reduction of dynamic 10 DOF model

A 10 DOFs dynamic system is illustrated in Fig. 17.3. The constants are $m = 50 \text{ kg}$ and $k = 5 \times 10^9 \text{ N/m}$. The dynamic system will be fixed in x_{10} .

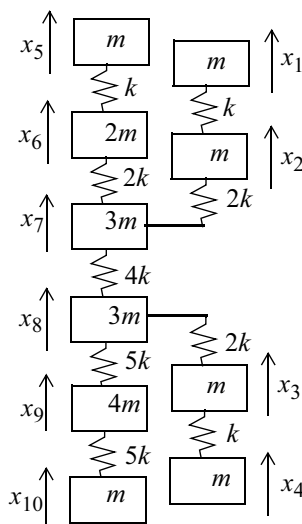


Fig. 17.3. 10 DOF mass-spring system

- Calculate the modal characteristics of the complete system (natural frequencies, vibration modes, modal effective masses).
- Calculate a reduced dynamic modal using the static condensation method. The remaining physical DOFs are $x_1, x_4, x_5, x_7, x_5, x_{10}$.
 - Calculate the modal characteristics (x_{10} fixed).
- Calculate a reduced dynamic modal using the SEREP method. The remaining physical DOFs are $x_1, x_4, x_5, x_7, x_5, x_{10}$.
 - Calculate the modal characteristics (x_{10} fixed).
- Calculate a reduced dynamic modal using the CB method. The remaining physical DOF is x_{10} , and four mathematical co-ordinates $\{\eta_p\}$ (modes).
 - Calculate the modal characteristics (x_{10} fixed).

18 Dynamic Substructuring, Component Mode Synthesis

18.1 Introduction

The component mode synthesis (CMS) or component modal synthesis [Hintz 1975] or modal coupling technique [Maia 1997] is used when components (substructures) are described by the mode displacement method (MDM) and coupled together (synthesis) via the common boundaries $\{x_b\}$ in order to perform a dynamic analysis (e.g. modal analysis, responses) on the complete structure (assembly of substructures). The CMS method can only be applied to linear structures. The component mode synthesis method can also be applied on components for which the modal characteristics were measured in combination with finite element reduced dynamic models. Many papers and reports are available in the open literature; e.g. [Craig 1968, Craig 1976, Craig 1977, MacNeal 1971, Craig 2000].

In general, a component or substructure is a recognisable part of the structure (e.g. for a spacecraft; the primary structure, the solar arrays, the antenna, large instruments, etc.).

In the past, the CMS method was applied to significantly reduce the number of DOFs due to the imposed limitations on computers, however, nowadays, these limitations are more or less removed, however, the CMS method is still popular. Sub-contractors deliver their reduced FE dynamic models to the prime contractor who will combine (synthesise) all these models to the spacecraft dynamic FE model to perform the dynamic analysis on the complete spacecraft. The same applies to the coupled dynamic load analysis (CDLA) when the reduced FE model of the complete spacecraft is placed on top of the launch vehicle. In general, the dynamic FE model of the launch vehicle is a reduced dynamic FE model too.

Dynamic properties of substructures may be defined by experiment and may be coupled to other dynamic FE models of other substructures.

Hence, there are many reasons to apply the CMS method.

For dynamic analyses the components may be obtained by reducing the number of DOFs by applying the MDM. The physical DOFs $\{x\}$ are, in general, depicted on a small number of kept modes (eigenvectors), the modal base,

$$\{x\} = [\Phi]\{\eta\}, \quad (18.1)$$

where $[\Phi]$ the modal base consists of the kept mode and $\{\eta\}$ the generalised or principal coordinates.

The number of generalised coordinates $\{\eta\}$ is, in general, much less than the number of physical DOFs $\{x\}$.

In this chapter an introduction to the CMS method will be given and a number of methods will be discussed. We will assume undamped components, however, in a later stage during the synthesis the modal damping ratios can be introduced.

The chapter is partly taken from [Wijker 2004].

18.2 Special CMS Methods

In this section three special CMS methods will be presented:

- The Craig–Bampton fixed-interface method.
- The free-interface method with improved accuracy
- The general CMS method, which combines the fixed- and free-interface CMS methods.

18.2.1 Craig–Bampton Fixed-Interface Method

The fixed-interface method (Craig–Bampton method) is discussed in several publications [Craig 1968, Craig 1977, Craig 1981, Craig 2000, Gordon 1999] and is one of the favourite methods used in the CMS.

The general undamped equations of motion are

$$[M]\{\ddot{x}\} + [K]\{x\} = \{F\} \quad (18.2)$$

We denote the external or boundary degrees of freedom with the index b and the internal degrees of freedom with the index i . The matrix equations of motion may be partitioned as follows

$$\begin{bmatrix} M_{ii} & M_{ib} \\ M_{bi} & M_{bb} \end{bmatrix} \begin{Bmatrix} \ddot{x}_i \\ \ddot{x}_b \end{Bmatrix} + \begin{bmatrix} K_{ii} & K_{ib} \\ K_{bi} & K_{bb} \end{bmatrix} \begin{Bmatrix} x_i \\ x_b \end{Bmatrix} = \begin{Bmatrix} F_i \\ F_b \end{Bmatrix}. \quad (18.3)$$

In [Craig 1968] it is proposed to depict the displacement vector $\{x(t)\}$ on a basis of static or constraint modes $[\Phi_c]$ with $\{x_b\} = [I]$ and elastic mode shapes

$[\Phi_i]$ with fixed external degrees of freedom $\{x_b\} = \{0\}$ and the eigenvalue problem $[[K_{ii}] - \langle \lambda_p \rangle [M_{ii}]] [\Phi_{ii}] = [0]$. $\{x\}$ can be expressed as

$$\{x\} = [\Phi_c] \{x_b\} + [\Phi_i] \{\eta_i\} = [\Phi_c, \Phi_i] \begin{Bmatrix} x_b \\ \eta_i \end{Bmatrix}. \quad (18.4)$$

The static modes can be obtained, assuming zero inertia effects, $\{F_i\} = \{0\}$, and successively prescribe a unit displacement for the boundary degrees of freedom, thus $\{x_b\} = [I]$. Therefore the static part of (18.3) may be written as follows

$$\begin{bmatrix} K_{ii} & K_{ib} \\ K_{bi} & K_b \end{bmatrix} \begin{Bmatrix} x_i \\ x_b \end{Bmatrix} = \begin{Bmatrix} 0 \\ R_b \end{Bmatrix}. \quad (18.5)$$

From the first equation of (18.5) for $\{x_i\}$ it can be found

$$[K_{ii}] \{x_i\} + [K_{ib}] \{x_b\} = 0, \quad (18.6)$$

hence

$$\{x_i\} = -[K_{ii}]^{-1} [K_{ib}] \{x_b\}, \quad (18.7)$$

and therefore

$$[\Phi_{ib}] = -[K_{ii}]^{-1} [K_{ib}] [I] = -[K_{ii}]^{-1} [K_{ib}]. \quad (18.8)$$

The static transformation now becomes

$$\{x\} = \begin{Bmatrix} x_i \\ x_b \end{Bmatrix} = \begin{bmatrix} \Phi_{ib} \\ I \end{bmatrix} \{x_b\} = [\Phi_c] \{x_b\}. \quad (18.9)$$

Assuming fixed external degrees of freedom $\{x_b\} = \{0\}$ and also assuming harmonic motions $x(t) = X(\omega) e^{j\omega t}$ the eigenvalue problem can be stated as

$$([K_{ii}] - \omega_i^2 [M_{ii}]) \{\Phi_{ii}\} = \{0\}. \quad (18.10)$$

The internal degrees of freedom $\{x_i\}$ will be projected on the set of orthogonal mode shapes (modal matrix) $[\Phi_{ip}]$, thus

$$\{x_i\} = [\Phi_{ii}] \{\eta_i\}. \quad (18.11)$$

The modal transformation becomes

$$\{x\} = \begin{Bmatrix} x_i \\ x_b \end{Bmatrix} = \begin{bmatrix} \Phi_{ii} \\ 0 \end{bmatrix} \{\eta_i\} = [\Phi_i] \{\eta_i\}. \quad (18.12)$$

The Craig–Bampton (CB) transformation matrix is (18.4)

$$[\Phi_c \Phi_i] = \begin{bmatrix} -[K_{ii}]^{-1}[K_{ib}] & \Phi_{ii} \\ I & 0 \end{bmatrix}.$$

The Craig–Bampton (CB) transformation matrix is (18.4)

$$\{x\} = [\Phi_c \Phi_i] \begin{Bmatrix} x_b \\ \eta_i \end{Bmatrix} = [\Psi] \{X\}.$$

with $[\Phi_c]$ the static or constraint modes, $[\Phi_i]$ the modal matrix, $\{x_b\}$ the external or boundary degrees of freedom and $\{\eta_i\}$ the generalised coordinates. In general, the number of generalised coordinates i is much less than the total number of degrees of freedom $n = b + i$, $i \ll n$.

The CB transformation (18.4) will be substituted into (18.2) presuming equal potential and kinetic energies, hence

$$[\Psi]^T [M] [\Psi] \{\ddot{X}\} + [\Psi]^T [K] [\Psi] \{X\} = [\Psi]^T \{F(t)\}. \quad (18.13)$$

On further elaboration it is found that

$$\begin{bmatrix} \tilde{M}_{bb} & M_{bi} \\ M_{ib} & \langle m_i \rangle \end{bmatrix} \begin{Bmatrix} \ddot{x}_b \\ \ddot{\eta}_i \end{Bmatrix} + \begin{bmatrix} \tilde{K}_{bb} & K_{bi} \\ K_{ib} & \langle k_i \rangle \end{bmatrix} \begin{Bmatrix} x_b \\ \eta_i \end{Bmatrix} = \begin{bmatrix} \Phi_{ib} & \Phi_i \\ I & 0 \end{bmatrix}^T \begin{Bmatrix} F_i \\ F_b \end{Bmatrix}, \quad (18.14)$$

with $[\tilde{M}_{bb}]$ the Guyan reduced-mass matrix (b -set), $[\tilde{K}_{bb}]$ the Guyan reduced-stiffness matrix (b -set), $\langle m_i \rangle$ the diagonal matrix of generalised masses, $\langle m_i \rangle = \Phi_i^T [M] [\Phi_i]$, $\langle k_i \rangle$ the diagonal matrix of generalised stiffnesses, $\langle k_i \rangle = [\Phi_i]^T [K] [\Phi_i] = \langle \lambda_i \rangle \langle m_i \rangle = \langle \omega_i^2 \rangle \langle m_i \rangle$, $[K_{ib}] = [\Phi_{ib}]^T [K_{ii}] [\Phi_i] + [K_{bi}] [\Phi_i] = (-[K_{ib}]^T [K_{ii}]^{-1} [K_{ii}] + [K_{bi}]) [\Phi_i] = [0]$ and $[K_{ib}] = K_{bi}^T = [0]$.

Thus (18.14) becomes

$$\begin{bmatrix} \tilde{M}_{bb} & M_{bi} \\ M_{ib} & \langle m_i \rangle \end{bmatrix} \begin{Bmatrix} \ddot{x}_b \\ \ddot{\eta}_i \end{Bmatrix} + \begin{bmatrix} \tilde{K}_{bb} & 0 \\ 0 & \langle k_i \rangle \end{bmatrix} \begin{Bmatrix} x_b \\ \eta_i \end{Bmatrix} = \begin{bmatrix} \Phi_{ib} & \Phi_i \\ I & 0 \end{bmatrix}^T \begin{Bmatrix} F_i \\ F_b \end{Bmatrix}. \quad (18.15)$$

Finally

$$[M_{CB}]\{\ddot{X}\} + [K_{CB}]\{X\} = [\Psi]^T\{F\} = \{F_{CB}\}, \quad (18.16)$$

with $[M_{CB}]$ the CB reduced-mass matrix and $[K_{CB}]$ the CB reduced-stiffness matrix.

The CB matrices are $b+i$, $b+i$ sized matrices.

If we look at the reduced-mass matrix $[M_{CB}]$ and the reduced-stiffness matrix $[K_{CB}]$ in more detail we observe only a mass coupling between the internal DOFs $\{x_i\}$ and the external DOFs $\{x_b\}$ in the reduced-mass matrix $[M_{CB}]$ via the submatrices $[M_{bi}]$ and $[M_{ib}]$ consisting of the modal participation factors. (18.2) can be written as follows

$$\begin{bmatrix} M_{CB}^A & 0 \\ 0 & M_{CB}^B \end{bmatrix} \begin{Bmatrix} \ddot{X}^A \\ \ddot{X}^B \end{Bmatrix} + \begin{bmatrix} K_{CB}^A & 0 \\ 0 & K_{CB}^B \end{bmatrix} \begin{Bmatrix} X^A \\ X^B \end{Bmatrix} = \begin{Bmatrix} F_{CB}^A \\ F_{CB}^B \end{Bmatrix} \quad (18.17)$$

$$[M_{\text{tot}}]\{\ddot{Q}_{\text{tot}}\} + [K_{\text{tot}}]\{Q_{\text{tot}}\} = \{F_{\text{tot}}\}, \quad (18.18)$$

or

$$\begin{bmatrix} \langle m_i \rangle^A M_{ib}^A & 0 & 0 \\ M_{bi}^A \tilde{M}_{bb}^A & 0 & 0 \\ 0 & 0 & \langle m_i \rangle^B M_{ib}^B \\ 0 & 0 & M_{bi}^B \tilde{M}_{bb}^B \end{bmatrix} \begin{Bmatrix} \dot{\eta}_i^A \\ \ddot{x}_b^A \\ \dot{\eta}_i^B \\ \ddot{x}_b^B \end{Bmatrix} + \begin{bmatrix} \langle k_i \rangle^A & 0 & 0 & 0 \\ 0 & \tilde{K}_{bb}^A & 0 & 0 \\ 0 & 0 & \langle k_i \rangle^B & 0 \\ 0 & 0 & 0 & \tilde{K}_{bb}^B \end{bmatrix} \begin{Bmatrix} \eta_i^A \\ x_b^A \\ \eta_i^B \\ x_b^B \end{Bmatrix} = \begin{Bmatrix} F_{CB,i}^A \\ F_{CB,b}^A \\ F_{CB,i}^B \\ F_{CB,b}^B \end{Bmatrix}. \quad (18.19)$$

For coupling the substructures A and B , equal displacement and acceleration of the external DOFs is assumed, $x_b^A = x_b^B$ and $\ddot{x}_b^A = \ddot{x}_b^B$. The total displacement vector can then be written as

$$\{Q_{\text{tot}}\} = \begin{Bmatrix} \eta_i^A \\ x_b^A \\ \eta_i^B \\ x_b^B \end{Bmatrix} = \begin{bmatrix} I & 0 & 0 \\ 0 & 0 & I \\ 0 & I & 0 \\ 0 & 0 & I \end{bmatrix} \begin{Bmatrix} \eta_i^A \\ \eta_i^B \\ x_b^A = x_b^B \end{Bmatrix} = [L]\{Q_{\text{red}}\} \quad (18.20)$$

The transformation matrix $[L]$ also applies to the acceleration. Using the equations of Lagrange or assuming equal potential and kinetic energies, (18.20) can be incorporated into (18.19).

$$[L]^T [M_{\text{tot}}] [L] \{\ddot{Q}_{\text{red}}\} + [L]^T [K_{\text{tot}}] [L] \{Q_{\text{red}}\} = [L]^T \{F_{\text{tot}}\} = \{F_{\text{red}}\} \quad (18.21)$$

$$\begin{aligned} & \left[\begin{array}{ccc} \langle m_i \rangle^A & 0 & M_{ib}^A \\ 0 & \langle m_i \rangle^B & M_{ib}^B \\ M_{bi}^A & M_{bi}^B & \tilde{M}_{bb}^A + \tilde{M}_{bb}^B \end{array} \right] \left\{ \begin{array}{c} \dot{\eta}_i^A \\ \dot{\eta}_i^B \\ \tilde{x}_b^A \end{array} \right\} + \left[\begin{array}{ccc} \langle k_i \rangle^A & 0 & 0 \\ 0 & \langle k_i \rangle^B & 0 \\ 0 & 0 & \tilde{K}_{bb}^A + \tilde{K}_{bb}^B \end{array} \right] \left\{ \begin{array}{c} \eta_i^A \\ \eta_i^B \\ x_b^A \end{array} \right\} \\ &= \left\{ \begin{array}{c} F_{\text{CB}, i}^A \\ F_{\text{CB}, i}^B \\ F_{\text{CB}, b}^A + F_{\text{CB}, b}^B \end{array} \right\}. \end{aligned} \quad (18.22)$$

The reduced-mass matrices $[\tilde{M}_{bb}^A]$, $[\tilde{M}_{bb}^B]$, the reduced_stiffness matrices $[\tilde{K}_{bib}]$ and $[\tilde{K}_{bb}]$, related to the common boundary DOFs $\{\tilde{x}_b^A\} = \{\tilde{x}_b^B\}$ and $\{x_b^A\} = \{x_b^B\}$ are added. The generalised masses $\langle m_i \rangle^A$ and $\langle m_i \rangle^B$ are coupled via the modal participation factors (matrices $[M_{bi}]$ and $[M_{ib}]$) to the reduced-mass matrix $[\tilde{M}_{bb}^A + \tilde{M}_{bb}^B]$. The generalised stiffnesses are not coupled with the reduced-stiffness matrix $[\tilde{K}_{bb}^A + \tilde{K}_{bb}^B]$.

The Craig–Bampton method is widely applied in the cases when the component dynamic properties are described by their mass and stiffness matrices.

Example

A linear free-free dynamic system consists of 19 DOFs; 1 to 19. The lumped masses at DOF 1 and DOF 19 are $m_1 = m_{19} = 0.5$ kg. The masses lumped to the other DOFs, 2 to 18, are $m_2 = m_3 = \dots = m_{17} = m_{18} = 1$ kg. The 18 springs between the DOFs 1 to 19 are equal, $k_{12} = k_{23} = \dots = k_{1718} = k_{1819} = 10000$ N/m. The free-free dynamic system is illustrated in Fig. 18.1.

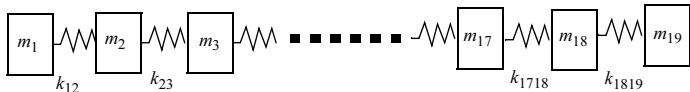


Fig. 18.1. Free dynamic system with 19 DOFs

A linear free-free substructure consists of 7 DOFs; 1 to 7. The lumped masses at DOF 1 and DOF 7 are $m_1 = m_7 = 0.5$ kg. The other masses lumped to the other

DOFs, 2 to 6, are $m_2 = \dots = m_6 = 1$ kg. The 6 springs between the DOFs 1 to 19 are equal, $k_{12} = k_{23} = \dots = k_{67} = 10000$ N/m. The substructure is shown in Fig. 18.2.

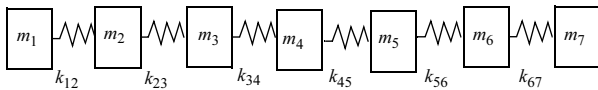


Fig. 18.2. Free-Free substructure with 7 DOFs

Three substructures will build up the total structure as illustrated in Fig. 18.1. The results of the analyses are shown in Table 18.1.

Table 18.1. Results of CMS natural-frequency calculations

#	Complete Model (Hz)	Model A	Model B
		1 mode per substructure (7 DOFs) (Hz)	2 modes per substructure (10 DOFs) (Hz)
1	0.0000	0.0000	0.0000
2	2.7743	2.7771 (0.1%)	2.7752 (0.0%)
3	5.5274	5.5803 (1.5%)	5.5316 (0.1%)
4	8.2385	8.9437 (9.5%)	8.2535 (0.2%)
5	10.8868	11.9825 (10.0%)	10.9253 (0.4%)
6	13.4524	15.5038	13.6279
7	15.9155	17.3217	17.3217
8	18.2575		19.7890
9	20.4606		22.5478
10	22.5079		23.7726

End of example

18.2.2 Free-Interface Method

The principle of CMS with the free-interface method (unconstrained boundaries) is discussed by Craig, [Craig 1976, Craig 1977, Craig 2000]. The basic free-free undamped equations of motion are taken from (18.2), simply written as

$$[M]\{\ddot{x}\} + [K]\{x\} = \{F\}. \quad (18.23)$$

The eigenvalue problem is

$$\{[K] - \omega_i^2 [M]\} \{\phi_i\} = \{0\}. \quad (18.24)$$

The n physical DOFs $\{x\}$ are projected on the linear independent set of eigenvectors, the so-called modal matrix

$$[\Phi] = [\phi_1, \phi_2, \dots, \phi_n], \quad (18.25)$$

hence

$$\{x\} = [\Phi] \{\eta\}. \quad (18.26)$$

The modal matrix $[\Phi]$ is orthogonal with respect to the mass matrix $[M]$, thus

$$[\Phi]^T [M] [\Phi] = \langle m \rangle, \quad (18.27)$$

and orthogonal with respect to the stiffness matrix $[K]$

$$[\Phi]^T [K] [\Phi] = \langle m \omega_i^2 \rangle. \quad (18.28)$$

(18.2) can be transformed (coordinate transformation) into a set of decoupled n SDOF equations of the generalised coordinates $\{\eta\}$

$$m_k \ddot{\eta}_k + m_k \omega_k^2 \eta_k = \{\phi_k\} \{F\}, \quad k = 1, 2, \dots, n, \quad (18.29)$$

with m_k the generalised or modal mass and $m_k \omega_k^2$ the generalised or modal stiffness.

In the frequency domain with

- $\{x(t)\} = \{X(\omega)\} e^{j\omega t}$
- $\{\eta(t)\} = \{\Pi(\omega)\} e^{j\omega t}$
- $\{F(t)\} = \{F(\omega)\} e^{j\omega t}$

the solution of $\Pi_k(\omega)$ is given by

$$\Pi_k(\omega) = \frac{\{\phi_k\}^T \{F(\omega)\}}{m_k(\omega_k^2 - \omega^2)}. \quad (18.30)$$

The solution for the vector of generalised coordinates $\{\Pi(\omega)\}$ in the frequency domain becomes

$$\{\Pi(\omega)\} = \left\langle \frac{1}{m_k(\omega_k^2 - \omega^2)} \right\rangle [\Phi]^T \{F(\omega)\}. \quad (18.31)$$

The physical displacement vector $\{X(\omega)\}$ is obtained from

$$\{X\{\omega\}\} = [\Phi]\{\Pi(\omega)\} = [\Phi]\left\langle \frac{1}{m_k(\omega_k^2 - \omega^2)} \right\rangle [\Phi]^T \{F(\omega)\}. \quad (18.32)$$

The modal matrix $[\Phi]$ may be partitioned in the remaining modes and the deleted modes:

$$[\Phi] = [\Phi_k, \Phi_d]. \quad (18.33)$$

Reconstructing the flexibility matrix $[G]$, with $\omega \rightarrow 0$

$$[G] = [\Phi_k]\left\langle m_k\omega_k^2 \right\rangle^{-1} [\Phi_k]^T + [\Phi_d]\left\langle m_d\omega_d^2 \right\rangle^{-1} [\Phi_d]^T = [G_k] + [G_r], \quad (18.34)$$

with $[G_r]$ the residual flexibility matrix, $[G_r] = [G] - [\Phi_k]\left\langle m_k\omega_k^2 \right\rangle^{-1} [\Phi_k]^T$ and $[G] = [K]^{-1}$ the flexibility matrix (the inverse of the stiffness matrix $[K]$ is only allowed if the structure is constrained such that rigid body motions are eliminated).

If the rigid-body modes are eliminated we can express $\{X(\omega)\}$, assuming for the modes $k > m$, $\omega_k^2 \gg \omega^2$

$$\{X(\omega)\} = \sum_{k=1}^m \{\phi_k\} \left(\frac{\{\phi_k\} \{F(\omega)\}}{m_k[\omega_k^2 - \omega^2]} \right) + \sum_{k=m+1}^n \{\phi_k\} \left(\frac{\{\phi_k\} \{F(\omega)\}}{m_k\omega_k^2} \right). \quad (18.35)$$

(18.35) can be transformed back in the time domain, such that

$$\{x(t)\} = [\Phi_k]\{\eta_k(t)\} + [G_r]\{F(t)\} \quad (18.36)$$

and this is done in combination with (18.29).

If a substructure has rigid-body modes, the flexibility matrix $[G]$ does not exist, however, an alternative formulation can be derived. We write the displacement vector $\{x\}$ as follows

$$\{x\} = [\Phi_r]\{\eta_r\} + [\Phi_e]\{\eta_e\}, \quad (18.37)$$

with $[\Phi_r]$ the rigid-body modes ($\omega_r = 0$), $[\Phi_e]$ the elastic modes of a free-free component ($\omega_e \neq 0$), $\{\eta_r\}$ generalised coordinates associated with the rigid body motions and $\{\eta_e\}$ generalised coordinates associated with the elastic motions.

The modal matrices $[\Phi_r]$ and $[\Phi_e]$ are orthonormal with respect to the mass matrix $[M]$, thus

$$[\Phi_r]^T [M] [\Phi_r] = \langle m_r \rangle, [\Phi_e]^T [M] [\Phi_e] = \langle m_e \rangle, [\Phi_r]^T [M] [\Phi_e] = [0], \quad (18.38)$$

and orthogonal with respect to the stiffness matrix $[K]$

$$[\Phi_r]^T [K] [\Phi_r] = [0], [\Phi_e]^T [K] [\Phi_e] = \langle m_e \omega_e^2 \rangle, [\Phi_r]^T [K] [\Phi_e] = [0]. \quad (18.39)$$

(18.23) can be written

$$[M][\Phi_r]\{\ddot{\eta}_r\} + [M][\Phi_e]\{\ddot{\eta}_e\} + [K][\Phi_r]\{\eta_r\} + [K][\Phi_e]\{\eta_e\} = \{F\}. \quad (18.40)$$

Taking into account that $[K][\Phi_r] = [0]$ (18.40) becomes

$$[M][\Phi_e]\{\ddot{\eta}_e\} + [K][\Phi_e]\{\eta_e\} = \{F\} - [M][\Phi_r]\{\ddot{\eta}_r\}. \quad (18.41)$$

Using (18.29), and referring to (18.38), it can be easily proved that

$$\{\ddot{\eta}_r\} = \langle m_r \rangle^{-1} [\Phi_r]^T \{F\}. \quad (18.42)$$

(18.41) now becomes

$$[M][\Phi_e]\{\ddot{\eta}_e\} + [K][\Phi_e]\{\eta_e\} = \{F\} - [M][\Phi_r]\langle m_r \rangle^{-1} [\Phi_r]^T \{F\} = [A]\{F\} \quad (18.43)$$

$$\langle m_e \rangle \{\ddot{\eta}_e\} + \langle m_e \omega_e^2 \rangle \{\eta_e\} = [\Phi_e]^T [A]\{F\} = [\Phi_e]^T \{F\}, \quad (18.44)$$

with $[A]$ the inertia-relief filter matrix with the following properties: $[\Phi_r]^T [A]\{F\} = [0]$ and $[\Phi_e]^T [A] = [\Phi_e]^T$. The first equation shows that $[A]\{F\}$ is an equilibrium force system.

Because the force system $[A]\{F\}$ is in equilibrium the free-free substructure may be constrained in an arbitrarily point "B", which will take out the rigid-body motions. This has no influence on the elastic deformation in the substructure. The elastic deformation, with respect to "B", is $\{x_{B,e}\}$ and can be calculated with

$$\{x_{B,e}\} = [G_{B,e}] [A]\{F\}. \quad (18.45)$$

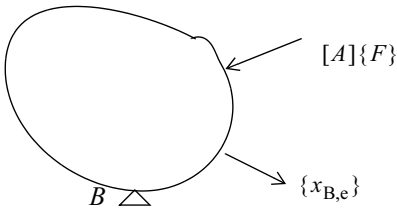


Fig. 18.3. Constrained substructure in point B

The stiffness matrix $[K]$ can be partitioned, giving

$$[K] = \begin{bmatrix} K_{ee} & K_{eB} \\ K_{Be} & K_{BB} \end{bmatrix}. \quad (18.46)$$

The DOFs in point B are constrained, so the rows and columns in the matrix $[K]$ with respect to DOFs associated with point B are removed. The stiffness matrix $[K_{ee}]$ is regular. To calculate the complete vector of deformation (including the DOFs associated with point B) we can define the constrained flexibility matrix $[G_{B,e}]$ as follows

$$[G_{B,e}] = \begin{bmatrix} K_{ee}^{-1} & 0 \\ 0 & 0 \end{bmatrix}. \quad (18.47)$$

The total displacement of the free-free substructure can be written as

$$\{x_{\text{rel}}\} = \{x_{B,e}\} + [\Phi_r]\{\theta_r\}. \quad (18.48)$$

The displacement $\{x_{\text{rel}}\}$ is forced to be mass orthogonal with the rigid-body modes $[\Phi_r]$, thus

$$[\Phi_r]^T [M] \{x_{\text{rel}}\} = \{0\}. \quad (18.49)$$

This will result in

$$\{\theta_r\} = -\langle m_r \rangle^{-1} [\Phi_r]^T [M] \{x_{B,e}\}. \quad (18.50)$$

Thus, the free-free displacement $\{x_{\text{rel}}\}$ becomes

$$\{x_{\text{rel}}\} = ([I] - [\Phi_r] \langle m_r \rangle^{-1} [\Phi_r]^T [M]) \{x_{B,e}\} = [A]^T [G_{B,e}] [A] \{F\} = [G] \{F\}. \quad (18.51)$$

The matrix $[G]$ in (18.51) is called the elastic flexibility matrix in inertia-relief format. (18.51) must be used when the substructure is unconstrained (free-free). (18.37) can now be written as

$$\{x\} = [\Phi_r]\{\eta_r\} + [\Phi_{e,k}]\{\eta_{e,k}\} + \{x_{\text{rel}}\}, \quad (18.52)$$

or the displacement vector $\{x\}$ becomes

$$\{x\} = [\Phi_r]\{\eta_r\} + [\Phi_{e,k}]\{\eta_{e,k}\} + [G]\{F\} = [\Phi_k]\{\eta_k\} + [G]\{F\}, \quad (18.53)$$

with $[\Phi_k]$ the kept elastic modes (including rigid-body modes).

(18.53) will be partitioned in internal DOFs $\{x_i\}$ and external or boundary DOFs $\{x_b\}$.

$$\begin{Bmatrix} x_i \\ x_b \end{Bmatrix} = \begin{bmatrix} \Phi_{k,i} \\ \Phi_{k,b} \end{bmatrix} \{\eta_k\} + \begin{bmatrix} G_{ii} & G_{ib} \\ G_{bi} & G_{bb} \end{bmatrix} \begin{Bmatrix} F_i \\ F_b \end{Bmatrix}, \quad (18.54)$$

and the associated undamped equations of motion expressed in the generalised coordinates $\{\eta_k\}$ (including the rigid-body modes, $\omega_k^2 = 0$)

$$\langle m_k \rangle \{\ddot{\eta}_k\} + \langle m_k \omega_k^2 \rangle \{\eta_k\} = [\Phi_k]^T \{F\} = \begin{bmatrix} \Phi_{k,i} \\ \Phi_{k,b} \end{bmatrix}^T \begin{Bmatrix} F_i \\ F_b \end{Bmatrix}. \quad (18.55)$$

Coupling of Two Substructures *A* and *B*

To couple the two substructures *A* and *B* we must force continuity with respect to the external or boundary displacement $\{x_b^A\}$ and $\{x_b^B\}$, hence

$$\{x_b^A\} = \{x_b^B\}, \quad (18.56)$$

and at the boundaries the external forces of substructure *A* $\{F_b^A\}$ and substructure *B* $\{F_b^B\}$ are at equilibrium, hence

$$\{F_b^A\} + \{F_b^B\} = \{0\}. \quad (18.57)$$

If the second part of (18.55) is substituted into (18.56) the following equation is found

$$\Phi_{k,b}^A \{\eta_k^A\} + [G_{bb}^A] \{F_b^A\} + [G_{bb}^A] \{F_b^A\} = \Phi_{k,b}^B \{\eta_k^B\} + [G_{bb}^B] \{F_b^B\} + [G_{bb}^B] \{F_b^B\}, \quad (18.58)$$

With the introduction of in equilibrium forces at the boundaries in (18.57), (18.58) can be rewritten as

$$\{F_b^A\} \{[G_{bb}^A] + [G_{bb}^B]\} = \Phi_{k,b}^B \{\eta_k^B\} - \Phi_{k,b}^A \{\eta_k^A\} + [G_{bi}^B] \{F_i^B\} - [G_{bi}^A] \{F_i^A\}, \quad (18.59)$$

or

$$\{F_b^A\} = \{[G_{bb}^A] + [G_{bb}^B]\}^{-1} (\Phi_{k,b}^B \{\eta_k^B\} - \Phi_{k,b}^A \{\eta_k^A\} + [G_{bi}^B] \{F_i^B\} - [G_{bi}^A] \{F_i^A\}). \quad (18.60)$$

and

$$\{F_b^B\} = -\{[G_{bb}^A] + [G_{bb}^B]\}^{-1} (\Phi_{k,b}^B \{\eta_k^B\} - \Phi_{k,b}^A \{\eta_k^A\} + [G_{bi}^B] \{F_i^B\} - [G_{bi}^A] \{F_i^A\}) \quad (18.61)$$

Substitution of the last two equations, (18.60) and (18.61) into (18.55) in substructures A and B respectively, with $[K_{bb}^{AB}] = \{[G_{bb}^A] + [G_{bb}^B]\}^{-1}$, it is found

$$\begin{aligned} \langle m_k^A \rangle \{ \ddot{\eta}_k^A \} + \langle m_k^A \omega_k^{2A} \rangle \{ \eta_k^A \} &= \begin{bmatrix} \Phi_{k,i}^A \\ \Phi_{k,b}^A \end{bmatrix}^T \begin{cases} F_i^A \\ F_b^A \end{cases} \\ &= \begin{bmatrix} \Phi_{k,i}^A \\ \Phi_{k,b}^A \end{bmatrix}^T \begin{bmatrix} F_i^A \\ [K_{bb}^{AB}]([\Phi_{k,b}^B] \{ \eta_k^B \} - [\Phi_{k,b}^A] \{ \eta_k^A \} + [G_{bi}^B] \{ F_i^B \} - [G_{bi}^A] \{ F_i^A \}) \end{bmatrix}, \quad (18.62) \end{aligned}$$

and

$$\begin{aligned} \langle m_k^B \rangle \{ \ddot{\eta}_k^B \} + \langle m_k^B \omega_k^{2B} \rangle \{ \eta_k^B \} &= \begin{bmatrix} \Phi_{k,i}^B \\ \Phi_{k,b}^B \end{bmatrix}^T \begin{cases} F_i^B \\ F_b^B \end{cases} \\ &= \begin{bmatrix} \Phi_{k,i}^B \\ \Phi_{k,b}^B \end{bmatrix}^T \begin{bmatrix} F_i^B \\ (-[K_{bb}^{AB}])([\Phi_{k,b}^B] \{ \eta_k^B \} - [\Phi_{k,b}^A] \{ \eta_k^A \} + [G_{bi}^B] \{ F_i^B \} - [G_{bi}^A] \{ F_i^A \}) \end{bmatrix}. \quad (18.63) \end{aligned}$$

Rewriting (18.62) and (18.63) the following is obtained

$$\begin{aligned} &\begin{bmatrix} \langle m_k^A \rangle & 0 \\ 0 & \langle m_k^B \rangle \end{bmatrix} \begin{cases} \ddot{\eta}_k^A \\ \ddot{\eta}_k^B \end{cases} \\ &+ \begin{bmatrix} \langle k_k^A \rangle + [\Phi_{k,b}^A]^T [K_{bb}^{AB}] [\Phi_{k,b}^A] & -[\Phi_{k,b}^A]^T [K_{bb}^{AB}] [\Phi_{k,b}^B] \\ -[\Phi_{k,b}^B]^T [K_{bb}^{AB}] [\Phi_{k,b}^A] & \langle k_k^B \rangle + [\Phi_{k,b}^B]^T [K_{bb}^{AB}] [\Phi_{k,b}^B] \end{bmatrix} \begin{cases} \eta_k^A \\ \eta_k^B \end{cases} \\ &= \begin{bmatrix} \left[[\Phi_{k,i}^A]^T - [\Phi_{k,b}^A]^T [K_{bb}^{AB}] [G_{bi}^A] \right] & [\Phi_{k,i}^A]^T [K_{bb}^{AB}] [G_{bi}^B] \\ [\Phi_{k,i}^B]^T [K_{bb}^{AB}] [G_{bi}^A] & \left[[\Phi_{k,i}^B]^T - [\Phi_{k,b}^B]^T [K_{bb}^{AB}] [G_{bi}^B] \right] \end{bmatrix} \begin{cases} F_i^A \\ F_i^B \end{cases} \quad (18.64) \end{aligned}$$

where $k_k = m_k \omega_k^2$.

In the final synthesised dynamic system (substructures A , B , etc.), only the generalised coordinates remain, while the interface DOFs have cancelled out. The coupling of the substructures is done via the stiffness matrix. The mass matrix is a diagonal matrix with the generalised masses on the main diagonal.

18.2.3 General-Purpose CMS Method

The general-purpose CMS method has been addressed by [Herting 1979]. Both constrained and unconstrained substructures are covered by this CMS method. We assume undamped substructures. The undamped equations of motion for a substructure or component can be written using (18.2)

$$[M]\{\ddot{x}\} + [K]\{x\} = \{F\}.$$

In the previous section the solution for the physical displacement vector in the frequency domain has been derived and is represented in (18.32)

$$\{X(\omega)\} = [\Phi] \left\langle \frac{1}{m_k(\omega_k^2 - \omega^2)} \right\rangle [\Phi]^T \{F(\omega)\}.$$

Three groups of responses can be considered:

1. The rigid-body modes; $\omega_k^2 = 0$, $[\Phi] = [\Phi_0]$ and $m_k = m_0$, $k = 1, 2, \dots, 6$
2. The kept elastic modes, the natural frequencies which are in the frequency range of interest; $\omega_k^2 \approx O(\omega^2)$, $[\Phi] = [\Phi_k]$ and m_k , $k = 6, 7, \dots, m$
3. The deleted elastic modes: $\omega_k^2 \gg \omega^2$, $[\Phi] = [\Phi_d]$ and m_d , $d = m+1, \dots$

(18.32) can be written

$$\begin{aligned} \{X(\omega)\} &= \left[[\Phi_0] \left\langle \frac{1}{-m_0 \omega^2} \right\rangle [\Phi_0]^T + [\Phi_k] \left\langle \frac{1}{m_k(\omega_k^2 - \omega^2)} \right\rangle [\Phi_k]^T \right] \{F(\omega)\} \\ &\quad \left[+ [\Phi_d] \left\langle \frac{1}{m_d(\omega_d^2)} \right\rangle [\Phi_d]^T \right] \{F(\omega)\}. \end{aligned} \quad (18.65)$$

The constant acceleration, when $\omega \rightarrow 0$, becomes

$$\ddot{x}_c = \lim_{\omega \rightarrow 0} \{\ddot{X}(\omega)\} = -\omega^2 \{X(\omega)\} = [\Phi_0] \left\langle \frac{1}{m_0} \right\rangle [\Phi_0]^T \{F(t)\}, \quad (18.66)$$

and the static displacement vector ($\omega \rightarrow 0$), premultiplied by the stiffness matrix $[K]$, is given by

$$\begin{aligned} [K]\{x_{\text{stat}}\} &= \lim_{\omega \rightarrow 0} [K]\{X(\omega)\} = [K] \left([\Phi_k] \left\langle \frac{1}{m_k \omega_k^2} \right\rangle [\Phi_k]^T \right) \{F(t)\} \\ &\quad + [K] \left([\Phi_d] \left\langle \frac{1}{m_d \omega_d^2} \right\rangle [\Phi_d]^T \right) \{F(t)\}. \end{aligned} \quad (18.67)$$

If (18.66) and (18.67) are substituted into (18.2), with $\omega \rightarrow 0$, $[K] \left([\Phi_d] \left\langle \frac{1}{m_d \omega_d^2} \right\rangle [\Phi_d]^T \right) \{F(t)\}$ can be expressed as follows

$$\begin{aligned} \left([\Phi_d] \left\langle \frac{1}{m_d \omega_d^2} \right\rangle [\Phi_d]^T \right) \{F(t)\} &= \{F(t)\} - [M][\Phi_0] \left\langle \frac{1}{m_0} \right\rangle [\Phi_0]^T \{F(t)\} \\ &\quad - [K] \left([\Phi_k] \left\langle \frac{1}{m_k \omega_k^2} \right\rangle [\Phi_k]^T + \dots \right) \{F(t)\}. \end{aligned} \quad (18.68)$$

(18.65) is transferred in the time domain giving:

$$\{x(t)\} = [\Phi_0]\{\eta_0(t)\} + [\Phi_k]\{\eta_k(t)\} + [\Phi_d] \left\langle \frac{1}{m_d \omega_d^2} \right\rangle [\Phi_d]^T \{F(t)\}. \quad (18.69)$$

If the result of (18.68) is substituted into (18.65) and if (18.69) is premultiplied by the stiffness matrix $[K]$ it follows that

$$[K]\{x(t)\} = [K][\Phi_0]\{\eta_0(t)\} + [K][\Phi_k]\{\eta_k(t)\} + \{F(t)\}$$

$$- [M][\Phi_0] \left\langle \frac{1}{m_0} \right\rangle [\Phi_0]^T \{F(t)\} - [K][\Phi_k] \left\langle \frac{1}{m_k \omega_k^2} \right\rangle [\Phi_k]^T \{F(t)\}. \quad (18.70)$$

Making use of $[K][\Phi_0] = \{0\}$, (18.70) can be written as

$$[K]\{x(t)\} = [K][\Phi_k](\{\eta_k(t)\} - \{\eta_{\text{stat}}(t)\}) - [M][\Phi_0] \left\langle \frac{1}{m_0} \right\rangle [\Phi_0]^T \{F(t)\} + \{F(t)\}, \quad (18.71)$$

or

$$[K]\{x(t)\} = [K][\Phi_k]\{\delta_k(t)\} - [M][\Phi_0]\{\delta_0(t)\} + \{F(t)\}, \quad (18.72)$$

with $\{\delta_k(t)\} = (\{\eta_k(t)\} - \{\eta_{\text{stat}}(t)\})$ the normal mode generalised coordinates and $\{\delta_0(t)\} = \left\langle \frac{1}{m_0} \right\rangle [\Phi_0]^T \{F(t)\}$ the inertia-relief coordinates ($n_0 \leq 6$), and have units of acceleration.

We return to (18.3)

$$\begin{bmatrix} M_{ii} & M_{ib} \\ M_{bi} & M_{bb} \end{bmatrix} \begin{Bmatrix} \ddot{x}_i \\ \ddot{x}_b \end{Bmatrix} + \begin{bmatrix} K_{ii} & K_{ib} \\ K_{bi} & K_{bb} \end{bmatrix} \begin{Bmatrix} x_i \\ x_b \end{Bmatrix} = \begin{Bmatrix} F_i \\ F_b \end{Bmatrix}.$$

With use of (18.72) $[K_{ii}]\{x_i\}$ can be expressed as follows

$$\begin{aligned} [K_{ii}]\{x_i\} &= \{F_i\} + ([K_{ii}][\Phi_{k,i}] + [K_{ib}][\Phi_{k,b}])\{\delta_k(t)\} \\ &\quad - ([M_{ii}][\Phi_{0,i}] + [M_{ib}][\Phi_{0,b}])\{\delta_0(t)\} - [K_{ib}]\{x_b\}, \end{aligned} \quad (18.73)$$

and furthermore,

$$\{x_i\} = [K_{ii}]^{-1}\{F_i\} + ([\Phi_{k,i}] - [G_{ib}][\Phi_{k,b}])\{\delta_k(t)\}$$

$$-[K_{ii}]^{-1}([M_{ii}][G_{ib}] + [M_{ib}])[\Phi_{0,b}]\{\delta_0(t)\} + [G_{ib}]\{x_b\}, \quad (18.74)$$

with $[G_{ib}] = -[K_{ii}]^{-1}[K_{ib}]$ and $[G_{ib}][\Phi_{0,b}] = [\Phi_{0,i}]$.

The displacement vector $\{x\}$, using (18.74), can be written as

$$\{x\} = \begin{Bmatrix} \bar{x}_i \\ x_b \end{Bmatrix} = [\Psi] \begin{Bmatrix} \delta_0 \\ \delta_k \\ x_b \end{Bmatrix} = [\Psi]\{\vartheta\}, \quad (18.75)$$

with

$$\{x_i\} = \{\bar{x}_i\} + [K_{ii}]^{-1}\{F_i\}. \quad (18.76)$$

Thus we can write for the transformation matrix $[\Psi]$

$$[\Psi] = \begin{bmatrix} -[K_{ii}]^{-1}([M_{ii}][G_{ib}] + [M_{ib}])[\Phi_{0,b}] & ([\Phi_{k,i}] - [G_{ib}][\Phi_{k,b}]) G_{ib} \\ 0 & 0 & I \end{bmatrix}. \quad (18.77)$$

Some remarks can be made;

- When the number of modes is zero and the inertia-relief effects are ignored, the transformation matrix $[\Psi]$ in (18.77) is the same as the Guyan reduction or matrix condensation transformation.
- Modes provide dynamic motion relative to the static deformation.
- Rigid-body motion and redundant constraint information are contained in the $[G_{ib}]$ transformation
- Inertia-relief deformation shapes are contained in the $-[K_{ii}]^{-1}([M_{ii}][G_{ib}] + [M_{ib}])[\Phi_{0,b}]$ matrix.
- The sum of rigid-body DOFs $\{\delta_0\}$ and elastic generalised DOFs $\{\delta_k\}$ must be less than or equal to the number of internal DOFs $\{x_i\}$.

The general undamped equations of motion are

$$[M]\{\ddot{x}\} + [K]\{x\} = \{F(t)\}.$$

If the transformation (18.75) is applied the following undamped equation of motion are obtained

$$[\Psi]^T[M][\Psi]\{\ddot{\vartheta}\} + [\Psi]^T[K][\Psi]\{\vartheta\} = [\Psi]^T\{F(t)\}, \quad (18.78)$$

or

$$[M_{\vartheta\vartheta}]\{\ddot{\vartheta}\} + [K_{\vartheta\vartheta}]\{\vartheta\} = \{F_\vartheta(t)\} \quad (18.79)$$

The data recovery of the physical DOFs, displacement $\{x\}$, velocities $\{\dot{x}\}$ and acceleration $\{\ddot{x}\}$, can be obtained as follows. The displacements $\{x\}$ becomes

$$\{x\} = \begin{Bmatrix} x_i \\ x_b \end{Bmatrix} = \begin{Bmatrix} \bar{x}_i \\ x_b \end{Bmatrix} + \begin{Bmatrix} x_{i, stat} \\ 0 \end{Bmatrix} = [\Psi] \begin{Bmatrix} \delta_0 \\ \delta_k \\ x_b \end{Bmatrix} + \begin{bmatrix} [K_{ii}]^{-1} \{F_i\} \\ 0 \end{bmatrix}, \quad (18.80)$$

and the velocities $\{\dot{x}\}$

$$\{\dot{x}\} = \begin{Bmatrix} \dot{x}_i \\ \dot{x}_b \end{Bmatrix} = \begin{Bmatrix} \dot{\bar{x}}_i \\ \dot{x}_b \end{Bmatrix} = [\Psi] \begin{Bmatrix} \dot{\delta}_0 \\ \dot{\delta}_k \\ \dot{x}_b \end{Bmatrix}, \quad (18.81)$$

and the accelerations $\{\ddot{x}\}$ are

$$\{\ddot{x}\} = \begin{Bmatrix} \ddot{x}_i \\ \ddot{x}_b \end{Bmatrix} = \begin{Bmatrix} \ddot{\bar{x}}_i \\ \ddot{x}_b \end{Bmatrix} = [\Psi] \begin{Bmatrix} \ddot{\delta}_0 \\ \ddot{\delta}_k \\ \ddot{x}_b \end{Bmatrix}. \quad (18.82)$$

The solution for the displacements $\{x\}$ may be improved by using the mode acceleration method [MAM]

$$\{x_{\text{MAM}}\} = \begin{Bmatrix} x_{i, \text{MAM}} \\ x_b \end{Bmatrix} = \begin{bmatrix} G_{ib} \\ I \end{bmatrix} \{x_b\} + \begin{bmatrix} [K_{ii}]^{-1} (\{F_i\} - [M_{ib}] \{\ddot{x}_b\} - [M_{ii}] \{\ddot{x}_i\}) \\ 0 \end{bmatrix}. \quad (18.83)$$

The damping effects are ignored here.

Example

A free-free dynamic system consists of 20 discrete masses, each $m = 1$ kg, connected with springs, each $k = 10000$ N/m. The total mass matrix and stiffness matrix are

$$[M] = \begin{bmatrix} 1 & 0 & \dots & 0 & 0 \\ 0 & 1 & \dots & 0 & 0 \\ \dots & \dots & \dots & \dots & \dots \\ 0 & 0 & \dots & 1 & 0 \\ 0 & 0 & \dots & 0 & 1 \end{bmatrix}, [K] = 10000 \begin{bmatrix} 1 & -1 & \dots & 0 & 0 \\ -1 & 2 & \dots & 0 & 0 \\ \dots & \dots & \dots & \dots & \dots \\ 0 & 0 & \dots & 2 & -1 \\ 0 & 0 & \dots & -1 & 1 \end{bmatrix}.$$

In this example only the natural frequencies of the complete and reduced models, using the general-purpose CMS method, will be given. The results of the reduction process are shown in Table 18.2. The number of elastic modes taken into account are reflected in the accuracy of the natural frequencies. The accuracy of the modes is not considered in this example.

Table 18.2. Results of reduction process, natural frequencies

#	Natural frequency (Hz)	Reduced model natural frequency (Hz)	Reduced model natural frequency (Hz)
	Complete model	$nb^a=2, nr^b=1, ne^c=5$	$nb=2, nr=1, ne=5$
1	0.0000	0.0000	0.0000
2	2.4974	2.4974	2.4974
3	4.9795	4.9795	4.9795
4	7.4308	8.8043	7.4308
5	9.8363	11.7091	9.8363
6	12.1812		12.1812
7	14.4510		16.8204
8	16.6316		19.0208
9	18.7098		
10	20.6726		

a. number of boundary DOFs, constraint modes

b. number of rigid-body modes

c. number of elastic modes

End Example

18.3 Literature

- Craig, R.R., Jr., Bampton, M.C.C., July 1968, *Coupling of Substructures for Dynamic Analysis*, AIAA Journal, Vol. 6, No. 7, pages 1313–1319.
- Craig, R.R., Jr., Chang, Ching-Jone, 1976, *Free-Interface Methods of Substructure Coupling for Dynamic Analysis*, AIAA Journal, Vol. 14, No. 11, pages 1633–1635.
- Craig, R.R., Jr., Chang, Ching-Jone, 1976, *Substructure Coupling for Dynamic Analysis and Testing*, NASA CR-2781.
- Craig, R.R., Jr., 2000, *Coupling of Substructure for Dynamic Analysis*, AIAA-2000-173.
- Hering, D.N., Morgan, M.J., 1979, *A General Purpose, Multi-stage Component Modal Synthesis Method*, AIAA/ASME/ASCE/AHS, 20th Structures, Structural Dynamics, and Materials Conference, April 6, presented by Universal Analytics, Inc.
- Hintz, R.M., 1975, *Analytical Methods in Component Modal Synthesis*, AIAA Journal, Vol. 13, No. 8, pages 1007–1016.
- MacNeal, R.H., 1971, *A Hybrid Method of Component Mode Synthesis*, Computer & Structures, Vol 1, pages 581–601.
- Maia, M.M.M., Silva, J.M.M., 1997, *Theoretical and Experimental Modal Analysis*, John Wiley, ISBN 0 47197067 0.
- Wijker, J.J., 2004, *Mechanical Vibrations in Spacecraft Design*, Springer, ISBN 3-54-40530-5.

18.4 Exercises

18.4.1 Substructure Analysis I

A linear free-free substructure consists of 7 DOFs; 1 to 7. The lumped masses at DOF 1 and DOF 7 is $m_1 = m_7 = 0.5 \text{ kg}$. The other masses lumped to the other DOFs, 2 to 6, are $m_2 = \dots = m_6 = 1 \text{ kg}$. The 6 springs between the DOFs 1 to 19 are equal, $k_{12} = k_{23} = \dots = k_{67} = 10000 \text{ N/m}$. The substructure is shown in Fig. 18.2.

Couple two substructures with each other, substructure 1 node 7 with node 1 of substructure 2, and calculate the natural frequencies and associated modes. There are no other boundary conditions (free-free structure). Use the following CMS methods:

1. Craig–Bumpkin method
2. Craig–Change method
3. Hurting method

18.4.2 Substructure Analysis 2

A structure may be identified with two components or substructures; component 1 and component 2, as illustrated in Fig. 18.4. The coupling of both components is shown in Fig. 18.5.

Calculate the modal characteristics (natural frequencies, mode shapes and effective masses). All masses have a mass $m = 1 \text{ kg}$ and all springs have a spring stiffness $k = 100000 \text{ N/m}$

Calculate all elastic modes per component (except for the Herting method).

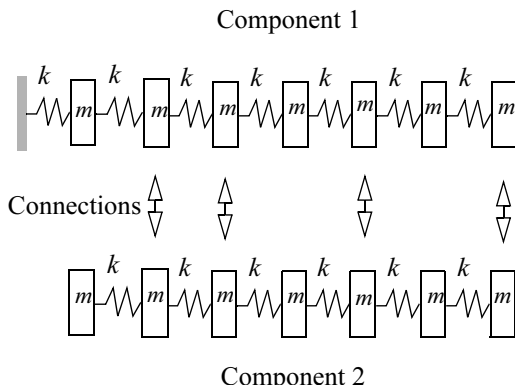


Fig. 18.4. Component 1 and component 2

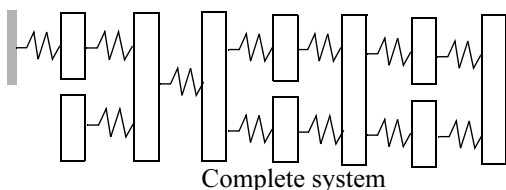


Fig. 18.5. Synthesised components

- Component 1
 - 1.Craig–Bampton method (using constraint modes)
 - 2.Herting method

- Component 2
 - 1.Craig-Bampton method (using constraint modes)
 - 2.Craig-Bampton method (free-free)
 - 3.Herting method
- Synthesis
 - 1.Component 1 – method 1, component 2 method 1
 - 2.Component 1 – method 1, component 2 method 2
 - 3.Component 1 – method 1, component 2 method 3
 - 4.Component 1 – method 2, component 2 method 3

19 Output Transformation Matrices

19.1 Introduction

The mathematical reduced (condensed) dynamic model consists of the reduced-mass and reduced-stiffness matrices. The damping matrix is, in general, not delivered in a reduced form because the damping characteristics will be introduced later in the dynamic response analyses.

Due to the fact that the reduced dynamic model only consists of reduced matrices during the dynamic response analyses no direct information about physical responses (e.g. forces, stresses) can be made available. The reduced dynamic model will only produce response characteristics of physical (e.g. I/F DOFs) and generalised degrees of freedom; displacements, velocities and accelerations.

To be able to produce responses, stresses and forces, in selected structural elements during the dynamic response analyses using (coupled) reduced dynamic models, the so-called load transformation matrix (LTM) can be used. The LTM defines a relation between forces and stresses in certain structural elements and the degrees of freedom of the reduced dynamic model. In general the transformation matrix is called the output transformation matrix (OTM) [Chung 1998, Fransen 2002]. Besides LTMs displacement transformation matrices (DTM), acceleration transformation matrices (ATM) can also be defined [Bray 1991], however, in this chapter only LTMs will be discussed. The creation of DTMs and ATMs is quite the same as the generation of LTMs.

In the following section a method to obtain LTMs will be discussed. The method is based upon the mode displacement method (MDM) and the mode acceleration method (MAM) [Craig 1981]. The method described is:

- The OTMs of a free-free reduced dynamic model. In general, six rigid-body motions will exist.

19.2 Reduced Free-Free Dynamic Model

The calculation of the stresses and forces that are related to the degrees of freedom at the unconstrained boundary DOFs $\{x_j\}$ and the generalised coordinates $\{\eta_p\}$ may be inaccurate when the contribution of the high natural frequency modes is neglected. With the aid of the MAM the stresses and forces in the structural elements become more accurate.

The equations of motion for a component or a substructure are:

$$\begin{bmatrix} M_{ii} & M_{ij} \\ M_{ji} & M_{jj} \end{bmatrix} \begin{Bmatrix} \ddot{x}_i \\ \ddot{x}_j \end{Bmatrix} + \begin{bmatrix} K_{ii} & K_{ij} \\ K_{ji} & K_{jj} \end{bmatrix} \begin{Bmatrix} x_i \\ x_j \end{Bmatrix} = \begin{Bmatrix} 0 \\ F_j \end{Bmatrix}. \quad (19.1)$$

The force vector $\{F_j\}$ represents the interface forces between components, $\{x_i\}$ the internal degrees of freedom and $\{x_j\}$ the external degrees of freedom (in general at the boundary).

The internal degrees of freedom $\{x_i\}$ may be written as [Klein 1988]:

$$\{x_i^*\} = -[K_{ii}]^{-1} \left\{ \begin{bmatrix} M_{ii} & M_{ij} \\ 0 & I \end{bmatrix} \begin{Bmatrix} \ddot{x}_i \\ \ddot{x}_j \end{Bmatrix} + [K_{ij}]\{x_j\} \right\}. \quad (19.2)$$

For a Craig–Bampton model [Craig 1968], [Craig 1981]

$$\begin{Bmatrix} \ddot{x}_i \\ \ddot{x}_j \end{Bmatrix} = \begin{bmatrix} \phi_p & \phi_{ij} \\ 0 & I \end{bmatrix} \begin{Bmatrix} \ddot{\eta}_p \\ \ddot{x}_j \end{Bmatrix}, \quad (19.3)$$

where $[\phi_{ij}] = -[K_{ii}]^{-1}[K_{ij}]$ are the constrained modes, $([K_{ii}] - \lambda_i[M_{ii}])\{\phi_{pi}\} = \{0\}$ are the eigenvalues problem of the internal degrees of freedom and $\{\eta_p\}$ are the generalised coordinates (modal amplitude coefficients). The acceleration transformation matrix [ATM] in the sense of the modal displacements method (MDM) is given by

$$[\text{ATM}] = \begin{bmatrix} \phi_p & \phi_{ij} \\ 0 & I \end{bmatrix}. \quad (19.4)$$

The displacement vector $\{x_i^*\}$ can be written as:

$$\{x_i^*\} = -[K_{ii}]^{-1} \left\{ \begin{bmatrix} M_{ii} & M_{ij} \\ 0 & I \end{bmatrix} \begin{bmatrix} \phi_p & \phi_{ij} \\ 0 & I \end{bmatrix} \begin{Bmatrix} \ddot{\eta}_p \\ \ddot{x}_j \end{Bmatrix} + [K_{ij}] \{x_j\} \right\}. \quad (19.5)$$

The complete displacement vector $\{x\}$ becomes:

$$\{x\} = \begin{bmatrix} x_i^* \\ x_j \end{bmatrix} = \left[\begin{bmatrix} -[K_{ii}]^{-1} [M_{ii} & M_{ij}] & \begin{bmatrix} \phi_p & \phi_{ij} \\ 0 & I \end{bmatrix} \begin{Bmatrix} \ddot{\eta}_p \\ \ddot{x}_j \end{Bmatrix} \\ 0 & I \end{bmatrix} \right] + \begin{bmatrix} -[K_{ii}]^{-1} [K_{ij}] \\ I \end{bmatrix} \{x_j\}. \quad (19.6)$$

The displacement transformation matrix DTM, using the mode acceleration, is given by

$$\{x\} = \begin{bmatrix} x_i^* \\ x_j \end{bmatrix} = [\text{DTM}_1] \begin{Bmatrix} \ddot{\eta}_p \\ \ddot{x}_j \end{Bmatrix} + [\text{DTM}_2] \{x_j\} \quad (19.7)$$

The stresses or forces in particular structural elements of the component can be expressed as:

$$\{\sigma\} = [D_\sigma] \{x\} = \begin{bmatrix} D_{\sigma i} & D_{\sigma j} \end{bmatrix} \begin{Bmatrix} x_i^* \\ x_j \end{Bmatrix}, \quad (19.8)$$

or

$$\{\sigma\} = \begin{bmatrix} D_{\sigma i} & D_{\sigma j} \end{bmatrix} \left\{ \begin{bmatrix} -[K_{ii}]^{-1} [M_{ii} & M_{ij}] & \begin{bmatrix} \phi_p & \phi_{ij} \\ 0 & I \end{bmatrix} \begin{Bmatrix} \ddot{\eta}_p \\ \ddot{x}_j \end{Bmatrix} \\ 0 & I \end{bmatrix} + \begin{bmatrix} -[K_{ii}]^{-1} [K_{ij}] \\ I \end{bmatrix} \{x_j\} \right\}, \quad (19.9)$$

or

$$\{\sigma\} = [\text{LMT}_1] \begin{Bmatrix} \ddot{\eta}_p \\ \ddot{x}_j \end{Bmatrix} + [\text{LMT}_2] \{x_j\}, \quad (19.10)$$

with:

$$[\text{LMT}_1] = \begin{bmatrix} D_{\sigma i} & D_{\sigma j} \end{bmatrix} \begin{pmatrix} -[K_{ii}]^{-1} & [M_{ii} & M_{ij}] \\ 0 & I \end{pmatrix} \begin{bmatrix} \phi_p & \phi_{ij} \\ 0 & I \end{bmatrix}, \quad (19.11)$$

and

$$[\text{LMT}_2] = \begin{bmatrix} D_{\sigma i} & D_{\sigma j} \end{bmatrix} \begin{pmatrix} -[K_{ii}]^{-1} & [K_{ij}] \\ I & I \end{pmatrix}, \quad (19.12)$$

The load transformation matrix $[\text{LMT}_1]$ can be defined by setting $\{x_j\} = \{0\}$

and $\begin{Bmatrix} \ddot{\eta}_p \\ \ddot{x}_j \end{Bmatrix} = [I]$, and the load transformation matrix $[\text{LMT}_2]$ by setting

$$\{x_j\} = \{I\} \text{ and } \begin{Bmatrix} \ddot{\eta}_p \\ \ddot{x}_j \end{Bmatrix} = \{0\}.$$

The term $[\text{LMT}]$ is more or less general, because the stresses may be replaced by forces.

For $\{x_j\} = \{0\}$ the external degrees of freedom have been fixed and if

$$\begin{Bmatrix} \ddot{\eta}_p \\ \ddot{x}_j \end{Bmatrix} = \{0\} \text{ no inertia forces are active.}$$

The delivery of a reduced dynamic model is frequently accompanied by the load transformation matrices. During the coupled dynamic loads analysis the stresses and forces may be calculated in selected structural elements.

Example

The undamped equations of motion of the “free-free” 4 mass–spring dynamic system are (shown in Fig. 19.1):

$$m \begin{bmatrix} 1 & 0 & 0 & 0 \\ 0 & 1 & 0 & 0 \\ 0 & 0 & 1 & 0 \\ 0 & 0 & 0 & 1 \end{bmatrix} \begin{Bmatrix} \ddot{x}_1 \\ \ddot{x}_2 \\ \ddot{x}_3 \\ \ddot{x}_4 \end{Bmatrix} + k \begin{bmatrix} 1.5 & -1 & -0.5 & 0 \\ -1 & 3 & -1 & -1 \\ -0.5 & -1 & 2.5 & -1 \\ 0 & -1 & -1 & 2 \end{bmatrix} \begin{Bmatrix} x_1 \\ x_2 \\ x_3 \\ x_4 \end{Bmatrix} = \begin{Bmatrix} 0 \\ 0 \\ 0 \\ F_4 \end{Bmatrix},$$

with:

- $\{x_i\} = \begin{Bmatrix} x_1 \\ x_2 \\ x_3 \end{Bmatrix}$ the internal degrees of freedom
- $x_j = x_4$ the external degrees of freedom
- F_4 the interface force

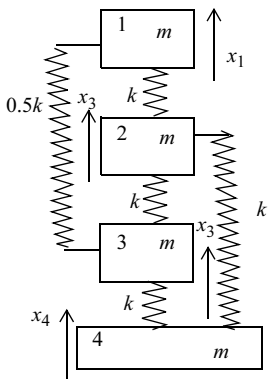


Fig. 19.1. 4 mass–spring dynamic system (free-free)

The partitioned mass matrices become:

$$[M_{ii}] = m \begin{bmatrix} 1 & 0 & 0 \\ 0 & 1 & 0 \\ 0 & 0 & 1 \end{bmatrix}, [M_{jj}] = m \text{ and } [M_{ij}] = [M_{ji}]^T = m \begin{Bmatrix} 0 \\ 0 \\ 0 \end{Bmatrix},$$

and the partitioned stiffness matrices:

$$[K_{ii}] = k \begin{bmatrix} 1.5 & -1 & -0.5 \\ -1 & 3 & 0 \\ -0.5 & 0 & 2.5 \end{bmatrix}, [K_{jj}] = 2k \text{ and } [K_{ij}] = [K_{ji}]^T = k \begin{Bmatrix} 0 \\ -1 \\ -1 \end{Bmatrix}.$$

The following eigenvalue problem for the $\{x_i\}$ degrees of freedom must now be solved. This eigenvalue problem for the internal degrees of freedom is defined as:

$$([K_{ii}] - \lambda[M_{ii}])\{x_i\} = \{0\}.$$

The eigenvalue λ_1 and the associated mode shape $\{\phi_1\}$ are:

$$\lambda_1 = 0.5539 \frac{k}{m}, \text{ and } \{\phi_1\} = \{\phi_p\} = \frac{1}{\sqrt{m}} \begin{Bmatrix} 0.7511 \\ 0.4886 \\ 0.4440 \end{Bmatrix}, \text{ with}$$

$$\{\phi_1\}^T [M] \{\phi_1\} = [I].$$

The force LTM will be based upon the first natural frequency and associated mode shape. Thus the reduced model will only consist of the first mode shape.

The constrained mode $[\phi_{ij}]$ is:

$$[\phi_{ij}] = -[K_{ii}]^{-1} [K_{ij}] = \begin{Bmatrix} 1 \\ 1 \\ 1 \end{Bmatrix}.$$

The forces in the springs can be calculated with:

$$\{\sigma\} = [D_\sigma] \{x\},$$

with a stress matrix $[D_\sigma]$ defined as follows:

$$[D_\sigma] = k \begin{bmatrix} 1 & -1 & 0 & 0 \\ 0 & 1 & -1 & 0 \\ 0 & 0 & 1 & -1 \\ 0.5 & 0 & -0.5 & 0 \\ 0 & 1 & 0 & -1 \end{bmatrix}, [D_{\sigma i}] = k \begin{bmatrix} 1 & -1 & 0 \\ 0 & 1 & -1 \\ 0 & 0 & 1 \\ 0.5 & 0 & -0.5 \\ 0 & 1 & 0 \end{bmatrix} \text{ and } [D_{\sigma j}] = k \begin{Bmatrix} 0 \\ 0 \\ -1 \\ 0 \\ -1 \end{Bmatrix}.$$

The load transformation matrices were defined as:

$$\{\sigma\} = [\text{LTM}_1] \begin{Bmatrix} \ddot{\eta}_p \\ \ddot{x}_j \end{Bmatrix} + [\text{LTM}_2] \{x_j\},$$

and are as follows:

$$[\text{LTM}_1] = [D_{\sigma i}] \left[-[K_{ii}]^{-1} \left\{ \begin{bmatrix} M_{ii} & M_{ij} \\ 0 & I \end{bmatrix} \begin{bmatrix} \phi_p & \phi_{ij} \end{bmatrix} \right\} \right] = k \begin{bmatrix} -0.4739 & -0.6364 \\ -0.0804 & -0.0909 \\ -0.8016 & -1.4545 \\ -0.2772 & -0.3636 \\ -0.8821 & -1.5455 \end{bmatrix},$$

and

$$[\text{LTM}_2] = \begin{bmatrix} D_{\sigma i} & D_{\sigma j} \end{bmatrix} \begin{bmatrix} -K_{ii}^{-1} K_{ij} \\ I \end{bmatrix} = \begin{Bmatrix} 0 \\ 0 \\ 0 \\ 0 \\ 0 \\ 0 \end{Bmatrix}.$$

$[\text{LTM}_2] = \{0\}$ means that the structure has a determinate interface.

End of example

19.3 References

- Bray, E.L., May 1991, *Specification for Dynamic Models of Polar Platform*, British Aerospace Ltd., Earth Observation and Science Division, SPE-1211368-003, Issue 3.
- Chung, Y.T., 1998, *Dynamic Loads Recovery using Alternative Mode Acceleration Approach*, AIAA-98-1719, 39th AIAA/ASME/ASCE/AHS/ASC/ Structures, Structural Dynamics, and Materials Conference and Exhibit and AIAA/ ASME/AHS Adaptive Structures Forum, Long Beach, California, April 20–23, 1998.
- Craig, R.R. Jr. Bampton, M.C.C., July 1968, *Coupling of Substructures for Dynamic Analysis*, AIAA Journal, Vol. 6 No. 7, pages 1313–1319.
- Craig, R.R. Jr., 1981, *Structural Dynamics, An Introduction to Computer Methods*, John Wiley & Sons, ISBN 0-471-04499-7.
- Fransen, S.H.J.A., 2002, *An Overview and Comparison of OTM Formulations on the Basis of the Mode Displacement Method and the Mode Acceleration Method*, paper 17, Proceedings of the Worldwide Aerospace Conference and Technology Showcase 2002, 810 April, 2002, Toulouse.
- Klein, M., Reynolds, J., Ricks, E., 1988, *Derivation of improved load transformation matrices for launchers-spacecraft coupled analysis, and direct computation of margins of safety*, Proc. Int. Conf.: "Spacecraft Structures and Mechanical testing", Noordwijk, The Netherlands, 1921 October 1988, pages 703–719.

19.4 Exercises

19.4.1 Problem 1

The dynamic system is illustrated in Fig. 19.1 with the degrees of freedom $x_1 = x_4 = 0$. A load F is applied in degree of freedom x_2 , however, in the opposite direction. The stress matrix $[D_\sigma]$ is defined as follows:

$$[D_\sigma] = k \begin{bmatrix} -1 & 0 \\ 1 & -1 \\ 0 & 1 \\ 0 & -0,5 \\ 1 & 0 \end{bmatrix}.$$

Calculate $[\text{LTM}_F]$ and $[\text{LTM}_\eta]$.

19.4.2 Problem 2

The dynamic system is illustrated in Fig. 19.1. The degrees of freedom are

$$\{x_j\} = \begin{Bmatrix} x_1 \\ x_4 \end{Bmatrix} \text{ and } \{x_i\} = \begin{Bmatrix} x_2 \\ x_3 \end{Bmatrix}. \text{ The stress matrix } [D_\sigma] \text{ is defined as follows}$$

$$[D_\sigma] = k \begin{bmatrix} 1 & -1 & 0 & 0 \\ 0 & 1 & -1 & 0 \\ 0 & 0 & 1 & -1 \\ 0.5 & 0 & -0.5 & 0 \\ 0 & 1 & 0 & -1 \end{bmatrix}.$$

Calculate $[[\text{LTM}_1]]$ and $[[\text{LTM}_2]]$.

20 Coupled Dynamic Loads Analysis

20.1 Introduction

The launch authority generally carries out a coupled dynamic load analysis (CDLA) also called the coupled load analysis (CLA). The coupled loads analysis is carried out in order to calculate the response behaviour and the dynamic loads occurring in the spacecraft during launch. The design loads that are mentioned in the user manual are obviously very general. The dynamic interaction between the launch vehicle and the spacecraft during launch is calculated with the coupled analysis. The results are also used to avoid the satellite structure from being over-tested during the qualification. The dynamic system of the shaker table and the spacecraft is not the same as the launch vehicle and the spacecraft.

A complete overview for the ESA/ESTEC ARIANE 5 CDLA is given in [Fransen 2006] and ARIANESPACE general specifications for payload dynamic models is given in [Boland 2001]. The modal reduction shall be based on the Craig and Bampton condensation [Craig 1968].

The launch authority (ARIANESPACE, NASA or the European space organization ESA) is in charge of the mathematical model and the dynamic launch loads of the launch vehicle that act on the mathematical model. The primary contractor provides the launch authority with the mathematical model of the spacecraft. The analysis stream diagram is illustrated in Fig. 20.1.

With the aid of Fig. 20.2, [Kabe 1995], it is possible to gain more insight into the size of the complete and reduced dynamic models, as well as the relative effort that is needed to carry out a coupled dynamic loads analysis.

Critical load-producing events during the launch phase [DiMaggio 2001]:

- Lift-off
- Atmospheric flight (gust, buffet, autopilot-induced, etc.)
- Engine ignition and shutdowns
- Staging and separation events

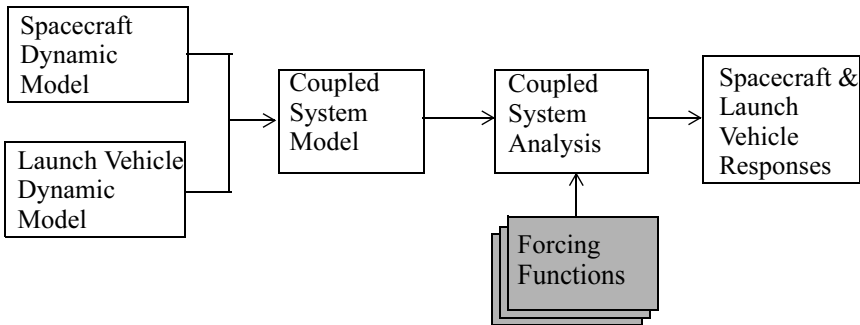


Fig. 20.1 CLA process (courtesy Quartus Engineering, USA)

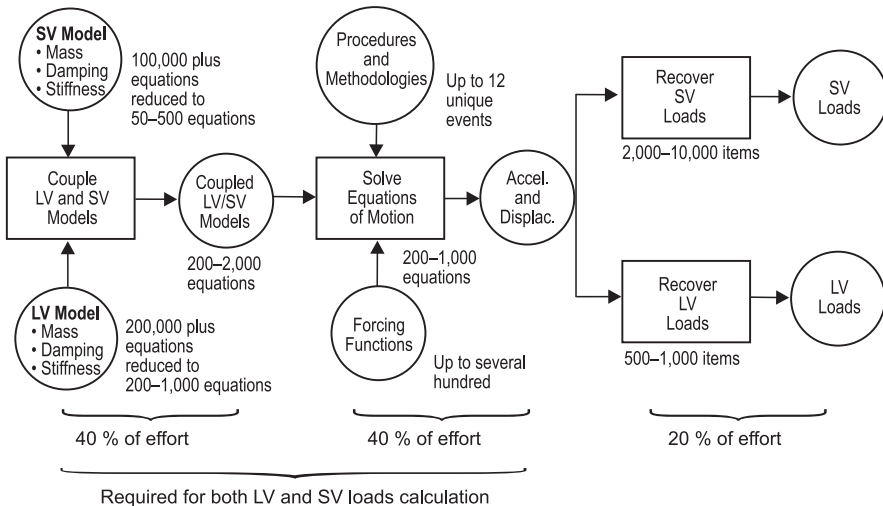


Fig. 20.2 Loads analysis flow (effort breakdown), [Kabe 1998]

The mathematical models of the launch vehicle as well as the spacecraft are converted to a so-called Craig-Bampton (CB) model. This is also done for the loads that act on the launch vehicle. Modal synthesis methods are applied to couple the CB reduced models and afterwards transient analysis are carried out for various phases of the launch. Results of the calculations are:

- Max/min values in time
 - interface (I/F) forces
 - accelerations for the selected degrees of freedom and in the interface
 - displacements for the selected degrees of freedom and in the interface

- Time-history plots
 - I/F forces
 - I/F accelerations
 - I/F displacements
- Max/min equivalent accelerations (load factors) and time histories
- Shock spectra plots of the I/F accelerations and max/min values. The I/F shock spectrum is the sinusoidal input for the spacecraft at the base.

20.2 Finite Element Validation

The finite element model used for the coupled load analysis must be test-verified and must satisfy the correlation requirements with the test results obtained from the modal survey test. The recommended correlation criteria for the analytical prediction and the test results include frequency and mode shape comparison [Chung 2002, NASA 1996, Ricks 1991, Fransen 2006].

- The natural frequency variation is required to be less than $\pm 5\%$
- The cross orthogonality matrix, $[XOR]$, of the analytical mode shapes $[\Phi_a]$ and the test modes $[\Phi_t]$ with respect to the analytical mass matrix $[M_a]$ of the test analysis model (TAM) is determined as follows

$[XOC] = [\Phi_a]^T [M_a] [\Phi_t]$ with $[\Phi_a]^T [M_a] [\Phi_a] = \langle I \rangle$ and the auto-correlation check of the test modes as defined by $[AOC] = [\Phi_t]^T [M_a] [\Phi_t]$ with unity terms on the diagonal and the off-diagonal terms less than 0.1.

A XOR value close to one indicates a high degree of correlation or consistency between two modes. A generally accepted requirement for the cross orthogonality correlation matrix is to have all diagonal terms larger than 0.9 and all the off-diagonal terms less than 0.2, [Ricks 1991].

Example

Two 2-DOFs systems need to be correlated with each other. The first system represents the analytical system and the second one the tested system. The system is illustrated in Fig. 20.3. We will apply the correlation specification as stated in [Ricks 1991].

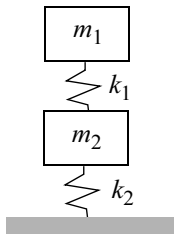


Fig. 20.3 2 DOFs dynamic system.

The characteristics of the dynamic systems are given in Table 20.1.

Table 20.1 Characteristics of dynamic system

Model	m_1 (kg)	m_2 (kg)	k_1 (N/m)	k_2 (N/m)
Analytical	1.0	1.0	10000	10000
Test	1.2	0.95	9500	11000

The intermediate results are given in Table 20.2.

Table 20.2 Intermediate results

Model	Natural frequencies		Mode Shapes $[\Phi]$
	$\{f\}$ (Hz)		
Analytical	$\{f_a\} = \left\{ \begin{array}{l} 9.8363 \\ 25.7518 \end{array} \right\}$		$[\Phi_a] = \begin{bmatrix} -0.8507 & -0.5257 \\ -0.5257 & 0.8507 \end{bmatrix}$
Test	$\{f_t\} = \left\{ \begin{array}{l} 9.5099 \\ 26.6358 \end{array} \right\}$		$[\Phi_t] = \begin{bmatrix} -0.8185 & -0.4891 \\ -0.5263 & 0.8807 \end{bmatrix}$

The auto orthogonality of the test modes with respect to the analytical mass matrix becomes

$$[AOC] = \Phi_a^T [M_a] [\Phi_a] = \begin{bmatrix} 1 & 0 \\ 0 & 1 \end{bmatrix},$$

$$[AOC] = \Phi_t^T [M_a] [\Phi_t] = \begin{bmatrix} 0.9469 & -0.0632 \\ -0.0632 & 1.0149 \end{bmatrix}.$$

The test modes are scaled such that the diagonal terms of $\Phi_t^T [M_a] [\Phi_t]$ become unity. Hence the scaled test mode shape becomes

$$[\Phi_t] = \begin{bmatrix} -0.8411 & -0.4855 \\ -0.5408 & 0.8743 \end{bmatrix},$$

and the $[AOC]$ becomes

$$[AOC] = \Phi_t^T [M_a] [\Phi_t] = \begin{bmatrix} 1.0000 & -0.0645 \\ -0.0645 & 1.0000 \end{bmatrix}.$$

The cross orthogonality matrix is

$$[XOC] = [\Phi_a]^T [M_a] [\Phi_t] = \begin{bmatrix} 0.9998 & -0.0467 \\ -0.0178 & 0.9989 \end{bmatrix}.$$

The differences of the natural frequencies between the analytical and test model is less than 5%, however, for the off-diagonal terms in the $[XOC]$, they are less than 0.2, [Ricks 1991].

End of example

20.3 Literature

- Boland, Ph., Bourgain, M., 2001, *General Specification for payload Dynamic Models*, AE/DI/S/ES No 102/01, A5-SG-0-01, Issue 4, ArianeSpace, France.
- Chung, Y.T., Foist, B.L. and Sernaker, M.L., 2002, *Validation of Payload Acoustic Model based on Acoustic Test Results*, AIAA-2002-1621.
- Craig, R.R., Jr., Bampton, M.C.C., July 1968, *Coupling of Substructures for Dynamic Analysis*, AIAA Journal, Vol. 6, No. 7, pages 1313–1319.
- DiMaggio, S., *Structural Design and Verification of Space and Launch Vehicles*, The Aerospace Corporation, Presentation at Columbia University New York, NY, April 29, 2002, www.civi.columbia.edu/CEE1201/02lect26SD.pdf
- Kabe, A.M., 1998, *Design and Verification of Launch and Space vehicle Structures*, AIAA-98-1718, pages 175–189.
- Fransen, S. H., J., A., 2006, *Methodologies for Launcher-Payload Coupled Dynamic Analysis*, ISBN 90-9020293-5, PhD work Delft University of Technology, European Space Agency.
- NASA, 1996, *Load Analysis of Spacecraft and Payloads*, NASA-STD-5002, June 21.
- Ricks, E.G., 1991, *Guidelines for Loads Analysis and Dynamic Model Verification of Shuttle Cargo Elements*, MSFC-HDBK-1974, October 15.

20.4 Exercises

20.4.1 Internet search

Find on the internet publications about coupled dynamic load analysis?

21 Random Vibrations Simplified Response Analysis

21.1 Introduction

Random mechanical loads are, in general, specified for payloads of spacecraft, electronic boxes, etc. These are specified at the base of the scientific instrument, box, etc. (see for example Table 21.1)

Table 21.1 Random vibrations

Frequency range (Hz)	Power Spectral Density (g ² /Hz)	rms acceleration (g)
20–150	+6dB/octave	
150–700	0.04	7.3
700–2000	–3dB/octave	

The frequency domain lies in the range 20–2000Hz for almost all launch vehicles.

In the high frequency bands the finite element method and boundary element method are unreliable. This depends strongly on the finite element model, boundary element model, that is used to model the spacecraft. In general, the reliable upper limit of the frequency domain for complex finite element models is 200–300Hz. This upper limit is significantly higher when modelling a plate or a beam.

If the response calculations are carried out over the entire frequency domain of the random loads, then the finite element method alone is not sufficient. In the frequency domain, the Statistical Energy Analysis (SEA) method [Lyon 1995] can be applied, complementing the finite element method and boundary element method.

21.2 Low frequency

The general theory of random vibrations will not be covered, see for example [Wirsching 1995]. However, some practical aspects will be discussed:

- The response of a single mass-spring system due to a random force or base excitation.
- The stresses in a plate structure as a result of acoustic loads.
- The number of passages through a certain level.
- Root mean square (rms) responses, accelerations, stresses, etc.

21.2.1 The response of a single mass-spring system due to a random force or base excitation

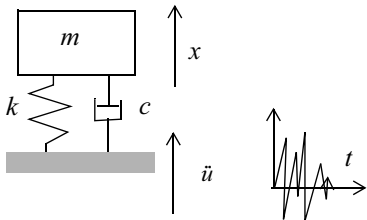


Fig. 21.1 SDOF system with enforced random acceleration

The relative displacement of the SDOF system (Fig. 21.1) with respect to the base is

$$z(t) = x(t) - u(t). \quad (21.1)$$

The rms acceleration of a single spring-mass system with respect to the base (relative) can be calculated with Miles' relation (equation) [Miles 1954]:

$$\ddot{z}_{\text{rms}} = \alpha \sqrt{\frac{\pi}{2} f_o Q W(f_o)}, \quad (21.2)$$

and

$$z_{\text{rms}} = \frac{\ddot{z}_{\text{rms}}}{(2\pi f_o)^2}, \quad (21.3)$$

where \ddot{z}_{rms} and z_{rms} are the rms acceleration and the rms displacement of the mass-spring system with respect to the base, α is a multiple of the standard deviation (1, 2, 3, ...). For fatigue calculations $\alpha=1$ is used, and to determine loads $\alpha=3$ is used. f_o is the natural frequency of the mass-spring system, Q is the amplification factor $Q = \frac{1}{2\zeta}$, $\zeta \leq 0.20$. $W(f_o)$ is the unchanging power spectral density function (white noise approximation) of the force or base excitation at a frequency

f_o . The 3σ acceleration results from the Miles' relation are often called the random vibration load factors (RVLF).

The absolute rms acceleration of the single mass-spring system due to the random base excitation can be calculated with the following formula:

$$\ddot{x}_{\text{rms}} = \sqrt{\frac{\pi}{2} f_o Q (1 + 4\zeta^2) W(f_o)} \approx \ddot{z}_{\text{rms}} (1 + 2\zeta^2) \approx \ddot{z}_{\text{rms}} \quad (21.4)$$

Example

A mass-spring system is excited at the base by a random acceleration a , with a power density function $W_a(f) = 0.1 \frac{g^2}{Hz}$, $f = 5 - 1000 \text{ Hz}$. The rms value of the base excitation is $a_{\text{rms}} = \sqrt{W_a(f) \Delta f} \approx 10 \text{ g}$. The natural frequency of the mass-spring system is $f_o = 30 \text{ Hz}$, and the mass of the mass-spring system is $m = 20 \text{ kg}$. The amplification factor becomes (with $\xi = 5\%$), $Q = \frac{1}{2\zeta} = 10$. The 3σ value of the relative acceleration

$$\ddot{z}_{\text{rms}} = \alpha \sqrt{\frac{\pi}{2} f_o Q W(f_o)} = 3 \sqrt{\frac{\pi}{2} \times 30 \times 10 \times 0.1} = 20.6 \text{ g.}$$

The 3σ value of the inertial force in the spring F_{rms} then becomes:

$$F_{\text{rms}} = m(2\pi f_o)^2 z_{\text{rms}} = m \ddot{z}_{\text{rms}} = 20 \times 20.6 \times 9.81 = 4041 \text{ N.}$$

End of example

Example

A beam without mass and a length L and a bending stiffness EI with a mass point m is excited at the base by a random acceleration $\ddot{u}(t)$, with a power spectral density function (PSD) $W_u(f)$. The response of the mass point is the deflection $z(t)$. The response $z(t)$ is relative to the restrained end.

In order to calculate the \ddot{z}_{rms} with the aid of Miles' formula, the beam is transformed to a mass-spring system with mass m , spring stiffness k and an added dashpot c . This is illustrated in Fig. 21.2.

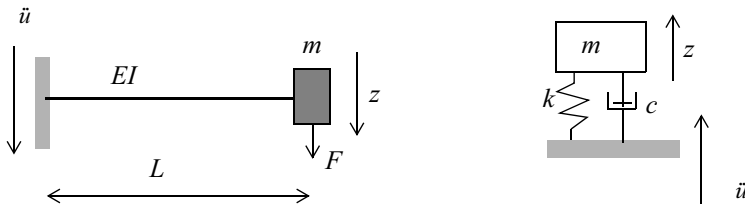


Fig. 21.2 Transformation of system into mass-spring-damper system

The static deflection z_{stat} at the far end of the beam due to a force F is:

$$z_{\text{stat}} = \frac{FL^3}{3EI}.$$

The spring stiffness k now becomes

$$k = \frac{F}{z_{\text{stat}}} = \frac{3EI}{L^3}.$$

It is then easy to determine the natural frequency f_o (Hz) of the system

$$f_o = \frac{1}{2\pi} \sqrt{\frac{k}{m}} = \frac{1}{2\pi} \sqrt{\frac{3EI}{mL^3}}.$$

The equation of motion of the mass-spring system can then be written as follows:

$$m\ddot{z} + c\dot{z} + kz = -m\ddot{u}, \quad z = x - u$$

By dividing the previous expression by m , we obtain the well-known normalized equation of motion of a mass-spring system

$$\ddot{z} + 2\zeta\omega_o\dot{z} + \omega_o^2 z = -\ddot{u},$$

Using $Q = \frac{1}{2\zeta}$, the rms acceleration \ddot{z}_{rms} at the far end of the beam can be calculated, with the aid of Miles' (21.2).

$$\ddot{z}_{\text{rms}} = \alpha \sqrt{\frac{\pi}{2} f_o Q W_{\ddot{u}}(f_o)}$$

$$\text{with } f_o = \frac{1}{2\pi} \sqrt{\frac{3EI}{mL^3}}.$$

When investigating the strength capability of the beam, in general, $\alpha = 3$ is taken.

A transverse force $m\ddot{z}_{\text{rms}}$ and a bending moment $m\ddot{z}_{\text{rms}}L$ are induced at the restrained end of the beam as a result of the rms acceleration \ddot{z}_{rms} of the mass.

End of example

Example

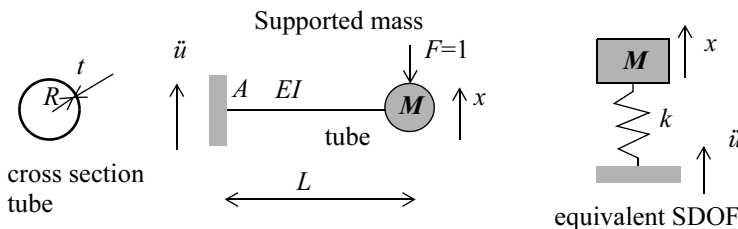


Fig. 21.3 Cantilevered tube

A cantilevered tube (see Fig. 21.3) made of an Al-alloy has a length $L = 0.6$ m, a Young's modulus $E = 70$ GPa. The discrete mass at the end of the tube has a mass $M = 20$ kg. The radius is $R = 0.09$ m and the wall thickness is $t = 0.004$ m. The mass of the tube is neglected. The second moment of area becomes $I = \pi R^3 t = 9.16 \times 10^{-6}$ m⁴.

The first natural frequency can be calculated by

$$f_o = \frac{1}{2\pi} \sqrt{\frac{3EI}{ML^3}} = 106 \text{ Hz.}$$

The stiffness of the spring k of the equivalent dynamic system applying the unit load $F = 1$ N becomes

$$k = \frac{3EI}{L^3} = 8.91 \times 10^6 \text{ N/m}$$

The ultimate stress of the applied material is $\sigma_U = 328$ MPa and the yield stress is $\sigma_Y = 216$ MPa.

The random design limit loads are given in Table 21.2.

Table 21.2 PSD enforced acceleration (design loads)

Frequency (Hz)	PSD (g ² /Hz)	m,n	Area (g ²)
20–100	9 dB/oct	3	$A_1=23.7$
100–250	0.95	N/A	$A_2=142.5$
250–2000	-15dB/oct	-5	$A_3=59.4$
Grms=15.0		$A=225.6$	

The factor of safety against yield loads is $j_Y = 1.1$ and the factor of safety against is $j_U = 1.25$ (ultimate loads).

Check the ability of the system shown in Fig. 21.3 to withstand for a time of 30 s the random enforced accelerations (design limit load) \ddot{u} . The damping ratio is $\zeta = 0.02$ ($Q=25$). The relative displacement between the instrument at the end of the tube and the supporting structure (fixation) must not exceed 4 mm.

The rms acceleration of the instrument using Miles' equation becomes

$$\ddot{x}_{\text{rms}} = \sqrt{\frac{\pi}{2} f_o Q W_{\ddot{u}}(f_o)}.$$

We have a very peaked response at the first natural frequency and no contribution of the responses at other natural frequencies are taken into account.

The power spectral density of the enforced acceleration at 106Hz is extracted from Table 21.2.

The g_{rms} response of the instrument becomes

$$\ddot{x}_{\text{rms}} \approx \sqrt{\frac{\pi}{2} f_o Q W_{\ddot{u}}(f_o)} = \sqrt{\frac{\pi}{2} x 106 x 25 x 0.95} = 62.9 \text{ Grms.}$$

The rms value of the displacement x_{rms} becomes

$$z_{\text{rms}} = \frac{\ddot{x}_{\text{rms}}}{(2\pi f_o)^2} = \frac{62.9 x 9.81}{(2\pi 106)^2} = 1.4 x 10^{-3} \text{ m.}$$

The rms displacement of the instrument is below the requirement of 4 mm.

The 3σ of the acceleration response is $\ddot{x}_{3\sigma} \approx 3 \sqrt{\frac{\pi}{2} f_o Q W_{\ddot{u}}(f_o)} = 188.7 \text{ g.}$

The inertia force at the instrument becomes $F_{3\sigma} = m\ddot{x}_{3\sigma} = 3.7 x 10^4 \text{ N}$ and the bending moment at A is $M_{3\sigma} = m\ddot{x}_{3\sigma}L = 2.22 x 10^4 \text{ Nm.}$

The maximum bending stress at the extreme fibre distance can be calculated by

$$\sigma_{b,3\sigma} = \frac{Me}{I} = \frac{M}{W} = \frac{M}{\pi R^2 t} = 2.18 x 10^8 \text{ Pa.}$$

The maximum shear stress in the cross section for a thin walled tube is [Shanley 1967]

$$\tau_{3\sigma} = \frac{2F_{3\sigma}}{A} = 2 \frac{F_{3\sigma}}{2\pi R t} = 3.27 x 10^7 \text{ Pa.}$$

The von Mises stress becomes

$$\sigma_{vM} = \frac{1}{\sqrt{2}} \sqrt{6\tau_{3\sigma}^2} = 5.67 x 10^7 \text{ Pa.}$$

The shear stress is at another location (neutral plane, bending stress is zero) and lower than the maximum occurring bending stress.

The margins of safety with respect to yield and ultimate loads, respectively, become

$$MS_Y = \frac{\sigma_Y}{j_Y \sigma_{b,3\sigma}} - 1 < 0$$

$$MS_U = \frac{\sigma_U}{j_U \sigma_{b, 3\sigma}} - 1 = 0.2$$

The MS value against the yield load is negative and a redesign of the tube is required to cover the yield load.

The main conclusion is that the random loads cause permanent deformation of the tube. This may be prevented increasing the radius R or the thickness t of the tube. As a consequence the mass of the tube will increase as well.

The fatigue aspects are not investigated.

End of example

21.2.2 Damping

In order to calculate the responses of structures due to random vibrations (acoustic, mechanic), NASA has established the following guidelines for damping of payloads (Table 21.3). The payloads will be launched with STS [Leung 1995].

Table 21.3 Modal damping ratio ζ for STS Payloads

Modal damping ratio ζ for STS Payloads	
Frequency (Hz)	Damping ratio ζ %
< 10	1
10–35	2
35–75	2–3
75–130	3–4
130–200	4–5

21.2.3 Static Assumed Mode Random Vibration Response Analysis

The random vibration structural response analysis may be simplified by using the static responses of structures assuming a static (assumed) mode comparable with a “significant” dynamic mode.

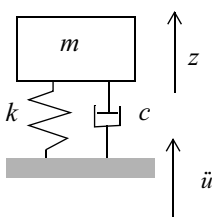


Fig. 21.4 Assumed static mode

The mass-spring system, as shown in Fig. 21.4, is loaded with an inertia field \ddot{u} . In the static analysis no damping influence will be considered. The inertia load applied to the mass m is $m\ddot{u}$. The relative static displacement z becomes

$$z = \frac{m\ddot{u}}{k} = \frac{m\ddot{u}}{m(2\pi f_o)^2} = \frac{\ddot{u}}{(2\pi f_o)^2} \quad (21.5)$$

The term $(2\pi f_o)^2$ may be expressed as follows, assuming $\ddot{u} = 1$

$$(2\pi f_o)_{\ddot{u}=1}^2 = \frac{1}{z}. \quad (21.6)$$

The rms acceleration response can be obtained using Miles' equation

$$\ddot{z}_{\text{rms}} = \alpha \sqrt{\frac{\pi}{2} f_o Q W_{\ddot{u}}(f_o)}.$$

The rms displacement z_{rms} can be derived with

$$z_{\text{rms}} = \frac{\alpha}{(2\pi f_o)^2} \sqrt{\frac{\pi}{2} f_o Q W_{\ddot{u}}(f_o)} = z_{\ddot{u}=1} \alpha \sqrt{\frac{\pi}{2} f_o Q W_{\ddot{u}}(f_o)}. \quad (21.7)$$

The relative static displacement $z_{\ddot{u}=1}$ may be replaced by any response variable due to the inertia load $\ddot{u} = 1$, e.g. loads, stresses, etc.

21.2.4 Passages

The number of expected passages per unit of time, in the positive direction, due to a certain level of the response, for example x with an amplitude $x = x_a$, is calculated by

$$v_a^+ = v_0^+ e^{-\frac{x_a^2}{2\sigma_x^2}}, \quad (21.8)$$

where σ_x^2 is the variance¹ of the response x . The response x can be anything, such as the displacement, the velocity, the acceleration, the force, the stress, etc. (21.9)

The expected frequency v_0^+ (number of characteristic passages with $x = 0$, characteristic frequency, zero-upcrossing rate) is calculated using

$$v_0^+ = \left(\frac{\int_0^\infty f^2 W_x(f) df}{\int_0^\infty W_x(f) df} \right)^{\frac{1}{2}}, \quad (21.10)$$

with $W_x(f)$ the PSD-function of x

If x is a displacement then, when $W_{\dot{x}}(f) = (2\pi f)^2 W_x(f)$:

$$v_0^+ = \left(\frac{\int_0^\infty f^2 W_x(f) df}{\int_0^\infty W_x(f) df} \right)^{\frac{1}{2}} = \frac{1}{2\pi} \frac{\dot{x}_{\text{rms}}}{x_{\text{rms}}} = \frac{1}{2\pi} \frac{\sigma_{\dot{x}}}{\sigma_x}. \quad (21.11)$$

If it is difficult to calculate the integrals numerically, then v_0^+ can quickly and easily be calculated using Miles' formula:

$$v_0^+ = \sqrt{\frac{\sum_{i=1}^n \frac{\pi f_i Q_i W_{\ddot{u}}(f_i)}{f_i^2}}{\sum_{i=1}^n \frac{\pi f_i Q_i W_{\ddot{u}}(f_i)}{f_i^4}}} \quad (21.12)$$

where f_i are the natural frequencies and Q_i is the amplification factor or the value of the transfer function $Q_i = H_{ij}(f_i)$, where the index i (for example) is the acceleration and j (for example) is the induced stress in the structure. When the indices i and j represent the same physical magnitude (such as the acceleration, for example), then one can speak of an amplification factor.

The standard deviation of x , σ_x , can thus be the standard deviation of anything, such as the displacement, the velocity, the acceleration, the force, the stress, etc.

1. The definition of the variance $\sigma_x^2 = E(x^2) - \mu_x^2$, with $\mu_x = \lim_{T \rightarrow \infty} \frac{1}{T} \int_0^T x(t) dt$ being the average of the response x and $E(x^2) = \lim_{T \rightarrow \infty} \frac{1}{T} \int_0^T x^2(t) dt$ the second moment of x . For mechanical vibrations $\mu_x = 0$, so $\sigma_x^2 = E(x^2) = x_{\text{rms}}^2$.

The probability and the number of positive passages for $x_a = n\sigma_x$ is shown in Table 21.4.

Table 21.4 Probability aspects

x_a	$P(x_a \geq n\sigma_x)$ %	$\frac{v_a^+}{v_0^+}$
σ_x	31.73	0.6065
$2\sigma_x$	4.55	0.1353
$3\sigma_x$	0.27	0.0111

The probability that $P(|x_a| \geq n\sigma_x)$ can be determined as follows:

$$P(|x| \geq n\sigma_x) = 1 - P(-n\sigma_x \leq x \leq n\sigma_x) . \quad (21.13)$$

If a normal distribution is concerned then:

$$P(-n\sigma_x \leq x \leq n\sigma_x) = \int_{-n\sigma_x}^{n\sigma_x} \frac{1}{\sigma_x \sqrt{2\pi}} e^{-\frac{x^2}{2\sigma_x^2}} . \quad (21.14)$$

The number of peaks per unit of time (s^{-1}) of x between a and $a + da$ is:

$$dn(a) = v_a^+ - v_{a+da}^+ = \frac{-dv_a^+}{da} da = v_0^+ \frac{a}{\sigma_x^2} e^{-\frac{x_a^2}{2\sigma_x^2}} . \quad (21.15)$$

The expected fatigue life of the structure can be calculated with the help of $dn(a)$.

The number of cycles per unit of time is now known. The total number of cycles can be calculated by multiplying v_o^+ by the duration of the launch or the test.

An approximate value of the average of the highest peaks \bar{x}_{peak} is given by [Lalanne 2002, Vol III]

$$\bar{x}_{peak} \approx \left(\sqrt{2 \ln \{v_0^+ T\}} + \frac{\epsilon}{\sqrt{2 \ln \{v_0^+ T\}}} \right) \sigma_x \quad (21.16)$$

with $\epsilon = 0.5772156649$ as Euler's constant and T is the duration of the random process.

The standard deviation of the peaks x_{peak} can be calculated with [Elishakoff 1991]

$$\frac{\sigma_{x_{\text{peak}}}}{\sigma_x} = \frac{\pi}{\sqrt{6}} \frac{1}{\sqrt{2 \ln v_0^+ T}}. \quad (21.17)$$

21.2.5 Calculation of the rms stresses / forces

It is important that the induced stresses σ due to the random loads / base excitations are determined directly from the PSD-values of the stresses $W_\sigma(f)$, thus with the aid of:

$$\sigma_{\text{rms}} = \sqrt{\int_0^\infty W_\sigma(f) df} \quad (21.18)$$

and not with the help of the rms-values of the inertial forces ($Mx a_{\text{rms}}$), where:

$$a_{\text{rms}} = \sqrt{\int_0^\infty W_a(f) df} \quad (21.19)$$

The aforementioned method produces internal stresses in the structure that are too high, and results in a structural design that is too heavy.

Example

A 3 mass-spring dynamic system, as shown in Fig. 21.5, is excited at the base with a constant band-limited random acceleration $W_{\ddot{u}}(f) = 0.01 \text{ g}^2/\text{Hz}$ in a frequency range $5 \leq f \leq 500 \text{ Hz}$. In [Chung 2001] is stated that integration of a cutoff frequency of 300 Hz is sufficient to obtain the rms values of the stresses and acceleration. The mass distribution is $m_1 = 200 \text{ kg}$, $m_2 = 150 \text{ kg}$ and $m_3 = 100 \text{ kg}$. The stiffness distribution is $k_1 = 3 \times 10^8 \text{ N/m}$, $k_2 = 2 \times 10^8 \text{ N/m}$ and $k_3 = 1 \times 10^8 \text{ N/m}$. The modal damping ratio for all modes is $\zeta = 0.05$ or $Q = 10$.

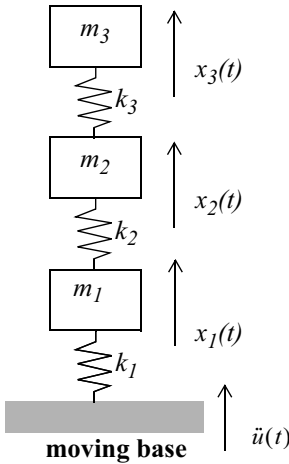


Fig. 21.5 3 mass-spring system with enforced acceleration at the base

The undamped equations of motion are

$$\begin{bmatrix} m_1 & 0 & 0 \\ 0 & m_2 & 0 \\ 0 & 0 & m_3 \end{bmatrix} \begin{Bmatrix} \ddot{x}_1 \\ \ddot{x}_2 \\ \ddot{x}_3 \end{Bmatrix} + \begin{bmatrix} k_1 + k_2 & -k_2 & 0 \\ -k_2 & k_2 + k_3 & -k_3 \\ 0 & -k_3 & k_3 \end{bmatrix} \begin{Bmatrix} x_1 \\ x_2 \\ x_3 \end{Bmatrix} = \begin{Bmatrix} 0 \\ 0 \\ 0 \end{Bmatrix}, \quad (21.20)$$

or (21.20) expressed in the relative motion \$\{z(t)\}\$ will result in

$$\begin{bmatrix} m_1 & 0 & 0 \\ 0 & m_2 & 0 \\ 0 & 0 & m_3 \end{bmatrix} \begin{Bmatrix} \ddot{z}_1 \\ \ddot{z}_2 \\ \ddot{z}_3 \end{Bmatrix} + \begin{bmatrix} k_1 + k_2 & -k_2 & 0 \\ -k_2 & k_2 + k_3 & -k_3 \\ 0 & -k_3 & k_3 \end{bmatrix} \begin{Bmatrix} z_1 \\ z_2 \\ z_3 \end{Bmatrix} = -\begin{bmatrix} m_1 & 0 & 0 \\ 0 & m_2 & 0 \\ 0 & 0 & m_3 \end{bmatrix} \begin{Bmatrix} 1 \\ 1 \\ 1 \end{Bmatrix} \ddot{u}(t). \quad (21.21)$$

The natural frequencies and associate mode shapes of the MDOF dynamic system are

$$\{f_n\} = \begin{Bmatrix} 94.35 \\ 201.73 \\ 299.53 \end{Bmatrix} \text{ Hz}, [\Phi] = \begin{bmatrix} -0.0224 & 0.0432 & -0.0513 \\ -0.0482 & 0.0386 & 0.0535 \\ -0.0743 & -0.0636 & -0.0210 \end{bmatrix}.$$

The effective masses, for, respectively modes shapes 1, 2 and 3, are

$$\{M_{eff}\} = \begin{Bmatrix} 366.13 \\ 64.97 \\ 18.90 \end{Bmatrix} \text{ kg.}$$

The most important mode shape represents the maximum effective mass. This first mode will show maximum responses. A 3×3 matrix $W_{\ddot{x}\ddot{x}}(f)$ of PSD and cross-PSD functions of the acceleration will be calculated for every frequency. The quadrature of diagonal terms of $W_{\ddot{x}\ddot{x}}(f)$ are the mean-square values of the acceleration. Taking the square root of the mean-square (auto-spectrum) values will result in the root mean square values of the acceleration of the DOFs x_1 , x_2 and x_3 . The plots of the PSD functions of the acceleration \ddot{x}_1 , \ddot{x}_2 and \ddot{x}_3 are shown in Fig. 21.6.

The integration, to obtain the mean-square values, is done with the trapezium rule with a frequency increment $\Delta f = 1$ Hz.

The rms values of the acceleration are

$$\{\ddot{x}\}_{rms} = \begin{Bmatrix} \ddot{x}_1 \\ \ddot{x}_2 \\ \ddot{x}_3 \end{Bmatrix} = \begin{Bmatrix} 30.27 \\ 41.72 \\ 60.52 \end{Bmatrix} \frac{m}{s^2}.$$

The force matrix of the dynamic system, shown in Fig. 21.5, is defined as

$$[D_\sigma] = \begin{bmatrix} k_1 & 0 & 0 \\ -k_2 & k_2 & 0 \\ 0 & -k_3 & k_3 \end{bmatrix} \text{ N.}$$

The diagonal terms of the PSD function matrix $W_{\sigma\sigma}(f)$ are plotted in Fig. 21.7.

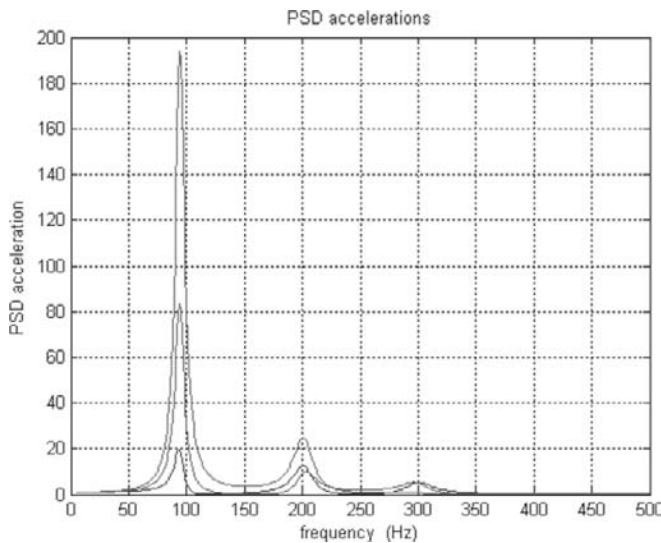


Fig. 21.6 PSD values of the acceleration \ddot{x}_1 , \ddot{x}_2 and x_3 (m/s^2) $^2/\text{Hz}$

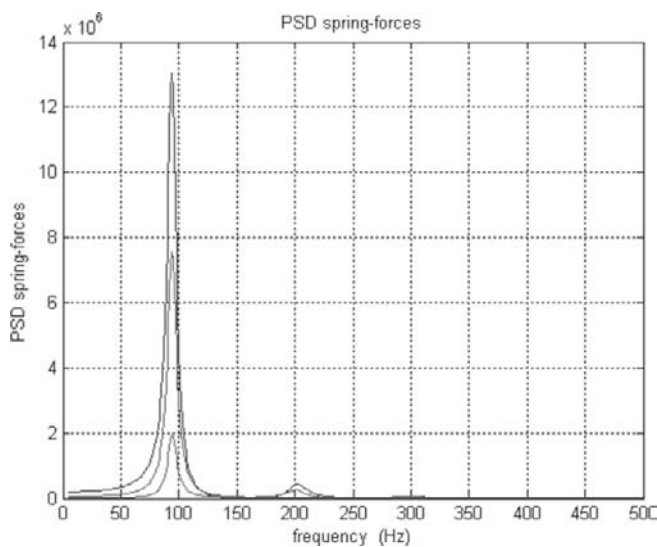


Fig. 21.7 PSD values of the spring forces F_1 , F_2 and F_3 (N^2/Hz)

The square root of the diagonal terms of the auto-spectrum functions of the spring forces is $\sqrt{\langle R_{\sigma\sigma}(0) \rangle} = \langle F_{\text{rms}} \rangle = \sqrt{\int_0^{500} \langle W_{\sigma\sigma}(f) \rangle df} = \begin{bmatrix} 14379 & 0 & 0 \\ 0 & 10706 & 0 \\ 0 & 0 & 6043 \end{bmatrix} \text{ N.}$

The positive zero-crossings of the spring forces are

$$\{v_0^+\} \Rightarrow \begin{Bmatrix} F_1 \\ F_2 \\ F_3 \end{Bmatrix} = \begin{Bmatrix} 105.7 \\ 105.0 \\ 127.8 \end{Bmatrix} \text{ Hz.}$$

The rms values of the forces in the springs are compared with the quasi-static forces in the spring in Table 21.5.

Table 21.5 Comparison of quasi-static spring forces with rms spring forces

Node #	Mass (kg)	$\ddot{x}_{i,\text{rms}}$ (m/s ²)	Quasi-static load (N)	Spring #	Quasi-static $F_{i,\text{rms}}$ (N)	Dynamic $F_{i,\text{rms}}$ (N)
1	200	30.27	6054	1	18364	14379
2	150	41.72	6258	2	12310	10706
3	100	60.52	6052	3	6052	6043

It turns out that the calculation of the stresses / forces using inertial forces is conservative with respect to the method where stresses/forces are calculated directly.

End of example

21.2.6 Reaction Forces

Chung proposed in [Chung 2001] the “mass participation approach” to obtain the root sum squared (RSS) reaction force at the base. This method requires the effective masses per mode. The RSS reaction force can be calculated by

$$F_{\text{RSS}} = \sqrt{\sum_{i=1}^n \left(M_{\text{eff},i} \sqrt{\frac{\pi}{2} f_i Q_i W_a(f_i)} \right)^2 + M_{\text{residual}}^2 \int_0^{f_{\max}} W_a(f) df}, \quad (21.22)$$

where the residual mass is given by $M_{\text{residual}} = M_{\text{total}} - \sum_{i=1}^n M_{\text{eff},i}$, n is the

number of modes involved, $M_{\text{eff},i}$ the modal effective mass associated with mode i , $W_a(f)$ is the power spectral density function of the enforced acceleration, f_i is the natural frequency and Q_i is the amplification factor both belonging to mode i .

Example

We take the analysis results of the previous example as shown in Fig. 21.5. The reaction force at the base will be calculated with (21.22). The results are shown in Table 21.6.

Table 21.6 RSS reaction forces, all modes included

Natural frequency (Hz)	Effective mass (kg)	Amplification factor	Enforced acceleration (g ² /Hz)	Force per mode (N)
94.35	366.13	10	0.01	13827
201.73	64.97	10	0.01	3588
299.53	18.9	10	0.01	1272
M_{residual}	0.0		F_{RSS}	14342 (14379)

The reaction force correlates very well with the force power spectral density function results integrated over 5–500Hz (number between brackets). The calculation may be repeated for example using the first mode.

21.3 Acoustic Analysis

The frequency spectrum of the acoustic loads for almost all launch vehicles is 20 – 10000Hz, given in the octave band.

Calculations using finite element methods have limitations with respect to the highest reliable frequency.

If the response calculations are carried out over the entire frequency domain of the acoustic loads, then the finite element method alone is not sufficient. In the frequency domain, complementing the finite element method, the Statistical Energy Analysis (SEA) method can or must be applied. The same holds for the responses as for the mechanical random vibrations.

21.3.2 Acoustic loads transformed into mechanical random vibrations

Large (sandwich) panels, with all kinds of instruments, electronic boxes, etc. mounted onto them, are fairly sensitive to acoustic loads. The acoustic loads are transformed into mechanical random vibrations by the panel. These mechanical random vibrations vibrate in tune with the mounted instruments, electronic boxes, etc. In this section we determine the applied mechanical vibrations due to the acoustic loads.

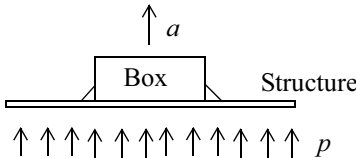
The sound pressure level (*SPL*) is expressed with respect to a reference pressure $p_{\text{ref}} = 2 \times 10^{-5}$ Pa, that is:

$$SPL = 10 \log \left(\frac{p}{p_{\text{ref}}} \right)^2 \text{ (dB).}$$

The *SPL* is usually given in the one octave- or one-third octave band. A certain centre frequency f_{centre} (Hz) is associated with a bandwidth Δf (Hz) (see Table 21.7).

Table 21.7 Bandwidth

x st -Octave band	Bandwidth (Hz)
x=1	$\Delta f = 0.7071 f_{\text{centre}}$
x=1/3	$\Delta f = 0.2316 f_{\text{centre}}$



$$\text{Acoustic Loading } F = pA\beta$$

Fig. 21.8 Model for the evaluation of the effects of acoustic pressure [Spann 1984]

The power spectral density $W_p(f)$, where p is the effective (rms) sound pressure for a specific centre frequency, and relative bandwidth Δf , is calculated as follows:

$$W_p(f) = \frac{p^2}{\Delta f} \text{ (Pa}^2/\text{Hz).} \quad (21.23)$$

The power spectral density of the acceleration of the box, due to the acoustic pressure (Fig. 21.8), is determined as follows [Spann 1984, Schaefer 1996, Lalanne 2002]:

$$W_a(f) = (\beta Q)^2 \left(\frac{A}{gM} \right)^2 W_p(f) \text{ (g}^2/\text{Hz)} \quad (21.24)$$

where $W_a(f)$ is the power spectral density of the acceleration of the box and the support structure, β is the effectiveness vibroacoustic factor [Lalanne 2002], Q is the amplification factor, A is the surface area of the panel exposed to the acoustic pressure (m^2), M is the total mass of the box and support structure (kg), and g is the gravitational acceleration (9.81 m/s^2). (21.24) is evaluated in Table 21.8.

Table 21.8 Conversion of acoustic pressure into mechanical accelerations

Reference	β	Q	(21.24) (g)
[Schaefer 1996] Sandwich panels	2.5	4.5	$W_a(f) = 126.6 \left(\frac{A}{gM} \right)^2 W_p(f)$
[Schaefer 1996] Sandwich panels, 95% probability level	2.5	5.0	$W_a(f) = 156.3 \left(\frac{A}{gM} \right)^2 W_p(f)$
[Spann 1984 ^a , Lallane 2002]	2.5	4.5	$W_a(f) = 126.6 \left(\frac{A}{gM} \right)^2 W_p(f)$

a. Based on 1/3 octave band

The wave length λ of an acoustic field is given by [Pain 1983]

$$\lambda = \frac{2\pi}{k}, \quad (21.25)$$

where k is the wave number and is given by

$$k = \frac{2\pi f}{c}, \quad (21.26)$$

with c the speed of sound in air, $c \approx 340 \text{ m/s}$. To apply the equations in Table 21.8 the wave length λ must be greater than a typical length of the plate structure. The wavelength λ is given in Table 21.9.

Table 21.9 Calculation of wave length

Frequency (Hz)	Wave number ($c=340$ m/s)	Wave length (m)
31.5	0.58	10.79
63	1.16	5.44
125	2.31	2.72
250	4.62	1.36
500	9.24	0.68
1000	18.48	0.34

21.3.3 Component Vibration Requirements

Spann proposed in [Spann 1984] two methods to establish component vibration requirements based on (21.24). The first and more conservative method, a complete enveloping procedure, the second partially enveloping method is less low frequency conservative. The two procedures will be described below.

Complete enveloping procedure (Fig. 21.9)

1. identify the peak frequency f_{peak} at which the power spectral density value $W_a(f)$ is maximum, PSD_1 .
2. draw a flat spectrum at the f_{peak} g²/Hz level between $0.5f_{\text{peak}}$ and $4.0f_{\text{peak}}$.
3. above $4.0f_{\text{peak}}$ vary the spectrum at minus 6 dB/Oct to a level (PSD_2) given by the following relationship.

$$PSD_2 = PSD_1 - 0.4 \left(6900 \frac{A}{gM} - 5 \right) \text{ dB} \quad (21.27)$$

or

$$10 \log \frac{PSD_2}{PSD_1} = -0.4 \left(6900 \frac{A}{gM} - 5 \right) \quad (21.28)$$

The factor 6900 is needed for the conversion from square inches and pounds to square meters and newtons $\frac{0.454 \times 9.81}{0.0254^2} = 6900$.

4. maintain this level (PSD_2) to 2000Hz.

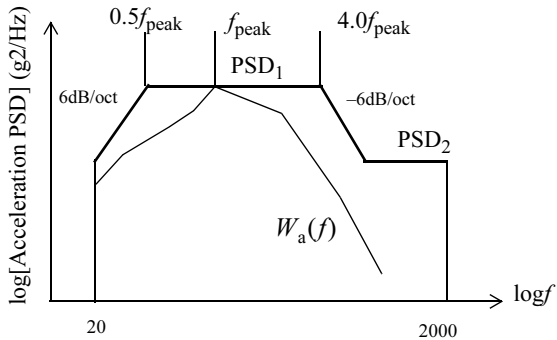


Fig. 21.9 Complete enveloping component acceleration requirement

Partially enveloping procedure (Fig. 21.10)

The partially enveloping procedure is an alternative to the complete enveloping

1. identify the peak frequency f_{peak} at which the power spectral density value of $W_a(f)$ is maximum, PSD_1 .
2. draw a flat spectrum at the f_{peak} g²/Hz level between f_{peak} and $4.0f_{\text{peak}}$.
3. below f_{peak} roll down the spectrum at 6 dB/Oct.
4. above $4.0f_{\text{peak}}$ vary the spectrum at minus 6 dB/Oct to a level (PSD_2) given by the following relationship.

$$PSD_2 = PSD_1 - 0.4 \left(6900 \frac{A}{gM} - 5 \right) \text{ dB},$$

or

$$10 \log \frac{PSD_2}{PSD_1} = -0.4 \left(6900 \frac{A}{gM} - 5 \right).$$

maintain this level (PSD_2) to 2000 Hz.

The frequency associated with PSD_2 can be calculated by

$$\frac{f_{PSD_2}}{4.0f_{\text{peak}}} = \left(\frac{PSD_1}{PSD_2} \right)^2. \quad (21.29)$$

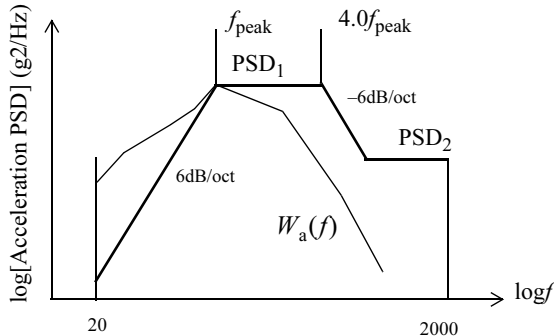


Fig. 21.10 Partially enveloping component acceleration requirement

The vibration prediction has been shown to be reasonably conservative for the derivation of component vibration criteria, [Spann 1984]. The method is primarily useful during the early design phase as a procedure to derive component test requirements.

21.3.4 Static approach

We consider a SDOF system with an area A placed in an acoustic chamber and we calculate the random response characteristics of the SDOF system. The SDOF system is illustrated in Fig. 21.11.

When the vibration is associated with the natural frequency f_o and mass m the rms acceleration of the panel due to a uniform pressure load $W_p(f)$ can be calculated using Miles' equation [Richard 1998]

$$\ddot{x}_{\text{rms}} = \frac{A}{mg} \sqrt{\frac{\pi}{2} f_o Q W_p(f_o)} (\text{g}), \quad (21.30)$$

where the amplification factor is, in general, $Q = 10$.

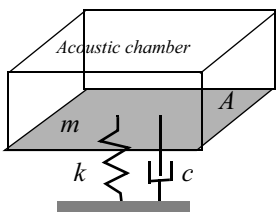


Fig. 21.11 SDOF system in a acoustic chamber [Richard 1998]

The calculated \ddot{x}_{rms} can be induced on the panel as a static acceleration field (inertia force).

21.3.5 The stress in an acoustically loaded panel

Based on [NASA 1986] guidelines, the following steps are to be followed for establishing acoustic loads of the planar components:

1. Estimate the panel fundamental natural frequency f_o .
 2. Convert the sound pressure levels to sound pressure power spectral density (21.23)
 3. Based on a realistic damping ratio ζ , determine the amplification factor Q for the panel.
 4. Use Miles equation to determine the rms equivalent static pressure P_{rms} with
- $$P_{\text{rms}} = \sqrt{\frac{\pi}{2} f_o Q W_p(f_o)}$$
5. The peak equivalent static pressure is given by the 3σ value

$P_{\text{peak}} = 3P_{\text{rms}} = 3\sqrt{\frac{\pi}{2} f_o Q W_p(f_o)}$. This assumes the panel fundamental mode is the same as the deflection for a uniform pressure and the spatial correlation of the acoustic pressure field over the panel is uniform.

Example

The maximum stress at the centre of a circular simply supported plate with a radius R , a thickness t and a uniform pressure p and a Poisson's ratio ν is given by [Timoshenko 1959, Prescott 1961]

$$\sigma_{\text{max}} = \frac{3(3 + \nu)pR^2}{8t^2}. \quad (21.31)$$

We assume a fundamental frequency $f_o = 100$ Hz, a one-octave sound pressure level at 125Hz, $SPL(125) = 135$ dB and an amplification factor $Q = 10$. The lower band frequency $f_{\text{min}} = \frac{1}{2}f_{\text{centre}}\sqrt{2} = 125 \times 0.7071 = 88.38$ Hz,

$$f_{\text{max}} = \frac{f_{\text{centre}}}{\frac{1}{2}\sqrt{2}} = \frac{125}{0.7071} = 176.8 \text{ and the bandwidth}$$

$\Delta f = \frac{1}{2}f_{\text{centre}}\sqrt{2} = \frac{1}{2}x125\sqrt{2} = 88.38 \text{ Hz}$. The fundamental frequency of 100Hz match with the one-octave band with $f_{\text{centre}} = 125$. The rms pressure in the an octave band, with the centre frequency $f_{\text{centre}} = 125 \text{ Hz}$,

$$p_{\text{rms}}^2 = p_{\text{ref}}^2 10^{\frac{SPL}{10}} = 4x10^{-10} 10^{\frac{135}{10}} = 1.265x10^4 \text{ Pa}^2. \text{ The power spectral density}$$

$$\text{function } W_p(125) = \frac{p_{\text{rms}}^2}{\Delta f} = \frac{1.265x10^4}{88.388} = 143.1 \text{ Pa}^2/\text{Hz}. \text{ The peak pressure can}$$

be calculated $P_{\text{peak}} = 3\sqrt{\frac{\pi}{2}f_o W_p(f_o)} = 3\sqrt{\frac{\pi}{2}x100x10x143} = 1422 \text{ Pa}$. The panel has radius $R = 0.5 \text{ m}$ and a thickness $t = 0.002 \text{ m}$. The Poisson's ratio $\nu = 0.33$. The maximum peak stress in the circular plate becomes

$$\sigma_{\max} = \frac{3(3+\nu)P_{\text{peak}}R^2}{8t^2} = \frac{3(3+0.33)x1422x0.5^2}{8x0.002^2} = 1.110x10^8 \text{ Pa}.$$

End of example

Blevins in [Blevins 1989, Blevins 1990, chapter 7] discussed a method to calculate rms stresses in plates exposed to random pressures.

The modal pressure (inertia load) \bar{p} is defined as follows:

$$\bar{p} = (2\pi f_o)^2 m |\delta| \quad (21.32)$$

where $m (\text{kg/m}^2)$ is the mass per unit area of the plate, $f_o (\text{Hz})$ is the fundamental natural frequency of the plate and δ is the maximum modal displacement of $\phi(x, y)$ which is the mode shape or vibration mode. The rms stress $\sigma_{\text{rms}}(x, y)$ at a certain point in the plate can be determined with the following equation:

$$\frac{\sigma_{\text{rms}}(x, y)}{\sigma_{\bar{p}}(x, y)} = \frac{1}{\bar{p}} \sqrt{\frac{\pi}{2} f_o Q W_p(f)} \quad (21.33)$$

with Q is the amplification factor, $W_p(f)$ is the power spectral density of the pressure and $\sigma_{\bar{p}}(x, y)$ is the stress at location (x, y) corresponding with the modal pressure \bar{p} .

Example

Again the simply supported panel with $R = 0.5 \text{ m}$ and the thickness $t = 0.002 \text{ m}$. The fundamental frequency is $f_o = 100 \text{ Hz}$. The power spectral density of the

sound pressure is $W_p(125) = 143 \text{ Pa}^2/\text{Hz}$. The assumed mode is

$$\phi(r) = \frac{(R^2 - r^2)^2}{64D} \left(\frac{5 + \nu}{1 + \nu} R^2 - r^2 \right), \quad [\text{Timoshenko 1959}].$$

The maximum modal dis-

placement at $r = 0$ is $\delta = \frac{(5 + \nu)R^4}{64(1 + \nu)D}$, and $D = \frac{Et^3}{12(1 - \nu^2)}$. The panel is made

of an Al-alloy with a density $\rho = 2800 \text{ kg/m}^3$ and a Young's modulus $E = 70 \times 10^9 \text{ Pa}$. The maximum displacement $\delta = \frac{(5 + \nu)R^4}{64(1 + \nu)D} = 7.473 \times 10^{-5}$.

The modal pressure now becomes $\bar{p} = (2\pi f_o)^2 m \delta = 165.2$. The associated stress

at the centre of the panel is $\sigma_{\max}(r=0) = \frac{3(3 + \nu)\bar{p}R^2}{8t^2} = 1.287 \times 10^7 \text{ Pa}$.

$\sigma_{\text{rms}}(r=0) = \frac{\sigma_{\bar{p}}(r=0)}{\bar{p}} \sqrt{\frac{\pi}{2} f_o Q W_p(f)} = 3.7 \times 10^7 \text{ Pa}$. The 3σ of the stress becomes $\sigma_{3\sigma}(r=0) = 3\sigma_{\text{rms}}(r=0) = 1.11 \times 10^8 \text{ Pa}$.

End of example

Example rectangular panel

A plate has the following characteristics, a is the width of the plate, b is the length of the plate, assuming $\frac{a}{b} \leq 1$, E is the modulus of elasticity (Young's modulus), I is the second moment of area against bending (m^4), W is the section factor against bending (m^3) and m is the mass per unit area (kg/m^2). The bending stiffness and the section factor of the plate are respectively $D = \frac{Et^3}{12(1 - \nu^2)}$ and

$$W = \frac{t^2}{6(1 - \nu^2)}.$$

Table 21.10 Blevins' method

Characteristic	Simply supported rectangular plate (e.g. printed circuit board)
Fundamental natural frequency f_o (Hz)	$\frac{\pi}{2} \left(\frac{1}{a^2} + \frac{1}{b^2} \right) \sqrt{\frac{D}{m}}$
Mode shape $\phi(x, y)$	$\sin\left(\frac{\pi x}{a}\right) \sin\left(\frac{\pi y}{b}\right)$
Maximum modal displacement $\delta\left(\frac{a}{2}, \frac{b}{2}\right)$ (m)	1.0
Modal pressure \bar{p}	$\pi^4 \left(\frac{1}{a^2} + \frac{1}{b^2} \right)^2 D$
Maximum modal stress $\sigma_{\bar{p}}\left(\frac{a}{2}, \frac{b}{2}\right)$ (Pa), $b > a$	$\frac{\beta \bar{p} a^2}{W} \quad b \geq a$ [Timoshenko 1959]
Miles stress $\sigma_{\text{rms}}\left(\frac{a}{2}, \frac{b}{2}\right)$ (Pa)	$\frac{\sigma_{\bar{p}}\left(\frac{a}{2}, \frac{b}{2}\right)}{\bar{p}} \sqrt{\frac{\pi f_o Q W_p(f)}{2}}$

End of example

21.4 Literature

- Blevins, R.D., 1989, *An Approximate Method for Sonic Fatigue Analysis of Plates and Shells*, Journal of Sound and Vibration 129(1), pages 51–71.
- Blevins, R.D., 1990, *Flow-Induced Vibration*, Second Edition, Van Nostran Reinhold, 1990.
- Crandall, S.H. and Mark, W.D., 1973, *Random Vibration in Mechanical Systems*, Academic Press.
- Chung, Y.T., et al, 2001, *Estimation of Payload Random Vibration Loads for proper Structure Design*, AIAA-2001-1667.
- Elishakoff, I., Lin, Y.K., 1991, *Stochastic Structural Dynamics 2*, pages 17–31, ISBN 0-387-54168-3, Springer-Verlag, Heidelberg.
- E. Kreyszig, 1993, *Advanced Engineering Mathematics*, 7th press, John Wiley & Sons.
- Lalanne, C., 2002, *Mechanical Vibration & Shock Volume III, Random Vibrations*, ISBN 1 9039 9605 8, Hermes Penton Ltd.
- K. Leung & B.L. Foist, 1995, *Prediction of Acoustically Induced Random Vibration Loads for Shuttle Payloads*, AIAA paper AIAA-95-1200-CP, pages 362–367.
- Lyon, R.H., DeJong, R.G., 1995, *Theory and Application of Statistical Energy Analysis*, 2nd edition, ISBN 0-7506-9111-5, Butterworths and Heineman..
- Miles, J.W., 1954, *On Structural Fatigue under Random Loading*, Journal of the Aeronautical Sciences, November 1954, pages 753–762.
- NASA, 1986, *Design and Verification Guidelines for Vibroacoustic and Transient Environments*, NASA TM-86538, MSFC.
- Pain, H.J., 1983, *The Physics of Vibrations and Waves*, third edition, John Wiley, ISBN0471901822.
- Richard, C., 1998, *The Concept of Effective Surfaces and its Application for a Quick Evaluation of Fluid Structure Coupling*, Proceedings European Conference on Spacecraft Structures, Materials and Mechanical Testing, Braunschweig, Germany, 4–6 November, 1998, ESA SP-428.
- Scheafer, E.D., 1996, *Evaluating the Vibroacoustic Response of Honeycomb Panels*, 19th Space Simulation Conference Cost Effective Testing for the 21st Century, Oct. 29–31, pages 149–158.
- Shanley, F.R., 1967, *Mechanics of Materials*, Mc-Graw-Hill.
- Spann, F., Patt, P., 1984, *Component Vibration Environment Predictor*, The Journal of Environment Sciences, September/October pages 19–24.
- Timoshenko, S., 1959, *Theory of Plates and Shells*, McGraw-Hill.
- Steinberg, D.S., 1988, *Vibration Analysis for Electronic Equipment*, second edition, John Wiley & Sons, ISBN 0-471-37685-X.
- Wirsching, P.H., et al, 1995, *Random Vibrations, Theory and Practice*, John Wiley, ISBN 0-471-58579-3

21.5 Exercises

21.5.1 Calculation of PSD Function

In Table 21.11 not all cells in the rows and columns are calculated. The objective of this exercise is to replace the question marks with the relevant numbers.

Table 21.11 Acoustic load specification

Octave band (Hz)	Qualification loads, SPL (dB), $p_{\text{ref}} = 2 \times 10^{-5}$ Pa	p_{rms}^2 (Pa ²)	PSD $W_p(f)$ (Pa ² /Hz)
31.5	124	?	?
63	128	?	?
125	129	?	?
250	127	?	?
500	127	?	?
1000	121	?	?
2000	114	?	?
OASPL	?		

21.5.2 Peak Pressure Values

With reference to Table 21.11 calculate the 3σ peak values of the pressures using the equation $P_{\text{peak}} = 3 \sqrt{\frac{\pi}{2} f_c W_p(f_c)}$, where f_c is the centre frequency and the amplification factor $Q = 10$. Generate a graph with the format shown in Fig. 21.12.

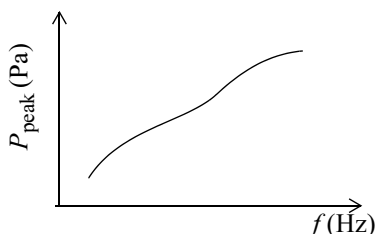


Fig. 21.12 3σ peak values of the pressure

21.5.3 Simply Supported Plate [Blevins 1989]

Consider a simply supported plate made of an Al-alloy with the following properties; the Young's modulus $E = 70 \times 10^9$ Pa, the Poisson's ratio $\nu = 0.33$, the density of the material $\rho = 2700$ kg/m³, the thickness of the plate $t = 1.25$ mm, the length of the plate is $b = 1$ m, the width $a = 0.5$ m. The plate is exposed to a random pressure field, uniform over the surface, with an overall sound pressure $OASPL=150$ dB. The random pressure field has a constant power spectral density over the frequency range from 20–1020Hz. The modal damping ratio $\zeta = 0.015$. The maximum bending stress at the centre of the plate, exposed to a uniform pressure p , is given by $\sigma_b = \frac{0.1017pa^2}{t^2} \frac{1}{6}$ [Timoshenko 1959].

- Calculate the PSD W_p of the pressure field.
- What is the first (fundamental) natural frequency f_o (Hz) associated with mode

$$\phi(x, y) = \sin \frac{\pi x}{a} \sin \frac{\pi y}{b}$$

- What is the maximum modal deflection δ at the centre of the plate?
- Calculate the modal pressure \bar{p} .
- What is the maximum stress at the centre of the plate exposed to the modal pressure \bar{p} ?
- Calculate the peak pressure of the random pressure field $p_{peak} = \sqrt{\frac{\pi}{2}} f_o Q W_p$.
- What is the maximum rms stress at the centre of the plate applying the Blevins approximation method?

Answers: 400 Pa²/Hz, $f_o = 60.5$ Hz, $\delta = 1$, $\bar{p} = 1.951 \times 10^6$ Pa,

1.191×10^{10} Pa, $p_{peak} = 616.6$ Pa, 3.76×10^6 Pa

21.5.4 Waves

A Sea-launch platform is exposed to a storm with waves of standard deviation, $\sigma = 2.5$ m and an average wave period $\bar{T}_0 = 10$ s. Design a platform height h , so that the deck is flooded only once per $\bar{T}_h = 15$ minutes. The diffraction of the waves a neglected, thus the incoming waves are not effected by the presence of the platform.

- Calculate the number of positive zero crossing v_0^+ .
- Calculate the number of positive crossing at h , v_h^+ .
- Calculate h .

Answers: $v_0^+ = \frac{1}{10}$ Hz, $v_h^+ = \frac{1}{900}$ Hz, $h = 7.50$ m.

22 Fatigue Life Prediction

22.1 Introduction

Vibration loads will cause oscillating stresses and forces internally in the spacecraft structure. Oscillating stresses can lead to fatigue problems. Mathematical models are available, such as the linear cumulative damage rule of Palmgren-Miner (published by Palmgren in 1924 and by M.A. Miner in 1945 [Juvinall 1967]) in combination with the fatigue (s-N) curve of a design material, to predict the so-called fatigue life of a structural part under a oscillating environment [Bishop 2000]. The linear cumulative damage rule assumes that the total life of a structural part can be predicted by merely adding up the percentage of life consumed by each stress cycle.

In this chapter the linear cumulative damage rule based on the stress-life approach is discussed. s-N fatigue analyses recapitulated are based on:

- Time domain stress-life fatigue life estimation
- Frequency domain model
- Random vibration narrow band solution

22.2 Palmgren-Miner Linear Cumulative Damage Rule

There are of course numerous failure modes. One of them is failure of the structure due to material fatigue. So the question remains as to what is fatigue actually? Fatigue is an occurrence where structures crack or even break (prematurely) due to alternating loads. Alternating micro plastic deformations that damage the material structure locally causes fatigue. As the alternating loads continue to increase, the deformations can accumulate to become micro cracks or fractures. The Palmgren-Miner rule (life-fraction rule) is applied to predict the lifetime of a structure or a structural part that is affected by linear cumulative damage. At a certain stress level s_i , making use of the so-called s-N (Wöhler or fatigue) curve, one can predict the

permissible number of cycles N_i . Additionally, one can calculate the number of real “cycles” that take place for a certain stress s_i during launch or the test. According to the cumulative damage model, the following must hold during the lifetime of a spacecraft structure (to prevent the structure from failing due to fatigue):

$$D = \sum_i \frac{n_i}{N_i} \quad (22.1)$$

where D is the cumulative damage at i load cases with n_i oscillations or cycles at the stress level s_i and N_i the allowable number of oscillations at the stress level s_i . Miner's rule states that $D = 1$ at fatigue failure. Miner cites numerous tests with factors at $0.7 \leq \sum_i \frac{n_i}{N_i} \leq 1.2$ [Juvinall 1967].

The total number of cycles which cause fatigue failure is N_T and is defined by

$$N_T = \sum_i n_i. \quad (22.2)$$

Equation (22.1) can be rewritten with $D = 1$ as follows, [Richards 1968]

$$N_T \sum_i \frac{n_i}{N_T N_i} = 1. \quad (22.3)$$

But the probability of occurrence of stress s_i is defined by

$$p_i = \frac{n_i}{N_T}. \quad (22.4)$$

Hence

$$N_T \sum_i \frac{p_i}{N_i} = 1 \quad (22.5)$$

The number of allowable cycles N_i at the stress level s_i can be obtained from the s-N curve, in general, described by the following equation

$$N(s)s^b = c. \quad (22.6)$$

A load event causes the same damage regardless of where it occurs in the overall load history.

22.3 Analysis of Load-time Histories

The time responses (time history) are in general rather irregular. Cycling counting is to be done for example by the rain flow method [Bishop 2000]. The rain flow or range pair-range counting method [Jonge 1982, AGARD 1983] is widely used to decompose the irregular time history into equivalent sets of block loading. The number of cycles in each block are recorded in a stress range histogram. The stress range histogram can then be used in the Palmgren-Miner calculations. We try to explain the procedure with the help of two examples [www.me.iastate.edu].

Example

Given a block of transient loading in Fig. 22.1 and

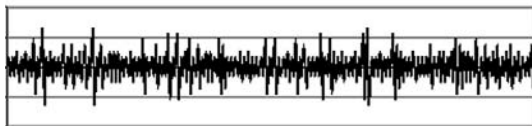


Fig. 22.1 Transient loading

assuming it is reduced in a constant amplitude events, i.e. with cycle counting, see Fig. 22.2.

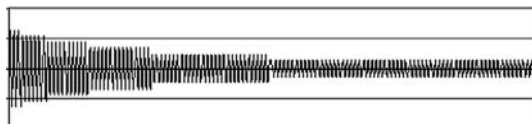


Fig. 22.2 Constant amplitude events

It is possible to extract a block of stress amplitudes associated with a number of cycles. This is shown in Table 22.1.

Table 22.1 Block of stress amplitudes and number of cycles

Block	
Stress amplitudes (Mpa)	Number of cycles
448	3
379	6
310	10
241	15
172	28
103	63

End of example

Example

A steel component has an endurance limit (10^6 cycles) at 207 Mpa and a 10^3 cycles strength of 510 Mpa. The s-N ($N_s^b = c$) curve is defined and based on the former information. If the known values are substituted in the expression for the s-N curve we obtain two equations

$$b \log(207 \times 10^6) - \log c = -\log(10^6)$$

and

$$b \log(510 \times 10^3) - \log c = -\log(10^3)$$

It is found that $c = 5.1011 \times 10^{69}$ and $b = 7.6609$.

Determine the life of the component (in number of blocks) and how much of the overall damage is contributed by each of the stress levels. Use the s-N method, linear damage rule and Miner's constant $D = 1$.

The block is given in Table 22.2.

Table 22.2 Block of stress amplitudes and cycles

Block	
Stress amplitudes (Mpa)	Number of cycles
482	3
400	8
310	50
269	350
221	1000

Table 22.3 Fatigue life prediction per block

Stress Amplitude s (MPa)	number of cycles n_i	N_i	$Ns^b = c$	$D_i = \frac{n_i}{N_i}$	Percent total Damage %
482	3	1540	0.0019	22.8	
400	8	6430	0.0012	14.6	
310	50	45330	0.0011	12.9	
269	350	134380	0.0026	30.5	
221	1000	605710	0.0017	19.3	
		5		0.0085	100.0
Total Damage per Block		$\sum_{i=1}^5 D_i$			
Blocks to failure		$\sum_{i=1}^5 D_i = 1$			

The cumulative damage per block associated with the Palgren-Miner rule block is calculated in Table 22.3. The predicted life is about 117 blocks.

22.4 Failure due to Sinusoidal Vibrations

The enforced acceleration at the base of the spacecraft, solar arrays, instruments, equipment, etc. will result in responses in the frequency domain.

This response is the steady state solution of the be equations of motion. The stress and or force responses in the structure are illustrated in Fig. 22.3.

The frequency responses in an elastic structure with damping is written as

$$\sigma(\omega) = H_{\sigma\ddot{u}}(\omega)\ddot{u}(\omega) \text{ and } F(\omega) = H_{F\ddot{u}}(\omega)\ddot{u}(\omega) \quad (22.7)$$

The frequency response function (FRF) $H_{\sigma\ddot{u}}(\omega)$ and $H_{F\ddot{u}}(\omega)$ can be evaluated with a general purpose finite element programme assuming a unitary base excitation $\ddot{u}(\omega) = 1$. In general, the sinusoidal base excitation is in a frequency range between 5–100 Hz.

On a shaker, the sinusoidal enforced acceleration is applied to a structure with a certain (logarithmic) sweep rate with the unit octave/min, see Fig. 22.4.

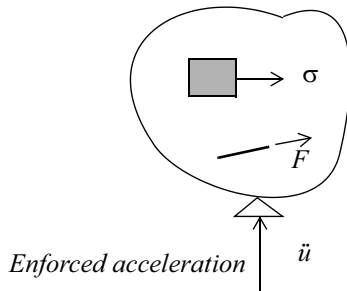


Fig. 22.3 Enforced acceleration

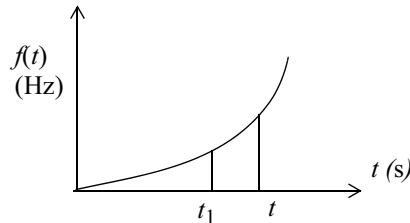


Fig. 22.4 Sweep rate

The logarithmic ratio of the frequency ratio is equal to a constant times the time difference

$$\ln\left\{\frac{f(t)}{f_1}\right\} = K(t - t_1). \quad (22.8)$$

From (22.8) we derive that

$$f(t)dt = \frac{df}{K}. \quad (22.9)$$

The sweep rate is defined as the number of octaves per minute, i.e. n Oct/min. If there are n Oct/min, (22.8) can be written $\ln(2^n) = K60$. Thus the constant K is

$$K = \frac{n \ln(2)}{60} = 0.0116n. \quad (22.10)$$

The number of cycles in a certain time domain can be obtained by

$$N(t) = \int_{t_{\text{ref}}}^t f(t) dt = \frac{1}{K} \int_{f_{\text{ref}}}^f df = \frac{f - f_{\text{ref}}}{K} = \frac{\Delta f}{K}. \quad (22.11)$$

The number of cycles per Hertz is constant all over the frequency range and is given by

$$N(\Delta f=1) = \frac{1}{K} = \frac{86.6}{n}.$$

If the frequency is swept from the frequency f_1 to f_2 the average stress becomes

$$\sigma_{\text{average}}(\Delta f_i) = \frac{1}{2} \{ \sigma(f_i) + \sigma(f_{i-1}) \}. \quad (22.12)$$

The number of allowable cycles at a stress level σ_{average} can be obtained from the fatigue curve $N(s)s^b = c$

$$N_{s-N}(\Delta f_i) = \frac{c}{\sigma_{\text{average}}^b(\Delta f_i)}. \quad (22.13)$$

The cumulative damage due to sinusoidal stresses, swept with a certain sweep rate n , can be calculated with the aid of the following expression

$$D_{\text{sinusoidal}} = \sum_i \frac{N(\Delta f_i)}{N_{s-N}(\Delta f_i)}. \quad (22.14)$$

The fatigue life associated with the cumulative damage $D_{\text{sinusoidal}}$ can be calculated by

$$T_{\text{sinusoidal}} = \frac{1}{K} \ln \left(\frac{f_{\max}}{f_{\min}} \right). \quad (22.15)$$

22.5 Failure due to Narrow-banded Random Vibrations

The expected damage due to the number of peaks, while the stress s lies between a certain stress level s and $s + ds$ during a time T , is given by:

$$D(s) = \frac{n(s)}{N(s)}, \quad (22.16)$$

where $n(s)$ is the number of cycles occurring at stress level $s = a$ and the number of allowable cycles $N(s)$ is taken from the s-N curve (22.6)

$$N(s) = \frac{c}{b} s . \quad (22.17)$$

The number of cycles occurring at stress level $s_a = a$ is given by

$$n(s_a) = v_a^+ T, \quad (22.18)$$

where

$$n(s) = v_s^+ - v_{s+ds}^+ = \frac{-d v_s^+}{ds} ds = v_0^+ \frac{s}{\sigma_s^2} e^{-\frac{s^2}{2\sigma_s^2}} ds . \quad (22.19)$$

The number of positive crossings at stress level $s_a = a$, for a narrow banded process, is given by

$$v_a^+ = v_0^+ e^{-\frac{s_a^2}{2\sigma_s^2}}, \quad (22.20)$$

with the number of positive zero crossings v_0^+ , with the power spectral density function $W_s(f)$ given by

$$v_0^+ = \left(\frac{\int_0^\infty f^2 W_s(f) df}{\int_0^\infty W_s(f) df} \right)^{\frac{1}{2}} . \quad (22.21)$$

The linear cumulative damage due to $n(s_a)$ can be calculated by

$$D(s) = \frac{n(s)}{N(s)} = \frac{v_s^+ T}{N(s)} = \frac{s v_0^+ T e^{-\frac{s^2}{2\sigma_s^2}}}{N(s) \sigma_s^2} ds \quad (22.22)$$

where σ_s^2 is the variance of the stress s .

According to Palmgren-Miner, the total expected cumulative damage amounts to:

$$E[D(T)] = \frac{v_0^+ T}{\sigma_s^2} \int_0^\infty \frac{s e^{-\frac{s^2}{2\sigma_s^2}}}{N(s)} ds . \quad (22.23)$$

In combination with (22.6), the s-N curve, (22.23) representing the expected value of the cumulative damage becomes

$$\bar{D}(T) = \frac{v_0^+ T}{c \sigma_s^2} \int_0^\infty s^{b+1} e^{-\frac{s^2}{2\sigma_s^2}} ds = \frac{v_0^+ T}{c} \{ \sqrt{2} \sigma_s \}^b \Gamma \left(1 + \frac{b}{2} \right) \quad (22.24)$$

with the Gamma function¹ $\Gamma(z) = \int_0^\infty e^{-t} t^{z-1} dt$ and σ_s is the rms value of the induced (to be investigated) stress component.

To find the fatigue damage due to a wide-banded process the damage based on the narrow-banded assumption can be estimated first, and correction is then made correspondingly [Jiao 1990].

Steinberg proposed in [Steinberg 1978] an approximation

$$D = v_0^+ T \left[\frac{0.683}{N_{1\sigma}} + \frac{0.271}{N_{2\sigma}} + \frac{0.043}{N_{3\sigma}} \right], \quad (22.25)$$

where $N_{1\sigma}$ is the number of allowable oscillations at a 1σ stress level, etc.

Assuming that available cumulative damage is $\bar{D}(T) \approx 1$ when the structure fails due to fatigue, then the expected life time \bar{T} can be calculated.

$$\bar{T} = \frac{c}{v_0^+ \{ \sqrt{2} \sigma_s \}^b \Gamma \left(1 + \frac{b}{2} \right)}. \quad (22.26)$$

With

$$h_1 = \frac{v_0^+}{c} \{ \sqrt{2} \sigma_s \}^b \Gamma \left(1 + \frac{b}{2} \right) \text{ and } h_2 = \frac{1}{c} \{ \sqrt{2} \sigma_s \}^b \Gamma \left(1 + \frac{b}{2} \right) \sqrt{\frac{v_0^+ \psi_1(b)}{\zeta}},$$

we are able to calculate the standard deviation of the fatigue life distribution [Sun 1996]

$$\sigma_T = \frac{h_2 \sqrt{h_2^2 + 4h_1}}{6h_1}, \quad (22.27)$$

with $\zeta = \frac{1}{2Q}$ the modal damping ratio, and $\psi_1(b)$ a function of b , tabulated in Table 22.4.

1. $\Gamma(z+1) = z\Gamma(z)$, $\Gamma(1) = 1$, $\Gamma(m+1) = m!$, $\Gamma\left(\frac{1}{2}\right) = \sqrt{\pi}$.

Table 22.4 $\psi_1(b)$ [Crandall 1963]

b	1	3	5	7
$\psi_1(b)$	0.0414	0.3690	1.2800	3.7200
b	9	11	13	15
$\psi_1(b)$	10.700	31.5000	96.7000	308.0000

Assume a Gaussian probability density function (pdf) of the fatigue life T , then

$$f_N = \frac{1}{\sigma_T \sqrt{2\pi}} e^{-\frac{1}{2} \left(\frac{T-\bar{T}}{\sigma_T}\right)^2}. \quad (22.28)$$

The normal distribution can be transferred to the standard normal pdf, using the transformation $z = \frac{T-\bar{T}}{\sigma_T}$, [Bain 1987], hence

$$\phi(z) = \frac{1}{\sqrt{2\pi}} e^{-\frac{1}{2} z^2}, \quad (22.29)$$

and the cumulative density function (CDF) becomes

$$\Phi(z) = \int_{-\infty}^z \phi(t) dt, \quad (22.30)$$

with [Stange 1970]

$$\Phi(-z) = 1 - \Phi(z). \quad (22.31)$$

The reliability with respect to fatigue life becomes

$$R_N = \int_T^\infty f_N(t) dt = 1 - \Phi\left(\frac{T-\bar{T}}{\sigma_T}\right) = 1 - \Phi(z). \quad (22.32)$$

Example

A mass-spring system, with a mass m and a spring stiffness k of the rod, is random excited at the base with $W_{\ddot{u}}(f)$. The amplification factor is $Q = 10$. A natural frequency of $f_o = 50\text{Hz}$ is selected and the spring stiffness of the spring is $k = \frac{EA}{L} = 1 \times 10^{-4} \text{ N/m}$, with a surface area of $A = 10^{-4} \text{ m}^2$. The mass m is

$$m = \frac{k}{(2\pi f_o)^2} = 101.3 \text{ kg.}$$

The random base excitation is $W_{\ddot{u}}(f) = 10 \text{ (m/s}^2)^2/\text{Hz.}$, in a frequency domain from 5–2000Hz.

With the aid of Miles' equation the acceleration of the mass m can be calculated:

$$\ddot{x}_{\text{rms}} = \sqrt{\frac{\pi}{2} f_o Q W_{\ddot{u}}(f_o)} = \sqrt{\frac{\pi}{2} \times 50 \times 10 \times 10} = 88.6 \text{ m/s}^2$$

The rms value of the stress $s_{\text{rms}} = \sigma_s$ in the rod then becomes:

$$s_{\text{rms}} = \sigma_s = \frac{m \ddot{x}_{\text{rms}}}{A} = \frac{101.3 \times 88.6}{1 \times 10^{-4}} = 8.98 \times 10^7 \text{ Pa}$$

For a simple mass-spring system $v_0^+ = f_0 = 50 \text{ Hz.}$

The expected lifetime T can be calculated as follows: The S-N curve is given and is $N(s)s^b = c$, with $b = 4$, $c = 1.56 \times 10^{37}$, $T = \frac{c}{v_0^+ \{ \sqrt{2} \sigma_s \}^b \Gamma \left(1 + \frac{b}{2} \right)} = 600 \text{ s.}$

$$\text{With } b = 4 \text{ the function } \psi_1(4) = \frac{\psi_1(3) + \psi_1(5)}{2} = 0.64$$

The standard deviation of the predicted expected fatigue life is

$$\sigma_T = \frac{h_2 \sqrt{h_2^2 + 4h_1}}{6h_1^2} = 12.4 \text{ s}$$

$$\text{Assume } z = \frac{T - \bar{T}}{\sigma_T} = \frac{\bar{T} - 3\sigma_T - \bar{T}}{\sigma_T} = -3, \text{ thus with } \Phi(-z) = 1 - \Phi(z),$$

$$\Phi(-3) = 1 - \Phi(3) = 1 - 0.9987 = 0.0013.$$

$$\text{Thus the reliability figure for a fatigue life } \bar{T} - 3\sigma_T \text{ becomes } R_N = 1 - \Phi(-3) = 0.9987.$$

The total number of cycles n then becomes $n = v_0^+ T = 50 * 600 = 30000$ after which the rod will collapse due to fatigue.

For a sinusoidal stress alternation with constant amplitude, constant frequency and a total of 30000 cycles, then it follows from the s-N curve that the permissible

$$\text{stress amplitude is equal to: } s = \left(\frac{c}{N} \right)^{\frac{1}{b}} = \left(\frac{1.56 \times 10^{37}}{30000} \right)^{\frac{1}{4}} = 1.51 \times 10^8 \text{ Pa.}$$

End of example

Example Steinberg approach

This example is taken from [Steinberg 1978]. A mounting bracket that is to hold a transformer of 3.5 kg.

The bracket and box are illustrated in Fig. 22.5. The total length of the bracket is $2L = 0.4 \text{ m}$, the width $b = 0.1 \text{ m}$ and the thickness $t = 0.01 \text{ m}$. The bracket has

been manufactured from Al-alloy with a Young's modulus $E = 70$ GPa. The mass of the box is $M = 3.5$ kg. The power spectral density of the enforced acceleration is constant in the frequency range between 50-200 Hz and is given by $W_{\ddot{u}} = 0.1 \text{ g}^2/\text{Hz}$. The assembly will be exposed to an enforced vibration test of duration $T = 10$ hrs. The amplification factor or transmissibility is $Q = 25$. The s-N curve of the construction material steel is given by $N_s^{1.585} = 1.4231 \times 10^{19}$

Determine whether the bracket design is satisfactory for the specified vibration level and duration of the test, and also how long it can withstand such a test.

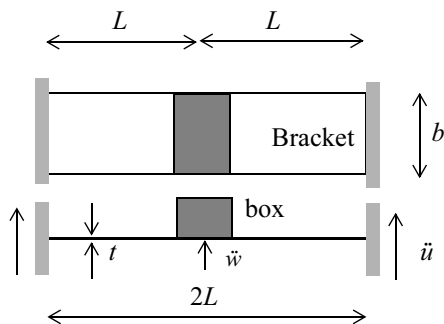


Fig. 22.5 Box mounted on bracket

Initially the natural frequency of the bracket is calculated while ignoring the mass of the bracket. The second moment of area I of the bracket is

$$I = \frac{1}{12}bt^3 = 8.333 \times 10^{-9} \text{ m}^4.$$

The deflection of the clamped-clamped beam in the mid of the beam under a gravitation load Mg is given by

$$\delta = \frac{MgL^3}{24EI},$$

where $g = 9.81 \text{ m/s}^2$.

The natural frequency can be calculated using

$$f_o = \frac{1}{2\pi}\sqrt{\frac{g}{\delta}} = \frac{1}{2\pi}\sqrt{\frac{24EI}{ML^3}} = 112.5 \text{ Hz.}$$

The M-line of a beam clamped at both sides with a force in the middle of the beam is illustrated in Fig. 22.6. The maximum absolute value of the bending

moment is $M_{\max} = \frac{FL}{4}$. The maximum corresponding bending stress at the extreme fibre distance $e = \frac{t}{2}$ is given by

$$\sigma_{\text{bending,max}} = \frac{M_{\max}e}{I} = \frac{M_{\max}t}{2I}.$$

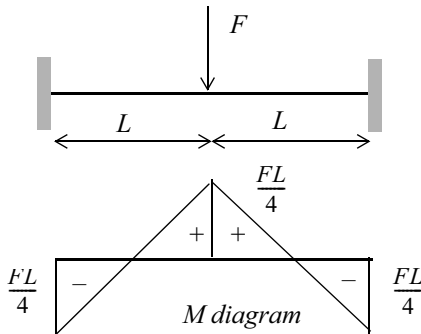


Fig. 22.6 M-line

It is now required to calculate the inertia force F . This rms value of the inertia force is given by

$$F_{\text{rms}} = M\ddot{w}_{\text{rms}}$$

where \ddot{w}_{rms} is the rms acceleration of the box. The rms acceleration can be calculated using the Miles' equation

$$\ddot{w}_{\text{rms}} = \sqrt{\frac{\pi}{2} f_o Q W_i(f_o)} = \sqrt{\frac{\pi}{2} \times 112.5 \times 25 \times 0.1} = 21.0 \text{ g}$$

The rms value of the inertia force F_{rms} becomes

$$F_{\text{rms}} = M\ddot{w}_{\text{rms}} = 3.5 \times 21.0 \times 9.81 = 721.8 \text{ N.}$$

If a stress concentration factor $K = 2.2$ is taken into account, the maximum bending stress is

$$\sigma_{\text{bending,rms}} = \frac{KM_{\max}t}{2I} = \frac{KFLt}{8I} = \frac{2.2 \times 721.8 \times 0.2 \times 0.010}{8.333 \times 10^{-9}} = 4.764 \times 10^7 \text{ Pa.}$$

The number of allowable cycles at stress levels can be obtained from the s-N curve $N_s^{1.585} = 1.4231 \times 10^{19}$:

- $1\sigma = \sigma_{\text{bending,rms}}$ is $N_{1\sigma} = 9.631 \times 10^6$
- $2\sigma = 2\sigma_{\text{bending,rms}}$ is $N_{2\sigma} = 3.21 \times 10^6$
- $3\sigma = 3\sigma_{\text{bending,rms}}$ is $N_{3\sigma} = 1.688 \times 10^6$

Finally it is possible to calculate the linear cumulative damage in accordance to the Palgren-Miner rule and applying (22.25)

$$D = f_0 T \left[\frac{0.683}{N_{1\sigma}} + \frac{0.271}{N_{2\sigma}} + \frac{0.043}{N_{3\sigma}} \right] = 0.733$$

How many hours the vibration test can last until the cumulative damage $D = 1$

$$T_{D=1} = \frac{T}{D} = \frac{10}{0.733} = 13.65 \text{ hrs.}$$

End of example

22.6 Literature

- AGARD, 1983, *Helicopter Fatigue Design Guide*, AGARD-AG-292
- Bishop, N.W., Sherratt, F., 2000, *Finite Element Based Fatigue Calculations*, NAFEMS Publication.
- Crandall, S.H. and Mark, W.D., 1973, *Random Vibration in Mechanical Systems*, Academic Press.
- Bain, L.J., Engelhardt, M, 1987, *Introduction to Probability and Mathematical Statistics*, PWS Publishers, ISBN 0-97-150067-1.
- Jiao, G., Moan, T., 1990, *Probabilistic analysis of fatigue due to Gaussian load process*, Probabilistic Engineering Mechanics, Vol.5, No 2.
- Jonge de, J.B., 1982, *The Analysis of Load Time by means of Counting Methods*, NLR report, NLR MP 82039 U.
- Juvinal, R.C., 1967, *Stress, Strain and Strength*, McGraw-Hill.
- Lyon, R.H., 1967, *Random Noise and Vibration in Space Vehicles*, SVM-1.
- Lyon, R.H., Dejong, R.G., 1995, *Theory and Application of Statistical Energy Analysis*, ISBN 0-7506-9111-05.
- Richards, E.J., Mead, D.J., 1968, *Noise and Acoustic Fatigue in Aeronautics*, John Wiley & Sons Ltd.
- Stange, K., 1970, *Angewandte Statistik, Eindimensionale Probleme*, Springer-Verlag.
- Steinberg D.S., 1978, *Quick way to predict Random Vibration Failures*, Machine Design, April 1978, pages 188-191.
- Sun, Feng-Bin, et al., 1996, *Fatigue Reliability Evaluation and Preventive Maintenance Policy for a Structural Element Under Random Vibration*, AIAA paper-96-1563-CP.

22.7 Internet

http://www.me.iastate.edu/me515_comer/Lecture/lecture25.pdf

22.8 Exercises

22.8.1 Fatigue life prediction sinusoidal vibration

A dynamic system is given in Fig. 22.7. A large mass M is supported by a simply supported beam with a total length of $2L$ with a bending stiffness EI and a mass m per unit of length. The beam is excited by an enforced acceleration \ddot{u} .

Obtain the natural frequency associated with the assumed mode

$$\phi(x) = A \sin\left(\frac{\pi x}{2L}\right),$$

with use of the Rayleigh quotient $R(\phi)$ given by

$$R(\Phi) \approx \omega_o^2 = \frac{\frac{1}{2} \int_0^{2L} EI(\phi'')^2 dx}{\frac{1}{2} \int_0^{2L} m\phi'^2 dx + \frac{1}{2} M\Phi^2(L)}.$$

$$\text{(answer: } \omega_o = \left(\frac{\pi}{2}\right)^2 \sqrt{\frac{EI}{L^4} \frac{1}{m + \frac{M}{L}}})$$

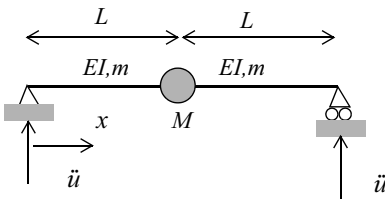


Fig. 22.7 Dynamic system

The beam has to carry a large mass \$M = 10\$ kg and the total length of the beam is \$L = 0.5\$ m. The mass per unit of length of the beam is assumed to be \$m = 0.2\$ kg/m. Design a beam with a bending stiffness \$EI\$ such that the lowest natural frequency \$f_o = 60\$ Hz.

$$\text{(answer: } EI = 2.9472 \times 10^4 \text{ Nm}^2)$$

The construction material of the beam shows an s-N curve given by

$$Ns^4 = 1.0 \times 10^{35}$$

The sinusoidal enforced acceleration \$\ddot{u}\$ has a constant amplitude of \$10\$ m/s\$^2\$ in the frequency range from 5-100 Hz. The damping ratio in the system may be represented by the amplification factor \$Q = \frac{1}{2\zeta} = 25\$.

The deflection \$w(x, t)\$ can be written as

$$w(x, t) = \sin\left(\frac{\pi x}{2L}\right) \eta(t).$$

Transform the continuous system of the beam carrying a big mass in a one degree of freedom system by applying the Lagrange equation

$$\frac{d}{dt} \frac{dL}{d\dot{\eta}} - \frac{dL}{d\eta} = 0.$$

The Lagrangian is given by

$$L = \frac{1}{2} \int_0^{2L} m \{ \dot{w}(x, t) + \dot{u} \}^2 dx + \frac{1}{2} M \{ \dot{w}(L, t) + \dot{u} \}^2 - \frac{1}{2} \int_0^{2L} EI w''^2 dx.$$

$$\text{(answer: } \ddot{\eta}(t) + \omega_o^2 \eta(t) = -\frac{\left(\frac{4mL}{\pi} + M\right)}{(mL + M)} \ddot{u}(t) \text{)}$$

Introduce the damping term $2\zeta\omega_o\dot{\eta}(t)$ in the equation of motion.

$$\text{(answer: } \ddot{\eta}(t) + 2\zeta\omega_o\dot{\eta}(t) + \omega_o^2 \eta(t) = -\frac{\left(\frac{4mL}{\pi} + M\right)}{(mL + M)} \ddot{u}(t) \text{)}$$

Calculate the sinusoidal responses in the frequency range from 5–100 Hz.

The maximum bending moment in the beam is at $x=L$ and is given by $M_{\text{bending}} = EIw''(L)$. The construction material has a Young's modulus $E = 70 \text{ GPa}$. The extreme fibre distance is $e = 0.05 \text{ m}$. The maximum bending stress can be obtained by the following equation

$$\sigma_{\text{bending}}(L, e) = \left| \frac{M_{\text{bending}}e}{I} \right|.$$

$$\text{(answer: } \sigma_{\text{bending}}(L, e) = \left(\frac{\pi}{2L} \right)^2 Ee \text{)}$$

The sinusoidal test is done with a sweep rate $n = 2 \text{ Oct/min}$.

Calculate the cumulative damage $D_{\text{sinusoidal}}$ and the associated time $T_{\text{sinusoidal}}$ needed to perform the sine vibration test.

$$\text{(answer: } T_{\text{sinusoidal}} = 129.7 \text{ s})$$

22.8.2 Fatigue life prediction random vibration

The following exercise uses all of the parameters of the dynamic system described in the previous exercise “Fatigue life prediction sinusoidal vibration” on page 363.

The system will be tested against random enforced vibrations with following levels $W_{\ddot{u}}(f)$:

- 20–50 Hz 3 dB/oct
- 50–300 Hz 0.05 g²/Hz (1g=10m/s²)
- 300–2000 Hz –3 dB/oct
- Test duration 120 s.

Calculate the G_{rms} value of the given spectrum.

(answer: $G_{\text{rms}} = 6.482 \text{ g}$)

What is the modified acceleration density function $\bar{W}_{\ddot{u}}(f)$?

$$\text{(answer: } \bar{W}_{\ddot{u}}(f) = \left(\frac{\frac{4mL}{\pi} + M}{mL + M} \right)^2 W_{\ddot{u}}(f) \text{)}$$

Using the derived single degree of freedom system the rms values of the deflection $w_{\text{rms}}(L)$ (using Miles' equation) and the bending stress $\sigma_{\text{bending,rms}}(L, e)$ respectively.

(answer: $w_{\text{rms}}(L) = 7.658 \times 10^{-4} \text{ m}$, $\sigma_{\text{bending,rms}}(L, e) = 2.645 \times 10^7 \text{ Pa}$)

Calculate the cumulative damage D_{random} for the time duration specified, applying (22.24). The number of positive zero crossings is equal to the natural frequency of the system.

(answer: $D_{\text{random}} = 0.282$)

23 Shock-Response Spectrum

23.1 Introduction

Separation of stages and the separation of the spacecraft from the last stage of the launch vehicle will induce very short duration loads in the internal structure of the spacecraft, the so-called shockloads. The duration of the shock load is, in general, very short with respect to the duration associated with the fundamental natural frequencies of the loaded dynamic mechanical system.

The effects of the shock loads are generally depicted in a shock-response spectrum (SRS). The SRS is essentially a plot that shows the responses of a number of single degree of freedom (SDOF) systems to an excitation. The excitation is usually an acceleration–time history.

A SRS is generated by calculating the maximum response of a SDOF system to a particular base transient excitation. Many SDOF systems tuned to a range of natural frequencies are assessed using the same input-time history. A damping value must be selected in the analysis. A damping ratio of $\zeta = 0.05$, $Q = 10$, is commonly used. The final plot, the SRS, looks like a frequency-domain plot. It shows the largest response encountered for a particular SDOF system anywhere within the analysed time. Thus the SRS provides an estimate of the response of an actual product and its various components to a given transient input (i.e. shock pulse) [Grygier 1997].

A typical example of a time-history acceleration and associated SRS as illustrated in Fig. 23.1 and Fig. 23.2, are extracted from NASA-STD-7003 [Mulville 1999].

In this chapter, the response of a SDOF system, due to enforced acceleration, will be reviewed. Furthermore, the calculation of a SRS will be discussed in detail. The maximum values occurring in time histories will be compared with the SRS approach and finally it will be shown how an existing SRS can be matched (with synthesised decaying sinusoids).

This chapter is based on chapter 10 of the book of Jaap Wijker [Wijker 2004].

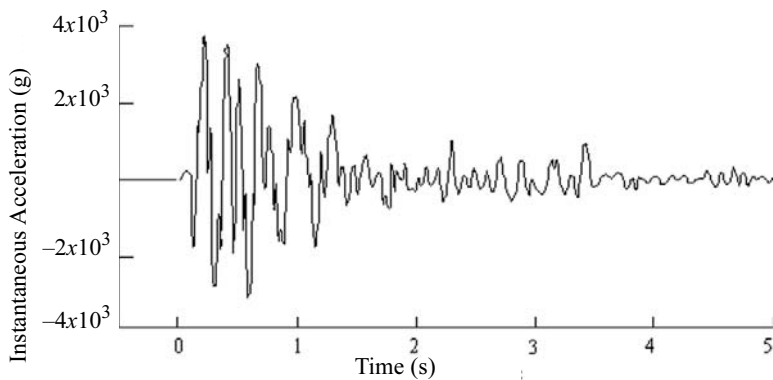


Fig. 23.1 Typical pyroshock acceleration time-history [Mulville 1999]

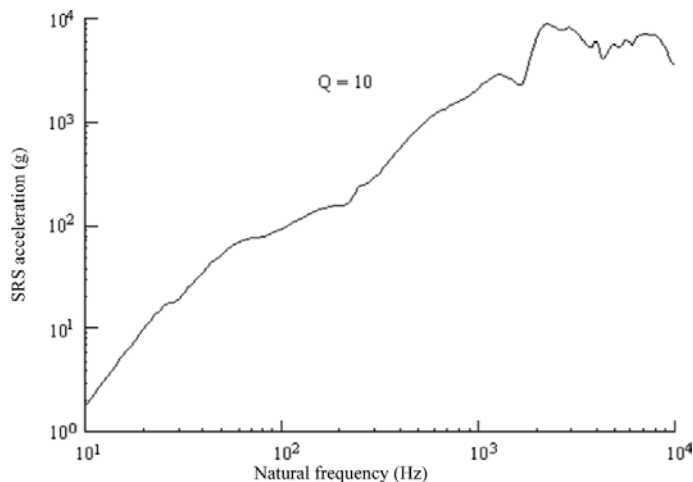


Fig. 23.2 Typical pyroshock maximum shock response spectrum (SRS) [Mulville 1999]

23.2 Enforced Acceleration

A SDOF system with a discrete mass m , a damper element c and a spring element k is placed on a moving base that is accelerated with an acceleration $\ddot{u}(t)$. The resulting displacement of the mass is $x(t)$. The natural (circular) frequency

$\omega_n = \sqrt{\frac{k}{m}}$, the damped circular frequency $\omega_d = \omega_n \sqrt{1 - \zeta^2}$, the critical damping constant $c_{crit} = 2\sqrt{km}$ and the damping ratio $\zeta = \frac{c}{c_{crit}}$ are then introduced. The amplification factor is defined as $Q = \frac{1}{2\zeta}$ where $Q = 10$ is generally assumed.

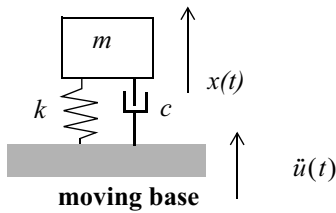


Fig. 23.3 Enforced acceleration on a damped SDOF system

We introduce a relative motion $z(t)$, which is the displacement of the mass with respect to the base. The relative displacement is

$$z(t) = x(t) - u(t). \quad (23.1)$$

The equation of motion for the relative motion $z(t)$ is

$$\ddot{z}(t) + 2\zeta\omega_n\dot{z}(t) + \omega_n^2 z(t) = -\ddot{u}(t). \quad (23.2)$$

The enforced acceleration of the SDOF system is transformed into an external force. The absolute displacement $x(t)$ can be calculated with

$$\ddot{x}(t) = \ddot{z}(t) + \ddot{u}(t) = -2\zeta\omega_n\dot{z}(t) - \omega_n^2 z(t). \quad (23.3)$$

The solution of (23.2), taking into account the initial condition with respect to displacement $z(0)$ and velocity $\dot{z}(0)$ is

$$z(t) = z(0)e^{-\zeta\omega_n t} \left(\cos \omega_d t + \frac{\zeta}{\sqrt{1 - \zeta^2}} \sin \omega_d t \right)$$

$$+ \dot{z}(0)e^{-\zeta\omega_n t} \frac{\sin \omega_d t}{\omega_d} - \int_0^t e^{-\zeta\omega_n \tau} \frac{\sin \omega_d \tau}{\omega_d} \ddot{u}(\tau) d\tau. \quad (23.4)$$

For SRS calculations $z(0) = \dot{z}(0) = 0$, hence

$$z(t) = - \int_0^t e^{-\zeta\omega_n\tau} \frac{\sin\omega_d\tau}{\omega_d} \ddot{u}(t-\tau) d\tau = - \int_0^t e^{-\zeta\omega_n(t-\tau)} \frac{\sin\omega_d(t-\tau)}{\omega_d} \ddot{u}(\tau) d\tau. \quad (23.5)$$

After differentiation of (23.5) with respect to time [Kelly 1969] the relative velocity $\dot{z}(t)$ becomes

$$\dot{z}(t) = - \int_0^t e^{-\zeta\omega_d(t-\tau)} \cos(\omega_d(t-\tau)) \ddot{u}(\tau) d\tau - \zeta\omega_n z(t). \quad (23.6)$$

The absolute acceleration $\ddot{x}(t)$ can be obtained by applying (23.3) [Kelly 1969]

$$\ddot{x}(t) = 2\zeta\omega_n \int_0^t e^{-\zeta\omega_n(t-\tau)} \cos(\omega_d(t-\tau)) \ddot{u}(\tau) d\tau + \omega_n(2\zeta^2 - 1)z(t). \quad (23.7)$$

The maximum acceleration $\ddot{x}(t)$ can be calculated by inserting the natural frequency $\omega_n = 2\pi f_n$ (Rad/s) of the SDOF system for every natural frequency. The maximum acceleration $\ddot{x}(t)$ will be plotted against the number of cycles per second f_n (Hz). This plot is called the shock-response spectrum (SRS) of the base excitation $\ddot{u}(t)$.

23.3 Numerical Calculation of the SRS, the Piece wise Exact Method

In this section, two similar methods of calculating numerically transient responses of SDOF dynamic systems, are discussed:

1. A method as discussed in [Nigam 1968, Ebeling 1997]
2. A method as discussed by [Kelly 1969]

In both methods the forcing function is assumed to vary linearly in a piece wise fashion and, based upon this assumption, an exact solution is determined.

The equation of relative $z(t)$ motion of the SDOF dynamic system exposed to a base acceleration $\ddot{u}(t)$ is given by (23.2)

$$\ddot{z}(t) + 2\zeta\omega_n\dot{z}(t) + \omega_n^2 z(t) = -\ddot{u}(t).$$

The base acceleration $\ddot{u}(t)$ is mostly given in a discrete form in a table: acceleration versus time. We assume a linear variation of the acceleration between two time steps t_j and t_{j+1} . The acceleration $\ddot{u}(t_{j+1})$ is expressed in terms of the accel-

eration $\ddot{u}(t_j)$. The time increment is $\Delta t_j = t_{j+1} - t_j$ and the increment of the acceleration is $\Delta \ddot{u}(t_j) = \ddot{u}(t_{j+1}) - \ddot{u}(t_j)$.

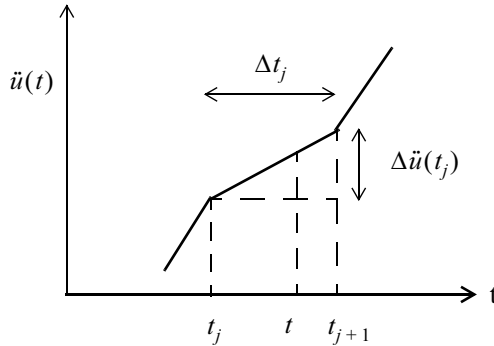


Fig. 23.4 Linearisation numerical scheme of acceleration $\ddot{u}(t)$

The acceleration $\ddot{u}(t_{j+1})$ at the time t_{j+1} becomes

$$\ddot{u}(t) = \ddot{u}(t_j) + \frac{\Delta \ddot{u}(t_j)}{\Delta t_j}(t - t_j), \quad t_j \leq t \leq t_{j+1}. \quad (23.8)$$

(23.2) will be rewritten

$$\ddot{z}(t) + 2\zeta\omega_n \dot{z}(t) + \omega_n^2 z(t) = -\ddot{u}(t_j) - \frac{\Delta \ddot{u}(t_j)}{\Delta t_j}(t - t_j), \quad t_j \leq t \leq t_{j+1}. \quad (23.9)$$

The solution of (23.9) is

$$\begin{aligned} z(t) &= z(t_j) e^{-\zeta\omega_n(t-t_j)} \left(\cos \omega_d(t-t_j) + \frac{\zeta}{\sqrt{1-\zeta^2}} \sin \omega_d(t-t_j) \right) \\ &\quad + \dot{z}(t_j) e^{-\zeta\omega_n(t-t_j)} \frac{\sin \omega_d(t-t_j)}{\omega_d} - \int_{t_j}^t e^{-\zeta\omega_n(t-\tau)} \frac{\sin \omega_d(t-\tau)}{\omega_d} \ddot{u}(\tau) d\tau \end{aligned} \quad (23.10)$$

The integral in (23.10) is given by [Kelly 1969].

$$\int_{t_j}^t e^{-\zeta\omega_n(t-\tau)} \frac{\sin \omega_d(t-\tau)}{\omega_d} \ddot{u}(\tau) d\tau =$$

$$\begin{aligned}
&= \frac{-\ddot{u}(t_j)}{\omega_n^2} \left[1 - e^{-\zeta \omega_n(t-t_j)} \left(\cos \omega_d(t-t_j) + \frac{\zeta}{\sqrt{1-\zeta^2}} \sin \omega_d(t-t_j) \right) \right] \\
&\quad \left(\frac{-\Delta \ddot{u}(t_j)}{\omega_n^2} \right) \left[1 - \frac{2\zeta}{\omega_n(t-t_j)} (1 - e^{-\zeta \omega_n(t-t_j)} \cos \omega_d(t-t_j)) \right] \\
&\quad + \frac{\Delta \ddot{u}(t_j)}{\omega_n^2} \left[\frac{(1-2\zeta^2)}{\omega_d(t-t_j)} e^{-\zeta \omega_n(t-t_j)} \sin \omega_d(t-t_j) \right]
\end{aligned} \tag{23.11}$$

The state vector $(z, \dot{z})^T$ at time t_{j+1} can be expressed in the state vector at time t_j and the piece wise linear given base acceleration \ddot{u} at both t_j and t_{j+1} [Nigam 1968, Gupta 1992, Ebeling 1997],

$$\begin{Bmatrix} z(t_{j+1}) \\ \dot{z}(t_{j+1}) \end{Bmatrix} = [A] \begin{Bmatrix} z(t_j) \\ \dot{z}(t_j) \end{Bmatrix} + [B] \begin{Bmatrix} \ddot{u}(t_j) \\ \ddot{u}(t_{j+1}) \end{Bmatrix}, \tag{23.12}$$

with

- $[A] = \begin{bmatrix} a_{11} & a_{12} \\ a_{21} & a_{22} \end{bmatrix}$

and

- $[B] = \begin{bmatrix} b_{11} & b_{12} \\ b_{21} & b_{22} \end{bmatrix}$

The absolute acceleration $\ddot{x}(t_{j+1})$ is given by (23.3)

$$\ddot{x}(t_{j+1}) = -2\zeta \omega_n \dot{z}(t_{j+1}) - \omega_n^2 z(t_{j+1}). \tag{23.13}$$

With $\Delta t_j = t_{j+1} - t_j$, the elements of the matrix $[A]$ are

- $a_{11} = e^{-\zeta \omega_n \Delta t_j} \left(\frac{\zeta}{\sqrt{1-\zeta^2}} \sin \omega_d \Delta t_j + \cos \omega_d \Delta t_j \right)$
- $a_{12} = e^{-\zeta \omega_n \Delta t_j} \frac{\sin \omega_d \Delta t_j}{\omega_d}$
- $a_{21} = -\frac{\omega_n}{\sqrt{1-\zeta^2}} e^{-\zeta \omega_n \Delta t_j} \sin \omega_d \Delta t_j$

- $a_{22} = e^{-\zeta \omega_n \Delta t_j} \left(\cos \omega_d \Delta t_j - \frac{\zeta}{\sqrt{1 - \zeta^2}} \sin \omega_d \Delta t_j \right)$

With $\Delta t_j = t_{j+1} - t_j$ the elements of the matrix $[B]$ are

- $b_{11} = e^{-\zeta \omega_n \Delta t_j} \left(\left[\frac{2\zeta^2 - 1}{\omega_n^2 \Delta t_j} + \frac{\zeta}{\omega_n} \right] \frac{\sin \omega_d \Delta t_j}{\omega_d} + \left[\frac{2\zeta}{\omega_n^3 \Delta t_j} + \frac{1}{\omega_n^2} \right] \cos \omega_d \Delta t_j \right) - \frac{2\zeta}{\omega_n^3 \Delta t_j}$
- $b_{12} = -e^{-\zeta \omega_n \Delta t_j} \left(\left[\frac{2\zeta^2 - 1}{\omega_n^2 \Delta t_j} \right] \frac{\sin \omega_d \Delta t_j}{\omega_d} + \frac{2\zeta}{\omega_n^3 \Delta t_j} \cos \omega_d \Delta t_j \right) - \frac{1}{\omega_n^2} + \frac{2\zeta}{\omega_n^3 \Delta t_j}$
- $b_{21} = e^{-\zeta \omega_n \Delta t_j} \left[\frac{2\zeta^2 - 1}{\omega_n^2 \Delta t_j} + \frac{\zeta}{\omega_n} \right] \left(\cos(\omega_d \Delta t_j) - \frac{\zeta}{\sqrt{1 - \zeta^2}} \sin \omega_d \Delta t_j \right)$
 $- e^{-\zeta \omega_n \Delta t_j} \left[\frac{2\zeta}{\omega_n^3 \Delta t_j} + \frac{1}{\omega_n^2} \right] (\omega_d \sin \omega_d \Delta t_j + \zeta \omega_n \cos \omega_d \Delta t_j) + \frac{1}{\omega_n^2 \Delta t_j}$
- $b_{22} = -e^{-\zeta \omega_n \Delta t_j} \left[\frac{2\zeta^2 - 1}{\omega_n^2 \Delta t_j} \left(\cos \omega_d \Delta t_j - \frac{\zeta}{\sqrt{1 - \zeta^2}} \sin \omega_d \Delta t_j \right) \right]$
 $- e^{-\zeta \omega_n \Delta t_j} \left(\frac{-2\zeta}{\omega_n^3 \Delta t_j} (\omega_d \sin \omega_d \Delta t_j + \zeta \omega_n \cos \omega_d \Delta t_j) \right) - \frac{1}{\omega_n^2 \Delta t_j}$

In [Gupta 1992] the following expressions for b_{21} and b_{22} are given:

- $b_{21} = -\frac{a_{11} - 1}{\omega_n^2 \Delta t_j} - a_{12}$
- $b_{22} = -b_{21} - a_{12}$

In [Kelly 1969] a very similar numerical approach, as discussed by [Nigam 1968, Gupta 92, Ebeling 97], is proposed

$$z(t_{j+1}) = B_1 z(t_j) + B_2 \dot{z}(t_j) + B_3 \ddot{u}(t_j) + B_4 \Delta \ddot{u}(t_j) \quad (23.14)$$

$$\frac{\dot{z}(t_{j+1})}{\omega_n} = B_6 z(t_j) + B_7 \dot{z}(t_j) + B_8 \ddot{u}(t_j) + B_9 \Delta \ddot{u}(t_j), \quad (23.15)$$

with (23.13)

$$\ddot{x}(t_{j+1}) = -2\zeta \omega_n \dot{z}(t_{j+1}) - \omega_n^2 z(t_{j+1})$$

where

- $\Delta t_j = t_{j+1} - t_j$
- $\Delta \ddot{u}(t_j) = \ddot{u}(t_{j+1}) - \ddot{u}(t_j)$
- $B_1 = e^{-\zeta \omega_n \Delta t_j} \left(\frac{\zeta}{\sqrt{1-\zeta^2}} \sin \omega_d \Delta t_j + \cos \omega_d \Delta t_j \right)$
- $B_2 = e^{-\zeta \omega_n \Delta t_j} \frac{\sin \omega_d \Delta t_j}{\omega_d}$
- $B_3 = \frac{1}{\omega_n^2} (1 - B_1)$
- $B_4 = \frac{1}{\omega_n^2} \left[1 - \frac{2\zeta}{\omega_n \Delta t_j} (1 - e^{-\zeta \omega_n \Delta t_j} \cos \omega_d \Delta t_j) - (1 - 2\zeta^2) \left(e^{-\zeta \omega_n \Delta t_j} \frac{\sin \omega_d \Delta t_j}{\omega_d \Delta t_j} \right) \right]$
- $B_6 = -\omega_n B_2$
- $B_7 = \frac{e^{-\zeta \omega_n \Delta t_j}}{\omega_n} \left(\cos \omega_d \Delta t_j - \frac{\zeta}{\sqrt{1-\zeta^2}} \sin \omega_d \Delta t_j \right)$
- $B_8 = -\frac{B_2}{\omega_n}$
- $B_9 = \frac{B_1 - 1}{\omega_n^3 \Delta t_j}$

For the calculation of the SRS the following parameters are important [Assink 1995]:

1. The damping ratio ζ of the SDOF dynamic system.
2. The number of SDOF systems for which the maximum response is calculated.
3. The minimum time frame of the transient T_{\min} (s). The minimum time frame is

the maximum of either $T_{\min} \geq \frac{1}{f_{\min}}$ or twice the maximum shock time

$$T_{\min} \geq 2t_{\text{shock}}.$$

4. The time increment Δt must be less than 10% of the reciprocal value of the maximum frequency f_{\max} (Hz) involved in the calculation of the SRS,

$\Delta t \leq \frac{0.1}{f_{\max}}$. The minimum number of time steps n within the time frame T_{\min} is

$$n = \frac{T_{\min}}{\Delta t} = 10 \frac{f_{\max}}{f_{\min}}.$$

A half-sine pulse $\ddot{u}_{\text{base}} = 200 \sin \frac{\pi t}{\tau}$, ($0 \leq t \leq \tau$) = 0.0005 s and $\ddot{u}_{\text{base}} = 0$, $t < 0, t > \tau$ is applied to the base of series of SDOF dynamic systems to calculate the SRS of the HSP. The total time is $t_{\text{end}} = 0.05$ s and $\Delta t = 0.00001 \leq \frac{0.1}{f_{\max}} = \frac{0.1}{3000} = 0.00003$ s. The damping ratio $\zeta = 0.05$, $Q = 10$. The Kelly method is applied to obtain the SRS.

The calculated SRS (absolute acceleration) is illustrated in Fig. 23.5.

23.4 Response Analysis in Combination with Shock-Response Spectra

A multi-DOF linear system, excited with an acceleration \ddot{u}_{base} at the base, is represented by the equation

$$[M]\{\ddot{x}\} + [C]\{\dot{x}\} + [K]\{x\} = \{0\}. \quad (23.16)$$

The matrix equation for the relative displacement vector $\{z\} = \{x\} - \{u\}$, the relative velocities $\{\dot{z}\} = \{\dot{x}\} - \{\dot{u}\}$ and the relative acceleration $\{\ddot{z}\} = \{\ddot{x}\} - \{\ddot{u}\}$, with respect to the base, can be written as

$$[M]\{\ddot{z}\} + [C]\{\dot{z}\} + [K]\{z\} = -[M]\{T\}\ddot{u}_{\text{base}}, \quad (23.17)$$

where $\{T\}$ is the rigid-body vector with respect to the base.

From the undamped eigenvalue problem (23.17)

$$([K] - \lambda_i[M])\{\phi_i\} = \{0\}, \quad (23.18)$$

the eigenvalues λ_i and associated modes $\{\phi_i\}$ can be obtained and used for the modal analysis (modal displacement method (MDM)) approach. We assume

$$\{z\} = [\phi_1, \phi_2, \phi_3, \dots] \begin{Bmatrix} \eta_1 \\ \eta_2 \\ \eta_3 \\ \vdots \end{Bmatrix} = [\Phi]\{\eta\}, \quad (23.19)$$

where $[\Phi]$ the modal matrix and $\{\eta\}$ the vector of generalised coordinates.

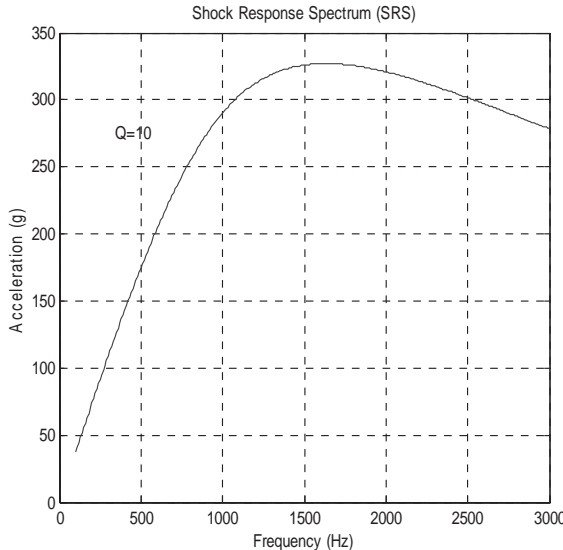


Fig. 23.5 The SRS of a half-sine pulse (HSP) with amplitude $A=200$ g and a time duration $\tau = 0.0005$ s

The modes are orthogonal with respect to the mass matrix $[M]$ and the stiffness matrix $[K]$,

$$[\Phi]^T [M] [\Phi] = \langle m \rangle, \quad [\Phi]^T [K] [\Phi] = \langle \lambda_i m_i \rangle = \langle \omega_i^2 m_i \rangle. \quad (23.20)$$

If the modal damping $c_i = 2\zeta_i\omega_i$ is introduced the equations of motion expressed in the generalised coordinates become

$$\ddot{\eta}_i + 2\zeta_i\omega_i\dot{\eta}_i + \omega_i^2\eta_i = \frac{-[\phi_i]^T [M] \{T\}}{[\phi_i]^T [M] [\phi_i]} \ddot{u}_{\text{base}} = -\Gamma_i \ddot{u}_{\text{base}}, \quad (23.21)$$

with ζ_i the modal damping ratio with respect to mode ' i ', ω_i the natural frequency corresponding with mode $\{\phi_i\}$ and Γ_i the modal participation factor.

Equation (23.21) is similar to (23.2). (23.2) is applied to calculate the maximum (peak) response of the SDOF system to obtain the SRS corresponding with the base acceleration \ddot{u}_{base} . The peak responses, or SRS of the SDOF dynamic systems as described by (23.21), will be a fraction Γ_i of the base acceleration SRS of \ddot{u}_{base} .

The acceleration SRS of the generalised coordinate $\ddot{\eta}_i$ is given by

$$SRS(\ddot{\eta}_i) = \Gamma_i SRS(\ddot{u}_{\text{base}}). \quad (23.22)$$

The modal contribution to the SRS of the physical degrees of freedom; $\{z\}$, $\{\dot{z}\}$, $\{\ddot{z}\}$ becomes

$$SRS(\ddot{z}, \omega_i) = \{\phi_i\} SRS(\ddot{\eta}_i), \quad (23.23)$$

and the contribution to the SRS of the velocities

$$SRS(\dot{z}, \omega_i) = \frac{\{\phi_i\} SRS(\ddot{\eta}_i)}{\omega_i}, \quad (23.24)$$

and the contribution to the SRS of the displacement

$$SRS(z, \omega_i) = \frac{\{\phi_i\} SRS(\ddot{\eta}_i)}{\omega_i^2}. \quad (23.25)$$

The SRS of the absolute acceleration $SRS(\ddot{x})$ can be obtained in a similar way as for the SRS for the relative acceleration $SRS(\ddot{z})$.

Example

A simply supported beam with a bending stiffness EI , mass m per unit of length and length L is excited by an enforced acceleration with a SRS shown in Fig. 23.2. The simply supported beam is illustrated in Fig. 23.6. This example is taken from [Biggs 1964]. The length $L = 1$ m, the bending stiffness $EI = 700 \text{ Nm}^2$ and the mass per unit of length $m = 0.3 \text{ kg/m}^2$. The beam is made of an Al-alloy with $E = 70 \times 10^9 \text{ Pa}$.

The equation of motion of the beam is

$$EI \frac{d^4}{dx^4} w + m(\ddot{w} + \ddot{u}) = 0$$

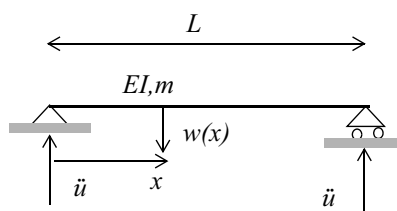


Fig. 23.6 Simply supported beam

Assume a vibration mode $\phi(x)$

$$\phi(x) = \sin \frac{\pi x}{L}$$

The physical deflection of the beam $w(x)$ will be expressed as follows

$$w(x, t) = \eta(t) \sin \frac{\pi x}{L}.$$

The following undamped equation of motion is obtained by multiplying with $\phi(x)$ and taking the integral from $0 \rightarrow L$

$$EI\ddot{\eta}(t)\left(\frac{\pi}{L}\right)^4 \int_0^L \phi^2(x) dx + m\ddot{\eta}(t) \int_0^L \phi^2(x) dx = -m\ddot{u}(t) \int_0^L \phi(x) dx.$$

The previous equation introducing $\omega_o^2 = \frac{EI}{m}\left(\frac{\pi}{L}\right)^4$ and the adhoc modal damping

$2\zeta\omega_o\dot{\eta}(t)$ now becomes

$$\ddot{\eta}(t) + 2\zeta\omega_o\dot{\eta}(t) + \omega_o^2\eta(t) = -\ddot{u}(t) \frac{\int_0^L \phi(x) dx}{\int_0^L \phi^2(x) dx} = -\Gamma\ddot{u}(t) = -\frac{4}{\pi}(\ddot{u}(t))$$

The natural frequency f_o with regard to the vibration mode $\phi(x) = \sin \frac{\pi x}{L}$ is

$$f_o = \frac{1}{2\pi} \sqrt{\frac{EI}{m}\left(\frac{\pi}{L}\right)^4} = 75.9 \text{ Hz.}$$

The acceleration from the acceleration SRS in Fig. 23.2 is

$\ddot{\eta} = SRS(75.9) \approx 90 \text{ g}$. The displacement becomes $\eta = \frac{\ddot{\eta}}{\omega_o^2}$, thus

$$\eta = \frac{90 \times 9.81}{(2\pi \times 75.9)^2} = 3.885 \times 10^{-3} \text{ m.}$$

The absolute value of the bending moment in the middle of the beam is

$$M_{\text{bending}}(L) = EI \frac{d^2}{dx^2} w(L) = \eta EI \left(\frac{\pi}{L}\right)^2 \sin \frac{\pi}{2} = \eta EI \left(\frac{\pi}{L}\right)^2 = 26.8 \text{ Nm.}$$

The extreme fibre of the beam is $e = 0.05 \text{ m}$, so the bending stress becomes

$$\sigma_{\text{bending}}(L) = \frac{M_{\text{bending}}(L)e}{I} = 1.34 \times 10^8 \text{ Pa.}$$

End of example

The total SRS for the absolute acceleration is a particular summation over all the modal contributions $SRS(\ddot{x}, \omega_i)$. In [Gupta 1992] two summation methods were discussed. The first one is an absolute summation taking all modes into account

$$SRS(\ddot{x}) = \sum_{i=1}^n |SRS(\ddot{x}, \omega_i)|, \quad (23.26)$$

and the second one is the Square Root of the Summation of the Squared values, the SRSS value

$$SRS(\ddot{x}) = \sqrt{\sum_{i=1}^n \{SRS(\ddot{x}, \omega_i)\}^2}. \quad (23.27)$$

A combination of (23.26) and (23.27) is given by [Lalanne 2002]

$$SRS(\ddot{x}) = \frac{\sqrt{\sum_{i=1}^n \{SRS(\ddot{x}, \omega_i)\}^2 + p \sum_{i=1}^n |SRS(\ddot{x}, \omega_i)|}}{p+1}, \quad (23.28)$$

where p is a weighting factor.

Example

A four mass-spring system with the discrete mass $m = 5$ kg, the spring stiffness $k = 1000000$ N/m and the damping ratio is $\zeta = 0.05$ ($Q = 10$) is illustrated in Fig. 23.7.

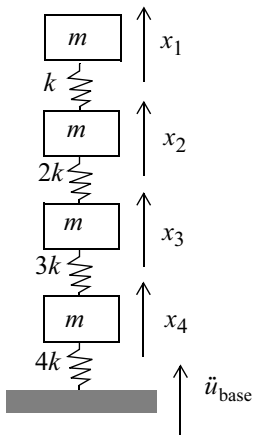


Fig. 23.7 Four mass-spring-system

The base acceleration is:

1. A half-sine pulse $\ddot{u}_{\text{base}} = 200 \sin \frac{\pi t}{\tau}$, $0 = t \leq \tau$ g and $\ddot{u}_{\text{base}} = 0$, $t < 0, t > \tau$
with $\tau = 0.0005$ s.
2. A Shock Response Spectrum based upon a HSP with an amplitude $A = 200$ g,
a time duration $\tau = 0.0005$ s and $Q = 10$.

For both cases the acceleration transient responses $\{\ddot{x}\}$ and the SRS(\ddot{x}, f) will be calculated and compared.

We will solve (23.17)

$$[M]\{\ddot{z}\} + [C]\{\dot{z}\} + [K]\{z\} = -[M]\{T\}\ddot{u}_{\text{base}}$$

applying the modal displacement method (MDM) and taking all 4 modes into account. The absolute displacement vector is $\{x\} = \{z\} + \{u\}$, the absolute velocity vector $\{\dot{x}\} = \{\dot{z}\} + \{\dot{u}\}$ and the absolute acceleration vector $\{\ddot{x}\} = \{\ddot{z}\} + \{\ddot{u}\}$. To calculate the spring forces only the relative displacement vector $\{z\}$ is required. The force matrix $[S]$ is defined as

$$[S] = k \begin{bmatrix} 1 & -1 & 0 & 0 \\ 0 & 2 & -2 & 0 \\ 0 & 0 & 3 & -3 \\ 0 & 0 & 0 & 4 \end{bmatrix}.$$

The forces in the springs are $\{F\} = [S]\{z\}$.

The physical relative degrees of freedom $\{z\}$ are transformed into the generalised coordinates $\{\eta\}$ using the modal matrix $[\Phi]$, thus $\{z\} = [\Phi]\{\eta\}$.

The stress modes can be calculated with

$$[\Phi_\sigma] = [S][\Phi].$$

The decoupled equations of motion expressed in the generalised coordinates $\{\eta\}$ and adding the “ad hoc” modal damping ratio ζ become

$$\ddot{\eta}_i + 2\zeta_i \omega_i \dot{\eta}_i + \omega_i^2 \eta_i = \frac{-\{\phi_i\}^T [M]\{T\}}{\{\phi_i\}^T [M]\{\phi_i\}} \ddot{u}_{\text{base}} = -\Gamma_i \ddot{u}_{\text{base}} = f.$$

To solve the acceleration in the time domain, the Newmark- β method [Wood 1990] will be applied with $\beta = 0.25$ and $\gamma = 0.5$.

$$\{\eta\}_{n+1} = \{\eta\}_n + \Delta t \{\dot{\eta}\}_n + \frac{\Delta t^2}{2} (1 - 2\beta) \{\ddot{\eta}\}_n + \Delta t^2 \beta \{\ddot{\eta}\}_{n+1}$$

$$\{\dot{\eta}\}_{n+1} = \{\dot{\eta}\}_n + \Delta t (1 - \gamma) \{\ddot{\eta}\}_n + \Delta t \gamma \{\ddot{\eta}\}_{n+1}$$

$$[D] = [I] + \gamma \Delta t \langle 2\zeta_i \omega_i \rangle + \beta \Delta t^2 \langle \omega_i^2 \rangle$$

$$[D]\{\ddot{\eta}\}_{n+1} = \{f\}_{n+1} - \langle 2\zeta_i \omega_i \rangle (\{\dot{\eta}\}_n + \Delta t(1-\gamma)\{\ddot{\eta}\}_n) \\ - \langle \omega_i^2 \rangle \left(\{\eta\}_n + \Delta t \{\dot{\eta}\}_n + \frac{\Delta t^2}{2}(1-2\beta)\{\ddot{\eta}\}_n \right).$$

At $t = 0$, $\{\ddot{\eta}\}_1 = \{\ddot{\eta}(0)\}$

$$\{\ddot{\eta}\}_1 = \{f\}_1 - \langle 2\zeta_i \omega_i \rangle \{\dot{\eta}\}_1 - \langle \omega_i^2 \rangle \{\eta\}_1,$$

with the initial conditions

- $\{\dot{\eta}\}_1 = \{\dot{\eta}(0)\} = ([\Phi]^T [\Phi])^{-1} [\Phi]^T \{\dot{z}(0)\}$
- $\{\eta\}_1 = \{\eta(0)\} = ([\Phi]^T [\Phi])^{-1} [\Phi]^T \{z(0)\}$

The natural frequencies $\{f_n\}$ (Hz) and associated mode shapes $[\Phi]$ of the dynamic system illustrated in Fig. 23.7 are

$$\{f_n\} = \begin{Bmatrix} 40.4 \\ 94.0 \\ 151.6 \\ 218.2 \end{Bmatrix} \text{ Hz, } [\Phi] = \begin{bmatrix} 0.7766 & -0.5978 & 0.1972 & -0.0232 \\ 0.5261 & 0.4458 & -0.6974 & 0.1950 \\ 0.3160 & 0.5785 & 0.4372 & -0.6118 \\ 0.1420 & 0.3303 & 0.5325 & 0.7663 \end{bmatrix}.$$

The stress modes become $[\Phi_\sigma] = [S][\Phi]$

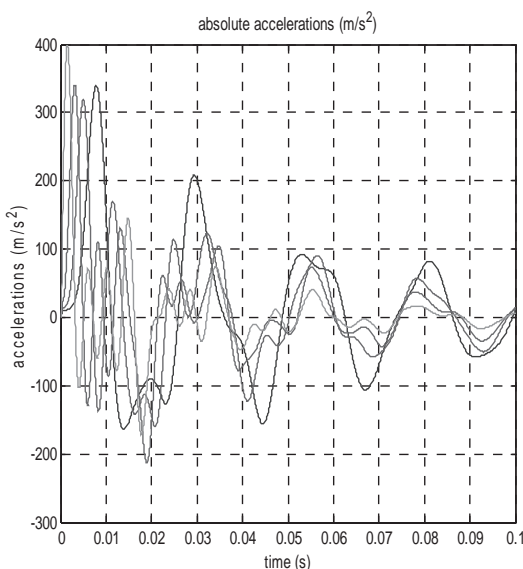


Fig. 23.8 Accelerations

$$[\Phi_\sigma] = 10^6 \begin{bmatrix} 0.2505 & -1.0437 & 0.8946 & -0.2182 \\ 0.4202 & -0.2653 & -2.2693 & 1.6134 \\ 0.5221 & 0.7446 & -0.2857 & -4.1342 \\ 0.5679 & 1.3213 & 2.1299 & 3.0651 \end{bmatrix}.$$

The vector of modal participation factors $\{\Gamma\}$ is

$$\{\Gamma\} = \begin{Bmatrix} 1.7608 \\ 0.7568 \\ 0.4695 \\ 0.3262 \end{Bmatrix}.$$

Question 1

With the initial conditions $z(0) = 0$ and $\dot{z}(0) = 0$ the time accelerations $\{\ddot{x}(t)\}$ are calculated and illustrated in Fig. .2.3.8.

The relative displacement $\{z(t)\}$ is calculated and shown in Fig. 23.9. The time histories of the spring forces $\{F(t)\}$ are illustrated in Fig. 23.10.

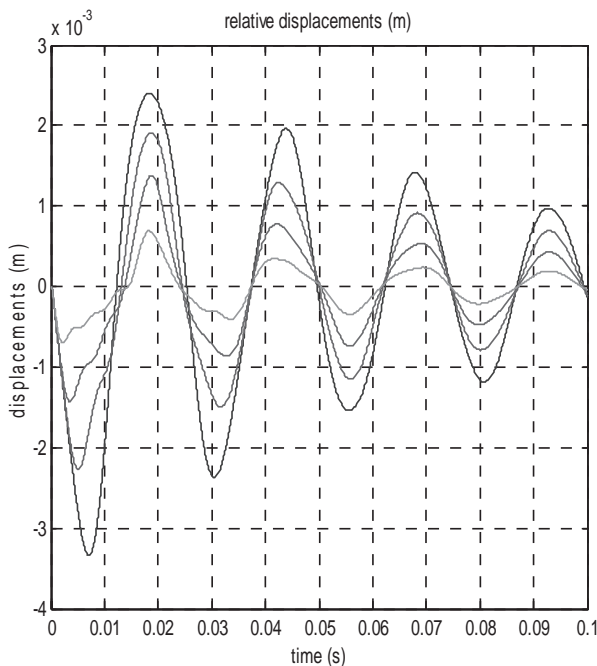
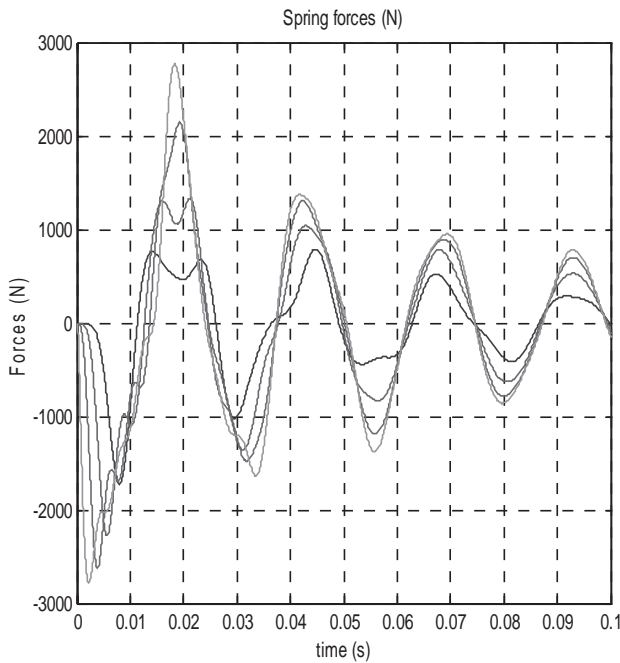


Fig. 23.9 Relative displacements

**Fig. 23.10** Spring forces

The maximum values of the time histories of the absolute acceleration $\{\ddot{x}(t)\}$ and the spring forces $\{F(t)\}$ are given in Table 23.1

Table 23.1 Maximum values of the accelerations and the spring forces

Node #	Absolute acceleration (m/s ²)	Spring #	Spring force (N)
x ₁	340	x ₁ -x ₂	786
x ₂	319	x ₂ -x ₃	1331
x ₃	342	x ₃ -x ₄	2145
x ₄	400	x ₄	2774

Question 2

The Shock spectra for the acceleration and the displacement per mode are given in Table 23.2. The shock spectra per mode are given in Table 23.3, and the absolute and SRSS values of the acceleration in Table 23.4. The calculation of the shock spectra values of the spring force can be found in Table 23.5, and the absolute and SRSS values are given in Table 23.6.

Table 23.2 SRS acceleration/displacement generalised coordinates (Continued)

Mode #	Natural frequency f_i (Hz)	SRS (f_i) (m/s ²)	Modal participation factor Γ_i	Γ_i SRS (f_i) (m/s ²)	$\frac{\Gamma_i \text{SRS}(f_i)}{(2\pi f_i)^2}$ (m)
1	40.4233	147.6260	1.7608	259.9357	4.0294e-3
2	94.0432	342.8672	0.7568	259.4977	0.7432e-3
3	151.6007	550.8845	0.4695	258.6392	0.2851x10 ⁻³
4	218.1650	788.2119	0.3262	257.1538	0.1369x10 ⁻³

Observations

The SRS approach, absolute and SRSS values, bounds the maximum values of the time histories

Table 23.3 Acceleration

Node #	Mode 1 $\{\phi_i\} \Gamma_i \text{SRS}(f_i)$ (m/s ²)	Mode 2 $\{\phi_i\} \Gamma_i \text{SRS}(f_i)$ (m/s ²)	Mode 3 $\{\phi_i\} \Gamma_i \text{SRS}(f_i)$ (m/s ²)	Mode 4 $\{\phi_i\} \Gamma_i \text{SRS}(f_i)$ (m/s ²)
x ₁	201.8738	-155.1394	51.0037	-5.9718
x ₂	136.7599	115.6969	-180.3807	50.1338
x ₃	82.1471	150.1255	113.0865	-157.3186
x ₄	36.9065	85.7168	137.7211	197.0530

Table 23.4 SRS(\ddot{x}) acceleration

Node #	(m/s ²)	(m/s ²)
x ₁	414	260
x ₂	483	259
x ₃	503	259
x ₄	457	258

Table 23.5 Forces per mode (Continued) (Continued)

Spring #	Mode 1 (N)	Mode 2 (N)	Mode 3 (N)	Mode 4 (N)
x_1-x_2	1009.4	-775.7	255.0	-29.9
x_2-x_3	1693.2	-197.2	-646.9	220.8
x_3-x_4	2103.9	553.4	-81.5	-565.8
x_4	2288.4	982.0	607.2	419.5

Table 23.6 Spring forces

Spring #	Sum Absolute values (N)	SRSS (N)	Combination with $p = 1$, (23.28) (N)
x_1-x_2	2070	1299	1685
x_2-x_3	2758	1837	2298
x_3-x_4	3305	2249	2777
x_4	4297	2597	3447

End of example

23.5 Matching Shock Spectra with Synthesised Time Histories

It is not possible to run an SRS on a shaker table, because it has no time history. The calculation of a time history from a given or specified SRS (time-history synthesis) is not unique and the recalculation of a time history is a process of trial and error [Smallwood 1974a]. It is assumed that a time history that results in a SRS in accordance with the given or specified SRS will cause the same damage in the structure under test. However, the time-history synthesis is very much dependent on the physical limitations of the exciter. These limitations are illustrated in Table 23.7 [Smallwood 1974a]:

Table 23.7 Exciter limitations

Limitation #	Initial	Final	Maximum
1	$\ddot{u}_{\text{base}}(0) = 0$	$\ddot{u}_{\text{base}}(T) = 0$	limited
2	$\dot{u}_{\text{base}}(0) = 0$	$\dot{u}_{\text{base}}(T) = 0$	limited
3	$u_{\text{base}}(0) = 0$	$u_{\text{base}}(T) = 0$	limited

The acceleration is actually limited by the force capabilities of the exciter and the start and the final acceleration, velocity and displacement of the applied transient must be zero.

Smallwood [Smallwood 1974a] lists a number of possible transients that meet the limitations indicated in Table 23.7:

- Sums of decaying sinusoids
- Sum of waveforms
- Shaker optimised cosines
- Fast sine sweeps
- Modulated random noise
- Classical pulses

A discussion of all possible techniques for time-history synthesis is beyond the scope of this book. Only summation of decaying sinusoids will be discussed.

Decaying sinusoids

The equation of motion for the relative motion $z(t)$ is (23.2)

$$\ddot{z}(t) + 2\zeta\omega_n\dot{z}(t) + \omega_n^2 z(t) = -\ddot{u}(t).$$

The solution of (23.2), with initial condition with respect to displacement $z(0)$ and velocity $\dot{z}(0)$ is (23.4)

$$\begin{aligned} z(t) &= z(0)e^{-\zeta\omega_n t} \left(\cos\omega_d t + \frac{\zeta}{\sqrt{1-\zeta^2}} \sin\omega_d t \right) \\ &\quad + \dot{z}(0)e^{-\zeta\omega_n t} \frac{\sin\omega_d t}{\omega_d} - \int_0^t e^{-\zeta\omega_n(\tau-t)} \frac{\sin\omega_d(\tau-t)}{\omega_d} \ddot{u}(\tau) d\tau. \end{aligned}$$

For SRS calculations $z(0) = \dot{z}(0) = 0$, hence

$$z(t) = - \int_0^t e^{-\zeta\omega_n(\tau-t)} \frac{\sin\omega_d(\tau-t)}{\omega_d} \ddot{u}(\tau) d\tau = - \int_0^t e^{-\zeta\omega_n(t-\tau)} \frac{\sin\omega_d(t-\tau)}{\omega_d} \ddot{u}(\tau) d\tau$$

If the base excitation \ddot{u} is equal to the Dirac delta function $\delta(\tau)$ then

$$\ddot{z}(t) = -e^{-\zeta\omega_n t} \frac{\sin\omega_d t}{\omega_d} = -h(t), \quad t \geq 0. \quad (23.29)$$

Assuming $\ddot{z}(t)$ is the acceleration response of one of the generalised coordinates of the uncoupled equations of motion, the transient response of a structure consists of the superposition of decaying sinusoids that have been exposed to shocks (delta functions). Thus, excitation consisting of sums of decaying sinusoids appears to be a natural choice [Nelson 1974] as a transient vibration test of sub-

structures and components exposed to shock environments. The usual basic decaying sinusoid is given by [Smallwood 1974b]

$$g_i(t) = \begin{cases} A_i e^{-\zeta_i \omega_i t} \sin(\omega_i t) & , t \geq 0 \\ 0 & , t < 0 \end{cases}. \quad (23.30)$$

The associated velocity $v_i(t) = \int_0^t g_i(\tau) d\tau$, with $v_i(0) = 0$ becomes

$$v_i(t) = \frac{A_i \{e^{-\zeta_i \omega_i t} [\cos(\omega_i t) + \zeta_i \sin(\omega_i t)] - 1\}}{\omega_i (\zeta_i^2 + 1)}, \quad (23.31)$$

and the corresponding displacement $s_i(t) = \int_0^t v_i(\tau) d\tau$, with $s_i(0) = 0$ is

$$s_i(t) = \frac{A_i \left\{ e^{-\zeta_i \omega_i t} [2\zeta_i \cos(\omega_i t) - \sin(\omega_i t) + \zeta_i^2 \sin(\omega_i t)] + \zeta_i^2 \omega_i t + \zeta_i \omega_i t - 2\zeta_i \right\}}{\omega_i^2 (\zeta_i^2 + 1)^2}, \quad (23.32)$$

with $A_i = 1 \text{ m/s}^2$ the amplitude, $\zeta_i = 0.05$ the decay rate and $\omega_i = 25 \text{ Rad/s}$, circular frequency.

The plot in Fig. 23.11 shows that the velocity and the displacement transients do not converge to zero with increasing time, i.e. the constraints as stated in Table 23.7 are thus violated when basis decaying sinusoids are applied.

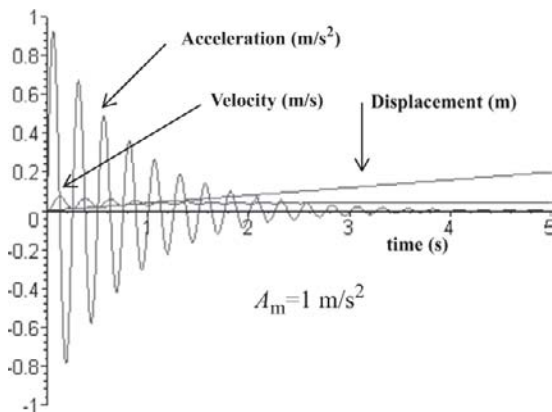


Fig. 23.11 Acceleration, velocity and displacement associated with the associated decaying sinusoids.

Velocity and displacement compensation is needed to achieve zero velocity and displacement with increasing time. Smallwood and Nord [Smallwood 1974b] and Nelson and Prasthofer [Nelson 1974] suggested compensation methods to obtain zero velocity and displacement with increasing time.

Smallwood and Nord

$$\ddot{u}_{\text{base}} = \sum_{i=1}^n g_i(t) + U(t+\tau) A_m e^{-\zeta_m \omega_m (t+\tau)} \sin \omega_m (t+\tau) \quad (23.33)$$

$$g_i(t) = A_i U(t-\tau_i) e^{-\zeta_i \omega_i (t-\tau_i)} \sin \omega_i (t-\tau_i), \quad (23.34)$$

with

- $A_m = -\omega_m (1 + \zeta_m^2) \sum_{i=1}^n \frac{A_i}{\omega_i (1 + \zeta_i^2)}$.
- $\tau = \frac{\omega_m (1 + \zeta_m^2)}{A_m} \left\{ \frac{2\zeta_m A_m}{\omega_m^2 (1 + \zeta_m^2)^2} + \sum_{i=1}^n \left[\frac{A_i \tau_i}{\omega_i (1 + \zeta_i^2)} + \frac{2\zeta_i A_i}{\omega_i^2 (1 + \zeta_i^2)^2} \right] \right\}$.
- $U(t)$ is the unit step function, $U(t) = 0, t < 0$ and $U(t) = 1, t \geq 0$.
- The decaying sinusoids $g_i(t)$ are in fact $g_i(t-\tau)$ and start after τ (s), and the correcting time history $A_m e^{-\zeta_m \omega_m (t+\tau)} \sin \omega_m (t+\tau)$ is, in fact, $A_m e^{-\zeta_m \omega_m t} \sin \omega_m (t)$ and starts at $t=0$.

The magnitude A_m and the shift τ of the velocity and the displacement compensating pulse are fixed by the other parameters.

Nelson and Prasthofer

$$\ddot{u}_{\text{base}} = \sum_{i=1}^n g_i(t) \quad (23.35)$$

$$g_i(t) = A_i \{(K_1 e^{-at} - K_2 e^{-bt}) + K_3 e^{-ct} \sin(\omega_i t + \theta)\}, \quad (23.36)$$

with

$$\bullet \quad K_1 = \frac{\omega_d a^2}{(a-b)[(c-a)^2 + \omega_d^2]}$$

- $K_2 = \frac{\omega_d b^2}{(a - b)[(c - b)^2 + \omega_d^2]}$
- $K_3 = \sqrt{\frac{(c^2 - \omega_d^2)^2 + 4c^2\omega_d^2}{[(b - c)^2 + \omega_d^2][(a - c)^2 + \omega_d^2]}}$
- $\theta = \text{atan}\left(\frac{-2c\omega_d}{c^2 - \omega_d^2}\right) - \text{atan}\left(\frac{\omega_d}{a - c}\right) - \text{atan}\left(\frac{\omega_d}{b - c}\right)$
- $a = \frac{\omega_i}{2\pi}$
- $b = 2\zeta_i\omega_i$
- $c = \zeta_i\omega_i$
- $\omega_d = \omega_i\sqrt{1 - \zeta_i^2}$

The normalised peak acceleration response of decaying sinusoids is the SRS divided by the maximum value of the decaying sinusoid $g_i(t)$. The maximum value of the decaying sinusoid (g) is

$$g_{\max} = A_i e^{-\zeta_i \omega_i \text{atan}\left(-\frac{1}{\zeta_i}\right)} \sin\left\{\omega_i \text{atan}\left(-\frac{1}{\zeta_i}\right)\right\} \quad (23.37)$$

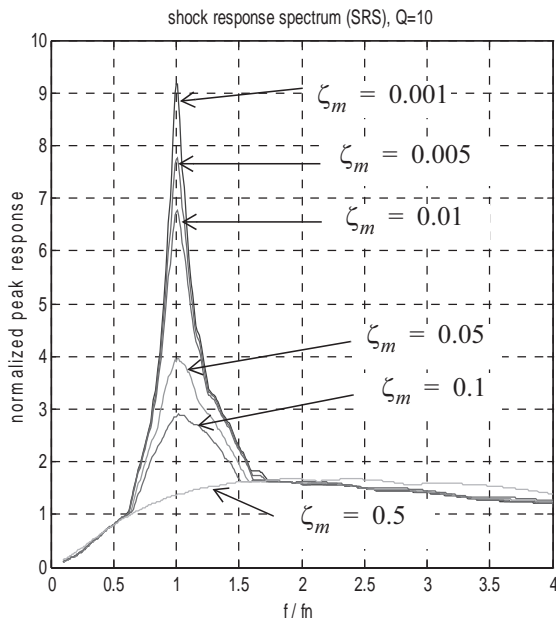


Fig. 23.12 Normalised peak response of a decaying sinusoid

The normalised peak acceleration response of a decaying sinusoid is illustrated in Fig. 23.12. Fig. 23.13 [Smallwood 1974a] proposes a flow diagram that can be applied to select decaying sinusoids to match a given shock response-spectrum to estimate the amplitude A_i in conjunction with the frequency ω_i and the decay rate ζ_i .

Example

In this example the decaying sinusoids of Smallwood and Nord will be applied to match the SRS as illustrated in Fig. 23.5

This SRS is based upon the half-sine pulse (HSP), $\ddot{u}_{base} = 200 \sin \frac{\pi t}{\tau}$ g,

$0 \leq t \leq \tau = 0.0005$ s. The procedure, as illustrated in Fig. 23.13, will be used to match the SRS with decaying sinusoids.

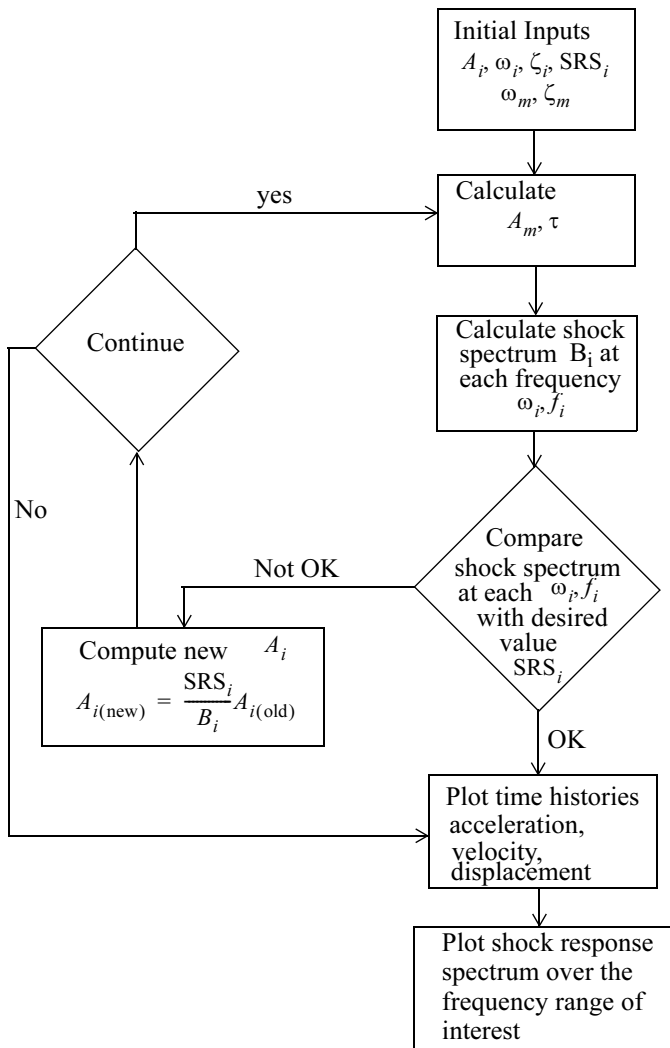


Fig. 23.13 Flow diagram for selecting decaying sinusoids to match a given shock-response spectrum [Smallwood 1974b]

The SRS will be matched with the following values, see Table 23.8.

Table 23.8 Components of decaying sinusoids [Smallwood 1974b]

Frequency #	f_i ((Hz))	ζ_i (%)	A_i (g)	τ_i (s)
1	250	20	35	0
2	500	10	50	0
3	750	10	68	0
4	1000	5	47	0
5	1250	5	47	0
6	1500	5	46	0
f_m (Hz)		ζ_m (%)	A_m (g)	τ (s)
7	100	100	-87.7	0.0015

The matched acceleration time history of the combined Smallwood decaying sinusoids is illustrated in Fig. 23.15. The trapezoidal rule [Schwarz 1989] was applied to calculate the velocity $v(t)$ and displacement $s(t)$ time histories.

$$v(t + \Delta t) = v(t) + 0.5\Delta t\{\ddot{u}(t) + \ddot{u}(t + \Delta t)\} \quad (23.38)$$

$$s(t + \Delta t) = s(t) + 0.5\Delta t\{v(t) + v(t + \Delta t)\}. \quad (23.39)$$

Several numerical integration methods, trapezoidal rule, Simpson's rule and the Newton–Cotes method, are described in [Hairer 1996]. A very popular numerical integration method is Simpson's rule, with $x_k = a + kh$, $x_n = b$,

$$\int_a^b f(x)dx \approx h[f(x_0) + 4f(x_1) + 2f(x_2) + 4f(x_3) + 2f(x_4) + \dots + f(x_n)]. \quad (23.40)$$

The velocity time history is shown in Fig. 23.17, and the displacement time history in Fig. . The original SRS and the matched SRS are both shown in Fig. 23.18.

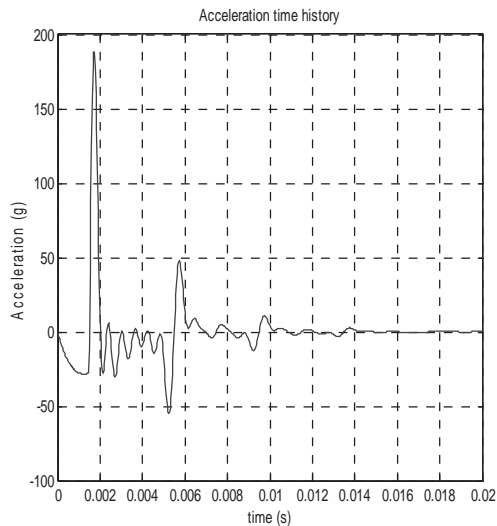


Fig. 23.14 Displacement time history of combined Smallwood decaying sinusoids

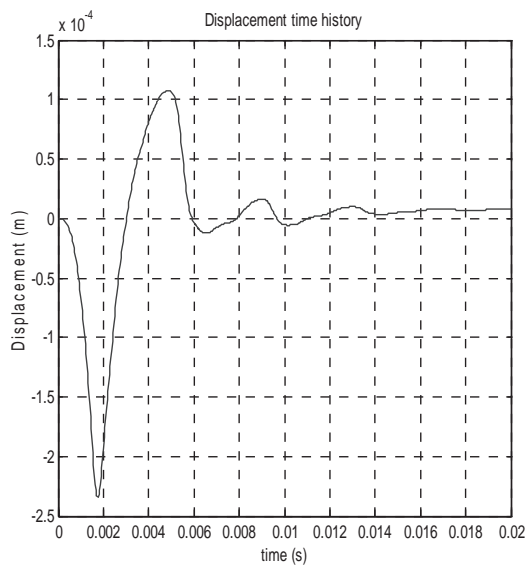


Fig. 23.15 Matched acceleration time history of combined Smallwood decaying sinusoids

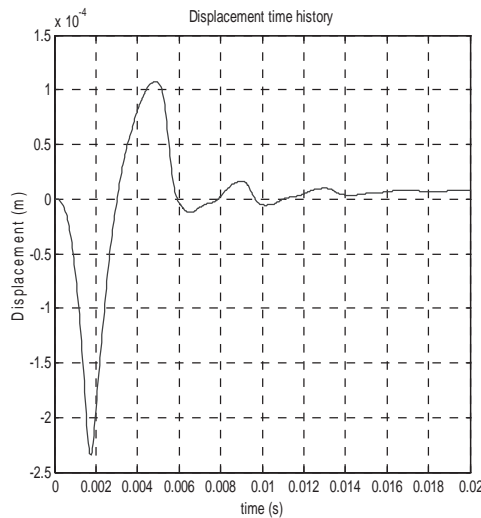


Fig. 23.16 Displacement time history of combined Smallwood decaying sinusoids

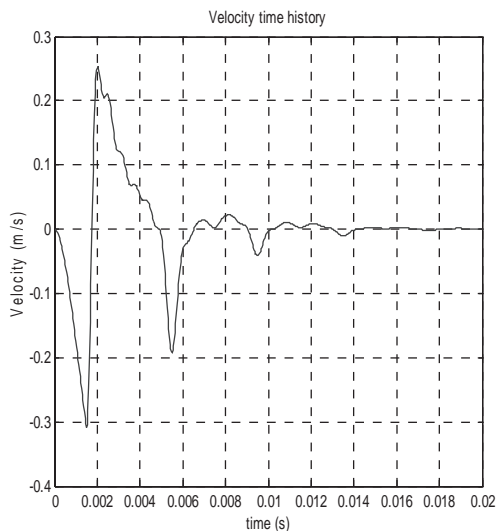


Fig. 23.17 Velocity time history of combined Smallwood decaying sinusoids

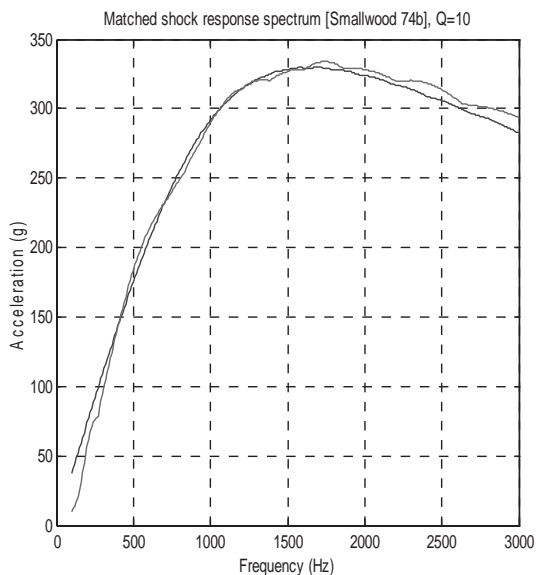


Fig. 23.18 Original and matched SRS

23.6 Literature

- Assink, F.C.J., 1995, *Guidelines for the calculation of Shock Response Spectra*, Memo Environmental Test Laboratory, Signaal, RDT/950828/02, The Netherlands, [in Dutch].
- Biggs, J.M., 1964, *Introduction to Structural Dynamics*, Mc-Graw-Hill.
- Ebeling, R.M., Green, R.A., French, S.E., 1997, *Accuracy of Response of Single-Degree-of-Freedom Systems to Ground Motion*, Technical Report ITL-97-7, US Army Corps of Engineers, WES.
- Grygier, M.S., 1997, *Payload Loads Design Guide*, Lyndon B. Johnson Center, NASA.
- Gupta, A.K., 1992, *Response Spectrum Method in Seismic Analysis and Design of New Structures*, ISBN 0-8493-8628-4, CRC Press.
- Hairer, E., Wanner, G., 1996 *Analysis by Its History*, ISBN 0-387- 94551-2, Springer.
- Kelly, R.D., Richman, G., 1969, *Principles and Techniques of Shock Data Analysis*, SVM-5, The Shock and Vibration Information Centre, US DoD.
- Lalanne, C., 2002, *Mechanical Vibration & Shock, Mechanical Shock, Volume II*, HPS, ISBN 1 9039 9604 X.
- Mulville, D.R., 1999, *Pyroshock Test Criteria*, NASA Technical Standard, NASA-STD-7003, May 18, <http://standards.nasa.gov>.
- Nelson, D.B., Prasthofer, P.H., 1974 *A Case for Damped Oscillatory Excitation as a Natural Pyrotechnic Shock Simulation*, Shock and Vibration Bulletin, No 44, Part 3, pages 67–71.
- Nigam, N.C., Jennings, P.C., 1968, *Digital Calculation of Response from Strong-Motion Earthquake Records*, California Institute of Technology, printed in STARDYNE Theoretical Manual, III. DYNRE5 Program Analysis.
- Schwarz, H.R., 1989, *Numerical Analysis, A Comprehensive Introduction*, Wiley, ISBN 0 471 92064 9, Third edition.
- Smallwood, D.A., 1974 a, *Time History Synthesis for Shock Testing on Shakers*, Shock and Vibration Bulletin, No 44, Part 3, pages 23–41.
- Smallwood, D.A., Nord, A.R., 1974 b, *Matching Shock Spectra with Sums of Decaying Sinusoids Compensated for Shaker Velocity and Displacement Limitations*, Shock and Vibration Bulletin, No 44, Part 3, pages 43–56.
- Wood, W.L., 1990, *Practical Time-stepping Schemes*, Oxford Applied Mathematics and Computing Science Series, ISBN 0-19-853208-3.
- Wijker, J.J., 2004, *Mechanical Vibrations in Spacecraft Design*, Springer, ISBN 3-540-40530-5.

23.7 Exercises

23.7.1 Calculation of Shock Response Curves

Calculate, using the Wilson-θ method, the absolute acceleration SRS of the following 4 pulses:

1. Rising triangular pulse
2. Decaying triangular pulse
3. Rectangular pulse
4. Half-sine pulse

and illustrate the SRSs in one figure. The pulses start at $t = \tau = 0.0005$ s and the duration $t_{\text{duration}} = \tau$. The amplitudes of the pulses are unity. The results obtained with Kelly's numerical approach are illustrated in Fig. 23.19.

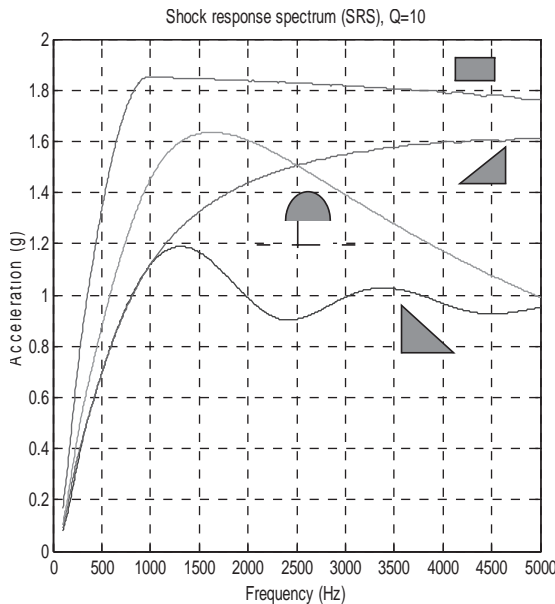


Fig. 23.19 SRS of rising and decaying triangular pulse, rectangular pulse and the half sine pulse

The equation of relative motion $z(t)$ of an SDOF dynamic system, exposed to a base acceleration $\ddot{u}(t)$, is given by (23.2)

$$\ddot{z}(t) + 2\zeta\omega_n\dot{z}(t) + \omega_n^2 z(t) = -\ddot{u}(t).$$

The constant time increment is $\Delta t = t_{j+1} - t_j$.

The Wilson-θ method is defined as follows [Wood 1990]

$$\{Z_{j+1}\} = [A_\theta]\{Z_j\} + \{F_\theta\},$$

with

- $\{Z_j\} = \begin{bmatrix} z_j \\ \Delta t \dot{z}_j \end{bmatrix}$
- $[A_\theta] = D_\theta^{-1} \begin{bmatrix} 1 + 2\Delta t \theta \zeta \omega_n - \theta(1-\theta) \Delta t^2 \omega_n^2 & 1 \\ -\Delta t^2 \omega_n^2 & 1 - (1-\theta)2\Delta t \zeta \omega_n - \theta(1-\theta) \Delta t^2 \omega_n^2 \end{bmatrix}$
- $D_\theta = 1 + 2\Delta t \theta \zeta \omega_n + \theta^2 \Delta t^2 \omega_n^2$

- $\{F_\theta\} = -\Delta t^2 D_\theta^{-1} \begin{bmatrix} \theta \{\theta \ddot{u}_{j+1} + (1-\theta) \ddot{u}_j\} \\ \{\theta \ddot{u}_{j+1} + (1-\theta) \ddot{u}_j\} \end{bmatrix}$

- $\theta = 0.5$
- j is the time step

and the absolute acceleration \ddot{x} of the SDOF system is

$$\ddot{x}_{j+1} = -2\zeta\omega_n \dot{z}_{j+1} - \omega_n^2 z_{j+1}.$$

23.7.2 Problem 2

Match the SRS of a half-sine pulse (Fig. 23.5) with decaying sinusoids using the proposed method of Nelson and Prasthofer [Nelson 1974],

$$\ddot{u}_{\text{base}} = 200 \sin \frac{\pi t}{\tau} \text{ g}, \quad 0 \leq t \leq \tau = 0.0005 \text{ s}, \quad \text{elsewhere } \ddot{u}_{\text{base}} = 0.$$

24 Damage to Spacecraft by Meteoroids and Orbital Debris

24.1 Introduction

Millions of meteoroids orbit around the sun and cross the orbit of the Earth around the sun.

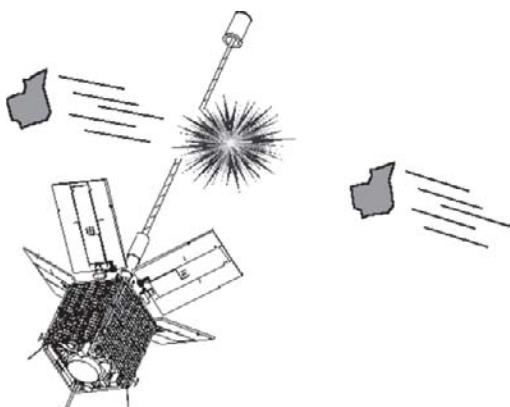


Fig. 24.1 Space debris collision with CERISE micro satellite stabilisation boom at 14 km/s in LEO (Courtesy SSTL)

Surrey Satellite Technology Ltd (SSTL) manufactured the CERISE micro satellite for Alcatel Espace (France) and the French MoD to carry out broad band radiometric measurements. CERISE was launched by Ariane in July 1995.

Many aspects about meteoroids and orbital debris environmental conditions and counter measures are discussed [IADC 2004].

24.2 Micro-Meteoroids and Space Debris Environment

The flux of particles for micro meteoroids and orbital debris are given in terms of the integral flux, which is the number of particles per m^2 per year of mass larger than or equal to m or diameter equal to or larger than d , impacting a randomly-orientated flat plate under a viewing angle of 2π radians.

24.2.1 Micro-Meteoroids Environment

The flux of micro-meteoroids (MM) is not constant but varies through the years. This is due to the micro-meteoroid showers (see Table 24.1). This happens if the orbit of the Earth crosses the orbits of the comets.

Table 24.1 Meteor showers [Tribble 2003]

Name	Date
Quantrantids	January 1–6
Lyrids	April 19–24
Eta Aquarids	May 2–7
Delta Aquarids	July 15–August 15
Perseids	July 27–August 17
Orionids	October 12–16
Taurids	October 26–November 25
Leonids	November 15–19
Geminids	December 7–14

Spacecraft have mission durations varying from some weeks to several years, therefore the mean flux of the MM's is sufficient to analyse the effects of MM's on spacecraft. The interplanetary flux of MM can be defined with the following Gruens formula [Drolshagen 1992, Tribble 2003]

$$F_{\text{MM}} = c_0 \{F_1(m) + F_2(m) + F_3(m)\} \text{ m}^{-2}/\text{year} \quad (24.1)$$

where

$$F_1(m) = (c_1 m^{0.306} + c_2)^{-4.38}$$

$$F_2(m) = c_3 (m + c_4 m^2 + c_5 m^4)^{-0.36}$$

$$F_3(m) = c_6 (m + c_7 m^2)^{-0.85}$$

$$c_0 = 3.15576 \times 10^7, c_1 = 2.2 \times 10^3, c_2 = 15, c_3 = 1.3 \times 10^{-9},$$

$$c_4 = 1 \times 10^{11}, c_5 = 1 \times 10^{27}, c_6 = 1.3 \times 10^{-16} \text{ and } c_7 = 1 \times 10^6$$

The function F_1 refers to large particles ($m > 1 \times 10^{-9}$ g), function F_2 to intermediate-sized particles ($1 \times 10^{-14} \leq m \leq 1 \times 10^{-9}$ g) and function F_3 to small particles ($m \leq 1 \times 10^{-14}$ g).

The average velocity of the MM particles is about 17 km/s. The velocity ranges from 11 to 72 km/s. The NASA 90 velocity density is analytically defined by

$$f(v) = \begin{cases} 0.112 & \text{if } 11.1 \leq v \leq 16.3 \text{ km/s} \\ 3.328 \times 10^5 v^{-5.34} & \text{if } 16.3 \leq v \leq 55 \text{ km/s} \\ 1.695 \times 10^{-4} & \text{if } 16.3 \leq v \leq 72.2 \text{ km/s} \end{cases} \quad (24.2)$$

The MM flux F_{MM} shall be corrected to account for Earth shielding. The correction parameter $\xi(h)$ is given by

$$\xi_{\text{mean}}(h) = \frac{1 + \cos \theta}{2}, \quad (24.3)$$

where h (km) is the height of the orbit and the angle θ is defined as

$$\sin \theta = \frac{R_E + 100}{R_E + h}, \quad (24.4)$$

with R_E the mean radius of the Earth (6378 km) and $h \geq 100$ km.

Due to the gravitational field of the Earth, meteoroid particles are attracted and the flux increases compared with deep space. This effect is taken into account by the defocusing factor G_E , that is

$$G_E = 1 + \frac{R_E + 100}{R_E + h}. \quad (24.5)$$

For planes pointing to Earth the MM flux will be reduced with a factor of 10. The reduction factor F_{dir} is defined by

$$F_{\text{dir}}(h) = \frac{1.8 + 3 \sqrt{1 - \left(\frac{R_E + 100}{R_E + h}\right)^2}}{4} \quad (24.6)$$

Considering the Earth shielding, the gravitational defocussing and the direction reduction factor will lead to a particle flux

$$F_C(m, h) = F_{\text{MM}}(m) G_E(h) \xi_{\text{mean}}(h) F_{\text{dir}}(h) \quad (24.7)$$

24.2.2 Orbital debris Environment

The orbital debris (OD) is encountered in orbits around the Earth with an approximate velocity 8 km/s. The OD is dependent on the diameter d (cm) of the OD particle and is given in a number of OD particles per year and per m^2

$$F_{\text{OD}} = H(d)\Phi(h, S)\Psi(i)[F_1(d)g_1(t) + F_2(d)g_2(t)] \quad (24.8)$$

where

$$H(d) = \sqrt{\left[10^{e^{-\frac{(\log d - 0.78)^2}{0.637}}} \right]}, \quad \text{this function is called the Henize function}$$

$$H(x, y) = \sqrt{10^{e^{\frac{x^2}{y}}}}$$

$$\Phi(h, S) = \frac{\Phi_1(h, S)}{\Phi_1(h, S) + 1}, \quad \text{and } \Phi_1(h, S) = 10^{\left(\frac{h}{200} - \frac{S}{140} - 1.5\right)}$$

$$F_1(d) = 1.22 \times 10^{-5} d^{2.5}, \quad \text{and } F_2(d) = (8.1 \times 10^{10})(d + 700)^{-6}$$

$$g_1(t) = (1 + q)^{(t - 1988)}, \quad \text{and } g_2(t) = 1 + p(t - 1988)$$

The height is $h < 2000$ (km), the angle of orbital inclination i is in degrees, the time t is n years with $t \leq 2011$. The assumed growth rate of intact objects is $p \approx 0.05$ and the estimated growth rate of fragments is $q \approx 0.02$.

The function $\Psi(i)$ gives the relation between the orbital inclination and the OB flux.

The function is given in the following Table 24.2.

Table 24.2 Inclination dependent function $\Psi(i)$

Inclination i (degrees)	$\Psi(i)$
up to 28.5	0.91
30	0.92
40	0.96
50	1.02
60	1.09
70	1.26
80	1.71
90	1.37
100	1.78
120	1.18
up to 360	1.18

S , the 13-month smoothed solar radio flux with a wave length of 10.7 cm ($F_{10.7}$) for year $t - 1$, is expressed in 1×10^4 J. A typical value of the solar radio flux is $S = 100$.

The solar radio flux $F_{10.7}$ is given in Table 24.3.

Table 24.3 $F_{10.7}$ in year $t - 1$

$F_{10.7}$ in year		$F_{10.7}$ in year	
Year	$t - 1$	Year	$t - 1$
2005	118	2014	180
2006	80	2015	137
2007	76	2016	118
2008	74	2017	80
2009	75	2018	76
2010	106	2019	74
2011	163	2020	75
2012	198	2021	106
2013	190	2022	163

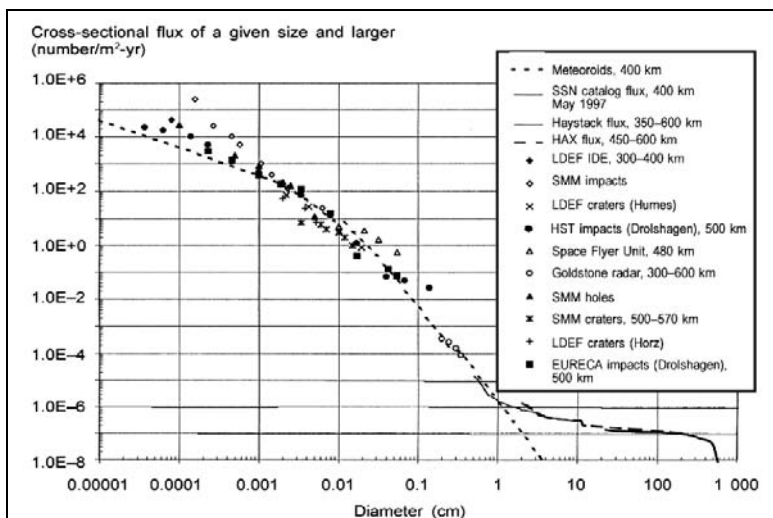


Fig. 24.2 Approximate measured debris flux in low Earth orbit, by object size [ISIS 2000]

For bodies in LEO, whether orbital debris or spacecraft, there is only a small change in speed versus altitude even out to 2000 km, and the average speed is about 7.7 km/s (at 500 km). However, because different objects are in different orbits, collisions are possible between 0–15.4 km/s, with an average speed of about 10 km/s.

Fig. 24.2 presents a compilation of the results of many of the measurement systems described in previous sections. It shows the cross-sectional flux (number of objects per year per square metre) for objects of a given size and larger. The figure summarizes measurements in LEO near an altitude of 500 km.

The development of MOD protection systems allows the designers to reduce the risk of spacecraft failure. Risk may be defined as the probability of critical failure or loss of spacecraft, or simply the probability of any spacecraft malfunction. The decision to protect a spacecraft is governed by the compromise between accepting a reasonable level of risk, and the cost of implementing protection methods. A flowchart which illustrates the general algorithm involved in the development of MOD threat assessment is shown in Fig. 24.3.

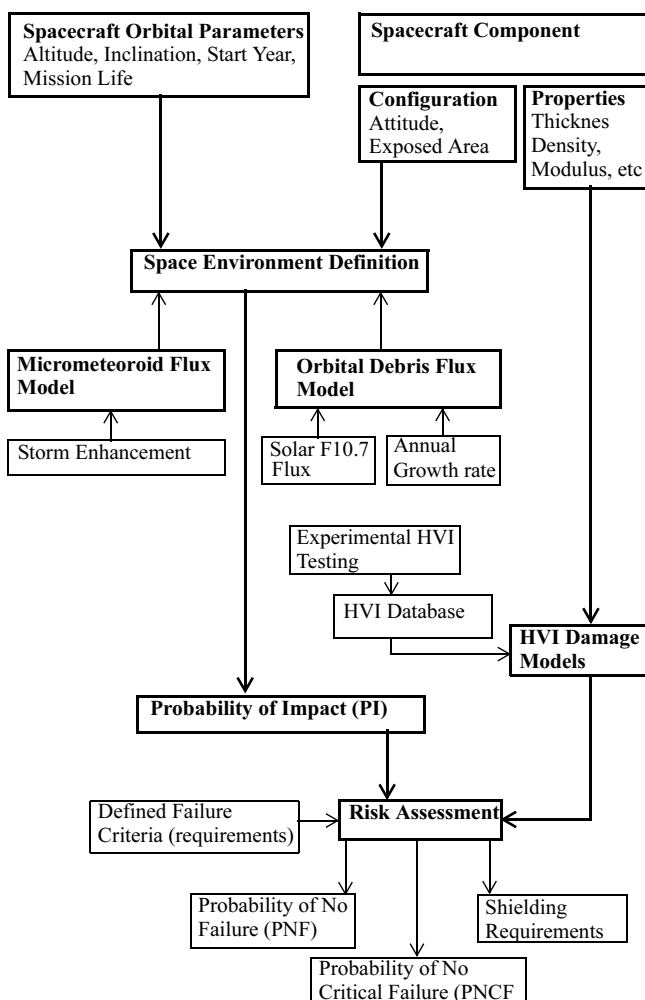


Fig. 24.3 MOD threat assessment flowchart

24.3 Hyper Velocity Impact Damage Models

Many impact damage models are discussed in [Elfer 1996, IADC 2004].

24.3.1 Single Plate Penetration Equations

The following equation was developed by Fish and Summers [Hayashida 1991]. They used test results with velocities which ranged from 0.5–8.5 km/s, metallic targets which ranged in density from magnesium-lithium alloy to beryllium-copper alloy, and with aluminium alloy. The velocity vector is perpendicular to the plate. This equation was recommended for design to establish the threshold penetration (ballistic limit) of thin, ductile, metal plates.

$$t = K_1 m_p^{0.352} v_p^{0.875} \rho_p^{\frac{1}{6}}, \quad (24.9)$$

where t is the target thickness (cm), m_p is the projectile mass (gr), v_p is the impact velocity (km/s), ρ_p is the projectile density (gr/cm³) and K_1 is a constant $K_1 = 0.57$ for Al-alloys such as 2024-T3, 2024-T4, 6061-T6 and 7075-T6. $K_1 = 0.70$ was used to determine the plate thickness to prevent penetration from spalling (spallation limit).

The mass density ρ_p (gr/cm³) of the projectile is discussed in [Drolshagen 1992] and can be obtained by the following equation

$$\rho_p(d) = \frac{2.8}{d^{0.74}}, \quad (24.10)$$

where the projectile diameter d is in (cm).

If a spherical particle is assumed, the mass m_p (gr) can be expressed in the density ρ_p (gr/cm³) and the diameter d_p (cm)

$$m = \frac{1}{6}\pi\rho d^3. \quad (24.11)$$

The cratering or depth of penetration p (cm) in a single wall is given by [Elfer 1996]

$$p = K_1 m_p^{0.352} v_p^{0.667} \rho_p^{\frac{1}{6}}, \quad (24.12)$$

where $K_1 = 0.42$ for Al-alloys and $K_1 = 0.25$ for 304 and 316 stainless steel.

The entry crater diameter D_c (mm) for composite materials in space is given by [Tennyson 1997]

$$D_c = 1.05 \sqrt[3]{\frac{E_{\text{kin}} t \rho_t}{D_p \rho_p}}. \quad (24.13)$$

where E_{kin} the kinetic energy of the projectile (J), $E_{\text{kin}} = \frac{1}{2} m_p v_p^2$, D_p diameter of projectile (mm), ρ_t and ρ_p are the target and projectile densities and t the target thickness (mm).

The model is applicable to PEEK and epoxy matrix based composites. The carbon fibres used all have a modulus in between 135–235 GPa. Applicable laminate thicknesses range from 0.5–6.7 mm. The model is independent of the laminate lay-up. The model is consistent for a broad band of projectile diameters, extending from 0.4–9.13 mm, travelling at velocities ranging from 4–7.5 km/s. Al-alloy, glass, nylon and steel projectiles are compatible with the model.

24.3.2 Multi-shock shield

The **Whipple Shield** is the first spacecraft shield ever implemented. It was introduced by Fred Whipple back in the 1940s, and is still in use today. Basically, it consists of placing a sacrificial bumper, usually aluminium, in front of the spacecraft, thus allowing it to absorb the initial impact. The Whipple bumper shocks the projectile and creates a debris cloud containing smaller, less lethal, bumper and projectile fragments. The full force of the debris cloud is diluted over a larger area on the spacecraft rear wall. The Whipple shield is illustrated in Fig. 24.4.

The **Stuffed Whipple Shield** is a variation of the simple Whipple shield. Layers of Nextel and Kevlar are inserted in between the bumper and the rear wall. These additional layers further shock and pulverize the debris cloud such that any fragments reaching the rear wall are benign.

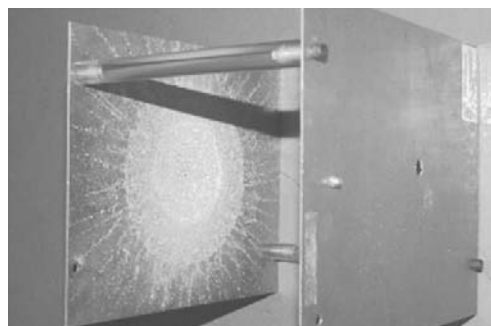


Fig. 24.4 Whipple Shield [hitf.jsc.nasa.gov]



Fig. 24.5 Stuffed Whipple Shield

In this section only the equations for the whipple shield are given. The equations for other type of shield can be found in [Elfer 1996].

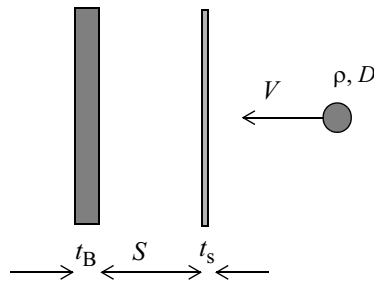


Fig. 24.6 Whipple shield

Examples from the International Space Station (ISS) [NRS 1997]. These applications are shown in Fig. 24.7.

Whipple Shield

The distance between the rear wall is in general $S \geq 15D$ and the thickness of the bumper shield

$$t_b = \frac{c_b m_p}{\rho_b} = \frac{c_b D \rho_p}{\rho_b}, \quad (24.14)$$

where t_b is the thickness of the bumper shield (cm), m_p is the mass of the particle (gr), ρ_b is the density of the bumper material (g/cm^3) and ρ_p is the density of the particle (g/cm^3). The constant c_b depends upon the ratio of the distance S and the particle diameter D .

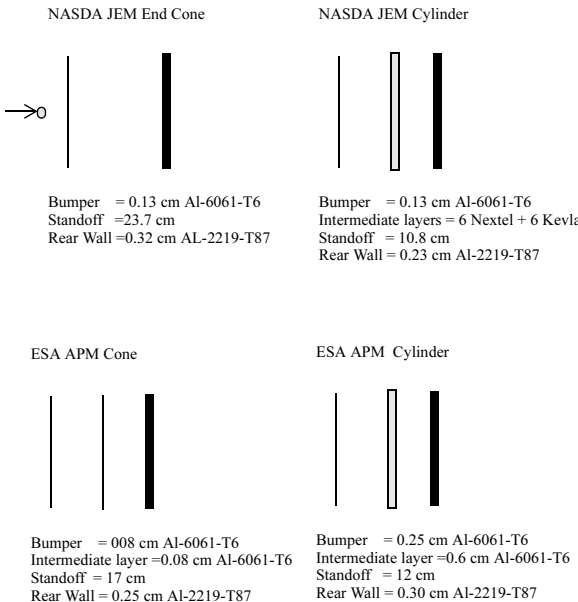


Fig. 24.7 Examples ISS shield configurations [NRC 1997]

$$c_b = \begin{cases} 0.25 & \frac{S}{D} < 30 \\ 0.20 & \frac{S}{D} \geq 30 \end{cases} \quad (24.15)$$

The thickness of the rear wall t_w , to prevent spall detachment, can be calculated [Drolhagen 1992]

$$t_w = c_w (\rho_p \rho_b)^{\frac{1}{6}} m_p^{\frac{1}{3}} \frac{V}{\sqrt{S}} \sqrt{\frac{70}{\sigma_y}} \quad (24.16)$$

where

- t_w is the threshold rear wall sheet thickness (cm)
- ρ_b is the rear wall material density (g/cm^3)
- ρ_p is the projectile density (g/cm^3)
- S the spacing between shield and rear wall
- V the speed of the projectile $6 < V < 9.8 \text{ km/s}$
- σ_y the yield stress in (ksi)

Equations for multi shock shield can be found in the literature, especially in [Elfer 1996].

24.4 Probability of Impacts

The probability that k meteoroids or particles of orbital debris will have a collision with a spacecraft can be estimated with Poisson (Simeon-Denis Poisson 1781–1840) probability density function

$$p_k = e^{-\lambda} \frac{\lambda^k}{k!}, k = 0, 1, \dots . \quad (24.17)$$

The probability density function of Poisson is illustrated in Fig. 24.8.

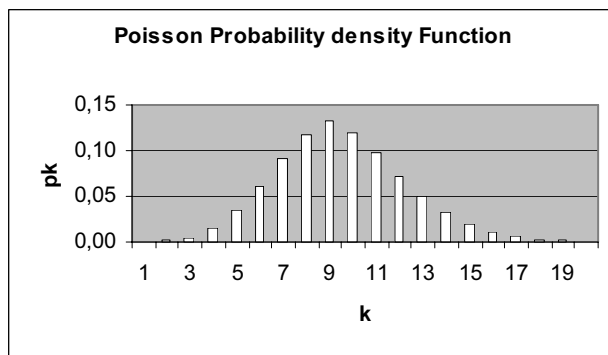


Fig. 24.8 Poisson Probability Density Function, $\lambda = 9$

If a stochastic variable X indicates the total number of successes in case of a large number of independent executions of an experiment with a very little probability of success, then the probability can be approximated by

$$P(X=k) = e^{-\lambda} \frac{\lambda^k}{k!}, \quad (24.18)$$

for which the value for λ is the product of the number of experiments and the probability of success.

The probability $P(X \leq k)$ is given by

$$P(X \leq k) = e^{-\lambda} \left(1 + \frac{\lambda}{1!} + \frac{\lambda^2}{2!} + \dots + \frac{\lambda^k}{k!} \right), \quad (24.19)$$

thus

$$P(X \leq \infty) = 1 \quad (24.20)$$

The average or expected value $E(X) = \mu_X = \lambda$ and the variance $\sigma_X^2 = \lambda$.

The probability of no impact (PNI) $P(k=0)$, or no collisions is given by

$$P(k=0) = e^{-\lambda} \quad (24.21)$$

where the total number of impacts, or fluence λ , a spacecraft can expect to experience is the product of the flux F (number of particles per year per m²), the spacecraft's exposed area A (m²) and the mission duration T_M (years). The relationship is expressed as

$$\lambda = F A T_M \text{ (particles).} \quad (24.22)$$

The probability of impact (PI), at least one impact is expressed as the complement of the PNI (see (24.19))

$$P(k=1) = 1 - e^{-\lambda}, \quad (24.23)$$

where $F(x)$ is given by (24.1) and (24.8) or Fig. 24.2.

24.5 Literature

- Drolshagen, G. and Borde, J., 1992, *ESABASE/DEBRIS, Meteoroids/Debris Impact Analysis, Technical Description*, ESABASE-GD-01/1.
- Elfer, N.C., 1996, *Structural Damage Prediction and Analysis for Hypervelocity Impacts–Handbook*, NASA CR-4706.
- Hayashida, K.B. and Robinson, J.H., 1991, *Single Wall Penetration Equations*, NASA TM-103565.
- IADC WG3, 2004, *Protection Manual*, Inter-Agency Space Debris Coordination Cie, IADC-WD-00-03, Version 3.3, April.
- Lambert, M., 1990, *Shielding Against Orbital Bebris- A Challenging Problem*, ESA SP-303, June 1990, pages 319–328.
- NASA CP-1408, 1997, *Meteoroids and Orbital Debris: Effects on Spacecraft*, August 1997.
<http://sn-callisto.jsc.nasa.gov>, NASA Orbital Debris Programme Office.
<http://hitf.jsc.nasa.gov/hitfpub/shielddev/whippleshield.html>
- NRC, 1995, *Orbital Debris, A technical Assessment*, National Research Council, ISBN 0-309-05125-8, National Academy Press.
- NRC, 1997, *Protecting Space Station from Meteoroids and Orbital Debris*, National Research Council, ISBN 0-309-52352-4, National Academy Press.
- Orbital Debris Quarterly News, NASA Johnson Space Center Houston, Texas 77058, www.orbit-aldebris.jsc.nasa.gov/newsletter/news_index.html
- Stange, K., 1970, *Angewandte Statistik, Eindimensionale Probleme*, Springer-Verlag.
- Tennyson, R.C., Shortliffe, G., 1997, *MOD Impact Damage on Composite Materials in Space*, 7th International Symposium ‘Materials in Space’, Toulouse, France, 16–20 June, ESA SP-399.
- Tribble, A.C., 2003, *The Space Environment, Implications for Spacecraft Design* Princeton University Press, ISBN 0690102996.
- Tijms, H, Heierman, 2000, F. and Nobel, R., *Poisson, de Pruisen en de Lotto*, Epsilon Uitgaven, ISBN 90-5041-059-6 (dutch).
- ISIS, International Space Information Service , 2000, <http://www.oosa.unvienna.org/isis/pub/sdtechrep1/sect01c.html>

25 Prescribed Averaged Temperatures

25.1 Introduction

The temperature distribution in a spacecraft is calculated with the aid of a thermal analysis programme such as SINDA and ESATAN. The thermal analysis program makes use of the lumped parameter method (LPM). That means that thermal properties are assigned to thermal nodes. The properties are equally distributed over the surface area of the node. The calculated temperature is thus constant over a thermal node. The transfer of thermal energy takes place among others by radiation and is proportional to the absolute temperature to the power of four, T^4 . This makes the thermal calculations non-linear. That is the reason why the thermal engineer limits the temperatures (nodes) that need to be computed [Tsai 2004].

The mechanical engineer, on the contrary, generally applies the linear laws of elasticity to his finite element model in order to calculate the thermal deformations and thermal stresses.

It is therefore possible that the ratio of the number of thermal nodes to the number of finite element model nodes (the temperature is the degree of freedom) is 1:25–50. Such a ratio makes it difficult to display the temperatures of the thermal model on the finite element model.

Dutch Space B.V. developed a method called “Prescribed Averaged Temperatures” (PAT) for ESA-ESTEC. The PAT method is used to display the temperatures of the thermal model on the nodes of the finite element model very systematically.

In the following sections the PAT method will be explained and illustrated with the aid of a few simple examples.

25.2 PAT method

The temperatures of the nodes, calculated with the aid of the thermal model (lumped parameter method), are referred to by the temperature vector $\{T^t\}$ (t for thermal) and the temperatures in the nodes of the finite element model (the mathe-

mathematical model of the spacecraft structure) with $\{T^s\}$ (s for structure). The relation between the temperatures $\{T^t\}$ and the temperatures $\{T^s\}$ is given by:

$$[A]\{T^s\} = \{T^t\} \quad (25.1)$$

where the weighting matrix $[A]$ is called the A-matrix. For a specific row of the previous expression the following holds:

$$\sum_{j=1}^N a_{ij} T_i^s = T_i^t \quad (25.2)$$

That means that the weighed average of the temperatures $\{T^s\}_i$, which coincide with a thermal node i is equal to the temperature T_i^t of the thermal node i .

N is the number of structural nodes overlapping with thermal node i .

If the temperature T_i^t is equal to the temperatures $T_j^s, j = 1, 2, \dots, N$, then the following must hold for a row of the A-matrix:

$$\sum_{j=1}^N a_{ij} = 1 \quad (25.3)$$

If V refers to the volume of a thermal node, then the temperature T_i^t of the thermal node i can be written as:

$$T_i^t = \frac{\int_{V_i} T^c(\vec{x}) dV}{\int_{V_i} dV} \quad (25.4)$$

where $T^c(\vec{x})$ is the varying temperature equivalent to the volume of thermal node i and \vec{x} is the position vector. An analogous relation exists for surface areas.

The continuous temperature $T^c(\vec{x})$ in a finite element, can be expressed in terms of the temperatures in the structural nodes of the finite element model of the structure:

$$T^c(\vec{x}) = \sum_{k=1}^{N_e} \sum_{j=1}^n \lfloor \Psi_{k,j} \rfloor \{T_j^s\}_k, \quad (25.5)$$

where:

N_e the number of finite elements, with n structural nodes, that coincide with the volume or surface of thermal node i

$\left[\Psi_{k,j} \right]$ the shape functions that describes the temperature in the finite element k ,

$$T^e(\vec{x})_k = \Psi_k \{ T^s \}_k.$$

$\{ T^s \}_k$ the temperatures in the structural nodes of the finite element k .

Example

A 1-D truss element as shown in Fig. 25.1 has two structural nodes 1 and 2.

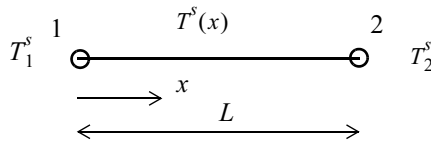


Fig. 25.1 Temperature distribution truss element

The temperature distribution in the truss element is given by

$$T^s(x) = \left[\left(1 - \frac{x}{L} \right), \frac{x}{L} \right] \begin{Bmatrix} T_1^s \\ T_2^s \end{Bmatrix} = \left[\Psi_1, \Psi_2 \right] \begin{Bmatrix} T_1^s \\ T_2^s \end{Bmatrix}$$

The finite element model of the structure has been converted into a conduction model (conduction matrix $[C]$ and nodal temperatures $\{ T^s \}$). Without radiation, the steady-state heat problem, where $\{ Q^s \}$ is the heat flow in the structural nodes, becomes:

$$[C] \{ T^s \} = \{ Q^s \} \quad (25.6)$$

Example

The conduction matrix of a truss as shown in Fig. 25.1 with a cross section A and material conduction property $k \left(\frac{W}{m^2 C} \right)$.

$$[C] = \frac{kA}{L} \begin{bmatrix} 1 & -1 \\ -1 & 1 \end{bmatrix}$$

End of example

However, later in this section a more detailed discussion about the derivation of the conduction matrix $[C]$ will be held.

Two mathematical models now exist separately:

- The thermal mathematical model (TMM)
- The finite element model of the spacecraft structure

Both models are coupled by means of the A-matrix (see Fig. 25.2).

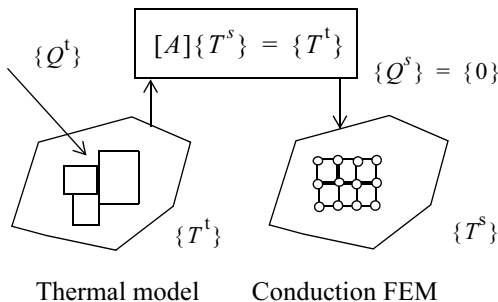


Fig. 25.2 Coupling of Thermal Model with the Conduction Model

Thermal Model

The temperatures $\{T^t\}$ in the nodes of the thermal model represent heat flows to and from the thermal nodes, referred to by $\{Q^t\}$.

Conduction Model of the Structure

The temperatures $\{T^s\}$ in the structural nodes are coupled to the temperatures $\{T^t\}$ of the thermal model by means of the A-matrix. No heat is transported to or away from the nodes or elsewhere, thus $\{Q^s\} = \{0\}$. The conduction matrix $[C]$ of the finite element model is used to lead through heat flows due to the prescribed temperatures $\{T^t\}$. The conduction matrix is used as an interpolation function.

Thermal Functional

We define the following thermal functional $J(T^t, T^s, q)$, where $\{q^t\}$ are Lagrange multipliers in order to include the relation $[A]\{T^s\} = \{T^t\}$ in the thermal functional as a side-condition, and $\{Q^t\}$ is regarded as external heat flow:

$$J(T^t, T^s, q) = \frac{1}{2} [T^s, T^t] \begin{bmatrix} C & 0 \\ 0 & 0 \end{bmatrix} \begin{Bmatrix} T^s \\ T^t \end{Bmatrix} - [T^s, T^t] \begin{Bmatrix} 0 \\ Q^t \end{Bmatrix} + [T^s, T^t] \begin{bmatrix} A^T \\ -E \end{bmatrix} \{q^t\}, \quad (25.7)$$

where

$\frac{1}{2} [T^s, T^t] \begin{bmatrix} C & 0 \\ 0 & 0 \end{bmatrix} \begin{Bmatrix} T^s \\ T^t \end{Bmatrix}$ represents the internal thermal energy

$[T^s, T^t] \begin{Bmatrix} 0 \\ Q^t \end{Bmatrix}$ represents thermal work done by the external heat flow, and

$[T^s, T^t] \begin{bmatrix} A^T \\ -E \end{bmatrix} \{q^t\}$ the additional term to force the side relations between thermal and structural node temperatures, and finally

$$\{T\} = \begin{Bmatrix} T^s \\ T^t \end{Bmatrix}$$

The state is in equilibrium when:

$$\delta J = \frac{\partial J}{\partial T} \delta T + \frac{\partial J}{\partial q} \delta q = 0 \quad (25.8)$$

The Interpolation matrix

The stationary value of the thermal functional J gives:

- $\frac{\partial J}{\partial T} = \begin{bmatrix} C & 0 \\ 0 & 0 \end{bmatrix} \begin{Bmatrix} T^s \\ T^t \end{Bmatrix} + \begin{bmatrix} A^T \\ -E \end{bmatrix} \{q^t\} - \begin{Bmatrix} 0 \\ Q^t \end{Bmatrix} = 0$

- $\frac{\partial J}{\partial q} = [T^s, T^t] \begin{bmatrix} A \\ -E \end{bmatrix} = [A, -E] \begin{Bmatrix} T^s \\ T^t \end{Bmatrix} = 0$

or written in matrix notation

$$\begin{bmatrix} C & 0 & A^T \\ 0 & 0 & -E \\ A & -E & 0 \end{bmatrix} \begin{Bmatrix} T^s \\ T^t \\ q^t \end{Bmatrix} = \begin{Bmatrix} 0 \\ Q^t \\ 0 \end{Bmatrix}. \quad (25.9)$$

The second equation shows that the Lagrange multipliers are equal to $\{q^t\} = -\{Q^t\}$. Subsequently, $\{Q^t\}$ is eliminated from (25.9) and the resulting interpolation matrix becomes:

$$\begin{bmatrix} C & A^T \\ A & 0 \end{bmatrix} \begin{Bmatrix} T^s \\ q^t \end{Bmatrix} = \begin{Bmatrix} 0 \\ T^t \end{Bmatrix}. \quad (25.10)$$

Using the previous matrix expression, the temperatures in the nodes of the thermal model are displayed on the finite element model of the structure. In addition, the temperatures in the nodes of the thermal model are interpolated along all the nodes by means of the conduction matrix, provided the average temperature of the nodes coinciding with a thermal node are equal to the temperature of that thermal node. The A-matrix defines the relationship between the thermal model and the finite element model of the structure.

25.3 PAT Method Applied to a Simplified Solar Array

Applying the PAT method to a simplified solar panel is an example of a temperature interpolation of the temperatures of the thermal model, to the nodes of the finite element model of the structure. The thermal model consists of two nodes: the yoke, node 1 and the panel, node 2 with respectively thermal node temperatures T_1^t and T_2^t . It is illustrated in Fig. 25.3.

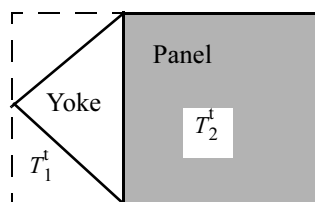


Fig. 25.3 Thermal model, two thermal nodes

The finite element model of the solar panel consists of 12 nodes, 1 to 12, 4 line-elements and 4 quadrilateral elements. The cross-section of the rod elements is A (m^2) and the thickness of the panel is t (m). The yoke as well as the panel have a level of conductivity k (W/m^2). The finite element model is illustrated in Fig. 25.4.

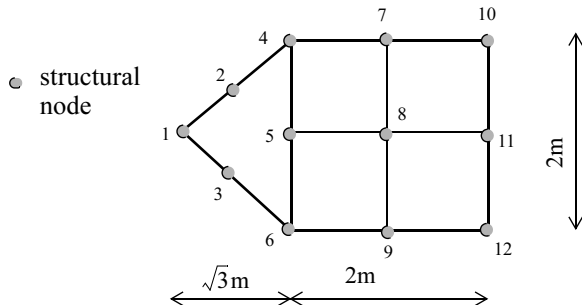


Fig. 25.4 Structural finite element model

The yoke consist of four 1-D structural elements with a length $L = 1$ m and the panel is built up of 4 rectangular panels with a length $a=1$ m and a width $b=1$ m.

The temperatures in the two nodes of the thermal model are as follows (see Table 25.1):

Table 25.1 Thermal node temperatures

Temperature load case	T_1^t	T_2^t
1	1.0	0.0
2	0.1	1.0

Two element types are used in the structural finite element model of the solar panel. The line-elements (rod) with cross-section A and length L , and a rectangular quadrilateral element (membrane) with length a , width b and thickness t . Both types of elements are illustrated in Fig. 25.5.

The temperature function of the line-element, with $\xi = \frac{x}{L}$ and a temperature T_1^s in node 1 and T_2^s in node 2, is:

$$T^s(\xi) = (1 - \xi)T_1^s + \xi T_2^s = [\Psi_1(\xi), \Psi_2(\xi)] \begin{Bmatrix} T_1^s \\ T_2^s \end{Bmatrix} \quad (25.11)$$

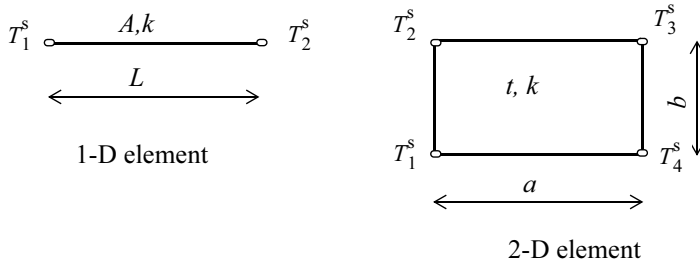


Fig. 25.5 1-D and 2-D conduction elements

The equation for conservation of energy for a continuum can be found in [Thornton 1996] and finite element relations may be derived from these equations.

The relationship between the nodal temperatures and the heat flows in the nodes per element is $[C]\{T\} = \{Q\}$, where $[C]$, the conduction matrix, can be derived with the aid of the stationary value of the heat functionality [Cook 1989]:

$$\int_{V_e} \frac{\delta dT^s}{dx} k \frac{dT^s}{dx} dV = \sum_{i=1}^2 \delta T^s_i Q_i. \quad (25.12)$$

The derivative of the temperature $T^s(\xi)$,

$$\frac{\delta dT^s}{dx} = \frac{\delta dT^s}{d\xi} \frac{d\xi}{dx} = \frac{1}{L} [-\delta T^s_1 + \delta T^s_2] = \left[\frac{-1}{L}, \frac{1}{L} \right] \begin{Bmatrix} \delta T^s_1 \\ \delta T^s_2 \end{Bmatrix} \quad (25.13)$$

$$\frac{dT^s}{dx} = \frac{dT^s}{d\xi} \frac{d\xi}{dx} = \frac{1}{L} [-T^s_1 + T^s_2] = \left[\frac{-1}{L}, \frac{1}{L} \right] \begin{Bmatrix} T^s_1 \\ T^s_2 \end{Bmatrix} \quad (25.14)$$

The conduction matrix of the line-element is:

$$[C] = \frac{Ak}{L} \begin{bmatrix} 1 & -1 \\ -1 & 1 \end{bmatrix} \quad (25.15)$$

If the structural node temperatures are equal, there is no heat flow into or out of the structural nodes, which means that the sum of one row or column must vanish.

$$\sum_{j=1}^n c_{ij} = \sum_{i=1}^n c_{ij} = 0 \quad (25.16)$$

Suppose that the thermal node overlaps with one line-element, then:

$$V_i T_i^t = \int_{V_i} T^s(x) dV = A \int_0^1 T^s(\xi) |J| d\xi = AL \int_0^1 T^s(\xi) d\xi = AL \int_0^1 [1 - \xi, \xi] d\xi \begin{Bmatrix} T_1^s \\ T_2^s \end{Bmatrix}$$

$$ALT_i^t = AL \int_0^1 [1 - \xi, \xi] d\xi \begin{Bmatrix} T_1^s \\ T_2^s \end{Bmatrix} = \frac{1}{2} AL(T_1^s + T_2^s) = \bar{a}_{i1} T_1^s + \bar{a}_{i2} T_2^s = \bar{a}_{ij} T_j^s , \quad (25.17)$$

where the Jacobian $|J| = \left| \frac{dx}{d\xi} \right| = L$. (25.18)

$$(25.3), \sum_{j=1}^N a_{ij} = 1, \text{ must be satisfied, thus } a_{ij} = \frac{\bar{a}_{ij}}{AL}.$$

Assume two associated structural elements with one thermal node

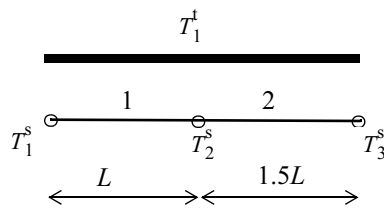
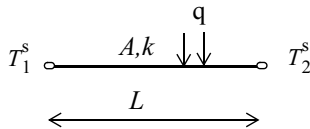


Fig. 25.6 Two one-line structural elements overlap one thermal node

$$T_i^t = \frac{A \int_0^1 T_1^s(\xi) |J| d\xi + 1.5A \int_0^1 T_2^s(\xi) |J| d\xi}{2.5AL} = \frac{AL \int_0^1 T_1^s(\xi) d\xi + 1.5AL \int_0^1 T_2^s(\xi) d\xi}{2.5AL},$$

$$T_i^t = 0.2 T_1^s + 0.5 T_2^s + 0.3 T_3^s = a_{11} T_1^s + a_{12} T_2^s + a_{11} T_3^s.$$

If a distributed heat flow q (J/m³) is applied to the 1-D (Fig. 25.7) structural element, the lumped heat flows at the structural nodes can be calculated.



1-D element

Fig. 25.7 Distributed heat flow in 1-D element

The lumped heat input in nodes 1 and 2 can be calculated using the principle of virtual work

$$A \int_0^1 q \delta T^s(\xi) |J| d\xi = AqL \int_0^1 [\Psi_1(\xi), \Psi_2(\xi)] \begin{Bmatrix} \delta T_1^s \\ \delta T_1^s \end{Bmatrix} d\xi = \sum_{i=1}^2 \delta T_i^s Q_i \quad (25.19)$$

or

$$qAL \int_0^1 [\Psi_1(\xi), \Psi_2(\xi)] \begin{Bmatrix} \delta T_1^s \\ \delta T_1^s \end{Bmatrix} d\xi = qAL \left[\frac{1}{2}, \frac{1}{2} \right] \begin{Bmatrix} \delta T_1^s \\ \delta T_1^s \end{Bmatrix} = [Q_1^s, Q_2^s] \begin{Bmatrix} \delta T_1^s \\ \delta T_1^s \end{Bmatrix} \quad (25.20)$$

Assuming a unit distributed heat flow $q = 1$ then

$$\begin{Bmatrix} Q_1^s \\ Q_2^s \end{Bmatrix}_{q=1} = AL \begin{Bmatrix} a_{i1} \\ a_{i2} \end{Bmatrix} = AL \begin{Bmatrix} \frac{1}{2} \\ \frac{1}{2} \end{Bmatrix} \quad (25.21)$$

For a 1-D line element the A-matrix elements are proportional to the equivalent nodal heat flow divided by the length L of the 1-D line element.

Example

Three structural line elements can be associated with one thermal node T_1^t and

T_2^t

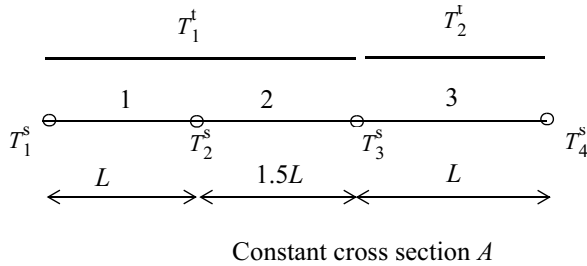


Fig. 25.8 One thermal overlaps two line elements

$$\begin{Bmatrix} Q_1^s \\ Q_2^s \end{Bmatrix}_{q=1} = \begin{Bmatrix} \tilde{a}_{11} \\ \tilde{a}_{12} \end{Bmatrix} = AL \begin{Bmatrix} \frac{1}{2} \\ \frac{1}{2} \end{Bmatrix}, \begin{Bmatrix} Q_2^s \\ Q_3^s \end{Bmatrix}_{q=1} = \begin{Bmatrix} \hat{a}_{12} \\ \hat{a}_{12} \end{Bmatrix} = 1.5AL \begin{Bmatrix} \frac{1}{2} \\ \frac{1}{2} \end{Bmatrix}.$$

The row in the A-matrix with respect to thermal **node 1** becomes

$$\begin{Bmatrix} Q_1^s \\ Q_2^s \\ Q_3^s \end{Bmatrix}_{q=1} = \begin{Bmatrix} \bar{a}_{11} \\ \bar{a}_{12} \\ \bar{a}_{13} \end{Bmatrix} = \begin{Bmatrix} \tilde{a}_{11}AL \\ \tilde{a}_{12}AL + \hat{a}_{12}1.5AL \\ \hat{a}_{13}1.5AL \end{Bmatrix} = AL \begin{Bmatrix} \frac{1}{2} \\ \frac{1}{2} + 0.75 \\ 0.75 \end{Bmatrix} = AL \begin{Bmatrix} \frac{1}{2} \\ 1.25 \\ 0.75 \end{Bmatrix}.$$

N

We have to satisfy (25.3), $\sum_{j=1}^3 a_{ij} = 1$,

but the result is $\sum_{j=1}^3 \bar{a}_{1j} = 2.5AL$, thus $a_{1j} = \frac{\bar{a}_{1j}}{2.5AL}$.

The A-matrix (see (25.1)) can be written as

$$[A]_{node-1} = [a_{11}, a_{12}, a_{13}] = [0.2, 0.5, 0.3]$$

The row in the A-matrix with respect to thermal **node 2** becomes

$$\begin{Bmatrix} Q_3^s \\ Q_4^s \end{Bmatrix}_{q=1} = \begin{Bmatrix} \bar{a}_{23} \\ \bar{a}_{24} \end{Bmatrix} = 2AL \begin{Bmatrix} \frac{1}{2} \\ \frac{1}{2} \end{Bmatrix},$$

but the result is $\sum_{j=3}^4 \bar{a}_{2j} = 2AL$, thus $a_{2j} = \frac{\bar{a}_{2j}}{2AL}$.

The A-matrix (see (25.1)) can be written as

$$\lfloor A \rfloor_{node-2} = \lfloor a_{23}, a_{24} \rfloor = \lfloor 0.5, 0.5 \rfloor$$

The total A-matrix becomes

$$[A] = \begin{bmatrix} 0.2 & 0.5 & 0.3 & 0 \\ 0 & 0 & 0.5 & 0.5 \end{bmatrix}.$$

End of example

The temperature function in the rectangular element is (where $\xi = \frac{x}{a}$, $\eta = \frac{y}{b}$,

with a temperature T_1^s in node 1, T_2^s in node 2, T_3^s in node 3 and T_4^s in node 4):

$$T(\xi, \eta) = (1 - \xi)(1 - \eta)T_1^s + (1 - \xi)\eta T_2^s + \xi\eta T_3^s + \xi(1 - \eta)T_4^s, \quad (25.22)$$

or written as

$$T(\xi, \eta) = \Psi_1(\xi, \eta)T_1^s + \Psi_2(\xi, \eta)T_2^s + \Psi_3(\xi, \eta)T_3^s + \Psi_4(\xi, \eta)T_4^s. \quad (25.23)$$

The conduction matrix $[C]$ can be derived with the aid of the stationary value of the heat functional:

$$\int_V \left[\frac{\delta \partial T^s}{\partial x}, \frac{\delta \partial T^s}{\partial y} \right] \begin{bmatrix} k & 0 \\ 0 & k \end{bmatrix} \begin{Bmatrix} \frac{\partial T^s}{\partial x} \\ \frac{\partial T^s}{\partial y} \end{Bmatrix} dV = \sum_{i=1}^4 \delta T_i^s Q_i. \quad (25.24)$$

The conduction matrix $[C]$ of the rectangular element becomes:

$$[C] = kt \begin{bmatrix} \frac{1}{3}\left(\frac{b}{a} + \frac{a}{b}\right) & \frac{1}{6}\frac{b}{a} - \frac{1}{3}\frac{a}{b} & -\frac{1}{6}\frac{b}{a} - \frac{1}{6}\frac{a}{b} & -\frac{1}{3}\frac{b}{a} + \frac{1}{6}\frac{a}{b} \\ \frac{1}{6}\frac{b}{a} - \frac{1}{3}\frac{a}{b} & \frac{1}{3}\left(\frac{b}{a} + \frac{a}{b}\right) & -\frac{1}{3}\frac{b}{a} + \frac{1}{6}\frac{a}{b} & -\frac{1}{6}\frac{b}{a} - \frac{1}{6}\frac{a}{b} \\ -\frac{1}{6}\frac{b}{a} - \frac{1}{6}\frac{a}{b} & -\frac{1}{3}\frac{b}{a} + \frac{1}{6}\frac{a}{b} & \frac{1}{3}\left(\frac{b}{a} + \frac{a}{b}\right) & \frac{1}{6}\frac{b}{a} - \frac{1}{3}\frac{a}{b} \\ -\frac{1}{3}\frac{b}{a} + \frac{1}{6}\frac{a}{b} & -\frac{1}{6}\frac{b}{a} - \frac{1}{6}\frac{a}{b} & \frac{1}{6}\frac{b}{a} - \frac{1}{3}\frac{a}{b} & \frac{1}{3}\left(\frac{b}{a} + \frac{a}{b}\right) \end{bmatrix}. \quad (25.25)$$

If a distributed heat flow q (J/m^3) is applied to the 2-D structural element the lumped heat flows at the structural nodes represent the A-matrix terms per element like the 1-D line structural element.

$$t \int_0^1 \int_0^1 q \delta T^s(\xi, \eta) |J| d\xi d\eta = \sum_{i=1}^4 \delta T^s_i Q_i, \quad (25.26)$$

or

$$qabt \int_0^1 \int_0^1 [\Psi_1(\xi, \eta), \Psi_2((\xi, \eta), \Psi_3(\xi, \eta)), \Psi_4(\xi, \eta)] \begin{Bmatrix} \delta T_1^s \\ \delta T_1^s \\ \delta T_1^s \\ \delta T_1^s \end{Bmatrix} d\xi d\eta = \sum_{i=1}^4 \delta T^s_i Q_i, \quad (25.27)$$

thus

$$qabt \int_0^1 \int_0^1 [\Psi_1(\xi, \eta), \Psi_2((\xi, \eta), \Psi_3(\xi, \eta)), \Psi_4(\xi, \eta)] \begin{Bmatrix} \delta T_1^s \\ \delta T_1^s \\ \delta T_1^s \\ \delta T_1^s \end{Bmatrix} d\xi d\eta = qabt \left[\frac{1}{4}, \frac{1}{4}, \frac{1}{4}, \frac{1}{4} \right] \begin{Bmatrix} \delta T_1^s \\ \delta T_1^s \\ \delta T_1^s \\ \delta T_1^s \end{Bmatrix}. \quad (25.28)$$

The A-matrix components can be calculated assuming $q = 1$, thus

$$\begin{Bmatrix} Q_1^s \\ Q_2^s \\ Q_2^s \\ Q_2^s \end{Bmatrix} = abt \begin{Bmatrix} a_{j1} \\ a_{j2} \\ a_{j3} \\ a_{j4} \end{Bmatrix} = abt \begin{Bmatrix} \frac{1}{4} \\ \frac{1}{4} \\ \frac{1}{4} \\ \frac{1}{4} \end{Bmatrix}.$$

Example

Calculate the row of the A-matrix of two quadrilateral structural element, covered by one thermal node (Fig. 25.9).

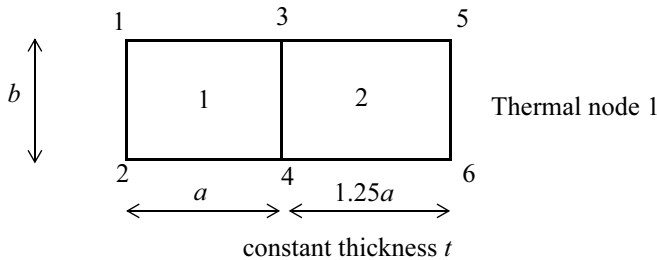


Fig. 25.9 Two 2-D structural elements associated with one thermal node

The A-matrix is given by:

$$\begin{bmatrix} \bar{a}_{11}, \bar{a}_{12}, \bar{a}_{13}, \bar{a}_{14}, \bar{a}_{15}, \bar{a}_{16}, \bar{a}_{17}, \bar{a}_{18} \end{bmatrix} = abt \begin{bmatrix} \frac{1}{4}, \frac{1}{4}, \frac{2.25}{4}, \frac{2.25}{4}, \frac{1.25}{4}, \frac{1.25}{4} \end{bmatrix}$$

$$\sum_{j=3}^8 \bar{a}_{1j} = 2.25abt, \sum_{j=3}^8 a_{1j} = 1, a_{1j} = \frac{\bar{a}_{1j}}{2.25abt}$$

$$\begin{bmatrix} a_{11}, a_{12}, a_{13}, a_{14}, a_{15}, a_{16}, a_{17}, a_{18} \end{bmatrix} = \begin{bmatrix} 0.111, 0.111, 0.25, 0.25, 0.139, 0.139 \end{bmatrix}$$

End of example

To continue, a solar array example will be outlined. The conduction matrix of one 1-D structural element with $\frac{Ak}{L} = 1 \times 10^{-3}$ W/m becomes

$$[C] = 1 \times 10^{-3} \begin{bmatrix} 1 & -1 \\ -1 & 1 \end{bmatrix}.$$

The conduction matrix of the rectangular element with $a=b=1$ m and $kt = 1 \times 10^{-3}$ W/m.

$$[C] = 1 \times 10^{-3} \begin{bmatrix} \frac{2}{3} & -\frac{1}{6} & -\frac{2}{6} & -\frac{1}{6} \\ -\frac{1}{6} & \frac{2}{3} & -\frac{1}{6} & \frac{2}{6} \\ \frac{2}{6} & -\frac{1}{6} & \frac{2}{3} & -\frac{1}{6} \\ -\frac{1}{6} & -\frac{2}{6} & -\frac{1}{6} & \frac{2}{3} \end{bmatrix}.$$

The generation of the A-matrix will be illustrated hereafter with $L=1$ m and $a=b=1$ m. A unit heat flux is applied to the 1-D and 2-D elements $q=1$ J/m³.

Table 25.2 Generation A-matrix components associated with thermal node 1

Node #	1-D element nodes 1–2	1-D element nodes 1–3	1-D element nodes 2–4	1-D element nodes 3–6	\bar{a}_{1j}	$\sum_i \bar{a}_{ij}$
1	0.25A	0.25A	0.00A	0.00A	0.50A	0.25
2	0.25A	0.00A	0.25A	0.00A	0.50A	0.25
3	0.00A	0.25A	0.00A	0.25A	0.50A	0.25
4	0.00A	0.00A	0.25A	0.00A	0.25A	0.125
6	0.00A	0.00A	0.00A	0.25A	0.25A	0.125
					2.00A	1.00
				$\sum_j \bar{a}_{ij}$		

To begin with, the A-matrix components associated with thermal node 1 and the 4 associated 1-D elements (Fig. 25.3 and Fig. 25.4) are generated.

Following this, the A-matrix components associated with thermal node 2 will be generated.

Table 25.3 Generation A-matrix components associated with thermal node 2

Node #	2-D element nodes 5–4-7–8	2-D element nodes 6–5–8–9	2-D element nodes 8–7–10–11	2-D element nodes 9–8–11–12	\bar{a}_{1j}	$\sum_i \bar{a}_{ij}$
4	0.25t	0.00t	0.00t	0.00t	0.25t	0.0625
5	0.25t	0.25t	0.00t	0.00t	0.50t	0.125
6	0.00t	0.25t	0.00t	0.00t	0.25t	0.0625
7	0.25t	0.00t	0.25t	0.00t	0.50t	0.125
8	0.25t	0.25t	0.25t	0.25t	1.00t	0.25
9	0.00t	0.25t	0.00t	0.25t	0.50t	0.125
10	0.00t	0.00t	0.25t	0.00t	0.25t	0.0625
11	0.00t	0.00t	0.25t	0.25t	0.50t	0.125
12	0.00t	0.00t	0.00t	0.25t	0.25t	0.0625
					4.00t	1.00
				$\sum_j \bar{a}_{ij}$		

The complete A-matrix looks as follows

$$[A]^T = \begin{bmatrix} 0.25 & 0.00 \\ 0.25 & 0.00 \\ 0.25 & 0.00 \\ 0.125 & 0.0625 \\ 0.00 & 0.125 \\ 0.125 & 0.0625 \\ 0.00 & 0.125 \\ 0.00 & 0.25 \\ 0.00 & 0.125 \\ 0.00 & 0.0625 \\ 0.00 & 0.125 \\ 0.00 & 0.0625 \end{bmatrix}.$$

The complete conduction matrix $[C]$ of the total finite element model of the solar array shown in Fig. 25.4 with $\frac{Ak}{L} = 1 \times 10^{-3}$ W/m and $kt = 1 \times 10^{-3}$ W/m is given by

$$[C] = \frac{1 \times 10^{-3}}{3} \begin{bmatrix} 6 & -3 & -3 & 0 & 0 & 0 & 0 & 0 & 0 & 0 & 0 & 0 & 0 \\ -3 & 6 & 0 & -3 & 0 & 0 & 0 & 0 & 0 & 0 & 0 & 0 & 0 \\ -3 & 0 & 6 & 0 & 0 & -3 & 0 & 0 & 0 & 0 & 0 & 0 & 0 \\ 0 & -3 & 0 & 5 & -\frac{1}{2} & 0 & -1 & -\frac{1}{2} & 0 & 0 & 0 & 0 & 0 \\ 0 & 0 & 0 & -\frac{1}{2} & 4 & -\frac{1}{2} & -\frac{1}{2} & -2 & -\frac{1}{2} & 0 & 0 & 0 & 0 \\ 0 & 0 & -3 & 0 & -\frac{1}{2} & 5 & 0 & -\frac{1}{2} & -1 & 0 & 0 & 0 & 0 \\ 0 & 0 & 0 & -1 & -\frac{1}{2} & 0 & 4 & -1 & 0 & -1 & -\frac{1}{2} & 0 & 0 \\ 0 & 0 & 0 & -\frac{1}{2} & -2 & -\frac{1}{2} & -1 & 8 & -1 & -\frac{1}{2} & -2 & -\frac{1}{2} \\ 0 & 0 & 0 & 0 & -\frac{1}{2} & -1 & 0 & -1 & 4 & 0 & -\frac{1}{2} & -1 \\ 0 & 0 & 0 & 0 & 0 & 0 & -1 & -\frac{1}{2} & 0 & 2 & -\frac{1}{2} & 0 \\ 0 & 0 & 0 & 0 & 0 & 0 & -\frac{1}{2} & -2 & -\frac{1}{2} & -\frac{1}{2} & 4 & -\frac{1}{2} \\ 0 & 0 & 0 & 0 & 0 & 0 & -\frac{1}{2} & -1 & 0 & -\frac{1}{2} & 2 \end{bmatrix}.$$

The temperature distribution $\{T^s\}$ is determined with the following interpolation matrix (25.10):

$$\begin{bmatrix} C & A^T \\ A & 0 \end{bmatrix} \begin{Bmatrix} T^s \\ q^t \end{Bmatrix} = \begin{Bmatrix} 0 \\ T^t \end{Bmatrix},$$

and is solved with the known temperatures in both nodes of the thermal model. The results of the calculations are shown in Table 25.4.

Table 25.4 Structural node temperature results

Structural node #	$T_1^t = 1$	$T_1^t = 0$
T^s	$T_2^t = 0$	$T_2^t = 1$
1	1.2013	-0.2013
2	1.0671	-0.0671
3	1.0671	-0.0671
4	0.6644	0.3356
5	0.0067	0.9933
6	0.6644	0.3356
7	-0.1007	1.1007
8	-0.0366	1.0366
9	-0.2081	1.2081
10	-0.1946	1.1946
11	-0.2081	1.2081
12	-0.1946	1.1946

The temperature distribution turns out to be very systematic with the aid of the conduction matrix of the finite element model of the structure.

25.4 Literature

- Appel, S., 1996, *Interpolation of Lumped Parameter Temperatures for Thermo-elastic FEM Analysis with SINAS*, Proceedings Conference on Spacecraft Structures & Mechanical Testing, ESA SP-386, pages 277–281.
- Bathe, K.J., 1986, *Finite Element Methods*, Springer-Verlag, 1986.
- Cook, D., Malkus, D.S., Plesha, M.E., 1989, *Concepts and Applications of Finite Element Analysis*, third edition, John Wiley & Sons, ISBN0-471-84788-7.
- Thronton, E.A., 1996, *Thermal Structures for Aerospace Application*, ISBN 1-56347-6, AIAA Education Series.
- Tsai, J.R., 2004, *Overview of Satellite Thermal Model*, Journal of Spacecraft & Rockets, Vol 41, No. 1, pages 120–125.

25.5 Exercises

25.5.1 Temperature interpolation in finite element model

A flexible deployable solar array consists of two side bars, a spreader bar and the membrane covered with solar cells. The bars are made of an Al-alloy with a conduction property $k = 150 \text{ W/mC}^0$. The area of the side bars is $A = 1 \times 10^{-4} \text{ m}^2$ and of the spreader bar is $A = 2 \times 10^{-4} \text{ m}^2$. The membrane is made of a Ti-alloy with a conduction property $k = 10 \text{ W/mC}^0$. The length of the side bars is $L = 5 \text{ m}$ and the length of the spreader bar is $L = 1.6 \text{ m}$. The thickness of the membrane is $t = 0.2 \text{ mm}$, the width is $b = 1.2 \text{ m}$, and the length is equal to the length of the side bars. The space between the side bars and the membrane is 0.2 m. The bars are modelled with bar elements and the membrane with quadrilateral elements. This structural finite element mode is illustrated in Fig. 25.10 and the thermal model is shown in Fig. 25.11.

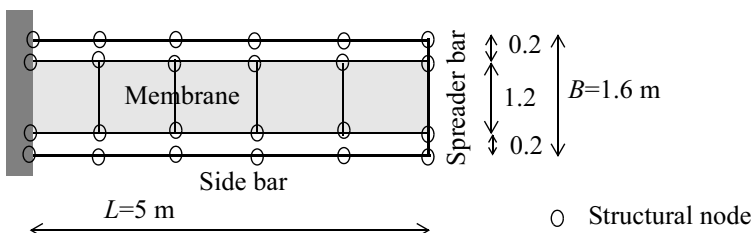


Fig. 25.10 Structural finite element model

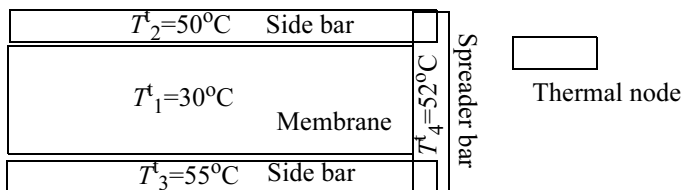


Fig. 25.11 Thermal model

With the PAT method, perform a temperature interpolation for the temperature distribution in the structural finite element model based on the thermal model.

26 Thermal-elastic Stresses

26.1 Introduction

For straightforward cases it is possible to analytically determine the thermal deformations and thermal stresses due to temperature gradients [Thorton 1996]. In most cases, however, it is very difficult or impossible, unless large simplifications are applied to the mathematical model. The finite element method is very suitable for determining thermal deformations and thermal stresses due to temperature variations. Generally, a static finite element model is available. In the following section, a schematic overview is given on how thermal deformations and thermal stresses due to temperature variations can be calculated with the aid of the finite element method. Temperature variations along the cross-section of a beam or the thickness of a plate fall beyond the scope of this book.

The principle of virtual work is used to write the equations for the finite element method. $\Delta T = T - T_{\text{ref}}$ is the temperature difference with respect to the surroundings, where T is the actual temperature in °C or K and T_{ref} the reference temperature. This reference temperature is usually the room temperature.

The mechanical strain is referred to by ε and the thermal strain by ε_T and the thermal strain equals $\varepsilon_T = \alpha \Delta T$, where α is the coefficient of thermal expansion.

For an aluminium alloy $\alpha = 24 \times 10^{-6}$ m/m/K.

In the finite element method the thermal stress is

$$\sigma_T = E \alpha \Delta T. \quad (26.1)$$

The internal thermal stress will be converted to nodal forces and superimposed on the mechanical forces. If a structure has a stress free state due to the thermal-elastic deformation, the thermal strain must be subtracted from the strain calculated from the nodal displacements equivalent thermal modal forces. The net strain $\bar{\varepsilon}$ consist of the total strain due to the total nodal forces (mechanical + thermo-elastic) ε the thermal strain ε_T shall be subtracted, hence

$$\bar{\varepsilon} = \varepsilon - \varepsilon_T . \quad (26.2)$$

The principle of virtual work is a condition for equilibrium. The internal virtual work is equal to the external virtual work. The principle of virtual work is given by the following formula

$$\int_V \sigma \delta(\varepsilon - \varepsilon_T) dV - \int_A F \delta u dA = 0 . \quad (26.3)$$

F and u are the applied loads and the unspecified displacement on the surface A respectively. The thermal strain $\varepsilon_T = \alpha \Delta T$ is specified and the variation $\delta \varepsilon_T = 0$. The formula for the virtual work is then (26.3):

$$\int_V \sigma \delta \varepsilon dV - \int_A F \delta u dA = 0 . \quad (26.4)$$

To illustrate the application of virtual work, some calculations will be done for a simple tension- and compression member (truss). The truss finite element is shown in Fig. 26.1.

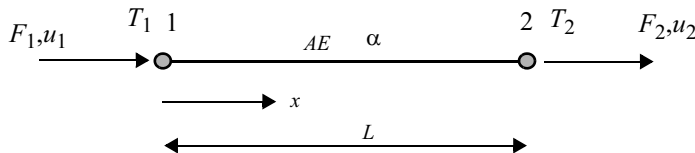


Fig. 26.1 Tension- and compression element (truss)

The finite element model of the tension- and compression member consists of two nodes. The displacement field and the temperature field can both be written as a linear function expressed in the nodal variables; the nodal displacements u_1, u_2 and the nodal temperatures T_1, T_2 . The displacement function is:

$$u(x) = \left(1 - \frac{x}{L}\right) u_1 + \frac{x}{L} u_2 , \quad (26.5)$$

and for the temperature field is taken:

$$T(x) = \left(1 - \frac{x}{L}\right) T_1 + \frac{x}{L} T_2 . \quad (26.6)$$

The mechanical strain in the truss is

$$\bar{\varepsilon} = (\varepsilon - \varepsilon_T) = \frac{du}{dx} - \alpha \Delta T = \frac{u_2 - u_1}{L} - \alpha \Delta T . \quad (26.7)$$

The strain is constant over the length of the strut.

The stress in the truss becomes:

$$\sigma = E\bar{\varepsilon} = E \left[\frac{u_2 - u_1}{L} - \alpha \Delta T \right] \quad (26.8)$$

The expression for the virtual work, (26.3), becomes:

$$\int_V \sigma \delta(\varepsilon - \varepsilon_T) dV = AE \int_0^L \frac{u_2 - u_1}{L} - \alpha \left\{ \left(1 - \frac{x}{L} \right) T_1 + \frac{x}{L} T_2 - T_{ref} \right\} \frac{\delta u_2 - \delta u_1}{L} dx,$$

and

$$\int_A F \delta u dA = F_1 \delta u_1 + F_2 \delta u_2.$$

If the terms associated with the virtual displacement δu_1 and δu_2 are equated and the following two equations are obtained

$$-AE \int_0^L \left[\frac{u_2 - u_1}{L} + \alpha \left\{ \left(1 - \frac{x}{L} \right) T_1 + \frac{x}{L} T_2 - T_{ref} \right\} \frac{\delta u_1}{L} \right] dx = F_1 \delta u_1, \quad (26.9)$$

and

$$AE \int_0^L \left[\frac{u_2 - u_1}{L} - \alpha \left\{ \left(1 - \frac{x}{L} \right) T_1 + \frac{x}{L} T_2 - T_{ref} \right\} \frac{\delta u_2}{L} \right] dx = F_2 \delta u_2. \quad (26.10)$$

If the integration is performed and the virtual magnitudes are arranged then:

$$\frac{AE}{L} \begin{bmatrix} 1 & -1 \\ -1 & 1 \end{bmatrix} \begin{Bmatrix} u_1 \\ u_2 \end{Bmatrix} = \frac{\alpha EA}{2} \begin{bmatrix} -1 & -1 \\ 1 & 1 \end{bmatrix} \begin{Bmatrix} T_1 - T_{ref} \\ T_2 - T_{ref} \end{Bmatrix} + \begin{Bmatrix} F_1 \\ F_2 \end{Bmatrix}. \quad (26.11)$$

In this matrix equation (26.11) the thermal strain has been converted to nodal forces. The thermal stress is

$$\sigma = E\bar{\varepsilon} = E(\varepsilon - \varepsilon_T). \quad (26.12)$$

Two simple problems are used as an illustration:

- A truss that is restrained at one end ($u_1 = 0$) with a constant temperature field $\Delta T = T - T_{ref}$, and a nodal force $F_3=F$ at the other side. The truss is idealised with two truss finite elements as describe with (26.11). Calculate element stresses and nodal displacements.
- A rod that is restrained at both ends ($u_1 = 0, u_3 = 0$) and with a constant temperature field $\Delta T = T - T_{ref}$. Calculate element stresses and nodal displacements. No external loads are applied.

The idealisation of the truss is shown in Fig. 26.2.

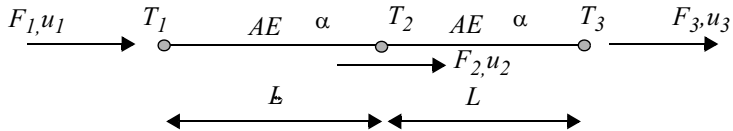


Fig. 26.2 Two truss elements, constant temperature

The equilibrium equations then become:

$$\frac{AE}{L} \begin{bmatrix} 1 & -1 & 0 \\ -1 & 2 & -1 \\ 0 & -1 & 1 \end{bmatrix} \begin{Bmatrix} u_1 \\ u_2 \\ u_3 \end{Bmatrix} = \frac{\alpha AE \Delta T}{2} \begin{bmatrix} -1 & -1 & 0 \\ 1 & 1 & -1 \\ 0 & 1 & 1 \end{bmatrix} \begin{Bmatrix} 1 \\ 1 \\ 1 \end{Bmatrix} + \begin{Bmatrix} 0 \\ 0 \\ F \end{Bmatrix}$$

The nodal displacements become for:

Case 1

The nodal displacements become

$$\begin{Bmatrix} u_1 \\ u_2 \\ u_3 \end{Bmatrix} = \alpha \Delta T L \begin{Bmatrix} 0 \\ 1 \\ 2 \end{Bmatrix} + \frac{FL}{AE} \begin{Bmatrix} 0 \\ 1 \\ 2 \end{Bmatrix},$$

and the total strains can be derived from the nodal displacement vector

$$\begin{Bmatrix} \varepsilon_1 \\ \varepsilon_2 \end{Bmatrix} = \left(\alpha \Delta T + \frac{F}{AE} \right) \left(\begin{bmatrix} 1 & -1 & 0 \\ 0 & 1 & -1 \end{bmatrix} \begin{Bmatrix} u_1 \\ u_2 \\ u_3 \end{Bmatrix} \right).$$

The strain corrected with the thermal strain becomes

$$\begin{Bmatrix} \bar{\varepsilon}_1 \\ \bar{\varepsilon}_2 \end{Bmatrix} = \frac{F}{AE} \left(\begin{bmatrix} 1 & -1 & 0 \\ 0 & 1 & -1 \end{bmatrix} \begin{Bmatrix} u_1 \\ u_2 \\ u_3 \end{Bmatrix} \right),$$

thus the stresses are $\{\sigma\} = [E]\{\bar{\varepsilon}\}$

$$\begin{Bmatrix} \sigma_1 \\ \sigma_2 \end{Bmatrix} = \frac{F}{A} \left(\begin{bmatrix} 1 & -1 & 0 \\ 0 & 1 & -1 \end{bmatrix} \begin{Bmatrix} u_1 \\ u_2 \\ u_3 \end{Bmatrix} \right).$$

In case 1 only the mechanical load will introduce stresses in the truss. There are no thermal stresses introduced if the truss is constrained so that it is statically determinate.

A finite element model can be checked with the aid of the method of expansion without stress. The statically determinate model is restrained and a homogeneous temperature distribution with respect to a reference temperature is subsequently induced. If all the materials are now made equal to each other (coefficient of expansion, modulus of elasticity, etc.) then the model will expand without stress.

Case 2

The nodal displacement vector becomes

$$\begin{Bmatrix} u_1 \\ u_2 \\ u_3 \end{Bmatrix} = \alpha \Delta T L \begin{Bmatrix} 0 \\ 0 \\ 0 \end{Bmatrix}.$$

And the total strain

$$\begin{Bmatrix} \varepsilon_1 \\ \varepsilon_2 \end{Bmatrix} = \begin{Bmatrix} 0 \\ 0 \end{Bmatrix}.$$

The corrected strain obtained is

$$\begin{Bmatrix} \bar{\varepsilon}_1 \\ \bar{\varepsilon}_2 \end{Bmatrix} = \begin{Bmatrix} 0 \\ 0 \end{Bmatrix} - \alpha \Delta T \begin{Bmatrix} 1 \\ 1 \end{Bmatrix},$$

and the stresses

$$\begin{Bmatrix} \sigma_1 \\ \sigma_2 \end{Bmatrix} = -\alpha E \Delta T \begin{Bmatrix} 1 \\ 1 \end{Bmatrix}.$$

The aforementioned example can also be used for other types of finite elements, depending of course on the finite element program.

Example

The following example is taken from the book of Peery and Azar [Peery 1982].

Consider an indeterminate truss frame as shown Fig. 26.3. Assume member 1 has an area A and is heated to a constant temperature T with respect to zero reference temperature. The area of members 2 and 3 is \sqrt{A} each. The equivalent external loads at both ends of member 1 are $\alpha A E T$, see (26.11). α is the coefficient of thermal expansion and E is the Young's modulus of the material. The problem will be solved using the energy method (Castigliano). This may be accomplished by making the structure redundant, as shown in Fig. 26.3. For compatibility of deformation, the relative displacement in the direction of R_1 must be zero. Thus from Castigliano's theorem

$$\delta_1 = \frac{dU}{dR_1} = 0,$$

where U is the total strain energy stored in the structure and R_1 is the unknown equivalent internal load in member 1.

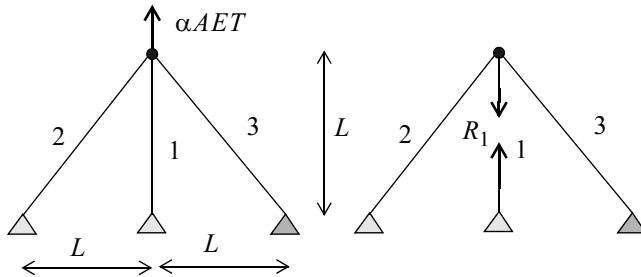


Fig. 26.3 Indeterminate truss frame

From the equations of equilibrium in conjunction with the joint method, the equivalent internal loads in members 2 and 3 can be calculated.

$$\bar{F}_2 = \bar{F}_3 = \frac{\alpha AET - R_1}{\sqrt{2}}.$$

The total strain energy becomes

$$U = \frac{1}{2} \frac{R_1^2 L}{AE} + \frac{1}{AE\sqrt{2}} \left[\left(\frac{\alpha AET - R_1}{\sqrt{2}} \right)^2 L\sqrt{2} \right].$$

Performing the differentiation with respect to R_1 and setting the result equal to zero yields

$$R_1 = \frac{\alpha AET}{2} = \bar{F}_1, \text{ and } \bar{F}_2 = \bar{F}_3 = \frac{\alpha AET}{2\sqrt{2}}.$$

The stresses in the members can be obtained as follows using (26.8)

$$\sigma_1 = \frac{\bar{F}_1}{A} - \alpha ET = \frac{\alpha ET}{2}, \text{ and } \sigma_2 = \sigma_3 = \frac{\bar{F}_2}{A\sqrt{2}} - 0 = \frac{\bar{F}_3}{A\sqrt{2}} - 0 = \frac{\alpha ET}{4}$$

End of example

26.2 Material properties

In the following Table 26.1 typical values (modulus of elasticity, the coefficient of expansion and the conduction coefficient) for various alloys are given.

Table 26.1 Material properties

Material	Young's modulus E (MPa)	CTE ($\frac{\mu m}{mK}$)	Conduction coefficient k ($\frac{J}{mK}$)
Al-alloys	70	24	150
Mg-alloys	45	26	44
Ti-alloys	110	9	7
Be-alloys	330	11	180

26.3 Literature

- Peery, D.J., Azar, J.J., 1982, *Aircraft Structures*, ISBN 0-07-049196-8, MacGraw-Hill.
 J.S. Przemieniecki, 1985, *Theory of Matrix Structural Analysis*, Dover Publications, Inc.
 Thorton, E.A., 1996, *Thermal Structures for Aerospace Application*, ISBN 1-56347-6, AIAA Education Series.
 K. Washizu, 1968, *Variational Methods in Elasticity and Plasticity*, Pergamon Press.

26.4 Exercises

26.4.1 Thermal stress in beam

Consider a beam that is heated uniformly from a reference temperature T_{ref} to a final temperature $T(\text{K})$. The elongation of beam with cross-section A , Young's modulus is E (Pa) and coefficient of thermal expansion is α (m/m/K) is hindered by a spring with spring stiffness k . This system is shown in Fig. 26.4.

Derive expressions for the following parameters:

- the stress in the beam
- the displacement at point C, δ_C

$$\text{Answer: } \sigma = -\frac{\alpha k E L (T - T_{\text{ref}})}{kL + AE}, \quad \delta_C = \frac{\sigma A}{k}$$

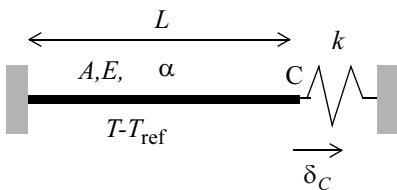


Fig. 26.4 Heated beam

26.4.2 Self Strained Structure

The side of a “spacecraft” structure exposed to the sun is heated by radiation heat transfer. The truss-frame structure is shown in Fig. 26.5. All rods have the same extensional stiffness EA . The length of rod 1-3 is L and is heated above the stress

free temperature with ΔT . The rods 1-2 and 2-3 are not heated. The coefficient of thermal expansion is α . The following needs to be calculated:

- The reaction forces in the supports
- The unknown displacements in the nodes 1 and 3
- The forces in the rods (trusses)

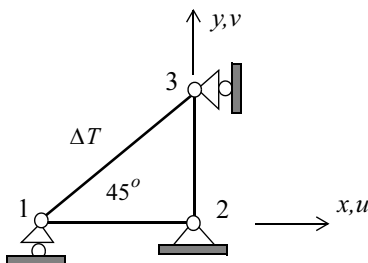


Fig. 26.5 Heated truss-frame structure

$$\text{Answers: } \begin{Bmatrix} R_{1y} \\ R_{2x} \\ R_{2y} \\ R_{3x} \end{Bmatrix} = AE\alpha\Delta T \begin{Bmatrix} \frac{\sqrt{2}}{2+\sqrt{2}} \\ \frac{\sqrt{2}}{2+\sqrt{2}} \\ \frac{-\sqrt{2}}{2+\sqrt{2}} \\ \frac{\sqrt{2}}{2+\sqrt{2}} \end{Bmatrix}, \quad \begin{Bmatrix} u_1 \\ v_2 \end{Bmatrix} = \alpha\Delta TL \begin{Bmatrix} \frac{-\sqrt{2}}{2+\sqrt{2}} \\ \frac{\sqrt{2}}{2+\sqrt{2}} \end{Bmatrix},$$

$$\begin{Bmatrix} N_{1-2} \\ N_{1-3} \\ N_{2-3} \end{Bmatrix} = AE\alpha\Delta T \begin{Bmatrix} \frac{\sqrt{2}}{2+\sqrt{2}} \\ \frac{-\sqrt{2}}{2+\sqrt{2}} \\ \frac{\sqrt{2}}{2+\sqrt{2}} \end{Bmatrix}.$$

27 Coefficients of thermal & moisture expansion

27.1 Introduction

Thermal distortions in spacecraft structures may be of great importance. They are dependent on temperature gradients and the coefficient of thermal expansion (CTE). In this chapter the definition of CTE will be discussed:

Distortions in spacecraft structures may occur when moisture is absorbed into the material (coefficient of moisture expansion, CME), e.g. CFRP and/or GFRP manufactured structural parts. However, the calculations of distortions due to moisture are analog to thermal distortion analysis techniques.

27.2 Coefficient of thermal expansion

In this section two definitions of CTE will be discussed:

- The CTE α [m/m/ $^{\circ}$ C] as a derivative of the thermal expendability $\beta(\Delta T)$ as a function of the temperature difference ΔT [$^{\circ}$ C, K]
- The secant CTE α_c [m/m/ $^{\circ}$ C]

27.2.1 The CTE as a derivative of the thermal expansibility

The thermal expendability β is defined as the increase or decrease of length $\Delta L(\Delta T) = L(T) - L_{ref}(T_{ref})$ [m] of a bar of a material with respect a reference length L_{ref} [m], with $\Delta T = T - T_{ref}$ [$^{\circ}$ C, K], hence

$$\beta = \frac{\Delta L(\Delta T)}{L_{ref}(T_{ref})} . \quad (27.1)$$

The definition of the thermal expendability is the same as the definition of the engineering strain ε [m/m] due to an external load F [N], thus

$$\varepsilon(F) = \frac{\Delta L}{L_{ref}}. \quad (27.2)$$

The infinite increase $d\varepsilon$ of the engineering strain is defined as

$$d\varepsilon(T) = \alpha(T)dT, \quad (27.3)$$

$$\varepsilon(T) = \int_{T_{ref}}^T \alpha(T)dT. \quad (27.4)$$

It can now be written

$$\alpha(T) = \frac{d\varepsilon(T)}{dT} \approx \frac{\Delta(\varepsilon(T))}{\Delta T} = \frac{\Delta(\beta(T))}{\Delta T}, \quad (27.5)$$

or

$$\alpha(T) = \frac{1}{L_{ref}} \frac{\{L(T + \Delta T) - L(T)\}}{\Delta T} = \frac{1}{L_{ref}} \frac{\{\Delta L(\Delta T)\}}{\Delta T}. \quad (27.6)$$

27.2.2 The Secant CTE

The secant CTE $\alpha_c(T)$ is defined as

$$\varepsilon(T) = \alpha_c(T)(T - T_{ref}) = \alpha_c(T)\Delta T \quad (27.7)$$

$$\alpha_c(T) = \frac{1}{(T - T_{ref})} \int_{T_{ref}}^T \alpha(z)dz \quad (27.8)$$

When using the secant CTE, the temperature dependent thermal coefficient of expansion is linearised between the current temperature T and T_{ref} . By the introduction of the secant CTE the non linear deformation is linearised and the thermal distortion and associated stresses can be calculated with linear elastic calculations.

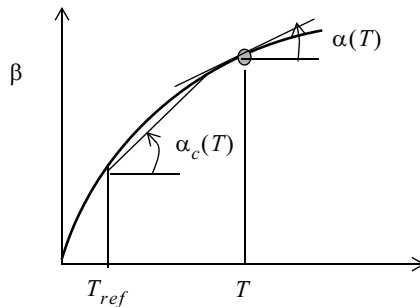


Fig. 27.1 Illustration of CTE and secant CTE

Example

The elongation ΔL of a bar with length L_{ref} is given by

$$\Delta L(T - T_{ref}) = a_1(T - T_{ref}) - a_2(T - T_{ref})^2,$$

with all coefficients $a_i > 0$

The CTE $\alpha(T)$ becomes

$$\alpha(T) = \frac{d\varepsilon(T)}{dT} = \frac{d\Delta L(T)}{L_{ref}dT} = a_1 - 2a_2(T - T_{ref}).$$

The secant CTE is defined by

$$\alpha_c(T) = \frac{1}{(T - T_{ref})} \int_{T_{ref}}^T (a_1 - 2a_2(\Theta - T_{ref})) d\Theta = a_1 - a_2(T - T_{ref}).$$

27.3 Moisture coefficient of expansion (CME)

The matrix of fibre materials, e.g. CFRP, GFRP, etc. absorbs moisture in an earth environment and will increase in size. However, in orbit the moisture contents in the matrix will decrease and the structure will shrink. Due to the shrinkage, stresses will be build up in statically indeterminate structures.

The phenomena of moisture is comparable with thermal expansion.

The alteration in length and width of a structure due to the fact that materials will absorb moisture can be calculated with

$$\Delta L = L_{ref}\beta(M_f - M_{ref}) \quad (27.9)$$

where

- ΔL the alteration in length [m]
- L_{ref} the reference length [m]

- β the coefficient of moisture expansion [m/m/%]
- M_f the percentage of moisture in the final situation [%]
- M_{ref} the percentage of moisture in the reference state [%]

The percentage of moisture can be calculated with

$$M_f = 100 \left(\frac{W_f - W_{ref}}{W_{ref}} \right) \quad (27.10)$$

where

- W_f The weight of the structure in the final state [kg]
- W_{ref} The weight of the structure in the reference state [kg]

The strain ε due to the moisture is

$$\varepsilon = \frac{\Delta l}{L_{ref}} = \beta(M_f - M_{ref}) \quad (27.11)$$

Note that (27.11) is very similar to (27.7).

For CFRP the percentage of moisture M varies between 0.5–1%.

The Coefficient of Moisture Expansion (CME) β of the resin is about $\beta = 2.5 \times 10^{-3}$ [m/m/%].

28 Venting Holes

28.1 Introduction

To avoid over-pressurising in a box, venting holes must be applied. In this chapter a method is presented to calculate the cross-section of the venting hole needed to prevent an over pressure in the enclosure. Also a rule of thumb expression is given to estimate the cross-section of the venting hole.

28.2 Venting Holes

28.2.1 Beryline method

The velocity of the air at a reduced section just behind the hole is given by the Beryline relation (air considered as incompressible when going out)

$$v = \sqrt{\frac{2\Delta p}{\rho_{int}}}, \quad (28.1)$$

where Δp is the pressure difference between inside and outside (P.a.), ρ_{int} is the density of the air inside the box (kg/m^3) and v the gas velocity (m/s).

The pressure inside the box is given by

$$p_{int} = RT_{int}\rho_{int} = RT_{int} \frac{m}{V}, \quad (28.2)$$

where m is the total mass of air inside the box, R is the gas constant and the temperature T_{int} (K) is considered as constant inside the box. The internal pressure will be

$$p_{int}(t) = RT_{int} \frac{m_{int}(t)}{V}. \quad (28.3)$$

The rate of decrease of the total mass of air inside the box is

$$-\frac{dm_{int}(t)}{dt} = v(t)\rho_{int}(t)A_{vh}, \quad (28.4)$$

where A_{vh} is the area of the venting hole.

The total mass of air inside $m_{int}(t)$ becomes

$$m_{int}(t) = m_{int}(0) - \int_0^t v(\tau)\rho_{int}(\tau)A_{vh}d\tau. \quad (28.5)$$

The alteration (decrease) of the internal pressure p_{int} , using (28.4) is

$$-\frac{dp_{int}(t)}{dt} = -\frac{RT_{int}}{V} \frac{dm_{int}(t)}{dt} = \frac{RT_{int}}{V} v(t)\rho_{int}(t)A_{vh}. \quad (28.6)$$

Substituting (28.1) in (28.6) we obtain

$$-\frac{dp_{int}(t)}{dt} = \frac{RT_{int}}{V} \sqrt{\frac{2\Delta p(t)}{\rho_{int}(t)}} \rho_{int}(t)A_{vh} = \frac{RT_{int}}{V} \sqrt{2\rho_{int}(t)\Delta p(t)} A_{vh}. \quad (28.7)$$

The cross-section (area) of the venting hole can be calculated by

$$A_{vh}(t) = \frac{dp_{int}(t)}{dt} \frac{V}{RT_{int}} \frac{1}{\sqrt{2\rho_{int}(t)\Delta p(t)}}. \quad (28.8)$$

Example

To avoid over pressure in a box the need for venting holes is foreseen. The diameter is defined to limit the over-pressure at 20mBar. The volume of the box is 33 litres. The characteristic constant of the air at room temperature, $T_{RT} = 300$ K, is $R = 287$. The pressure reduction versus time outside the box after lift off is limited to 20mBar/s.

The internal pressure reduction versus time is given to be $\frac{dp_{int}(t)}{dt} = -2 \times 10^3$ P.a./s.

Equation (28.8) is applied to calculate the required cross-section A_{vh}

$$A_{vh}(t) = \frac{dp_{int}(t)}{dt} \frac{V}{RT_{int}} \frac{1}{\sqrt{2\rho_{int}(t)\Delta p(t)}} = 2 \times 10^3 \frac{33 \times 10^{-3}}{287 \times 300} \frac{1}{\sqrt{\rho_{int}(t)}} \frac{1}{\sqrt{4 \times 10^3}}$$

This function rises to a maximum at low pressure $p = 1 \times 10^3$ Pa, hence the density of the air at this pressure can be obtained by (28.2)

$$\rho_{int}(t) = \frac{p(t)}{RT} = \frac{2 \times 10^3}{287 \times 300} = 0.012 \text{ kg/m}^3$$

thus

$$A_{vh} = 2 \times 10^3 \frac{33 \times 10^{-3}}{287 \times 300} \frac{1}{\sqrt{0.012}} \frac{1}{\sqrt{4 \times 10^3}} = 1.125 \times 10^{-4} \text{ m}^2$$

In case of a circular hole the diameter d becomes, with $A_{vh} = \frac{\pi}{4} d^2$,
 $d = 12 \text{ mm}$.

End of example

28.2.2 The convergent Nozzle

Consider now the fractiousness flow of gas from a large tank ($A_1 \sim \infty$, $V_1 \sim 0$) through a convergent nozzle into a region of pressure, p'_2 (P.a.), see Fig. 28.1. The sonic velocity is not achieved unless the pressure drop between the inside and the outside of the tank is large enough.

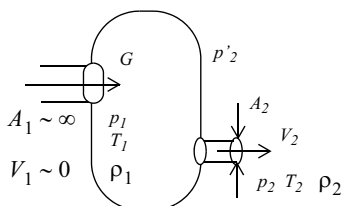


Fig. 28.1 Large tank, fractiousness flow of gas

For small pressure drops the pressures p'_2 and p_2 are the same, and the velocity at the nozzle (venting hole) exit may be calculated by [Vineyard 1975]

$$\frac{V_2^2}{2} = \frac{p_1}{\rho_1 k - 1} \left[1 - \left(\frac{p_2}{p_1} \right)^{\frac{k-1}{k}} \right], \quad (28.9)$$

where for air $k = 1.4$.

The flow rate $G = \rho_2 V_2 A_2$ can be computed by

$$G = \begin{cases} A_2 \sqrt{\frac{2k}{k-1} p_1 \rho_1 \left[\left(\frac{\rho_2}{\rho_1} \right)^{\frac{2}{k}} - \left(\frac{p_2}{p_1} \right)^{\frac{k+1}{k}} \right]} & \frac{p_2}{p_1} > \left[\frac{2}{(k+1)} \right]^{\frac{k}{k-1}}, \\ \frac{A_2 p_1}{\sqrt{T_1}} \sqrt{R} \left(\frac{2}{k+1} \right)^{\frac{(k+1)}{(k-1)}} & \frac{p_2}{p_1} < \left[\frac{2}{(k+1)} \right]^{\frac{k}{k-1}} \end{cases}, \quad (28.10)$$

where R is the characteristic constant of air. The semitropical relation between pressures and densities is given by

$$\frac{p_2}{p_1} = \left(\frac{\rho_2}{\rho_1} \right)^k. \quad (28.11)$$

28.2.3 Rule of Thumb

The venting hole cross-section with respect to the volume to be vented is given by

$$\frac{A}{V} \geq 17-20 \times 10^{-4} \text{ 1/m}, \quad (28.12)$$

where A is the total area of venting hole(s) (m^2) and V the total volume to be vented (m^3), [Droner 1995, Eliot 2002].

28.3 Literature

- Droner Dumb, 1995, *Envisage-1*, document PO-RP-DOR-PL-0038.
- Eliot, A., 2002, *General Design and Interface Requirement Specification* (GDIR), Austrian, AE.RS.ASU.SY.004, issue 2.
- Vineyard, J.K., Street, R.L., 1975, *Elementary Fluid Mechanics*, John Welly & Sons, Inc., ISBN 0-471-90587-9.

29 Examples

29.1 Introduction

In this chapter examples of typical spacecraft related topics are outlined. The examples are defined in such a way that solutions can be achieved by analytical methods and by hand calculations. The classical hand calculations can be done using PC computer tools like EXCEL®, MATLAB®, MATHCAD®, etc.

To set-up the geometrical design of components of a spacecraft structure it is very useful to start with simple strength and stiffness analyses. Most of the examples have this intention, i.e.

- Calculation of natural frequency using the displacement method
- Design example fixed-free beam (strength and stiffness)
- Equivalent dynamic systems
- Comparison of two random vibration specifications
- Enforced random acceleration (strength and stiffness)
- Strength and stiffness analysis of SIMPSAT
- Stiffness calculations using Castigliano's second theorem

Other examples are included to show analysis procedures:

- Modal effective mass of a cantilevered beam
- Component mode synthesis (Craig-Bampton method)

In some examples used references are listed at the end.

This chapter with examples is certainly not complete and may be extended later on.

29.2 Natural Frequencies, an Approximation

29.2.1 Displacement method

A shaft from a mechanism is supported by two bearings and may be idealised as a beam supported by two springs, as illustrated in Fig. 29.1.

The lowest natural frequency of that system is calculated whilst neglecting the mass of the shaft (beam).

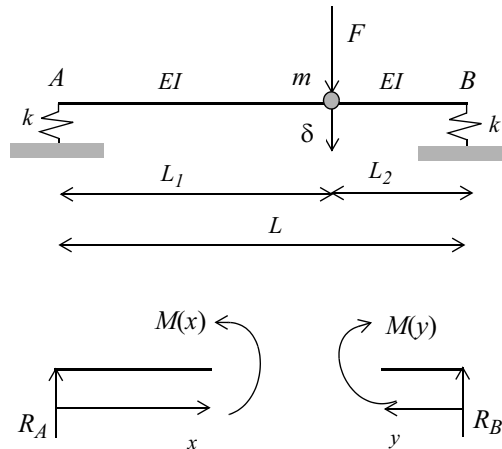


Fig. 29.1 Beam supported by springs

Calculate the displacement δ with the aid of Castigliano's theorem.

The reaction forces at point A and B are

$$R_A = \frac{L_2}{L}F \text{ and } R_B = \frac{L_1}{L}F.$$

The bending moments $M(x)$ and $M(y)$ are

$$M(x) = xR_A = \frac{xL_2}{L}F \text{ and } M(y) = yR_B = \frac{yL_1}{L}F.$$

The total strain energy U can be written as follows

$$U = \int_0^{L_1} \frac{M^2(x)}{2EI} dx + \int_0^{L_2} \frac{M^2(y)}{2EI} dy + \frac{R_A^2}{2k} + \frac{R_B^2}{2k}.$$

The deflection δ due to the applied load F becomes

$$\delta = \frac{\partial U}{\partial F} = \frac{F}{2EIL^2}(L_1^5 + L_2^5) + \frac{F}{k} \left[\left(\frac{L_1}{L} \right)^2 + \left(\frac{L_2}{L} \right)^2 \right].$$

The results may be checked by assuming $L_1 = L_2 = \frac{L}{2}$ and $k \rightarrow \infty$. The deflection δ becomes

$$\delta = \frac{FL^3}{48EI}.$$

If $L_1 = L_2 = \frac{L}{2}$ and $EI \rightarrow \infty$ the deflection δ becomes

$$\delta = \frac{F}{2k},$$

The displacement Δ at an unit load $F = 1$ is given by

$$\Delta = \frac{1}{2EIL^2} (L_1^5 + L_2^5) + \frac{1}{k} \left[\left(\frac{L_1}{L} \right)^2 + \left(\frac{L_2}{L} \right)^2 \right].$$

The natural frequency of the system with the discrete mass m , neglecting the mass of the beam, can be obtained by

$$f_o = \frac{1}{2\pi} \sqrt{\frac{1}{\Delta m}} \text{ (Hz)}.$$

29.3 Design Example Fixed-Free Beam

29.3.1 Introduction

A discrete mass $M = 30$ kg is supported by a fixed-free beam with length $L = 500$ mm. This is illustrated in Fig. 29.2. The cross section of the beam is a square pipe with length L and width b and wall thickness t . The beam is made of an Al-alloy with a Young's modulus $E = 70$ GPa, yield strength $\sigma_Y = 400$ MPa and an ultimate strength $\sigma_U = 525$ MPa.

The flight limit load factors are 20g simultaneously in all three directions (x, y and z).

The minimum natural frequencies in bending are $f \geq 20$ Hz (y- and z-direction) and in tension/compression (x-direction) $f \geq 35$. For the time being the mass of the beam is neglected.

Design the support beam as illustrated in Fig. 29.2.

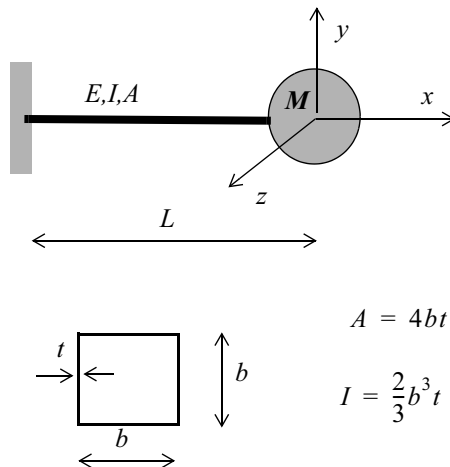


Fig. 29.2 Fixed-free beam with discrete mass

29.3.2 Stiffness calculations

At first the cross section of the beam will be calculated according to the stiffness requirements. The natural frequency with a bending mode in y - and z -direction can be calculated with

$$f_B = \frac{1}{2\pi} \sqrt{\frac{3EI}{ML^3}} \text{ (Hz)}, \quad (29.1)$$

and the natural frequency with a mode in x -direction (longitudinal) can be calculated with

$$f_L = \frac{1}{2\pi} \sqrt{\frac{EA}{ML}} \text{ (Hz)}. \quad (29.2)$$

The stiffness may be expressed as follows

$$EI \geq (2\pi f_B)^2 \left(\frac{ML^3}{3} \right)$$

and

$$AE \geq (2\pi f_L)^2 (ML)$$

To start with, the bending stiffness needed to fulfil the stiffness requirement $f \geq 20 \text{ Hz}$ can be calculated.

$$EI \geq (2\pi f_B)^2 \left(\frac{ML^3}{3} \right) = (2\pi 20)^2 \left(\frac{30 \times 0.5^3}{3} \right) = 1.974 \times 10^4 \text{ Nm}^2$$

$$I = \frac{2}{3}b^3 t = (2\pi f_B)^2 \left(\frac{ML^3}{3E} \right) = 2.82 \times 10^{-7} \text{ m}^4$$

Assuming a wall thickness $t = 0.75$ mm, the length and width of the cross section of the beam becomes $b = 83$ mm.

The cross section becomes $A = 4bt = 2.49 \times 10^{-4} \text{ m}^2$.

The natural frequency in the longitudinal direction is then

$$f_L = \frac{1}{2\pi} \sqrt{\frac{EA}{ML}} = \frac{1}{2\pi} \sqrt{\frac{2.49 \times 10^{-4} \times 70 \times 10^9}{30 \times 0.5}} = 171 \text{ Hz}$$

The bending stiffness EI is dominant with respect to the tension/compression stiffness. The natural frequency with an associated bending mode, with $t = 0.75$ mm and $b = 90$ mm becomes

$$f_{B,1} = \frac{1}{2\pi} \sqrt{\frac{3EI}{ML^3}} = \frac{1}{2\pi} \sqrt{\frac{3 \times 70 \times 10^9 \times \frac{2}{3} \times 0.090^3 \times 0.00075}{30 \times 0.5^3}} = 22.6 \text{ Hz}$$

The fixed-free beam, with a mass m per unit of length (kg/m), has a lowest natural frequency associated with a bending mode given by

$$f_B = \frac{3.516}{2\pi} \sqrt{\frac{EI}{mL^4}} \quad (29.3)$$

The density of Al-allow is $\rho = 2800 \text{ kg/m}^3$, thus the mass per unit of length $m = A\rho = 4bt\rho = 4 \times 0.090 \times 0.00075 \times 2800 = 0.756 \text{ kg/m}$

The minimum natural frequency of the fixed-free beam becomes

$$f_{B,2} = \frac{3.516}{2\pi} \sqrt{\frac{EI}{mL^4}} = \frac{3.516}{2\pi} \sqrt{\frac{70 \times 10^9 \times \frac{2}{3} \times 0.090^3 \times 0.00075}{0.756 \times 0.5^4}} = 411 \text{ Hz}$$

Using the Dunkerley's equation the final natural frequency with a bending mode can be calculated

$$\frac{1}{f_{\text{final}}^2} = \frac{1}{f_{B,1}^2} + \frac{1}{f_{B,2}^2}. \quad (29.4)$$

The final natural frequency associated with bending becomes

$$\frac{1}{f_{\text{final}}^2} = \frac{1}{f_{B,1}^2} + \frac{1}{f_{B,2}^2} = \frac{1}{22.6^2} + \frac{1}{411^2}, f_{\text{final}} = 22.5 \text{ Hz}.$$

The strength requirements will now be investigated.

29.3.3 Strength calculations

Design philosophy

The following design philosophy and factors of safety, illustrated in Fig. 29.3, will be applied.

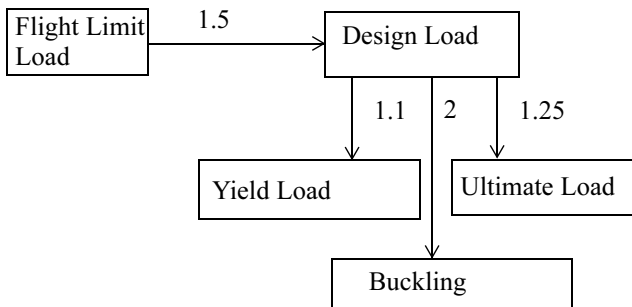


Fig. 29.3 Loads and factors of safety

The design loads are 30g simultaneously in all three directions.

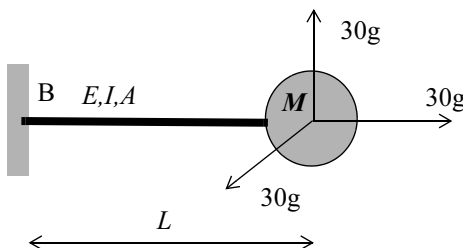


Fig. 29.4 Inertia loads

The cross-section at point *B* (fixed side of the beam) is shown in Fig. 29.5

The normal stress caused by the normal force *N* in x-direction is

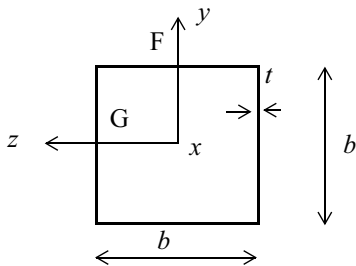
$$\sigma_{xx} = \frac{N}{A} = \frac{Mg_x}{4bt} = 3.27 \times 10^7 \text{ Pa}$$

The maximum bending moment about the y-axis is

$$M_{yy} = Mg_z L = 30 \times 30 \times 9.81 \times 0.5 = 4.415 \times 10^3 \text{ Nm}$$

The maximum bending moment about the z-axis is

$$M_{zz} = Mg_y L = 30 \times 30 \times 9.81 \times 0.5 = 4.415 \times 10^3 \text{ Nm}$$

**Fig. 29.5** Cross section at B

The maximum bending stress (at F and G) in x -direction becomes

$$\sigma_{xx, F} = \frac{\frac{1}{2}M_{zz}b}{I_{zz}} = \frac{\frac{1}{2}M_{zz}b}{\frac{2}{3}b^3t} = \frac{3M_{zz}}{4b^2t} = 5.45 \times 10^8 \text{ Pa.}$$

The shear stresses at the points F and G are

$$\tau_{xy, G} = \tau_{xy, F} = \tau_{xy} = \frac{9D}{16bt} = 2.453 \times 10^6 \text{ Pa.}$$

29.3.4 Effective stress

The 3-D stress state at the point F is

$$[\sigma] = \begin{bmatrix} \sigma_x & 0 & \tau_{xz} \\ 0 & 0 & 0 \\ \tau_{zx} & 0 & 0 \end{bmatrix}$$

The principle stresses are

$$\sigma_1 = \frac{\sigma_x}{2} + \frac{1}{2}\sqrt{\sigma_x^2 + 4\tau_{xz}^2} = 5.777 \times 10^8 \text{ Pa,}$$

$$\sigma_2 = \frac{\sigma_x}{2} - \frac{1}{2}\sqrt{\sigma_x^2 + 4\tau_{xz}^2} = -1.041 \times 10^4 \text{ Pa.}$$

The Von Mises stress becomes

$$\sigma_{VM} = \sqrt{\sigma_x^2 + 3\tau_{xz}^2} = 5.777 \times 10^8 \text{ Pa}$$

The 3-D stress state in G is

$$[\sigma] = \begin{bmatrix} \sigma_x & \tau_{xy} & 0 \\ \tau_{yx} & 0 & 0 \\ 0 & 0 & 0 \end{bmatrix}$$

The principle stresses are

$$\sigma_1 = \frac{\sigma_x}{2} + \frac{1}{2}\sqrt{\sigma_x^2 + 4\tau_{xy}^2} = 5.777 \times 10^8 \text{ Pa},$$

$$\sigma_2 = \frac{\sigma_x}{2} - \frac{1}{2}\sqrt{\sigma_x^2 + 4\tau_{xy}^2} = -1.041 \times 10^4 \text{ Pa}.$$

The von Mises stress becomes

$$\sigma_{VM} = \sqrt{\sigma_x^2 + 3\tau_{xy}^2} = 5.777 \times 10^8 \text{ Pa}.$$

The von Mises stress is too high with respect to the yield stress because, in general, $1.1\sigma_{VM} \leq \sigma_Y$ and $\sigma_Y = 400 \text{ MPa}$. The margin of safety becomes

$$MS = \frac{400}{1.1 \times 559.7} - 1 < 0 \text{ and yielding will occur.}$$

29.3.5 Iterations

The bending stress is quite dominant so b will be dimensioned with respect to the bending stress $\sigma_{xx,F}$ and $\sigma_{xx,G}$.

$$\sigma_{xx,F} = \sigma_{xx,G} = \frac{3M_{zz}}{4b^2 t} = \frac{3M_{yy}}{4b^2 t}$$

thus

$$b \geq \sqrt{\frac{3M_{yy}}{4\sigma_y t}} = \sqrt{\frac{3 \times 4.414e3}{4 \times 400e6 \times 0.00075}} = 0.105 \text{ m.}$$

It is assumed that $b = 120 \text{ mm}$.

The normal stress caused by the normal force N in x-direction is

$$\sigma_{xx} = \frac{N}{A} = \frac{Mg_x}{4bt} = \frac{30x30x9.81}{4x0.120x0.00075} = 2.453 \times 10^7 \text{ Pa}$$

The bending stresses at the points F and G will be

$$\sigma_{xx,F} = \sigma_{xx,G} = \frac{3M_{zz}}{4b^2 t} = \frac{3x4.415e3}{4x0.120^2 x0.00075} = 3.066 \times 10^8 \text{ Pa.}$$

The shear stresses at the points F and G are

$$\tau_{xy,G} = \tau_{xy,F} = \tau_{xy} = \frac{9D}{16bt} = 1.839 \times 10^6 \text{ Pa.}$$

The total normal stress

$$\sigma_{x,F} = \sigma_{xx} + \sigma_{xx,F} = 3.311 \times 10^8 \text{ Pa},$$

$$\sigma_{x,G} = \sigma_{xx} + \sigma_{xx,G} = 3.311 \times 10^8 \text{ Pa}.$$

The von Mises stress becomes

$$\sigma_{VM} = \sqrt{\sigma_x^2 + 3\tau_{xy}^2} = 3.311 \times 10^8 \text{ Pa}.$$

The MS value now obtained is

$$MS = \frac{400}{1.1 \times 344.5} - 1 = 0.098.$$

The Euler buckling load can be calculated with

$$F_{buckling} = \frac{\pi^2 EI}{4L^2} \quad (29.5)$$

With $b = 120 \text{ mm}$ and $t = 0.75 \text{ mm}$, the second moment of area is then

$$I = \frac{2}{3}b^3t = \frac{2}{3} \times 0.120^3 \times 0.00075 = 8.64 \times 10^{-7} \text{ m}^4.$$

The Euler buckling load for a fixed-free beam is

$$F_{buckling} = \frac{\pi^2 EI}{4L^2} = \frac{\pi^2 \times 70 \times 10^9 \times 8.64 \times 10^{-7}}{4 \times 0.5^2} = 5.97 \times 10^5 \text{ N}.$$

The MS value against buckling of the beam is given by

$$MS = \frac{F_{buckling}}{2Mg_x} - 1 = \frac{5.97 \times 10^5}{2 \times 30 \times 30 \times 9.81} - 1 = 32$$

The MS value against buckling is very high, therefore no problems with respect to buckling are expected.

The bending stiffness EI is dominant with respect to the tension/compression stiffness. The natural frequency with an associated bending mode, with $t = 0.75 \text{ mm}$ and $b = 120 \text{ mm}$ becomes

$$f_{B,1} = \frac{1}{2\pi} \sqrt{\frac{3EI}{ML^3}} = \frac{1}{2\pi} \sqrt{\frac{3 \times 70 \times 10^9 \times \frac{2}{3} \times 0.120^3 \times 0.00075}{30 \times 0.5^3}} = 34.8 \text{ Hz}.$$

The density of Al-allow is $\rho = 2800 \text{ kg/m}^3$, thus the mass per unit of length $m = A\rho = 4bt\rho = 4 \times 0.120 \times 0.00075 \times 2800 = 1.008 \text{ kg/m}$.

The minimum natural frequency of the fixed-free beam becomes

$$f_{B,2} = \frac{3.516}{2\pi} \sqrt{\frac{EI}{mL^4}} = \frac{3.516}{2\pi} \sqrt{\frac{70 \times 10^9 \times \frac{2}{3} \times 0.120^3 \times 0.00075}{1.008 \times 0.5^4}} = 548 \text{ Hz}$$

Using Dunkerley's equation the final natural frequency with a bending mode can be calculated

$$\frac{1}{f_{\text{final}}^2} = \frac{1}{f_{B,1}^2} + \frac{1}{f_{B,2}^2}.$$

The final natural frequency associated with bending becomes

$$\frac{1}{f_{\text{final}}^2} = \frac{1}{f_{B,1}^2} + \frac{1}{f_{B,2}^2} = \frac{1}{34.8^2} + \frac{1}{548^2}, f_{\text{final}} = 34.7 \text{ Hz.}$$

29.4 Equivalent dynamic systems

29.4.1 Introduction

For dynamic response analysis, the cantilevered beam with the discrete mass at the end of the beam will be transferred into three single degree of freedom systems:

1. Bending in y-direction
2. Bending in z-direction
3. Tension/compression in x-direction

To calculate the spring stiffness, unit loads are applied at the location of the discrete mass M ; $F_y = 1 \text{ N}$, $F_z = 1 \text{ N}$ and $N = 1 \text{ N}$. The displacement will be calculated using second theorem of Castigliano, $\delta = \frac{\partial U}{\partial F}$

where: U is the strain energy with $U = \frac{1}{2} \int_V \sigma \epsilon dV$, F is generalised force, δ is

the displacement, σ is the stress and ϵ is the strain.

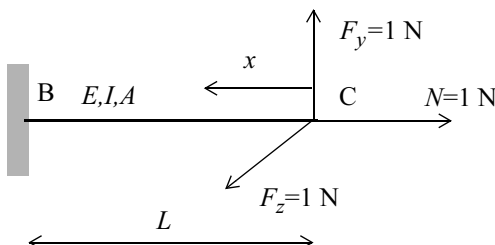


Fig. 29.6 Unit loads

The strain energy in the cantilevered beam (rod) can be expressed as follows

$$U = \frac{1}{2} \int_0^L \frac{(F_y x)^2}{EI} dx + \frac{1}{2} \int_0^L \frac{(F_z x)^2}{EI} dx + \frac{1}{2} \int_0^L \frac{N^2}{EA} dx$$

$$U = \frac{1}{2} \left[\frac{F_y L^3}{EI} + \frac{F_z L^3}{EI} + \frac{NL}{EA} \right]$$

The displacements in x, y and z-direction can now be calculated

- $\delta_x = \frac{\partial U}{\partial N} = \frac{NL}{EA} = \frac{L}{EA}$
- $\delta_y = \frac{\partial U}{\partial F_y} = \frac{F_y L^3}{3EI} = \frac{L^3}{3EI}$
- $\delta_z = \frac{\partial U}{\partial F_z} = \frac{F_z L^3}{3EI} = \frac{L^3}{3EI}$

In case of a dominant discrete mass, the spring stiffness can now be derived in a very straight forward way, $k = \frac{1}{\delta}$ (N/m). The mass of the beam/rod has been neglected.

The equivalent single degree of freedom (SDOF) dynamic systems are shown Table 29.1.

Table 29.1 Equivalent single degree of freedom systems

SDOF dynamic system	x-direction	y-direction	z-direction
	k	k	k
	$\frac{EA}{L}$	$\frac{3EI}{L^3}$	$\frac{3EI}{L^3}$
	m	m	m
	M	M	M

The undamped equation of motion of the equivalent SDOF system, with an enforced acceleration $\ddot{u}(t)$ is with $y(t) = x(t) - u(t)$

$$\ddot{y}(t) + \frac{k}{M}y(t) = \ddot{y}(t) + \omega_o^2 y(t) = -\ddot{u}(t)$$

29.5 Random Vibrations

29.5.1 Comparison of two random vibration specifications

ESA specifications

The unit specification as specified by ESA to test a unit against random vibrations is given with:

Frequency Domain [Hz]	PSD [g^2/Hz]
20–100	3 dB/oct
100–400	$0.05 \frac{(m + 20)}{(m + 1)}$
400–2000	–3dB/oct

With m the total mass of the unit [kg].

NASA specifications

The unit specifications as outlined by NASA to test a unit against random vibrations are given with:

Frequency Domain [Hz]	PSD [g^2/Hz]
20–50	6 dB/oct
50–800	0.16
800–2000	–6 dB/oct

Unit

A unit (dynamic system) with a mass $m=5$ kg and a first natural frequency $f_o = 140$ Hz shall be tested against either the ESA or NASA specifications. Find out for which specifications the unit the acceleration causes maximum loads in the unit?

Tasks

1. Calculate for both specifications the g_{rms} (g)
2. For which m have both specifications equal g_{rms} (g)?
3. For which m have both specifications equal maximum PSD values (g^2/Hz)?
4. Find out the worst case random vibration acceleration specification for the given unit?
5. What is the 3σ reaction force for the worst case random acceleration for the given unit? The amplification factor $Q = 10$.

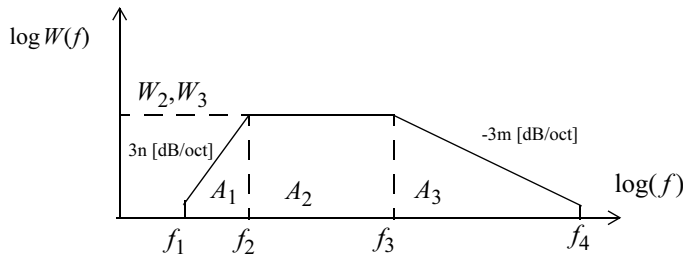


Fig. 29.7 PSD function $W(f)$ versus frequency f (Hz)

The g_{rms} of both specifications can be calculated by (see Fig. 29.7)

$$g_{\text{rms}}^2 = \int_0^\infty W(f) df = A_1 + A_2 + A_3. \quad (29.6)$$

where

$$A_1 = \frac{W_2 f_2}{n+1} \left[1 - \left(\frac{f_1}{f_2} \right)^{n+1} \right], \quad n > 0,$$

$$A_2 = W_2(f_3 - f_2),$$

$$A_3 = \frac{W_3 f_3}{m+1} \left[\left(\frac{f_4}{f_3} \right)^{m+1} - 1 \right], \quad m < 0, \quad (m \neq -1).$$

For $m = -1$ (with the help of the rule of l'Hôpital):

$$A_3 = W_3 f_3 \ln \left(\frac{f_4}{f_3} \right) = 2.303 W_3 f_3 \log \left(\frac{f_4}{f_3} \right).$$

The random vibration specification given by NASA is independent of the mass. We have the following properties; $n = 2$, $m = -2$, $f_1 = 20$, $f_2 = 50$, $f_3 = 800$ and $f_4 = 2000$ Hz. The PSD values are respectively $W_2 = W_3 = 0.16 \text{ g}^2/\text{Hz}$. The areas now become

$$A_1 = \frac{W_2 f_2}{n+1} \left[1 - \left(\frac{f_1}{f_2} \right)^{n+1} \right] = 2.5 \text{ g}^2,$$

$$A_2 = W_2(f_3 - f_2) = 120 \text{ g}^2,$$

$$A_3 = \frac{W_3 f_3}{m+1} \left[\left(\frac{f_4}{f_3} \right)^{m+1} - 1 \right] = 76.8 \text{ g}^2.$$

Thus the

$$g_{\text{rms}} = \sqrt{\int_0^\infty W(f) df} = \sqrt{A_1 + A_2 + A_3} = 14.1 \text{ g}.$$

If we assume $g_{\text{rms}}^{\text{ESA}} = g_{\text{rms}}^{\text{NASA}}$ we have to calculate the value of the PSD values $W_2 = W_3$ at the frequencies f_2 and f_3 (Hz). The random vibration specifications given by ESA have the following properties; $n = 1, m = -1, f_1 = 20, f_2 = 100, f_3 = 400$ and $f_4 = 2000$ Hz.

$$g_{\text{rms}}^{\text{ESA}} = \sqrt{W_2} \sqrt{\frac{f_2}{n+1} \left[1 - \left(\frac{f_1}{f_2} \right)^{n+1} \right] + f_3 - f_2 + f_3 \ln \left(\frac{f_4}{f_3} \right)} = 31.5 \sqrt{W_2}.$$

It is known that

$$g_{\text{rms}}^{\text{ESA}} = 31.5 \sqrt{W_2} = g_{\text{rms}}^{\text{NASA}} = 14.1 \text{ g}, \text{ thus } W_2 = W_3 = 0.2003 \text{ g}^2/\text{Hz}.$$

The ESA specification states that $W_2 = 0.05 \frac{m+20}{m+1}$. From this it is possible to

calculate the mass $m = 5.3$ kg. This is the answer to question 2.

The answer to question 3 is not so difficult. It is known that

$$PSD_{\text{ESA}} = PSD_{\text{NASA}} = 0.05 \frac{(m+20)}{(m+1)} = 0.16 \text{ g}^2/\text{Hz}. \quad (29.7)$$

From (29.7) it is possible to calculate the mass $m = 7.6$ kg for which the maximum PSD values are equal.

For the unit with a mass $m = 5$ kg and a natural frequency of $f_o = 140$ Hz the worst specification concerning the random vibration at the base of that dynamic system must be found. This will define the worst random response characteristics of the unit for both the ESA and NASA specification. The Miles' equation will be applied. The PSD value applicable for ESA with a mass $m = 5$ kg becomes

$$W_{\text{ESA}}(f_o) = 0.05 \frac{(m+20)}{(m+1)} = 0.21 \text{ g}^2/\text{Hz}.$$

The ratio of responses can be calculated

$$\frac{\sqrt{\frac{\pi}{2} f_o Q W_{\text{ESA}}(f_o)}}{\sqrt{\frac{\pi}{2} f_o Q W_{\text{NASA}}(f_o)}} = \sqrt{\frac{W_{\text{ESA}}(f_o)}{W_{\text{NASA}}(f_o)}} = \sqrt{\frac{0.21}{0.16}} = 1.14,$$

and it can be concluded that the ESA specification will result in higher responses with respect to the NASA specification.

For the fifth question, the rms acceleration of the unit is calculated using Miles' equation. The 3σ reaction force F_{reaction} due to the base excitation becomes

$$F_{\text{reaction}} = 3m \sqrt{\frac{\pi}{2} f_o Q W_{\text{ESA}}(f_o)} = 3 \times 5 \times 9.81 \sqrt{\frac{\pi}{2} \times 140 \times 10 \times 0.21} = 3162 \text{ N}.$$

29.5.2 Enforced random Acceleration

The nutation damper is used to damp out the nutations of a spinning satellite. The nutation damper consist of two reservoirs connected by two tubes with non-equal diameters (Figure 29.8, “Nutation damper,” on page 467). A fluid flows through the pipes which causes the damping forces.

In the structural analysis example the tube with the greatest diameter will be considered with respect to strength and stiffness. The tube is filled with fluid.

The goal of this example is to show a design analysis procedure in the case where random vibrations are involved.

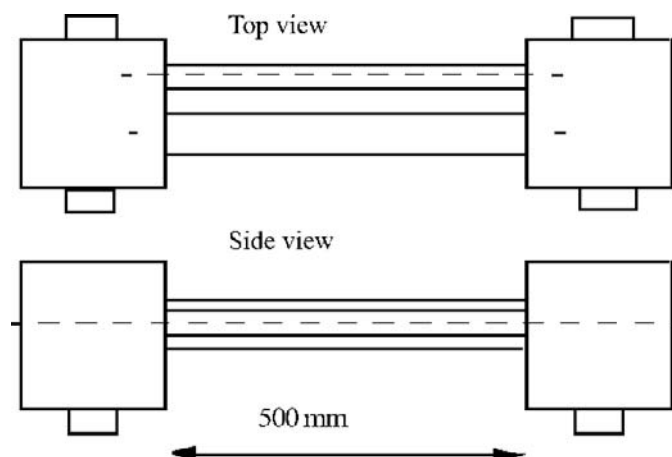


Fig. 29.8 Nutation damper

The following activities are to be done:

1. The calculation of the lowest natural frequency of the tube with the greatest diameter d (m), assuming clamped-clamped conditions.
2. Representation of the clamped-clamped tube in a simple mass-spring-damper system
3. Calculation of the rms responses of the mass-spring-damper system
4. Translation of mass-spring-damper responses to the clamped-clamped tube; bending moments and stresses.

The nutation will be excited with random enforced vibrations via the houses to which both tubes are connected.

Table 29.2 Random vibrations

Frequency Domain (Hz)	Acceleration Spectral Density ($\frac{g^2}{Hz}$)
20–50	6 dB/oct
50–800	0.2
800–2000	-6dB/oct
Grms	13.3 Grms

Clamped-Clamped Tube

The clamped-clamped tube and its characteristics are illustrated in Fig. 29.9.

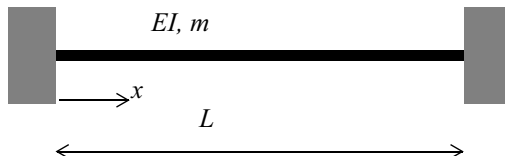


Fig. 29.9 Clamped-clamped beam

Natural Frequency

The natural frequency f_o (Hz) of a clamped-clamped beam, with a constant mass distribution m (kg/m) over the length L (m) and bending stiffness EI (Nm²), can be calculated by [Harris 1976]

$$f_o = \frac{22.4}{2\pi} \sqrt{\frac{EI}{mL^4}}. \quad (29.8)$$

The associated mode shape is:

$$\phi(x) = (\cos \kappa x - \cosh \kappa x) - 0.9825(\sin \kappa x - \sinh \kappa x) \quad (29.9)$$

and:

$$\kappa = \frac{\omega^2 m}{EI}, \quad (29.10)$$

with ω the radian frequency (Rad/s).

Rayleigh Quotient

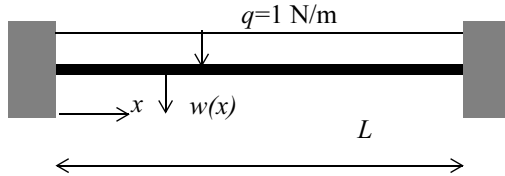


Fig. 29.10 Clamped-clamped beam with unit distributed loading

The static deflection $w(x)$ of the beam with a constant bending stiffness EI , due to the constant distributed load per unit length $q=1 \text{ N/m}$, is [Prescott 1924, Ludolph 1961]:

$$EIw(x) = \frac{1}{24}x^4 - \frac{1}{12}x^3L + \frac{1}{24}xL^2 \quad (29.11)$$

The Rayleigh quotient represents in fact the eigenvalue problem of a discrete or continuous dynamic system. For a bending beam the Rayleigh quotient is as follows:

$$R(u) = \frac{\frac{1}{2} \int_0^L EIu''^2 dx}{\frac{1}{2} \int_0^L mu^2 dx} \quad (29.12)$$

where u is the assumed eigenfunction or mode shape and u'' is the second derivative of the eigenfunction with respect to x .

An eigenfunction u is assumed to represent the static deflection of a clamped-clamped beam statically loaded with a constant unit distributed running load $q = 1 \text{ N/m}$. The assumed eigenfunction will be:

$$u(x) = \left(\frac{x}{L}\right)^4 - 2\left(\frac{x}{L}\right)^3 + \left(\frac{x}{L}\right)^2 \quad (29.13)$$

With the assumed eigenfunction $u(x)$ the Rayleigh quotient becomes

$$\omega^2 \cong R(u) = \frac{\frac{1}{2} \int_0^L EIu''^2 dx}{\frac{1}{2} \int_0^L mu^2 dx} = 504.10 \frac{EI}{mL^4}, f = \frac{22.4}{2\pi} \sqrt{\frac{EI}{mL^4}}.$$

The approximation is very close to the result obtained in (29.8).

Equations of Motion

With aid of the Lagrange equation it is possible to set up the equations of motion for the clamped-clamped bending beam. The total (absolute) displacement of the bending beam is the deflection of the beam $w(x, t)$ complemented with the displacement of the base $v(t)$. The total displacement $y(x, t)$ is given with:

$$y(x, t) = w(x, t) + v(t) = u(x)q(t) + v(t) \quad (29.14)$$

where $q(t)$ is the generalized coordinate or coefficient of modal amplitude.

The strain (potential) energy in the beam is:

$$U = \frac{1}{2}q^2 \int_0^L EIu''^2 dx = \frac{1}{2}\left(\frac{0.8EI}{L^3}\right)q^2 \quad (29.15)$$

The kinetic energy T is given with:

$$\frac{1}{2} \int_0^L m(u\ddot{q} + \ddot{v})^2 dx = \frac{1}{2}(0.001587mL\ddot{q}^2 + 0.03333mLv\dot{q} + mL\ddot{v}^2) \quad (29.16)$$

The Lagrange equation for the parameter $q(t)$ and $v(t)$:

$$\frac{\partial}{\partial t} \frac{\partial T}{\partial \dot{q}} - \frac{\partial T}{\partial q} + \frac{\partial U}{\partial q} = 0 \text{ and } \frac{\partial}{\partial t} \frac{\partial T}{\partial \dot{v}} - \frac{\partial T}{\partial v} + \frac{\partial U}{\partial v} = 0 \quad (29.17)$$

will give the equations of motion:

$$mL \begin{bmatrix} 0.001587 & 0.03333 \\ 0.03333 & 1 \end{bmatrix} \begin{bmatrix} \ddot{q} \\ \ddot{v} \end{bmatrix} + \frac{0.8EI}{L^3} \begin{bmatrix} 1 & 0 \\ 0 & 0 \end{bmatrix} \begin{bmatrix} q \\ v \end{bmatrix} = \begin{bmatrix} 0 \\ 0 \end{bmatrix} \quad (29.18)$$

Finally the equation of motion can be written as:

$$0.001587mL\ddot{q} + \frac{0.8EI}{L^3}q = -0.03333mL\ddot{v} \quad (29.19)$$

or

$$\ddot{q} + \frac{504.10EI}{mL^4}q = -21.1238\ddot{v} \quad (29.20)$$

$$\ddot{q} + \omega_o^2 q = -21.1238\ddot{v} \quad (29.21)$$

The equivalent mass-spring of the dynamic system

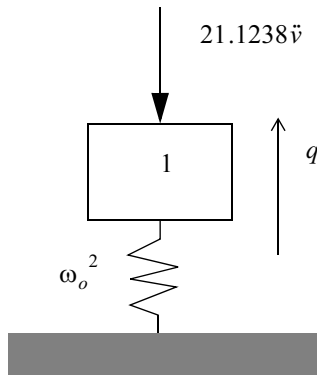


Fig. 29.11 Equivalent mass-spring system

After introduction of the ad-hoc modal viscous damping, the following mass-spring-damper system can be derived

$$\ddot{q} + 2\xi\omega_o\dot{q} + \omega_o^2 q = -21.1238\ddot{v}. \quad (29.22)$$

Enforced Random Vibrations

The dynamic system can be described with the following equation:

$$\ddot{q} + \omega_o^2 q = -\beta\ddot{v} \quad (29.23)$$

The modal viscous damping is added on an ad-hoc basis, thus

$$\ddot{q} + 2\xi\omega_o\dot{q} + \omega_o^2 q = -\beta\ddot{v} \quad (29.24)$$

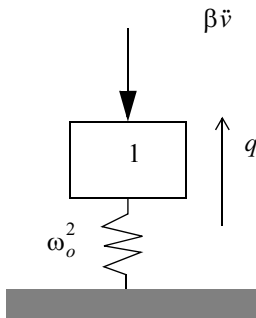


Fig. 29.12 Equivalent mass-spring system with base excitation $\beta \ddot{v}$

The 3x rms (3σ) acceleration of the mass may be calculated with Miles' formula

$$\ddot{q}_{3rms} = 3|\beta| \sqrt{\frac{\pi}{2} f_o Q W_{\ddot{v}}(f_o)} \quad (29.25)$$

and:

$$q_{rms} = \frac{\ddot{q}_{rms}}{\omega_o^2} \quad (29.26)$$

where q is the generalised coordinate (displacement of mass with respect to base), rms is the root mean square, f_o is the natural frequency of mass-spring system $f_o = \frac{\omega_o}{2\pi}$ (Hz), Q is the amplification factor $Q = \frac{1}{2\xi}$ (in general a value $Q=10$ is used in Miles' formula) and $W_{\ddot{v}}(f_o)$ is the Power Spectral density (PSD) $\left(\frac{g^2}{Hz}\right)$

of the enforced acceleration \ddot{v} at the natural frequency f_o

Accelerations

The physical acceleration is

$$\ddot{w}(t) = u(x)\ddot{q}(t). \quad (29.27)$$

The rms value of the acceleration $w(x, t)$ is:

$$\ddot{w}(x)_{rms} = u(x)\ddot{q}_{rms}. \quad (29.28)$$

At the position $x = \frac{L}{2}$ the acceleration is $\ddot{w}\left(\frac{L}{2}\right)_{rms} = u\left(\frac{L}{2}\right)\ddot{q}_{rms} = \frac{1}{16}\ddot{q}_{rms}$.

Displacements

The physical displacement is

$$w(t) = u(x)q(t).$$

The rms value of the acceleration $w(x, t)$ is:

$$w(x)_{rms} = u(x)q_{rms}. \quad (29.29)$$

At the position $x = \frac{L}{2}$ the acceleration is $w\left(\frac{L}{2}\right)_{rms} = u\left(\frac{L}{2}\right)q_{rms} = \frac{1}{16}q_{rms}$

Forces

The forces and stresses at the clamped interfaces ($x = 0, L$) and in the middle of the $\left(x = \frac{1}{2}L\right)$ are calculated.

The bending moment is defined with:

$$M(x) = -EIw''(x) \quad (29.30)$$

and the shear force:

$$D(x) = -EIw'''(x) \quad (29.31)$$

The bending moment $M(x)$ and the shear force $D(x)$ are expressed in the assumed mode $u(x)$ and the generalized coordinate $q(t)$, hence the bending moment is:

$$M(x, t) = -EIu''(x)q(t) = -EI\left[\frac{12}{L^2}\left(\frac{x}{L}\right)^2 - \frac{12}{L^2}\left(\frac{x}{L}\right) + \frac{2}{L^2}\right]q(t)) \quad (29.32)$$

and the shear force:

$$D(x, t) = -EIu'''(x)q(t) = -EI\left[\frac{24}{L^3}\left(\frac{x}{L}\right) - \frac{12}{L^3}\right]q(t)) \quad (29.33)$$

Expressed in the rms value of the generalized coordinate $q(t)$:

$$M_{rms}(x) = EI\left[\frac{12}{L^2}\left(\frac{x}{L}\right)^2 - \frac{12}{L^2}\left(\frac{x}{L}\right) + \frac{2}{L^2}\right]q_{rms} \quad (29.34)$$

and the shear force:

$$D_{rms}(x) = EI\left[\frac{24}{L^3}\left(\frac{x}{L}\right) - \frac{12}{L^3}\right]q_{rms} \quad (29.35)$$

At the locations $x = 0, L$ and $x = \frac{1}{2}L$ the rms values of the bending moment

and the shear forces are:

$$x = 0$$

$$M_{rms}(0) = EI\left[\frac{2}{L^2}\right]q_{rms}, \quad (29.36)$$

$$D_{rms}(0) = EI\left[\frac{12}{L^3}\right]q_{rms}. \quad (29.37)$$

$$x = \frac{L}{2}$$

$$\left|M_{rms}\left(\frac{L}{2}\right)\right| = EI\left[\frac{1}{L^2}\right]q_{rms}, \quad (29.38)$$

$$D_{rms}\left(\frac{L}{2}\right) = 0. \quad (29.39)$$

$$x = L$$

$$M_{rms}(L) = EI \left[\frac{2}{L^2} \right] q_{rms}, \quad (29.40)$$

$$D_{rms}(L) = EI \left[\frac{12}{L^3} \right] q_{rms}. \quad (29.41)$$

Stresses

The bending stresses σ_{bend} (Pa) in the extreme fibre e of the tube with a diameter d (m) and a wall-thickness t (m) can be calculated with:

$$\sigma_{bend} = \frac{M(x)e}{I} = \frac{4M(x)}{\pi d^2 t} \quad (29.42)$$

with I the second moment of area $I = \frac{\pi d^3 t}{8}$ (m^4) and e the extreme fibre distance $e = \frac{d}{2}$ (m).

The maximum shear stress τ (Pa) at the neutral plane (the plane with zero bending stress) of the tube with diameter d and wall thickness t is given by:

$$\tau_{max} = \frac{D(x)S}{It} = \frac{4D(x)}{\pi dt} \quad (29.43)$$

where S the first moment of area with respect to the neutral plane of the tube $S = \frac{d^2 t}{2}$ (m^3).

Numerical calculations

The nutation damper and materials used have the following physical properties:

- Tube is made of an Al-alloy
 - E modulus $E = 70 \times 10^9$ Pa
 - Poisson's ratio $\nu = 0.33$
 - Yield stress $\sigma_{0.2} = 250 \times 10^6$ Pa
 - Density $\rho = 2800$ kg/m³
- Averaged diameter tube $d = 15$ mm
- Wall thickness $t = 0.5$ mm
- Length of tube $L = 500$ mm
- Tube is for 100% filled with fluid with a density of $\rho = 1100$ kg/m³

Questions

1. Calculate the mass per unit length m
2. Calculate the second moment of inertia I
3. Calculate the natural frequency f_o corresponding to the assumed mode $u(x)$
4. Estimate PSD value of the base acceleration at f_o
5. Calculate the 3σ value of q , $Q = 10$
6. Calculate the relative 3σ acceleration $w\left(\frac{L}{2}\right)$
7. Calculate the 3σ bending moment $M(0) = M(L)$
8. Calculate the 3σ shear force $D(0) = D(L)$
9. Calculate stresses and compare with $\sigma_{0.2}$

Answers

1. The mass per unit of length m [kg/m] is

$$m = 2\pi dt \rho_{al} + \frac{\pi}{4} d^2 \rho_{fluid} = 0.26 \text{ kg/m}$$

2. The second moment of area of the tube is

$$I = \frac{\pi}{8} d^3 t = 6.6268 \times 10^{-4} \text{ m}^4$$

3. The first natural frequency of the clamped-clamped tube filled with fluid is

$$f_o = \frac{22.4}{2\pi} \sqrt{\frac{EI}{mL^4}} = 190 \text{ Hz}$$

$$u(x) = \left(\frac{x}{L}\right)^4 - 2\left(\frac{x}{L}\right)^3 + \left(\frac{x}{L}\right)^2$$

4. The PSD of the base acceleration at f_o is

$$W(f_o) = 0.2 \frac{\text{g}^2}{\text{Hz}}$$

5. The 3σ value of \ddot{q} and q are

$$\ddot{q}_{3\sigma} = 3 \sqrt{\frac{\pi}{2} f_o Q W(f_o)} = 73.3 \text{ g},$$

$$q_{3\sigma} = \frac{\ddot{q}_{3\sigma}}{(2\pi f_o)^2} = 5.0 \times 10^{-4} \text{ m.}$$

6. The 3σ bending moment $M(L)$ is

$$M_{3\sigma}(L) = EI \left[\frac{2}{L^2} \right] q_{3\sigma} = 0.19 \text{ Nm.}$$

7. The 3σ bending moment $D(0)$ is

$$D_{3\sigma}(L) = EI \left[\frac{12}{L^3} \right] q_{3\sigma} = 2.25 \text{ N.}$$

8. The bending stress and shear stress are

$$\sigma_{bend} = \frac{M(x)e}{I} = \frac{4M(x)}{\pi d^2 t} = 2.04 \times 10^6 \text{ Pa,}$$

$$\tau_{max} = \frac{D(x)S}{It} = \frac{4D(x)}{\pi dt} = 3.82 \times 10^5 \text{ Pa.}$$

The yield stress is $\sigma_{0.2} = 250 \times 10^6 \text{ Pa}$. We have to compare the 2-D stress state with the 1-D stress state. This can be done using the von Mises stress, $\sigma_{VM} = \sqrt{\sigma_{bend}^2 + 3\tau_{max}^2}$, which is low compared with the yield stress.

Literature

Harris, C.M., Crede, C.E., 1976, *Shock and Vibration Handbook*, second edition, McGraw-Hill, ISBN 0-07-026799-5.

Ludolph, G.L., Potma, A., Legger, J., 1961, *Leerboek der Mechanica*, Wolters, Groningen.

Prescott, J., 1924, *Applied Elasticity*, Dover Publications.

29.6 Strength and Stiffness Analysis SIMPSAT

29.6.1 Introduction

Using a simplified satellite structure the design structural analysis will be illustrated. The SIMPSAT satellite will be launched with the ARIANE 4 launch vehicle (L/V). The Arianespace design specifications [Arianespace 1999] will be applied.

SIMPSAT major payload is an experiment with total mass of $M = 500 \text{ kg}$ and is placed on a beam-like structure. The length between the interface (I/F) and the centre of gravity (CoG) of the experiment is $L = 1000 \text{ mm}$. We assume a point mass $M = 500 \text{ kg}$ and the total length of the beam structure $L = 1000 \text{ mm}$. SIMPSAT is illustrated in Fig. 29.13. We assume only loads in plane, respectively in x- and y-direction. This is of course a simplification, however, the approach with respect to the design analysis will not change if the approach is 2-D instead of 3-D.

The goal of this example is to show the approach used to design a load carrying structure. Strength and stiffness will be considered and margins of safety calculated.

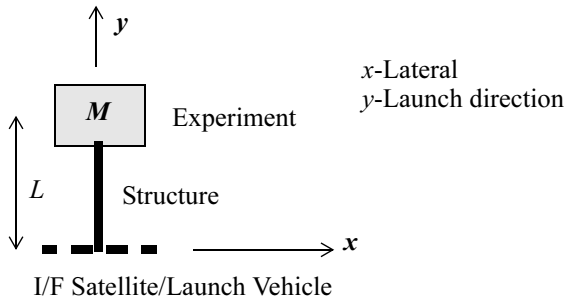


Fig. 29.13 SIMPSAT; Experiment and Structure

29.6.2 Design Philosophy

In Fig. 29.14 the relation between different kinds of loads is indicated. In case of a preliminary design of the structure the design loads will be used to dimension the satellite structure and in fact determine the design of the structure.

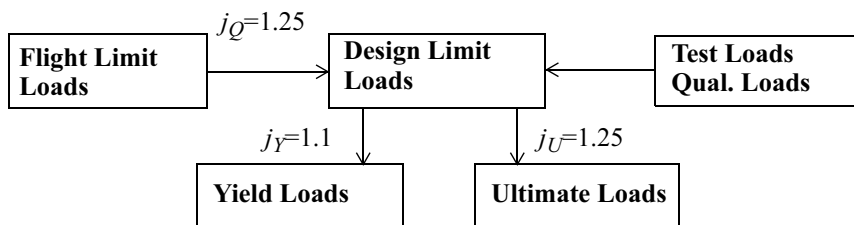


Fig. 29.14 Factors of Safety (FoS)

The Margins of Safety (MS) values shall be $MS \geq 0$ for the yield and ultimate loads respectively. The factors of safety will strongly depend upon the space project and mission, however, for SIMPSAT the FoS are defined in Fig. 29.14. The MS is defined as

$$MS = \frac{\sigma_{allowable}}{j\sigma_{stress_analysis}} - 1 \quad (29.44)$$

where j is the appropriate factor of safety (yield, ultimate), $\sigma_{allowable}$ is the allowable stress (yield, ultimate, buckling,...) and $\sigma_{stress_analysis}$ is the calculated stress (design limit loads)

29.6.3 Quasi-Static Loads (QSL)

The QSL are the static design limit loads (DLL) to be used for initial spacecraft structure design. The load factors are in (g).

Table 29.3 QSL

Accelerations (g) QSL		
ARIANE 4	Launch Direction	Lateral
Maximum Acceleration	-5.5	±1.5

29.6.4 Minimum Natural Frequencies

The stiffness requirements are in general translated into minimum natural frequencies:

- Launch direction (y-axis) $f_y \geq 35 \text{ Hz}$
- Lateral direction (x-axis) $f_x \geq 15 \text{ Hz}$

29.6.5 Material properties

The beam structure (load carrying structure) will be constructed from an isotropic Al-alloy with the following properties:

- Modulus of Elasticity (Young's modulus) $E = 70 \text{ GPa}$
- The ultimate stress $\sigma_{ultimate} = 480 \text{ MPa}$
- The yield stress $\sigma_{yield} = 410 \text{ MPa}$
- Density $\rho = 2770 \text{ kg/m}^3$
- Poisson's ratio $\nu = 0.3$
- The shear modulus $G = \frac{E}{2(1+\nu)} = 26.9 \text{ GPa}$

29.6.6 Natural Frequencies

The requirements about the minimum natural frequencies are specified both for the launch and lateral direction.

Launch direction

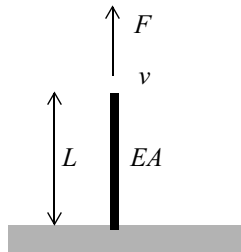


Fig. 29.15 Stiffness in launch direction

A force F (N) applies to the rod (bar) in y -direction. The rod has a cross-section A (m^2) and a length L (m). The elongation of the rod, due to the applied force F , is denoted with v m. The stiffness of the rod k (N/m) is defined with

$$k = \frac{F}{v}. \quad (29.45)$$

The total strain ε is

$$\varepsilon = \frac{v}{L}. \quad (29.46)$$

The strain ε is the ratio between the occurring stress and the modulus of elasticity (Hooke's Law)

$$\varepsilon = \frac{\sigma}{E} = \frac{F}{AE}. \quad (29.47)$$

Thus the elongation v of the rod now becomes

$$v = \varepsilon L = \frac{FL}{AE}, \quad (29.48)$$

and therefore the stiffness k (N/m)

$$k = \frac{AE}{L}. \quad (29.49)$$

The natural frequency can be calculated with

$$f_n = \frac{1}{2\pi} \sqrt{\frac{k}{M}} = \frac{1}{2\pi} \sqrt{\frac{AE}{ML}} \quad (29.50)$$

It follows that

$$\frac{AE}{L} \geq M(2\pi f_n)^2 \quad (29.51)$$

The mass of the structure will be neglected for the time being, therefore an uncertainty factor $j=1.25$ will be taken into account. The required stiffness must be

$$\frac{AE}{L} \geq 500(2\pi 1.25 * 35)^2 = 3.778 \times 10^7 \text{ N/m} \quad (29.52)$$

The conclusion is that the minimum area of the cross-section of the rod (tension and compression) must be $A \geq 5.397 \times 10^{-4} \text{ m}^2$.

Lateral direction

The deflection u (m) at the end of the clamped bending beam with bending stiffness EI (Nm^2), is illustrated in Fig. 29.16.

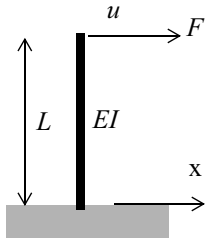


Fig. 29.16 Stiffness in lateral direction

The deflection u , due to the bending of the beam can be calculated with

$$u = \frac{FL^3}{3EI}. \quad (29.53)$$

The stiffness k (N/m) is defined with

$$k = \frac{F}{u} = \frac{3EI}{L^3}, \quad (29.54)$$

the natural frequency can be calculated with

$$f_n = \frac{1}{2\pi} \sqrt{\frac{k}{M}} = \frac{1}{2\pi} \sqrt{\frac{3EI}{ML^3}}. \quad (29.55)$$

It follows that

$$\frac{3EI}{L^3} \geq M(2\pi f_n)^2. \quad (29.56)$$

The mass of the structure will be neglected for the time being, therefore an uncertainty factor $j=1.25$ will be taken into account. The required stiffness must be

$$\frac{3EI}{ML^3} \geq 500(2\pi 1.25 \cdot 15)^2 = 6.940 \times 10^6 \text{ N/m} \quad (29.57)$$

The conclusion is that the minimum second moment of area of the cross-section of the bending beam must be $I \geq 3.305 \times 10^{-5} \text{ m}^4$.

29.6.7 Selection of the type of structure

Cylinder

If we select a cylinder with radius R (m), wall-thickness t (m) and length L (m), the area A (m^2) and the second moment of area I (m^4) of the cross-section can be calculated.

- The area $A = 2\pi R t$ (m^2)
- The second moment of area $I = \pi R^3 t$ (m^4)

It follows that

$$R = \sqrt[3]{\frac{I}{\pi t}}, \quad (29.58)$$

and

$$t = \sqrt{\frac{A^3}{8\pi^2 I}}. \quad (29.59)$$

In previous sections A and I were calculated, a cross-section with $t=0.5$ mm and $R=300$ mm and with an area $A = 9.42 \times 10^{-4} \text{ m}^2$ is chosen and the second moment of area becomes $I = 4.24 \times 10^{-5} \text{ m}^4$, which are both greater than the required section properties.

The natural frequencies both in launch and lateral directions become

- launch direction $f_n = \frac{1}{2\pi} \sqrt{\frac{k}{M}} = \frac{1}{2\pi} \sqrt{\frac{AE}{ML}} = 57.8 \text{ Hz}$
- lateral direction $f_n = \frac{1}{2\pi} \sqrt{\frac{k}{M}} = \frac{1}{2\pi} \sqrt{\frac{3EI}{ML^3}} = 21.2 \text{ Hz}$

Both calculated natural frequencies fulfill the requirements.

29.6.8 Strength aspects

Cylinder

In Fig. 29.17 the inertia loads which will act on the mass of the experiment of the satellite are illustrated. The cylinder defines the load path and will transfer the inertia loads to the interface with the launcher.

The inertia loads in y-direction will introduce bending at the interface with the launcher and in combination with the inertia loads in y-direction maximum compression stresses will be calculated at the interface. Also the buckling behaviour of the cylinder will be investigated.

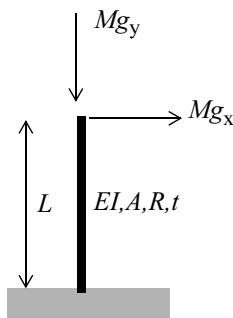


Fig. 29.17 Loaded cylinder

Following properties and facts will be taken into account to calculate the maximum stresses:

- Wall-thickness $t=0.5 \text{ mm}$
- Radius $R=300 \text{ mm}$
- Second moment of area $I = 4.24 \times 10^{-5} \text{ m}^4$
- Area cross-section $A = 9.42 \times 10^{-4} \text{ m}^2$

Design Loads

The loads at the interface are given in Fig. 29.18.

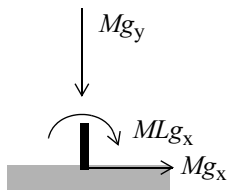


Fig. 29.18 Design Loads

The inertia forces and bending moment are

- In x -direction $Mg_x = 500*9.81*5.5=26978 \text{ N}$
- In y-direction $Mg_y = 500*9.81*1.5=7378 \text{ N}$
- About z-axis $MLg_x = 500*9.81*5.5=26978 \text{ Nm}$
- Maximum stress (compression) $\sigma_o = \frac{n_y}{t} = \frac{Mg_y}{A} + \frac{MLg_x R}{I} = 28.7 \text{ MPa}$

where the section modulus $W = \frac{I}{R} = \pi R^2 t$.

At this moment the shear stress at the interface is neglected.

Margins of Safety Yield

The MS value against the yield stress is

$$MS = \frac{\sigma_y}{j_y \sigma_o} - 1 = \frac{410}{1.1 * 28.7} - 1 > 10$$

Margins of Safety Ultimate

The MS value against the ultimate stress is

$$MS = \frac{\sigma_u}{j_u \sigma_o} - 1 = \frac{480}{1.25 * 28.7} - 1 > 10$$

Buckling of the cylinder under compression loads

The allowable buckling stress of a monocoque cylindrical shell will be calculated [NASA SP-8007, Marty 1986]. At first the sensitivity to imperfections is estimated with

$$\gamma = 1 - 0.901(1 - e^{-\alpha}), \quad (29.60)$$

$$\text{with } \alpha = \frac{1}{16} \sqrt{\frac{R}{t}}.$$

The allowable buckling stress of a monocoque cylinder with radius R and wall-thickness t is

$$\sigma_{buck} = \frac{\gamma E}{\sqrt{3(1 - v^2)}} \left(\frac{t}{R} \right) \quad (29.61)$$

The MS value against the allowable buckling stress is

$$MS = \frac{\sigma_{buck}}{j_y \sigma_o} - 1 \geq 0$$

With a radius $R=300 \text{ mm}$, an ultimate factor of safety $j_u=1.25$ and $\sigma_o = 28.7 \text{ MPa}$. A sensitivity analysis is performed on the wall-thickness t .

We select a cylinder with a wall-thickness $t=0.75$ mm.

Table 29.4 Trade-off wall-thickness t (mm)

t (mm)	$\sqrt{\frac{R}{t}}$	α	γ	σ_{buck} (MPa)	MoS
0.5	600	1.53	0.294	20.8	-0.42
0.75	400	1.25	0.357	37.8	0.05
1.0	300	1.08	0.405	57.2	0.59

The minimum second moment of area required is $I = 5.397 \times 10^{-4} \text{ m}^4$. A new value for the radius can be calculated with (29.58), $R = \sqrt[3]{\frac{I}{\pi t}} \Rightarrow 0.25 \text{ m}$.

With a radius $R=250$ mm, an ultimate factor of safety $j_u=1.25$ and $\sigma_o = 28.7 \text{ MPa}$ we perform a sensitivity analysis on the wall-thickness t .

Table 29.5 Trade-off wall-thickness t (mm)

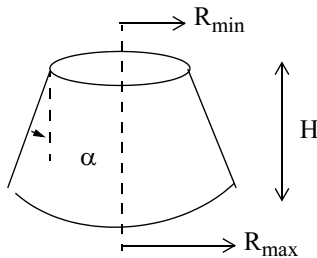
t (mm)	$\sqrt{\frac{R}{t}}$	α	γ	σ_{buck} (MPa)	MoS
0.5	500	1.40	0.321	27.2	-0.25
0.75	333.7	1.14	0.387	49.1	0.36

We select a cylinder with wall-thickness $t=0.75$ mm and radius $R=250$ mm. The second moment of area $I = \pi R^3 t = 3.68 \times 10^{-5} \text{ m}^4$ and the area of the cross-section $A = 2\pi R t = 1.18 \times 10^{-3} \text{ m}^2$.

Cone

Strength properties

Assuming that the diameter at the interface with the launcher $D=900$ mm and the interface with the experiment is $D=400$ mm, then the load carrying structure must be conical. It is assumed to design a cone with a minimum radius $R_{min}=200$ mm and a maximum radius $R_{max}=450$ mm. The height of the cone is $H=1000$ mm.

**Fig. 29.19** Cone

The allowable buckling axial load for long conical shells can be expressed as [Seide 1968]

$$F_{cr} = \gamma \frac{2\pi Et^2(\cos\alpha)^2}{\sqrt{3(1-v^2)}}, \quad (29.62)$$

where γ is an experimental factor with recommended value $\gamma = 0.33$ for $(10^\circ < \alpha < 75^\circ)$

- t wall-thickness (m)
- E modulus of elasticity $E=70$ (GPa)
- v Poisson's ratio =0.3

The angle α becomes

$$\alpha = \tan^{-1}\left(\frac{R_{\max}-R_{\min}}{H}\right) = \tan^{-1}\left(\frac{225-100}{1000}\right) = 14,04^\circ.$$

Neglecting the shear load, it can be stated that

$$F_{cr} \geq j_u Mg_y = 1.25 * 500 * 9.81 * 5.5 = 33722 \text{ N}.$$

It follows that the wall-thickness of the cone must be chosen to be $t=0.7$ mm.

The buckling load F_{cr} (N) becomes

$$F_{cr} = \gamma \frac{2\pi Et^2(\cos\alpha)^2}{\sqrt{3(1-v^2)}} = 0.33 \frac{2\pi 70e90.0007^2(\cos 14.04)^2}{\sqrt{3(1-v^2)}} = 40510.$$

The MS value can be calculated

$$MS = \frac{F_{cr}}{j_u Mg_y} - 1 = \frac{40510}{1.25(500)9.81(5.5)} - 1 = 0.20.$$

Stiffness

The flexibility of the cone in launch direction (y-axis) is [Seide 1972, Girard 1999]

$$G_y = \frac{1}{k} = \frac{\ln\left(\frac{R_{max}}{R_{min}}\right)}{2\pi \sin\alpha (\cos\alpha)^2 Et}. \quad (29.63)$$

The associated natural frequency is $f_y = \frac{1}{2\pi\sqrt{G_y M}}$

After some ample manipulation $f_y = \frac{1}{2\pi\sqrt{G_y M}} = 66 \text{ Hz}$

The MS value is

$$MS = \frac{66}{35} - 1 = 0.88$$

The flexibility of the cone in lateral direction (x-axis) is [Seide 1972, Girard 1999]

$$G_x = \frac{1}{k} = \frac{\ln\left(\frac{R_{max}}{R_{min}}\right) - 2\left(1 - \frac{R_{min}}{R_{max}}\right) + \left(1 - \left\{\frac{R_{min}}{R_{max}}\right\}^2\right)\left(\frac{1}{2} + (1 + v)(\sin\alpha)^2\right)}{\pi(\sin\alpha)^3 Et}. \quad (29.64)$$

The associated natural frequency is $f_x = \frac{1}{2\pi\sqrt{G_x M}}$

After some ample manipulation $f_y = \frac{1}{2\pi\sqrt{G_x M}} = 26 \text{ Hz}$

The MS value is

$$MS = \frac{26}{15} - 1 = 0.73$$

29.6.9 Summary MS values

Table 29.6

Structure	Strength/stiffness	Calculated	Required	MS
Cylinder	Nat. freq. lateral (Hz)	19.8	15	0.32
	Nat. freq. launch-direction (Hz)	64.6	35	0.85
	Buckling (MPa)	49.1	28.7	0.36
Cone	Buckling (N)	40510	33722	0.20
	Nat. freq. lateral (Hz)	26	15	0.73
	Nat. freq. launch-direction (Hz)	66	35	0.88

Literature

- Arianespace, 1999, ARIANE 4 User's Manual, Issue 2.
 Girard, A. and Pawłowski, M., *Optimum Conical Shell For Dynamic Behaviour*, Vibrations in Launchers, Conference, Toulouse, 1999, pages 265–272.
 Marty, D., 1986, *Conception des Vehicles Spatiaux*, Masson
 NASA SP-8007, *Buckling of Thin-Walled Circular Cylinders*, 1968.
 Seide, P., 1972, *Influence Coefficients for End-Loaded Conical Shells*, AIAA Journal, Vol. 10, No.12, 1972, pages 1717–1718.
 Seide, P., Weingarten, V.I., 1968, *Buckling of Thin-Walled Truncated Cones*, NASA Space Vehicle Design Criteria (Structures, NASA SP-8019, 1968)

29.7 Stiffness calculations using Castiglano's second theorem

The stiffness of the truss system both in x and y direction will be calculated using the Castiglano's second theorem

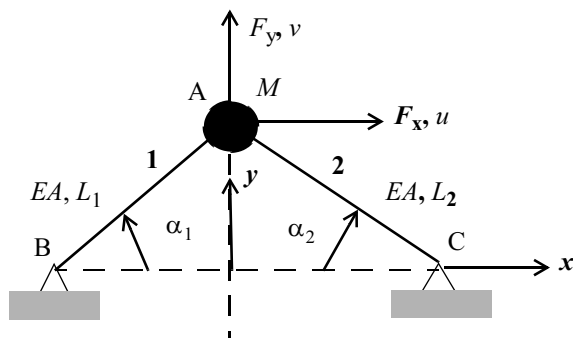


Fig. 29.20 Symmetrical Truss System with concentrated mass.

The complementary energy in the truss system is denoted by $U(E, A, L, F_y, F_y, \alpha)$. For linear systems the complementary energy is equal to the potential energy or strain energy.

The strain energy in a strut with a constant load N (N) is given by

$$U = \frac{1}{2} \int_0^L \frac{N^2(x)}{E(x)A(x)} dx, \quad (29.65)$$

with $N(x)$ the variable load in longitudinal direction of the strut, $E(x)$ the variable Young's modulus of the strut and $A(x)$ the variable cross section of the strut.

For a constant stiffness EA and load N the strain energy for one strut is

$$U = \frac{1}{2} \frac{N^2 L}{EA}. \quad (29.66)$$

The total strain energy in the truss system is

$$U = \frac{1}{2} \frac{N_1^2 L_1}{EA} + \frac{1}{2} \frac{N_2^2 L_2}{EA}. \quad (29.67)$$

The displacement u and v can be calculated with Castigliano's second theorem

$$u = \frac{\partial U}{\partial F_x}, \quad v = \frac{\partial U}{\partial F_y} \quad (29.68)$$

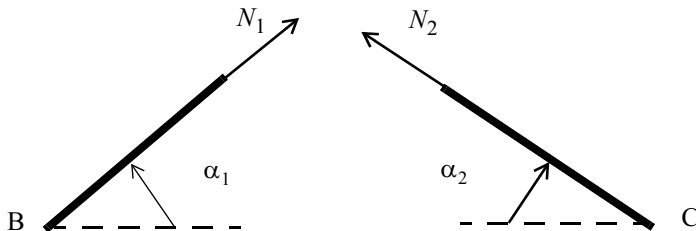


Fig. 29.21 Strut Loads

The equilibrium equations in point A are

$$\begin{bmatrix} \sin \alpha_1 & \sin \alpha_2 \\ \cos \alpha_1 & -\cos \alpha_2 \end{bmatrix} \begin{bmatrix} N_1 \\ N_2 \end{bmatrix} = \begin{bmatrix} -F_y \\ -F_x \end{bmatrix}. \quad (29.69)$$

The solution of (29.69) is, when $\alpha_1 = \alpha_2 = \alpha$,

$$N_1 = -\frac{F_x}{2\cos\alpha} - \frac{F_y}{2\sin\alpha}, N_2 = \frac{F_x}{2\cos\alpha} - \frac{F_y}{2\sin\alpha}. \quad (29.70)$$

The strain energy in the truss system becomes

$$U = \frac{1}{2} \frac{\left(-\frac{F_x}{2\cos\alpha} - \frac{F_y}{2\sin\alpha}\right)^2 L}{EA} + \frac{1}{2} \frac{\left(\frac{F_x}{2\cos\alpha} - \frac{F_y}{2\sin\alpha}\right)^2 L}{EA}.$$

The displacement u is

$$u = \frac{\partial U}{\partial F_x} = \frac{1}{2(\cos\alpha)^2 EA} P_x L \quad (29.71)$$

and the displacement v is

$$v = \frac{\partial U}{\partial F_y} = \frac{1}{2(\sin\alpha)^2 EA} P_y L \quad (29.72)$$

The stiffness in x -direction is k_{xx} and the stiffness in y -direction is k_{yy} , and are defined as

$$k_{xx} = \frac{F_x}{u} = \frac{1}{2(\cos\alpha)^2} \frac{EA}{L}, \quad (29.73)$$

and

$$k_{yy} = \frac{F_y}{v} = \frac{1}{2(\sin\alpha)^2} \frac{EA}{L}, \quad (29.74)$$

where L is the length of the struts.

The natural frequencies (Hz) in both directions are;

- x-direction $f_x = \frac{1}{2\pi} \sqrt{\frac{k_{xx}}{M}}$,
- y-direction $f_y = \frac{1}{2\pi} \sqrt{\frac{k_{yy}}{M}}$,

with M the mass at point A (kg).

The stresses in strut 1 and strut 2 are

$$\sigma_1 = \frac{N_1}{A}, \quad \sigma_2 = \frac{N_2}{A}.$$

29.8 Modal Effective Mass of a Cantilevered Beam

A cantilevered beam with bending stiffness EI and length L is shown in Fig. 29.22. The modal deformation is given by

$$\phi(x) = 2\left(\frac{x}{L}\right)^2 - \frac{4}{3}\left(\frac{x}{L}\right)^3 + \frac{1}{3}\left(\frac{x}{L}\right)^4 \quad (29.75)$$

The mass per unit of length of the cantilevered beam is m (kg/m).

- Calculate the natural frequency (Hz) associated with the modal deformation $\phi(x)$ using the Rayleigh Quotient
- Calculate the modal participation with respect to point A respectively in w and Θ direction
- Calculate generalised mass associated with the modal deformation $\phi(x)$.
- Calculate the 2×2 modal effective mass matrix.

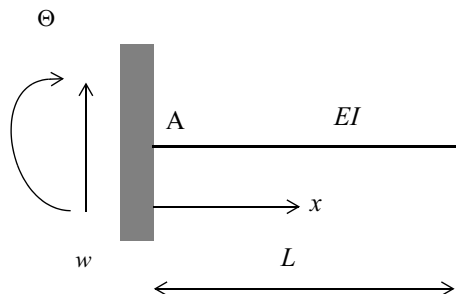


Fig. 29.22 Clamped beam

An approximation of the natural frequency can be obtained with the aid of Rayleigh's quotient $R(\omega)$ which is given by

$$R(\phi) \approx \omega_0^2 = \frac{\int_0^L EI \{\phi''(x)\}^2 dx}{\int_0^L m \{\phi(x)\}^2 dx} = 12.46 \frac{EI}{mL^4} \quad (29.76)$$

where

$$\phi'(x) = \frac{4}{L}\left(\frac{x}{L}\right) - \frac{4}{L}\left(\frac{x}{L}\right)^2 + \frac{4}{3L}\left(\frac{x}{L}\right)^3 \text{ and}$$

$$\phi''(x) = \frac{1}{L^2} \left[4 - 8\left(\frac{x}{L}\right) + 4\left(\frac{x}{L}\right)^2 \right].$$

The nominator of (29.76) now becomes

$$\int_0^L EI\{\phi''(x)\}^2 dx = \frac{EI}{L^4} \int_0^L \left\{ 4 - 8\left(\frac{x}{L}\right) + 4\left(\frac{x}{L}\right)^2 \right\}^2 dx = 3.2 \frac{EI}{L^3}. \quad (29.77)$$

The denominator of (29.76) becomes

$$\int_0^L m\{\phi(x)\}^2 dx = m \int_0^L \left\{ 2\left(\frac{x}{L}\right)^2 - \frac{4}{3}\left(\frac{x}{L}\right)^3 + \frac{1}{3}\left(\frac{x}{L}\right)^4 \right\}^2 dx = 0.2568mL. \quad (29.78)$$

The natural frequency of the bending beam becomes

$$f_o = \frac{\omega_o}{2\pi} = \frac{1}{2\pi} \sqrt{R(\omega)} = \frac{1}{2\pi} \sqrt{\frac{3.2 \frac{EI}{L^3}}{0.2568mL}} = \frac{3.53}{2\pi} \sqrt{\frac{EI}{mL^4}} = 0.56 \sqrt{\frac{EI}{mL^4}} \quad (29.79)$$

The modal participation factor is the coupling between the rigid body motion $\phi_R(x)$ ($\omega = 0$) and the elastic mode $\phi(x)$. The coupling matrix $[L]^T$ can be obtained by

$$[L]^T = \begin{Bmatrix} m \int_0^L \phi_{Ru}(x)\phi(x)dx \\ m \int_0^L \phi_{R\theta}(x)\phi(x)dx \end{Bmatrix}. \quad (29.80)$$

The rigid body mode associated with the translation U is set to $\phi_{RU}(x) = 1$ and the rigid body mode associated with the rotation θ is set to $\phi_{R\theta}(x) = x$. The mass matrix as rigid body modes (with respect to point A) can be calculated by

$$[M_R] = \begin{bmatrix} m \int_0^L \phi_{Ru}(x)\phi_{Ru}dx & m \int_0^L \phi_{Ru}(x)\phi_{R\theta}dx \\ m \int_0^L \phi_{R\theta}(x)\phi_{Ru}dx & m \int_0^L \phi_{R\theta}(x)\phi_{R\theta}dx \end{bmatrix} = \begin{bmatrix} mL & \frac{m}{2}L^2 \\ \frac{m}{2}L^2 & \frac{m}{3}L^3 \end{bmatrix}. \quad (29.81)$$

The vector with the modal participation factors (29.80) becomes

$$[L]^T = \begin{Bmatrix} m \int_0^L \left(2\left(\frac{x}{L}\right)^2 - \frac{4}{3}\left(\frac{x}{L}\right)^3 + \frac{1}{3}\left(\frac{x}{L}\right)^4 \right) dx \\ m \int_0^L x \left\{ 2\left(\frac{x}{L}\right)^2 - \frac{4}{3}\left(\frac{x}{L}\right)^3 + \frac{1}{3}\left(\frac{x}{L}\right)^4 \right\} dx \end{Bmatrix} = \begin{Bmatrix} 0.4mL \\ 0.29mL^2 \end{Bmatrix}. \quad (29.82)$$

The generalised mass is (29.78)

$$m_g = \int_0^L m \{ \phi(x) \}^2 dx = m \int_0^L \left\{ 2\left(\frac{x}{L}\right)^2 - \frac{4}{3}\left(\frac{x}{L}\right)^3 + \frac{1}{3}\left(\frac{x}{L}\right)^4 \right\}^2 dx = 0.2568mL.$$

Finally it is possible to calculate the modal effective mass matrix with regards to the assumed mode shape $\phi(x)$. The modal effective mass matrix is defined as

$$[M_{\text{eff}}] = \frac{[L]^T [L]}{m_g} = \frac{\begin{Bmatrix} 0.4mL \\ 0.29mL^2 \end{Bmatrix} \begin{Bmatrix} 0.4mL & 0.29mL \end{Bmatrix}}{0.2568mL} = \begin{bmatrix} 0.62mL & 0.45mL^2 \\ 0.45mL^2 & 0.33mL^3 \end{bmatrix}. \quad (29.83)$$

If the modal effective mass matrix $[M_{\text{eff}}]$ is compared with the mass matrix as rigid body with respect to point A $[M_{RR}]$ it can be concluded that with one mode $\phi(x)$ 62% of the mass is represented and about 100% of the second moment of mass.

29.9 Component Mode Synthesis (Craig-Bampton Method)

Consider the discrete dynamic system with 5 DOFs, which is illustrated in Fig. 29.23. Study its dynamic behaviour and compare the results obtained using component mode synthesis retaining different numbers of modes.

The fixed-free Craig-Bampton method will be applied. For simplicity the spring stiffnesses are equal $k_1 = k_2 = k_3 = k_4 = k_5 = k = 1$ and the discrete masses are $m_1 = m_2 = m_3 = m_4 = 1$ and $m_5 = 0.5$. The system matrices, the mass and stiffness matrix respectively, are:

$$[M] = \begin{bmatrix} 1 & 0 & 0 & 0 & 0 \\ 0 & 1 & 0 & 0 & 0 \\ 0 & 0 & 1 & 0 & 0 \\ 0 & 0 & 0 & 1 & 0 \\ 0 & 0 & 0 & 0 & 0.5 \end{bmatrix}, [K] = \begin{bmatrix} 2 & -1 & 0 & 0 & 0 \\ -1 & 2 & -1 & 0 & 0 \\ 0 & -1 & 2 & -1 & 0 \\ 0 & 0 & -1 & 2 & -1 \\ 0 & 0 & 0 & -1 & 1 \end{bmatrix}.$$

By directly solving the eigenvalue problem, the following eigenvalues are extracted

$$\{\lambda\} = \begin{Bmatrix} 0.0979 \\ 0.8244 \\ 2.0000 \\ 3.1756 \\ 3.9021 \end{Bmatrix}.$$

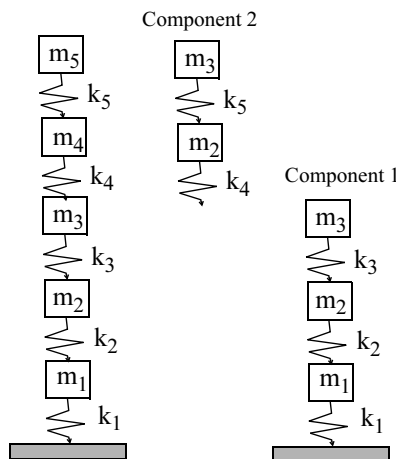


Fig. 29.23 Sketch of the system and components

Component 1

Component 1 includes nodes 1, 2 and 3 with the associated masses and springs. The displacements at nodes 1 and 2 are the internal DOFs $[x_1, x_2]$ while the displacement at node 3 is a boundary DOF x_3 . The mass and stiffness matrix of the component 1, partitioned first with the boundary DOFs and then the internal ones, are

$$\begin{aligned}
[M_1] &= \begin{bmatrix} 1 & 0 & 0 \\ 0 & 1 & 0 \\ 0 & 0 & 1 \end{bmatrix}, [K_1] = \begin{bmatrix} 1 & -1 & 0 \\ -1 & 2 & -1 \\ 0 & -1 & 2 \end{bmatrix}, \\
[K_{ii,1}] &= \begin{bmatrix} 2 & -1 \\ -1 & 2 \end{bmatrix}, [K_{ib,1}] = \left\{ \begin{array}{c} -1 \\ 0 \end{array} \right\}, [M_{ii,1}] = \begin{bmatrix} 1 & 0 \\ 0 & 1 \end{bmatrix}, \\
\{\Phi_{c,1}\} &= \left\{ \begin{array}{c} 1 \\ \frac{1}{3} \\ \frac{2}{3} \end{array} \right\}, \{\Phi_{i,1}\} = \begin{bmatrix} 0 & 0 \\ \frac{\sqrt{2}}{2} & \frac{-\sqrt{2}}{2} \\ \frac{\sqrt{2}}{2} & \frac{\sqrt{2}}{2} \end{bmatrix}, \\
[M_{CB,1}] &= \begin{bmatrix} 1.5556 & 0.7071 & -0.2357 \\ 0.7071 & 1 & 0 \\ -0.2357 & 0 & 1 \end{bmatrix}, [K_{CB,1}] = \begin{bmatrix} 0.3333 & 0 & 0 \\ 0 & 1 & 0 \\ 0 & 0 & 3 \end{bmatrix}.
\end{aligned}$$

Component 2

The second component includes nodes 3, 4 and 5 with the associated masses and springs. The mass at node 3 is set to zero because it will be represented in component 1. The displacements at nodes 4 and 5 are the internal DOFs $[x_4, x_5]$ while the displacement at node 3 is a boundary DOF x_3 . The mass and stiffness matrix of the component 1, partitioned with the boundary DOFs first and then the internal ones, are

$$\begin{aligned}
[M_2] &= \begin{bmatrix} 1 & 0 & 0 \\ 0 & 1 & 0 \\ 0 & 0 & 0.5 \end{bmatrix}, [K_2] = \begin{bmatrix} 1 & -1 & 0 \\ -1 & 2 & -1 \\ 0 & -1 & 1 \end{bmatrix}, \\
[K_{ii,2}] &= \begin{bmatrix} 2 & -1 \\ -1 & 1 \end{bmatrix}, [K_{ib,2}] = \left\{ \begin{array}{c} -1 \\ 0 \end{array} \right\}, [M_{ii,2}] = \begin{bmatrix} 1 & 0 \\ 0 & 0.5 \end{bmatrix}, \\
\{\Phi_{c,2}\} &= \left\{ \begin{array}{c} 1 \\ 1 \\ 1 \end{array} \right\}, \{\Phi_{i,2}\} = \begin{bmatrix} 0 & 0 \\ \frac{\sqrt{2}}{2} & \frac{-\sqrt{2}}{2} \\ 1 & 1 \end{bmatrix}, \\
[M_{CB,2}] &= \begin{bmatrix} 1.5 & 1.2071 & -0.2071 \\ 1.2071 & 1 & 0 \\ -0.2071 & 0 & 1 \end{bmatrix}, [K_{CB,2}] = \begin{bmatrix} 0 & 0 & 0 \\ 0 & 0.5858 & 0 \\ 0 & 0 & 3.412 \end{bmatrix}.
\end{aligned}$$

The components can be assembled the same as the elements. The following map can be written:

Table 29.1 Map of components DOFs

Component #	Boundary DOF #	Internal DOF #	Global DOF #
1	1	1	1
		2	2
		3	3
2	1	1	1
		2	4
		3	5

The map of the DOFs will yield the following stiffness and mass matrix

$$[K_{\text{CMS}}] = \begin{bmatrix} 0.3333 & 0 & 0 & 0 & 0 \\ 0 & 1 & 0 & 0 & 0 \\ 0 & 0 & 3 & 0 & 0 \\ 0 & 0 & 0 & 0.5858 & 0 \\ 0 & 0 & 0 & 0 & 3.1442 \end{bmatrix}$$

$$[M_{\text{CMS}}] = \begin{bmatrix} 3.0556 & 0.7071 & -0.2357 & 1.2071 & -0.2071 \\ 0.7071 & 1 & 0 & 0 & 0 \\ -0.2357 & 0 & 3 & 0 & 0 \\ 1.2071 & 0 & 0 & 0.5858 & 0 \\ -0.2071 & 0 & 0 & 0 & 3.1442 \end{bmatrix}$$

The matrices have been partitioned in such a way as to separate the boundary displacements DOFs from the modal DOFs. If the third and fifth rows and columns are cancelled, only one internal DOF is taken into account for each component. If the matrices are used in complete form, all modes are considered and the result must coincide except for computing approximations, with the exact ones (complete model). The results obtained in terms of eigenvalues (square of natural frequency) are

Table 29.2 Eigenvalues

Size of matrices	5 (exact)	3 (1 mode)	5 (2 modes)
Mode 1	0.0979	0.0979	0.0979
Mode 2	0.8244	0.8245	0.8244
Mode 3	2.0000	2.2150	2.0000
Mode 4	3.1756		3.1756
Mode 5	3.9021		3.9021

This example is taken from the book of Genta, [Genta 1995].

Literature

Genta, G., 1995, *Vibration of Structures and Machines*, ISBN 0-387-94403-6, Springer Verlag.

Subject Index

A

Abort limit 82
Absolute
 acceleration 60, 248, 370
 displacement 32, 59, 248, 369
 temperature 413
Acceleration
 transformation matrix 303
Accelerometer 73
Acceptance test 72
Acoustic
 analysis 334
 load 28, 73, 334
 test 72, 83
Admissible vector 232
Allowable
 cycles 350
 stress 20
Alternative Dunkerley's equation 238
Altitude 403
Aluminium
 alloy 207
 honeycomb core 207
A-matrix 414
Amplification factor 320
Analytical
 mass matrix 315
 mode shape 315
ARIANE 5 10
Assumed mode 232, 325
ATLAS 10
ATM 303
Atmospheric flight 313
Attitude
 control 2
Attitude control system 14, 215
A-value 21

Average speed 403

B

Balance weight 216
Bandwidth 49
Base acceleration 370
Bending
 beam 127
 stiffness 160
 stress 133
Bernoulli method 447
Beryllium alloy 208
Block
 of stress amplitude 352
 of stress cycles 352
Boron fibres 209
Boundary degrees of freedom 250
Buckling
 load 20
 of cone 147
 of cylinder 143
 of sandwich cylinder 164
 safety factor 20
Bumper 407
B-value 21

C

Carbon fibres 209
Castiglano's first theorem 126
CB
 reduced-mass matrix 285
 reduced-stiffness matrix 285
CDLA 281, 313

- Centre
 frequency 49
 of gravity 215
 of mass 215
- Centrifuge test 76
- Characteristic
 constant 448
 equation 235
 passages 326
- CLA 313
- Classical pulses 386
- CME 443
- CMS 281
- Coefficient
 of moisture expansion 443
 of thermal expansion 443
- Collision 403
- Combination of load conditions 114
- Component
 modal synthesis 281
 mode synthesis 281
 vibration requirement 337
- Composite material 207
- Conduction
 coefficient 439
 matrix 415
- Confidence interval 21
- Conservation of energy 420
- Constraint modes 284
- Continuous dynamic system 310
- Convergent nozzle 449
- Coordinate system 189
- Correlation requirement 315
- Coupled load analysis 119, 281, 313
- Craig–Bampton 266
 method 282
 model 304, 314
 transformation matrix 252, 284
- Crater diameter 406
- Cratering 405
- Critical
 damping 187
 design review 7, 216
- Cross
 orthogonality 86, 193
 orthogonality check 265
 orthogonality matrix 315
 second moments of mass 217
- CTE 443
- Cumulative
 damage rule 349
 density function 358
- D**
- Damping
 constant 187
 energy 181
 property 186
 ratio 187
- Data system 14
- Debris flux model 64
- Decaying sinusoid 386
- Decibel 42
- Degrees of freedom 186
- DELTA 10
- Deployable mechanism 2
- Design
 consideration 212
 criteria 111
 development plan 6
 drawing 6
 element 101
 limit load 19, 72
 load 106
 process 5
 specification 5
 study 6
- Detrimental deformation 20
- Diffuse sound field 46
- Dimpling of face sheet 166
- Displacement
 compensation 388
 field 434
 function 176
 transformation matrix 303
- Distributed
 heat 422
 mass 230
- Dry mass 216
- DTM 303
- Dunkerley's equation 229
- Dutch Space B.V. 413
- Dynamic analysis 118
- E**
- Effective pressure 52
- Elastic
 deformation 290
 mode shape 250
- Electrical
 ground support equipment 6
 model 6
- Enforced acceleration 32, 248
- Engine ignition 313

- Engineering strain 444
- Euler load 128
- Exciter 386
- Expendable launch vehicle 9
- Exposed area 410
- External
 - degree of freedom 250
 - heat flow 417
 - load vector 176
- F**
- Face
 - dimpling 159
 - sheet 157
- Facing failure 162
- Factor of safety 19, 110
- Fail-safe 23
- Failure mode 113, 162
- Fast sine sweep 386
- Fatigue
 - curve 349
 - life 349
 - problem 349
- Fibreglass 209
- Fill factor 55
- Filtered plots 98
- Finite element
 - analysis 118
 - mass matrix 225
 - method 175
 - model 175, 315, 413
 - model check 117
 - model requirements 189
 - strain energy 176
 - type 185
 - work 176
- First moment of mass 217
- Fixed-interface method 282
- Flexibility matrix 202, 289
- Flight
 - acceptance load 23
 - acceptance test 71
 - limit load 19, 72
 - model 6, 74
- Foldable structure 28
- Force
 - exciter 86
 - limiting 96
 - vector 178
- Fractile 22
- Free-free
 - elastic body 250
- Free-interface method 287
- Fuel mass 217
- Functional requirement 105
- G**
- Gamma function 357
- Generalised
 - coordinate 252, 282
 - mass 252
 - stiffness 252
- Geometric matrix 227
- Geostationary orbit 1
- Global mass matrix 225
- Growth rate 402
- Guyan reduced stiffness matrix 252
- H**
- Half sine pulse 85
- Highest peak 328
- Honeycomb
 - core 157, 211
 - core properties 170
- I**
- I/F
 - accelerations 315
 - displacements 315
 - forces 315
- Imperfections 20
- Inertia-relief
 - coordinates 295
 - effect 296
- Insert 168
- Interface forces 314
- Internal
 - degree of freedom 250
 - thermal energy 417
- Internal load 123
- Interplanetary flux 400
- Interpolation
 - function 416
 - matrix 418

J

Jacobian 421
 Johnson column equation 129
 Joint 186

K

Kinetic energy 181
 Knock down factor 20, 144, 149

L

Lagrange 175
 multiplier 418
 Lagrangian function 181
 Lap joint 150
 Launch
 authority 313
 mission 103
 system 9
 vehicle 9
 vehicle adapter 104
 vehicles catalogue 11
 Life-fraction rule 349
 Lift-off 313
 Lightsat 216
 Limit stress 19
 Load
 transformation matrix 303
 Local
 buckling 139
 crushing of core 162
 Low level sine sweep test 73
 LTM 303
 Lumped
 heat input 422
 mass 230
 parameter method 413

M

MAC 109
 Magnesium alloy 207
 Margin of safety 23, 113
 Mass
 acceleration curve 109
 budget 215
 coupling 285
 matrix 182
 participation approach 333
 Matched SRS 392
 Material strength 20

Mathematical model 184, 313, 414

Max/min values 314

Maximum
 acceleration 60, 370
 shocktime 60, 374

Measurement plan 73

Mechanical
 dynamic load 28
 engineer 413

Metal

 alloy 207
 matrix 211
 threads 209

Micro meteoroid 28, 63
 flux 64

Micro metreonoid
 shower 400

Microphone 83

Miles' equation 320

Miner's constant 352

Minimum

 mass optimisation 160
 stiffness 199

Mission duration 410

Modal

 analysis 71
 assurance criteria 193, 265, 270
 base 282
 characteristics 86
 contribution 377
 coupling technique 281
 damping ratio 253, 325
 effective mass 94, 247, 254, 334
 matrix 252, 284
 participation factor 253, 285, 376
 reaction force 255
 survey 71, 85
 transformation 283

Mode

 displacement method 281, 303

Modulated random noise 386

Moisture contents 445

Moment of inertia 215

Myosotis formulae 127

N

Narrow-banded Random Vibration 355
 Natural frequency 35, 106, 107, 123, 229,
 249, 320
 Newmark-beta method 380
 Newton-Cotes Method 392

- Nodal temperature 415
 Normal mode generalised coordinates 295
 Normalised cross orthogonality 270
 Notching 86
 Numbering scheme 190
- O**
 OASPL 52
 Octave band 48
 One-third octave band 48
 Operational condition 207
 Orbital debris 63
 Organic fibres 209
 Orbital debris
 flux 402
 Orthogonality test 86
 OTM 303
 Output transformation matrix 303
 Overall sound pressure level 52
- P**
 Palgren-Miner 349
 Passages 320, 326
 PAT 413
 Payload 2
 separation system 104
 Permanent deformation 20
 Permissible bending moment 215
 Pilot accelerometer 82
 Poisson 409
 Positive zero crossings 356
 Potential energy 176
 Power spectral density 319
 function 40
 Power supply 14
 Preliminary
 design review 7, 216
 sizing 123
 Preliminary design 105
 Prescribed averaged temperatures 413
 Pressure change 28
 Primary
 contractor 313
 structure 27
 Principal
 axis of inertia 224
 coordinates 282
 direction 203
 second moments of mass 217
- Probability
 density function 358
 of impact 409
 Probability (*cont.*)
 of no impact 410
 of occurrence of stress 350
 Production document 6
 Proof load 20
 Propulsion system 15
 Protection method 404
 Proto flight model 75
 PSD 40
 Pyroshock 57, 368
- Q**
 Qualification
 model 6, 74
 test 71
 Quasi-static
 load 108
 load factor 123
- R**
 Rain flow method 351
 Random
 mechanical load 319
 vibration 38, 319
 vibration level 110
 vibration load factors 321
 vibration test 72, 82
 Range pair-range counting method 351
 Rankine allowable load 131
 Rayleigh's
 method 132
 quotient 229
 Reaction force 248
 Reduced
 dynamic model 281
 mass matrix 303
 model 193
 stiffness matrix 202, 303
 Reference
 coordinate system 218
 pressure 52
 Relative
 displacement 248
 motion 248
 velocity 59, 370
 Reliability 21

- Residual
 - flexibility matrix 289
 - mass 94
- Reverberant
 - chamber 72, 83
 - sound field 46
- Rigid body
 - mass matrix 254
 - mode 179, 252, 289
 - motion 226
 - motion energy 190
 - vector 375
- Ring 141
- Root
 - mean square 320
 - sum squared 333
- RSS 333
- Running load 146

- S**
- Safe-life 23
- Safety plan 74
- Sandwich
 - column 163
 - construction 157
- S-basis 22
- Scaled test mode 316
- Secant coefficient of thermal expansion 443
- Second moment of mass 215
- Secondary
 - notching 86
 - structure 27, 73
- Selection of material 114, 207
- Separation test 73
- SEREP 266
- Service module 2
- Shaker 71
- Shear
 - crimping 166
 - force 162
 - stress 134, 162
- Shell of revolution 143
- Shock
 - load 28, 56, 73, 367
 - response spectrum 56
 - spectra plot 315
 - test 72, 85
- Shut down 313
- Sicilian carbide fibres 209
- Side-condition 416
- Simpson's rule 392
- Sine
 - burst test 75
 - dwell test 75
 - vibration test 71, 78
- Single mass-spring system 320
- Sinusoidal vibration 30
- Smallsat 216
- s-N curve 349
- Solar radio flux 403
- Sound
 - pressure level 46, 335
- SOYUZ 10
- Space
 - debris 28
 - flight 1
 - transportation system 9
- Spacecraft
 - configuration 101
 - construction 2
 - structure 123
- Speed of sound 336
- Spinning satellite 215
- SPL 46, 335
- SRS 56, 367
- SRSS 379
- Stability of cone 147
- Staging 313
- Standard
 - deviation 21
 - structural element 112
- Static
 - condensation method 266
 - displacement method 229
 - mode 251, 283
 - test 71, 75
 - transformation 283
- Statistical Energy Analysis 319
- Steady-state
 - acceleration 29
 - heat problem 415
 - static load 28
- Steel 208
- Steinberg's approximation 357
- Stiffness
 - matrix 177
 - of cone 147
 - of cylinder 145
 - requirement 108, 200
- Strain
 - energy 176
 - gauge 73
 - vector 177

- S**
- Strength
 - analysis 118
 - of materials 124
 - Stress
 - cycle 349
 - range histogram 351
 - Structural
 - analyse 116
 - damping 187
 - member 123
 - model 6, 72, 74
 - test 71
 - Structure 2, 15
 - efficiency 115
 - mass 217
 - shrink 445
 - Stuffed Whipple Shield 406
 - Substructure 281
 - Subsystem 5, 13
 - S-Value 22
 - Sweep rate 79, 354
 - System equivalent reduction expansion process 266
- T**
- TAM 265
 - Tapered strut 131
 - Telecommunication system 15
 - Telemetry 2
 - Temperature
 - distribution 415
 - field 434
 - function 419
 - gradient 443
 - variation 433
 - Test
 - analysis model 265, 315
 - article 74
 - condition 74
 - facility 74, 98
 - mode 315
 - model 6
 - plan 6, 73
 - prediction 73
 - preparation phase 86
 - procedure 6, 74
 - rig 75
 - sequence 73
 - success criteria 73
 - tolerance 82
 - verification 120
- Thermal**
- control 2
 - control system 14
 - deformation 433
 - distortion 443
 - engineer 413
 - functional 416
 - model 6, 416
 - node 413
 - stress 413, 433
 - work 417
- Thermo-elastic Analysis** 118
- T**ime
- frame 60, 374
 - history 315, 351
 - history synthesis 385
- TITAN** 10
- T**itanium alloy 207
- T**olerance limit 62
- T**orsion in beam 136
- T**race of matrix 235
- T**ransformation matrix 180
- T**ransient response 370
- T**ransverse shear failure 162
- T**rapezoidal rule 392
- T**russ frame 124
- U**
- Ultimate load 20
 - Uncertainty factor 216
 - Unfiltered plots 98
 - Unit 189
 - displacement method 202
 - force method 201
 - Universal file 98
 - Upper bound 233
 - User's manual 10, 123
- V**
- Variation static pressure 62
 - Velocity compensation 388
 - Venting hole 447
 - Vibroacoustic Analysis 119
 - Virtual work 181, 433

W

- Wave
 form 386
 length 336
 number 336
Weight factor 22
Whiffle tree 76
Whipple Shield 406
Wöhler curve 349
Wrinkling of face sheet 166

Y

- Yield load 20
Yoke 419

Z

- Zero inertia effects 251
Zero to peak 78
Zero-upcrossing rate 326